Behaviour-dependent neuronal network activity in a novel *Cyfip1* haploinsufficient rat model of psychiatric risk

Julia Rita Heckenast

A thesis presented for the degree of

Doctor of Philosophy

June 2018

Word count: 67,700

Abstract

Advances in psychiatric genetics have begun to reveal the complex biological underpinnings of psychiatric disorders. Rare but penetrant copy number variants offer particularly direct mechanistic clues. The deletion at 15q11.2(BP1-BP2) has a 13% penetrance for developmental delay, congenital malformation, autism or schizophrenia. Reduced dosage of *CYFIP1,* one of four genes within this deletion, has emerged as a likely contributor to cognitive dysfunction seen in 15q11.2(BP1-BP2) deletion patients. However, the route from *CYFIP1* haploinsufficiency to impaired behaviour has not been fully mapped.

While synaptic deficits have been identified in mice haploinsufficient for *Cyfip1* (*Cyfip1*$^{+/-}$), circuit-level phenotypes have not been investigated. Using multi-site chronic electrode implants I recorded local field potential data simultaneously from prefrontal cortex, hippocampus and nucleus accumbens in a novel *Cyfip1*$^{+/-}$ rat model during a behavioural task and during sleep.

Cyfip1$^{+/-}$ rats show normal performance accuracy on a discrete-trial alternation T maze task, but require more trials to achieve criterion during training. Task-dependent hippocampal-prefrontal network coordination remains intact in well-trained *Cyfip1*$^{+/-}$ rats, although theta-gamma phase-amplitude coupling within dorsal hippocampus is reduced compared to WTs. While circadian patterns and sleep architecture appear normal, hippocampal non-REM ripples are diminished in *Cyfip1*$^{+/-}$ rats compared to WTs, and preliminary data from the related *Fmr1* (Fragile X Mental retardation 1) knockout rat also show aberrant ripples.

Disrupted interactions are seen in the cortico-hippocampal-accumbal network, most prominently during approach to sucrose reward locations. Altered N-methyl-D-aspartate receptor signalling is implicated, as *Cyfip1*$^{+/-}$ rats show an exaggerated response to acute ketamine injection in the form of an enhanced surge in high frequency oscillations in nucleus accumbens and prelimbic cortex.

Overall, abnormal behaviour- and ketamine-dependent network dynamics in hippocampus, prefrontal cortex and nucleus accumbens of *Cyfip1*$^{+/-}$ rats are reminiscent of some features of neuropsychiatric disorders, and lend weight to causal roles for *CYFIP1* haploinsufficiency in predisposing patients to cognitive dysfunction.

Acknowledgements

I would like to thank my supervisors, Prof Matt Jones, Prof Jeremy Hall and Prof Lawrence Wilkinson for their unwavering support and for opening the doors to some fantastic opportunities over the past four years.

Thanks also go to past and present members of the Jones Lab in Bristol for their friendship and support in and out of the lab. In particular, Dr Alice Fodder, Dr Emilie Werlen, Dr Aleks Domanski, Dr Flavie Kersanté, Dr Tom Jahans-Price, Dr Ullrich Bartsch, Emma Roscow, Ed Morrell, Dr Ross Purple and Dr Tim Howe. In Cardiff, thanks to Jenny Carter, Dr Nichola Brydges and Dr Trevor Humby for their technical support and helpful discussions, and to Dr Nick Clifton and Anna Moon for their friendship.

Thanks to Debi Ford and Leah Cook for their help with the histology, and to the undergraduate students who helped with sleep recordings.

I would like to thank my family for their support through the ups and downs, and finally, Petar, thanks for *everything*.

This project was jointly funded by Cardiff University School of Psychology and School of Medicine, with additional support from an MRC Senior Non-clinical Research Fellowship awarded to Matt Jones.

Declarations

Statement 1

This work has not been submitted in substance for any other degree or award at this or any other university or place of learning, nor is being submitted concurrently in candidature for any degree or other award.

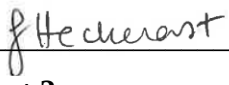
(Julia Heckenast) Date 15/5/2018

Statement 2

This thesis is being submitted in partial fulfillment of the requirements for the degree of Doctor of Philosophy.

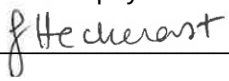
(Julia Heckenast) Date 15/5/2018

Statement 3

This thesis is the result of my own independent work/investigation, except where otherwise stated, and the thesis has not been edited by a third party beyond what is permitted by Cardiff University's Policy on the Use of Third Party Editors by Research Degree Students. Other sources are acknowledged by explicit references. The views expressed are my own.

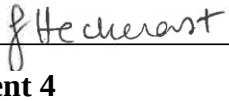
(Julia Heckenast) Date 15/5/2018

Statement 4

I hereby give consent for my thesis, if accepted, to be available online in the University's Open Access repository and for inter-library loan, and for the title and summary to be made available to outside organisations.

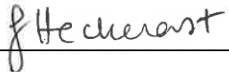
(Julia Heckenast) Date 15/5/2018

Acknowledgement of assistance received during the course of this thesis

Training in techniques and laboratory practice and subsequent mentoring:

Prof Matt Jones: discussions and advice with reference to systems neuroscience, behavioural neuroscience, surgical, behavioural and electrophysiological laboratory techniques and Matlab analysis.

Prof Lawrence Wilkinson: discussions and advice with reference to psychiatric molecular genetics and behavioural neuroscience.

Dr Ullrich Bartsch, Dr Lucy Carracedo, Dr Aleks Domanski, Dr Alice Fodder, Dr Jo Haddon, Dr Tom Jahans-Price, Dr Flavie Kersanté, Dr Emilie Werlen and Emma Roscow: discussions, advice and practical assistance with reference to electrophysiological and behavioural experiments and Matlab analysis.

Experimental assistance:

Anna Bickerton, Emilia Piwek and Joseph Moore (final year project students): assistance with preparing implants and conducting *Fmr1* KO rat sleep recordings reported in Chapter 7.

Debi Ford and Leah Cook: Majority of histological preparation of brain slices.

Data and analysis provided by others:

Prof Lawrence Wilkinson, Dr Simon Trent and Cardiff colleagues: Data regarding generation and molecular validation of *Cyfip1*$^{+/-}$ rat model.

Jenny Carter: Genotyping

Dr Gareth Banks: Ran my actigraphy data through the ClockLab data analysis package.

Any illustrations taken from external sources are explicitly acknowledged in the text of this thesis.

Contents

List of Tables

List of Figures

List of Abbreviations

ACC.....anterior cingulate cortex

AMPA.....α-amino-3-hydroxy-5-methyl-4-isoxazolepropionic acid

ANOVA.....analysis of variance

ARC.....activity-regulated cytoskeleton-associated

ARP2/3 .....actin-related proteins 2/3

BDNF .....brain-derived neurotrophic factor

Bdr .....blind-drunk

BOLD .....blood-oxygen-level dependent

BP1-BP2 .....base-pair 1 – base-pair 2

CA1.....Cornu Ammonis 1

CA3.....Cornu Ammonis 3

CANTAB.....Cambridge Neuropsychological Test Automated Battery

CNV.....copy number variation

CRISPR .....clustered regularly interspaced short palindromic repeats

Cyfip1 .....cytoplasmic FMR1 interacting protein 1

dCA1.....dorsal Cornu Ammonis 1

DISC1 .....disrupted in schizophrenia 1

DLG.....discs large

DNA .....deoxyribonucleic acid

ECoG .....electrocorticography

EEG .....electroencephalography

EHMT1.....euchromatic histone-lysine N-methyltransferase 1

eIF4E .....eukaryotic translation initiation factor 4E

EPSC.....excitatory post-synaptic current

ERBB4.....Erb-B2 receptor tyrosine kinase 4

F-actin.....filamentous actin

Fmr1 .....fragile X mental retardation 1

fMRI .....functional magnetic resonance imaging

FMRP .....fragile X Mental Retardation Protein

GABA.....γ-aminobutyric acid

G-actin ..... globular actin
GAD67 ..... glutamate decarboxylase
GSK3 ..... glycogen synthase kinase 3
GWAS ..... genome-wide association study
HFO ..... high frequency oscillations
HPC ..... hippocampus
Hz ..... Hertz
IL ..... infralimbic
IQ ..... intelligence quotient
KB ..... kilobase
KO ..... knock out
LED ..... light-emitting diode
LFP ..... local field potential
LTD ..... long-term depression
LTP ..... long-term potentiation
MAM ..... methylazoxymethanol acetate
MEG ..... magnetoencephalography
Mg^{2+} ..... magnesium ions
mGluR ..... metabotropic glutamate receptor
mPFC ..... medial prefrontal cortex
MRI ..... magnetic resonance imaging
mRNA ..... messenger ribonucleic acid
mTOR ..... mammalian target of rapamycin
NAc ..... nucleus accumbens
NIPA1 ..... non imprinted in Prader-Willi/Angelman Syndrome 1
NIPA2 ..... non imprinted in Prader-Willi/Angelman Syndrome 2
NMDA ..... N-methyl-D-aspartate
NMDAR ..... N-methyl-D-aspartate receptor
NREM ..... non-rapid eye movement
NRG1 ..... neuregulin 1
PAC ..... phase-amplitude coupling

PCP .....phencyclidine

PET .....positron emission tomography

PFC .....prefrontal cortex

PIR .....passive infrared sensor

PPI .....pre-pulse inhibition

PRL .....prelimbic

PV .....parvalbumin

Rac1 .....Ras-related C3 botulinum toxin substrate 1

REM .....rapid eye movement

SCN .....suprachiasmatic nucleus

SLc12A2 .....solute carrier family 12 member 2

SNAP-25.....synaptosomal-associated protein 25

SNARE .....SNAP receptor

SNP.....single nucleotide polymorphism

SWD .....spike-wave discharge

TRN .....thalamic reticular nucleus

TUBGCP5 .....tubulin gamma complex associated protein 5

vHPC .....ventral hippocampus

VTE .....vicarious trial and error

WT.....wild-type

Zdhhc8 .....zinc finger DHHC-type containing 8

ZNF804A.....zinc finger protein 804A

1

Chapter 1 Introduction

This chapter introduces the genetic and genomic insights that are having a major impact on our understanding of complex psychiatric disorders, followed by an introduction to the gene of interest, *CYFIP1,* and the *in vivo* circuit-level analysis approach which together represent the focus of this thesis. Sections of this chapter have been published in Heckenast et al. (2015).

1.1 Psychiatric molecular genetics: an inroad to complex psychiatric disorders

Many psychiatric disorders carry a significant genetic risk, apparent through classical family, twin and adoption studies (Gottesman, 1991; Kendler and Eaves, 2005). Together with environmental influences, genetic predisposition can significantly increase the chances of falling ill. As an example, schizophrenia is a severe disorder characterised by hallucinations and delusions (positive symptoms), a reduction in affect (negative symptoms) and cognitive deficits, with a lifetime prevalence of 1% (American Psychiatric Association, 2013; Tandon et al., 2009). The extent to which genetic makeup contributes to schizophrenia risk, i.e. the heritability of the disorder, is estimated to be 60-80% (Sullivan et al., 2012). Therefore, in principle, identifying which genes and variants contribute to risk and the mechanisms through which they impact brain function should allow rational design of new therapies. This is particularly critical for treatment of cognitive

deficits, the symptom domain most predictive of longer term prognosis (Green et al., 2000), which is not alleviated by currently available medications (Insel, 2010, 2012; Keefe et al., 2007). The pathophysiology of schizophrenia and other psychiatric conditions needs to be better understood before new targeted treatments can be designed.

One significant inroad to understanding the pathogenesis of schizophrenia, and increasingly other diagnosed psychiatric conditions such as bipolar disorder and autism, therefore lies with advances in psychiatric molecular genetics. Making use of large sample sizes and the integration of data within large-scale international consortia, modern day association studies are beginning to reveal the specific DNA variants that give rise to the genetic component of risk for disorder. These studies, most mature for schizophrenia, have seen great advances in cataloguing associated loci, with suspected candidate genes confirmed, new ones discovered and importantly convergent evidence implicating key, possibly causal, molecular pathways (Hall et al., 2015; Need and Goldstein, 2014; Pocklington et al., 2015; Rees et al., 2014; Ripke et al., 2014). Two emerging general conclusions are that the genetic architecture underlying psychiatric risk is highly multi-genic and complex, with contributions from, typically, hundreds of individually low penetrance single nucleotide polymorphism (SNP) variants that are common in the population (known as the 'polygenic' risk) together with a much lower number of rare but much more damaging variants (discussed further below). Secondly it appears there can be substantial genetic overlap between diagnosed conditions, whereby the same variants can confer risk across multiple clinically defined disorders including, to varying degrees, schizophrenia, bipolar disorder, autism, ADHD, developmental delay and intellectual disability (Kirov, 2015; Lee et al., 2013). Notwithstanding their emerging complexity, the genomic findings have stimulated the creation of new genetic models in order to delineate the biological mechanisms by which genetic variants can contribute to risk for disorder. Concurrently, the rapid progress in genome editing technologies, such as CRISPR, have enabled epidemiological studies of psychiatric genetics to inform mechanistic studies in cellular and animal models (McCarthy et al., 2014) by increasing the ease

and efficiency of genetic manipulation in a wider range of model species, including rats (Hamra, 2010).

Broadly, this thesis aims to understand the neural and behavioural consequences of *Cyfip1* haploinsufficiency, a gene within the recently identified risk-carrying 15q11.2 copy number variant (CNV), with a view to defining mechanisms of cognitive impairment in 15q11.2 CNV carriers. The work presented here is part of a major research programme at Cardiff University that aims to harness the recent advances in understanding the genomics underlying complex psychiatric conditions such as schizophrenia to generate novel animal models that could help in understanding the pathophysiology of disease processes and ultimately develop better treatments. In this chapter, following an overview of the genetic architecture of complex psychiatric disorders, I will introduce the 15q11.2 deletion syndrome and outline the rationale that led to the creation of the *Cyfip1*$^{+/-}$ rat model. Finally, I will introduce electrophysiological recording from behaving animals as the main experimental approach in this thesis, which provides one of the most directly translatable measures with which to investigate the activity of neural networks underlying cognitive processes and may represent useful disease biomarkers (Rosen et al., 2015).

1.2 The allelic architecture of genetic risk for psychiatric disorder

The genetic architecture of psychiatric conditions such as schizophrenia, bipolar disorder and autism is highly complex: risk alleles have varying frequencies in the population, different penetrance levels and interacting properties both with other genes and the environment, all of which contribute to the intricate relationship between genotype and phenotype. In broad terms, the main sources of genetic risk can be divided into: 1) genetic "nudges": alleles that are common in the population but have small individual effect sizes; 2) genetic "shoves": rare alleles with a larger effect on disease risk (McCarroll and Hyman, 2013) (Figure 1.1). It has been proposed that this basic genetic architecture arises from the effects of natural selection, whereby common alleles persist because they are individually less damaging to fecundity, whereas rarer, more damaging variants, such as CNVs, are

under negative selection because they adversely impact on fecundity (Kirov, 2015). In support of this notion, *de novo* rare variants have particularly high penetrance, potentially because they have not yet been subjected to the rigours of selection (Sullivan, Daly, and O'Donovan 2012). Genome-wide association studies (GWAS) using microarray-based methods and more recently sequencing methods are being used to identify the variants associated with an increased risk for psychiatric disorder.

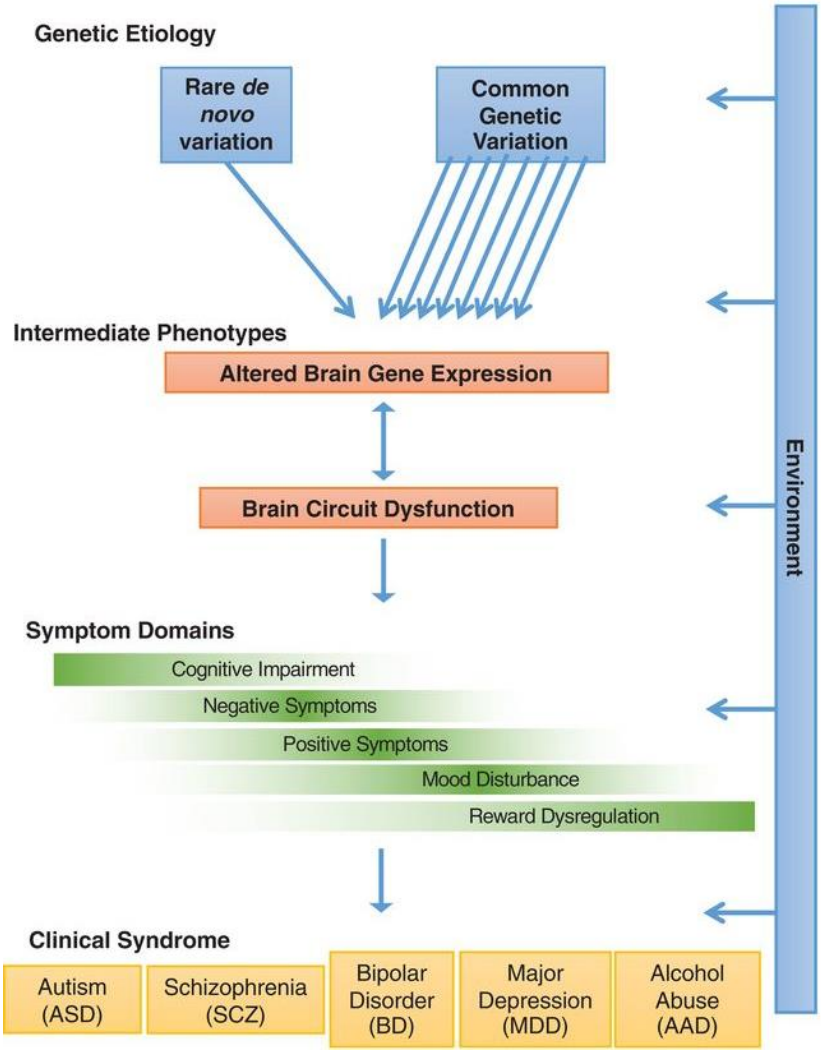

Figure 1.1 | **The pathogenesis of psychiatric disorders.** Figure taken from Gandal et al., (2018).

1.2.1 Genetic nudges: common, low penetrance single nucleotide polymorphisms

Successive GWAS in schizophrenia and other conditions have seen the number of significantly associated SNPs increase in parallel with sample sizes. The largest GWAS to date, which included 36,989 patients diagnosed with schizophrenia and 113,075 controls (Ripke et al., 2014), identified 108 risk loci for schizophrenia. The data were amassed through huge collaborative efforts among many research groups to combine phenotype-genotype datasets, and it is likely that as sample sizes increase further, more risk loci will be identified (Owen, 2014). The currently known 108 SNP risk loci are located both within genes (coding [exons] and non-coding [introns] regions) and between genes. As a proportion of the SNP variance is likely to reflect markers for risk genes in close genomic proximity, the 108 loci are estimated to implicate at least 350 genes (or more, depending on how liberally the associations are defined, see Need and Goldstein (2014)) across a number of putative pathogenic pathways.

These implicated genes include some previously suspected biological systems based on non-genetic evidence, as well as highlighting new associations. In line with a major theory of schizophrenia, which suggests aberrant dopamine signalling, the gene coding for the dopamine D2 receptor was in a risk locus. The most statistically significant association related to genes in the major histocompatibility complex, some of which are involved in innate immunity, lending support to an increasingly recognized hypothesis regarding the immune system's role in schizophrenia (reviewed in Patterson (2009), and Sperner-Unterweger and Fuchs (2015)). A subsequent study was able to ascertain which gene was driving this association (Sekar et al., 2016): the gene coding for the C4 complement protein which is, amongst a range of functions, interestingly also associated with synaptic pruning during development (Sekar et al., 2016). Other risk SNP loci implicate genes and pathways in other biological systems, notably those involved in glutamatergic neurotransmission, calcium signalling, epigenetic modification and synaptic function and plasticity, findings which demonstrate a degree of convergence with recent data from the analyses of rare variants, as described below.

The emerging picture of common risk variants suggests there is significant overlap in risk SNPs between schizophrenia, bipolar disorder, autism, major depression and ADHD, with cases from one disorder showing higher genetic similarity to the cases of another disorder than with their controls (Lee et al., 2013) (Figure 1.1). Following from this, analysing data from several psychiatric conditions helps improve predictions of polygenic risk (Maier et al., 2015) and a recent meta-analysis found similar overlap in transcriptomic profiling (Gandal et al., 2018). These findings suggest that current diagnostic categories do not align with genetically distinct pathophysiological states (Sullivan et al., 2018).

1.2.2 Genetic shoves: rare, higher penetrance genetic variants

CNVs are rare, sub-microscopic deletions or duplications of short stretches of chromosome, caused by unbalanced rearrangements during meiosis, leading to carriers having a structural variation on one of the chromosome pairs. CNVs range from hundreds of base pairs to several megabases in length and often span multiple genes. Schizophrenia patients have a 1-3-fold genome-wide enrichment of relatively rare CNVs, indicating significant contributions of these structural abnormalities to schizophrenia risk (Walsh et al. 2008; International Schizophrenia Consortium. 2008; Stefansson et al. 2008). This increased CNV burden is evident in several other neurodevelopmental and psychiatric disorders, including intellectual disability, autism spectrum disorders and attention-deficit/hyperactivity disorder (Kirov, 2015).

The deletion at 22q11.2 was the first identified schizophrenia-associated CNV, and larger sample sizes have allowed at least 15 more pathogenic loci to be identified (Rees et al., 2014). While only around 2.5% of patients with schizophrenia carry a pathogenic CNV, their odds ratios (the fold change in risk compared to the general population) are between 2 and 60 (Rees et al., 2015), a substantially larger effect size than SNPs. Almost all CNVs are also associated with a range of other neurodevelopmental disorders, such as autism spectrum disorder and intellectual disability (Girirajan et al., 2012; Kirov et al., 2014) (Figure 1.2).

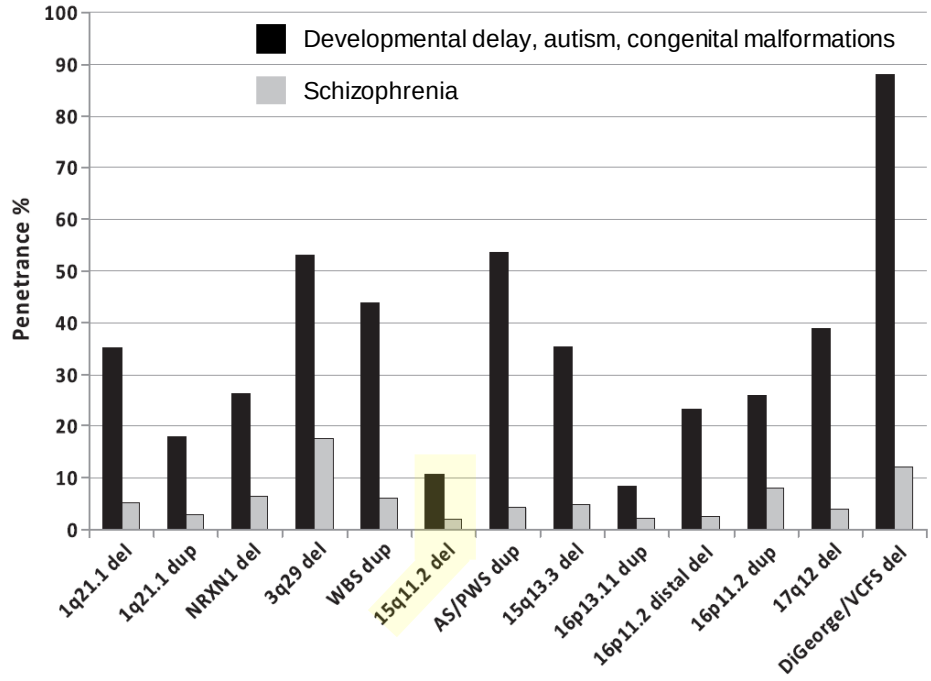

Figure 1.2 | **Penetrance of schizophrenia-associated copy number variants.** Taken from Kirov et al. (2014). AS/PWS, Angelman/Prader-Willi syndrome; del, deletion; dup, duplication; VCFS, velo-cardio-facial syndrome; WBS, Williams-Beuren syndrome.

While much of the overall population genetic risk for schizophrenia and other disorders is accounted for by alleles present in one or both of the parents, the hardest hitting, most penetrant individual mutations found in a small fraction of patients are often *de novo* (Kirov 2015), i.e. not present in the somatic cells of the parents but arising in their germ line during meiosis. The method used to study *de novo* CNVs, for example, is a proband-parent trio design, where CNVs which occur in the child but neither of the parents are identified. This design has proven successful in identifying *de novo* mutations in autism spectrum disorder and intellectual disability (Rauch et al., 2012; Sanders et al., 2012), while in a sample of 662 schizophrenia proband-parent trios and 2623 controls, Kirov et al. (2012) found rare *de novo* CNVs to be significantly more common in cases that in controls (5.1% vs 2.2%). Further *de novo* mutations were located at known schizophrenia risk loci, 3q29, 15q11.2, 15q13.3 and 16p11.2, while others included genes for the discs large (DLG) protein family, which are part of the post synaptic density, and euchromatic histone-lysine N-methyltransferase 1 (EHMT1), a histone methyl transferase which interacts directly with DLG proteins.

Rare and *de novo* mutations can also occur as single nucleotide variants (SNVs) and tiny insertions and deletions (indels) which, until recently, were undetectable due to their rarity and miniscule size. Whole genome sequencing now allows rapid and higher-resolution scanning in order to detect these mutations. Initially, sequencing research was limited to the exome, where data from schizophrenia trios showed enrichment of small *de novo* mutations in the N-methyl-D-aspartate receptor (NMDA) signalling complex, interactors with activity-regulated cytoskeleton-associated protein (ARC) at the synapse, and in the targets of the fragile X mental retardation protein (FMRP)-CYFIP1 complex involved in translation regulation. Further evidence supporting these findings came from a large scale case-control exome sequencing study, which found enrichment of small rare mutations in PSD-95, an NMDA receptor associated protein, and targets of the FMRP-CYFIP1 complex (Purcell et al., 2014). In addition they also found an enrichment in voltage-gated calcium channels, which have also been strongly implicated in previous GWAS analyses (Ripke et al., 2014) and play a key role in synaptic plasticity (Berger and Bartsch, 2014).

The largest whole genome sequencing study to date found that disruptive and damaging rare variants in schizophrenia cases were enriched in brain-specific genes, specifically in neuron-expressed genes, and within neurons were more enriched in synaptic genes, such as targets of FMRP (Genovese et al., 2016). So far only one gene passed the stringent statistical threshold to be confirmed by the whole genome sequencing approach (SETD1A, (Singh et al., 2016)), and it is likely that even greater sample sizes are needed when looking for such rare variants (Gratten, 2016). Nevertheless, these studies support the implication of synaptic pathways underlying schizophrenia (Hall et al., 2015).

1.3 Putting psychiatric genetics to work

An important next step in order to take advantage of the recent progress in identifying risk genes is the creation of animal and cellular models able to reveal the mechanisms by which genetic variants influence risk for disorder. While animal models in psychiatry in particular have encountered significant hurdles (Arguello and Gogos, 2006; Nestler and Hyman, 2010; Wong and Josselyn, 2015), the high

construct-validity of genetic approaches still holds strong potential to shed light on the mechanisms underlying disease aetiology.

An initial challenge arose in prioritising exactly which genetic animal models should be created. There has been some debate regarding the most advantageous genetic strategy for modelling purposes. By modelling common variants, with an individually small contribution to risk, it may prove difficult to see their effect on the phenotype, despite their significant overall contribution to risk in concert with other common and rare variants. However, it should not be forgotten that common variants have the potential to implicate genes and pathways of large effect, which can then be investigated and other elements of the pathway targeted by drugs (McCarroll and Hyman, 2013). An alternative basic strategy, one now widely supported (Karayiorgou et al. 2012; Need & Goldstein 2014; although see Hyman 2018), is to focus on the rare, highly penetrant mutations. While CNVs are the strongest contributing genetic factor in only a small fraction of schizophrenia cases, it is proposed that identifying the mechanism of these (predicted) stronger phenotypes will lead to finding convergent disturbances at the mechanistic level. In addition to the 22q11.2 mouse model, which has been intensively studied (Mukai et al., 2008; Nilsson et al., 2016a; Sigurdsson et al., 2010; Tamura et al., 2016; Van et al., 2017), a handful of mouse models have been created to model the recently identified, high penetrance CNVs (or single genes within them) for neuropsychiatric disorders, such as 7q11.23 (Li et al., 2009), 15q11-13 (Nakatani et al., 2009), 16p11.2 (Horev et al., 2011), 15q13.3 (Fejgin et al., 2014; Forsingdal et al., 2016; Nilsson et al., 2016b; Thelin et al., 2017), 1q21.1 (Nielsen et al., 2017) and finally, the key risk variant of this thesis, 15q11.2 (Bozdagi et al., 2012; DeRubeis et al., 2013; Hsiao et al., 2016; Pathania et al., 2014).

Following the decision to pursue highly penetrant CNV variants, the next challenge is to identify the causative, and mechanistically interesting individual genes within the CNVs responsible for the observed risk phenotype. While it is important to investigate all genes affected by the CNV, it makes practical sense to prioritize ones which other lines of evidence suggest may be mechanistically important. This was

the motivation behind the creation of the novel rat model investigated in this thesis, a rat heterozygous for *Cyfip1* (*Cyfip1*$^{+/-}$) designed to model the reduced gene dosage of *CYFIP1* in 15q11.2(BP1-BP2) deletion carriers.

1.4 15q11.2

The primary genetic lead of this thesis is the 15q11.2(BP1-BP2) CNV. This region is a risk locus for several neuropsychiatric and neurological disorders: intellectual disability, autism spectrum disorder, schizophrenia, developmental delay and epilepsy (Chaste et al., 2015; Fromer et al., 2014; Horsthemke and Wagstaff, 2008; Kirov et al., 2012; Leblond et al., 2012; Stefansson et al., 2014; Tam et al., 2010; Vanlerberghe et al., 2015; Zhao et al., 2013b). A deletion in this region is one of the most common CNVs linked to schizophrenia, with an odds ratio of 2.15 (Rees et al., 2014), while the reciprocal duplication contributes more to ASD risk (Malhotra and Sebat, 2012). This chromosomal segment has previously been of interest due to its involvement in Prader-Willi and Angelman syndromes, both imprinting disorders. Type I deletions of these syndromes include the BP1-BP2 segment, in addition to the imprinted region, and are associated with more severe neurodevelopmental symptoms than Type II deletions, where this segment is spared, revealing the critical nature of the BP1-BP2 deletion (Butler, 2017).

1.4.1 Carriers of the 15q11.2(BP1-BP2) CNV

Carriers of the 15q11.2(BP1-BP2) microdeletion may be identified when they present for genetic services due to varying degrees of developmental delay or intellectual disability (Abdelmoity et al., 2012; Burnside et al., 2011; Cox and Butler, 2015; Doornbos et al., 2009; von der Lippe et al., 2011; Madrigal et al., 2012; Picinelli et al., 2016; Rudd et al., 2014; Sempere Pérez et al., 2011; Vanlerberghe et al., 2015; van der Zwaag et al., 2010). A proportion of these carriers are diagnosed with schizophrenia or ASD at ~20% and ~27% respectively, with ~73% reporting developmental delay, estimated from a review of clinical case studies (Butler, 2017). However, not all carriers share a clinical phenotype, indicating that the CNV has incomplete penetrance with variable expressivity.

The above numbers were likely subject to ascertainment bias (referring to the non-random sampling that arises from studying subjects referred to genetic clinics) and lower power. Data from a much larger cohort (~13,000-32,000 cases, ~18,000 controls) led to a penetrance estimation for developmental delay, congenital malformation, ASD or schizophrenia, of 13% (Kirov et al., 2014). It is suggested that incomplete penetrance is seen due to the 'two-hit' hypothesis, whereby those with clinical phenotypes have a further pathogenic mutation or environmental insult that confers additional risk (Girirajan et al., 2012; Rudd et al., 2014). Incomplete penetrance offers the opportunity to study the effects of the CNV in controls, separately from disease states. A database of genotype data from a third of the Icelandic population provides an opportunity to study these carriers. Stefansson et al. (2014) identified 47 15q11.2(BP1-BP2) deletion carriers without a current clinical diagnosis of schizophrenia, ASD or intellectual disability from an Icelandic sample of 101,655 genotyped subjects, and found them to have marginally lower IQ than population controls as well as deficits in overall level of daily functioning (as assessed by the general assessment of function scale (Hall, 1995)) and cognitive deficits relating to dyslexia and dyscalculia, even after adjusting for IQ. In fact, these control carriers fell between population controls and schizophrenia patients on a number of tests, suggesting the presence of sub-clinical effects.

Structural MRI was assessed in 15 carriers of the 15q11.2(BP1-BP2) deletion and revealed reduced grey matter volume in the perigenual anterior cingulate cortex (ACC) and the left insula, as well as bilateral white matter reductions in the temporal lobe and increased white matter in the corpus callosum. The changes seen in ACC, a key region for cognitive and emotional processing and executive function (Bersani et al., 2014; Tamminga et al., 2000), are reminiscent of reduced grey matter volume observed in schizophrenia patients (Baiano et al., 2007). Similarly, temporal white matter reductions are associated with early-stage schizophrenia (Bora et al., 2011), although the white matter changes in the corpus callosum appear to be in the opposite direction to that found in schizophrenia patients (Arnone et al., 2008). The literature on structural correlates of dyslexia and dyscalculia, deficits observed in 15q11.2(BP1-BP2) deletion carriers, also reveals some overlap, such

as grey matter reductions in ACC associated with dyscalculia (Rotzer et al., 2008). Considering the clear neurodevelopmental impact of the 15q11.2(BP1-BP2) CNV, the next question is to identify which genes contribute to the phenotype.

1.4.2 The case for *CYFIP1* contributing to the 15q11.2 CNV phenotype

The 15q11.2(BP1-BP2) CNV extends over ~500kb and spans four non-imprinted genes: *NIPA1*, *NIPA2*, *CYFIP1* and *TUBCGP5* (Chai et al., 2003) (although one study did report parent of origin effects (Chung et al., 2015) implicating the possibility of imprinting). All genes are expressed in the central nervous system, with *CYFIP1*, *NIPA1* and *NIPA2* widely expressed, and *TUBGCP5* expressed specifically in the subthalamic nuclei (Nagase et al., 2001). *NIPA1* and *NIPA2* are both involved in Mg^{2+} transport (Goytain et al., 2007), and mutations in *NIPA1* cause autosomal dominant hereditary spastic paraplegia (Rainier et al., 2003) while *NIPA2* mutations cause childhood absence epilepsy (Jiang et al., 2012). *TUBGCP5* is involved in microtubule nucleation at the centrosome during mitosis (Izumi et al., 2008) has been implicated in other disorders including attention deficit hyperactivity disorder and obsessive compulsive disorder (De Wolf et al., 2013). All four genes have the potential to play roles in brain development and function, but at present it is unclear to what extent they each contribute to the risk of psychiatric disorder in carriers of the 15q11.2(BP1-BP2) deletion/duplication (Cox and Butler, 2015).

CYFIP1 has emerged as a prominent candidate for having a significant contribution to the cognitive dysfunction seen in the 15q11.2(BP1-BP2) deletion phenotype, primarily due to being first identified as an interacting partner of FMRP. Functional loss of FMRP causes the most common type of monogenic ID in the form of Fragile X Syndrome, where 30%-72% of cases exhibit ASD symptoms (Rosti et al., 2014). As mentioned, rare, disruptive point mutations are enriched in genes encoding targets of the FMRP/CYFIP1 complex, including ARC (Fromer et al., 2014; Genovese et al., 2016; Purcell et al., 2014). In addition, transcriptional profiling in human induced pluripotent stem cells with reduced *CYFIP1* expression revealed the dysregulation of genes associated with schizophrenia and epilepsy, providing

further support for the role of *CYFIP1* in disorders associated with 15q11.2(BP1-BP2) deletion (Nebel et al., 2016).

Cyfip1 is widely expressed in the nervous tissue (Hsiao et al., 2016; Köster et al., 1998; Yoon et al., 2014) but also other cell types, where it has been linked to cell migration in cancer metastasis (Bramham et al., 2016). CYFIP1 has been shown to have a role in two main functional complexes involved in the development and maintenance of neuronal structures at the synapse. On the one hand it interacts with the WAVE complex to mediate actin polymerization, and on the other, in combination with FMRP it exerts translational control on FMRP target mRNAs (Napoli et al., 2008; Schenck et al., 2001a, 2003) (Figure 1.3). Given these roles, what impact might reduced *CYFIP1* expression, as seen in 15q11.2(BP1-BP2) deletion carriers (Chai et al., 2003), have on brain structure, function and development, and how might these changes lead to the 15q11.2(BP1-BP2) deletion phenotype? An emerging literature of *CYFIP1* has started answering these questions using *in vivo* and *in vitro* modelling approaches.

1.4.3 Functions of *CYFIP1* in the brain

CYFIP1 is expressed widely in the brain from embryonic development through to adulthood (Köster et al., 1998) and, while it is present in all neuronal and glial cells (Hsiao et al., 2016; Pathania et al., 2014; Yoon et al., 2014), it is ~90% enriched at excitatory synapses compared to all dendrites (Pathania et al., 2014). Expression levels measured in cerebellum and cortex peak at 3 weeks old, a period important in the activity-dependent stabilization of synapses (Bonaccorso et al., 2015).

As mentioned above, CYFIP1 has two main functional states at the synapse, and broadly speaking acts as a molecular brake in both states (Figure 1.3). The small Rho GTPase RAC1 appears to act as a switch, regulating which complex CYFIP1 binds to (Di Marino et al., 2015). When CYFIP1 is bound to the WAVE complex, it renders it inactive. RAC1 can bind to (Kobayashi et al., 1998) and trigger a conformational change in CYFIP1 (DeRubeis et al., 2013; Di Marino et al., 2015), releasing the WAVE complex to interact with ARP2/3 and begin actin

polymerisation forming F-actin (Di Marino et al., 2015; Schenck et al., 2003). At this point, CYFIP1 is free to interact with other proteins, specifically FMRP (encoded by the *FMR1* gene) and the mRNA cap-binding protein eIF4E. FMRP recruits target mRNAs to CYFIP1, which then binds eIF4E, thus preventing translation initiation (Napoli et al., 2008). Translation is regulated by brain-derived neurotrophic factor (BDNF) or activation of group 1 metabotropic glutamate receptors (mGluRs), which, via activation of RAC1, trigger the dissociation of CYFIP1 and eIF4E, releasing the CYFIP1 brake and allowing translation to proceed (Napoli et al., 2008). Importantly, CYFIP1 can only interact with one of these pathways at one time (DeRubeis et al., 2013), therefore it will be necessary to understand which phenotypes are linked to the disruption of actin polymerisation, or the dysregulation of FMRP-target mRNA translation, or both.

1.4.4 *Cyfip1* animal models

The first animal modelling a reduction in the evolutionarily highly conserved *CYFIP1* gene, a *drosophila* with *dCyfip* mutation, was reported in 2003 (Schenck et al., 2003), and it was using this model that the dual role of CYFIP1 was first identified (Schenck et al., 2001b, 2003). Over ten years later, renewed interest in this region following genetic advances linking it to schizophrenia and other neurodevelopmental disorders, Bozdagi et al. (2012) generated a heterozygous mouse model that is haploinsufficient for *Cyfip1*, reflecting the low dosage of *CYFIP1* in 15q11.2(BP1-BP2) CNV deletion carriers. The *Cyfip1*-homozygous null mutant is lethal in mice during early embryonic development (Bozdagi et al., 2012; Pathania et al., 2014) .

Cyfip1 is expressed both in axons and dendrites, therefore we can expect it to have an impact both pre- and post-synaptically. A collection of studies in recent years have begun to elucidate the consequences of *Cyfip1* haploinsufficiency and the broad pattern emerging indicates that presynaptic phenotypes are present early in development, up to ~3 weeks, at which point presynaptic function appears normal while post-synaptic phenotypes emerge (Hsiao et al., 2016). The importance of developmental stages has also been highlighted by studies using human induced

pluripotent stem cells, showing *Cyfip1*-linked deficits in the development of neural progenitor cells (Yoon et al., 2014).

1.4.4.1 Presynaptic effects

Cyfip1 haploinsufficiency appears to impact synaptic development. Hippocampal sections from P10 *Cyfip1*$^{+/-}$ mice showed enlarged glutamatergic terminals with higher release probability compared to wild-type (WT) littermates due to increased vesicle pool size (Hsiao et al., 2016), which is not evident in mature neurons (Bozdagi et al., 2012). Postsynaptic strength was not affected as measured by miniature excitatory post-synaptic current amplitude (Hsiao et al., 2016). These presynaptic effects in cultured neurons were rescued when transfecting with a mutant version of *Cyfip1* that contains only the WAVE-associated binding region, but not with a mutant where neither the eIF4E nor the WAVE-associated binding region were present (Hsiao et al., 2016). These findings suggest that *Cyfip1* has a role in restraining the size and release probability in immature synapses, and that these presynaptic effects are likely mediated by Cyfip1's interaction with the WAVE regulatory complex, rather than via the FMRP-linked translation repression pathway. Furthermore, inhibition of RAC1 rescued this phenotype in cultured neurons and slices, indicating these effects are downstream of RAC1.

Enlarged presynaptic terminals may be a consequence of the higher levels of polymerized actin (F-actin) compared to soluble (G-actin) found in *Cyfip1*$^{+/-}$ hippocampal lysates compared to WT (Hsiao et al., 2016). This finding is consistent with the role of Cyfip1 as a repressor of actin polymerisation via the WAVE complex. However, it should be noted that there has been some conflicting evidence on the direction of the change in F-actin levels. De Rubeis et al. (2013) found cortical neurons from 15 day old *Cyfip1*$^{+/-}$ mice had longer dendrites with reduced levels of F-actin, while Pathania et al. (2014) saw longer dendrites with increased F-actin in spines in hippocampal cultured neurons from *Cyfip1*$^{+/-}$ mouse embryos, and in the Drosophila *cyfip* mutants, presynaptic terminals of the neuromuscular junction had higher F-actin levels (Schenck et al., 2003; Zhao et al., 2013a).

Consistent with the role of Cyfip1 as a repressor of protein translation (Napoli et al., 2008), cultured *Cyfip1*$^{+/-}$ neurons had greater levels of newly synthesised proteins, indicating higher levels of translation compared to WT (Hsiao et al., 2016). However, given that the eIF4E binding region was not necessary to rescue the presynaptic phenotype of enlarged terminals and increased release probability, the increased translation of Cyfip1 targets is independent of this phenotype.

In addition to defects at the synaptic terminal, evidence from the *drosophila cyfip1* null mutant model showed abnormal axonal growth, pathfinding and axonal branching. For example, in 79% of mutant fly embryos, axons abnormally crossed the midline, which was rescued by reinsertion of the *Cyfip1* gene (Schenck et al., 2003).

1.4.4.2 Postsynaptic effects

Cyfip1$^{+/-}$ mice show features akin to key characteristics of the *Fmr1* knockout mouse. Bozdagi et al. (2012) found enhanced mGluR-dependent long-term depression (LTD) in hippocampal slices from 4-6-week-old *Cyfip1*$^{+/-}$ mice, which is unusually independent of protein synthesis and mammalian target of rapamycin (mTOR), while long-term potentiation (LTP) was unaffected. Due to the similarity of this finding to the *Fmr1* phenotype, it would seem this feature is mediated via the FMRP-linked translation pathway. Hippocampal neurons, both *in vivo* from P55–60 *Cyfip1*$^{+/-}$ mice and *in vitro*, show decreased dendritic complexity, with more immature dendritic spines, although spine density was unchanged (Pathania et al., 2014). *Cyfip1* haploinsufficiency in cultured neurons leads to increased F-actin assembly in dendritic spines, which may partly underlie the dendritic dysmorphology seen (Pathania et al., 2014). Cortical neuron dendrites were also abnormal, with more immature, long spines (DeRubeis et al., 2013). There may be a dose-dependent effect of *Cyfip1*, as when *Cyfip1* expression levels were more extremely knocked-down by 70-80% vs. 40% seen in heterozygote neurons, cortical neurons showed a more profoundly reduced dendritic complexity, including reduced spine density (Abekhoukh et al., 2017). Pathania et al. (2014) suggested reduced dendritic complexity may be linked to Cyfip1's interaction with

RAC1, as the Rho GTPase has also been implicated in spine maturation (Cingolani and Goda, 2008). De Rubeis et al. (2013) attempted to parse out which Cyfip1 pathway is responsible for spine defects, and found that neither Cyfip1 mutant protein (missing either the WAVE- or FMRP-interacting region, respectively) could restore normal morphology. This suggests that both Cyfip1 pathways are important for correct dendritic development.

Expression of *ARC*, a key target protein of the FMRP-CYFIP1 complex, was found to be increased by ~30% at cortical synapses from *Cyfip1*$^{+/-}$ mice, consistent with the role of CYFIP1 as a translational repressor (DeRubeis et al., 2013). *ARC* is a dendritically-targeted mRNA that is enriched at active synapses (Steward and Worley, 2001) and has multiple roles in synaptic plasticity and actin polymerization. Decreasing *Arc* in the hippocampus leads to reduced F-actin levels (Messaoudi et al., 2007). Thus, while the overexpression of *Arc* in *Cyfip1*$^{+/-}$ mice supports the role of Cyfip1 as a translational repressor, dysregulation of *Arc* also demonstrates the converging routes by which Cyfip1 can influence F-actin polymerisation and subsequent morphological changes.

Spine shrinkage, which normally follows NMDA receptor activation, was absent in *Cyfip1*$^{+/-}$ cultured hippocampal neurons, suggesting a role for Cyfip1 in the structural reorganisation seen during synaptic plasticity, possibly via its regulation of actin dynamics (Pathania et al., 2014). *Cyfip1*$^{+/-}$ neurons also showed increased α-amino-3-hydroxy-5-methyl-4-isoxazolepropionic acid (AMPA) receptor mobility, indicating a lack of stabilization of the receptors (Pathania et al., 2014), which can impact synaptic plasticity (Huganir and Nicoll, 2013). Disruptions to the receptor-stabilizing cytoskeletal architecture might be a downstream effect of dysregulated actin dynamics. Furthermore, ARC has also been shown to regulate AMPA receptor mobility (Chowdhury et al., 2006). These findings support an important role for Cyfip1 in the development of normal dendritic morphology and function.

While this thesis focuses on understanding the consequences of *Cyfip1* haploinsufficiency, copy number variations at the 15q11.2 locus also include duplications of the BP1-BP2 region. It is worth noting that at the synaptic level, neurons from transgenic *Cyfip1*-overexpressing mice show opposite effects. For example, Oguro-Ando et al. (2014) showed more complex dendritic morphology in *Cyfip1*-overexpressing mice.

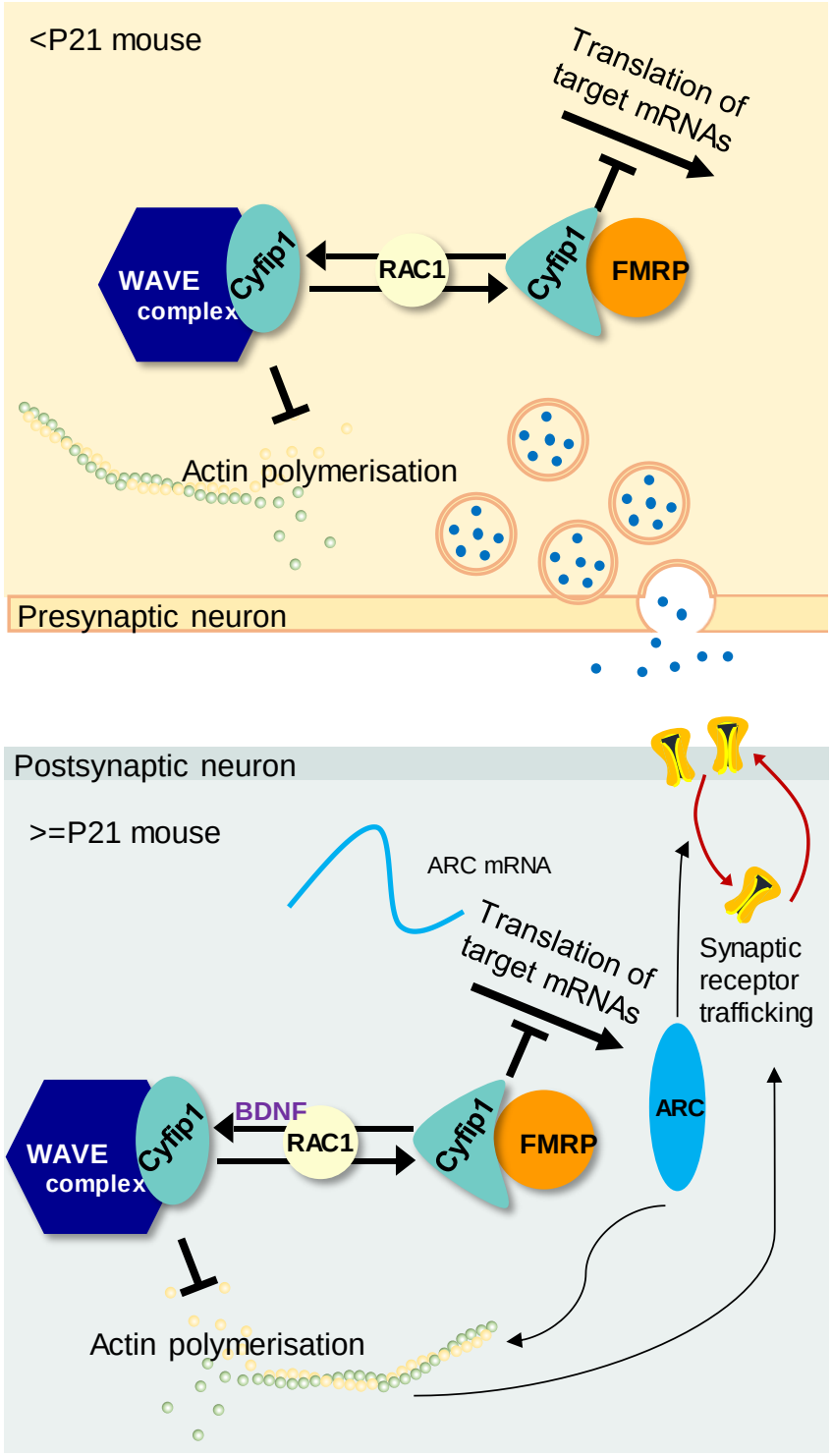

Figure 1.3 | **Role of *Cyfip1* at the synapse**. A simplified diagram of *Cyfip1*'s role pre- and post-synaptically. Presynaptic effects, observed in cells from P10 *Cyfip1* haploinsufficient mice but not P21, include increased glutamatergic terminal size and increased vesicle release probability, mediated via RAC1 and the Cyfip1-WAVE pathway. Postsynaptic effects, seen in P21 *Cyfip1* haploinsufficient mice but not P10, show increased translation of CYFIP1-FMRP target mRNAs, such as ARC, and most studies see increased actin polymerisation. Translation is regulated by BDNF, which promotes the CYFIP1-WAVE

interaction via RAC1, which acts as a conformational switch shuttling CYFIP1 from one complex to the other.

1.4.4.3 Behavioural effects

Behavioural findings in *Cyfip1*$^{+/-}$ mice are subtle and comparable to those seen in the *Fmr1* knockout model. *Cyfip1*$^{+/-}$ mice showed no anxiety phenotypes, as tested by open field analysis, and elevated zero maze (Bozdagi et al., 2012). Cognitive behavioural tests found no effect in the Y maze and Morris water maze, but observed an enhanced extinction of inhibitory avoidance, findings that parallel those seen in the *Fmr1* KO mouse (Bozdagi et al., 2012; Dölen et al., 2007). In this task the experimenters measured latency to enter the dark side of a box (that has previously been paired with a shock) in 3 post-acquisition extinction training sessions, during which a shock is no longer delivered. *Cyfip1*$^{+/-}$ mice had shorter latencies by the third post-acquisition session, displaying faster extinction of the memory to avoid the dark side of the box (Bozdagi et al., 2012).

1.4.5 From disrupted synapses to network-level deficits

Our current understanding of *Cyfip1* demonstrates its important role in the development of normal synapses, and while the exact mechanisms are still being investigated (Abekhoukh et al., 2017), these findings suggest a possible route by which *Cyfip1* haploinsufficiency could give rise to a network-level dysfunction that leads to psychiatric symptoms. Disruptions in actin remodelling and synaptic protein translation impact dendritic morphogenesis and synaptic plasticity which in turn are essential for normal development of neural networks (Jan and Jan, 2010; Kasai et al., 2010). To demonstrate with an example, we can follow the consequences of *Arc* disruption on network functioning (Peebles et al., 2010). Overexpression of *Arc* in hippocampal neurons (which is known to follow *Cyfip1* haploinsufficiency (DeRubeis et al., 2013)) leads to thinner spines, reminiscent of the increase in immature spines seen in *Cyfip1*$^{+/-}$ mutants – this follows what we would expect if Cyfip1 negatively regulates *Arc* expression. *Arc* is also important in regulating AMPA receptor cycling, and therefore elements of homeostatic plasticity, critical when responding to hyperexcitable events such as seizures.

Neural networks in *Arc*$^{-/-}$ mutant mice are indeed hyperexcitable, linking *Arc*'s role to the aetiology of epilepsy (Peebles et al., 2010).

Together, the above findings suggest that the negative consequences of *Cyfip1* haploinsufficiency on plasticity and spine dynamics could lead to a detrimental reorganisation of neural networks, ultimately leading to a psychiatric condition.

1.5 *In vivo* circuit-level analysis as a phenotyping strategy

This thesis presents experiments using a novel rat model haploinsufficient for *Cyfip1*. The rat model was created using CRISPR-Cas9 mediated genomic engineering leading to a 4 base pair deletion in the *Cyfip1* gene resulting in the generation of a premature-stop codon (further details in Appendix 1). Such new models require extensive phenotyping to understand the impact of the engineered mutation on brain function. One major aim of animal models is to identify biomarkers of fundamental disease processes, and where possible provide translationally relevant observations, which could inform patient stratification and give better measures of drug efficacy. As mentioned, the synaptic impact of *Cyfip1* could give rise to network level deficits, which could then link the molecular and cellular changes to any behavioural consequences of the genetic mutation. In this thesis I utilize an *in vivo* electrophysiology approach to observe the impact of *Cyfip1* haploinsufficiency in the context of an intact network in a behaving animal, a technique which also has potential to reveal translatable biomarkers through the analysis of neuronal oscillations. Next, I will introduce *in vivo* circuit-level analysis as a first line phenotyping strategy. Here, as in much of the discussion in the thesis, the main focus will be on schizophrenia, reflecting that the large majority of work in both psychiatric genomics and allied systems level analysis has been done in schizophrenia. However, as discussed previously, there can be overlap of symptoms and to an extent clinical conditions with respect to effects of the same genetic lesion, in the case of 15q11.2(BP1-BP2) CNV depending on the dosage effects (i.e. low dosage in the deletion or high dosage in the duplication) the increased risk is shared mainly between schizophrenia, autism and intellectual disability, together in some instances with motor deficits (Butler, 2017).

1.5.1 Neural oscillations and coherence

Cognitive processing is supported by neural oscillations: population activity patterns emerging from the coordinated, periodic summed sub-threshold electrical activity of a population of neurons and synapses (Buzsáki and Draguhn, 2004). Oscillations originate in distributed brain areas, and their synchrony presents a framework for short- and long-range circuit interactions (Buzsáki and Watson, 2012), as proposed by the influential 'communication through coherence' hypothesis (Fell and Axmacher, 2011; Fries, 2005; Friston et al., 2015a). This hypothesis posits that the pace of cognitive flexibility we require must depend on a method of communication between brain areas other than anatomical connections, which at these timescales are relatively fixed. It is proposed that a flexible communication mechanism can arise from the coherence between neuronal populations. Coherence captures the extent to which the phase relationships of the two regional oscillations remain consistent as well as correlations in power (Harris and Gordon, 2015) (Figure 1.4a). Oscillations reflect the changing excitability of the neuronal population, modulating the likelihood of firing and its sensitivity to inputs. Therefore, neuron firing is often phase-locked to the oscillation, reliably firing at a preferred phase of the oscillation – the archetypal example being phase locking of hippocampal pyramidal neuron spike times to the local theta rhythm (O'Keefe and Recce, 1993). The recurring windows of excitability allow inputs from a distant but coherent brain region to influence its target (Fries, 2005). Oscillations of different frequencies can occur at the same time, and this mechanism might allow selective communication by operating in different frequency bands, ranging delta (1-4 Hz), theta (6-10 Hz) and beta (15-30 Hz), to faster gamma (30-90Hz) and high frequency oscillations above 100Hz.

Oscillations in the theta and gamma frequency bands in particular have been associated with mnemonic processing in rodents, humans and monkeys (Düzel et al., 2010). For example, theta coherence between hippocampus and prefrontal cortex is selectively increased during the retrieval phase of a working memory task in rats (Benchenane et al., 2010; Jones and Wilson, 2005; Sigurdsson et al., 2010), while gamma coherence peaks during the encoding phase (Spellman et al., 2015).

Intra-hippocampal gamma coherence between CA1 and CA3 is also increased during the retrieval phase of a maze task (Montgomery and Buzsáki, 2007). Human electroencephalogry (EEG) studies show that theta coherence between the prefrontal cortex and temporal lobe increases during encoding and retrieval, persists during the delay phase of a working memory task, and correlates with increasing working memory load (Axmacher et al., 2008). Gamma coherence in humans was initially noted for its role in visual 'binding' and perceptual processing (Engel and Singer, 2001), but intracranial recordings from epileptic patients allowed recording from the medial temporal lobe, showing that increased gamma coherence between hippocampus and rhinal cortex predicted successful encoding during a verbal memory task (Fell et al., 2001). In monkeys it was shown that hippocampal neurons showed enhanced phase-locking to gamma during successful encoding (Jutras et al., 2009).

Oscillatory coherence has also been specifically linked to memory encoding through enhanced plasticity (Jutras and Buffalo, 2010). The precise neuronal firing that can arise from cells phase-locked to an ongoing rhythm can facilitate spike timing-dependent plasticity (STDP). Gamma oscillations are particularly well-placed for inducing STDP (Abbott and Nelson, 2000; Axmacher et al., 2006; Jutras and Buffalo, 2010), as the temporal window where phase-locked neurons fire is on the scale of the 10-20ms window required for STDP to occur (Markram et al., 1997). LTP can also be induced by delivering burst stimulation to the CA1 at the peak of theta oscillations, while inputs arriving during the trough induce LTD (Huerta and Lisman, 1995; Hyman et al., 2003).

Networks oscillating at different frequencies can be further associated through cross-frequency coupling, such as theta-gamma phase-amplitude coupling, whereby gamma amplitude is modulated by theta phase (Bragin et al., 1995; Colgin, 2015) (Figure 1.4b). This phase-amplitude coupling has been associated with working memory processes in rats (Tort et al., 2009) and humans (Axmacher et al., 2010; Canolty and Knight, 2010)

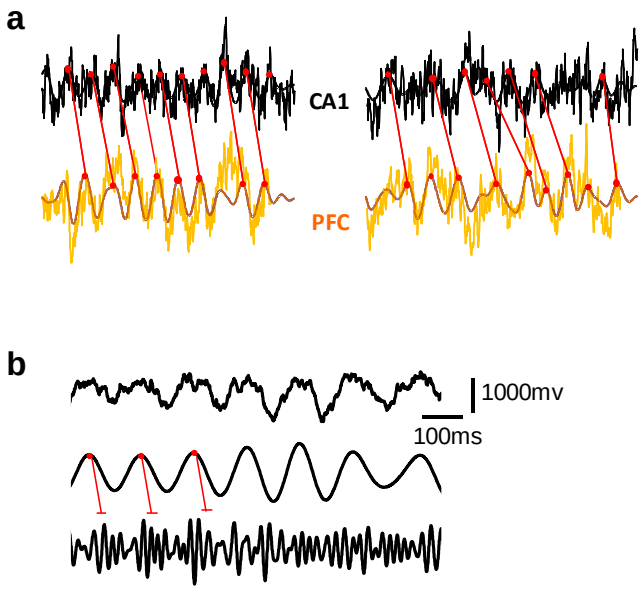

Figure 1.4 | **Coherence and phase amplitude coupling of oscillations. a,** Raw traces from hippocampal CA1 (black) and prefrontal cortex (yellow), with data filtered at theta frequency (6-10Hz) overlaid in a thicker line. Peaks of the theta oscillations are marked with red circles and red lines highlight the relationship between the phase of theta in the two regions. The left traces are more coherent than the right. Figure provided by M.W. Jones. **b,** Data from hippocampal CA1 showing the raw trace (top), theta filtered signal (6-10Hz, middle) and gamma filtered signal (30-90Hz, bottom). Gamma amplitude is more coupled to theta peaks (as highlighted by red lines) in the first three theta cycles than in the later ones.

1.5.2 Aberrant oscillations in 15q11.2 CNV-associated psychiatric disorders

To my knowledge, there have been no studies directly examining oscillatory activity in 15q11.2(BP1-BP2) deletion carriers. However, the literature contains extensive analyses of these phenomena in schizophrenia and to a lesser extent autism and intellectual disability.

The idea that schizophrenia may be caused by pathological interactions between brain regions was first proposed by Wernicke early in the 20th century (Wernicke, 1906). It is only in recent years that this hypothesis has been corroborated by observations of abnormalities in oscillations and their synchronization in schizophrenia patients from imaging and electrophysiological studies (Pettersson-Yeo et al., 2011), coupled with anatomical evidence of altered white matter organisation (Kubicki et al., 2007). This aberrant connectivity is increasingly thought to play a role in the causes of cognitive deficits seen in patients (Haenschel and Linden, 2011), supporting the idea of schizophrenia as a 'functional

disconnection syndrome' (Friston and Frith, 1995; Friston et al., 2016). Findings have seen deficits in local synchrony, measured as the power of oscillations within a brain region, or in synchrony between distinct brain regions (reviewed in Spellman and Gordon, 2015). In autism, more recent work in imaging, electrophysiology and white matter tractography points towards abnormal connectivity, with a combination of long-range hypo-connectivity and local hyper-connectivity findings (Hughes, 2007; O'Reilly et al., 2017).

A significant problem in drug trials for schizophrenia is the lack of reliable and objective biomarkers to measure improvement in disease state (Hyman, 2014). Crucially, neural network activity as measured by electro/magnetoencephalography (EEG/MEG) and functional magnetic resonance imaging (fMRI) have the potential to be highly informative biomarkers for diagnosis and efficacy of treatment, paving the way to patient stratification and the discovery of new therapies (Haenschel and Linden 2011; Jones, Menniti, and Sivarao 2015).

The important functional relevance to cognition of theta and gamma oscillations has led to an interest in these frequency bands in schizophrenia research. Studies investigating oscillations in humans can be divided into three broad experimental paradigms, 1) perception related paradigms, such as auditory steady-state responses and stimulus-evoked potentials, 2) spontaneous oscillations, i.e. during resting state or during sleep, and 3) during cognitive tasks, such as working memory (Phillips and Uhlhaas, 2015). Studies reporting on oscillatory activity during working memory tasks and during sleep are particularly relevant to this thesis, as the experiments presented herein utilize these behavioural contexts.

Abnormal gamma band spectral power is consistently reported in schizophrenia, but different paradigms lead to mixed findings. A general pattern has emerged where cortical gamma power is reduced in perception-related tasks and during cognitive processes (Uhlhaas and Singer, 2010), including working memory (Haenschel et al., 2009), but increased in spontaneously occurring gamma during resting (Kikuchi et al., 2011) (although reports inconsistent with this pattern,

showing increased gamma during task performance (Barr et al., 2010) and reduced resting state gamma also exist (Rutter et al., 2009)). Gamma oscillations are driven by recurrent excitatory/inhibitory circuits between parvalbumin-positive (PV) interneurons and glutamatergic pyramidal cells (Cardin et al., 2009; Sohal et al., 2009). Indeed, several findings point to impaired excitatory/inhibitory balance in schizophrenia, such as disrupted N-methyl-D-aspartate receptor (NMDAR) mediated transmission and post-mortem studies finding a reduction in PV interneurons and GAD67 expression, the enzyme that turns glutamate into γ-aminobutyric acid (GABA) (Cohen et al., 2015).

Aberrant theta activity is also commonly reported in schizophrenia, but again with mixed results on the direction of change (Hunt et al., 2017; Kim et al., 2015). During an N-back working memory task, unlike healthy participants, schizophrenia patients did not show an increase in frontal theta activity with working memory load (Schmiedt et al., 2005). Theta generation in the rodent hippocampus depends on cholinergic and GABAergic input from the medial septum or local interneuron/pyramidal cell recurrent networks (Buzsáki, 2002), while in the cortex, slice recordings suggest theta may be generated by layer 5 neurons (Carracedo et al., 2013). Frontal midline theta oscillations are prominent in human scalp EEG recordings and have been implicated in memory encoding and retrieval (Hsieh and Ranganath, 2014). Direct links between pathological changes in schizophrenia and in theta generating systems are currently unclear (Hunt et al., 2017).

Network oscillations have been shown to have a strong genetic determination, as exemplified by highly correlated, fingerprint-like gamma oscillation characteristics in identical twins (van Pelt et al., 2012). Indeed, many of the genetic pathways being implicated in psychiatric illness have significant roles in the generation of oscillations, such as NMDAR signalling and GABAergic signalling (Pocklington et al., 2015). Furthermore, numerous genetic animal models have found abnormal changes in neural network activity, which in some cases have been directly linked to a causal mutation (e.g. *Erbb4* and *Zdhhc8* mutations, discussed further in Chapter 3).

1.5.3 Using circuit-level analysis to investigate the *Cyfip1*$^{+/-}$ rat

Skull surface EEG recordings from genetic animal models allow relatively direct translation to human studies, as well as using implanted electrodes to record directly from specific brain regions. Implanted electrodes can record local field potentials (LFP, local population activity) and individual spiking of neurons in behaving animals. Importantly, the characteristics of oscillations and mechanisms of generation have been conserved across species (Buzsáki et al., 2013), supporting the translatability of these measures. In addition, the high spatial and temporal resolution of this approach means that while it cannot give information regarding the entire brain it is well suited to investigate one or multiple brain areas. Multi-site electrophysiology particularly benefits from the larger size of a rat model compared to mice.

LFP signals reflect the extracellular voltage changes generated by the excitatory and inhibitory post-synaptic potentials of a population of neurons surrounding the recording electrode. Reports of the spatial region from which cells contribute to the LFP ranges on the scale of tens to thousands of micrometres (Kajikawa and Schroeder, 2011; Katzner et al., 2009), depending on brain region, recording condition and the level of synchronous activity of local cells (Lindén et al., 2011).

As in the human literature, the various paradigms used to investigate neural circuit function in animal models fall into a similar three categories: evoked oscillations such as event related potentials, spontaneous activity during rest or sleep, and observation of oscillations during behaviour (Phillips and Uhlhaas, 2015). The work in this thesis represents the first exploration of the consequences of *Cyfip1* haploinsufficiency on neural circuit function. I decided to focus on two broad networks which are known to be compromised in psychiatric conditions. Firstly, the hippocampal-prefrontal cortex circuit, which has received particular attention as disruptions of this network are associated with cognitive impairments in several psychiatric disorders, including schizophrenia, fragile X syndrome, major depression and post-traumatic stress disorder (Godsil et al., 2013; Park and Holzman, 1992; Wang et al., 2012). Secondly, nucleus accumbens-associated

networks, which are crucial to mediate normal reward-processing and decision-making have been shown to be disrupted in schizophrenia and autism, as well as several relevant animal models (Dölen, 2015; Fletcher and Frith, 2009; Fuccillo, 2016; Goda et al., 2015; Kohls et al., 2013; Lee et al., 2017; Radua et al., 2015). Furthermore, emerging findings from unpublished diffusion tensor imaging data highlight significant white matter tract changes in the *Cyfip1*$^{+/-}$ rats, which could lead to hypothesised functional connectivity changes.

1.5.3.1 Hippocampal-prefrontal interactions

Interactions between the prefrontal cortex and hippocampus have been extensively studied with regards to their roles in learning, memory and decision making, whereby oscillatory synchrony couples the two regions and is considered to reflect the bidirectional flow of information during cognitive processing (reviewed in Godsil et al. 2013, and discussed further in Chapter 3). Evidence for this stems partly from ipsilateral disconnection studies, where the prefrontal cortex and hippocampus are inactivated in opposing hemispheres to disrupt ipsilateral interactions (Floresco et al., 1997; Wang and Cai, 2006a). Subsequently, landmark findings in rats highlighted a key reflection of hippocampal-prefrontal interaction, describing strong oscillatory synchrony between these regions during memory retrieval, particularly in the theta band (Benchenane et al., 2010; Jones and Wilson, 2005; Sigurdsson et al., 2010). Comparable oscillatory interactions have been observed in humans (Anderson et al., 2010).

As mentioned, abnormalities in the hippocampal-prefrontal circuit have been linked to cognitive deficits in a number of psychiatric conditions. Evidence from structural and functional imaging studies, as well as EEG recordings in schizophrenia patients, has demonstrated the relevance of this circuit for cognition (Hao et al., 2009; Meyer-Lindenberg et al., 2005; Qiu et al., 2010; Wolf et al., 2009; Zhou et al., 2008). Furthermore, the existence of aberrant hippocampal-prefrontal circuit activity in currently healthy carriers of risk alleles suggests the network deficit is a core component of psychiatric illness that is strongly influenced by genetic risk, and may have potential as a biomarker (Callicott et al., 2013; Cousijn et al., 2015;

Esslinger et al., 2009). The hippocampal-prefrontal network has been extensively studied in rodent models, and a number of studies have begun to investigate the consequences of psychiatric risk on this network. Most notably, Sigurdsson et al. (2010) examined the functional connectivity in the *Df16(A)*$^{+/-}$ mouse, a model of the highly penetrant 22q11.2 CNV, and observed impaired hippocampal-prefrontal synchrony during a working memory task. These findings prompted the experiments described in Chapter 3, to explore the impact of *Cyfip1* haploinsufficiency on the hippocampal-prefrontal circuit during working memory.

1.5.3.2 Nucleus accumbens circuits

The nucleus accumbens (NAc), located in the ventral striatum, is widely considered as an interface between the limbic and motor systems (Mogenson et al., 1980). It integrates reward and motivation related information processed by frontal and temporal regions to serve action selection and goal-directed behaviours, via afferents to motor-output structures (Floresco, 2015; Groenewegen et al., 1993).

The NAc has been implicated in symptoms of schizophrenia and autism, including cognitive functions such as prediction-error based learning and flexible decision-making (Floresco et al., 2009; Fuccillo, 2016; Rausch et al., 2014; Salamone et al., 2005; Stopper and Floresco, 2015), and elements of psychosis, namely aberrant salience (Kapur, 2004). Impairments in reinforcement learning seen in schizophrenia may be due to reward-processing deficiencies, such as abnormal representations of the expected value of rewards and actions, or disrupted reward prediction errors (Gold et al., 2008; Waltz and Gold, 2016) (discussed further in Chapter 4). Indeed, initial studies finding increased striatal dopamine in schizophrenia patients prompted an interest in this brain area (Hietala et al., 1995; Lindström et al., 1999), and decreased grey matter volume and white matter abnormalities have since been observed in schizophrenia patients (van Erp et al., 2016; Okada et al., 2016; Quan et al., 2013).

The role of the NAc has also been investigated in the scope of the NMDAR hypofunction theory of schizophrenia (Kantrowitz and Javitt, 2010). Animal

models that recapitulate a deficit in NMDAR function, such as administration of ketamine or phencyclidine (PCP), show cognitive deficits in the novel object recognition task, coupled with disrupted NAc and cortico-accumbal network activity (Asif-Malik et al., 2017; Hunt et al., 2006; Rajagopal et al., 2013) (discussed further in Chapter 5). In particular, acute NMDAR blockade can increase the frequency and power of high-frequency oscillations in NAc, also affecting hippocampus and prefrontal cortex (Hunt and Kasicki, 2013; Lee et al., 2017), while sub-chronic PCP treatment led to reduced cortico-accumbal synchrony. Similarly, the MAM neurodevelopmental model of schizophrenia also shows increased high-frequency oscillations in the NAc (Goda et al., 2015). These convergent phenotypes in different models may suggest abnormal NAc network activity underlies some psychiatric symptoms, which prompted its investigation in the *Cyfip1*$^{+/-}$ rat.

1.5.3.3 Importance of sleep circuit activity

In addition to studying the network activity during awake behaviour, sleep-dependent network activity is also of significant interest. Sleep neurophysiology in the context of psychiatric research is an emerging field, primarily driven by the consistent reports of sleep disturbances in schizophrenia patients (Kaskie et al., 2017), autism (Cortesi et al., 2010; Verhoeff et al., 2018) and other severe psychiatric and neurodegenerative disorders (Wulff et al., 2010). In addition, sleep-specific neural activity is also disrupted in schizophrenia, autism and intellectual disability, and it is suggested that disrupted network processes that can be observed during sleep may contribute towards the aberrant waking brain (Castelnovo et al., 2016; Ferrarelli, 2015). The study of network activity in the sleeping brain offers a key advantage in that it reflects a resting state, unimpeded by confounds of variations of attention or motivation (Ferrarelli, 2015; Gardner et al., 2014) (discussed further in Chapter 6).

Characteristic oscillation events during the non-rapid eye movement (NREM) phase of sleep include slow waves, spindles and ripples. These oscillation events can be disrupted in psychiatric conditions (Castelnovo et al., 2016; Ferrarelli and

Tononi, 2017), which reflect abnormalities in the corticothalamic and cortico-hippocampal circuits, offering a further opportunity to investigate the functioning of the latter network in a different context. Furthermore, these sleep oscillation events have been implicated in learning and memory consolidation, and the disruptions to these phenomena observed in patients suggests they may contribute to their cognitive deficits (D'Agostino et al., 2018; Manoach et al., 2014; Marshall et al., 2006; Niknazar et al., 2015). A growing number of psychiatric illness-relevant animal models have been shown to have circadian or sleep neurophysiology disruptions, and it has been suggested that a common mechanism binds sleep disturbances and mnemonic function (Jagannath et al., 2013). Therefore, it is of interest to investigate the possible consequences of *Cyfip1* haploinsufficiency on circadian rhythms and sleep oscillations.

1.6 Thesis aim

The broad aim of this thesis is to explore how psychiatric disorder-linked genetic alterations might impact the function of networks across the brain, as assessed by changes in local field potential oscillations in key brain regions, and whether any changes manifest as a behavioural deficit. For the majority of this thesis I will focus on the novel *Cyfip1*$^{+/-}$ rat model and investigate how haploinsufficiency of *Cyfip1* might lead to network level effects using multi-site *in vivo* electrophysiology.

Following an outline of the general methods used in this thesis in Chapter 2, in Chapter 3 I will describe behavioural performance and hippocampal-prefrontal network activity in *Cyfip1*$^{+/-}$ rats during a working memory task. In Chapter 4, I examine activity of the nucleus accumbens and its afferent inputs in relation to the approach and receipt of reward on the same task. In the following two chapters, some of these networks are revisited in a different context. Chapter 5 describes a 'double-hit' experiment, where network activity changes following an acute dose of the NMDAR antagonist ketamine are investigated. In Chapter 6, I turn to assessing the impact of *Cyfip1* haploinsufficiency on circadian activity patterns and the sleeping brain, as sleep architecture disruptions can be symptomatic of underlying network abnormalities. Finally, in Chapter 7 I present data from a pilot

circadian activity and sleep study using the *Fmr1* knockout rat model, to compare and contrast the impact of depleting these two interacting proteins on these parameters.

2

Chapter 2 General Methods

This chapter describes general methods that apply to more than one chapter in this thesis. Individual chapters contain more information pertaining to specific methods.

2.1 Animals

All procedures were carried out in accordance with the UK Animals Scientific Procedures Act (1986) and University of Bristol Ethical Review Group. *Cyfip1*$^{+/-}$ rats were on a Long Evans background, with central colonies maintained at Charles River, UK. Prior to experiments, adult male rats were shipped to Biomedical Sciences Building, Bristol and group-housed (max 3 prior to surgery, single housed thereafter) in a room with 10:14 hour light cycle (lights on at 5am, off at 7pm), with ad libitum food and water. Animals were handled regularly from date of arrival and throughout the experiments.

2.2 Creation of the *Cyfip1*$^{+/-}$ rat

The *Cyfip1*$^{+/-}$ rat model was created by Cardiff University in collaboration with Horizon Discovery (St Louis, USA) using CRISPR-Cas9 targeting (https://www.horizondiscovery.com/) and supported by a Wellcome Trust Strategic Award, DEFINE. Briefly, CRISPR-Cas9 targeting of exon 7 of the *Cyfip1* gene on chromosome 1 was used to generate a founder female Long Evans rat with a 4bp out of frame heterozygous deletion in exon 7, that in turn created an early premature

stop codon in exon 8. Off target effects were assessed and excluded. The engineered genomic changes were confirmed to result in haploinsufficiency in brain tissue using qPCR and Western Blot to assess mRNA and protein levels, respectively. Subsequent F2 generation positive Long Evans rats were shipped from Horizon to Charles River Lyon (France) for re-derivation to SPF status and then on to Charles River, (Margate, UK) where they were held for breeding, employing a wild type x heterozygous cross design, giving rise to 1:1 heterozygous/wild-type littermate control Long Evans offspring that were shipped to Bristol at around 6-8weeks. Details pertaining to the creation of the model, confirmation of the heterozygous deletion, assessment of off-target effects, re-derivation, breeding and genotyping can be found in Appendix 1 (these data were kindly provided by colleagues in Cardiff).

2.3 Behaviour

2.3.1 T maze discrete-trial alternation

The T maze consisted of a stem arm (140 cm), 2 goal arms (60 cm), reward zones, and return arms (140 cm) leading back to the base of the stem arm (Figure 2.1a). Plastic divider doors slotted in at the required positions on the maze. The maze was custom built from plastic cable trunking and wooden support beams and spray-painted black.

A discrete-trial alternation task was used, and the protocol was a modified version of that presented in McHugh et al. (2008). Three-to-four-month-old rats were food-restricted to ≥85% of their free-feeding weight and habituated to the T maze apparatus for 3-5 days. They were allowed to explore one half of the maze, i.e. running either left or right loops, ensuring that the animals did not experience the decision point between the stem and goal arms of the maze during the habituation phase. Animals progressed to the task phase once they were comfortably running loops in each direction and consuming sucrose solution from the reward zone.

During the task phase, each trial consisted of two runs, the sample and the choice. During the sample run, one of the goal arms was blocked at the T junction, forcing

the rat to take the open arm where it received a 150 µl sucrose reward before returning to the start box via the return arm. During the rat's return, the T junction block was removed from the goal arm. Next, the rat initiated the choice run by entering the stem arm again and was then faced with an option of which goal arm to take. Taking the previously unvisited arm was rewarded, while choosing the same arm visited in the sample run was not. After consuming the reward, rats would return to the start box via the return arm and wait there while the next trial was set up, with an inter-trial interval of ~1-2 minutes. Left or right arm allocations for the sample run were pseudo-randomized over ten trials, with no more than two consecutive sample runs to the same side.

Animals were required to reach 80% accuracy over 2 consecutive sessions before they underwent surgery. Following recovery from surgery and when they had regained pre-surgery weight (less the weight of the implant which was around 25g), rats were food restricted for 3 days before their recording session. During the T maze section of the recording, rats ran as many trials as they could in 40 minutes, with left and right sample runs pseudo-randomized as during training.

2.3.2 Delayed T maze discrete-trial alternation

The day before running the delayed T maze task, rats had a session of the no delay task where they were required to show a baseline ≥80% accuracy. Those who did not meet this criterion had additional sessions until they did. Electrophysiology data was not recorded during these baseline sessions.

The delay T maze task was then run as before, but when the animals returned to the start box following the sample run, they were placed back into their home cage, which was situated behind the start box. After a 5 minute delay, during which the block was removed, the animals were replaced to the start box for the choice run. All animals ran 20 trials.

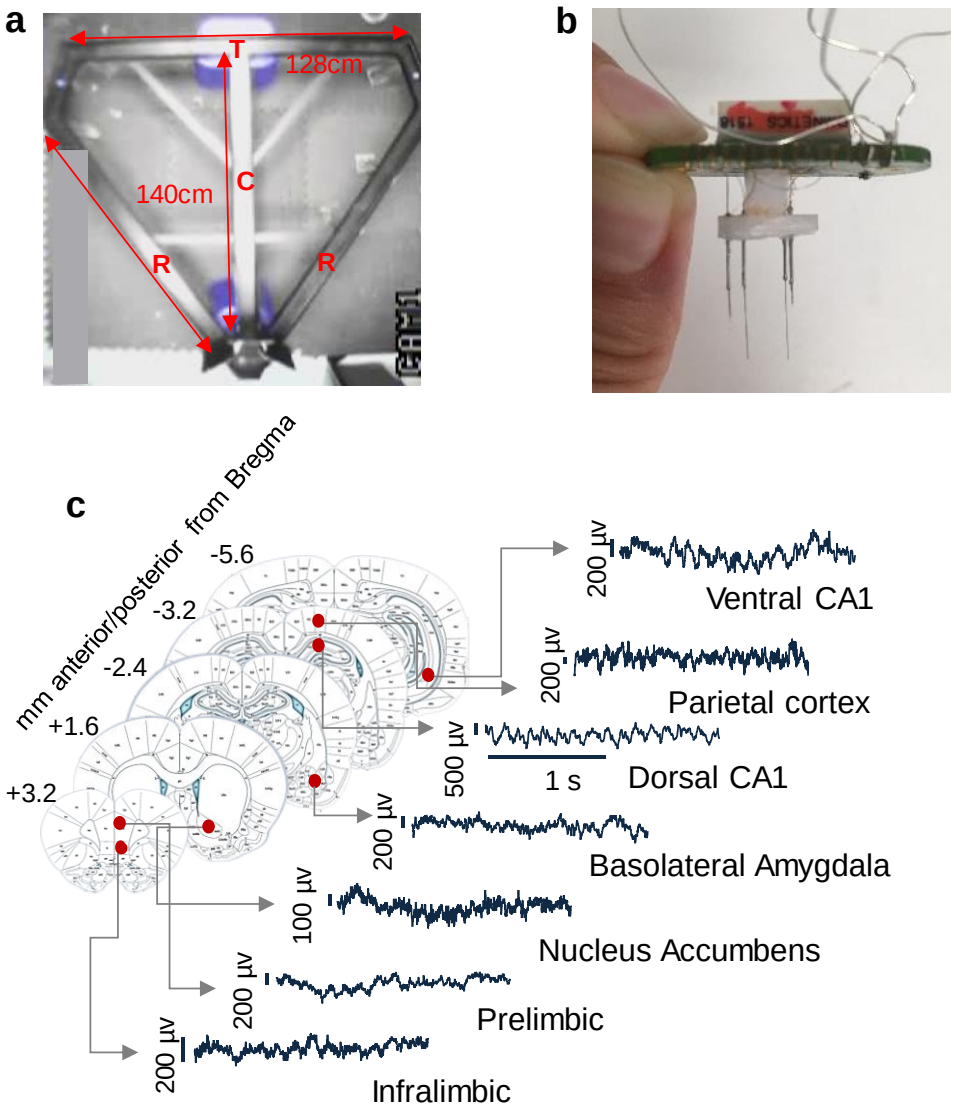

Figure 2.1 | **T maze and electrophysiology recording**. **a,** Snapshot from the video of the maze recording session. Main dimensions are shown in red. Blue bases support the maze at the top and bottom. Wooden support beams run between the central arm 'C', T junction and goal arms 'T', and return arms 'R'. Small blue circles at the top left and right corners of the maze are the reward wells. **b,** An LFP implant, showing green electrode interface board at top, white delrin in the middle, and stereotaxically arranged stainless steel cannulae holding nichrome wire at the bottom. **c,** Rat brain section diagrams from the Rat Atlas (Paxinos and Watson, 2007), indicating recording sites and example local field potential traces during wake.

2.4 *In vivo* electrophysiology

2.4.1 Multisite LFP electrode drive implants

The custom-built LFP electrode drives comprised five 30G cannulae of 8 mm length inserted into a Delrin platform, housing nichrome wires to be implanted into

the brain (Figure 2.1b). Holes in the 2 mm thick platform were 0.3 mm diameter and were drilled using a milling machine (Roland EGX-300) according to stereotaxic coordinates for chosen brain regions based on the Rat Brain Atlas (Paxinos and Watson, 2007) (Table 1). Cannulae were glued in place with superglue such that 4 mm extended ventrally. A small 2 mm x 2 mm Delrin block was glued onto the platform, and an electrode interface board (EIB, Neuralynx or TBSI) was glued on top using a stereotax, taking care to make sure the EIB was horizontal and its edges parallel to the platform. To load the drive, Formvar-insulated nichrome wire (60 μm diameter, A-M systems) was inserted through the respective cannulae and into the gold-plated pin channels on the EIB. The wire was glued in place such that the length extending from the bottom of the cannula corresponded to the depth of the target brain region. Finally, an electrical connection was made between the EIB and the wire by securing it with a gold pin (Neuralynx or TBSI). Prior to the surgery, electrodes were gold-plated (non-cyanide gold solution, SIFCO) to reduce the impedance to ~200-300 kΩ.

Table 1 Stereotaxic coordinates

Structure	**Anterior-Posterior coordinate (mm)**	**Medial-Lateral coordinate (mm)**	**Dorsal-Ventral coordinate (mm)**
Prelimbic	+3.2	+0.6	-2.8
Infralimbic	+3.2	+0.6	-4.4
Nucleus accumbens Shell	+1.6	+1.2	-6.6
Nucleus accumbens Core	+1.6	+1.2	-7.7
Basolateral amygdala	-2.4	+5.0	-8.4

Dorsal CA1	-3.2	+2.2	-2.2
Parietal cortex	-3.2	+2.2	-1.0
Ventral CA1	-5.6	+5.0	-7.8
Frontal skull screw	+3.5	-2.0	n/a
Occipital skull screw	-6.5	-5.2	n/a

Note – not all structures were used for each experiment, refer to results chapters for details.

2.4.2 Surgery

One day before surgery, animals were single-housed in a high-top cage (Techniplast) to allow for enough space for the implanted animal. Surgery was carried out using aseptic technique to minimise risk of infection. Anaesthesia was induced using 4% isoflurane in oxygen, and maintained at 2-3% isoflurane. After weighing the animal, the head was shaved, and the animal was transferred to the sterile bench and head-fixed onto the stereotaxic frame (Kopf model 1900). Body temperature was maintained at ~36.5°C using a heatmat and rectal probe, while heart rate and blood oxygen concentration were monitored with a paw sensor (PhysioSuite, Kent Scientific). Eyes were protected from drying out using LacriLube (Allergan) and shielded from the strong surgery lights using tape. The animal was given 5 ml 0.9% saline subcutaneously at the beginning of the surgery and subsequently every 2-3 hours until the end of the surgery. The scalp was cleaned using chlorhexidine, followed by subcutaneous injection of 0.1 ml lidocaine with adrenaline (Norbrook Laboratories) along the midline of the scalp.

A ~3 cm scalpel incision was made, and sutures were used to hold the skin open. Connective tissue was pushed aside using the scalpel and sterile cotton buds. The skull surface was cleaned by scraping with a curette, then levelled using the stereotax alignment indicator. Target region positions were marked on the surface of the skull, before seven skull screw (NewStar Fastenings) holes were drilled. Two

of these were over the cerebellum for ground screws, three were supporting screws, and the final two were placed over the motor cortex and parietal cortex to record EEG activity. Ground screws (screws with a short segment of silver wire soldered to their head) were lowered and the impedance checked to confirm a good connection.

Four craniotomies were made, one slightly larger anterior one to accommodate the PRL and NAc cannulae, and three smaller ones for the remaining cannulae. Subsequently, the dura was carefully removed using fine tweezers and a bent-tipped 30 gauge needle. Small cut pieces of absorption spears (Sugi, Fine Science Tools) were used to protect each craniotomy while the supporting screws and EEG screws were inserted. The drive was lowered over the skull and the wires were monitored as they each entered the brain. As the wires were of the correct length, the drive was lowered until the medial cannulae were resting flat of the surface of the brain. Craniotomies were covered with silicone gel (UniMed), and a strong dental adhesive was applied to the base of the screws (C&B Metabond). Gentamicin-containing dental cement (DePuy) was built up around the drive and the screws to secure it to the skull, and the silver wires from the EEG screws and ground screws were soldered to the EIB. An aluminium cone was attached using dental cement to protect the drive; this was grounded to the EIB. Nylon discontinuous sutures were made in the skin anterior and posterior to the implant, and an antibiotic/antipruritic gel applied to the wound edges (Surolan, Janssen), before turning off the anaesthetic. Once the animal had regained consciousness and was able to move around the clean cage, buprenorphine (0.025mg/kg, Vetergesic) was administered subcutaneously. Following surgery, recovery gel and mashed rat chow were provided for three days, while water intake and weight gain was monitored.

2.4.3 Data acquisition

All experiments involved home cage recordings, either for standalone sleep recordings, or for sleep recordings before and after a task. For home cage recordings the cage was placed in a sleep box, a wooden, sound-attenuating chamber. Rats were habituated to the sleep box for 10 minutes one week prior to recordings.

Electrophysiological data were acquired using Digital Lynx hardware, comprising a headstage (HS-36), tether (Litz) and an acquisition system (Digital Lynx SX) to digitise and amplify the signal. Cheetah software (Neuralynx) sampled the data at 2kHz and bandpass filtered between 0.1 and 600Hz (Figure 2.1c). Small cameras monitored behaviour in the sleep box at 720 x 576 pixel resolution, 30 frames per second and timestamped by Cheetah. The tether was supported by a counterbalanced pulley system which ensured uninhibited movement of the animal.

2.4.4 Perfusion

At the end of the experiments, rats were terminally anaesthetised with sodium pentobarbital (60 mg/kg), and a positive 30 µA current was passed down each LFP wire for ~10 s to create a lesion at the tip. Rats were perfused transcardially first with ~ 300 ml 0.9% saline, then with ~300 ml 4% paraformaldehyde in phosphate buffered saline. Once the brain was dissected out, it was refrigerated in 4% paraformaldehyde. A few days prior to sectioning, brains were transferred to 30% sucrose/phosphate buffered saline solution.

2.4.5 Histological verification of electrode placement

Coronal sections of 50 µm were cut with a freezing microtome and mounted on SuperFrost Plus slides (Thermo Scientific). Following drying, slides were Nissl-stained with thionin, and lesions were identified using a digital camera linked to an optical microscope (DM100, Leica) (Figure 2.2). Lesion sites were cross-checked with the Rat Brain Atlas (Paxinos and Watson, 2007). Ventral CA1 site lesions showed electrode placement was not always in the cell layer, therefore these signals will be referred to as ventral hippocampus rather than CA1. Three NAc Shell lesions could not be located, but as the NAc Core lesion was in the correct position, and the signals were not anomalous, the position for these sites was inferred (marked with x, see Figure 2.3 legend). Similarly, two parietal cortex lesions could not be identified as the cortex above the hippocampus was missing from the slice (possibly due to the lesioning process), but as the nearby dorsal CA1 lesion was present and signals appeared normal, the location of these were inferred (marked with x). One IL electrode lesion (rat M.2) was found to be too ventral, located in the dorsal

peduncular cortex, and the signal looked substantially different from the other animals, therefore this animal was excluded for analyses including the IL channel.

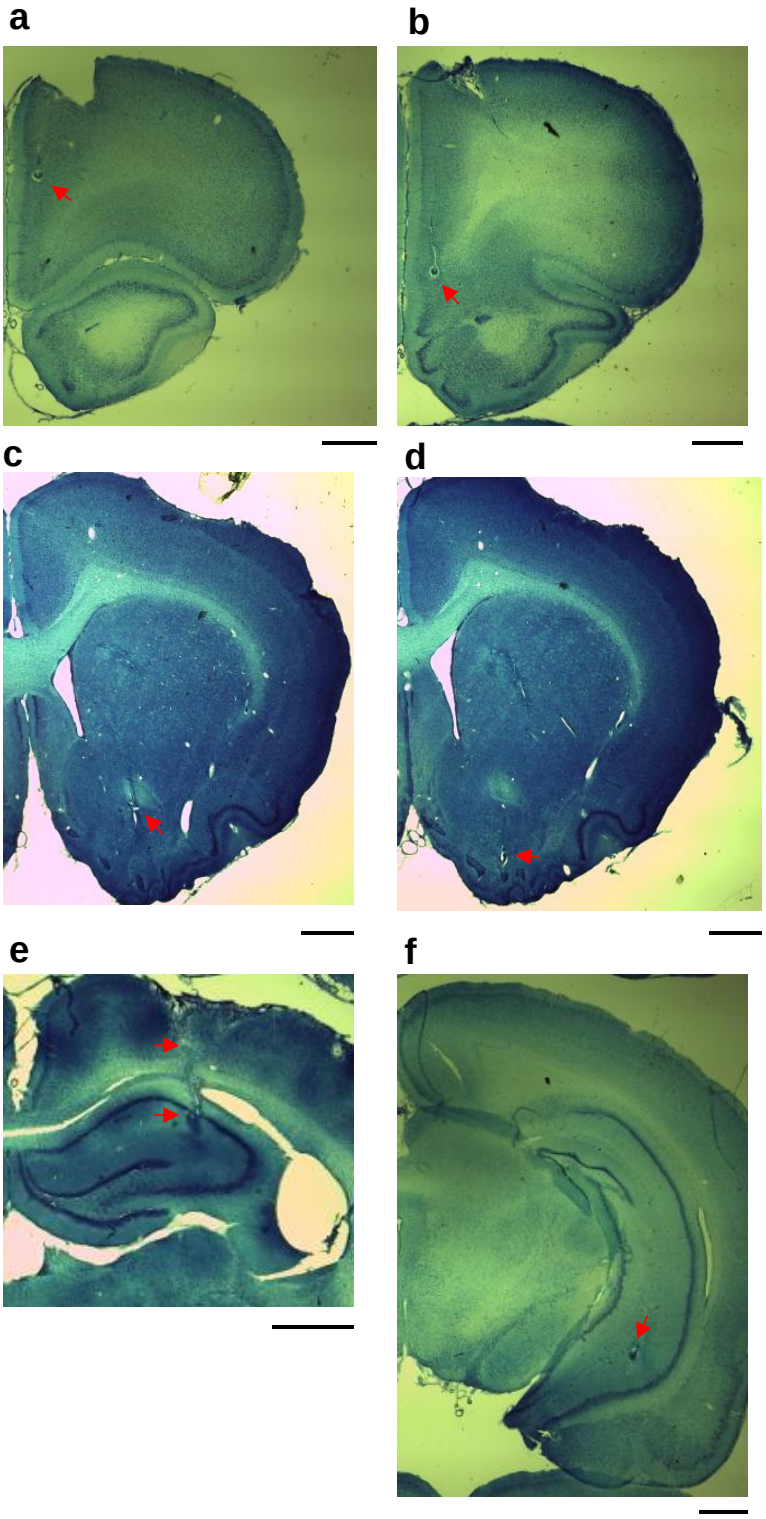

Figure 2.2 | **Examples of histological verification of electrode placement.** Nissl-stained coronal sections with red arrows indicating lesions in **a**, PRL, **b**, IL, **c**, NAc Core, **d**, NAc Shell, **e**, dCA1 of hippocampus (lower) and parietal cortex (upper), **f**, vHPC. Black scale bar = 1mm.

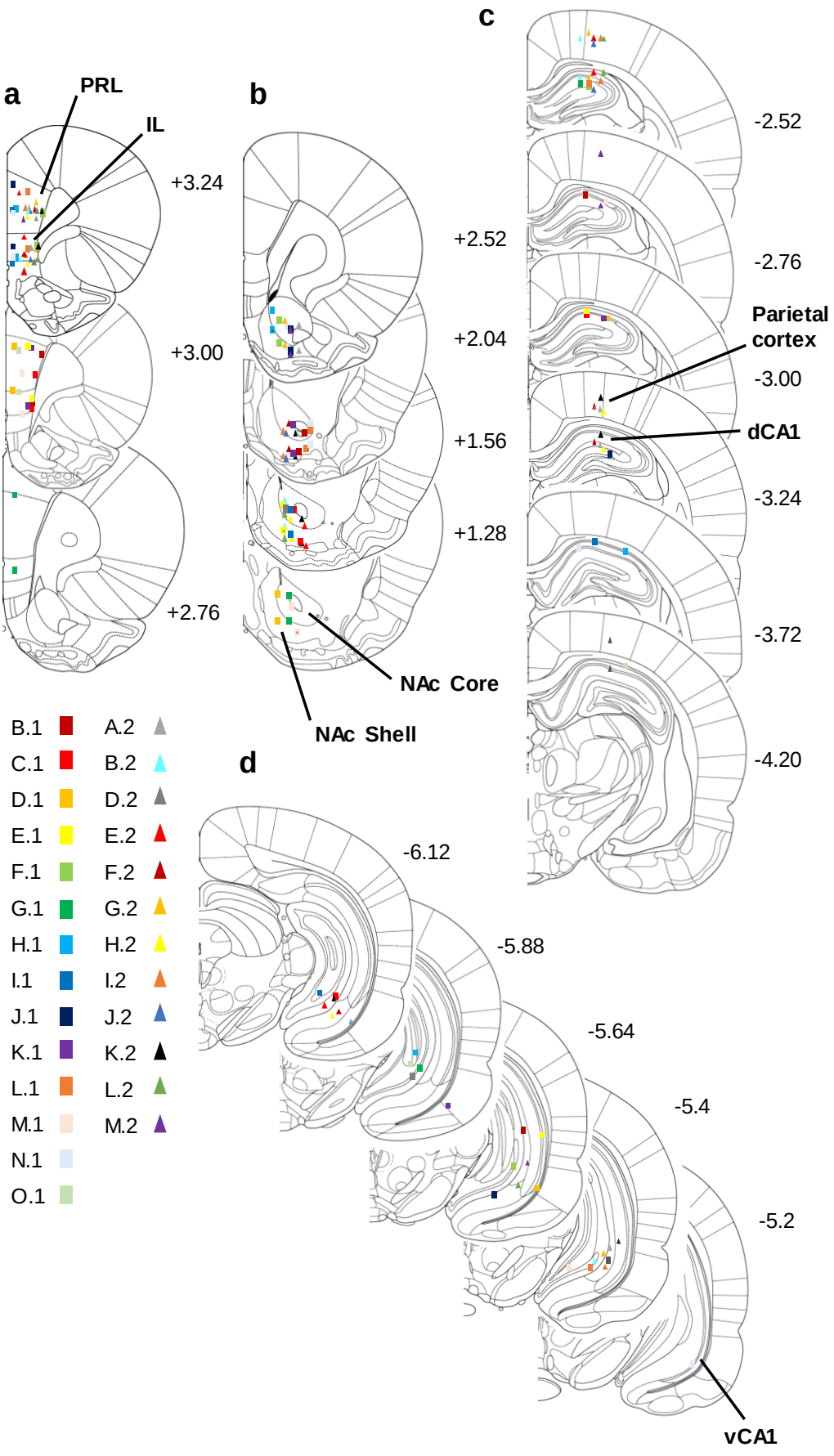
a
PRL
IL
+3.24
+3.00
+2.76
b
+2.52
+2.04
+1.56
+1.28
NAc Core
NAc Shell
c
-2.52
-2.76
Parietal cortex
-3.00
dCA1
-3.24
-3.72
-4.20
d
-6.12
-5.88
-5.64
-5.4
-5.2
vCA1
B.1
C.1
D.1
E.1
F.1
G.1
H.1
I.1
J.1
K.1
L.1
M.1
N.1
O.1
A.2
B.2
D.2
E.2
F.2
G.2
H.2
I.2
J.2
K.2
L.2
M.2

Figure 2.3 | **Histological verification of electrode placement. a,** Serial section diagrams of structures with the position of electrodes from each rat indicated with coloured squares (from first round of surgeries) or triangles (from second round of surgeries). Distances from bregma in mm shown on right. Figures taken from the Rat Atlas (Paxinos & Watson 2007). A small x in 3 NAc lesion marks and two parietal cortex lesion marks indicates that these locations were inferred (see text). The ventral IL lesion for rat M.2 that led to the exclusion of this data has a red outline.

2.5 Data analysis

Electrophysiological and tracking data were analysed using custom-written Matlab scripts and open source toolboxes such as the Chronux toolbox (http://chronux.org) (Mitra and Bokil, 2008).

2.5.1 LFP data

2.5.1.1 Pre-processing of LFP data

Data epochs to be analysed were inspected by eye for high-amplitude movement noise. When analysing many trials, epochs containing noise were discarded. For analysing single time windows, if the initially chosen time window contained noise, the window was shifted to exclude the noisy segment.

2.5.1.2 Power analysis

Power spectra were calculated in Matlab using the Chronux function *mtspectrumc*. Parameters were based on the length of the window to be analysed. For analysing time windows 2-9 seconds long, parameters were set as follows: bandwidth = 2 Hz, window = 1 s, constant = 1, providing three tapers for multi-taper spectral estimates.

To allow for effective comparison across animals, power spectra were normalized so that the integral of the spectrum (ranging from the bandwidth parameter (2 or 3 Hz) to the maximum frequency analysed) was equal to 1. This is a commonly used approach that can help account for variance in signal amplitude due to electrode impedance (Arbab et al., 2018; Dickerson et al., 2010; Malkki et al., 2016; Maurer et al., 2017; Russell et al., 2006).

Power spectrograms were calculated to show the time course of power changes, using the *mtspectgramc* function and a moving window of 0.05 seconds for analyses of 2-9 second epochs.

2.5.1.3 Coherence analysis

Coherence of two signals measures the extent to which they maintain a fixed phase relationship with each other. It is calculated by dividing the cross-spectrum of two signals by the product of the power spectral density of the two signals.

Coherency plots were created using the *coherencyc* function, which includes the calculation of jack-knife error bars, while changes in coherence over time were displayed in a coherogram using the *cohgramc* function (both Chronux functions). These functions are influenced by covarying amplitudes (Srinath and Ray, 2014). Therefore, when changes in coherence were found, changes in power were analysed to see to what extent they contributed to the change in coherence.

2.5.1.4 Granger causality

Granger causality analysis is a method used to infer the directionality of coherent activity between two signals. Using a multivariate autoregressive time series model to estimate spectral quantities, Granger analysis can indicate that one LFP (S_1) 'causes' the second signal (S_2) if the predictability of S_2 is improved by including earlier values of S_1. Granger causality values were obtained for each direction (S_1 to S_2 and S_2 to S_1) (Gregoriou et al., 2009). Peak values for Granger causality at theta frequency were tested for significance using a bootstrapping procedure. One of the two signals was shuffled 1000 times by shifting a pseudorandom 1-1.5 second section from the end of the signal to the beginning. The peak value for Granger causality in the theta band was considered significant if its value fell in the top 5% of shuffled peaks (Adhikari et al., 2010; Gregoriou et al., 2009).

2.5.1.5 Phase-amplitude coupling

A phase-amplitude coupling (PAC) detection toolbox was used to assess PAC (Onslow et al., 2011). A modulation index is calculated which signifies the extent to which the phase of a slower oscillation, e.g. theta, modulates the amplitude of a higher oscillation, e.g. gamma. Signals filtered for a range of lower and higher frequencies, using a filter via convolution with complex Morlet wavelets, are used to calculate a matrix of PAC values. Significance of PAC was assessed by using 50

shuffled gamma envelope signals to generate a distribution of PAC values, where values lying within the top 5% were taken as significant.

2.5.1.6 Sleep/wake state detection

Recordings were manually scored to identify periods of active wake, quiet wake, NREM and REM sleep. Movement data and electrophysiological data from hippocampus and PRL were used to define sleep/wake state, with specific features used to score sleep presented in Table 2. Movement was detected from the video recording, where after splitting each video into 1 second frames, the number of pixels varying from one frame to the next by more than 25 greyscale values was calculated. A Matlab-based software, Sleepscorer (Gross et al., 2009), was used to score the recording in 10s windows by identifying relevant features of the signals that correspond to each state (Figure 2.4).

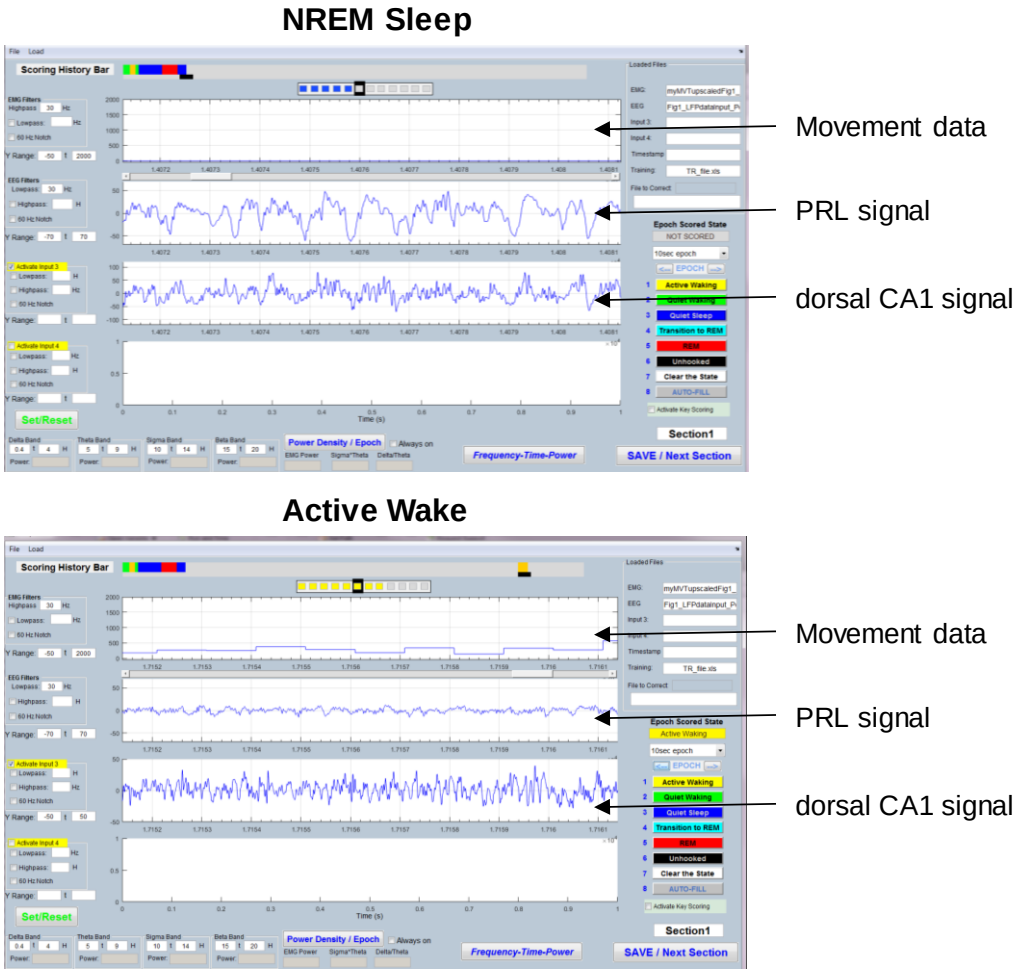

Figure 2.4 | **Manual sleep scoring with SleepScorer.** Two screenshots from the Matlab-based scoring software SleepScorer (Gross et al. 2009) showing a 10 second NREM epoch and active wake epoch. Note characteristic features of signals from PRL and dorsal CA1 during these states, and that movement data is at zero on the upper panel when the rat is asleep.

Table 2 Features used to manually score sleep/wake states

State	LFP data	Movement data
Active wake	Theta on dCA1 channel	High movement
Quiet Wake	No sleep signatures on PRL channel	Low movement

NREM sleep	Slow waves and spindles on PRL channel; ripples on dCA1 channel	Low movement
REM sleep	Theta on dCA1 channel	Low movement

2.5.1.7 Oscillation event detection algorithm

NREM sleep events (slow waves, spindles and ripples) were identified using an automated detection algorithm, based on frequency, amplitude and duration criteria, which was first developed in the lab by Dr Ullrich Bartsch (Phillips et al., 2012a). The signal was first band-pass filtered for the relevant frequency range, then rectified, and an amplitude envelope calculated. To detect events at this frequency, two envelope thresholds were set from the mean and standard deviation of the rectified, filtered signal. An 'upper threshold' was used as the detection threshold, while a 'lower threshold' was used to capture the start and end of sleep events (see Table 3). A putative sleep event occurred every time the amplitude envelope surpassed the detection threshold. The putative event was assessed further before being confirmed as a valid detection. Firstly, if a putative event occurred close to another (less than a 'minimum gap' threshold), these events were merged into one. The start and end times of an event were defined by when the envelope crossed the 'lower threshold' immediately before and after the 'upper threshold' crossing. Putative events that did not satisfy minimum and maximum duration criteria were discarded. Figure 2.5 shows an example from the spindle detection method. Mean frequency (calculated by dividing the number of peaks in the filtered LFP signal by the event duration) and amplitude (the greatest peak-to-trough difference) were calculated for each sleep event.

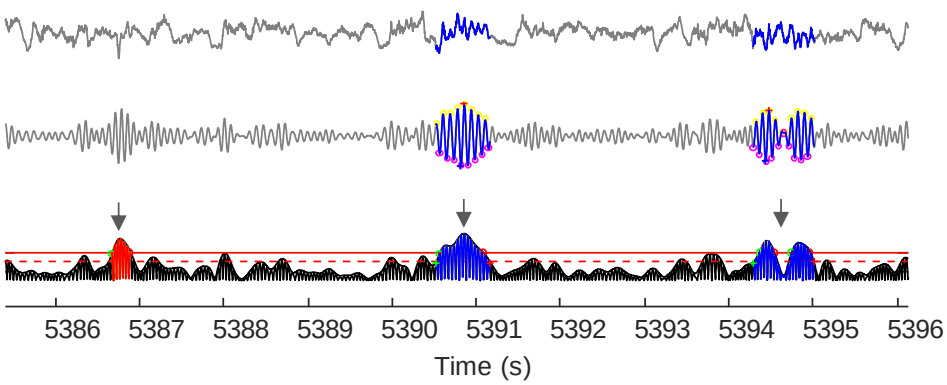

Figure 2.5 | **Sleep event detection method.** Example of spindle detection to illustrate sleep oscillation detection algorithm. Raw signal from PRL channel (top trace) was filtered at 10-16 Hz (middle trace) and its power envelope calculated (bottom trace). Horizontal solid red line indicates upper threshold for spindle detection (mean +2.8 standard deviations). Horizontal dashed red line indicates lower threshold for detection of start and end of events. Putative events indicated by grey arrows. First putative event (left) was discarded as it was too short. Second putative event (middle) was detected as a spindle as it met length, duration and frequency criteria. In the third putative event (right), two shorter events were merged and detected as one spindle, as they were closer to each other than the set threshold of 400ms.

Table 3 Parameters used to detect oscillation events

Event	Filterband (Hz)	Upper threshold : mean + n SDs	Lower threshold: mean + n SDs	Minimum gap (ms)	Duration (s)
Slow wave	0.5-4	2.5	1	500	0.25-3
Spindle	10-16	2.8	1.4	400	0.4-3
Ripple	120-250	5	0.5	50	0.025-0.5

2.5.2 Statistics

Statistics were run in SPSS. Data were confirmed to be normally distributed using the Shapiro-Wilk test unless otherwise stated. Outliers were assessed by inspection of a boxplot for values > 1.5 box-lengths from the edge of the box. Unless otherwise stated, they were excluded except in cases where they did not violate assumptions of statistical tests and did not affect the outcome of the statistical test. Mixed ANOVAs were used to compare genotype groups under different conditions. For lack of a valid non-parametric alternative, non-normal data were log-transformed to bring them within a normal distribution and this is noted in each case. Equality of error variances was confirmed using Levene's test, equality of covariance matrices was confirmed using Box's test. Any post-hoc tests for simple main effects were run using Tukey's post-hoc test for repeated measures.

2.6 Actigraphy monitoring

Actigraphy data were recorded using passive infra-red sensors (PIRs), which detect changes in background heat radiation, thus picking up the animal's movements. This home-cage activity monitoring setup is based on the COMPASS system (Brown et al., 2016). The sensors were positioned in a way that the field of detection of the sensor was confined to a single cage, 28cm above the floor of the cage and 17cm from the front of the cage (Figure 2.6a). To minimize obstructing the sensor, food was placed inside the cage rather than in the hopper. While cardboard tubes do obscure the animal, they were not removed to maintain animal welfare.

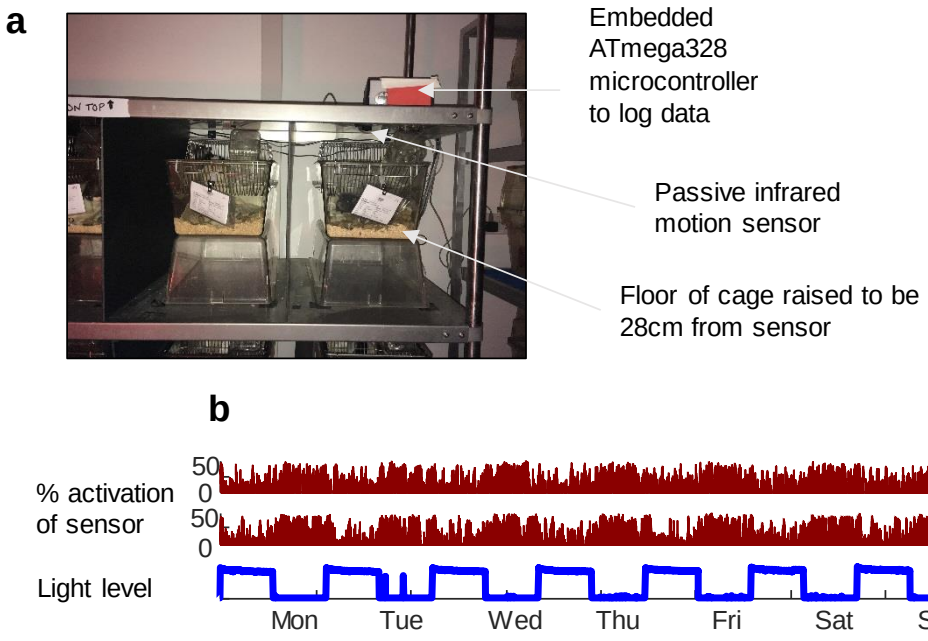

Figure 2.6 | **Actigraphy monitoring setup and example data**. **a,** Image of the actigraphy setup showing 2 of 12 cages. **b,** Upper and middle trace: Representative activity data from a *Cyfip1*$^{+/-}$ and WT rat respectively, showing activity counts in 10 s bins, recorded over 7 days. Lower trace: Data from ambient light level sensor showing light on (8pm) and off (8am) times, arbitrary light level units. Bursts of light in Tuesday's dark period represent someone accidentally letting light in.

Data was collected in 10 s bins, and with a measurement interval of 100 msec, each bin had 100 separate measurements. A percentage activation of the sensor for each time bin was calculated, herein referred to as activity counts. Movement data, the ambient light level and a timestamp were recorded and logged by an embedded ATmega328 microcontroller (Arduino) (Figure 2.6a and b).

Pilot recordings were done in normal light holding rooms. However, it appeared that the animals' sleep patterns were being disrupted by people coming in and out of the room. As sleep behaviour in the light phase was of particular interest, all subsequent recordings were made in a reverse light room, where most entries to the room were limited to the dark hours. The data in this thesis are from reverse light room actigraphy recordings. Animals required 12 days to adjust to the new light cycle.

1.1.1 Inferring sleep status from activity data

Previous work using video monitoring has shown that inactivity of ≥40s in mice can predict sleep with ~90% accuracy as compared to assessment using EEG/EMG (Fisher et al., 2012; Pack et al., 2007). Brown et al. (2016) also found a high correlation with sleep as assessed by infrared sensor and EEG/EMG in mice. However, this method has not been validated for rats, so movement data was recorded simultaneously with EEG recording to assess the degree of concordance between EEG-defined and immobility-defined sleep.

1.1.2 Actigraphy data analysis

2.6.1.1 Hourly means

Total activity counts or immobility-defined sleep parameters were averaged over hourly bins across monitoring days to generate a circadian activity profile.

2.6.1.2 ClockLab

With acknowledgements to Gareth Banks (Oxford) who had access to the software, actigraphy data were put through the ClockLab analysis software (Actimetrics). Results of the Lombe-Scargle periodogram were analysed, where a peak at the 24hr mark gives a measure of the strength of the circadian component of the rhythm. Time of activity onset and offset were also calculated, as was the average length of the active phase (alpha).

2.6.1.3 Non-parametric measures

Non-parametric methods are commonly used to analyse the actigraphy data, providing variables for interdaily stability (IS), relative amplitude (RA) and intradaily variability (IV) (Van Someren et al., 1999). IS quantifies the strength of the activity coupling to the daily light changes, where high IS values indicate that the animal is well synchronized to the light cycle. It is calculated as the variance of the average daily profile divided by the total variance. IV is a measure of the fragmentation of the rest-activity rhythm. Large differences between hours, such as sleep during the dark phase or highly active behaviour during the light phase increases the value of IV. It is calculated by taking the root mean square of the first derivative of hourly activity data and dividing by the total variance. RA captures the amplitude of the circadian rhythm, calculated by finding the difference between the most active ten hour and least active 5 hour periods of the 24 hour cycle. The equations for these variables are found in Van Someren et al. (1999), and the method discussed in detail by Gonçalves et al. (2015). Actigraphy data was processed and analysed using custom-written Matlab scripts.

3

Chapter 3 The hippocampal-prefrontal network in *Cyfip1*$^{+/-}$ rats during spatial working memory

This chapter explores spatial working memory and its neural network correlates in *Cyfip1*$^{+/-}$ rats. *Cyfip1*$^{+/-}$ rats took longer to achieve criterion during training on a T maze task, but hippocampal-prefrontal interactions were largely normal. However, theta-gamma phase amplitude coupling within hippocampus was reduced in *Cyfip1*$^{+/-}$ rats.

3.1 Introduction

3.1.1 The hippocampal-prefrontal network

3.1.1.1 Anatomical connectivity in the hippocampal-prefrontal network

Considerable evidence suggests that interactions between hippocampus and prefrontal cortex are mediated via coordinated oscillations of neural activity. There are several known direct and indirect anatomical pathways underlying this interaction. Hippocampal-prefrontal connections are comparable across rodents and primates, with reciprocal connections between the medial prefrontal cortex and hippocampus best characterized in rats (reviewed in Eichenbaum 2017; Sigurdsson & Duvarci 2015, Figure 3.1).

From hippocampus to medial prefrontal cortex, the densest direct monosynaptic projection originates from the ventral hippocampus (Hoover and Vertes, 2007; Jay and Witter, 1991; Jay et al., 1989). Bidirectional connections exist between dorsal and ventral hippocampus and medial prefrontal cortex via the reciprocally connected thalamic nucleus reuniens (Cassel et al., 2013; Dolleman-Van Der Weel and Witter, 1996; Vertes et al., 2007), as well as the perirhinal and lateral entorhinal cortex (Burwell and Amaral, 1998; Witter et al., 2000). However, a recent study has found evidence for a monosynaptic projection from the anterior cingulate part of the prefrontal cortex to dorsal hippocampus in mouse (Rajasethupathy et al., 2015), while an important mnemonic role has been associated with a direct dorsal/intermediate CA1 to PRL projection in rats (Barker et al., 2017; Hoover and Vertes, 2007).

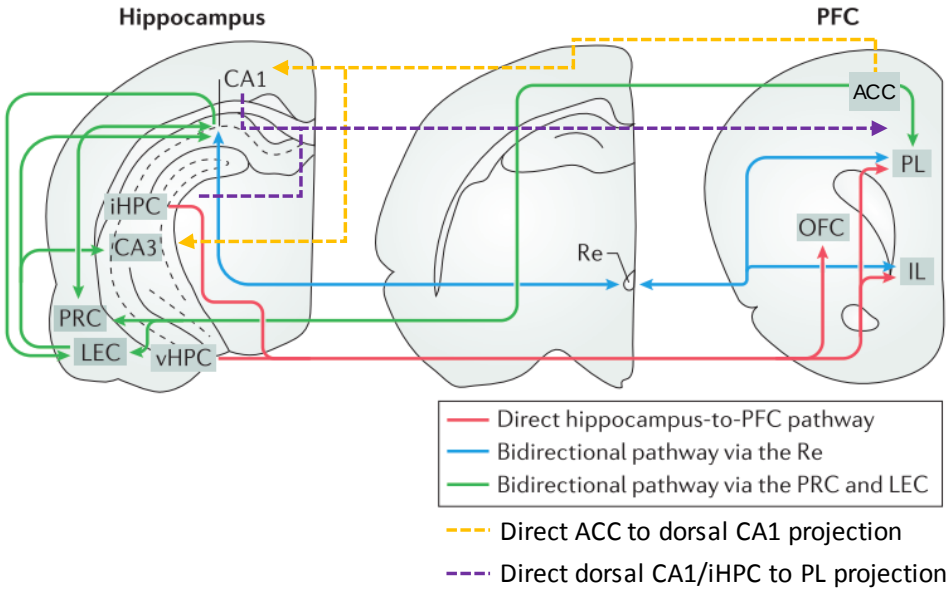

Figure 3.1 | **Anatomical connections between the hippocampus and prefrontal cortex.** The major well-known direct connection from the hippocampus to prefrontal cortex originates in the vHPC (including more dorsal regions in the intermediate hippocampus), and projects to the prelimbic, infralimbic and orbitofrontal areas. Two bidirectional connections are shown, one via the thalamic nucleus reuniens, and one via perirhinal cortex and lateral entorhinal cortex. More recently identified projections are a direct projection from anterior cingulate cortex to dCA1 and CA3 in mice (Rajasethupathy et al. 2015), and a direct dCA1/intermediate hippocampus projection to prelimbic cortex in rats (Barker et al. 2017). iHPC = intermediate hippocampus, PRC = perirhinal cortex, LEC = lateral entorhinal cortex, vHPC = ventral hippocampus, Re = nucleus reuniens, OFC =

orbitofrontal cortex, PL = prelimbic cortex, ACC = anterior cingulate cortex, IL = infralimbic cortex. Adapted from Eichenbaum et al. 2017.

3.1.1.2 Role of the hippocampus

Hippocampus and prefrontal cortex make distinct contributions to memory. Since the landmark case of patient H.M., whose amnesia following bilateral surgical removal of the hippocampus highlighted the importance of hippocampus in memory (Scoville and Milner, 1957), studies in rodents, monkeys and humans have identified a role for hippocampus in learning and declarative memory (e.g. Eichenbaum 2004; Smith & Mizumori 2006). A second dominant literature emerged following the discovery of spatially localised firing neurons in the hippocampus (place cells) (O'Keefe and Nadel, 1978) establishing the 'cognitive map' theory of hippocampal function, which proposed a role for hippocampus in navigation. These two theories have been reconciled to some extent following evidence that place cell representations can extend beyond just location, with place cell firing modulated by, for example, changes in the task or goals within the same environment (Eichenbaum et al., 1987; Hampson et al., 1993; Otto and Eichenbaum, 1992; Wood et al., 2000). Indeed, studies in rodents show the importance of hippocampus for memory with a spatial and temporal context, where rats with hippocampal lesions are able to recognise familiar objects in a familiar context, but not in a novel location or novel context (Butterly et al., 2012; Eacott and Norman, 2004; Langston and Wood, 2010). This and other evidence has led to the suggestion that the hippocampus acts as a 'relational processing system', integrating events over time in a 'memory space', or spatial trajectories into a contextual cognitive map (Buzsáki and Moser, 2013; Eichenbaum and Cohen, 2014; Eichenbaum et al., 1999).

The hippocampus has been implicated in spatial working memory, a short-term type of memory discussed in more detail later in this section. The contribution of dorsal hippocampus to spatial working memory has been demonstrated through lesion studies (Brito et al., 1983; Czerniawski et al., 2009; Rawlins and Olton, 1982; Stanton et al., 1984) and evidence of working memory coding in hippocampal cell firing. For example, during the central arm run or the delay phase of a spatial

alternation T maze task, dCA1 hippocampal cells showed discriminative firing modulated by the direction of the upcoming run (Ainge et al., 2007a, 2007b; Frank et al., 2000; Markus et al., 1995; Wood et al., 2000), and cell assembly sequences predicted future run direction and trial outcome (Hallock and Griffin, 2013; Pastalkova et al., 2008).

Numerous graded changes are evident along the dorsal-ventral axis of the hippocampus, including gene expression, connectivity and functional effects (Fanselow and Dong, 2010; Strange et al., 2014). The ventral hippocampus is thought to be more involved in emotional and motivational behaviours, such as anxiety (Adhikari et al., 2010; Bannerman et al., 2004, 1999); however, lesion and disconnection studies were inconsistent regarding its role in spatial working memory (Bannerman et al., 2002; Felix and Levin, 1997; Moser et al., 1995; Wang and Cai, 2006b). A recent study demonstrated a role for ventral hippocampus in spatial working memory by optogenetically silencing ventral hippocampus to prefrontal cortex pathway, which caused impairments in performance (Spellman et al., 2015).

3.1.1.3 Roles of the prefrontal cortex

Patient K.M., whose prefrontal cortex damage lead to poor performance in the Wisconsin Card Sorting Test, was important in highlighting the role of this region in 'executive' function, including decision-making, goal-directed and flexible behaviour (Lange et al., 2017; Milner, 1963). The rodent medial prefrontal cortex is thought to be roughly homologous to the dorsolateral prefrontal cortex of primates (Dalley et al., 2004; Uylings and van Eden, 1990). Lesions or inactivations of the medial prefrontal cortex affect performance of extinction tasks (Burgos-Robles et al., 2007; Griffin and Berry, 2004), task rule switching (Dias and Aggleton, 2000; Rich and Shapiro, 2009), and attentional set shifting (Birrell and Brown, 2000; Floresco et al., 2008), among others, which require suppression of a learned response. It has been suggested that such deficits in flexibility are key to the working memory deficits also observed following medial prefrontal cortex

lesions (Churchwell and Kesner, 2011; Floresco et al., 1997; Kolb et al., 1994; Ragozzino et al., 1999; Wang and Cai, 2006b).

The role of medial prefrontal cortex in working memory processes is highlighted by evidence showing persistent firing of medial prefrontal cortex neurons during the delay period of a task, thought to have a role in maintaining information during the delay (Funahashi, 2017; Fuster and Alexander, 1971; Goldman-Rakic, 1995). It was later shown that the activity of these 'delay cells' correlates with upcoming behaviour (Baeg et al., 2003; Chang et al., 2002). For example, Baeg et al., (2003) showed that neural ensemble activity in the medial prefrontal cortex could decode the recent and upcoming run direction, and this improved in parallel with the animal's task performance.

3.1.1.4 Hippocampal-prefrontal interactions

The roles of the hippocampus in episodic and spatial memory, combined with the medial prefrontal cortex's role in executive function, decision-making and flexible behaviour are well placed to subserve cognitive functions, such as spatial working memory (Colgin, 2011; Gordon, 2011; Sigurdsson and Duvarci, 2015; Spellman et al., 2015). Classic crossed lesion studies showed the importance of their interaction by compromising the largely ipsilateral hippocampal-prefrontal pathway, which leads to delay-dependent deficits in spatial working memory tasks (Floresco et al., 1997; Wang and Cai, 2006a), novel object location memory (Barker et al., 2007) and episodic memory (Barker et al., 2017; Chao et al., 2016).

Cell cross-correlation, phase-locking of units to oscillations and oscillatory coherence between hippocampus and prefrontal cortex were identified as reflecting an interaction (Hyman et al., 2005; Jones and Wilson, 2005; Siapas et al., 2005). Studies were then able to link this interaction directly to working memory processes and cognitive performance, further supporting the importance of this network (Benchenane et al., 2010; Jones and Wilson, 2005; O'Neill et al., 2013). Jones and Wilson (2005) were first to demonstrate that phase-locking of medial prefrontal cortex neurons to hippocampal theta oscillations was increased in the working

memory-dependent choice phase of a maze task. This effect was also reflected in the local field potential (LFP) signal with increased theta-frequency coherence between hippocampus and medial prefrontal cortex. It has since been shown that this coherence, seen both between dorsal and ventral hippocampus and medial prefrontal cortex develops in strength as mice acquire a spatial working memory task (Benchenane et al., 2010; O'Neill et al., 2013; Sigurdsson et al., 2010). More recent work suggests the hippocampal-prefrontal interactions are also involved in cue encoding via gamma band oscillations. Spellman et al. (2015) observed increases in gamma coherence during the sample phase of a T maze task, which correlated with behavioural performance. Optogenetically inhibiting the direct ventral hippocampal-prefrontal pathway disrupted coherent gamma activity and the encoding of task-relevant cues in the medial prefrontal cortex, leading to a behavioural deficit and abolished neural representation in the medial prefrontal cortex. Theta coherence, in contrast, was unaffected by the disruption of this pathway, suggesting other pathways mediate this interaction e.g. via the nucleus reuniens (Griffin, 2015; Hallock et al., 2016). Theta coherence has also been observed during the delay periods of spatial working memory tasks (Myroshnychenko et al., 2017), linking the hippocampal-prefrontal interaction with the earlier observed 'delay cells'. Thus, gamma and theta coherence in this network could support the encoding, maintenance and retrieval of information in spatial working memory tasks.

This network has mainly been explored in rodents, but hippocampal-prefrontal interactions are also observed in non-human primates and humans (Anderson et al., 2010; Axmacher et al., 2008; Brincat and Miller, 2015), although the modes of interaction do not always align exactly with the rat literature. Rhesus monkeys performing an object paired-associate learning declarative memory task showed trial-outcome related oscillatory synchrony at theta (in monkeys ~2-6 Hz) for incorrect trials and alpha/beta (~9-16 Hz) for correct trials, highlighting different functional roles for different frequency bands. Intracranial recordings from epilepsy patients showed a memory-load dependent increase in synchrony between hippocampus and anterior parahippocampal gyrus, in the low gamma range (26-50

Hz) (Axmacher et al., 2008). In addition, theta coherence between medial temporal lobe and prefrontal cortex was increased during the recall phase of a verbal memory task, closely mirroring findings in rodents (Anderson et al., 2010).

Functional connectivity analysis of human fMRI data corroborates the importance of hippocampal-prefrontal interactions during working memory and encoding and retrieval of episodic memory (Bähner et al., 2015; Gazzaley et al., 2004; Grady et al., 2003; Nee and Jonides, 2008; Rissman et al., 2008). One study involved subjects navigating a virtual reality radial arm maze while in the fMRI scanner, and the sample phase of the task was associated with the strongest hippocampal-prefrontal functional connectivity, with the magnitude correlating with performance accuracy (Bähner et al., 2015). This echoes the enhanced gamma synchrony seen in the sample phase of a T maze task in rats (Spellman et al., 2015). Earlier studies using non-spatial working memory tasks also found that increases in functional connectivity can be correlated with increasing working memory load (Rissman et al., 2008), although the opposite relationship has also been reported, where reduced connectivity predicts working memory load (Axmacher et al., 2008; Meyer-Lindenberg et al., 2005). The nature of the different working memory tasks used is likely to affect the role of the hippocampal-prefrontal network (Bähner and Meyer-Lindenberg, 2017), leading to some inconsistencies with the rodent literature. Furthermore, direct comparison between fMRI and electrophysiology data is constrained by the slow time course of the BOLD signal, limiting the timescale of neuronal correlations to <0.1 Hz (Fox and Raichle, 2007). Simultaneous electrophysiology and fMRI studies are addressing the problem of how to compare these two methods (Logothetis et al., 2013).

By what mechanism can increased synchrony between two brain regions enhance information transfer? When oscillations in two regions are coherent, a spike from one area to another will arrive when the second area is more excitable, i.e. at the peak of an LFP wave where the population activity is high, increasing the likelihood of this spike being integrated by receiving neurons, and plasticity occurring. However, when the regions fall out of phase synchrony, the spike would arrive to a

less excitable neuron (Fries, 2005) (see also Chapter 1). What is the function of this increase in synchrony? The working theory is that it facilitates transfer of task-related information, such as spatial location and reward-contingency, to mediate goal-directed behaviour. Some evidence to support this includes overlap in the population of medial prefrontal cortex neurons that phase-lock to hippocampal theta and the population that shows task-related activity (Hyman et al., 2005). The fact that error trials see reduced coupling within these regions also supports this (Hyman, 2010; Jones and Wilson, 2005). Furthermore, individual differences in task performance become evident in theta hippocampal-prefrontal coherence – the strength of coherence correlated with days to criterion (Mukai et al., 2015; Sigurdsson et al., 2010).

Phase-amplitude coupling (PAC), where the amplitude of a faster oscillation is increased at a certain phase of a slower oscillation, has been put forward as a further reflection of hippocampal-prefrontal interaction, by which local computations can be integrated across brain regions (Bragin et al., 1995; Canolty and Knight, 2010; Canolty et al., 2006; Lakatos et al., 2005; Lisman and Jensen, 2013; Palva et al., 2005; Sirota et al., 2008). Theta oscillations strongly modulate gamma oscillations within rodent and human hippocampus (Axmacher et al., 2010; Belluscio et al., 2012; Bragin et al., 1995; Buzsáki et al., 2003; Tamura et al., 2017; Tort et al., 2008), within medial prefrontal cortex in rodents (Li et al., 2012b; Tamura et al., 2017) and within neocortex in humans (Canolty et al., 2006; Cohen et al., 2009a; Lakatos et al., 2005; Palva et al., 2005). Furthermore, brain region and task demands have been shown to affect the frequencies involved in local phase amplitude coupling (Canolty and Knight, 2010). This coupling between oscillations at different frequency bands also occurs across brain regions (Sirota et al., 2008; Stujenske et al., 2014; Tort et al., 2008). Theta-gamma PAC is observed between the hippocampus and prefrontal cortex, with the gamma oscillations strongest at specific phases of the theta (Sirota et al., 2008). While this has not been shown directly in humans, EEG studies have also identified long-range theta-gamma phase amplitude coupling between frontal and posterior regions (Friese et al., 2013). This PAC has increasingly been linked to performance accuracy and learning in animals

and humans (Axmacher et al., 2010; Friese et al., 2013; Köster et al., 2014; Nishida et al., 2014; Schomburg and Fernández-Ruiz, 2014; Tamura et al., 2017; Tort et al., 2009), and the pattern of firing produced by theta-gamma coupling is well-placed to induce long-term synaptic potentiation (Canolty and Knight, 2010).

With a clear link between hippocampal-prefrontal interactions and cognitive function, these findings raise the possibility that dysfunctions in this network underlie cognitive deficits seen in psychiatric illness. Following the emergence of a more sophisticated genetic exploration psychiatric disorders, the field has started to link the synchrony in the hippocampal-prefrontal network to cross-diagnostic cognitive phenotypes.

3.1.1.5 Hippocampal-prefrontal interactions and psychiatric disorder

Abnormalities in the hippocampal-prefrontal circuit are most commonly observed in schizophrenia patients, using structural and functional imaging and EEG recordings. Meta-analyses have confirmed reduced grey matter volume, enlarged lateral ventricles and white matter volume reduction in first episode schizophrenia patients (De Peri et al., 2012). Grey matter reductions are seen in anterior cingulate, frontal and temporal lobes, including hippocampus and amygdala, thalamus and insula that appear to deteriorate over time (Shepherd et al., 2012). In addition, structural changes in anterior hippocampus and prefrontal cortex correlated with symptom severity (Qiu et al., 2010). Parvalbumin-positive (PV) interneurons are abnormal in schizophrenia patients and have received much attention thanks to their role in gamma oscillations, which are also disrupted in patients (Uhlhaas and Singer, 2010).

Functional coupling between hippocampus and medial prefrontal cortex has been assessed during working memory tasks in schizophrenia patients, but the nature of the abnormal coupling has not always been consistent between studies and is markedly different to the rodent literature, constraining its utility as a translational phenotype. Meyer-Lindenberg et al. (2005) assessed functional coupling using positron emission tomography (PET) while schizophrenia patients and healthy

controls performed the n-back working memory task. Controls showed increased activation of the prefrontal cortex, decreased activation of the hippocampus, and functional uncoupling during increased memory load. Schizophrenia patients showed opposite effects in prefrontal cortex and hippocampus, and abnormally persistent negative functional connectivity (anti-correlation) between hippocampal-prefrontal with increased memory load. The authors suggested the uncoupled state was advantageous in controls as it might prevent interference between cognitive processes. These findings were supported by Rasetti et al. (2011), although with a slightly different pattern in controls. Using a different measure of coupling, Benetti et al. (2009) saw reduced hippocampal-prefrontal connectivity in first episode patients during working memory. Findings during episodic memory tasks and in the resting state have also shown abnormalities in hippocampal-prefrontal interaction, observing both increased and decreased functional connectivity (Bähner and Meyer-Lindenberg, 2017; Wolf et al., 2007; Zhou et al., 2008). This network has also been implicated in Fragile X syndrome, as decreased levels of FMRP correlated with reduced parahippocampal activation and decreased functional connectivity between hippocampus and prefrontal cortex (Wang et al., 2012).

Furthermore, emerging evidence suggests cortical theta-gamma PAC is disrupted in schizophrenia, although results appear to depend on conditions (Barr et al., 2017; Hirano et al., 2018; Popov et al., 2015; Won et al., 2018). During an N-back task and the Stroop colour interference task, PAC was impaired in schizophrenia patients (Barr et al., 2017; Popov et al., 2015), while resting-state theta-gamma PAC was increased in schizophrenia patients. During a 40 Hz auditory steady-state stimulation PAC was unchanged in schizophrenia patients (Hirano et al., 2018; Kirihara et al., 2012).

Evidence supports the suggestion that circuit abnormalities may represent a biomarker for schizophrenia (Bähner and Meyer-Lindenberg, 2017). Esslinger et al. (2009) found that healthy carriers of a risk SNP in the gene ZNF804A had abnormally increased functional connectivity between hippocampus and

dorsolateral prefrontal cortex. These results were further supported by a study which found the risk allele to be associated with increased hippocampal-prefrontal connectivity and decreased intrahippocampal theta, through simultaneous fMRI and MEG measures (Cousijn et al., 2015). Callicott et al. (2013) looked at healthy subjects carrying two risk alleles SLC12A2 and DISC1, both involved in neural development, which together interact to increase schizophrenia risk. During a recognition memory task, these carriers showed decreased hippocampal-prefrontal connectivity. Overall, these findings highlight a link between the cognitive deficits of schizophrenia and aberrant hippocampal-prefrontal connectivity.

3.1.1.6 Hippocampal-prefrontal interactions in animal models of psychiatric disorder

To date, only a handful of animal models have investigated electrophysiological biomarkers *in vivo,* particularly in the hippocampal-prefrontal network. Sigurdsson et al. (2010) examined the functional connectivity in the Df16(A)$^{+/-}$ mouse, a model of the highly penetrant 22q11.2 CNV. They assessed synchronization of network activity between hippocampus and prefrontal cortex during a working memory task, discrete-trial alternation in the T maze. Synchrony was impaired as measured by phase-locking of prefrontal neurons to the hippocampal theta rhythm and coherence between hippocampus and prefrontal cortex LFP. Furthermore, Df16(A)$^{+/-}$ mice were impaired in the acquisition of the task, and the extent to which synchrony was impaired correlated with the extent of the behavioural deficit. A further study from the same group narrowed down the genetic origin of the deficits seen in hippocampal-prefrontal synchrony, by studying a mouse model heterozygous for *Zdhhc8*. *Zdhhc8* is one of the key genes within the 22q11.2 CNV, and functions as a transmembrane palmitoyltransferase, implicated in regulating normal axonal branching and dendritic growth (Mukai et al., 2004, 2008). Mice heterozygous for *Zdhhc8* showed reduced branching of neurons, paralleled with impaired hippocampal-prefrontal synchrony, which also correlated with impaired acquisition of the working memory task (Mukai et al., 2015). Furthermore, preventing these branching deficits by inhibition of glycogen synthase kinase-3 (GSK3) in the Df16(A)$^{+/-}$ mouse rescued hippocampal-prefrontal coherence deficits as well as task

performance and medial prefrontal cortex encoding of spatial representations (Tamura et al., 2016). In addition, the role of phase-amplitude coupling in spatial working memory was recently examined in this model, where an abnormally increased coupling was seen on choice runs of correct trials, suggesting a compensatory role of increased coupling (Tamura et al., 2017).

Interestingly, there appears to be some overlap in the molecular pathways involving Zdhhc8 and Cyfip1. The proteins known to be subject to palmitoyltransferase activity by Zdhhc8 were identified and, of the two target proteins which saw the greatest reductions in palmitoylation, one was Rac1. As seen in Chapter 1, this is the small Rho GTPase responsible for regulating the conformational change in Cyfip1 which sets which protein complex it binds to (Di Marino et al., 2015). Given that reduced Zddhc8 leads to disrupted Rac1 signalling, reduced functional connectivity in the HPC-PRL network and impaired spatial working memory, I hypothesised that disruptions downstream of Rac1 due to Cyfip1 haploinsufficiency may lead to similar outcomes.

Further genetic animal models have seen changes in the hippocampal-prefrontal network. Genes coding for neuregulin-1 (NRG1), a neurotrophic factor, and ERBB4, the synaptic protein it binds to, have been identified as psychiatric risk genes (Walsh et al. 2008; Stefansson et al. 2003). ERBB4 is expressed predominantly on parvalbumin-positive (PV+) interneurons (Fazzari et al. 2010), which have a role in mediating gamma oscillations (Sohal et al. 2009). Conditional PV+ ERBB4 knockout mice showed reduced hippocampal-prefrontal theta coherence under anaesthesia, while also finding increased baseline gamma oscillations in freely moving mice coupled with deficits in social and cognitive functions reminiscent of schizophrenia (Del Pino et al. 2013). In contrast, mice with DISC1 mutation, a risk gene for schizophrenia and depression with an important synaptic role (Brandon & Sawa 2011), have impairment of theta and low-gamma synchrony and power within the PRL, but normal theta coherence across HPC-PRL network. This is in line with normal working memory in DISC1 mice.

Recent work in the *Fmr1* KO mouse, which is of particular interest considering the close molecular interaction between CYFIP1 and FMRP, investigated hippocampal network activity during spatial exploration. The authors first reported that Fmr1-KO mice had disrupted place cell activity, namely impaired stability and reduced specificity of spatial representation (Arbab et al., 2017). In this study they showed increased hippocampal theta power, and increased intra-hippocampal coherence in the gamma band, while interneuron spikes were hypersynchronized to the ongoing theta and gamma oscillations. No studies have as yet investigated hippocampal-prefrontal interactions in this model.

Animal models can also reflect environmental impacts known to increase risk for psychiatric disorders (McDonald and Murray, 2000). The maternal immune activation model recapitulates the impact of a viral infection during pregnancy, which has been linked to increased risk of schizophrenia for the child (Brown and Derkits, 2010). This model showed impaired dorsal hippocampal-prefrontal synchrony and phase-locking in delta, theta and low gamma frequency bands (Dickerson et al., 2010). A gene x environment double-hit model carrying a DISC1 mutation as well as exposure to maternal immune activation further exacerbated the disruption to hippocampal-prefrontal coupling (Hartung et al., 2016). At postnatal day 8-10 double-hit animals had diminished hippocampal-prefrontal theta coherence, while by pre-juvenile age this switched to augmented coherence and increased hippocampal theta-prelimbic gamma PAC. This highlights the role of gene-environment interactions on the hippocampal-prefrontal network.

Neurodevelopmental models aim to assess the impact of disruptions in neural development on network activity in adulthood. The mitotoxin methylazoxymethanol ecetate (MAM) model, where the toxin is administered during gestation at a sensitive time for limbic-cortical network development, shows impaired hippocampal-prefrontal interactions during sleep, as measured by disruptions in hippocampal ripple-cortical spindle synchrony (Phillips et al., 2012a). While theta coherence during appeared normal during NREM sleep, task-related changes in theta coherence were not examined in this study.

Collectively, these studies reveal that disruptions to hippocampal-prefrontal synchrony are common in a variety of genetic, environmental and neurodevelopmental models of psychiatric illness. A key question arises: by what mechanism do these diverse manipulations lead to disruptions in hippocampal-prefrontal synchrony? The answer is still unclear. It could be through different mechanisms or a convergence on a common mechanism. The closest mechanistic link is that seen in the *Zdhhc8*$^{+/-}$ mice, where abnormalities seen in hippocampal projections to the cortex were shown to be directly responsible for impaired synchrony (Mukai et al., 2015; Tamura et al., 2016). Nonetheless, in the wider field there appears to be a convergence of risk genes onto pathways involved in synaptic plasticity and synaptic development (Hall et al., 2015), suggesting these studies are asking the right questions (Rosen et al., 2015).

3.1.2 Spatial working memory and the discrete-trial alternation T Maze task

Many of the above mentioned rodent studies linked deficits in the hippocampal-prefrontal network to the spatial working memory demands of an alternation T maze task. Before discussing the T maze task, it is worth defining in more detail the cognitive demands it is thought to harness. Baddeley & Hitch (1974) first introduced the concept of working memory, defining it as a system to provide temporary storage and manipulation of information. In animal studies working memory acquired a slightly different definition, considered as a system that retains information that is necessary for only one trial, versus reference memory, where the memory is useful over more than a single trial (Olton et al., 1979). Spatial alternation in the T maze is an example of the former, while the Morris water maze is an example of the latter. The authors ascribed the memory system required for T maze alternation as working memory, because they argued that animals need to remember cues presented (i.e. did I go right or left?) but also when the cue was presented so it does not interfere with upcoming performance (i.e. did I go right or left *in the last trial*?). However, the underlying psychology of this task has been disputed. Sanderson & Bannerman (2012) present a thorough discussion of this issue and suggest alternation behaviour rather relies on short-term habituation to spatial stimuli, reflecting aspects of attentional processing. Nevertheless, the likely

contribution of the hippocampal-prefrontal network makes this a suitable task to explore any network disruptions as a consequence of Cyfip1 haploinsufficiency. Thought this caveat is important to note, to conform to the majority of the literature in the psychiatric genetics/*in vivo* electrophysiology fields, I will refer to the cognitive demands of this task as spatial working memory.

An array of T maze-based tasks are commonly used in uncovering cognitive deficits linked to the hippocampal-prefrontal network in animal models. Alternation tasks, where the animal is required to choose the opposite arm to the one last visited, rely on a form of spatial working memory which harnesses the rodent's natural tendency to explore recently unvisited areas. These types of tasks are sensitive to lesions of the dorsal hippocampus (Bannerman et al., 1999; McHugh et al., 2008; Rawlins and Olton, 1982) and prefrontal cortex (Granon et al., 1994), although there are mixed findings regarding the effect of lesions or inactivations of the ventral hippocampus (McHugh et al., 2008; Wang and Cai, 2006a).

Alternation tasks can broadly be divided into continuous alternation and discrete-trial alternation (Figure 3.2). Continuous alternation is often not rewarded (in this case it is referred to as spontaneous alternation) and does not use barriers at the choice point: on the first run, a rat will choose one arm, and in the subsequent run the correct choice is the opposite arm. Subsequent runs must alternate based on which arm the rat last visited, and each run constitutes a trial. In contrast, discrete-trial alternation involves the use of a barrier at the T-junction in the first run, which guides the animal into one of the arms. In the next run, the barrier is removed, and the correct choice is to enter the opposite arm. In this version, each trial constitutes two runs, a guided and a choice run (Rawlins and Olton, 1982). A significant advantage of the discrete-trial alternation task is the presence of identical behaviour coupled with context-dependent cognitive demands. The ability to tease apart runs where spatial memory is invoked, i.e. in the choice run, is particularly useful when analysing network activity. Therefore, I decided to use a modified version of this task to investigate cognitive deficits in the *Cyfip1*$^{+/-}$ rat.

3.1.2.1 Use of the return arm T maze

Discrete-trial alternation is typically run using a classical T maze, with a central stem arm, and two goal arms. The addition of return arms, connecting the reward location back to the base of the central arm (Jung et al., 1998a), has been particularly useful in simultaneous electrophysiology and behaviour experiments, as it does not require potentially noise-inducing handling of the rat after each trial (Ainge et al., 2007a; Griffin et al., 2012; Hallock and Griffin, 2013; Lee et al., 2006; Shoji et al., 2012; Wood et al., 2000). Its use in continuous T maze alternation, however, indicated that a no-delay version of the task may be independent of hippocampus (Ainge et al., 2007a), rather involving striatal circuitry mediating learning of a motor pattern to run figure-of-8 loops (Moussa et al., 2011). Combining the return-arm T maze with a discrete-trial alternation task should interrupt the learning of a continuous motor pattern, generating a task that is hypothesised to be hippocampal-dependent and compatible with electrophysiological recording.

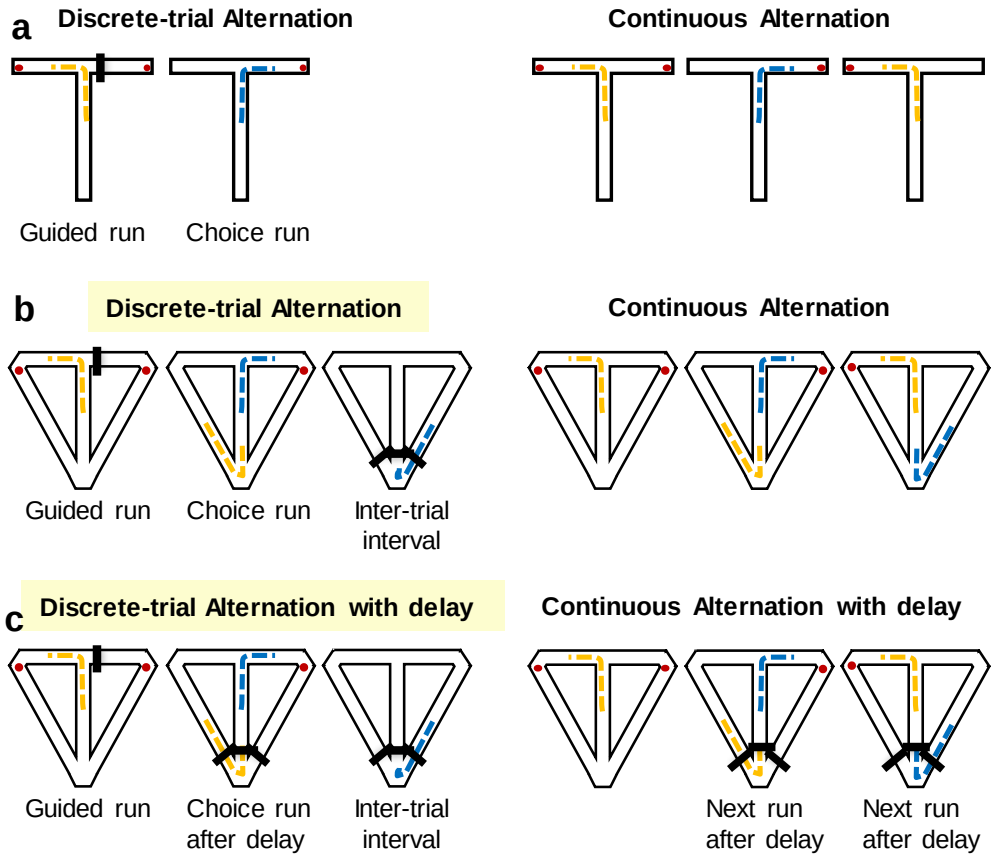

Figure 3.2 | **Schematics of different variations of T maze task. a,** Discrete-trial alternation and continuous alternation in a classical T maze. Black bar indicates a barrier, red dot indicates food reward, yellow dashed line illustrates rat's path on first run, blue line indicates subsequent run. **b,** Discrete-trial alternation and continuous alternation on the return arm T maze. In the rewarded alternation task, rats are held at the base of the T during the inter-trial interval while the next trial is set up, whereas in continuous alternation the rats run continuous loops. **c,** A delay can be added between the guided and choice runs in discrete-trial alternation, or between each run in continuous alternation. Experiments in this chapter use the tasks highlighted in yellow.

3.1.3 Chapter aims

In this chapter, I investigated the behavioural and neural network correlates of spatial working memory in *Cyfip1*$^{+/-}$ rats. Animals learned a discrete-trial alternation task on a return arm T maze and hippocampal-prefrontal network interactions were assessed during task performance. In addition, the impact of increasing task difficulty by introducing a delay was assessed.

Key hypotheses:

- Cyfip1 haploinsufficiency has a negative impact on spatial working memory performance.
- Hippocampal-prefrontal interactions necessary for this cognitive process are disrupted in *Cyfip1*$^{+/-}$ rats.
- *Cyfip1*$^{+/-}$ rats are more sensitive than wild types (WT) to increases in task difficulty by the introduction of a delay.

3.2 Methods

3.2.1 Behaviour and surgery

The discrete-trial alternation T maze task was run as described in Section 2.3 (page 58) in General Methods. Animals were implanted with multisite LFP electrode drives, including targets to dorsal CA1 (dCA1), ventral HPC (vHPC) and prelimbic cortex (PRL), as described in Section 2.4 (page 60).

3.2.2 Analysis

3.2.2.1 Tracking data

Tracking data were acquired by detecting coloured LEDs mounted on the headstage of each rat, sampled at 30 frames per second, time-locked to the electrophysiological data. Tracking data had to be manually cleaned by removing erroneous data points (caused by the camera detecting bright objects other than the LEDs), thus reducing the sampling frequency at some points. Due to slight movements of the maze between animals, tracking data needed to be aligned for group analysis purposes, by shifting and rotating each animal's tracking data.

3.2.2.2 LFP data

Half of the animals were recorded at 1017 Hz sampling frequency, while others at 2000 Hz due to updated hardware. Therefore, all data was down-sampled to 1017 Hz. For further details on power, coherence, granger causality and phase-amplitude coupling analysis, see Section 2.5 (page 68).

3.2.2.3 Maze segment analysis

For maze-based analyses, tracking data was segmented into 12 roughly equal segments using 13 trigger lines (Figure 3.4a). Using the Maze Query Language toolbox (Tom Jahans-Price, www.cs.bris.ac.uk/Research/MachineLearning/mql/), timestamps could be extracted for every crossing of the trigger lines, enabling analyses of behaviour and electrophysiology time-locked to different points on the maze (i.e. different trigger lines).

3.2.2.4 Granger causality

Trial-by-trial 6 second LFP epochs centred on trigger line 5 were concatenated to provide a single signal from the central arm of the maze for each animal. Granger causality values for the theta frequency band in the HPC→PFC direction and PFC→HPC direction were calculated and significance tested using a bootstrapping method as described in Chapter 2. Taking a ratio of the significant values for each direction showed which direction was more dominant.

3.3 Results

3.3.1 Behaviour

3.3.1.1 Performance accuracy normal in Cyfip1$^{+/-}$ rats

A group of 16 WT and 17 *Cyfip1*$^{+/-}$ began habituation on the T maze. Three *Cyfip1*$^{+/-}$ and one WT rat did not pass the habituation stage as they showed excessive freezing behaviour on the maze and did not consume the sucrose solution. One further *Cyfip1*$^{+/-}$ animal had to be excluded during the delay training due to apparent extreme anxiety on the maze. A Fisher's Exact test confirmed a similar proportion of drop outs from each group ($p = 0.165$).

The remaining animals progressed to running the reward alternation task (as described in Chapter 2) (Figure 3.3a). Performance accuracy during the first session of 10 trials was similarly high in *Cyfip1*$^{+/-}$ and WT rats, (WT: 83 ± 4%, Cyfip1$^{+/-}$: 81 ± 4%, $p=0.69$, independent sample t-test, Figure 3.3b) indicating that the task harnesses their natural tendency to alternate which arms to explore. Animals then

ran further daily sessions of 10 trials until achieving criterion (2 consecutive days of 80% or higher accuracy), after which they underwent surgical implantation.

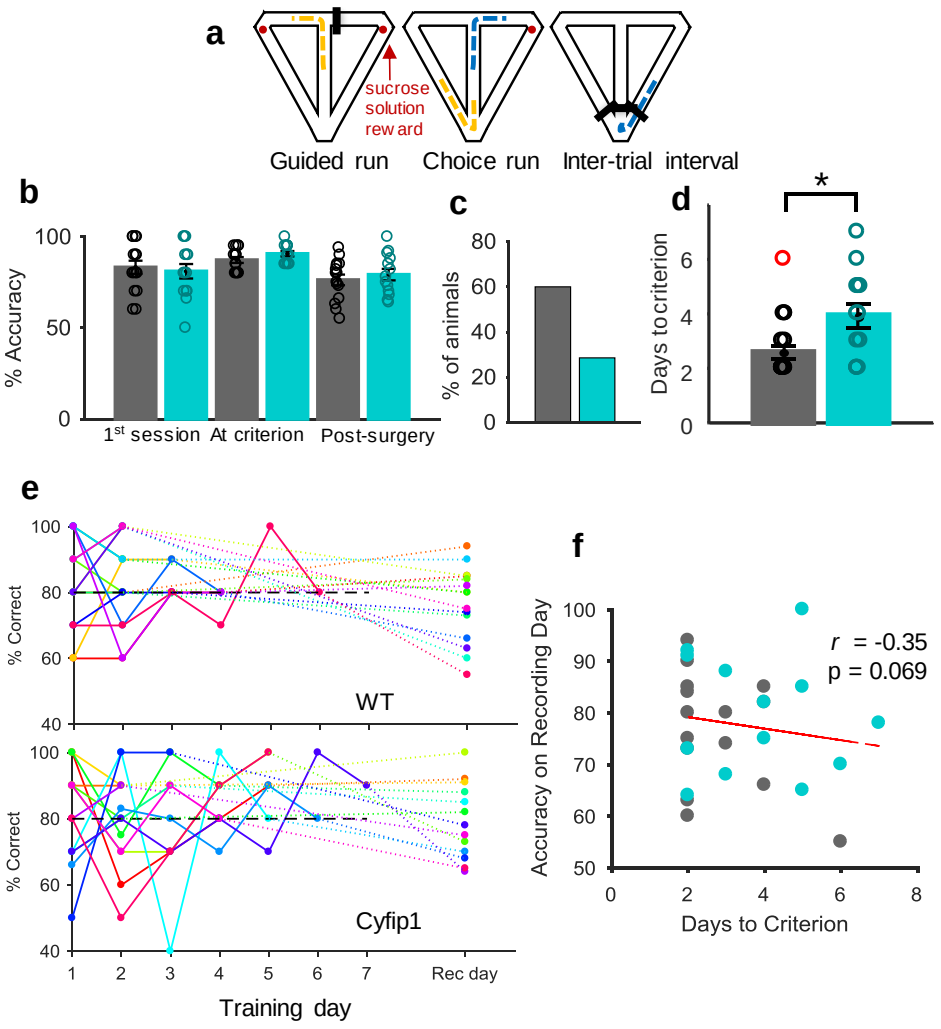

Figure 3.3 | **T maze performance of *Cyfip1*$^{+/-}$ and WT rats**. **a,** Schematic of return arm T maze task. **b,** Performance accuracy across three behaviour sessions. On first day and at criterion, WT (grey): n = 15, Cyfip1 (cyan): n = 14. Post-surgery, WT: n = 15 Cyfip1: n = 13. **c,** Percent of animals who achieved 2 consecutive sessions of 80% within the first 2 sessions. **d,** Days to criterion, WT outlier in red is not included in the group mean. **e,** Performance accuracy for individual animals (top WTs, bottom Cyfip1) over consecutive training sessions, each animal represented by a different colour. Thin dotted lines connect the score from the last training session to the score on the recording day. **f,** Correlation of days each animal took to reach criterion *vs* performance accuracy on the recording day. Red line shows line of best fit.

Performance accuracy during the post-surgery session was similar in both groups (WT: 76 ± 3%, Cyfip1: 79 ± 3%, p = 0.51, t-test, Figure 3.3b). Comparing criterion performance, taken as the mean of the last 2 sessions pre-surgery, to the first post-

surgery recording session, showed a significant drop in performance accuracy in both groups ($F_{1,26}$ = 20.20, p < 0.001, no genotype effect or interaction, ANOVA, Figure 3.3b). This could relate to a natural drop in performance accuracy due to lack of training in the peri-surgical period. Alternatively, it may relate to the fact that the first maze session post-surgery incorporated simultaneous electrophysiological data recording, which requires the rat being connected to a tether. While every effort was made to allow uninhibited movement while connected to the tether, the presence of the tether may have acted as a distraction. It is likely that a combination of these two factors led to the drop in performance on the recording day; however, this opened up the opportunity to analyse electrophysiological data from a more substantial number of error trials (see below). These results demonstrate that overall performance of the task was normal in *Cyfip1*$^{+/-}$ rats.

3.3.1.2 Cyfip1$^{+/-}$ *rats took longer to reach criterion performance*

While overall performance accuracy was similar across genotypes, there were some behavioural differences to note. Considering how quickly rats achieved criterion, ideal performance constitutes achieving ≥80% immediately in the first two days, i.e. 'passing first time'. Of the WT rats, 60% passed first time, vs. only 29% of *Cyfip1*$^{+/-}$ rats, although a chi square test for association between genotype and passing first time did not reach significance ($\chi 2(1) = 2.89$, p = 0.089, Figure 3.3c). Following from this, comparing days to criterion between groups, *Cyfip1*$^{+/-}$ rats took significantly more days to reach criterion (p = 0.024, Mann-Whitney U test, Figure 3.3d; one WT was excluded as an outlier). I next tested whether the number of days to criterion related to the performance during the post-surgery recording session: there was a trending negative correlation between these variables (Spearman's rho = -0.35, p = 0.069, Figure 3.3f), and in both groups animals who took the most days to reach criterion performed the worst on the recording session (Figure 3.3e). This suggests *Cyfip1*$^{+/-}$ rats were less able to maintain consistent performance over consecutive sessions.

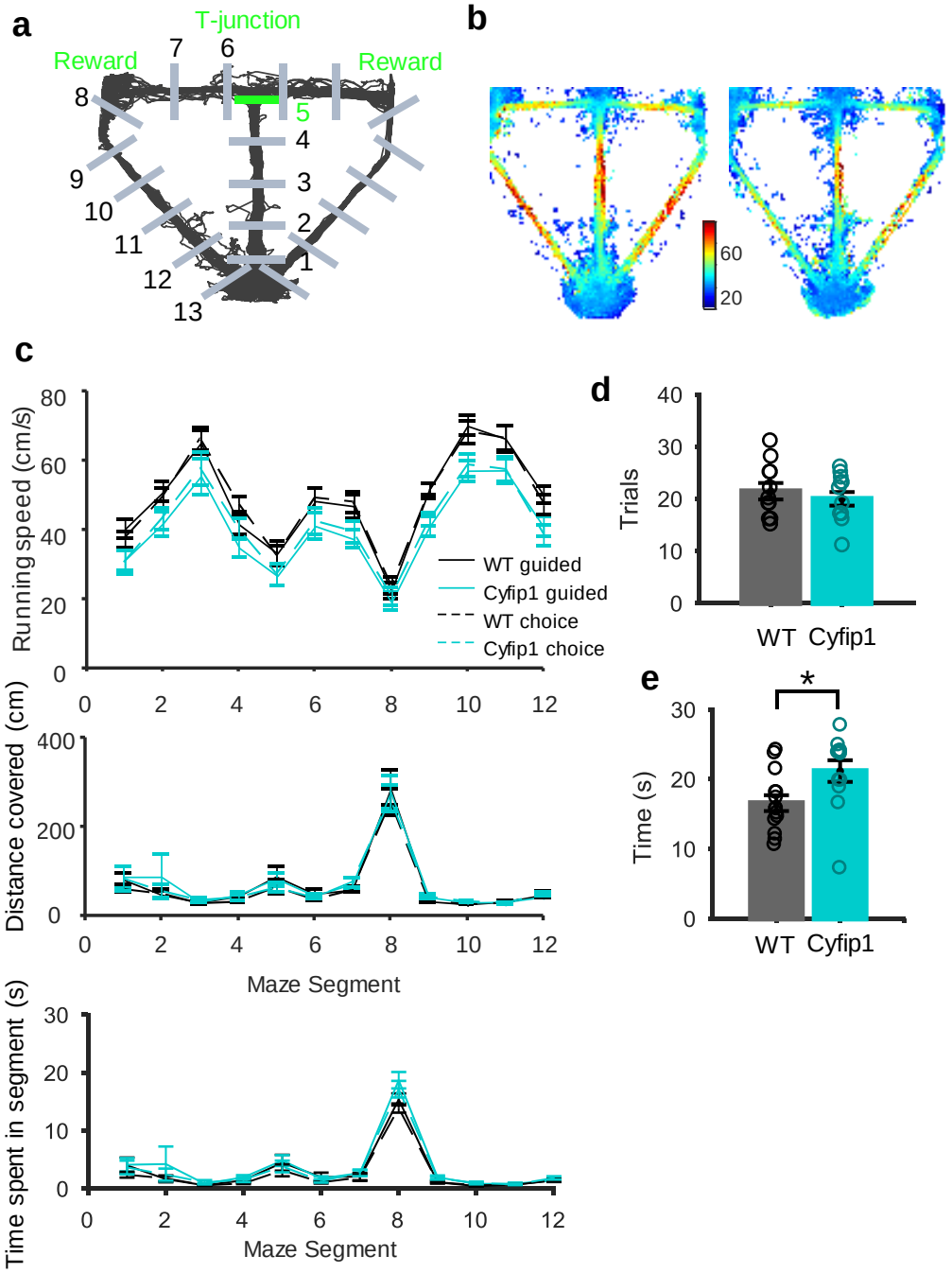

Figure 3.4 | **T maze running speed**. **a,** Representative tracking data from the return arm T maze, with trigger lines used for analyses marked and numbered. The segment of the same number always comes *after* the associated trigger line. T-junction analyses centre around trigger line 5 (green). **b,** Heatmaps showing instantaneous speed at different segments of the maze, averaged over trials for each animal, and over animals. **c,** Upper, running speed in each segment of the maze (segments numbers follow corresponding trigger line in **a**), averaged over trials and animals. Solid lines represent guided runs, dashed lines represent choice runs. Middle, distance covered by head movements in each segment of the maze, averaged over trials and animals. Lower, time spent in each segment of the maze. **d,** Number of trials during the recording session. **e,** Median time between

crossing trigger line 8 and trigger line 13, averaged over trials. *p<0.05. WT: n = 15, Cyfip1: n = 13.

3.3.1.3 Cyfip1$^{+/-}$ rats had slower running speeds on the maze

Behavioural data are presented from the post-implantation recording session, with one recording session per animal, from 15 WT and 13 *Cyfip1*$^{+/-}$ rats. One *Cyfip1*$^{+/-}$ rat died during surgery.

During the recording session, *Cyfip1*$^{+/-}$ rats had overall significantly slower running speeds compared to WT animals ($p = 0.017$, t-test, data not shown). This difference in running speed, however, did not impact the overall number of trials run in the 40 minute session, with average trial number similar between genotypes (WT: 21 ± 1.6%, Cyfip1$^{+/-}$: 20 ± 1.3%, $p=0.48$, t-test, Figure 3.4d). To explore whether running speed on different segments of the maze differed during guided or choice runs (Figure 3.4a), I ran a three-way mixed ANOVA with within-subject factors of run type and maze segment. This test confirmed that *Cyfip1*$^{+/-}$ rats ran slower than WT (main effect of genotype: $F_{1,24} = 6.81$, $p = 0.015$); while there was no main effect of run type ($F_{1,24} = 1.36$, $p = 0.26$) or genotype by run type interaction ($F_{1,24} = 1.9$, $p = 0.18$) , there was a significant run type by segment interaction ($F_{11,264} = 7.71$, $p < 0.001$) (Figure 3.4b, c).

To explore where on the maze there were run type-dependent speed differences, a series of paired t-tests were run to confirm the simple main effects. In maze segments 12 and 1, guided runs were faster than choice runs by 2-3 cm/s ($p < 0.05$), while in maze segments, 4, 7 and 8 choice runs were faster ($p < 0.05$). The effect size was greatest in segment 4, where there was an increase in speed of 5.7 ± 0.76cm/s, which reflects a faster run in the latter part of the central arm during choice runs. This difference between guided and choice runs on this segment of the maze may impact interpretation of electrophysiological findings that are affected by speed, as discussed below.

Analysing distance covered by the head-mounted LED in each maze segment, or time spent in each segment, could shed light on whether animals were running

straight through a segment, or exploring beyond the maze track, such as rearing and leaning over the maze wall (Figure 3.4c). Distance moved data were log transformed to bring them within a normal distribution. There was no main effect of genotype ($F_{1,24} = 0.48$, $p = 0.49$), but a significant segment by run type interaction ($F_{11,264} = 3.5$, $p < 0.001$), and analysis of simple effects revealed that in guided runs animals covered slightly more distance in segments 4 and 5 ($p < 0.05$, paired t-test). The difference was small (average of 2-6cm more distance covered in guided runs than in choice runs [segment length ~35cm]) and likely due to animals sniffing the barrier before they made the turn. Segment 8 has a notable increase in distance covered, which is explained by a behaviour typically observed in many rats. The 8th trigger line was positioned immediately before the reward. Rats would typically run directly to the reward point, cross the trigger line, consume the reward, and then instead of continuing through segment 8, they would rotate back and show exploratory behaviour towards the corner of the room. This can be seen in the example tracking data in Figure 3.4a as a cluster of position data points in the corners of the maze. The observation that this interest in this corner was higher on the left of the maze than on the right, suggests there is something of interest to the rats here. I believe this could be explained by the fact that the sleepbox, where their homecage was sitting, is in the far left corner of the room, and perhaps the rats could detect the presence of their homecage. This issue may have been resolved if I had used a black curtain to surround the maze, but this would still not have masked the scent of their homecage, which presumably is what they detected in the dimly lit room.

Together, these data indicate that *Cyfip1*$^{+/-}$ rats consistently run slower on most segments of the maze, although their exploratory behaviour on the maze was consistent with WTs.

3.3.1.4 Cyfip1$^{+/-}$ *rats have longer intervals between guided and choice runs*

The exploratory behaviour following reward consumption introduced an unintended delay between reward consumption and the start of the choice run (following a guided run) or the end of the trial (following a choice run). A difference

in the delay between guided and choice runs could impact the demands on the working memory system. While the shortest return arm time interval between reward consumption (trigger line 8) and start box return (trigger line 13) was 3-4 seconds, actual times for this interval on guided runs ranged between 4-108 seconds for WT and 3-106 seconds for *Cyfip1*$^{+/-}$ rats. Each animal's return arm run times were positively skewed, so the median was taken to represent the average. Comparing these medians between groups revealed a significant difference between genotypes in the time taken to run the return arm (WT: 16.6 ± 1 s, Cyfip1: 21.1 ± 2 s, p = 0.011, Mann-Whitney U test, Figure 3.4e). This may complicate the interpretation of the behaviour seen in this task, as cognitive deficits can be delay dependent. However, as the difference in the average 'delay' between groups is only ~5 seconds, I consider this of limited consequence, particularly as delays are normally introduced at greater intervals, e.g. 30s, 60s, 90s (Aggleton et al., 1997; Aultman and Moghaddam, 2001; Clinton et al., 2006). Furthermore, it does not appear that performance is affected by this difference.

3.3.2 Hippocampal-prefrontal network during maze task

To explore the impact of Cyfip1 haploinsufficiency on the hippocampal-prefrontal network during working memory, I examined LFP signals from this network during the T maze task. Analyses focussed on central arm and T-junction decision point of the maze, where rats presumably harness spatial working memory to inform their decision at the T-junction. To extract the relevant segments of behaviour, I extracted 6 s or 2 s epochs centred around the timestamp at trigger line 5, i.e. immediately before the turn. While the behaviour could be quite variable, with animals sniffing the maze or barrier, the 6 second windows generally captured paths of the rat spanning the central arm, turn, and T arm (Figure 3.5a), while the two second windows captured latter part of central arm, turn, and some of the T arm. The following analyses refer to data from correct trials only.

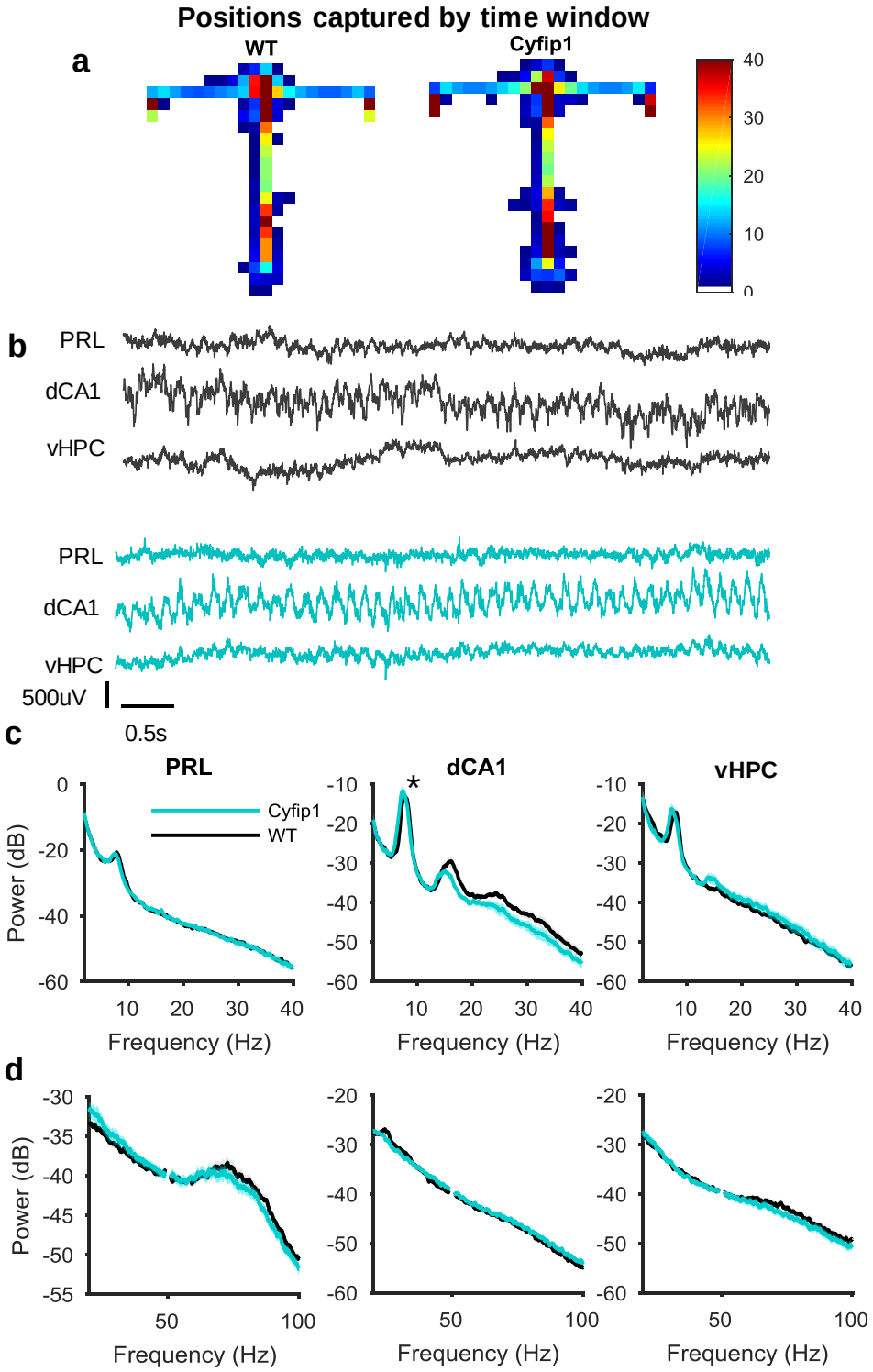

Figure 3.5 | **Power spectra for PRL, dCA1, and vHPC on T maze. a,** Heatmaps indicating paths captured by extracting a 6 s time window centred on trigger line 5, immediately before the T-junction. Colour represents the average number of times each pixel was visited, averaged across trials and animals. **b**, Representative (WT in grey, Cyfip1 in cyan) raw LFP traces from PRL, dCA1 and vHPC from the 6 second window as in a. **c**, Normalized power spectrums for PRL, dCA1 and vHPC in the 0-40 Hz range during the 6 s window.

*refers to significant difference in peak theta frequency, with Cyfip1 slightly slower. **d**, Normalized power spectrums for PRL, dCA1 and vHPC in the 20-100 Hz range during the 6 s window. Values between 49-51 Hz have been removed to mask 50Hz line noise. WT: n = 14, Cyfip1: n = 13.

3.3.2.1 Slower theta rhythm in CA1 of Cyfip1$^{+/-}$ rats, but normal power

Six second epochs centred on trigger line 5 around the T-junction were used to analyse oscillations in hippocampus and PRL (Figure 3.5b). Mean power at theta (6-10 Hz) and gamma (30-90 Hz) frequencies was not significantly different between genotypes (Figure 3.5c,d) in dCA1 (theta: p = 0.12, gamma: p = 0.27, t-tests), vHPC (theta [1 WT and 2 Cyfip1 outliers removed]: p = 0.28, gamma: 0.458, Mann-Whitney U test) or PRL (theta: p = 0.83, gamma: p = 0.65, t-tests). However, peak theta frequency in dCA1, identified in each rat as the frequency with maximum power within the theta frequency range, was found to be slightly slower in *Cyfip1*$^{+/-}$ rats (WT: 7.9 ± 0.08 Hz, Cyfip1: 7.5 ± 0.12, p = 0.029, t-test). This difference did not reach significance in the vHPC (WT: 7.71 ± 0.18 Hz, Cyfip1: 7.31 ± 0.17, p = 0.057, Mann-Whitney U test).

Theta frequency is known to be modulated by running speed (Li et al. 2012; Vanderwolf 1969; Morris et al. 1976; McFarland et al. 1975). As *Cyfip1*$^{+/-}$ rats tended to run more slowly on the maze, this difference in dCA1 theta frequency may be accounted for by a difference in running speed. I ran the analysis on a subset of runs where the average run speed was limited to a narrower speed range of 25-35 cm/s, thus eliminating group differences in run speed (p = 0.22, t-test, data not shown). On this subset of trials, the peak theta frequency was not significantly different between genotypes (p = 0.072, t-test). This suggests that while *Cyfip1*$^{+/-}$ rats had significantly slower theta rhythm, it is likely the difference in peak theta frequency is modulated by speed rather than by genotype.

3.3.2.2 Phase-amplitude coupling reduced in dCA1

PAC was assessed in WT and *Cyfip1*$^{+/-}$ rats to quantify the degree to which theta frequency is able to modulate gamma frequency within PRL, dCA1 and vHPC. There is some evidence that theta-gamma coupling within hippocampus may be modulated by memory demand (Montgomery and Buzsáki, 2007; Schomburg and

Fernández-Ruiz, 2014), therefore analysis was split over guided and choice runs. Timestamps for guided and choice runs were taken between trigger line 1 and 8, covering signals from the central arm to the reward point. Within PRL, a clear hot-spot of theta-gamma coupling was seen between theta and fast gamma in both genotypes (Figure 3.6a). Peak modulating (i.e. theta) frequency was equivalent between groups, as was peak modulated (i.e. gamma) frequency, as inspected from Figure 3.6b and c. By taking the mean of modulation index values bounded by a box encompassing 6-10 Hz phase frequency and 65-150 Hz amplitude frequency, theta-gamma coupling within PRL was compared between groups and across run types (Figure 3.6d), finding no effect of run type ($F_{1,25}$ = 0.47, p = 0.50) or genotype ($F_{1,25}$ = 0.061, p = 0.81), and no significant interaction ($F_{1,25}$ = 0.061, p = 0.80) . Two outliers were identified in the *Cyfip1*$^{+/-}$ group, but as they did not change the results of the test, were left in the analysis.

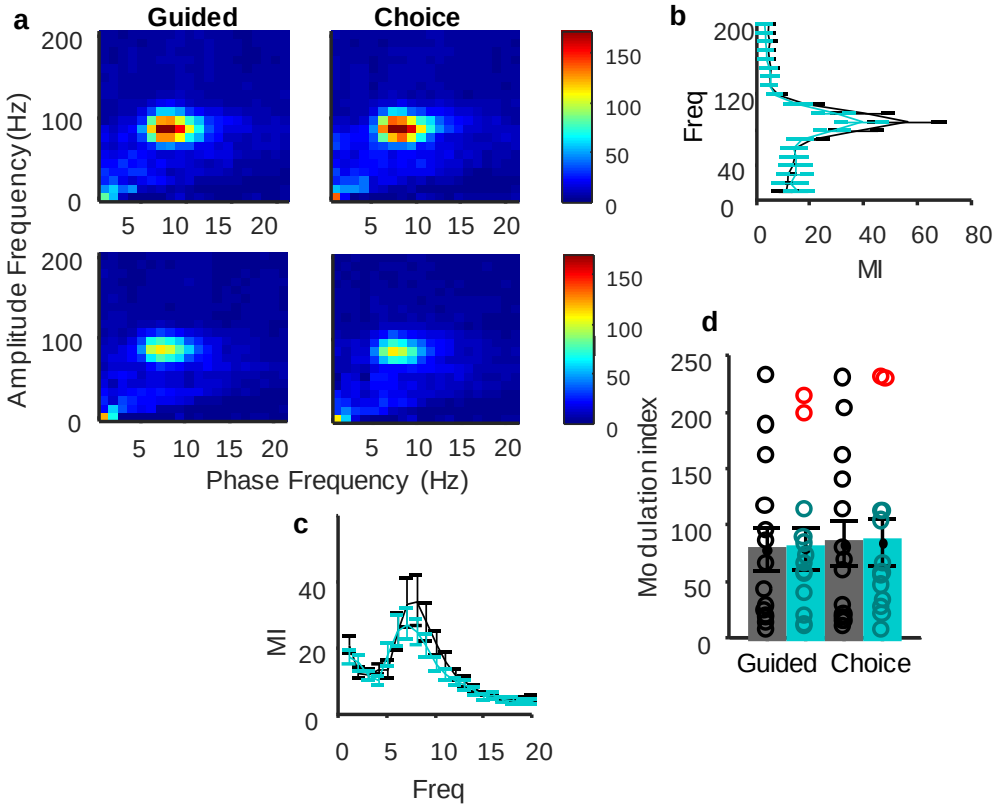

Figure 3.6 | **Theta-gamma phase-amplitude coupling within PRL. a,** Run and animal averaged comodulograms of WT (upper) and Cyfip1 (lower) showing theta-gamma coupling withinin PRL on guided and choice runs. Colour represents modulation index (MI).

b, Averaged modulation indices as a function of *modulated* frequencies (shown only for choice runs for clarity), i.e. the equivalent of collapsing the comodulograms in the x-direction. The peak *modulated* frequency can be seen. **c,** Averaged modulation indices as a function of modulating frequencies (shown only for choice runs for clarity), i.e. the equivalent of collapsing the comodulograms in the y-direction. The peak modulating frequency can be seen. **d,** Theta-fast gamma (65-150 Hz) coupling in the PRL. Outliers are circled in red, but were part of the group analyses as they did not affect the outcome. WT (grey): n = 14, Cyfip1 (cyan): n = 13.

Within dCA1, two distinct hot-spots of PAC were observed, as previously found (Colgin et al., 2009), so gamma frequency was divided into slow (25-60 Hz) and fast gamma (65-150 Hz) (Figure 3.7a). Peak modulating frequency was equivalent between groups, as was peak modulated frequency, as inspected from Figure 3.7b and c. Following removal of three *Cyfip1*$^{+/-}$ outliers, a significant reduction in theta-slow gamma coupling was seen in *Cyfip1*$^{+/-}$ rats (main effect of Genotype: $F_{1,22}$ = 6.80, p = 0.016) with no effect of run type ($F_{1,22}$ = 0.26, p = 0.61) and no interaction. While theta-fast gamma coupling was numerically lower in *Cyfip1*$^{+/-}$ rats, this was not significant ($F_{1,25}$ = 0.33, p = 0.57), and there was no effect of run type ($F_{1,25}$ = 0.22, p = 0.65) and no interaction.

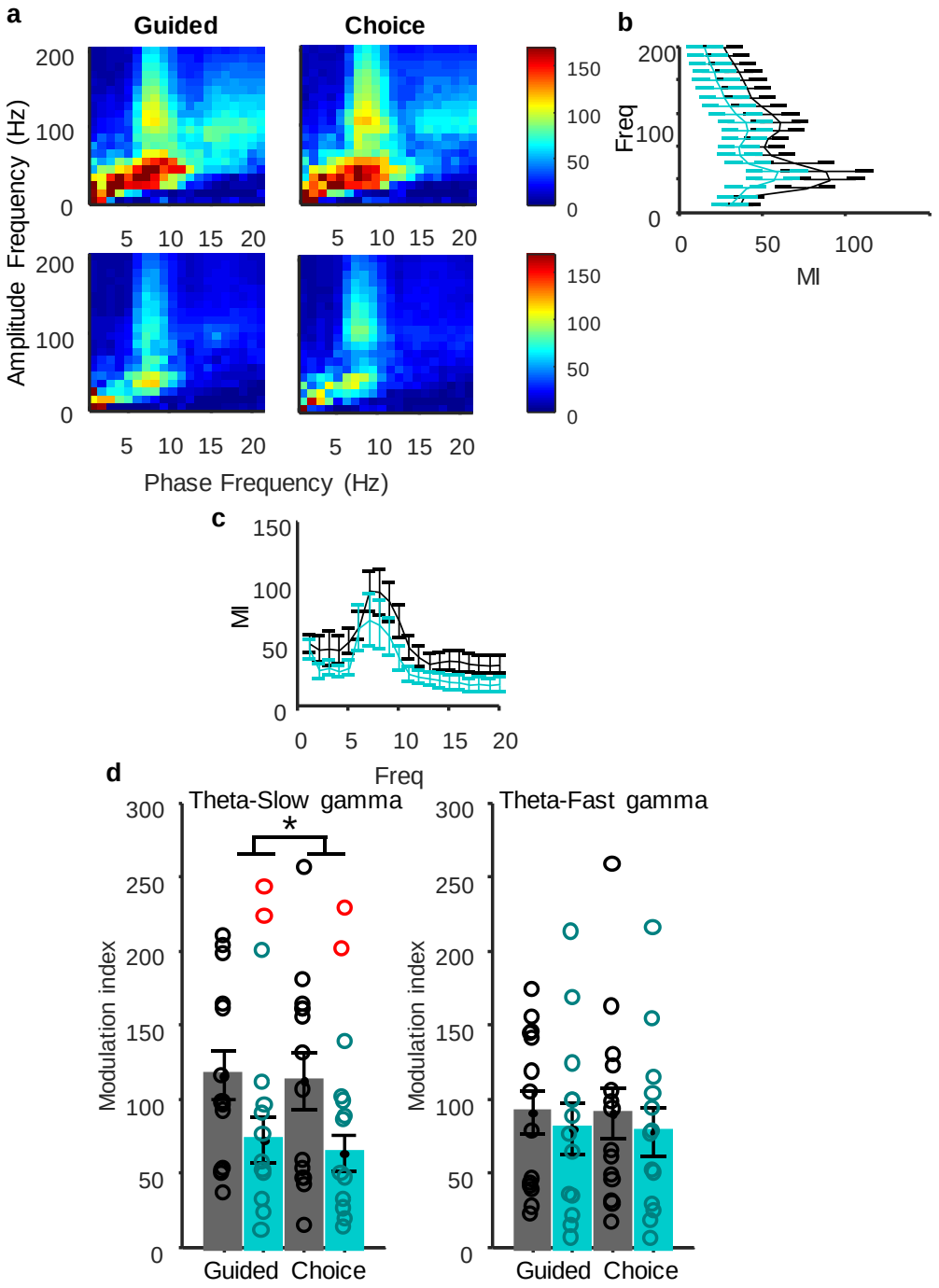

Figure 3.7 | **Theta-gamma phase-amplitude coupling within dCA1. a,** Run and animal averaged comodulograms of WT (upper) and Cyfip1 (lower) showing theta-gamma coupling withinin dCA1 on guided and choice runs. Colour represents modulation index. **b,** Averaged modulation indices as a function of *modulated* frequencies (shown only for choice runs for clarity), i.e. the equivalent of collapsing the comodulograms in the x-direction. The peak *modulated* frequency can be seen. **c,** Averaged modulation indices as a function of modulating frequencies (shown only for choice runs for clarity), i.e. the equivalent of collapsing the comodulograms in the y-direction. The peak modulating frequency can be seen. **d,** Left, theta-slow gamma (25-60 Hz) coupling in dCA1. Right,

theta-fast gamma (65-150 Hz) coupling in dCA1. Outliers are shown in red, these were not part of the group analyses. *p<0.05 for main effect of genotype, ANOVA. WT (grey): n = 14, Cyfip1 (cyan): n = 13.

Within vHPC, there were hotspots at theta-slow gamma and theta-fast gamma (Figure 3.8). Peak modulating frequency appeared slower in Cyfip1 rats (Figure 3.8c), corresponding to the slower theta seen in the power spectra between groups. Data was log-transformed to bring the data into a normal distribution, and following removal of 1 Cyfip1 outlier for slow gamma, and 2 Cyfip1 outliers and 1 WT outlier for fast gamma, there was no significant different between genotypes (slow gamma: $F_{1,24} = 0.063$, p = 0.804, fast gamma: $F_{1,22} = 0.005$, p = 0.95) or effect of run type (slow gamma: $F_{1,24} = 1.7$, p = 0.21, fast gamma: $F_{1,22} = 1.3$, p = 0.72) and no interaction (Figure 3.8d).

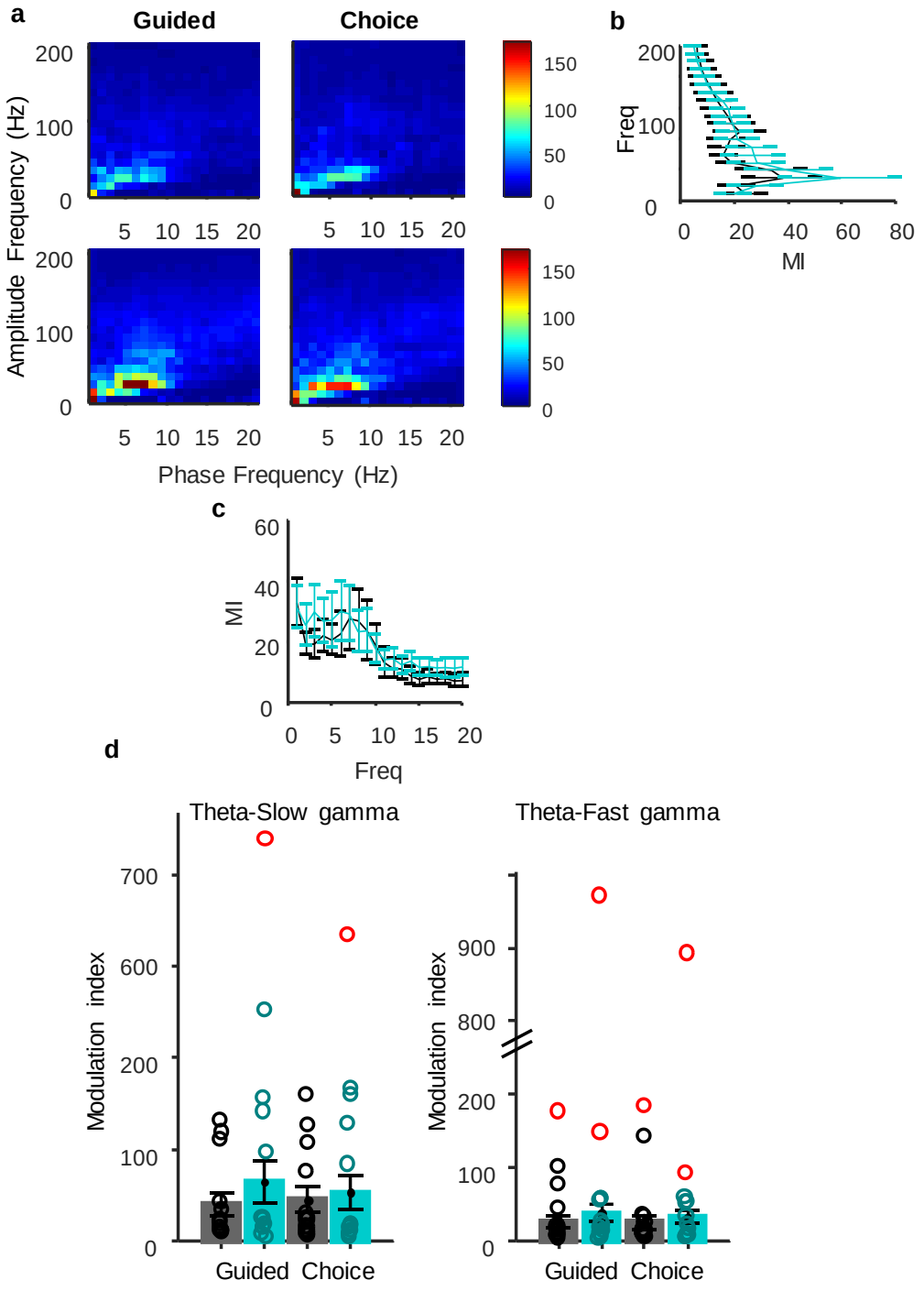

Figure 3.8 | **Theta-gamma phase-amplitude coupling within vHPC. a,** Run and animal averaged comodulograms of WT (upper) and Cyfip1 (lower) showing theta-gamma coupling withinin vHPC on guided and choice runs. Colour represents modulation index. **b,** Averaged modulation indices as a function of modulated frequencies (shown only for choice runs for clarity), i.e. the equivalent of collapsing the comodulograms in the x-direction. The peak *modulated* frequency can be seen. **c,** Averaged modulation indices as a function of modulating frequencies (shown only for choice runs for clarity), i.e. the equivalent of collapsing the comodulograms in the y-direction. The peak *modulating*

frequency can be seen. **d,** Left, theta-slow gamma (25-60 Hz) coupling in dCA1. Right, theta-fast gamma (65-150 Hz) coupling in dCA1. Outliers are shown in red, these were not part of the group analyses. WT(grey): n = 14, Cyfip1 (cyan): n = 13.

Together, these findings show that phase-amplitude coupling was disrupted within the dCA1 of *Cyfip1*$^{+/-}$ rats, although PAC was not modulated by run type as had previously been found.

3.3.2.3 Theta coherence normally modulated by context in Cyfip1$^{+/-}$ *rats*

Aside from a reduction in PAC in the hippocampus, *Cyfip1*$^{+/-}$ oscillations in hippocampus and PRL appear largely normal. Next, I investigated the interactions between hippocampus and PRL in *Cyfip1*$^{+/-}$ and WT rats. Analysing the 6 second window surrounding the decision point highlighted a hotspot of coherence in the centre of this time window (Figure 3.9a,b). Therefore, to narrow the focus of the analysis, subsequent analyses were based on a 2 second window centred around trigger line 5 i.e. immediately before the turn (Figure 3.9c). Theta coherence in this window was compared between guided and choice runs in WT and *Cyfip1*$^{+/-}$ rats.

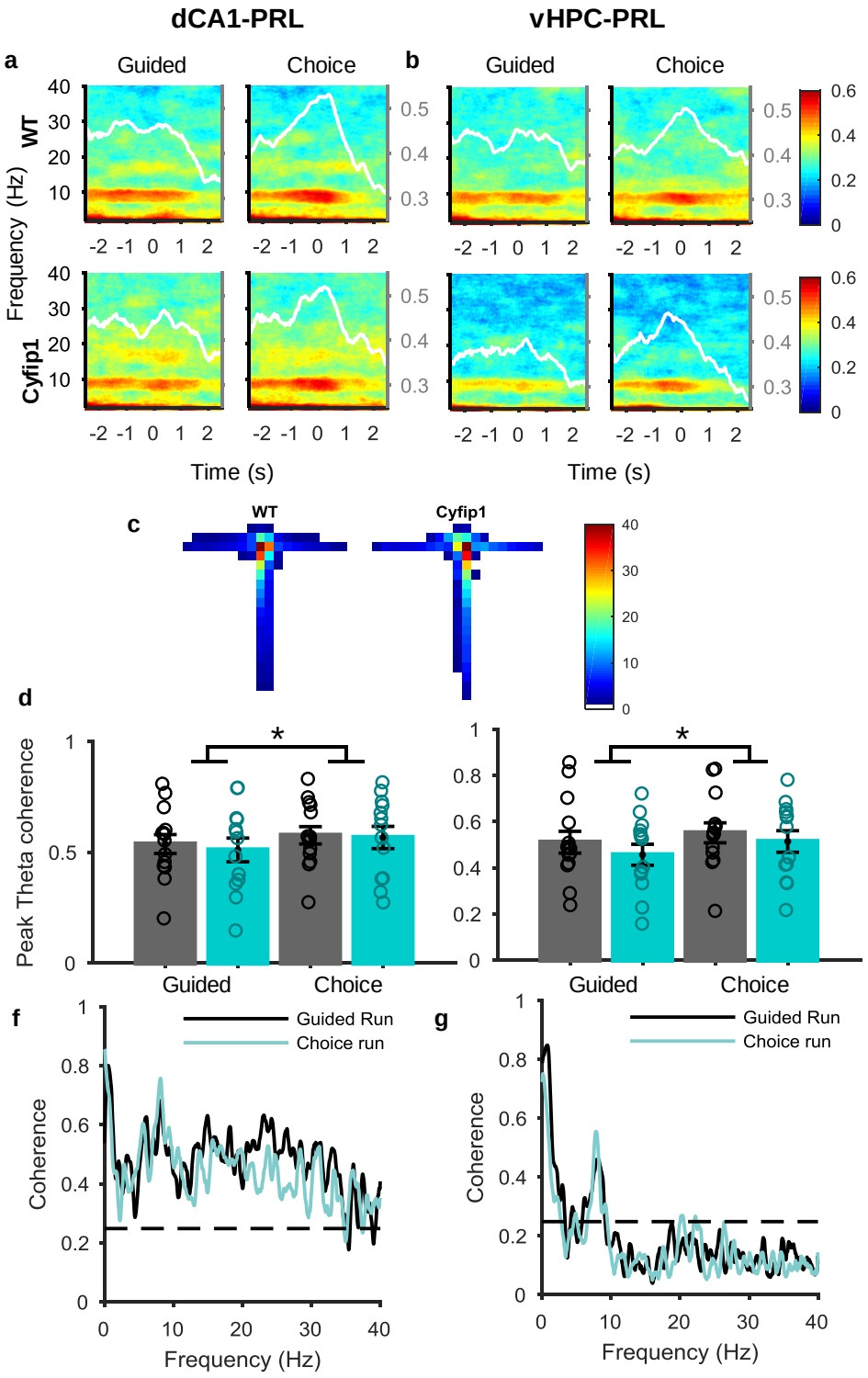

Figure 3.9 | **HPC-PRL coherence on T maze**. **a,** Trial and animal averaged coherograms for dCA1 and PRL, zero-aligned to trigger line 5, WT upper row, Cyfip1 lower row. Colour represents coherence, white trace represents mean theta (6-10 Hz) coherence during this time window, with values corresponding to right hand axis (Top row WT: n = 14, Bottom row Cyfip1: n = 13). **b,** Same as **a** for vHPC and PRL. **c,** Heatmaps indicating paths captured by extracting a 2 s time window centred on trigger line 5, immediately before the

T-junction. Colour represents the average number of times each pixel was visited, averaged across trials and animals. **d,e,** Peak theta coherence between dCA1 **(d)** and vHPC (**e**) and PRL. Taken from the central third of the coherograms in **a** and **b**, i.e. in the 2 s time window shown in **c,** split by guided or choice runs. *p<0.05 for main effect of run type. **f, g,** Representative coherency plots from an individual animal showing change in coherency in the theta range between guided and choice runs for dCA1-PRL (f) and vHPC-PRL (g) coherence. Dashed line represents confidence level at p = 0.05. WT (grey): n = 14, Cyfip1 (cyan): n = 13.

Peak theta coherence between dCA1 and PRL was significantly elevated in choice runs, but there was no difference between genotypes (WT Guided: 0.45 ± 0.445, WT Choice: 0.50 ± 0.044; Cyfip1 Guided: 0.43 ± 0.05, Cyfip1 Choice: 0.49 ± 0.05; Run type main effect: $F_{1,25}$ = 15.66, p < 0.001; Genotype main effect: $F_{1,25}$ = 0.054, p = 0.82), and no significant interaction ($F_{1,25}$ = 0.149, p = 0.70) (Figure 3.9d). The equivalent pattern was seen for vHPC and PRL coherence (WT Guided: 0.41 ± 0.048, WT Choice: 0.45 ± 0.046; Cyfip1 Guided: 0.37 ± 0.039, Cyfip1 Choice: 0.42 ± 0.045; Run type main effect: $F_{1,25}$ = 13.26, p = 0.001; Genotype main effect: $F_{1,25}$ = 0.387, p = 0.539), and no significant interaction ($F_{1,25}$ = 0.19, p = 0.667) (Figure 3.9d). Three outliers were identified within the vHPC-PRL guided coherence, but as the results of the ANOVA were unaffected by their removal, they were kept in the analysis.

It has been shown that amplitude covariations between theta-frequency signals could artificially increase coherence (Srinath and Ray, 2014). Therefore, it was important to confirm that changes in theta power in these regions was not biasing the changes seen in coherence. Hippocampal theta power and PRL theta power were not modulated by run type (dCA1: Run type main effect: $F_{1,25}$ = 8.41, p = 0.37; Genotype main effect: $F_{1,25}$ = 0.302, p = 0.59, no significant interaction; vHPC: Run type main effect: $F_{1,25}$ = 1.54, p = 0.23; Genotype main effect: $F_{1,25}$ = 0.05, p = 0.83, no significant interaction; PRL: Run type main effect: $F_{1,25}$ = 0.005, p = 0.94; Genotype main effect: $F_{1,25}$ = 0.302, p = 0.59, no significant interaction) (Figure 3.10).

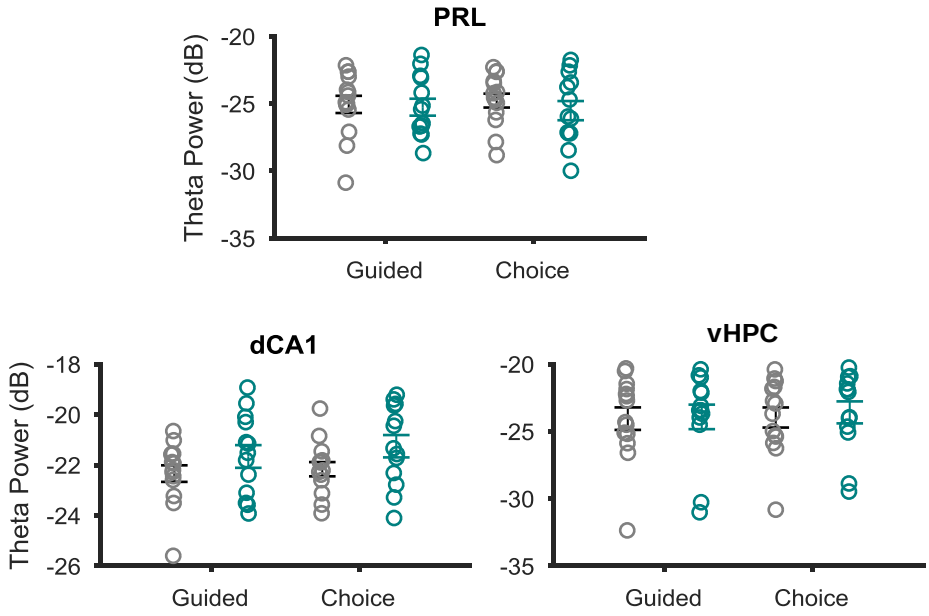

Figure 3.10 | **Theta power by run.** Normalized theta power in the PRL, dCA1 and vHPC regions. WT (grey): n = 14, Cyfip1 (cyan): n = 13.

Others have found that HPC-PRL functional connectivity prior to training could predict the number of days to criterion (Mukai et al., 2015; Sigurdsson et al., 2010). While in this study, network activity recordings were not made during the acquisition of the task, the greater number of days required to reach criterion may reflect a deficit in the HPC-PRL network which could persist beyond training. However, there was no significant correlation between dorsal or vHPC-PRL theta coherence and days to criterion on a rat-by-rat basis (dCA1-PRL : Spearman's rho = -0.109, p = 0.59, vHPC-PRL: Spearman's rho = 0.079, p = 0.70) (Figure 3.11).

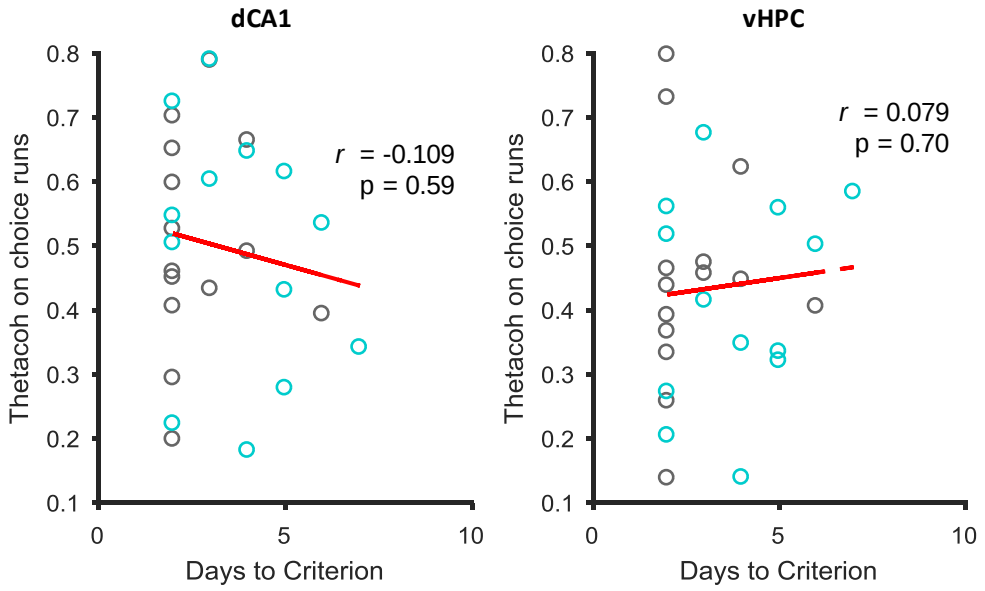

Figure 3.11 | **Relationship between theta coherence and days to criterion**. Correlation showing days to criterion *vs* theta coherence on choice runs in dorsal and vHPC. Each data point represents one animal, WT in grey, Cyfip1 in cyan. Red line represents line of best fit. WT: n = 14, Cyfip1: n = 13.

3.3.2.1 Hippocampus leads prelimbic signal

Granger causality was calculated to infer the directionality of the synchrony observed between HPC and PRL during choice runs (Figure 3.12). Consistent with the anatomy, in both genotypes, dCA1 leading PRL was significantly more dominant than PRL leading dCA1 in the theta frequency band (main effect of leading direction: $F_{1,25} = 17.3$, $p < 0.001$), but no main effect of genotype ($F_{1,25} = 0.049$, $p = 0.83$) (Figure 3.12a). Bootstrapping showed that theta frequency causality in the dCA1→PRL direction was significant in 13/14 WT rats, *vs* only 10/13 *Cyfip1*$^{+/-}$ rats, although a Fisher's exact test to show a difference between groups was not significant (p = 0.37,data not shown). Analysing only animals with a significant dCA1→PRL lead, the ratio of dCA1:PRL leading was similar in WT and *Cyfip1*$^{+/-}$ rats (p = 0.124, t-test, Figure 3.12b).

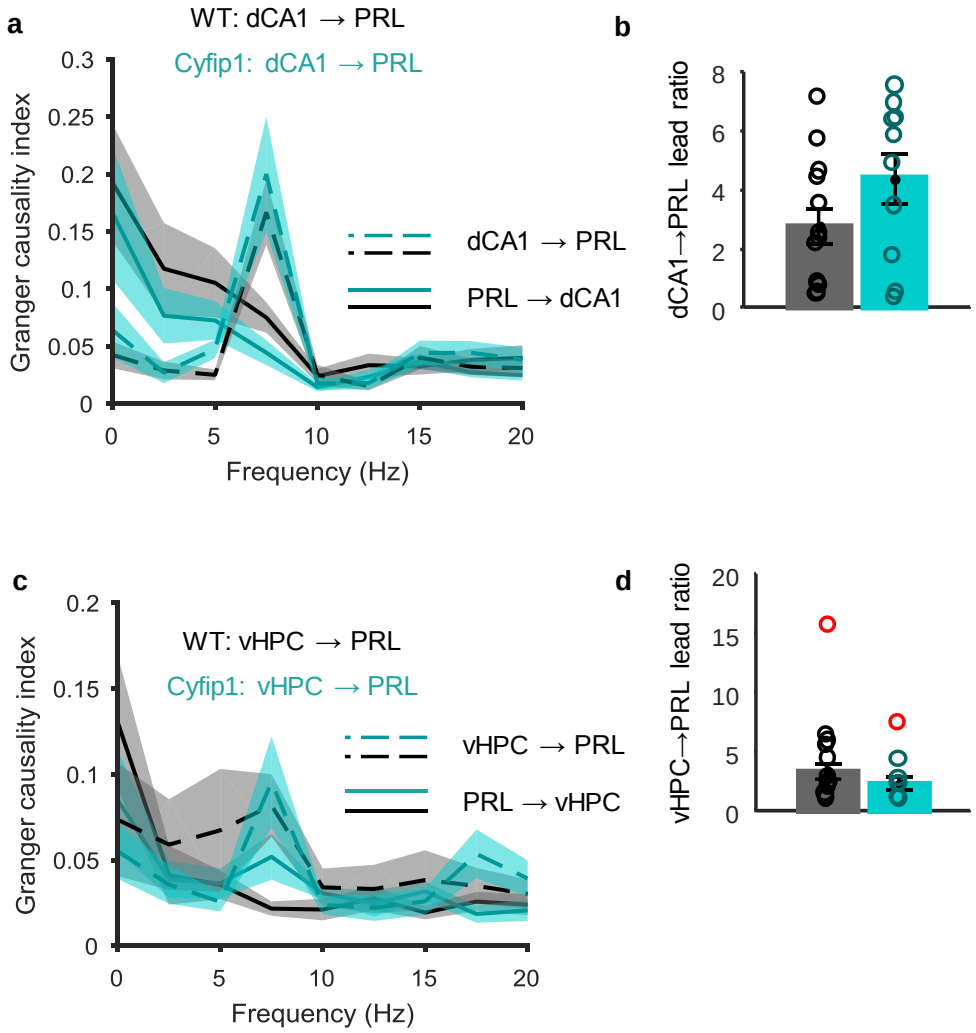

Figure 3.12 | **HPC-PRL coherence on T maze**. **a,c,** Granger causality showing directionality of the interaction between dCA1-PRL (**a**) and vHPC-PRL (**c**). Dashed lines represent causality from HPC to PRL, while solid lines represent causality from PRL to HPC. Text at top of figure summarises dominant directionality at theta frequency in each genotype. **b,d,** Ratio of HPC → PRL *vs* PRL→ HPC directionality. Outliers in **d** are marked in red and are not included in the group analysis. WT: n = 14, Cyfip1: n = 13.

Similarly, vHPC leading PRL was the more dominant direction (main effect of leading direction: $F_{1,25} = 6.24$,p = 0.019), with no genotype effect (: $F_{1,25} = 0.94$, p = 0.34, 2 WT and 1 Cyfip1 outlier did not affect results) (Figure 3.12c). However, bootstrapping showed that theta frequency causality in the vHPC→PRL direction was significant in 11/14 WT rats, but only 6/13 *Cyfip1*$^{+/-}$ rats, although this was not significant (p = 0.12, Fisher's exact test, data not shown). Analysing only animals with a significant vHPC→PRL lead, the ratio of vHPC:PRL leading was not

significantly different between genotypes (p = 0.241,t-test, 1 Cyfip1, 1 WT outliers removed, Figure 3.12d). Thus, for most animals, the dominant directionality of the signal was from hippocampus to cortex, but genotype did not affect this.

3.3.2.2 Running speed and theta coherence changes

As theta power can be affected by running speed (Li et al. 2012; Vanderwolf 1969; Morris et al. 1976; McFarland et al. 1975), it was important to assess whether running speed might modulate coherence. Analysing running speed in the 6 second window around the decision point shows that choice runs were faster than guided runs in both genotypes (run type main effect: $F_{1,25} = 15.98$, $p < 0.001$). While an earlier analysis found *Cyfip1*$^{+/-}$ rats ran slower (see Section 3.3.1.3, page 101), the genotype main effect only approached significance for this segment ($F_{1,25} = 3.74$, $p = 0.064$, Figure 3.13a). This difference in behaviour across guided and choice runs is problematic, as it complicates the dissociation of overt behavioural differences from differences in network activity in general and theta coherence in particular.

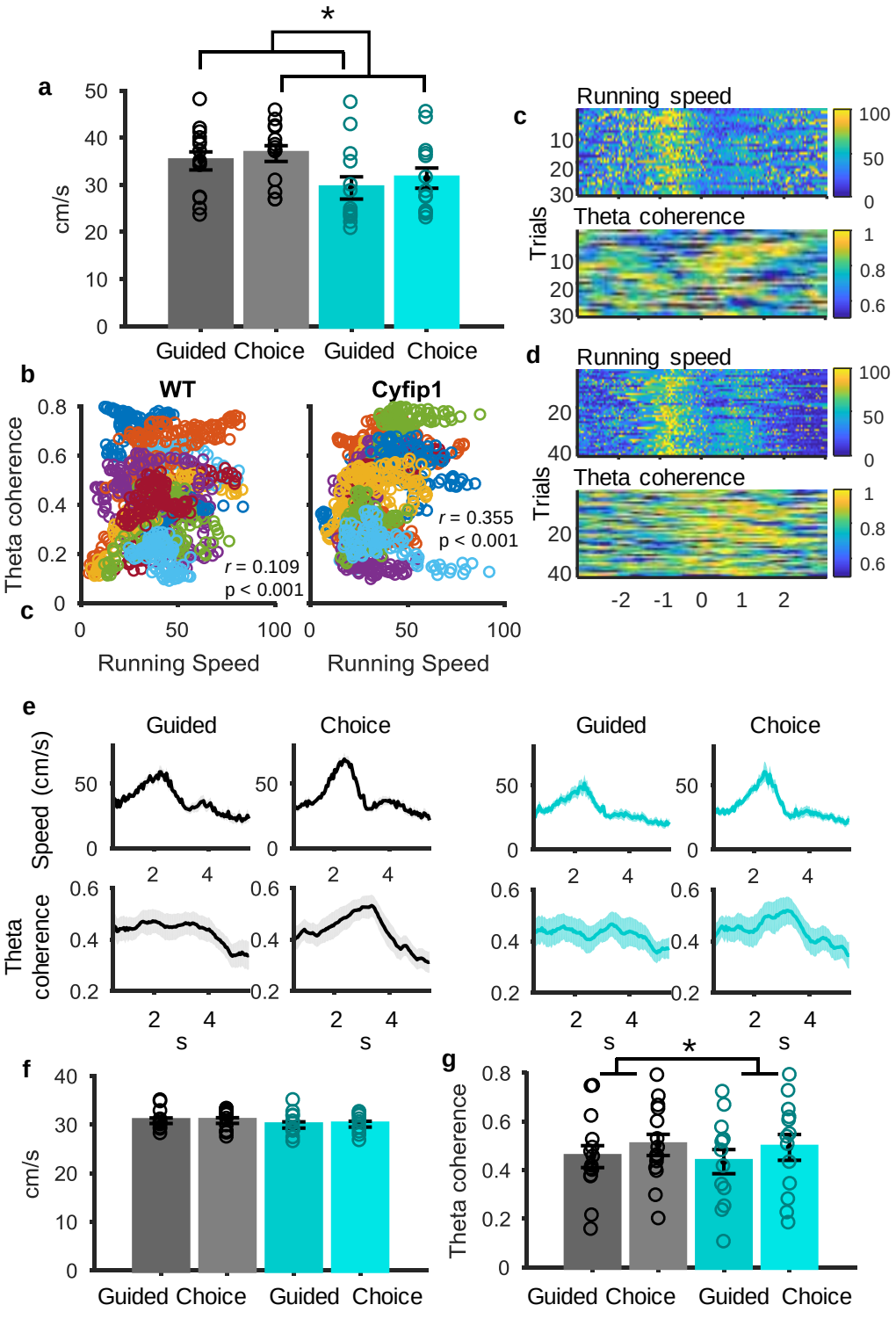

Figure 3.13 | **Running speed difference during guided and choice runs. a,** Running speed in guided and choice runs from a 6 s window centred around trigger line 5, immediately before the T-junction (WT grey, Cyfip1 cyan). *p<0.05 for main effect of run type, ANOVA. **b,** Scatter plot between average running speed over the 6 s window vs the average dCA1-PRL theta coherence in the same window, WT left, Cyfip1 right. Each

animal's trials are represented by datapoints in the same colour. **c,d,** Speed (upper) and theta coherence (lower) for all runs by one representative WT (**c**) and Cyfip1 (**d**) rat. Each row represents one run. Note the peaks in speed and coherence do not occur at the same point. **e,** Instantaneous running speed and dCA1-PRL theta coherence over the 6 s window, averaged over trials and animals. Note that the peak in running speed does not align with the peak in theta coherence in either run type or genotype **f,** A subset of runs within the 25-40 cm/s speed range were analysed, showing no difference between running speed between guided and choice runs. **g,** dCA1-PRL theta coherence in the running speed regulated subset of trials in **f.** *p<0.05 for main effect of run type, ANOVA. WT: n = 14, Cyfip1: n = 13.

To explore whether running speed might contribute to the enhanced coherence seen in choice runs, I correlated instantaneous running speed with instantaneous dCA1-PRL theta coherence for each rat. Taking all run types, there is a significant positive correlation between running speed and theta coherence (WT: $r = 0.109$, $p < 0.001$, Cyfip1: $r = 0.355$, $p < 0.001$, Pearson's correlation, Figure 3.13b). This prompted me to explore this possible caveat further. As rats approach the T-junction on the maze they often accelerate and, while this broadly coincides with the increase in theta coherence, I asked whether the peak running speed coincided with peak theta coherence. In both genotypes and across both types of run, mean instantaneous running speed peaks just before the turn, whereas mean theta coherence peaks just after the turn (Figure 3.13c,d,e). This provides some evidence that the peak in theta coherence is dissociable from increased running speed.

Furthermore, by excluding runs outside of the 25-40 cm/s speed range, thereby restricting analyses to runs where there was no significant speed difference between guided and choice runs (run type main effect: $F_{1,25} = 1.435$, $p = 0.24$, Figure 3.13f), I was able to dissociate any theta coherence differences from running speed. On this subset of trials, the main effect of guided *vs*. choice run type on dCA1-PRL theta coherence was still present ($F_{1,25} = 9.418$, $p = 0.005$, Figure 3.13g).

3.3.2.3 Theta coherence is not modulated by run type in error trials

Data from 72 error trials from 14 WT and 53 error trials from 12 *Cyfip1*$^{+/-}$ rats were analysed. Interestingly, during error trials, running speed was slower in choice runs than in guided runs, the opposite to what is seen in correct trials (run type main effect: $F_{1,24} = 9.51$, $p = 0.005$, genotype main effect: $F_{1,24} = 2.20$, $p = 0.15$, no interaction) (Figure 3.14a). This may be due to distraction during these trials,

leading to an error, or it might reflect uncertainty in the upcoming choice. Theta coherence between dCA1 and PRL was not modulated by run type in error trials (run type main effect: $F_{1,24} = 2.81$, $p = 0.107$, genotype main effect: $F_{1,24} = 0.254$, $p = 0.619$, no interaction; note: Levene's test for equality of error variance was violated in error choice trials) (Figure 3.14b,d), nor was vHPC-PRL coherence (trial type main effect: $F_{1,24} = 2.33$, $p = 0.14$, genotype main effect: $F_{1,24} = 0.57$, $p = 0.46$, no interaction) (Figure 3.14c,e). Previously, error trials have been found to correlate with reduced coherence compared to correct trials (Jones and Wilson, 2005). In contrast to these findings, my data show an increase in coherence in error choice runs compared to correct choice (trial outcome main effect: $F_{1,24} = 8.41$, $p = 0.008$, genotype main effect: $F_{1,24} = 0.19$, $p = 0.67$, no interaction) (data not shown). It is not clear why this would be the case, but considering there were significantly fewer error than correct trials per animal (WT: 17.1 ± 1.5 correct, 5 ± 0.6 error, Cyfip1: 16.6 ± 1.2 correct, 4.4 ± 0.7 error; main effect of trial outcome: $F_{1,24} = 93.4$, $p < 0.001$, no genotype effect or interaction), error trial data are inherently less reliable. Thus, while overall coherence was higher in error trials, it appears that an increase in theta coherence during choice *relative* to guided runs correlated with making a correct choice.

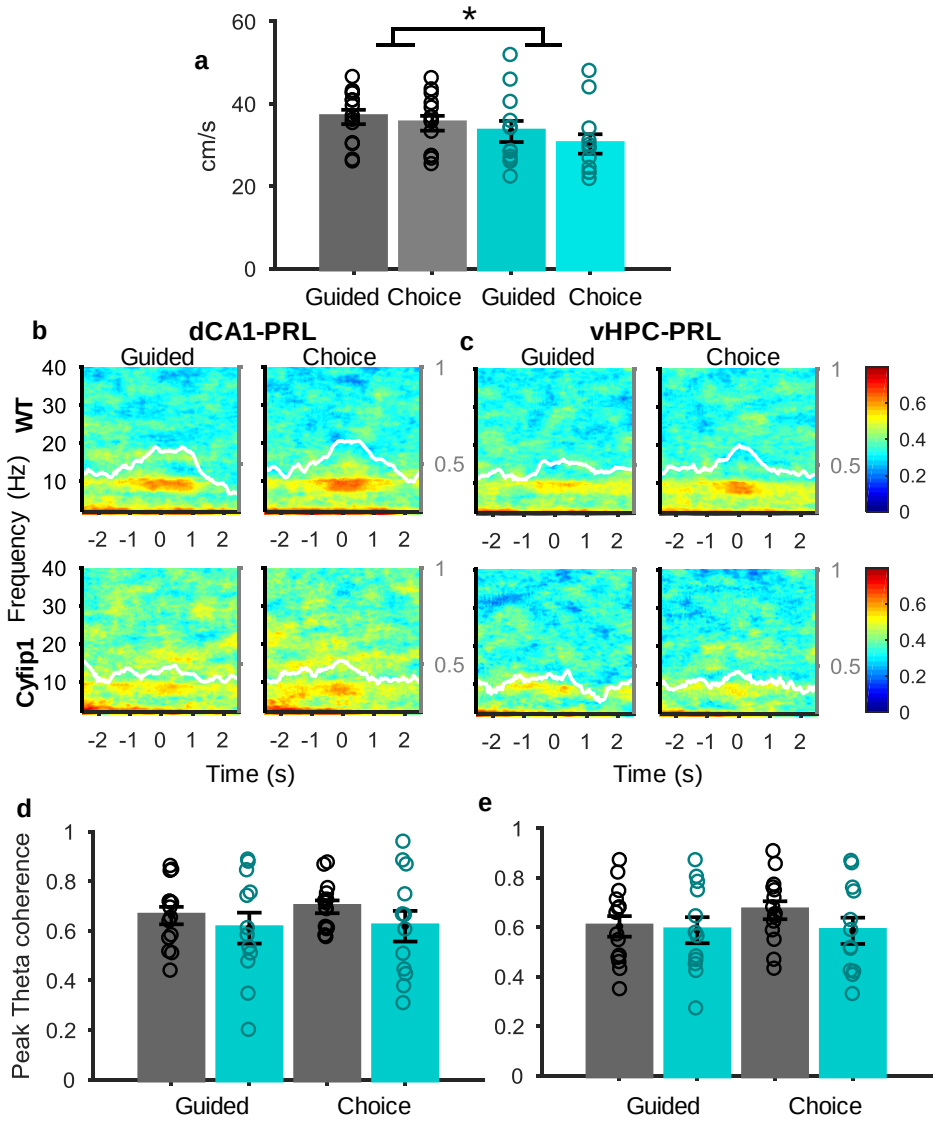

Figure 3.14 | **HPC-PRL coherence on T maze during error trials**. **a,** Running speed in the 6 s window centred on trigger line 5, split by guided and choice runs. *p<0.05 for main effect of run type, ANOVA **b,** Trial and animal averaged coherograms for dCA1 and PRL, zero-aligned to trigger line 5, WT upper row, Cyfip1 lower row. Colour represents coherence, white trace represents mean theta (6-10 Hz) coherence during this time window, with values corresponding to right hand axis (Top row WT: n = 14, Bottom row Cyfip1: n = 12). **c,** Same as **b** for vHPC and PRL. **d,e,** Mean theta coherence between dCA1 **(d)** and vHPC (**e**) and PRL. Taken from the central third of the coherograms in **a** and **b**,**,** split by guided or choice runs. WT (grey): n = 14, Cyfip1 (cyan): n = 12.

3.3.2.4 Phase-amplitude coupling between HPC-PRL normal in Cyfip1$^{+/-}$ rats

PAC was assessed in WT and *Cyfip1*$^{+/-}$ rats as a further means to interrogate the functional coupling across the HPC-PRL network (Figure 3.15). As before,

timestamps for each guided and choice runs were taken between trigger line 1 and 8, encompassing signals from the central arm to the reward point. Cross-regional hippocampal theta-prefrontal gamma coupling was assessed. There was a clear hot-spot in the theta-fast gamma range for dCA1-PRL, and log-transformed data showed it was unaffected by genotype ($F_{1,25}$ = 0.33, p = 0.57) or run type ($F_{1,25}$ = 0.003, p = 0.96), with no interaction (Figure 3.15a,b). vHPC-PRL theta-fast gamma coupling data was log-transformed and was similarly unaffected by genotype ($F_{1,23}$ = 0.018, p = 0.89) or run type ($F_{1,23}$ = 2.33, p = 0.14) (Figure 3.15c,d). Two Cyfip1 outliers did not affect this result. The striking similarity between the local PRL comodulogram and the cross-regional comodulograms raises the possibility that theta from the hippocampus is volume conducted to the PRL (Sirota et al., 2008), therefore it would be difficult to disentangle whether local PRL gamma is modulated by local theta, volume conducted hippocampal theta, or theta imposed via long-range projections. However, the fact that previous analyses of coherence, which would be expected to be impacted by volume conduction, are largely consistent with previous studies, suggests volume conduction does not play a significant role in these PAC analyses.

These findings suggest there is no effect on coupling across the HPC-PRL network, which is consistent with the lack of changes seen in overall theta coherence.

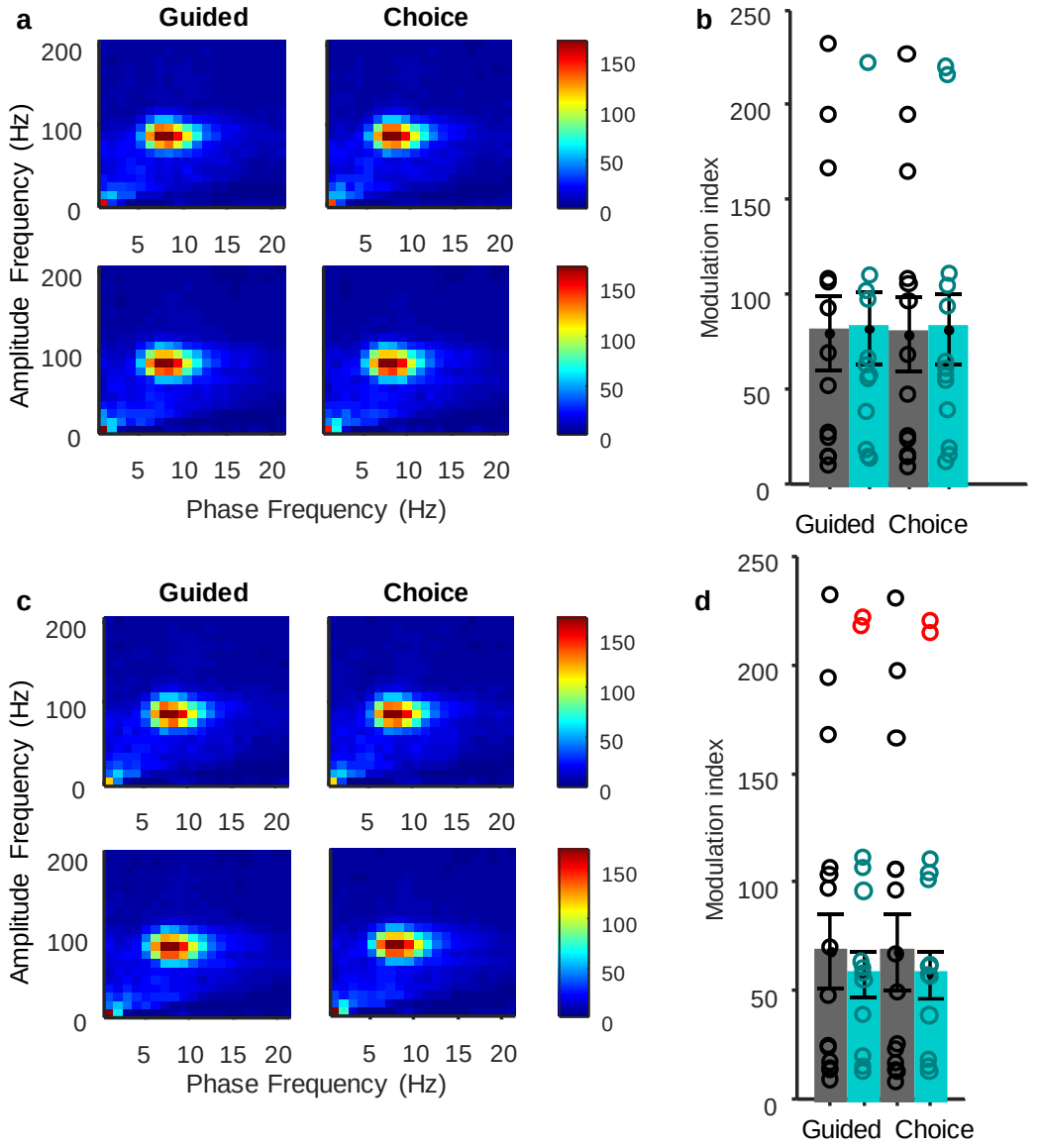

Figure 3.15 | **Theta-gamma phase-amplitude coupling across hippocampus and PRL. a,c,**Trial and animal averaged comodulogram of WT (top) and Cyfip1 (bottom) showing dCA1 (**a**) and vHPC (**c**) theta-PRL gamma coupling . Colour represents modulation index. **b,d** Theta-fast gamma coupling across dCA1-PRL (**b**) and vHPC-PRL (**d**) . Red makers were outliers that were not included in group analyses. WT in grey, Cyfip1 in cyan.

3.3.3 Delayed T maze

Introducing a delay between the guided and choice run of a T maze increases task difficulty by augmenting spatial working memory demands (Shoji et al., 2012). Therefore, to challenge the *Cyfip1*$^{+/-}$ rats I ran a pilot study with a 5 minute delay version of the task with a subset of the animals. Data are presented from one recording session per animal, from 8 WT and 5 *Cyfip1*$^{+/-}$ rats. A sixth *Cyfip1*$^{+/-}$ rat

began a delayed trial but was not able to complete 10 baseline trials in a practicable time, due to apparent anxiety on the maze.

3.3.3.1 Behaviour drops to 50% in both groups

Rats were given a baseline "reminder" training session with the no-delay task, where both groups achieved above 80% criterion (WT: 83.8 ± 1.8%, Cyfip1: 90.0 ± 4.5%). Twenty trials of the delay task session were run the following day. Strikingly, both groups had a significant drop in performance to chance levels (WT: 51.3 ± 4.0%, Cyfip1: 52.0 ± 4.4%; session main effect: $F_{1,11} = 117.64$, $p < 0.001$, main effect of genotype: $F_{1,11} = 0.727$ $p = 0.41$, interaction: $F_{1,11} = 0.716$, $p = 0.42$) (Figure 3.16a).

It appeared during the delay task session that some rats might have developed a side preference, as they often made errors in the same direction. I explored this by calculating a side preference index (Equation 1).

$$Side\ preference\ index = \frac{Right\ side\ errors - Left\ side\ errors}{Total\ errors} \qquad (1)$$

Thus, a positive side preference index means the rat would more often make an error by entering the left arm, whereas a negative side preference index indicates more errors made by entering the right arm. There was not a clear bias towards one side, so the absolute values of the side preference index were taken to ask whether a general side preference existed. A t-test for unequal variances showed a trend for *Cyfip1*$^{+/-}$ rats to be more likely to develop a side preference ($p = 0.079$), and one-sample t-tests showed both groups had side preferences, as their indexes were significantly different from zero(WT: $p = 0.001$, Cyfip1: $p = 0.022$) (Figure 3.16b). Notably, two *Cyfip1*$^{+/-}$ animals had side preference index scores of -1 and 1 respectively, meaning they chose their preferred arm on every single trial.

3.3.3.2 Normal running speed, theta frequency, and power spectra

Analysing running speed in the 6 second window around the decision point found no difference between guided and choice runs ($F_{1,11} = 0.165$, $p = 0.69$), or between

genotypes ($F_{1,11}$ = 0.321, p = 0.58) (Figure 3.16c). Dorsal CA1 peak theta frequency was not different between genotypes (p = 0.502, t-test, data not shown), which lends support to the suggestion from the no-delay task that any differences in peak theta frequency were due to changes in running speed.

As before, 6 second epochs centred around the T-junction were used to analyse oscillations in hippocampus and PRL. Mean power at theta (6-10 Hz) and gamma (30-90 Hz) frequencies was not significantly different between genotypes in dCA1 (theta: p = 0.17 [1 WT outlier did not affect result], gamma: p = 0.95,t-tests), PRL (theta: p = 0.14, gamma: p = 1.0, Mann Whitney U test, following removal of 1 *Cyfip1*$^{+/-}$ outlier), or vHPC (theta: p = 0.19, gamma: p = 0.45, t-tests).

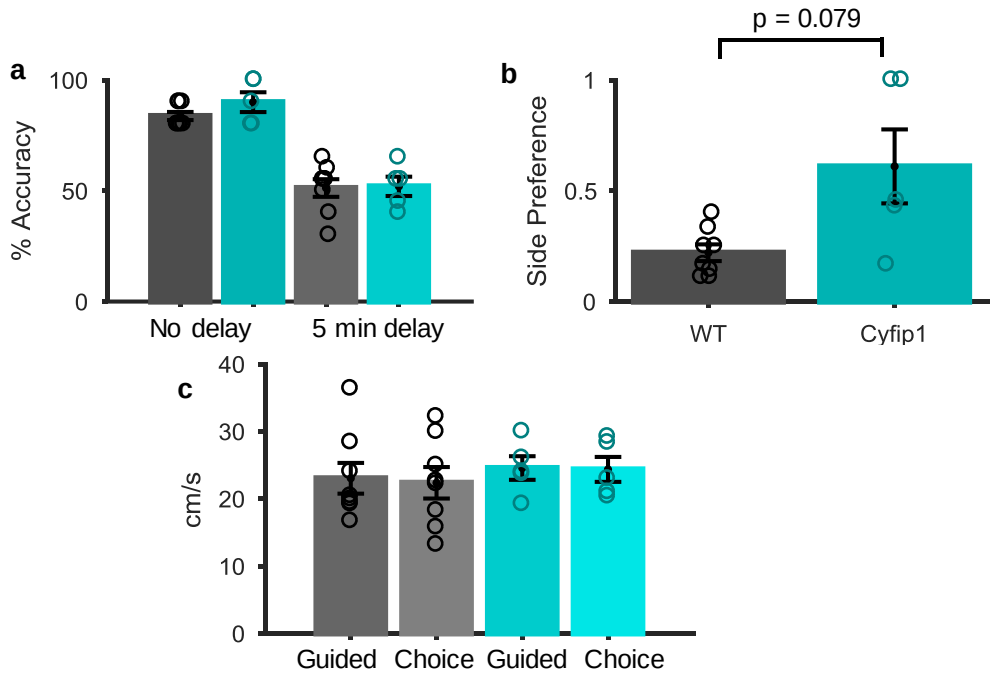

Figure 3.16 | **Behaviour on T maze with 5 minute delay. a,** Performance accuracy at the baseline session with no delay, and the session with the 5 minute delay. **b,** Side preference index, calculated as the difference between right and left errors divided by total errors. **c,** Running speed in guided and choice runs from a 6 s window centred around trigger line 5, immediately before the T-junction. WT in grey, Cyfip1 in cyan.

3.3.3.3 No modulation of theta coherence by run type in either group

As in the no delay task, theta coherence prior to the T-junction was compared between guided and choice runs in WT and *Cyfip1*$^{+/-}$ rats (theta and gamma power

were similar between genotypes, p>0.05, Figure 3.17a and b). In contrast to the no delay task, during the delay task dCA1-PRL peak theta coherence was not increased in choice relative to guided runs (WT Guided: 0.46 ± 0.54, WT Choice: 0.51 ± 0.046; *Cyfip1*$^{+/-}$ Guided: 0.66 ± 0.11, *Cyfip1*$^{+/-}$ Choice: 0.65 ± 0.12; Run type main effect: $F_{1,11} = 0.977$, p = 0.344; Genotype main effect: $F_{1,11} = 2.407$, p = 0.149), and no significant interaction ($F_{1,11} = 4.54$, p = 0.056) (Figure 3.17c,e). It should be noted that the assumption of equality of error variances was violated, as shown by Levene's test, for the choice run data (p = 0.037). While the two-way ANOVA is somewhat robust to these violations, these data should be interpreted cautiously also due to the low n numbers.

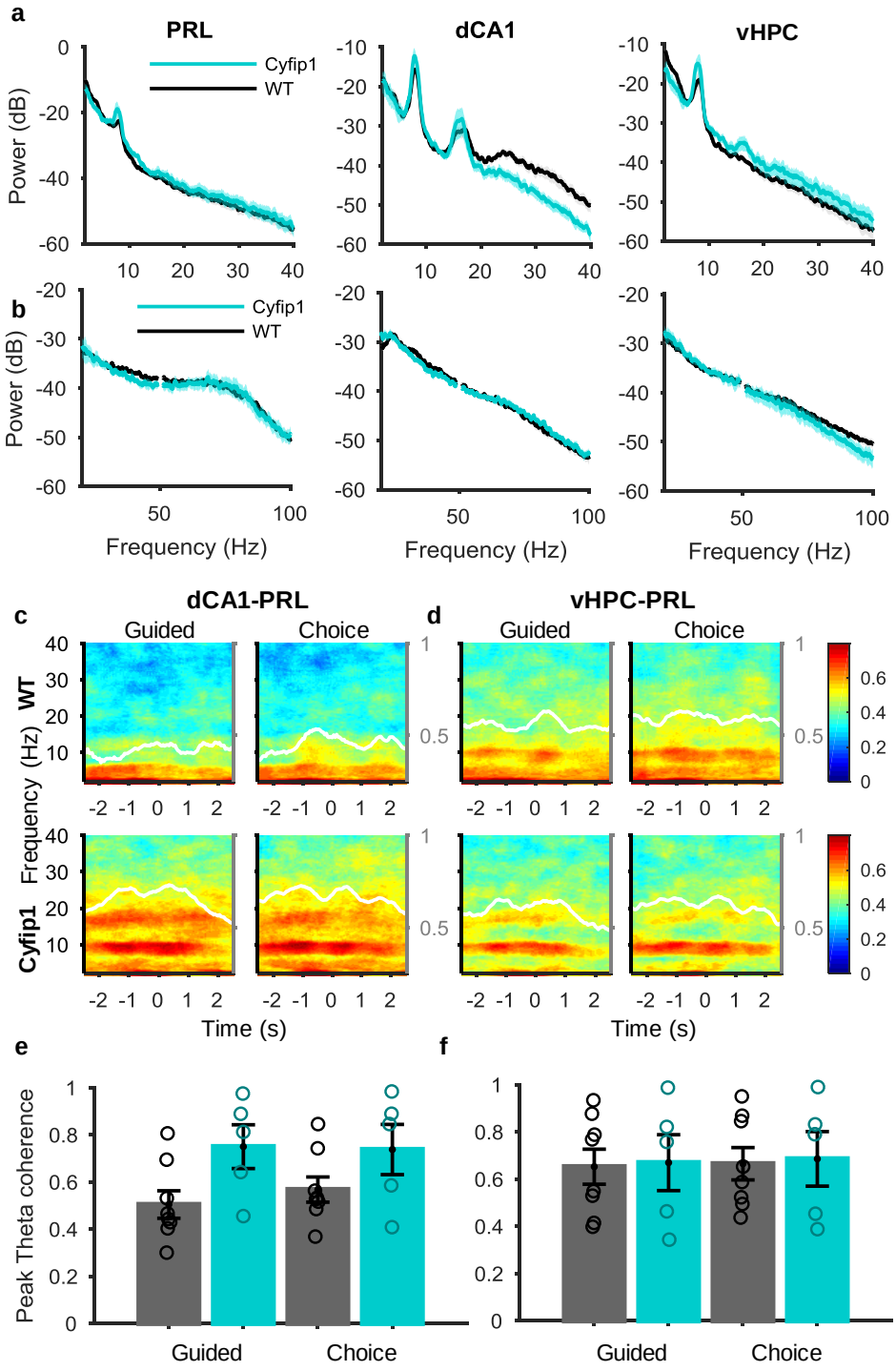

Figure 3.17 | **Power and HPC-PRL coherence on T maze with 5 minute delay. a,** Normalized power spectrums for PRL, dCA1 and vHPC in the 0-40 Hz range during the 6 s window. **b,** Normalized power spectrums for PRL, dCA1 and vHPC in the 20-100 Hz range during the 6 s window. Values between 49-51 Hz have been removed to mask 50Hz line noise. **c,** Trial and animal averaged coherograms for dCA1 and PRL, zero-aligned to trigger line 5, WT upper row, Cyfip1 lower row. Colour represents coherence, white trace represents mean theta (6-10 Hz) coherence during this time window, with values corresponding to right hand axis (Top row WT: n = 8, Bottom row Cyfip1: n = 5). **d,** Same

as **c** for vHPC and PRL. **e,f,** Mean theta coherence between dCA1 **(e)** and vHPC (**f**) and PRL. WT in grey, Cyfip1 in cyan.

Similarly, vHPC-PRL theta coherence was also not modulated by run type (WT Guided: 0.57 ± 0.08, WT Choice: 0.59 ± 0.077; *Cyfip1*$^{+/-}$ Guided: 0.60 ± 0.13, *Cyfip1*$^{+/-}$ Choice: 0.61 ± 0.13; Run type main effect: $F_{1,11}$ = 1.69, p = 0.221; Genotype main effect: $F_{1,11}$ = 0.027, p = 0.873; Interaction: $F_{1,11}$ = 0.204, p = 0.66) (Figure 3.17d,f).

Thus, introducing a 5 minute delay lead to the performance of both groups to drop to chance levels, with several rats developing strong side preferences, perhaps indicating they were no longer engaged in the task. Accordingly, theta coherence was no longer modulated by run type.

3.4 Discussion

Results from this chapter show:

- *Cyfip1*$^{+/-}$ rats have normal initial performance in a discrete-trial alternation T maze task but take longer to achieve criterion performance when tested over multiple days.
- Running speed on the maze is slower in *Cyfip1*$^{+/-}$ rats, particularly on the central arm; this is likely to contribute to the slower theta rhythm seen in dCA1 during this phase of the task.
- Theta-gamma phase-amplitude coupling within dCA1 is reduced in *Cyfip1*$^{+/-}$ rats.
- Run-type dependence of hippocampal-prefrontal theta coherence is normal in *Cyfip1*$^{+/-}$ rats, with increased theta coherence on choice runs relative to guided runs.
- *Cyfip1*$^{+/-}$ rats showed normal inter-regional phase-amplitude coupling between HPC-PRL.
- In a 5 minute delay version of the task, performance of both genotypes dropped to chance levels, and theta coherence was no longer modulated by run type.

3.4.1 Behaviour

Both genotypes performed at a high accuracy level in the very first session of the discrete-trial alternation task. This indicates their natural tendency to alternate, and others have seen similar initial performance (Bannerman et al., 2002). The finding that *Cyfip1*$^{+/-}$ rats took more sessions to achieve criterion is therefore difficult to interpret as a learning deficit. Rather, it appears that *Cyfip1*$^{+/-}$ rats could not consistently maintain high accuracy levels, which might point towards an attentional or motivational deficit. Nevertheless, the fact that both genotypes performed at comparable accuracy levels on the initial session and on the subsequent recording day shows that *Cyfip1*$^{+/-}$ rats are able to encode and enact the contingencies of the discrete-trial alternation task. This is consistent with the finding that *Cyfip1*$^{+/-}$ mice were unimpaired in a Y maze task for spatial working memory (Bozdagi et al., 2012), although the discrete-trial alternation variant of the T maze task has not previously been run in any *Cyfip1* models.

Studies investigating the impact of the 22q11.2 deletion, also linked to cognitive deficits, ran a similar discrete-trial alternation task in mice (Mukai et al., 2015; Sigurdsson et al., 2010; Stark et al., 2008), enabling comparison with *Cyfip1*$^{+/-}$ rats in the context of highly penetrant genetic variants. Mice with the broader Df(16)A$^{+/-}$ mutation and mice with deletion of one of the key genes in this deletion, *Zdhhc8*$^{+/-}$ (Mukai et al., 2015) took longer to reach criterion (Stark et al., 2008), though this phenotype did not reach significance in (Sigurdsson et al., 2010). These findings were interpreted as a learning deficit, although neither study showed data relating to differences in the initial session of the maze, which would allow direct comparison with the *Cyfip1*$^{+/-}$ findings.

While it is difficult to directly relate the underlying psychology of the T maze to human cognitive tasks, it is interesting to note a parallel finding in healthy carriers of the 15q11.2(BP1-BP2) deletion. They performed normally in a spatial working memory test from the CANTAB cognitive test battery, where subjects must use process of elimination to uncover a hidden token beneath 6 coloured squares. The measure used in this study, the number of times the subject revisits a box where a

token has previously been found, has been associated with spatial memory systems not unlike the T maze, where the location is remembered through a delay and interferences. This is thought to be analogous to spatial working memory in rats (Feigenbaum et al., 1996). However, these carriers were found to have cognitive deficits, including reduced IQ, dyslexia and dyscalculia (Stefansson et al., 2014), and it is tempting to speculate whether the deficit in acquisition of the T maze task might be related to these deficits seen in humans.

One limitation to this study, which limits full understanding of the psychology underlying T maze acquisition, is the lack of information on any differences in motivation levels in *Cyfip1*$^{+/-}$ rats, particularly following the finding that *Cyfip1*$^{+/-}$ ran slower on average. It would be useful to ensure the groups are matched for the incentive value of the sucrose reward. This could be done by a simple sucrose preference test to see whether *Cyfip1*$^{+/-}$ rats may be differentially motivated to obtain reward. However, considering number of trials run per session was not different between animals, it is unlikely there is a significant impairment in this domain.

3.4.2 Dorsal CA1 phase-amplitude coupling abnormal

Cyfip1$^{+/-}$ rats show diminished theta-gamma PAC within dCA1, while maintaining normal coupling within vHPC, PRL and across regions. Disruptions to local theta-gamma coupling have been observed in other animal models of cognitive dysfunction, including Alzheimer's models (Booth et al., 2016; Zhang et al., 2016) a chronic ketamine pharmacological schizophrenia model (Michaels et al., 2018), following acute ketamine (Caixeta et al., 2013), as well as in cortex of schizophrenia patients (Barr et al., 2017; Hunt et al., 2017; Won et al., 2018), suggesting a role in cognitive deficits. The mechanism by which *Cyfip1* haploinsufficiency might lead to disrupted theta-gamma coupling only in the hippocampus is unclear. Interneurons underlie the generation of gamma, and to some extent theta oscillations (Pastoll et al., 2013; Whittington and Traub, 2003), and recent evidence suggests synaptic inhibition onto parvalbumin-positive basket cells is necessary for theta-gamma coupling (Wulff et al., 2009b). While *Cyfip1*$^{+/-}$ is expressed in

interneurons, it is to a much lesser extent than in glutamatergic neurons. Thus, how *Cyfip1* can impact this coupling despite not altering the intrinsic properties of the individual oscillations is unclear. However, it is of interest that a recent study in Fmr1 KO mice found a dysregulation of dCA1 theta-gamma PAC during a place avoidance paradigm (Radwan et al., 2016), which promotes a hypothesis that the disruption to PAC seen in *Cyfip1*$^{+/-}$ is mediated via the Cyfip1-Fmrp pathway.

It is interesting to note that the reduction in phase-amplitude coupling preferentially impacts the slow gamma frequency. While CA1 fast gamma originates from the medial entorhinal cortex, CA1 slow gamma originates from and is highly synchronous with CA3 (Colgin et al., 2009). CA3 is crucial for memory retention and retrieval (Steffenach et al., 2002; Sutherland et al., 1983), so it has been proposed gamma oscillations provide a means to transmit information to the CA1. In fact, CA1-CA3 gamma coherence has been shown to increase on the approach to the T-junction in a T maze task, suggesting a role for this oscillational synchrony in memory retrieval (Montgomery and Buzsáki, 2007; Schomburg and Fernández-Ruiz, 2014). The disruption of theta-slow gamma coupling in CA1 might reflect a disruption of signalling between CA3 and CA1 in *Cyfip1*$^{+/-}$ rats. Hence, simultaneous recording from CA3 and CA1 pyramidal and inhibitory neurons might reveal disrupted signalling, although any possible deficit does not manifest as a performance deficit in the current task.

Furthermore, I did not see a memory retrieval associated increase in theta-gamma coupling within hippocampus, as coupling was similar between guided and choice runs, perhaps suggesting this task did not necessitate an increase in coupling. However, there is some evidence linking learning with hippocampal phase-amplitude coupling, which could help explain the longer days to criterion seen in *Cyfip1*$^{+/-}$ rats (Nishida et al., 2014). Nishida et al. (2014) saw the strength of intrahippocampal theta-gamma coupling increase during learning of an operant spatial alternation task. It would be interesting to explore the development of theta-gamma coupling in *Cyfip1*$^{+/-}$ rats during acquisition of the task to ask if these neural and behavioural deficits are linked.

3.4.3 Impact of Cyfip1 haploinsufficiency on hippocampal-prefrontal theta coherence

Findings from the Df(16)A$^{+/-}$ and *Zdhhc8*$^{+/-}$ mouse models, which impact the Rac1 pathway which is also involved in Cyfip1 signalling, showed a significant reduction in hippocampal-prefrontal theta coherence. This led to the hypothesis that this network may be compromised in *Cyfip1*$^{+/-}$ rats. In particular, a causal link between impaired axonal growth and reduced functional connectivity has been demonstrated in this network (Mukai et al., 2015; Tamura et al., 2016).

However, it appears that functional connectivity between hippocampus and PRL cortex is largely normal in *Cyfip1*$^{+/-}$ rats. Both dCA1 and vHPC coherence with PRL was modulated by run type in both genotypes, as was originally found on other versions of the T maze (Jones and Wilson, 2005). This is, however, the first time it is shown using this variation of the T maze task. This might support this task being reliant on spatial memory and dependent on this network rather than a striatally learned motor pattern, as has been suggested for continuous alternation tasks using the return-arm T maze (Ainge et al., 2007a; Moussa et al., 2011). In contrast, error trials did not see theta coherence modulation by run type, which is again consistent with previous findings (Jones and Wilson, 2005).

While hippocampal-PRL coherence was normal at the stage when *Cyfip1*$^{+/-}$ rats had successfully acquired the task, there is a possibility that deficits would have been evident during the impaired acquisition of the task. The studies with *Df(16)A*$^{+/-}$ and *Zdhhc8*$^{+/-}$ mice both recorded network activity during the acquisition of the task, and Sigurdsson et al. (2010) found theta coherence to increase during the course of acquisition. In these studies, final theta coherence levels at criterion performance were still impaired, but it could be hypothesised that theta coherence in the *Cyfip1*$^{+/-}$ rat starts off slightly impaired, but the improvement over time, in parallel with learning, raises the level of functional connectivity into the normal range. To test this hypothesis, recordings would need to be made during the acquisition stage of the task.

A baseline measure of theta coherence was found to predict the subsequent learning rate in the discrete-trial alternation T maze task (Mukai et al., 2015; Sigurdsson et al., 2010). Here I found that post-acquisition theta coherence did not correlate with days to criterion, suggesting even if there had been a deficit, by the time rats achieved criterion performance theta coherence was normal.

This study is complicated by the variation in behaviour seen between animals at the decision point. The high theta coherence at the T-junction may reflect different processes for a rat that is turning straight into the reward arm, versus a rat displaying vicarious trial and error (VTE) behaviour at the choice point, turning their heads to look in both directions before making its choice (Redish, 2016), a behaviour that was anecdotally seen in both genotypes. The former suggests that at the point of peak theta coherence, the animals are already in the process of turning into a chosen arm, and that the decision had already been made. Conversely, the latter suggests coherence peaks during decision making. In fact, analysing coherence on single trajectories, (Benchenane et al., 2010) show that the animal is already veering towards the chosen arm as the coherence is greatest, which complicates previous interpretations of the role of theta coherence. Finally, strong coherence has been found during rearing behaviour (Young and McNaughton, 2009), and animals often displayed rearing behaviour at several points in the maze , including occasionally at the T-junction. A fine-scale coherence-by-behaviour analysis would shed light on the role of theta coherence in *Cyfip1*$^{+/-}$ rats compared to WTs, and would benefit from higher-resolution video data around the choice point, potentially alongside head-mounted accelerometer data.

3.4.4 Delay T maze

I decided to introduce a 5 minute delay between guided and choice trials to see if *Cyfip1*$^{+/-}$ rats showed a delay-dependent behavioural or network deficit. Delays of 30-90 seconds are typically used (Aggleton et al., 1997; Aultman and Moghaddam, 2001; Clinton et al., 2006), although WT rats have been shown to maintain above-chance performance at delays of 5 minutes (Dudchenko, 2001) and 10 minutes (Bannerman et al., 2002). As there was no indication of a performance deficit in the

no-delay version, which in reality had an average delay of 15-20 s, the delay was set at 5 minutes, to ensure a step-change in task difficulty that might be able to capture any behavioural deficit in *Cyfip1*$^{+/-}$ rats without a ceiling effect.

The finding that behaviour dropped to 50% in both groups may be a result of a flaw in the experimental design. Rats were run one by one, to avoid having to repeatedly connect/disconnect animals from the electrophysiology recording system. As such, the intertrial interval was only as long as it took to set up the next trial, i.e. ~1 minute. With a 5 minute inter-run delay, it is now clear that this could cause significant proactive interference. Proactive interference occurs when prior information learned in a similar context inhibits the full potential to retain new memories (Jonides and Nee, 2006; Keppel and Underwood, 1962). The relationship between inter-trial interval and inter-run delay has been shown to influence levels of proactive interference (Brito et al., 1987). In this case, when a rat is running the choice run, it needs to remember which arm it entered 5 minutes ago on the guided run, but ignore information about which arm it entered ~6 minutes ago on the last choice run, leading to high levels of proactive interference. This may be why these behavioural results conflict with other studies that have shown WT rats to perform this task with even longer delays (Bannerman et al., 2002), where inter-trial intervals were on the scale of ~2 hours (personal correspondence). The fact that some animals developed strong side preferences may also indicate that the animal had abandoned a working memory-based approach to the task. This was supported by the lack of run type-modulated theta coherence, suggesting that this network was no longer being engaged in the choice runs as before.

A further limitation of this study is the fact that there is no single unit data to corroborate the LFP coherence findings. Volume conduction artefacts can appear as strong coherence between brain regions, and a common way to confirm that coherence is not merely due to volume conduction is to show correlation between LFP and single-unit spikes (Buzsáki et al., 2012; Sirota et al., 2008). However, following a negative finding based on LFP coherence, it would be unlikely to then see an effect from single unit data.

3.4.5 Conclusions and future directions

In this chapter I explored the hypothesis that the hippocampal-prefrontal network, and therefore spatial working memory is disrupted in *Cyfip1*$^{+/-}$ rats. The findings show that this is not the case, with interactions in this network remaining intact during a working memory task that *Cyfip1*$^{+/-}$ rats can perform at normal accuracy levels. This is reminiscent of the finding that control 15q11.2 carriers perform normally in a spatial memory task (Stefansson et al., 2014). Challenging the network and the behaviour by introducing a delay did not reveal a delay dependent deficit; however, the experimental protocol of the delay-task may have created floor effects where neither genotype could solve the task. Therefore, future studies could look to run a delay task with longer inter-trial intervals, or attempting to increase difficulty in other ways. For example, Hölscher et al. (2004) did not see a working memory impairment in mGluR knockout mice on a T maze, but increasing working memory demands on a radial arm maze (Olton and Werz, 1978) revealed a significant deficit.

The reduced theta-slow gamma phase-amplitude coupling seen in *Cyfip1*$^{+/-}$ dCA1 leads to the hypothesis that CA3 to CA1 gamma coupling might be disrupted. Future electrophysiological studies could investigate this network by recording place cell and LFP data from CA3 and CA1 simultaneously. Any deficit in this network might manifest as a behavioural deficit on a more demanding hippocampal-dependent task.

4

Chapter 4 Nucleus accumbens interactions with hippocampus and prefrontal cortex during reward approach

In this chapter I explore neural oscillations surrounding the reward point on the T maze, focussing on the NAc and its hippocampal and cortical inputs. Gamma coherence between ventral hippocampus and NAc shell is significantly reduced and shows a diminished response to reward point arrival in *Cyfip1*$^{+/-}$ rats, while IL cortex-NAc shell beta coherence is increased.

4.1 Introduction

4.1.1 Nucleus accumbens networks

The primary goal of recording *in vivo* electrophysiology on the T maze was to invoke hippocampal-prefrontal interactions during spatial working memory. However, the presence of spatially distinct reward locations also presented an opportunity to analyse reward-related network oscillations. Unique patterns of gamma oscillations surrounding rewards on mazes have been recorded from the NAc (Berke, 2009; Kalenscher et al., 2010; van der Meer and Redish, 2009a), prompting me to investigate NAc and brain regions connected to it during reward approach on the T maze.

Early work led to a view of the NAc as a reward centre, but it appears the role of this region, described as a 'limbic-motor interface' (Mogenson et al., 1980) or 'switchboard' (Gruber et al., 2009), extends to mediating more general goal-directed behaviour, whether that is to obtain reward, avoid aversive outcomes or explore novel stimuli (Floresco, 2015). Evidence has accumulated implicating the NAc in motivation and invigoration of behaviours (Berridge and Robinson, 1998; McBride et al., 1999; Robbins and Everitt, 1996; Setlow et al., 2003), drug addiction (Bardo, 1998; Cooper et al., 2017; Robinson and Berridge, 1993), learning and memory and decision-making (Acheson et al., 2006; Cardinal et al., 2001; Pennartz et al., 2009).

It appears that the NAc is particularly important when behavioural flexibility or action selection in the context of uncertainty is required (Floresco et al., 2009). Interactions between NAc and cortex are critical for behavioural flexibility, and rule-reversal tasks have revealed unique roles for the NAc Core and Shell in enabling learning of a new strategy and suppression of behaviour that interferes with goal seeking, respectively (Floresco, 2015; Floresco et al., 2006). The discrete-trial alternation T maze task is relatively simple, not explicitly designed to require behavioural flexibility or rule-switching, and is likely not heavily dependent upon NAc (Schacter et al., 1989). Thus, in this context, I would not necessarily expect any deficiencies in NAc activity to manifest as frank behavioural deficits. Nevertheless, the NAc shows characteristic activity patterns at food reward points, and any abnormalities observed here in the *Cyfip1*$^{+/-}$ rats could indicate altered NAc function which could be explored in more targeted behavioural tests. I first introduce the connectivity of the NAc with cortical and hippocampal regions. Next, I discuss relevant functional interactions between these regions and finally, I will outline evidence linking aberrant NAc activity to disorders associated with 15q11.2 deletion as a rationale for investigating this region in the *Cyfip1*$^{+/-}$ rat.

4.1.1.1 Connectivity of nucleus accumbens and its network

The NAc is located in the most ventral part of the striatum, which represents the main input nucleus of the basal ganglia (Sesack and Grace, 2010). In both rodents

and humans, the NAc is subdivided into a more medial 'Shell' and more lateral 'Core' region, where the Shell lies medial and ventral to the Core (Baliki et al., 2013; Voorn et al., 2004; Zahm and Brog, 1992) (Figure 4.1). These subregions are thought to mediate distinct behavioural functions due to their distinct anatomical connectivity to frontal and temporal regions, as well as a broad literature of lesion and pharmacology studies (Brog et al., 1993; Groenewegen et al., 1987; Pennartz et al., 1994).

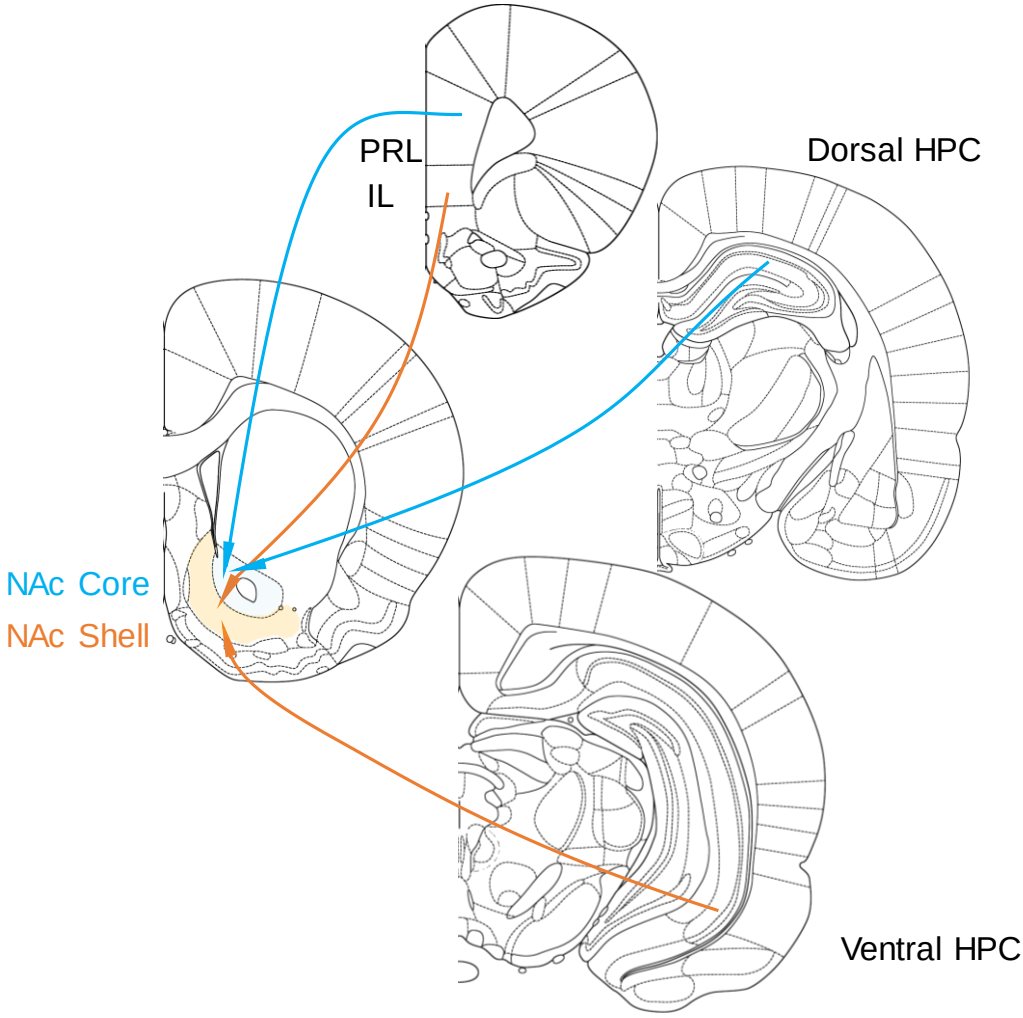

Figure 4.1 | **Inputs to the NAc investigated in this chapter.** The NAc receives projections from PRL, IL, dorsal and ventral hippocampus (shown on figure), basolateral amygdala and ventral tegmental area, with a high degree of convergence onto the same cells within the NAc (Britt et al., 2012; Floresco et al., 2001a; French and Totterdell, 2003; Groenewegen et al., 1999; O'Donnell and Grace, 1995). Hippocampal inputs are topographically arranged, with vHPC projecting mainly to NAc Shell, and dCA1 and parahippocampal regions projecting to NAc Core (Voorn et al., 2004).

Cortical-striatal connections are organised in topographic parallel loops (Alexander and Crutcher, 1990; Berendse et al., 1992; Groenewegen et al., 1993), where cortical projections begin the loop by targeting a region of the striatum and, via projections to midbrain and thalamus, projections arrive back to cortex in a similar area to their origin. The mPFC is divided into the prelimbic and the more ventral infralimbic cortices (Heidbreder and Groenewegen, 2003). These regions show distinct anatomical projections to limbic regions (Heidbreder and Groenewegen, 2003; Moorman et al., 2015; Vertes, 2004), with afferents from the prelimbic cortex and infralimbic cortex broadly projecting to NAc Core and Shell respectively (Brog et al., 1993; Mailly et al., 2013; Voorn et al., 2004). A broad functional dichotomy is also apparent, with prelimbic promoting the execution of behaviours and infralimbic involved in response inhibition, demonstrated most prominently in the fields of drug addiction and fear behaviour (reviewed in Peters et al. (2009)).

Projections from the VTA transmit dopaminergic prediction error signals in the form of phasic dopamine bursts (Schultz et al., 1997) and tonic dopamine which can modulate the impact of excitatory signals from other regions, gating and integrating inputs to the NAc, and thus affecting the promotion of different behaviours (Floresco, 2007; Pennartz et al., 1994).

NAc output is predominantly through GABAergic medium spiny neurons, which make up 95% of the neuronal cell population, along with a few interneuron subtypes (Voorn et al., 2004) which project to motor output regions, including the substantia nigra and ventral pallidum (Maurin et al., 1999; Zahm, 2000).

Medium spiny neurons in the striatum show typical periodic shifts in resting membrane potential from DOWN states to more depolarized UP states, which are not intrinsic but depend on excitatory synaptic inputs (O'Donnell and Grace, 1995; Wilson, 1993). Hippocampal inputs are key to driving these states, showing synchronous shifts in ventral hippocampal LFP and NAc membrane potentials (Goto and O'Donnell, 2001). Early results suggested the hippocampus is therefore able to gate the information flow from other inputs, such as the mPFC (O'Donnell

and Grace, 1995), but there is a complex interaction between hippocampal and mPFC inputs to the NAc, which depends on the timing of the inputs and modulation by dopamine (reviewed in Sesack & Grace (2010)).

4.1.1.2 Reward-related functions of nucleus accumbens

The NAc is thought to harness reward and context related information it receives from hippocampus and midbrain to guide goal-directed behaviour, through the NAc and mesolimbic dopamine pathway's role in associative learning about reward-predicting stimuli (Pennartz et al., 2011).

NAc neurons fire in response to reward consumption (Apicella et al., 1991), reward-predicting stimuli (Apicella et al., 1991; Roitman et al., 2005; Schultz et al., 1992; Setlow et al., 2003) and reward expectation, whereby NAc cells have been identified that ramp up their activity in an anticipatory manner during the approach to reward, with a sharp increase in firing rate coinciding with arrival at the reward point (Carelli and Deadwyler, 1994; Lavoie and Mizumori, 1994; van der Meer and Redish, 2009b, 2011; Miyazaki et al., 1998).

Simultaneous single unit and voltammetry recordings showed phasic dopamine transients occurred in regions where reward-related NAc cells fired (Owesson-White et al., 2009), supporting the suggested role of dopamine in modulating neuronal ensembles in the NAc (Nicola et al., 2000; Pennartz et al., 1994). Dopamine in the striatum is thought to strengthen salient inputs and inhibit weaker inputs, resulting in input selection that "could assist in preparing the animal to deal with the unexpected by promoting the switching of attentional and behavioural resources toward biologically significant stimuli", as proposed by Redgrave et al. (1999) (reviewed in Nicola et al. (2000); Bamford et al. (2018)).

At the behavioural level, the exact contribution of NAc dopamine signalling to reward-processing is unclear. Dopamine signals have been proposed to encode a reward prediction error that is necessary for learning associations between stimulus and reward (Bayer and Glimcher, 2005; Schultz et al., 1997). Other arguments

suggest that dopamine is not necessary for learning, rather to assign incentive salience to reward cues (Berridge, 2007; Redgrave et al., 1999; Saunders and Robinson, 2012). Either way, a general role of NAc in modulating approach behaviour to reward-associated stimuli is well supported by lesion studies and blocking of dopamine receptors (Blaiss and Janak, 2009; Everitt et al., 1991; Nicola, 2010; Parkinson et al., 2000; Saunders and Robinson, 2012). NAc lesions also abolish Pavlovian-to-instrumental transfer, whereby a previously Pavlovian conditioned stimulus associated with reward can invigorate operant lever pressing which has separately been associated with a reward (Corbit and Balleine, 2011; Keistler et al., 2015).

4.1.1.1 Reward-associated gamma oscillations

Prominent gamma oscillations in the human and rat ventral striatum have been associated with reward-processing. In humans, ventral striatal gamma was linked to a task where subjects had to process information regarding monetary gains and losses (Cohen et al., 2009b). In rats, gamma oscillations in the NAc and prefrontal cortex have been shown to be modulated by the presence or absence of reward, approach to reward sites and consumption of reward (Berke, 2009; Donnelly et al., 2014; Kalenscher et al., 2010; van der Meer and Redish, 2009a). The first three of these studies investigated gamma oscillations in relatively similar behavioural contexts, with freely moving rats running on a triangular track, a multiple T maze and a four-arm radial maze respectively; Donnelly et al. (2014) recorded reward-related gamma oscillations in NAc Shell and Core and prelimbic and infralimbic cortex during a lever-pressing task.

In the maze tasks, distinct activity of NAc gamma in the 50 Hz (gamma-50) and ~70-100 Hz (gamma-80) frequency bands was observed. van der Meer & Redish (2009b) found that gamma-50 showed a sharp spike in power at reward points, while gamma-80 ramped up gradually on approach to a reward site. Gamma-50 was sensitive to the absence of reward, showing no spike in power upon arrival at an empty reward site. In contrast, the gamma-80 ramping occurred regardless of whether a reward was received or not, suggesting it may be related to reward

anticipation. However, gamma-80 following reward site arrival did discriminate between rewarded and unrewarded trials. Reward consumption was followed by a sudden drop in gamma-80, which was absent without a reward.

The ramping of gamma power mirrors the ramping activity patterns seen in individual NAc neurons (Carelli and Deadwyler, 1994; Lavoie and Mizumori, 1994; van der Meer and Redish, 2009b, 2011; Miyazaki et al., 1998). Somewhat similar findings were observed by Berke (2009), with an increase of gamma-80 at reward sites, although without the preceding ramp, while gamma-50 decreased sharply following reward receipt. The findings of Kalenscher et al. (2010) broadly agreed with these results, with gamma-80 increased before reward delivery, and gamma-50 higher on rewarded *vs* unrewarded trials. Importantly, the three reward delivery sites on the triangular maze contained different rewards, and gamma power was differentially modulated between sites, despite identical behaviour (approach, stop, consumption), which supports the relevance of gamma oscillations to reward-seeking behaviour rather than movement or consumption (Kalenscher et al., 2010).

Findings in the operant box task also showed distinct reward and error-related gamma activity in NAc, infralimbic and prelimbic areas, with a sharp decrease and increase and decrease in ~60 Hz gamma power immediately after reward on correct trials, and a sustained increase following error trials (Donnelly et al., 2014). This gamma response reflects elements of the gamma-50 and gamma-80 response seen in earlier reports, but does not map clearly onto either, likely due to significant differences in the task, recording technique and rat strain.

The majority of fast-spiking interneurons (50-90%) and a smaller subset of medium spiny neurons (3%) in the NAc were phase-locked to the gamma oscillation (Kalenscher et al., 2010; van der Meer and Redish, 2009a). Distinct subpopulations of interneurons were identified that phase-locked to and were differentially modulated by gamma-50 and gamma-80 and it was further shown that unit firing was more likely to be entrained to gamma if their individual signals were reward related (Kalenscher et al., 2010). This suggests that at least a component of NAc

gamma is locally generated or a result of direct input from afferent areas that also show gamma oscillations, such as hippocampus, prefrontal cortex and amygdala (van der Meer et al., 2010), although a recent report suggest gamma might also originate from nearby piriform cortex (Berke, 2009; Carmichael et al., 2017).

Further behavioural correlates of gamma have been identified beyond reward related activity. Learning of the multiple T maze task showed differential changes in NAc gamma-50 and gamma-80, with gamma-80 associated with decision points on the maze early during learning (van der Meer and Redish, 2009a). As decision points coincide with forward sweeps of hippocampal place cells, as well as firing of NAc reward-related neurons (van der Meer and Redish, 2009b), this event has been suggested to be part of trajectory planning. Gamma-50 also showed a transient increase prior to movement initiation (van der Meer and Redish, 2009a). Distinct gamma bands in NAc have also been observed in a different paradigm, where gamma-60 was associated with an aversive location and gamma-80 with a preferred, safe location (Dejean et al., 2017).

4.1.1.2 Nucleus accumbens and the hippocampus

The interaction between hippocampus and NAc is thought to be critical for establishing place-reward associations, allowing a foraging rat to remember where rewarding stimuli were found. This is supported by, among others, a lesion study which found that disconnecting hippocampus and NAc Shell impaired learning of a conditioned place preference task (Ito et al., 2008).

Dopamine has an important role in modulating the hippocampus-NAc interaction (Floresco and Phillips, 1999). This hippocampal influence on dopamine signalling has been suggested to lead to the hyperdopaminergic striatal state seen in schizophrenia. Stimulating ventral hippocampus increases NAc activity, which, via GABAergic projections to the ventral pallidum, disinhibits the VTA, which projects back to the NAc and produces robust increases in dopamine (Blaha et al., 1997; Floresco et al., 2001b; Legault and Wise, 1999; Lodge and Grace, 2006, 2011). It

is thought that in schizophrenia, this process begins with aberrant regulation of ventral hippocampus activity by PV interneurons (reviewed in (Grace, 2016)).

This relationship between ventral hippocampus and NAc was recently explored in humans during reward anticipation (Bossong et al., 2018). They used proton magnetic resonance spectroscopy to monitor ventral hippocampus glutamate levels and fMRI to assess NAc activation and functional coupling between the two regions. They found that during reward anticipation, higher levels of glutamate correlated with 1) a greater NAc response to rewarding cues, 2) decreased functional coupling between ventral hippocampus and NAc. This might suggest that an overactive ventral hippocampus leads to reduced control of NAc activity during reward anticipation.

Neural activity in the rat NAc during approach to reward in a spatial task has been investigated by van der Meer et al. in a series of studies where animals were trained to run in a multiple-T maze with 4 choice points (van der Meer and Redish, 2009a, 2011). NAc reward-anticipatory ramping neurons show phase precession relative to the hippocampal theta oscillation, particularly on the approach to reward locations, suggesting that place and reward information from the hippocampus and NAc respectively could be linked via this temporal code (van der Meer and Redish, 2011). There is evidence to suggest that these place-reward associations are consolidated by simultaneous replay in the hippocampus and NAc, where hippocampus-NAc cell pairs with place and reward-related activity were preferentially reactivated (Lansink et al., 2009; Pennartz et al., 2004).

4.1.1.3 Nucleus accumbens and prefrontal cortex

Disconnection studies have revealed the role of the mPFC-NAc pathway in the regulation of reward-seeking behaviour. Neurons in the mPFC show correlates to a multitude of cues, ranging from correlates for action sequences, cues, spatial locations, prospective and retrospective encoding of trial outcome, delays and more, often with mixed selectivity of individual neurons (e.g. Baeg et al., 2003; Horst and

Laubach, 2012; Hyman et al., 2012; Jung et al., 1998; Rigotti et al., 2013). This rich information can be transferred to the NAc to guide reward-seeking.

Interactions between mPFC and NAc have a prominent role in flexible behaviour in attentional set-shifting tasks (Floresco et al., 2009). A more specific role in reward-seeking behaviour has also been investigated in rats. Inputs from prelimbic to NAc promotes conditioned drug-seeking behaviour, while infralimbic to NAc projections suppress this behaviour in a cocaine self-administration paradigm (reviewed in Peters et al., (2009)).

Further exploration of this network was prompted by the fact that anhedonia in schizophrenia and depression is associated with elevated activity of a part of the mPFC in humans (Dowd and Barch, 2010; Harvey et al., 2007; Keedwell et al., 2005; Mayberg et al., 2005), which is thought to modulate striatal output leading to loss of reward-seeking. The top-down inhibitory role of the infralimbic cortex in rodents has been noted in addictive drug seeking as described above, but also in impulsivity (Dalley et al., 2011; Donnelly et al., 2014) and anhedonia (Grace, 2016). The infralimbic has been shown to have a causative inhibitory influence on reward-seeking using a simultaneous optogenetic and fMRI paradigm. Using a stabilized step-function opsin (SSFO), Ferenczi et al. (2015) were able to induce subthreshold depolarization of pyramidal cells in the rat infralimbic cortex, enhancing the excitability of this region. Behaviourally, this led to a reduction in reward-seeking behaviour, such as diminished sucrose preference and reduced drive for social interaction. The SSFO-stimulation also led to increased functional coupling between infralimbic cortex and ventral striatum as measured by the BOLD response, also observed as abnormally increased gamma coherence between infralimbic cortex and ventral striatum. Simultaneous fMRI, optogenetic stimulation of VTA dopaminergic neurons and the SSFO infralimbic stimulation revealed that the elevated excitability of the infralimbic cortex suppressed the response to dopamine in the ventral striatum and, in terms of behaviour, prevented the development of a place preference usually elicited by stimulation of dopamine neurons. Another study used a similar SSFO technique to rescue the abnormally

high reward-seeking behaviour that occurs following acute sleep deprivation (Liu et al., 2016). These authors found that sleep deprivation leads to a reduction in the excitatory/inhibitory synaptic inputs onto NAc medium spiny neurons, specifically a reduction in presynaptic glutamate release probability. This glutamatergic tone was normalized following the SSFO-mediated elevation of excitability in the infralimbic, leading to reduced reward seeking.

The exact circuit mechanisms by which elevated prefrontal excitability leads to blunting of the response to dopamine in the striatum remains unclear, but these findings highlight the top-down inhibitory control the infralimbic cortex has on NAc function and reward-seeking behaviour.

4.1.2 Nucleus accumbens in 15q11.2-associated disorders

The NAc has been implicated in schizophrenia (Deserno et al., 2016; Goto and Grace, 2008; Grace, 2000) and autism (Dölen, 2015; Fuccillo, 2016; Kohls et al., 2013). Furthermore, changes in NAc BOLD activity are also seen in healthy participants with high polygenic risk scores for schizophrenia (Lancaster et al., 2016a, 2018) and psychosis (Lancaster et al., 2016b), suggesting an overlap between NAc function and genetic aetiology. The NAc was initially of interest for schizophrenia in the context of the dopaminergic theory of schizophrenia (Howes and Kapur, 2009), following the observation that striatal dopamine is elevated in schizophrenia patients presynaptically (Hietala et al., 1995; Lindström et al., 1999) and shows increased release following amphetamine-challenge (Abi-Dargham et al., 1998). Meta-analyses have also confirmed that NAc volume is reduced in patients (van Erp et al., 2016; Okada et al., 2016), and volume was recently shown to correlate with cognitive deficits in schizophrenia (Koshiyama et al., 2018). White matter abnormalities in the frontostriatal loop have been associated with symptom severity in schizophrenia (Quan et al., 2013). It appears the NAc may play a role in virtually all the symptom domains, including psychosis (Howes and Kapur, 2009), apathy (Caravaggio et al., 2018) and cognitive deficits (Deserno et al., 2016). In autism, aberrant NAc activity has been linked to social and monetary reward-processing deficits (Kohls et al., 2013).

Such reward-processing deficiencies, for example abnormal representations of the expected value of rewards and actions, or disrupted dopamine-mediated reward prediction errors, which have been observed in human ventral striatum (Pessiglione et al., 2006), could lead to impairments in reinforcement learning seen in these conditions (Gold et al., 2008; Waltz and Gold, 2016).

The dopamine dysregulation associated with schizophrenia is also implicated in the formation of delusions, whereby aberrant dopaminergic firing assigns salience to inappropriate cues (Kapur, 2003). Ventral striatal dysfunction has been consistently associated with psychosis, although reports of both increased (Richter et al., 2015; Sorg et al., 2013) and decreased striatal activity exist (Grimm et al., 2014; Radua et al., 2015). During reward anticipation, hypoactivation of ventral striatum has been linked to psychosis (Radua et al., 2015) and a blunted reward prediction error signal is typically seen in unmedicated patients (Morris et al., 2012; Murray et al., 2008; Schlagenhauf et al., 2014), although this is less consistent in medicated patients (Culbreth et al., 2016). It may seem counterintuitive that striatal dopamine is elevated, yet reduced reward-related activation is seen in the BOLD response to rewarding stimuli in SCZ patients. However, it was demonstrated in healthy volunteers receiving amphetamine, which causes an increase in striatal dopamine, that the BOLD response to rewarding cues was diminished, suggesting the high level of dopamine may 'drown out' cue-induced phasic release (Knutson et al., 2004).

As mentioned previously, a hyperexcitable PFC and hypoactivated ventral striatum have been linked to anhedonic symptoms in schizophrenia and depression (Dowd and Barch, 2010; Harvey et al., 2007; Keedwell et al., 2005; Mayberg et al., 2005), highlighting the role of this pathway in motivation in humans as well. Of course, a compromised cortico-striatal pathway can also impact on decision-making, thus disruptions to this network have been associated with deficient planning, for example in a delay discounting task (Avsar et al., 2013). Indeed, functional connectivity between cortical and ventral striatal regions is also disrupted in schizophrenia patients, with both increased and decreased connectivity findings

(Lin et al., 2018; Richter et al., 2015). Overall, the NAc is a major hub of for limbic and cortical inputs that is vulnerable to a range of disorders and contributes to a range of symptoms, particularly pertaining to cognition and reward-seeking.

4.1.3 Nucleus accumbens in animal models

NAc activity has not been investigated in the *Cyfip1*$^{+/-}$ mouse, and relatively few studies in schizophrenia- or autism-relevant animal models exist. Much of the interest in this region has come from pharmacological models using acute ketamine and other NMDA antagonists, which are discussed in the next chapter.

Aberrant mesolimbic dopamine network activity has been demonstrated in the methylazosymethanol acetate (MAM) developmental model of schizophrenia (Lodge and Grace, 2007), with a hyperactive ventral hippocampus leading to an augmented number of dopamine neurons spontaneously active in the VTA, via the NAc. This was reversed following ventral hippocampus inactivation. A maternal immune activation model (poly(I:C) treated dams) shows disrupted dopamine signalling in the accumbens, with increased baseline dopamine in the NAc but, in contrast to MAM animals, reduced activity of dopamine cells in the VTA (Luchicchi et al., 2016).

A recent study investigated the role of a schizophrenia risk gene, *Erbb4*, in the NAc (Geng et al., 2017). In Chapter 3, the consequence of *Erbb4* conditional knockout were described: reduced hippocampus-PFC theta coherence under anaesthesia and increased baseline gamma oscillations in freely moving mice coupled with deficits in social and cognitive functions reminiscent of schizophrenia (Del Pino et al., 2013). *Erbb4* is highly expressed in the medium spiny neurons of the striatum, and conditional local deletion of *Erbb4* in the NAc Core led to overexpression of the $GABA_A$ receptor α1 subunit and increased inhibitory synaptic transmission, which corresponded with a range of behavioural abnormalities including hyperactivity and impaired social behaviour.

Neuregulin 1 (*Nrg1*), a neurotrophic factor that binds to the Erbb4 synaptic receptor, has been implicated in schizophrenia risk (Stefansson et al., 2003) and regulates processes including neuronal migration and axonal pathfinding (Krivosheya et al., 2008; López-Bendito et al., 2006). Mice heterozygous for a disruption in the *Nrg1* gene (Het) show altered synaptic plasticity in hippocampal-NAc-cortical circuits (Zhong et al., 2008). In anaesthetized *Nrg1* Het mice, functional coupling between ventral hippocampus and NAc was compromised in the theta frequency band, as shown by reduced phase-locking of NAc cells to bursts of hippocampal theta seen under anaesthesia.

4.1.4 Chapter aims

In this chapter, I investigated the network activity of the NAc and its interaction with prefrontal cortex and hippocampus in *Cyfip1*$^{+/-}$ rats. Initial analyses were focused on the approach to a reward point on the T maze task introduced in Chapter 3.

Key hypotheses:

- Reward-approach and arrival associated gamma power is abnormal in *Cyfip1*$^{+/-}$ rats.
- The putative disruption to long-range connectivity causes *Cyfip1*$^{+/-}$ rats to show abnormal connectivity between the NAc and hippocampal and cortical regions.

4.2 Methods

4.2.1 Behaviour and surgery

This chapter analyses data from the same discrete-trial alternation T maze task in Chapter 3, which was run as described in Chapter 2. 14 WT and 13 *Cyfip1*$^{+/-}$ rats were implanted with multisite LFP electrode drives, including targets to NAc Core, NAc Shell, hippocampal dCA1, vHPC, PRL and IL. For analyses using the IL channel, 2 *Cyfip1*$^{+/-}$ animals were excluded: one had too much noise on this channel

and the other was excluded due to a misplaced electrode (see General Methods). Thus results for IL analyses are shown for WT = 14, *Cyfip1*$^{+/-}$ = 11.

4.2.2 Maze LFP analysis

Tracking, maze segment analysis, power and coherence spectra calculation were as described in Chapter 3 and Chapter 2.

4.2.2.1 Power time series

Gamma power time series were z-scored against gamma power throughout the maze task, in order to ensure these plots showed changes from the average gamma power level at the reward point, thus minimising the added variability that comes with using the absolute gamma power for each animal (van der Meer and Redish, 2009a).

4.2.2.2 Homecage wake data

A 10 minute segment of data during awake state in the homecage was analysed. This segment represents the first 10 minutes of the post-T maze 'sleep recording' session, during which rats were still awake and moving in their homecage. Power spectra were generated using the Chronux *mtspectrumsegc* function, which divided the 10 minutes into 10 second epochs, computed the fast fourier transform for each epoch and averaged over them. Similarly, coherency plots were generated using the *coherencysegc* function. Parameters were set as follows: bandwidth = 3 Hz, window = 2 s, constant = 3, providing nine tapers for multi-taper spectral estimates.

4.2.3 Novel object location task

Animals were habituated to a 1m^2 sawdust covered arena with three wooden walls painted grey, and one painted black to provide a spatial orientation cue. Black curtains covered the space above the front and back walls, while side walls remained open. A camera above the arena tracked the position of the LED on the animal's head. Animals were placed in the arena every day for 4 days and habituated for 10 minutes each day. The novel object location task was based on the protocol used by the Warburton lab (Barker et al., 2007) and consisted of a

sample and a test phase. Two identical DUPLO® objects were placed in adjacent corners of the arena, and the animal was allowed to explore the arena during the 4 minute sample phase. The sawdust was mixed and the objects sprayed with ethanol to minimise olfactory cues, before two identical objects were replaced in a new position whereby one object remained in the original location, and the other was placed in the opposite corner (Figure 4.2). Following a 10 minute delay in the home cage, the animal was placed in the centre of the arena for a 4 minute test phase. The object placement was pseudo-random and counterbalanced between rats.

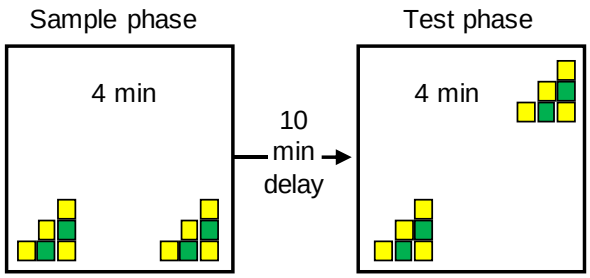

Figure 4.2 | **Novel object location task**

Behavioural scoring used a custom Matlab GUI, blind to genotype and the identity of the novel location. Behaviour was scored as object exploration when the rat's nose was oriented towards the object at close range. A discrimination ratio (DR) was used to assess performance, specifically the degree to which animals explored the novel location more. This was calculated using equation 2 below, such that a positive DR indicates the rat explored the novel location more, while a DR of 0 means the animal explored both objects equally.

$$DR = \frac{seconds\ exploring\ novel\ -seconds\ exploring\ familiar}{total\ seconds\ exploring} \qquad (2)$$

4.3 Results

4.3.1 LFP activity during reward site approach

In investigating the LFP activity in NAc and its interacting brain regions, I decided to focus my analyses on the theta and gamma frequency bands, consistent with the focus on these oscillation in the NAc literature (Catanese et al., 2016; Lansink et

al., 2009; van der Meer and Redish, 2009a; van der Meer et al., 2010; Tabuchi et al., 2000).

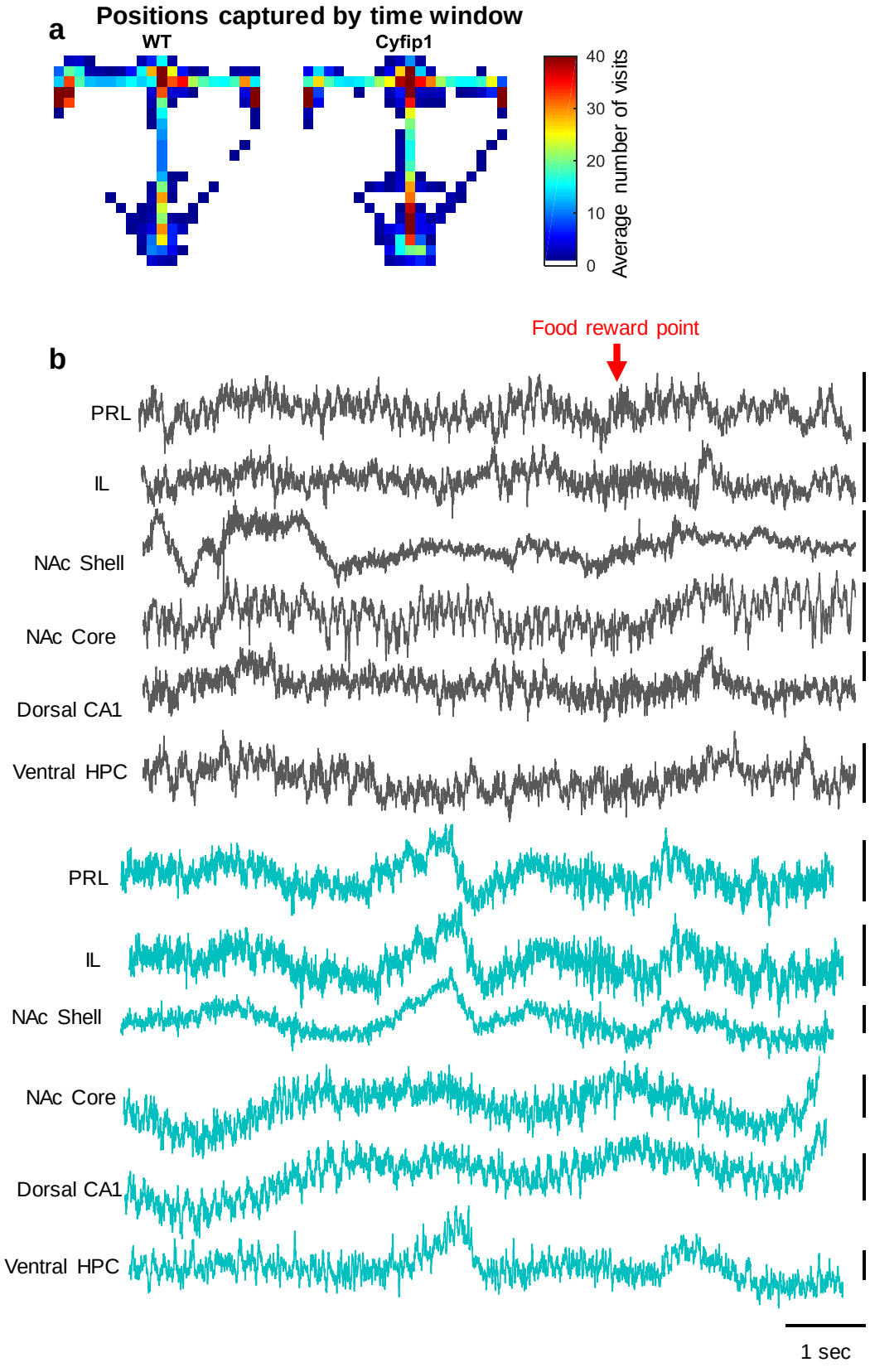
a
Positions captured by time window
WT
Cyfip1
40
30
20
10
0
Average number of visits
b
Food reward point
PRL
IL
NAc Shell
NAc Core
Dorsal CA1
Ventral HPC
PRL
IL
NAc Shell
NAc Core
Dorsal CA1
Ventral HPC
1 sec

Figure 4.3 **| Paths captured and raw traces. a**, Heatmaps indicating paths captured by extracting a 9 s time window centred on trigger line 8 (see text), at the reward point. Colour represents the average number of times each pixel was visited, averaged across trials and animals. WT: n = 14, Cyfip1: n = 13. **b**, Representative raw LFP traces (WT in grey, Cyfip1 in cyan) from PRL, IL, NAc Shell, NAc Core, dCA1 and vHPC from the 9 second window as in **a**. Timestamp of reward point arrival is marked with red arrow. Note heightened high frequency (gamma) activity at reward point.

In the initial analyses, I investigated whether my task elicits a similar ramp in gamma power as in van der Meer et al. (2009), where gamma power increased steadily from the beginning of the trial to the reward location. Therefore, I chose a window time-locked to the arrival at trigger line 8 (i.e. the reward delivery point): 6 seconds back, 3 seconds forward. This 9-second window was chosen to typically capture the central arm run, approach to reward, and consumption time (Figure 4.3a). Example traces from this window from NAc, hippocampus and mPFC are shown in Figure 4.3b. Analysing correct trials only, guided and choice runs were not found to differ in gamma power or coherence measures (data not shown), therefore all run types were analysed together. Previously, some studies identified activity in two distinct gamma power bands in the NAc, around 50 Hz and 80 Hz (Berke, 2009; Catanese et al., 2016; Kalenscher et al., 2010; van der Meer and Redish, 2009a), although this was not seen by others (Donnelly, 2014), perhaps due to various experimental differences. In my data, no distinct NAc gamma activity could be seen around 50 Hz, although this may have been affected by the AC line noise. However, prominent high gamma power was clear at ~70 Hz (Figure 4.5), therefore a gamma range of 65-85 Hz was used for all subsequent analyses.

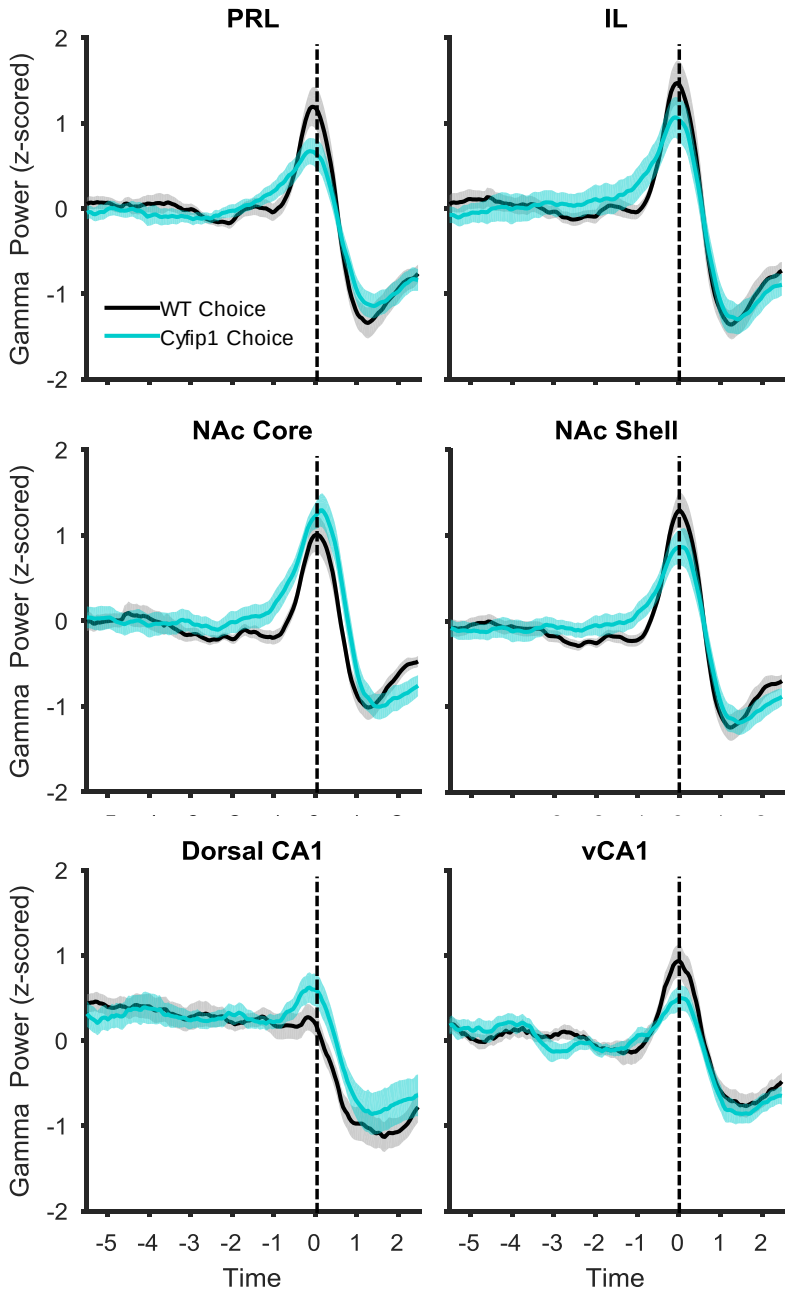

Figure 4.4 **| Gamma power on approach to reward point**. Amplitude of z-scored gamma power (65-85 Hz) envelope over time on each channel from the 9 second window capturing approach to the reward point. Time 0 marks arrival at reward point (trigger line 8). Only correct trials are shown, both guided and choice runs. WT: n = 14, Cyfip1: n = 13. In IL, Cyfip1 n = 11.

Figure 4.4 shows changes from the average gamma power in the window surrounding reward point arrival. While a ramping effect that started from the beginning of the run was absent, there was a striking rise in gamma power starting 1-2s before the reward point and peaking on arrival at the reward site, with a

subsequent drop in power, a pattern observed in the PRL, IL, NAc Core and Shell as well as the vHPC, but to a lesser extent in dCA1 (Figure 4.4). This pattern is broadly similar to what was seen in the gamma-50 band by others (Berke, 2009; Donnelly et al., 2014; Kalenscher et al., 2010; van der Meer and Redish, 2009a).

To test whether there was a genotype effect on the reward point increase in gamma power, I took the difference between the mean power in a window spanning -0.5 s to +0.5s surrounding trigger line 8, and the average 'baseline' gamma power prior to the reward point between -5 to -3 seconds. There was no significant genotype effect on the increase in gamma power at the reward point in any region ($p > 0.05$). Inspection of the gamma power profile suggested the rate of increase might be slower in *Cyfip1*$^{+/-}$ rats. A permutation test for a difference between genotypes in gamma power over time, with 1000 shuffles, showed no significant differences between genotypes in any brain region ($p > 0.05$ for all timepoints). Thus, gamma power changes evoked by arrival at the reward site appear normal in *Cyfip1*$^{+/-}$ rats.

4.3.2 Reward point analysis

Since I saw no indication of a gamma power ramp that starts earlier in the maze, I decided to narrow the window of analysis to focus on the reward point, with a 2 second window centred on arrival at the reward point (i.e. trigger line 8). This window captured the immediate approach and arrival at the reward point. This 2 second window was used to statistically analyse power and coherency spectra, while coherograms and figures showing change in power over time are shown over the full 9 second window to illustrate the change at the reward point. Mean power at theta (6-10 Hz) and gamma (65-85 Hz) frequencies was normal in all hippocampal, prefrontal and accumbal regions ($p > 0.05$ for all frequency bands in all regions, t-tests; Outliers: 1 WT and 2 Cyfip1 in NAc Shell gamma, 1 Cyfip1 in dCA1 gamma, 1 Cyfip1 in prelimbic gamma, none of the outliers in this analysis affected the result) (Figure 4.5).

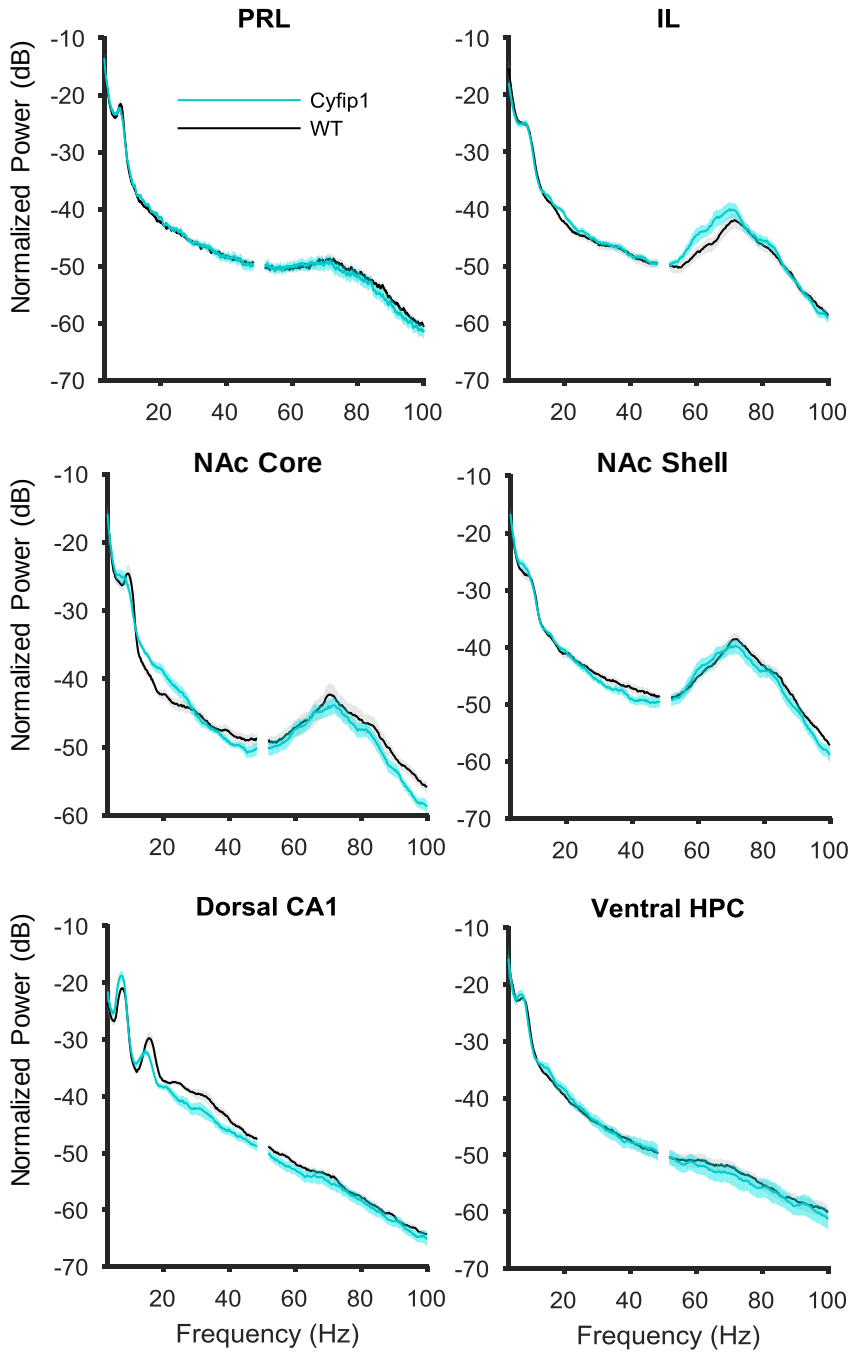

Figure 4.5 **| Power spectra**. Normalized power spectra for all channels taken from the 2 second window centred on the reward point. Values between 49-51 Hz have been removed to mask 50Hz line noise in the current figure and all subsequent power or coherency spectra. WT: n = 14, Cyfip1: n = 13. For IL Cyfip1: n = 11.

4.3.3 Nucleus accumbens-hippocampal interactions

Next, I analysed the oscillatory interaction between hippocampus and NAc regions by measuring coherence. The NAc receives dense projections from the

hippocampus, which is thought to provide contextual information critical for establishing place-reward associations (Ito et al., 2008; Voorn et al., 2004). Therefore, coherence between NAc Core-dCA1 and NAc Shell-vHPC regions in the 2 second window centred on reward point arrival were investigated, consistent with the known prominent anatomical connections between these subregions (Voorn et al., 2004).

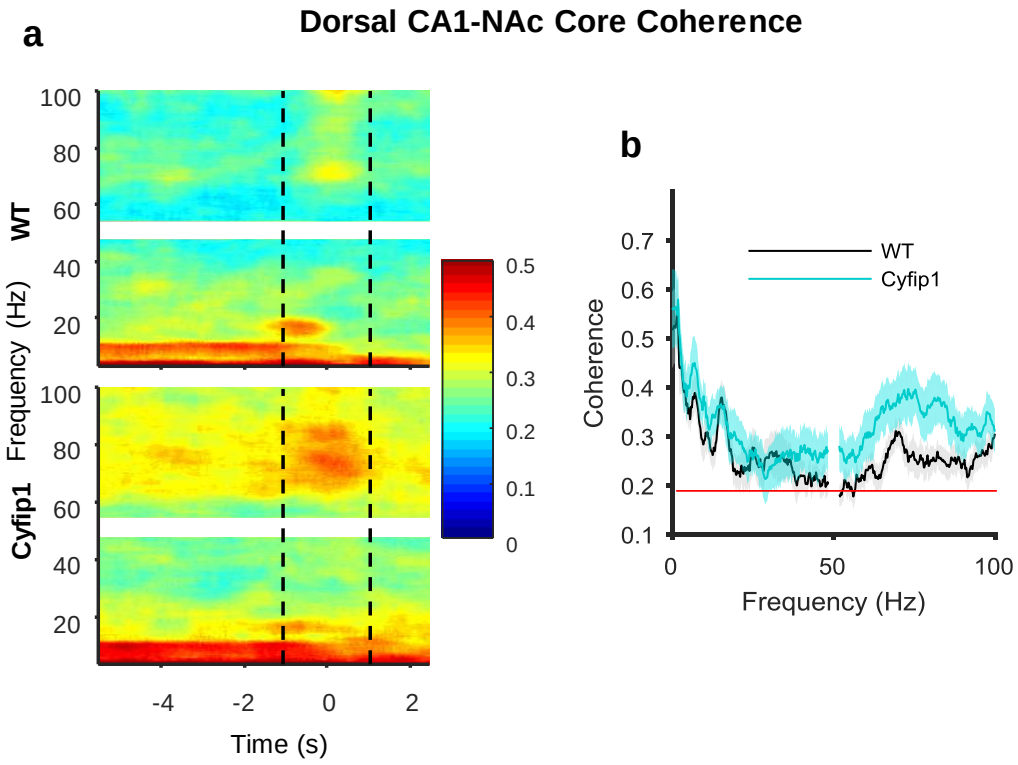

Figure 4.6 **| Dorsal CA1-NAc Core coherence**. **a**, Trial and animal averaged coherograms of the 9 second window capturing approach to the reward point. Time 0 marks arrival at reward point (trigger line 8). Upper: WT, Lower: Cyfip1. Colour represents coherence. Dashed lines indicate 2 second window used for analysis. Data at 50 Hz has been removed to mask 50Hz line noise in the current figure and all subsequent coherograms. **b,** Coherency spectrum for the 2 second window indicated by dashed black lines in **a.** Red line represents confidence level at p = 0.05. WT: n = 14, Cyfip1: n = 13

Theta coherence between NAc Core and dCA1 was normal (p = 0.46, t-test; 1 WT outlier did not affect result) (Figure 4.6). However, there was a trend for increased gamma coherence in *Cyfip1*$^{+/-}$ rats (p = 0.071, t-test).

In contrast, gamma coherence was significantly reduced between NAc Shell and vHPC in *Cyfip1*$^{+/-}$ rats ($p = 0.028$, t-test), with normal theta coherence ($p = 0.99$, t-test) (Figure 4.7). As might be expected from the similar profiles of gamma power over time, a similar pattern was also seen in the gamma coherence between vHPC and NAc Shell, with an increase in coherence immediately before the reward point (Figure 4.7c). However, the coherence increase at the reward point in *Cyfip1*$^{+/-}$ rats was weaker when comparing pre-reward coherence (average coherence between -3 to -1s) to the maximal coherence reached at reward arrival (maximum coherence between -0.5 to +2). Not only was gamma coherence significantly lower in *Cyfip1*$^{+/-}$ rats (genotype main effect: $F_{1,25} = 5.69$, $p = 0.025$), but the increase in coherence seen at the reward point was significantly smaller in *Cyfip1*$^{+/-}$ than WT rats (genotype x time interaction: $F_{1,25} = 4.62$, $p = 0.042$).

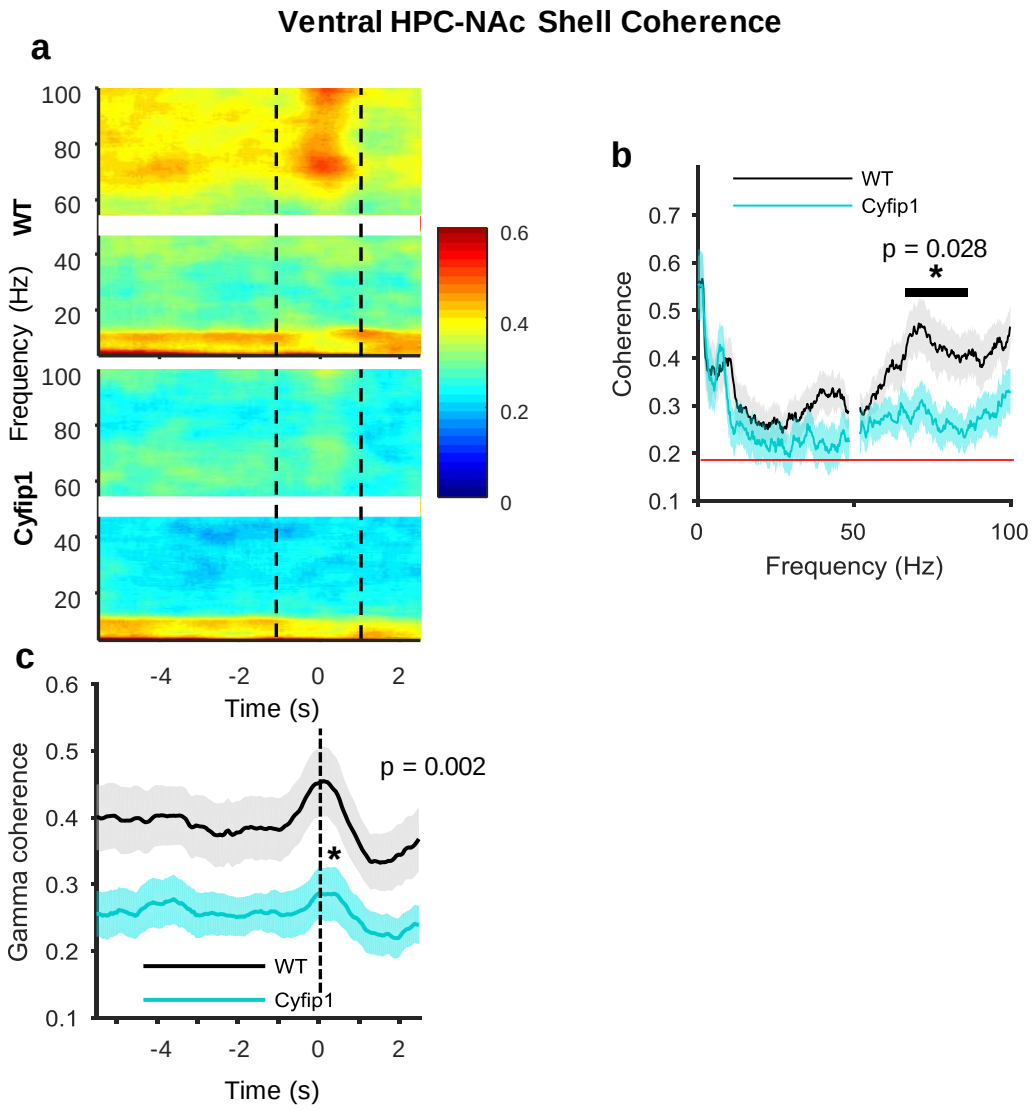

Figure 4.7 **| Ventral HPC-NAc Shell coherence**. **a**, Trial and animal averaged coherograms of the 9 second window capturing approach to the reward point. Time 0 marks arrival at reward point (trigger line 8). Upper: WT, Lower: Cyfip1. Colour represents coherence. Dashed lines indicate 2 second window used for analysis. **b,** Coherency spectrum for the 2 second window indicated by dashed lines in **a.** Black bar marks gamma (65-85 Hz) frequency range for which statistical test is shown. Red line represents confidence level at p = 0.05. **c,** Gamma (65-85 Hz) coherence during the 9 second window (as in **a**). * refers to a significant difference between groups in the magnitude of the increase in gamma power at the reward point. WT: n = 14, Cyfip1: n = 13.

Is the reduced vHPC-NAc Shell gamma coherence specific to the reward point context? I analysed two further contexts: during the return arm runs on the maze, and during awake states in the home cage. Return arm runs showed normal theta and gamma power ($p > 0.05$, t-tests; Outliers: 2 Cyfip1 outliers in NAc Shell gamma did not affect the result) and a trend for reduced gamma coherence ($p = 0.059$, t-

test) (Figure 4.8). A 10 minute epoch during wake in the homecage showed a similar pattern with normal theta and gamma power ($p > 0.05$ for both regions) and significantly reduced gamma coherence ($p = 0.046$, t-test) (Figure 4.9).

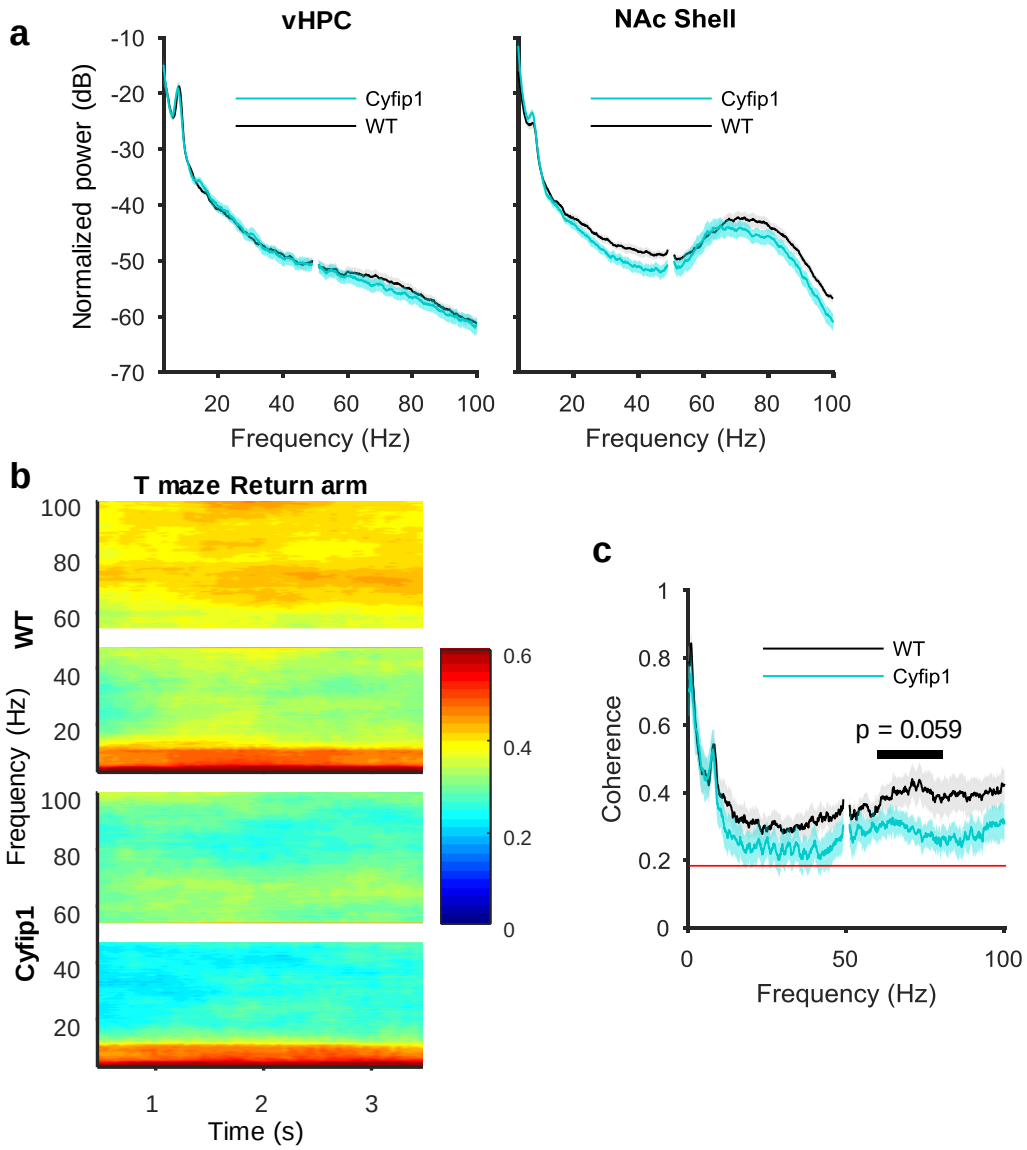

Figure 4.8 **| vHPC-NAc Shell coherence on return arms of T maze**. **a**, Normalized power spectra for for vHPC and NAc Shell taken from a 4 second window capturing return arm runs (4 seconds after trigger line 9). **b,** Trial and animal averaged coherograms of the 4 second window as in **a**. Upper: WT, Lower: Cyfip1. Colour represents coherence. Dashed lines indicate 2 second window used for analysis. **c,** Coherency spectrum for the 4 second window as in **a.** Black bar marks gamma (65-85 Hz) frequency range for which statistical test is shown. Red line represents confidence level at $p = 0.05$. WT: n = 14, Cyfip1: n = 13

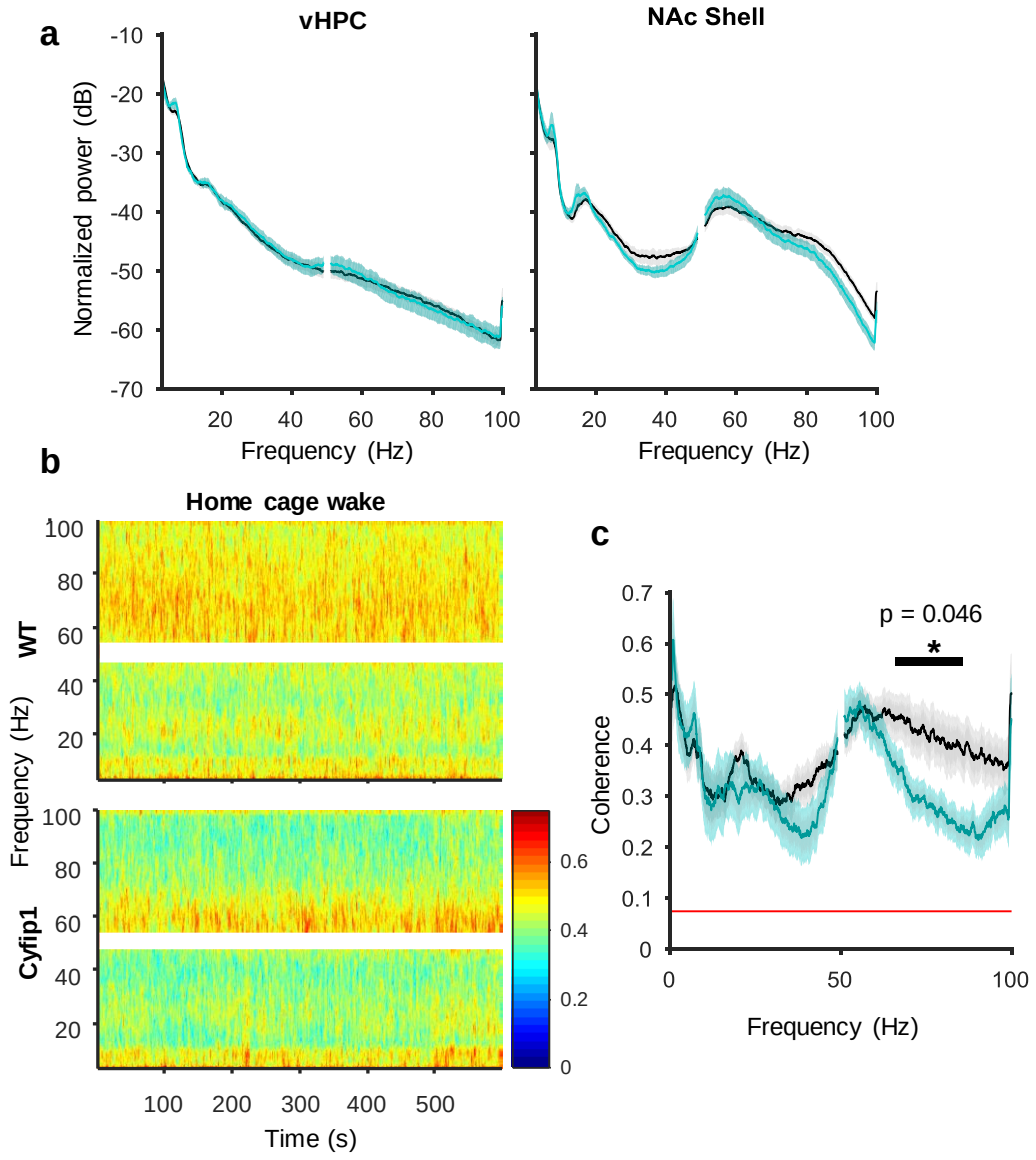

Figure 4.9 **| vHPC-NAc Shell coherence in homecage**. **a**, Normalized power spectra for for vHPC and NAc Shell taken from a 10 minute awake homecage recording. **b,** Trial and animal averaged coherograms of the 10 minute window as in **a**. Upper: WT, Lower: Cyfip1.Colour represents coherence. **c,** Coherency spectrum for the 10 minute window as in **a.** Black bar marks gamma (65-85 Hz) frequency range for which statistical test is shown. Red line represents confidence level at p = 0.05. WT: n = 14, Cyfip1: n = 13.

Taken together, these findings show globally reduced vHPC-NAc Shell gamma coherence in *Cyfip1*$^{+/-}$ rats relative to WT littermates, which becomes most prominent during goal-directed behaviour and may reflect aberrant signalling of reward approach and receipt.

4.3.3.1 Nucleus accumbens gamma coherence and running speed

As in Chapter 3, it is important to disentangle any running speed influences from the reduced vHPC-NAc Shell coherence in *Cyfip1*$^{+/-}$ rats, as running speed is known to affect gamma power (Ahmed and Mehta, 2012; Chen et al., 2011). There was no difference in average running speed between genotypes in the 9 second segment ($p = 0.185$, Mann Whitney U test), suggesting the reduced gamma coherence in *Cyfip1*$^{+/-}$ rats is independent of running speed (Figure 4.10a).

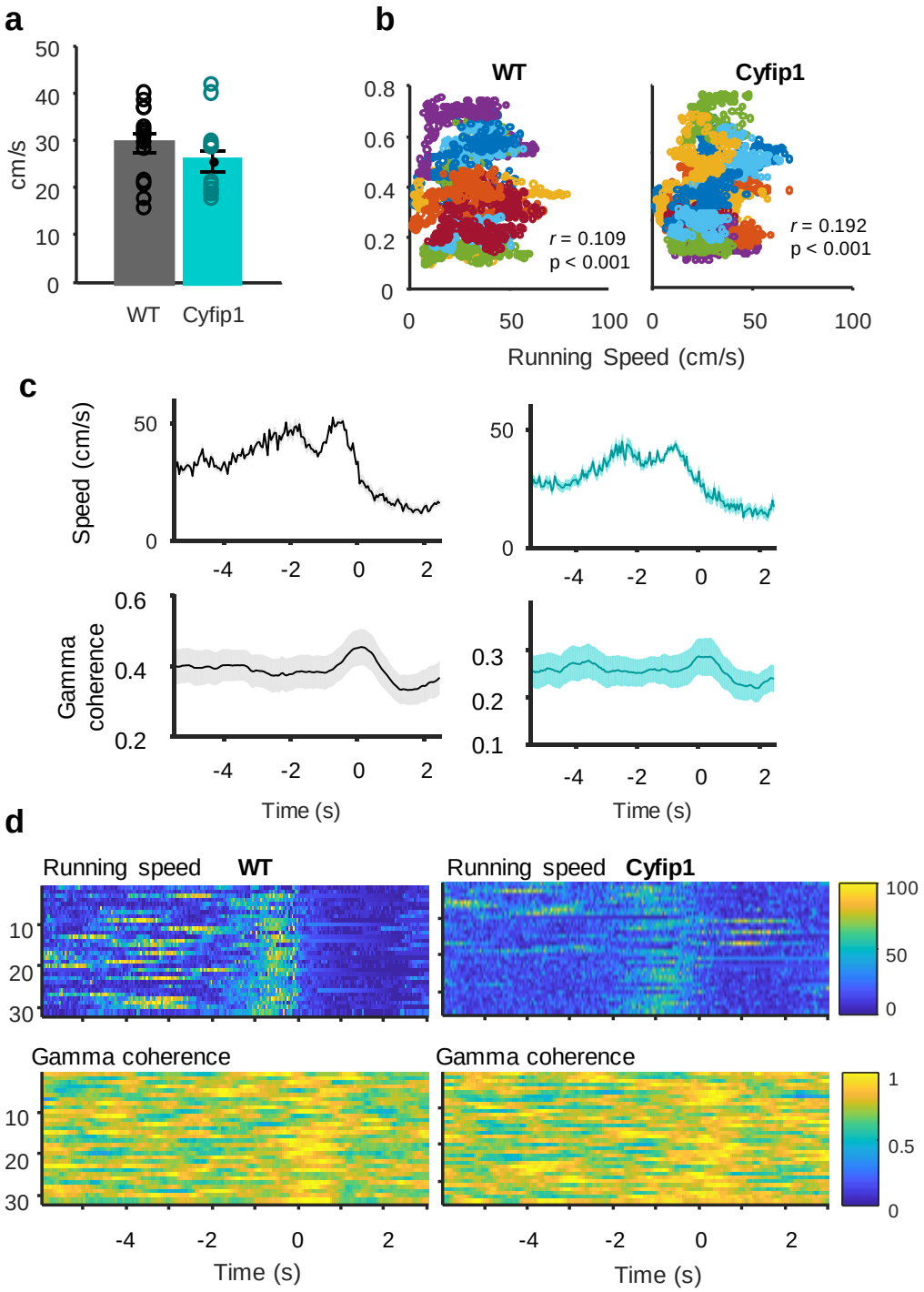

Figure 4.10 **| vHPC-NAc Shell gamma coherence and run speed**. **a**, Running speed in the 9 s window capturing approach to the reward point. **b,** Scatter plot between average running speed over the 9 s window *vs* the average vHPC-NAc Shell gamma (65-85 Hz) coherence in the same window. Each animal's trials are represented by datapoints in the same colour. **c,** Instantaneous running speed and vHPC-NAc Shell gamma coherence over the 9 s window, averaged over trials and animals. Note that the peak in running speed comes just before the peak in gamma coherence in both genotypes. **d,** Speed (upper) and gamma coherence (lower) for all runs by one representative WT and *Cyfip1*$^{+/-}$ rat. Each

row represents one run. Note the peaks in speed and coherence do not occur at the same point. WT: n = 14, Cyfip1: n = 13.

However, I noted that running speed showed a similar pattern to gamma power and coherence in this epoch, as rats tended to accelerate towards the reward point and then stop suddenly as they consumed it. This mirrors the increase and drop of gamma power and coherence, suggesting the striking peak seen in gamma power and coherence might be related to run speed. Furthermore, a scatter plot showed a small but significant positive correlation between running speed and gamma coherence (WT: $r = 0.109$, $p < 0.001$, Cyfip1: $r = 0.192$, $p < 0.001$, Pearson's correlation) (Figure 4.10b). However, it has been previously shown in a similar context that these two elements are dissociable (van der Meer and Redish, 2009a), and to demonstrate this here I plotted mean instantaneous running speed against mean gamma coherence (Figure 4.10c). This shows that the peaks are not temporally aligned, and can be seen in Figure 4.10d for individual trials in representative rats. Running speed drops significantly immediately before trigger line 8, reflecting the animals stopping to consume the reward, while gamma coherence peaks at or just after trigger line 8, appearing to coincide with actual consumption.

Similarly, analysing runs on the return arms, where there is no reward-related increase in gamma power or coherence, there are no clear patterns emerging from the speed and coherence plots, nor is there a significant correlation from the scatter plots (WT: $r = 0.033$, $p = 0.345$, Cyfip1: $r = 0.076$, $p = 0.062$, Pearson's correlation, data not shown). These observations support the suggestion that the peak in gamma coherence is not a direct result of increased running speed.

4.3.4 Nucleus accumbens – prefrontal cortex interactions

Top down cortical influence on the NAc has been shown to be important for regulation of reward-seeking behaviour (Ferenczi et al., 2016; Gruber et al., 2009; Liu et al., 2016; Peters et al., 2009). In particular, the IL to NAc Shell pathway appears to be involved in regulating reward-seeking behaviour (Ferenczi et al., 2016; Liu et al., 2016). Therefore, the interactions between NAc Shell-infralimbic

regions were investigated surrounding the reward point in the 2 s window described above (Figure 4.11). Theta coherence between NAc Shell-infralimbic was normal (p = 0.109, t-test), but there was a trend for increased gamma coherence in *Cyfip1*$^{+/-}$ rats (p = 0.09, t-test).

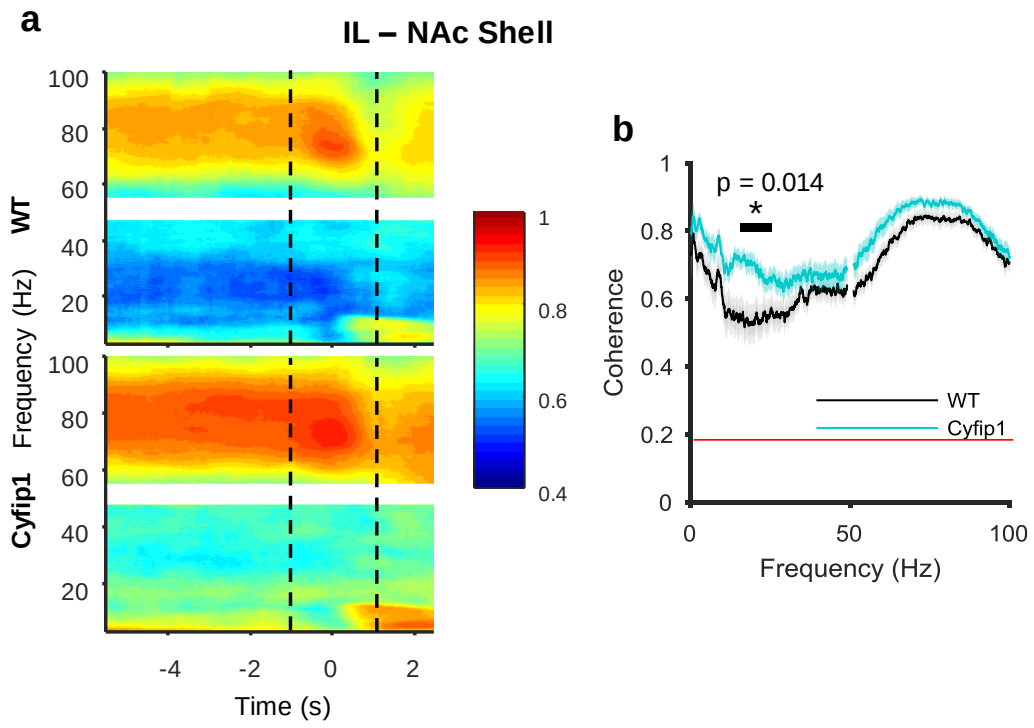

Figure 4.11 **| IL-NAc Shell coherence**. **a,** Trial and animal averaged coherograms of the 9 second window capturing approach to the reward point. Upper: WT, Lower: Cyfip1. Colour represents coherence. Dashed lines indicate 2 second window used for analysis. **b,** Coherency spectrum for the 2 second window shown in **a** (dashed lines)**.** Red line represents confidence level at p = 0.05. WT: n = 14, Cyfip1: n = 11.

Although beta oscillations were not a focus of the analysis presented here, the striking difference in beta coherence seen on the coherency plot for infralimbic-NAc Shell was tested. As this was an unplanned analysis, to control for multiple comparisons the significance level was adjusted to 0.0167 as per the Bonferroni correction ($\alpha = 0.05/3$, for three frequency bands tested). *Cyfip1*$^{+/-}$ rat beta coherence was significantly increased following correction (p = 0.014, t-test). Neurons in the NAc are modulated by hippocampal beta oscillations, and show increased phase-locking to beta upon presentation of reward-predicting cues

(Lansink et al., 2016), suggesting beta rhythms may be important in reward anticipation-related behaviours (Berke, 2009).

4.3.5 Error trials

I noticed that error trials showed a different gamma power profile following arrival at the reward point. In both genotypes prefrontal and accumbal regions showed a gamma power peak followed by a sharp drop on correct trials, but on error trials, this drop in gamma power was reduced (Figure 4.12). A very similar effect was seen by van der Meer & Redish (2009). It appeared there might be a genotype difference in the post-error gamma power. I compared the change in gamma power between the reward point (-0.5-0.5 s) and the period immediately following reward site arrival (at the point of minimal gamma on rewarded runs, 0.5-1.5 s after reward point arrival). All brain regions showed a main effect of run type ($F_{1,24} > 13$, $p =< 0.001$, mixed ANOVA). There was a trend for an interaction in the IL ($F_{1,22} = 13.4$, $p = 0.054$) and NAc Shell ($F_{1,24} = 18.7$, $p = 0.081$). This suggests that all brain regions had a differential response to error trials, but this was not significantly modulated by genotype.

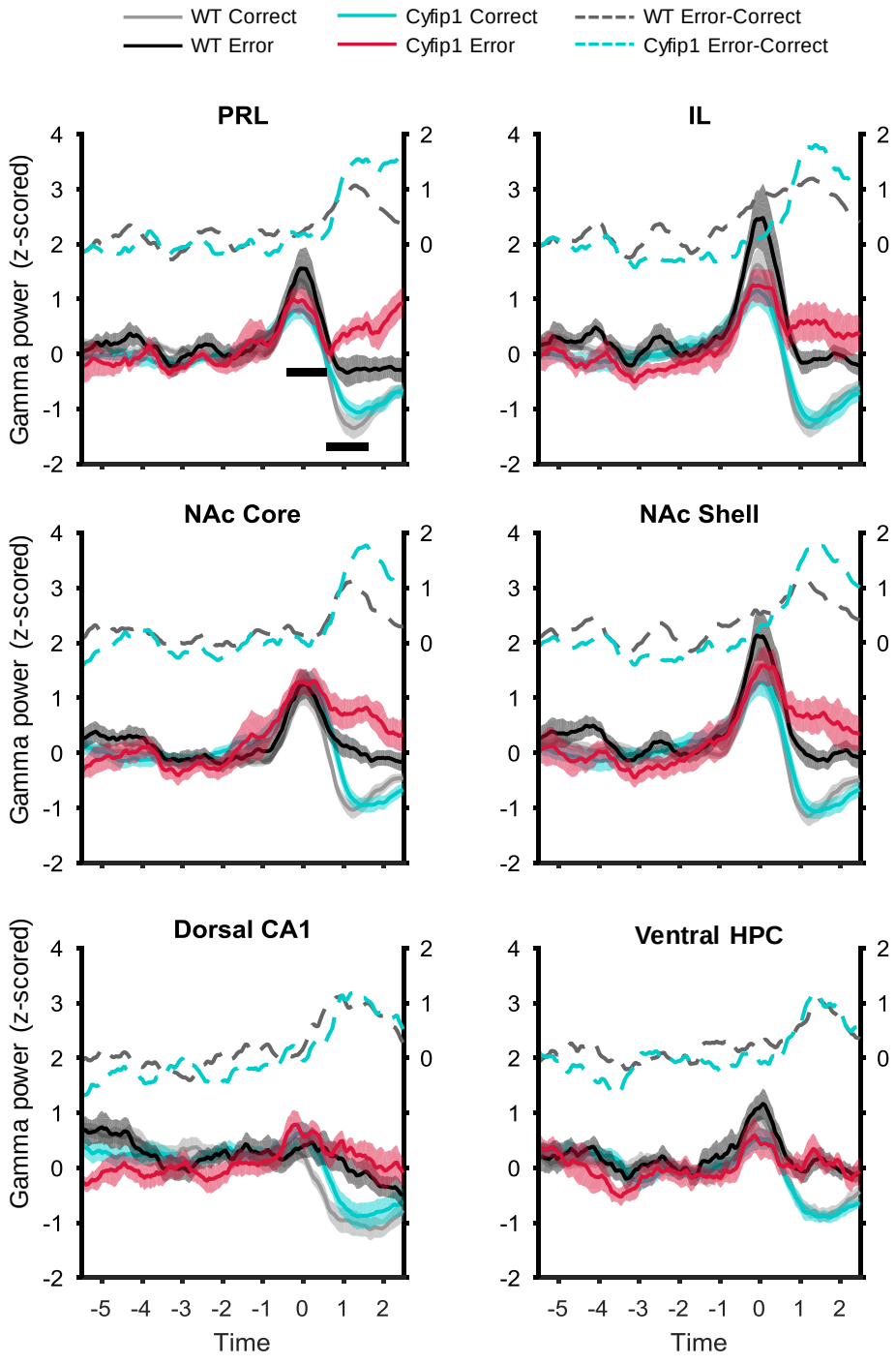

Figure 4.12 **| Gamma power on approach to reward point on error *vs* correct trials**. Amplitude of z-scored gamma power (65-85 Hz) envelope over time on each channel from the 9 second window capturing approach to the reward point. Time 0 marks arrival at reward point (trigger line 8). Correct trials are shown in light grey (WT) and cyan (Cyfip1), incorrect trials where rats did not receive a reward are shown in black (WT) and red (Cyfip1). Dashed lines represent the difference between gamma power on error and correct trials (right hand axis). WT: n = 14, Cyfip1: n = 13. In IL, Cyfip1 n = 11.

I next investigated whether the aberrant vHPC-NAc Shell coherence, which shows a similar profile to gamma power at the reward point, might be modulated differentially on error trials in *Cyfip1*$^{+/-}$ rats. Using a similar analysis of the drop in gamma coherence following reward point arrival, there was a main effect of run type ($F_{1,25} = 6.29$, $p = 0.019$) and genotype ($F_{1,25} = 6.9$, $p = 0.014$), but no interaction ($F_{1,25} = 0.033$, $p = 0.86$), suggesting that while gamma coherence is significantly lower in *Cyfip1*$^{+/-}$ rats as shown earlier, the response to error trials is not modulated by genotype (Figure 4.13).

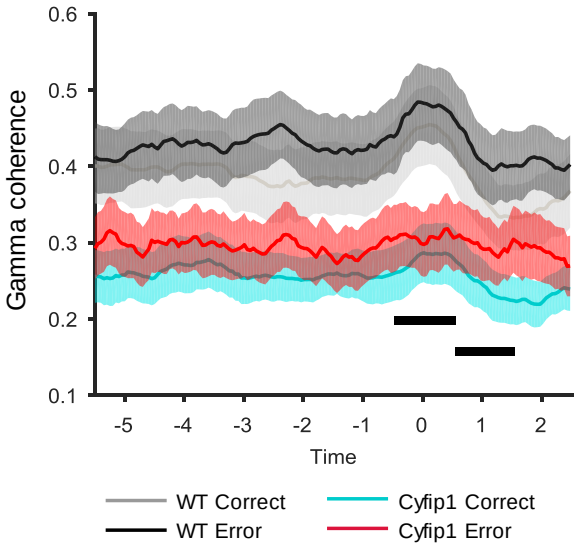

Figure 4.13 | **vHPC-NAc Shell gamma coherence on approach to reward point on error *vs* correct trials.** Gamma (65-85 Hz) coherence over time from the 9 second window capturing approach to the reward point. Time 0 marks arrival at reward point (trigger line 8). Correct trials are shown in light grey (WT) and cyan (Cyfip1), incorrect trials are shown in black (WT) and red (Cyfip1). Black bars indicate time windows compared statistically. WT: n = 14, Cyfip1: n = 13.

4.3.6 Novel object location task

Given the disturbed hippocampal-accumbal coherence seen in *Cyfip1*$^{+/-}$ rats, I next wanted to assess whether this disruption would manifest as a behavioural deficit in a task that involves this network. As mentioned in the introduction, the hippocampal-NAc Shell interaction is critical to the performance of spatial tasks (Ito et al., 2008), and the interaction likely relies on dopamine modulating hippocampal inputs to the NAc (Floresco and Phillips, 1999). One study explored

the impact on novel object location memory of dopamine depletion by NAc 6-hydroxydopamine infusions (Nelson et al., 2010). The task consists of a sample phase where animals explore a familiar environment containing two identical objects. After a delay of 10 minutes, the rats were returned to the environment, but one of the objects had been moved to the adjacent corner. The existence of object-in-place memory was inferred if the rats spent more time exploring the object in the novel location than the unmoved object. They found that depletion of dopamine in NAc Shell was correlated with a deficit in location memory, which could implicate the hippocampal-NAc Shell pathway in the novel object location task, seeing as this task is known to be hippocampal dependent (Barker et al., 2007). The deficit in the *Cyfip1*$^{+/-}$ rat network was specific to the vHPC-NAc Shell pathway, so this task is well-placed to probe the consequences of reduced coherence on object location memory.

I ran a pilot behavioural study with a subset of animals to assess novel object location memory (see Methods).

4.3.6.1 Sample phase

All animals explored objects for longer than the 15 second minimum criterion (Barker et al., 2007), and the average time exploring both objects was similar between groups ($p = 0.77$, t-test) (Figure 4.14a). During the sample phase there was no significant preference for either object. Accordingly, the discrimination ratio did not show a significant difference from zero in either group as shown by a one-sampled t-test (WT: $p = 0.41$, Cyfip1: $p = 0.46$, one-sample t-test, Figure 4.14c).

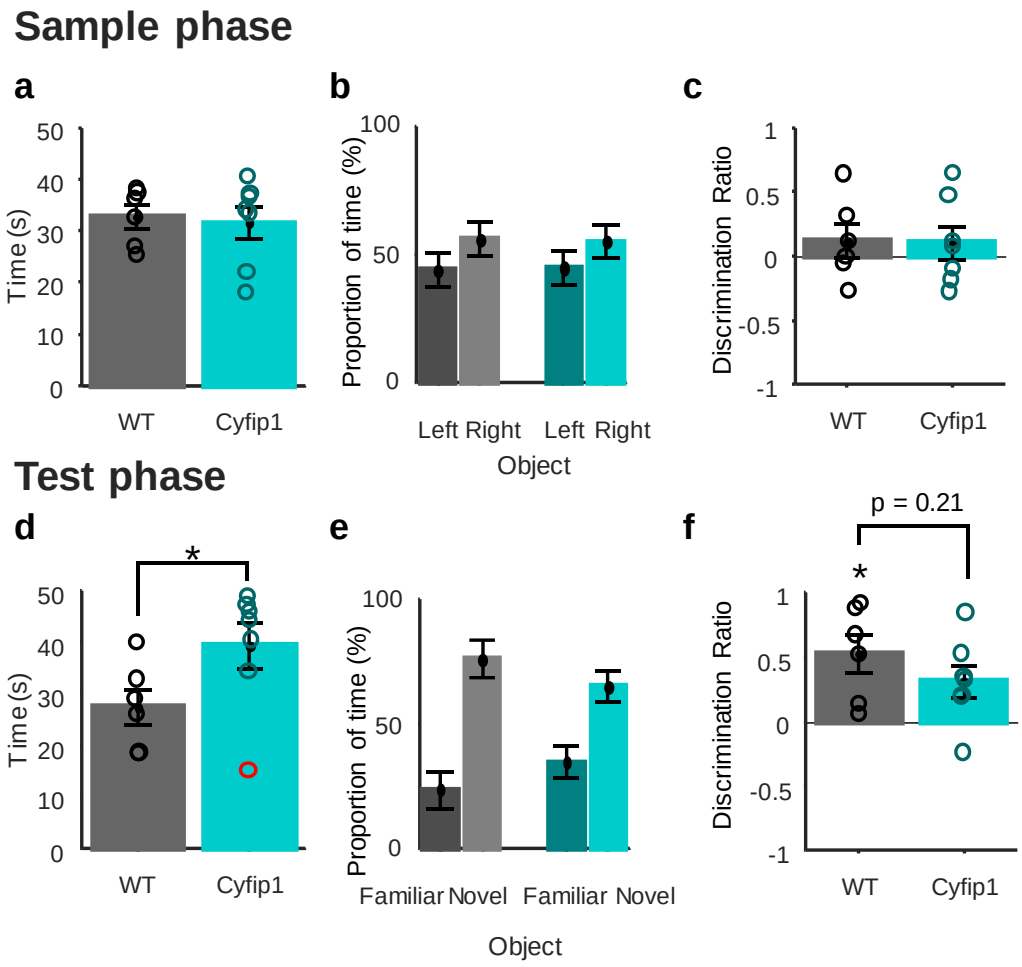

Figure 4.14 **| Novel object location pilot study**. **a,** Sample phase. Time spent exploring both objects. **b,** Proportion of time spent exploring left and right objects. **c,** Discrimination ratio. **d,** Test phase. Time spent exploring both objects. * p = 0.003 following removal of outlier in red. **e,** Proportion of time spent exploring left and right objects. **f,** Discrimination ratio. Two groups did not differ from each other. * p = 0.017, one sample t-test for WTs. One sample t-test not significant for Cyfip1 rats. WT: n = 6, Cyfip1: n = 7

4.3.6.2 Test phase

All animals explored objects for longer than the 15 second minimum criterion (Barker et al., 2007). Following the removal of one *Cyfip1*$^{+/-}$ outlier, *Cyfip1*$^{+/-}$ rats spent significantly longer exploring both objects than WTs (p = 0.003, t-test) (Figure 4.14d). This should not impact the result of the memory test however, as a more confounding issue arises if one group of animals explores objects less during the sample phase, which could lead to a weaker memory being established.

All animals, except one *Cyfip1*$^{+/-}$ rat, explored the novel location object more than the familiar location object. The discrimination ratio was not significantly different between groups (p = 0.21, t-test) (Figure 4.14f). However, a one-sample t-test showed that the WT discrimination ratio was significantly different from zero (p = 0.017), suggesting they discriminated between novel and familiar locations, while for *Cyfip1*$^{+/-}$ rats the discrimination ratio was not significantly different from zero (p = 0.134). Due to the lack of significant group differences however, it is not possible to conclude that the *Cyfip1*$^{+/-}$ rats performed worse than WTs in this task. The large variability between individuals and low n for this task means it is likely underpowered, therefore I hesitate to draw firm conclusions about object-location memory in *Cyfip1*$^{+/-}$ rats.

4.4 Discussion

Results from this chapter show:

- During a T maze task, gamma coherence between vHPC and NAc Shell is significantly reduced in *Cyfip1*$^{+/-}$ rats *vs* WTs.
- On approach to the reward site on the T maze, both genotypes show a sharp increase in gamma power coinciding with arrival at the reward site.
- A similar increase can be seen in vHPC-NAc Shell gamma coherence upon arrival at the reward site, and this is significantly diminished in *Cyfip1*$^{+/-}$ rats.
- Coherence between IL and NAc Shell showed enhanced beta coherence in *Cyfip1*$^{+/-}$ rats.
- Gamma power following reward point arrival is significantly different on error trials, but this is not affected by genotype. A similar finding was seen for vHPC-NAc Shell gamma coherence.
- The novel object task, used in a pilot study to probe the consequences of deficient hippocampus-NAc interaction, pointed towards a deficit in location memory in *Cyfip1*$^{+/-}$ rats, although this was inconclusive.

4.4.1 Disrupted hippocampal-accumbal network

The NAc is able to mediate optimal goal-directed behaviour when it receives the necessary information from its key inputs – including the hippocampus, prefrontal cortex and dopaminergic input from the VTA – and, importantly, when the balance between limbic and cortical inputs is maintained. The reduced gamma coherence between vHPC and NAc Shell observed in *Cyfip1*$^{+/-}$ rats suggests information transfer from the hippocampus is compromised and, following from this, the balance of hippocampal/cortical inputs may be disrupted. However, as behavioural results from the T maze presented in Chapter 3 demonstrate, this task was not impaired by this disruption to the network.

A similar asynchrony in this network was seen in the *Nrg1* heterozygous mouse, with reduced phase-locking of NAc cells to bursts of hippocampal theta, although this was under anaesthesia and gamma frequencies were not reported (Nason et al., 2011). Furthermore, the MAM model shows disrupted synaptic plasticity in the ventral hippocampus-NAc-PFC network, which is thought to contribute to the deficits in goal-directed behaviour seen in this model (Belujon et al., 2014). However, the fact that theta and gamma power were normal in *Cyfip1* hippocampus argues against a hyperactive ventral hippocampus as seen in the MAM model (Lodge and Grace, 2007, 2011).

Further experiments are required to explore the consequences of reduced vHPC-NAc Shell coupling and increased IL-NAc Shell coupling. Firstly, behavioural tests of motivation for reward would be needed to elucidate whether *Cyfip1*$^{+/-}$ rats have normal drives to obtain reward. A sucrose preference test, where animals are given the option to drink water or sucrose solution, can reveal an anhedonic phenotype where rats are less sensitive to rewarding stimuli (Barnes et al., 2017). A spatial test that invokes reward evaluation would also be predicted to rely on hippocampal and NAc activity, such as a T maze where reward value and probabilities are changed (e.g. (Kim et al., 2009)). In addition, a behavioural task that is known to engage the vHPC-NAc Shell network, such as place preference conditioning which was disrupted by the disconnection of these two regions by Ito et al. (2008), could shed

light on the consequences of reduced coherence on behaviour. The hippocampal-cortico-striatal network is important in enabling flexible behaviour (Floresco et al., 2009). Therefore, a task involving a rule-reversal could reveal behavioural deficits.

As mentioned in Chapter 3, the *Zdhhc8*$^{+/-}$ mouse model, which impacts the Rac1 pathway also involved in Cyfip1 signalling, showed a significant reduction in hippocampal-prefrontal theta coherence, which was causally linked to impaired axonal branching of ventral hippocampal projections to the prefrontal cortex both at P16 and at 12 weeks (Mukai et al., 2015; Tamura et al., 2016). It is conceivable therefore, that the reduction in hippocampal-accumbens gamma coherence seen in *Cyfip1*$^{+/-}$ rats might be caused by a similar disruption to the axons of the direct anatomical connections between these regions.

4.4.2 Beta band

Beta oscillations have been recorded in the NAc (Berke, 2009; Howe et al., 2011; Lansink et al., 2016) and mPFC (Benchenane et al., 2011), and this relatively understudied frequency band has been associated with movement and perceptual processes (Engel and Fries, 2010). However, the relevance of beta in the rat infralimbic-NAc Shell network is unknown. A recent paper electrically stimulated the rat prelimbic at frequencies ranging from 4-60Hz and measured evoked dopamine release in the NAc. They found that 20 Hz stimulation was able to trigger the greatest dopamine release in NAc when the stimulation lasted longer than 5s (Hill et al., 2017). Moreover, optogenetically stimulating mPFC-VTA projecting neurons at a range of frequencies when rats made a nose-poke showed that animals preferred the stimulation at 20 Hz over lower frequencies (Beier et al., 2015). This behaviour depended on dopamine release in the NAc. An obesity model also found changes in the beta band, observing increased beta power in the NAc and mPFC of rats fed on a high fat diet, which correlated with body weight, leptin and insulin levels, together with decreased beta coherence between these regions (Maurer et al., 2017). Together, these studies hint that beta frequency oscillations may be highly relevant to the cortico-limbic reward network. Therefore, the abnormally

high cortical-striatal beta coherence seen in *Cyfip1*$^{+/-}$ rats supports the notion that reward-signalling in the NAc network is disrupted.

4.4.3 Hippocampal-cortical-accumbal network

It has been proposed that the hippocampus and PFC compete for control over the NAc at the level of synaptic plasticity (Goto and Grace, 2005, 2008). High frequency stimulation of the hippocampus leads to long term potentiation (LTP) of the hippocampus-NAc synapse, while PFC-NAc synapses were subject to long term depression (LTD). Conversely, stimulation of the PFC leads to the opposite outcome: LTP in PFC-NAc synapses and LTD in hippocampus-NAc synapses (Goto and Grace, 2005). The authors suggest that this could be a mode of input integration that allows for fast expression of a well-learned behaviour. In light of this competitive relationship between hippocampal inputs and mPFC inputs in the NAc, it is interesting to note that *Cyfip1*$^{+/-}$ rats show a reduction in coherence between vHPC-NAc together with an increased coherence between infralimbic-NAc, which was highly significant in the beta band, but also numerically greater in the gamma band. While it is unknown whether these aberrant interactions indeed cause synaptic plasticity changes, one could speculate that reduced efficacy of information transfer from ventral hippocampus to NAc Shell could lead to cortical, specifically infralimbic, inputs exerting a stronger influence, thus inhibiting reward seeking, which this pathway has been shown to do (Ferenczi et al., 2016; Liu et al., 2016). This might explain the subtle yet significantly diminished response following reward site arrival, as seen by the reduced gamma coherence peak in *Cyfip1*$^{+/-}$ rats. Again, tasks explicitly designed to test the reward sensitivity of *Cyfip1*$^{+/-}$ rats could be used to test this directly.

4.4.4 Functional relevance and origin of reward-related gamma activity

4.4.4.1 Gamma-50 or gamma-80?

In my data, the reward site peak gamma power was highest at 70 Hz, thus gamma analyses focused on the 65-85 Hz frequency band (referred to as gamma-70). A number of other studies have differentiated between two types of gamma in the NAc, gamma-50 and gamma-80 (Berke, 2009; Catanese et al., 2016; Kalenscher et

al., 2010; van der Meer and Redish, 2009a). The fact that I did not observe two prominent gamma bands may be due to recording location, animals strain and task-related differences. However, I asked whether my gamma-70 behaved more like the observed gamma-50 or gamma-80 that others have observed. Prior to reward arrival, there is no distinct ramp, and the peak of gamma power occurs just after reward site arrival, which is similar to what is seen in the gamma-50 band. However, the profile of gamma-70 on error trials looks more like gamma-80 activity, with a gamma peak as usual, but without the following drop in gamma power seen on correct trials. Thus it appears that my gamma-70 band reflects both reward anticipatory processes as well as reward outcome processes.

In the current task it is difficult to disentangle whether the peak in gamma power and coherence seen across the limbic-cortical network is related to reward expectancy or reward consumption. However, there are some observations that speak to this. Firstly, in my data, the peaks in gamma power and coherence were seen on both correct (rewarded) and error (unrewarded) trials, with a peak in gamma power and gamma coherence seen upon arrival at the reward site despite an absence of sucrose solution. However, even on error trials rats appeared to interact with the reward site, so the gamma peak could still be related to licking behaviour. Secondly, in Kalenscher et al. (2010) where rats came across three different reward types on a triangular track, gamma-50 and gamma-80 power were modulated by the type of reward. As outward behaviour was the same at all reward sites, they suggested gamma power is related to reward-processing. Together, these observations suggest that gamma modulation is at least in part related to reward processes. In order to definitively isolate reward anticipation and reward consumption, a task involving unexpected reward could be used. Additionally, introducing a short 2 second delay between reward site arrival and reward delivery could help parse out these causes, such as in Howe et al. (2011).

4.4.4.2 Gamma power on error trials

The profile of gamma power following error trials is significantly different from correct trials. It appears the moment the rat detects a lack of reward, gamma power

drops to a lesser extent than when reward is present. Whether this reflects a reward-processing related signal, such as a prediction error type signal, or even some kind of regret (Steiner and Redish, 2014), or instead is related to differences in motor behaviour is unclear. Of course, outward behaviour following reward site arrival on a correct trial will differ from an error trial, in that rats lick the reward site for longer when there is reward present. However, rats also appeared to interact the reward site on error trials. While only a trend, the differential response to errors in infralimbic and NAc Shell gamma power seen in *Cyfip1*$^{+/-}$ rats could reflect an abnormal prediction error signal, which could lead to disrupted reward learning and would support an aberrant reward processing system in *Cyfip1*$^{+/-}$ rats.

4.4.4.3 Origin of reward-related gamma

The origin of the prominent reward-related gamma in NAc has been much-debated and investigated (Berke, 2009; Carmichael et al., 2017; Donnelly et al., 2014; van der Meer and Redish, 2009a). In particular, it is possible that volume conduction from the nearby piriform cortex could account for the gamma power observed in NAc, hippocampus and prelimbic (Carmichael et al., 2017). By obstructing olfactory input, Carmichael et al. demonstrated significant reductions in gamma-50 and gamma-80 bands in the NAc, although it appears from the figures that gamma-80 is not abolished in one subject. They also observed a consistent power gradient as recording distance from piriform cortex increases, and current source density analysis found no indication of sink-source gradients that would be indicative of local generation. However, a number of observations suggest at least part of the gamma oscillation is related to reward-processing.

As before, the consistent peak in gamma power/coherence seen in my data on error trials even when reward is absent, would suggest it is not an olfaction related phenomenon, given that there was nothing to smell at the reward site on error trials. However, there are some indications that gamma activity may be related to sniffing behaviour (Kay, 2003), which likely still occurs on error trials. Also, I cannot rule out that there are no residual olfactory cues on error trials, as I did not wipe the reward wells between trials.

Others have found gamma-locked spiking activity, suggesting that gamma oscillations are relevant to NAc processing, even if some component of the observed gamma is volume conducted. In fact, LFP traces with reward-related gamma had more unit phase-locking than LFPs that did not show gamma modulation around reward (Kalenscher et al., 2010). The suggestion that gamma oscillations could be locally generated comes from observation that the intrinsic membrane properties of striatal fast spiking interneurons show prominent subthreshold oscillations around 50 Hz (Bracci et al., 2003). Although, locally generated gamma is typically an output of recurrent excitatory-inhibitory loops (Fries et al., 2007). Alternatively, inputs from other brain regions that are known to generate gamma, such as mPFC, hippocampus or thalamus, could be the source of local NAc gamma. Kalenscher et al. (2010) noted regional differences in gamma activity within the NAc, which also argues against a common, volume-conducted source.

Finally, there is evidence that reward-related gamma in NAc changes throughout learning (Howe et al., 2011; van der Meer and Redish, 2009a), which would not necessarily be expected if the gamma reflected purely a sensory input.

4.4.5 NOL task

A pilot experiment used the NOL task to address any consequences of reduced hippocampal-NAc coherence on behavioural performance, given the known dependence of this task on NAc Shell dopamine signalling (Nelson et al., 2010), hippocampus (Barker et al., 2007) and other studies demonstrating the importance of the hippocampal-NAc interaction in spatial tasks (Floresco and Phillips, 1999; Ito et al., 2008). I hypothesised that the possible disruption of NAc dopamine signalling due to impaired vHPC-NAc Shell coherence could lead to a deficit in this task (Nelson et al., 2010). In addition, novelty itself has been suggested to be rewarding (Bevins, 2001; Bevins and Besheer, 2005; Bevins et al., 2002), so a general reward-related behaviour deficit might also be detected with this task. The results of this task, however, were inconclusive due to low n numbers. WT animals discriminated the novel location object significantly, while *Cyfip1*$^{+/-}$ rats did not,

but a group difference was not statistically significant. Nevertheless, this result prompts further behavioural investigation in a larger cohort.

4.4.6 Conclusions and future directions

This chapter explored the hypothesis that *Cyfip1* haploinsufficiency leads to long-range connectivity changes in the NAc network. The results suggest that both hippocampal-accumbal and cortical-accumbal networks are affected, with the former less coherent and the latter more coherent, perhaps reflecting their relative influence on the function of the NAc. It would be important to assess the impact of these network changes on dopamine signalling in the NAc, perhaps with voltammetry recordings. The T maze task provided an initial context to examine these networks, but a behavioural manifestation is more likely to be seen in tasks designed specifically to probe these network deficits. For example, the simple place-preference conditioning task that was shown to be disrupted by vHPC-NAc Shell lesion (Ito et al., 2008) would be a good place to start. Reward processing is such a central component of many behaviours that even subtle changes in the activity of the NAc, such as those observed in this chapter, could have dramatic effects on behaviour and symptoms over the lifetime of patients.

5

Chapter 5 A double-hit: assessing the sensitivity of *Cyfip1*$^{+/-}$ rats to ketamine

This chapter reports on the effects of acute, systemic S(+)-ketamine on behaviour and neural oscillations. The main findings were that ketamine induces greater power high frequency oscillations and increases hippocampal theta-gamma coupling more in *Cyfip1*$^{+/-}$ rats than in WT littermates.

5.1 Introduction

The ability of NMDA receptor (NMDAR) antagonists to elicit behavioural effects that partially mimic positive (e.g. hallucinations and paranoia), negative (e.g. blunted affect, emotional withdrawal) and cognitive symptoms (e.g. conceptual disorganisation, abstract thinking, poor attention and recall) of schizophrenia in healthy humans and exacerbate positive symptoms in patients (Adler et al., 1999; Krystal et al., 1994; Lahti et al., 1995; Luby et al., 1959; Malhotra et al., 1997) contributed to the hypothesis that dysregulation of NMDAR mediated neurotransmission might underlie some of the symptoms of schizophrenia (Javitt and Zukin, 1991; Olney et al., 1999). Importantly, unlike amphetamine-induced symptoms, NMDAR antagonists, such as ketamine and PCP, also elicit cognitive disruption similar to that seen in schizophrenia, such as conceptual disorganisation, abstract thinking and poor attention, alongside positive symptoms (Krystal et al., 2005). In rodents, NMDA antagonists lead to hyperlocomotion, stereotypic

behaviours such as staggering, abnormal social interaction and impaired cognitive function (Abi-Saab et al., 1998; Asif-Malik et al., 2017; Becker et al., 2003; Mansbach, 1991; Sams-Dodd, 1995). Together, the human and allied animal model findings led to the development of the influential 'glutamate hypofunction' theory of schizophrenia in the late 1980s (Javitt, 1987).

Ketamine is an example of a non-competitive antagonist acting primarily on NMDARs (Anis et al., 1983) (although it is not specific to these receptors, also acting on a number of other brain receptors including D_2 receptors, 5-HT_2 receptors and HCN1 channels (Chen et al., 2009; Kapur and Seeman, 2002)). NMDARs play a crucial role in synaptic plasticity and in inhibitory interneuron activity (Lüscher and Malenka, 2012; Malenka, 1994). In addition to the psychopharmacology studies noted above NMDARs have been implicated in schizophrenia from post-mortem studies finding altered NMDAR mRNA levels (Bitanihirwe et al., 2009; Woo et al., 2004), with a recent meta-analysis confirming decreased expression of GluN1 in prefrontal cortex in schizophrenia (Catts et al., 2016). Furthermore, and indicative of a likely causal relevance, genetic studies have highlighted that DNA variants in schizophrenia patients are enriched for genes coding for proteins in NMDAR signalling pathways, supporting the contribution of NMDARs in the pathophysiology of the disorder (Fromer et al., 2014; Pocklington et al., 2015; Purcell et al., 2014; Ripke et al., 2014).

The glutamate hypofunction theory of schizophrenia has become influential, in part, due to the plausible interactions with other neurotransmitter systems implicated in schizophrenia, such as reduced GABAergic transmission and aberrant dopamine signalling (Lisman et al., 2008). NMDARs contribute significantly to excitatory post-synaptic potentials in GABAergic interneurons, and blocking these receptors reduces the inhibitory output (Grunze et al., 1996). Thus, one net effect of NMDAR antagonism can be disinhibition of pyramidal cells (Homayoun and Moghaddam, 2007). Of particular relevance to schizophrenia, it has been suggested that through disinhibition of hippocampal neurons projecting to dopaminergic neurons in the ventral tegmental area, NMDAR hypofunction can lead to maladaptive dopamine

release (Lisman et al., 2008; Pawlowski et al., 1990). Indeed, a recent meta-analysis showed that acute ketamine increases firing of ventral tegmental area dopamine neurons leading to increased dopamine levels in the striatum, nucleus accumbens (NAc) and frontal cortex in rodents, with a substantial effect size (Kokkinou et al., 2018).

A number of animal models involving NMDAR antagonism have been developed, including acute administration of a range of NMDA antagonists with different specificities and doses, subchronic dosing regimens, and postnatal administration to add a neurodevelopmental element (Gilmour et al., 2012). The most well-studied experimental scenario is in relation to the acute administration, which is the model used in the experiments described in this chapter.

In very recent times ketamine has also emerged as a potential treatment for major depressive disorder (Zarate and Machado-Vieira, 2017). While the exact mechanism is as yet unknown, suggested routes include via regulation of AMPA receptors (Zanos et al., 2016) or via disinhibition of dopaminergic neurons (Belujon and Grace, 2014). In addition, post-mortem studies have found reductions in spine density in major depressive disorder (Kang et al., 2012; Penzes et al., 2011), and systemic ketamine has been shown to increase dendritic spine density in the mPFC by activating the mammalian target of rapamycin (mTOR) pathway (Li et al., 2010; Ruddy et al., 2015).

5.1.1 Ketamine affects neural oscillations

Subanaesthetic doses of ketamine and other NMDAR antagonists have been shown to evoke abnormal neural oscillations in humans, non-human primates and rodents (Goonawardena et al., 2016; Hong et al., 2010; Hunt and Kasicki, 2013; Muthukumaraswamy et al., 2015; Pinault, 2008; Rivolta et al., 2015; Shaw et al., 2015). While there are numerous findings of changes in gamma oscillations in both directions, a picture is emerging whereby the direction of change depends on brain state, measurement of spontaneous or evoked oscillations and chronic or acute treatment (McNally and McCarley, 2016). In this chapter I focus on the acute

effects of ketamine, and this has consistently been reported to enhance gamma oscillations in several cortical and subcortical brain regions, including NAc, prelimbic cortex (PRL) and hippocampus (Hunt et al., 2011; Kittelberger et al., 2012; Phillips et al., 2012b), and this has been shown to be dissociable from hyperlocomotion (Hakami et al., 2009; Páleníček et al., 2011). Similar increases in gamma power have also been seen in humans and monkeys in resting conditions (Goonawardena et al., 2016; Hong et al., 2010; Rivolta et al., 2015).

Further to the gamma power changes, augmented high frequency oscillations (130-180 Hz, HFOs) are evoked by acute ketamine in several regions, including PRL and hippocampus and most strikingly in the NAc (Hunt et al., 2011; Nicolás et al., 2011; Olszewski et al., 2013a). The mechanism of HFO generation is unclear (Lee et al., 2017; Olszewski et al., 2013a), although some evidence points to their origin in the NAc with passive spread to other regions which are not reciprocally connected to NAc yet still show coherent HFOs (Hunt et al., 2011). Evidence supporting a role for HFOs in schizophrenia symptoms comes from findings in animal studies that the antipsychotic agent clozapine can modulate the generation of HFOs in the NAc (Hunt et al., 2015; Olszewski et al., 2013b). HFO oscillations are also known to exist in the human brain having been identified using MEG and electrocorticography (ECoG) methods and linked to cognitive functions (Canolty et al., 2006). One study recorded HFO using deep electrodes in human NAc in major depression patients treated with deep brain stimulation (Cohen et al., 2009a). A study observing auditory evoked potentials following ketamine in healthy participants found an increase in cortical gamma power, but not in HFO band; however; abnormalities in HFO of schizophrenia patients have not been reported thus far.

Further to the changes in gamma and HFOs, NMDAR antagonists including ketamine can also distort normal oscillatory interactions as measured by phase-amplitude coupling (PAC) (Caixeta et al., 2013; Cordon et al., 2015; Michaels et al., 2018; Neymotin et al., 2011). In the rat hippocampus, Caixeta et al. (2013) found that theta-gamma coupling was affected in a dose-dependent manner, with

increased coupling at a 25mg/kg dose and decreased coupling at a 75mg/kg dose of ketamine but theta-HFO coupling was increased at all doses, while Michaels et al. (2018) saw increased hippocampal PAC at slower speeds on a rectangular track, and reduced PAC at faster running speeds.

Parvalbumin (PV) interneurons are known to be critical in the generation of gamma oscillations, demonstrated by their optogenetic activation and silencing leading to amplification and suppression of cortical gamma oscillations, respectively (Cardin et al., 2009; Sohal et al., 2009). Indeed, PV interneuron abnormalities have been linked to schizophrenia symptoms (Akbarian et al., 1995; Lewis et al., 2005), for example by reduced PV expression post mortem in the dorsolateral PFC and abnormal gamma oscillations in patients (Gonzalez-Burgos et al., 2015; Lisman et al., 2008). However, the precise mechanisms mediating ketamine-induced changes in gamma power are unclear. As mentioned above, emerging evidence suggests the disruption of NMDAR signalling on PV interneurons is critical. For example, specific ablation of NMDAR on PV interneurons leads to increased gamma activity and disrupts the gamma-inducing and behavioural effects of ketamine in these mice (Carlén et al., 2012; Korotkova et al., 2010). Homayoun & Moghaddam (2007) found that NMDAR antagonism preferentially decreases the activity of GABA interneurons and increases activity of pyramidal cells, causing cortical excitation by the disinhibition of pyramidal neurons. This specificity of action might occur if interneurons are more sensitive to the effects of ketamine via the NR2A subunit, which is more highly expressed on interneurons than pyramidal cells (Xi et al., 2009) although other subunits have also been implicated (Sapkota et al., 2016). As mentioned, ketamine also induces HFOs; however the mechanism of HFO generation is unknown. Similar frequencies have been recorded in cerebellar slice recordings, where 80-160 Hz oscillations were independent of synaptic connections, implicating the involvement of gap junctions (Middleton et al., 2008).

5.1.2 Double-hit models

Animal models related to CNV syndromes often show subtle phenotypes which may be exacerbated by an acute injection of ketamine. This can be viewed as an

additional liability, as it disrupts the NMDAR signalling known to be affected in schizophrenia. This 'double-hit' approach has been used in a handful of schizophrenia relevant models to date (Didriksen et al., 2017; Fejgin et al., 2014; Goda et al., 2015; Ji et al., 2013; Jones et al., 2017; Kocsis, 2012; Nielsen et al., 2017; Phillips et al., 2012b), including other deleterious CNV models. A novel mouse model for 22q11.2 deletion syndrome, *Df(h22q11)*$^{/+}$, displayed enhanced ketamine- and PCP-induced hyperlocomotion (Didriksen et al., 2017). Low-frequency cortical oscillations were unaffected, and while high frequency oscillations were not reported in this study, a conference abstract from one of the authors shows preliminary evidence for enhanced sensitivity to PCP/ketamine, especially in beta, gamma and HFO ranges (Lladó-Pelfort et al., 2014). In this model, there is no obvious mechanistic link of how these changes might be mediated. In contrast, another CNV lesion model (1q21.1) investigating the consequences of a ketamine/PCP challenge on hyperlocomotion did not find a difference to WT (Nielsen et al., 2017), although mutant mice were more sensitive to PCP-induced disruptions to pre-pulse inhibition (Nielsen et al., 2017), a commonly used schizophrenia-related behavioural assay to measure sensory gating, a low level form of attention. A further mouse model, for the 15q13.3 deletion, was tested for PCP-induced PPI disruption, but was no different to WTs (Fejgin et al., 2014).

Non-genetic neurodevelopmental models have also adopted this approach (Goda et al., 2015; Phillips et al., 2012b; Tagliabue et al., 2017). For example, the methyl-azoxymethanol acetate (MAM) treated neurodevelopmental model of schizophrenia showed a blunted ketamine-induced increase in gamma oscillations in the visual cortex but not in the motor cortex, which was paralleled with reductions in PV interneurons exclusively in the visual cortex (Phillips et al., 2012b). This model also showed greater sensitivity to ketamine in the HFO range, where the ketamine-induced HFO increase was enhanced in MAM animals. Another study explored the effects MK801 in a rat with neonatal tetrodotoxin inactivation of the prefrontal cortex, a neurodevelopmental model for disrupted cortical development linked to schizophrenia (Tagliabue et al., 2017). They found

augmented MK801-induced hyperlocomotion and increased dopamine release in the NAc compared to non-lesioned rats.

These studies highlight the use of NMDA-antagonist challenge as an assessment of the face, and to an extent construct, validity of schizophrenia models, even where mechanistic links are as yet not fully known. In line with this, I decided to investigate the consequences of ketamine challenge on hyperlocomotion and neural oscillations in the *Cyfip1*$^{+/-}$ rat model. The presence of Cyfip1 in GABAergic cells (albeit much less than in excitatory cells (Pathania et al., 2014)), together with findings that *Cyfip1* haploinsufficiency can block NMDAR dependent spine remodelling (Pathania et al., 2014) hint that Cyfip1 function may affect the mechanisms thought to be responsible for ketamine's effects. Furthermore, electrophysiological and molecular studies have identified deficits in the GABAergic system in *Fmr1* knockout models of Fragile X syndrome (Nomura et al., 2017; Paluszkiewicz et al., 2011). In line with a focus on gamma and HFO in the literature (Hunt et al., 2011; Kittelberger et al., 2012; Phillips et al., 2012b), I will primarily explore these frequency bands in cortical and subcortical brain regions. In addition, following the abnormalities in hippocampal theta-gamma PAC observed in Chapter 3, I will investigate any interaction of *Cyfip1* haploinsufficiency with ketamine on this phenotype.

5.1.3 Chapter Aims

This chapter investigates the consequences of an acute ketamine challenge on locomotor activity and electrophysiological signals in the PRL, hippocampus and NAc of the *Cyfip1*$^{+/-}$ rat.

Key hypothesis:

- *Cyfip1*$^{+/-}$ rats have a heightened sensitivity to the effects of ketamine as measured by locomotor activity and neural oscillations in the PRL, hippocampus and NAc.

5.2 Methods

5.2.1 Ketamine

S(+)-Ketamine (Sigma) was diluted in 0.9% saline to create a 10 mg/ml concentration solution, administered in a volume of 1 ml/kg to achieve a 10mg/kg dose. All recordings took place in the home cage within the sleep box (for further details on electrophysiological recording set up see Chapter 2). Following a 20 minute baseline period, ketamine or saline was administered intraperitoneally, the timestamp was recorded, and video and electrophysiology recording continued for another 80 minutes.

5.2.2 Locomotor activity

Movement was detected from the video recording, where after splitting each video into 1 second frames, the number of pixels varying from one frame to the next by more than 25 greyscale values was calculated. Movement activity data were log transformed to normalise the data and averaged over a series of bins where time 0 is the injection time: -20 min to 0, 0 to 10 min, 10 to 30 min, 30 to 50 min. A three-way repeated-measures ANOVA (genotype as between-subjects factor, time bin and treatment as within-subjects factor) was used, with Bonferroni-corrected post-hoc comparisons and t-tests.

5.2.3 Electrophysiology data analysis

5.2.3.1 Pre and post injection segment selection

One minute-long segments were compared pre- and post-injection. For the initial analyses presented here, a single post-injection timepoint was analysed. Pre-injection windows and post-vehicle injection windows often contained periods of quiet rest during which 16 Hz spike wave discharges (SWDs) dominated the signal, commonly seen in quietly resting animals (Kelly, 2004; Shaw, 2004). While the frequency ranges of interest (gamma and HFO) were unlikely to be affected by these 16 Hz oscillations, taking segments where these were not present increases the likelihood that behavioural state is similar across all compared segments, i.e. not quietly resting. To capture segments without high amplitude SWDs, a variation of the spindle detection algorithm (see Chapter 2) was used to identify epochs

containing SWDs. A 2 minute window immediately surrounding the injection timestamp was excluded from the analyses to eliminate artefacts that occurred during handling. For the pre-injection window, a series of one minute segments were assessed for presence of SWDs, moving in 10 s steps away from the injection timestamp. The first segment without SWDs was chosen as the baseline segment, and this fell within a 15 minute window prior to injection for all animals. For post-injection segments, a similar method was used, but the range of possible windows was limited to 6 minutes in order to capture a similar timepoint in all animals.

5.2.3.2 Power analyses

Power spectra were generated from the pre and post segments for each animal as described in Chapter 2. Subsequent group analyses were based on the percent change from baseline power. As such, it was not necessary to normalise individual power spectra. For these 1 minute windows, parameters were set as follows: bandwidth = 2 Hz, window = 3 s, constant = 3, providing nine tapers for multi-taper spectral estimates. Spectrograms were produced for the whole 100 minute recording and parameters were set as follows: bandwidth = 2 Hz, window = 6 s, constant = 13, providing eleven tapers. Power changes in gamma (55-90 Hz) and HFO (130-180 Hz) frequency bands were analysed with a two-way ANOVA.

5.2.3.3 PAC

PAC was calculated as described in Chapter 2 for the same one minute segments described above.

5.3 Results

An acute 10 mg/kg dose of ketamine or saline was administered to 14 WT and 13 *Cyfip1*$^{+/-}$ rats in a counterbalanced crossover design, such that all animals received both injections, with a minimum 5 day washout period.

5.3.1 Normal response in *Cyfip1*$^{+/-}$ rats to the locomotor effects of ketamine

Both WT and *Cyfip1*$^{+/-}$ rats showed a significant increase in locomotor activity, reaching a peak around 1-3 minutes post-injection, a timecourse for lomocotor

activity that is similar to that seen by others at this dose (Nicolás et al., 2011; Phillips et al., 2012b) (median WT: 89s, median Cyfip1: 150 s, Mann-Whitney U Test, p = 0.054) (Figure 5.1a). Analysing over 4 time bins, there was a significant treatment x time interaction ($F_{3,75}$ = 11.1, p < 0.001), although there was no treatment x time x genotype interaction ($F_{3,75}$ = 1.07, p = 0.34) or genotype effect ($F_{1,75}$ = 0.32, p = 0.58) suggesting the sensitivity of *Cyfip1*$^{+/-}$ rats to the locomotor effects of ketamine and the pharmacodynamic profile is normal (Figure 5.1b). Bonferroni pairwise comparisons showed that activity collapsed over genotypes in time bin 2 was significantly greater than all other time bins (p < 0.001), time bin 3 was not different from pre-injection (bin 1) and time bin 4 was significantly lower than all other bins (p<0.001). Bonferroni-corrected comparisons of the ketamine data between genotypes did not pass the adjusted alpha level of significance (α = 0.05/4) at any time point. Comparing total post-injection activity confirmed the increased locomotor effect of ketamine (treatment main effect: $F_{1,25}$ = 22.57, p < 0.001), but the treatment x genotype interaction did not reach significance ($F_{1,25}$= 3.51, p = 0.072) and there was no genotype main effect ($F_{1,25}$ = 1.68, p = 0.21) (Figure 5.1c).

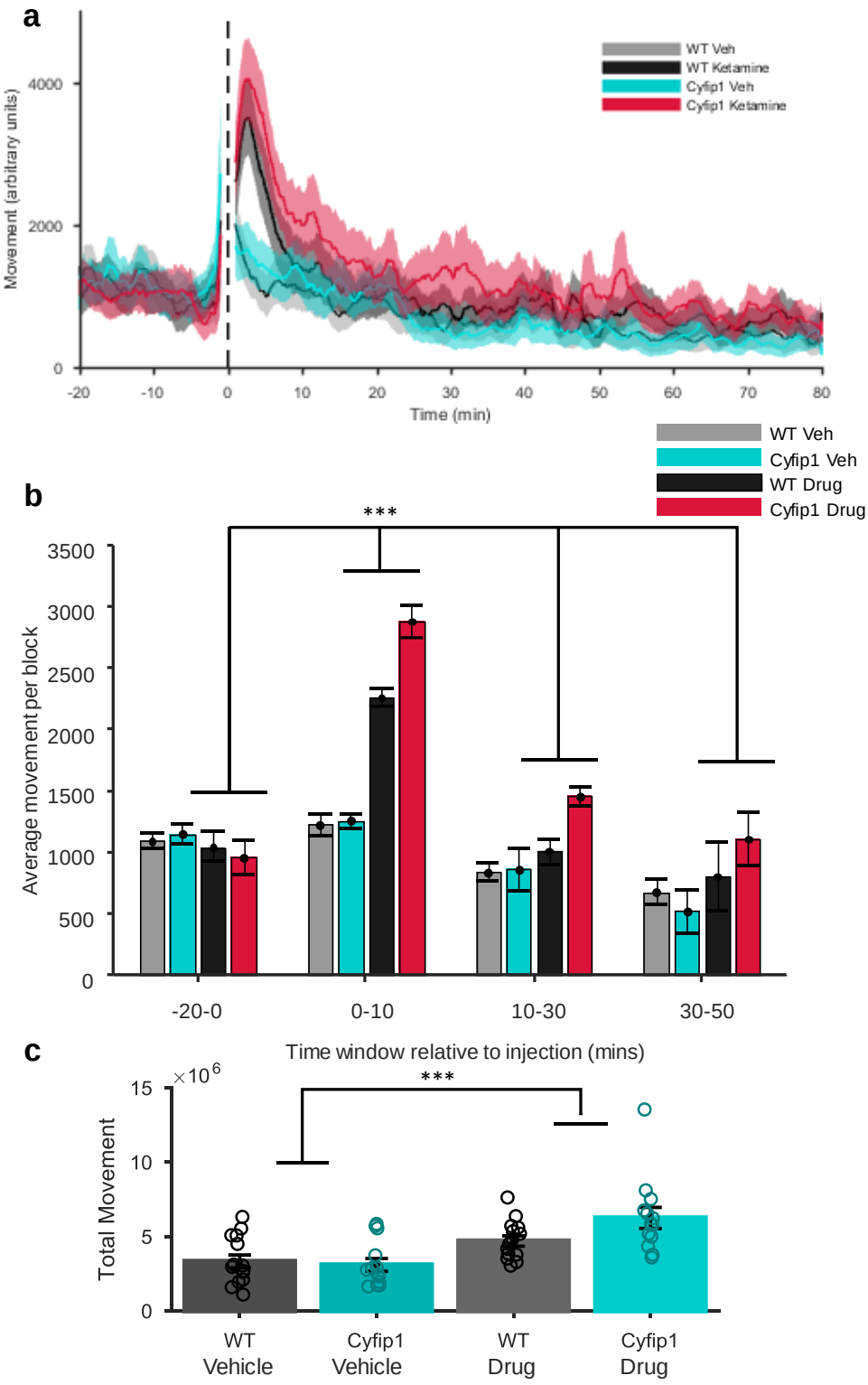

Figure 5.1 | **Locomotor activity following ketamine. a,** Group averaged movement data extracted from video recording shows increased locomotor activity following ketamine injection (dashed black line at 0). A two minute window was removed surrounding the injection to remove artefacts. **b,** Movement in the 0-10 time window was significantly

greater than all the other windows, ***p<0.001. Bonferroni-corrected t-tests found *Cyfip1*$^{+/-}$ Drug and WT Drug movement was not significantly different. Veh = Vehicle injection. **c,** Total post-injection movement counts (arbitrary units) in vehicle and drug conditions. ***p<0.001 for main effect of treatment. WT: n = 14, *Cyfip1*$^{+/-}$: n = 13.

5.3.2 Gamma and high frequency oscillations

The dose of ketamine used here has previously been shown to elicit increased gamma and HFOs (Hunt et al., 2006, 2011; Phillips et al., 2012b). Power changes were quantified by calculating a percent change from baseline power. One minute signal segments were selected (see Methods) from within a 15 minute window pre-injection, and from within a 6 minute post-injection window.

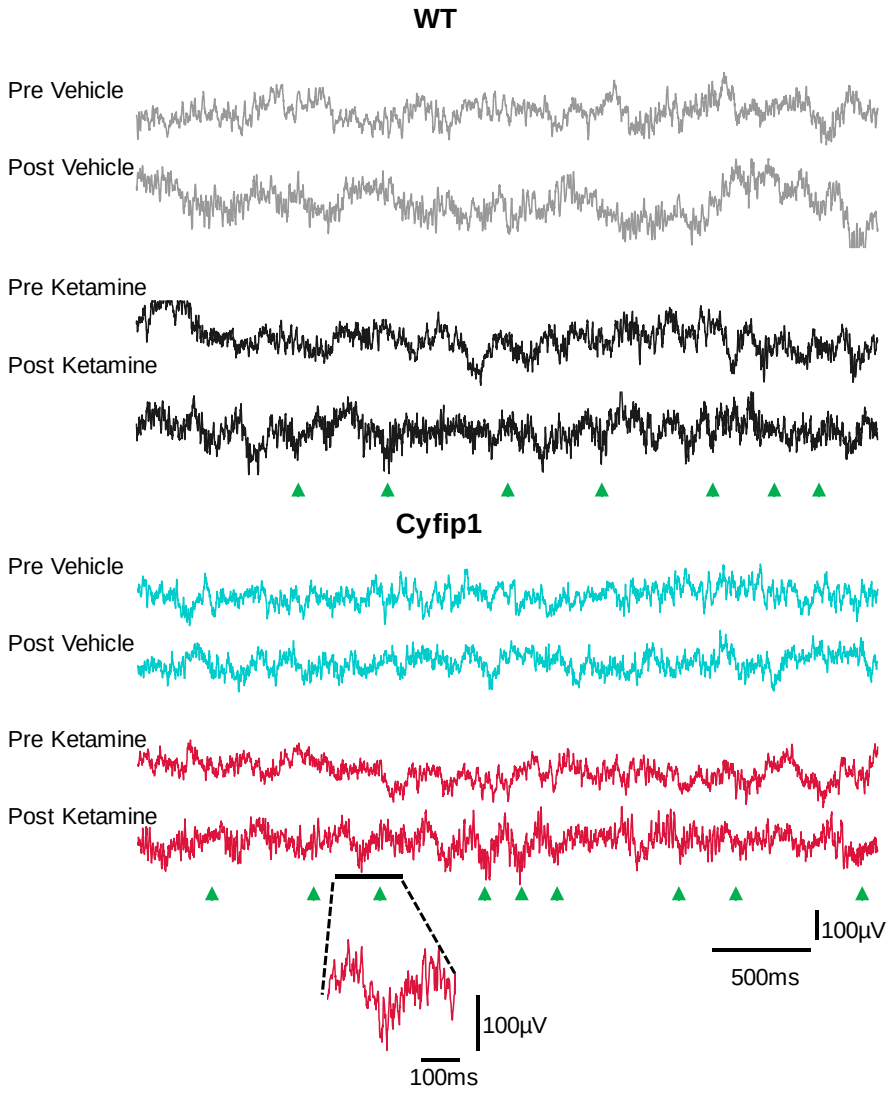

Figure 5.2 | **Representative raw traces from PRL**. Raw traces taken from the pre- and post-injection period in vehicle and ketamine injection sessions from one WT and one *Cyfip1*$^{+/-}$ rat, traces are 3.8 seconds long. Note the increase in gamma oscillation amplitudes in the post-ketamine injection segments, and more bursts of high frequency oscillations highlighted by green arrows. Bottom, an example of a high frequency burst in greater time resolution.

As previously reported, power changes were most striking in the gamma and HFO frequency bands (Hunt et al., 2006; Phillips et al., 2012b) (Figure 5.2). Example multi-taper spectrograms of power in NAc Core reveal clear increases in gamma power and HFO following ketamine injection (Figure 5.3). Ketamine injection led to a significant increase in gamma (55-90 Hz) power in PRL (drug effect: $F_{1,22}$ = 21.3, $p < 0.001$; 2 WT and 1 Cyfip1 outliers) NAc Core ($F_{1,24}$ = 15.9, $p = 0.001$; 2 WT and 1 Cyfip1 outliers), NAc Shell ($F_{1,24}$ = 11.6, $p = 0.002$; 1 WT outlier), vHPC

($F_{1,25}$ = 9.08, p = 0.006) and dCA1 ($F_{1,23}$ = 17.9, p < 0.001; following removal of 1 WT and 1 Cyfip1 outlier). There was no main effect of genotype (p > 0.05) or interaction (p > 0.05) in any brain region, suggesting ketamine- induced gamma power was normal in *Cyfip1*$^{+/-}$ rats (Figure 5.4).

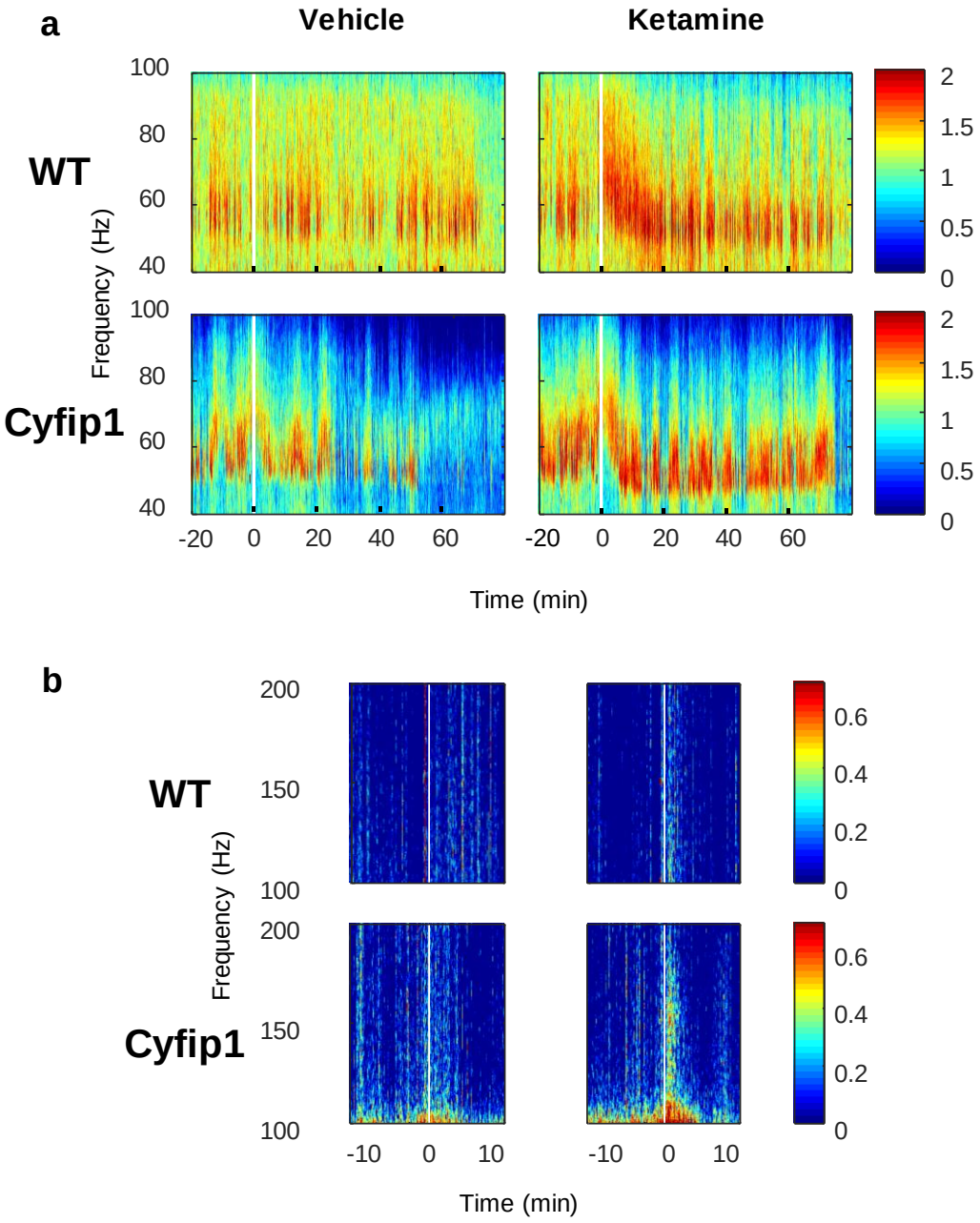

Figure 5.3 | **Representative spectrograms from the NAc core**. **a,** 40-100 Hz frequency range shows timecourse of gamma power following injection (white vertical line at injection time 0). Colour represents power (dB). **b,** High frequency oscillations (~150 Hz) shown on

a shorter timescale. Note the burst of high frequency power immediately following the ketamine injection in the *Cyfip1*$^{+/-}$ animal.

In contrast, HFO (130-180 Hz) in *Cyfip1*$^{+/-}$ rats were significantly more sensitive to ketamine (Figure 5.4). In PRL there was a significant genotype x treatment interaction ($F_{1,22}$ = 4.38, p = 0.048; 1 WT and 2 Cyfip1 outliers), but no main effect of genotype (p > 0.05) or treatment (p > 0.05), suggesting a crossover relationship. A significant interaction was present in both areas of NAc (Core: $F_{1,25}$ = 10.1, p = 0.032, Shell: $F_{1,25}$ = 19.7, p = 0.007), and genotype main effect was significant in the Shell ($F_{1,25}$ = 4.97, p = 0.035), but not the Core ($F_{1,25}$ = 2.15, p = 0.155). However, a Mann-Whitney U test comparing ketamine-induced HFO power showed a significant effect of genotype (Core: p = 0.033, Shell: p = 0.022). Dorsal CA1 showed a significant effect of ketamine on HFO power (treatment: $F_{1,22}$ = 4.54, p = 0.045; following removal of 1WT and 2 Cyfip1 outliers), but no genotype effect ($F_{1,22}$ = 0.12, p = 0.73) or interaction ($F_{1,22}$ = 3.27, p = 0.084). In contrast, vHPC HFO showed no significant effect of treatment ($F_{1,22}$ = 0.89, p = 0.36), genotype ($F_{1,22}$ = 0.47, p = 0.50) or interaction ($F_{1,22}$ = 1.07, p = 0.31; 1 WT and 2 Cyfip1 outliers). Unless stated, outliers did not affect the outcome of the statistical tests.

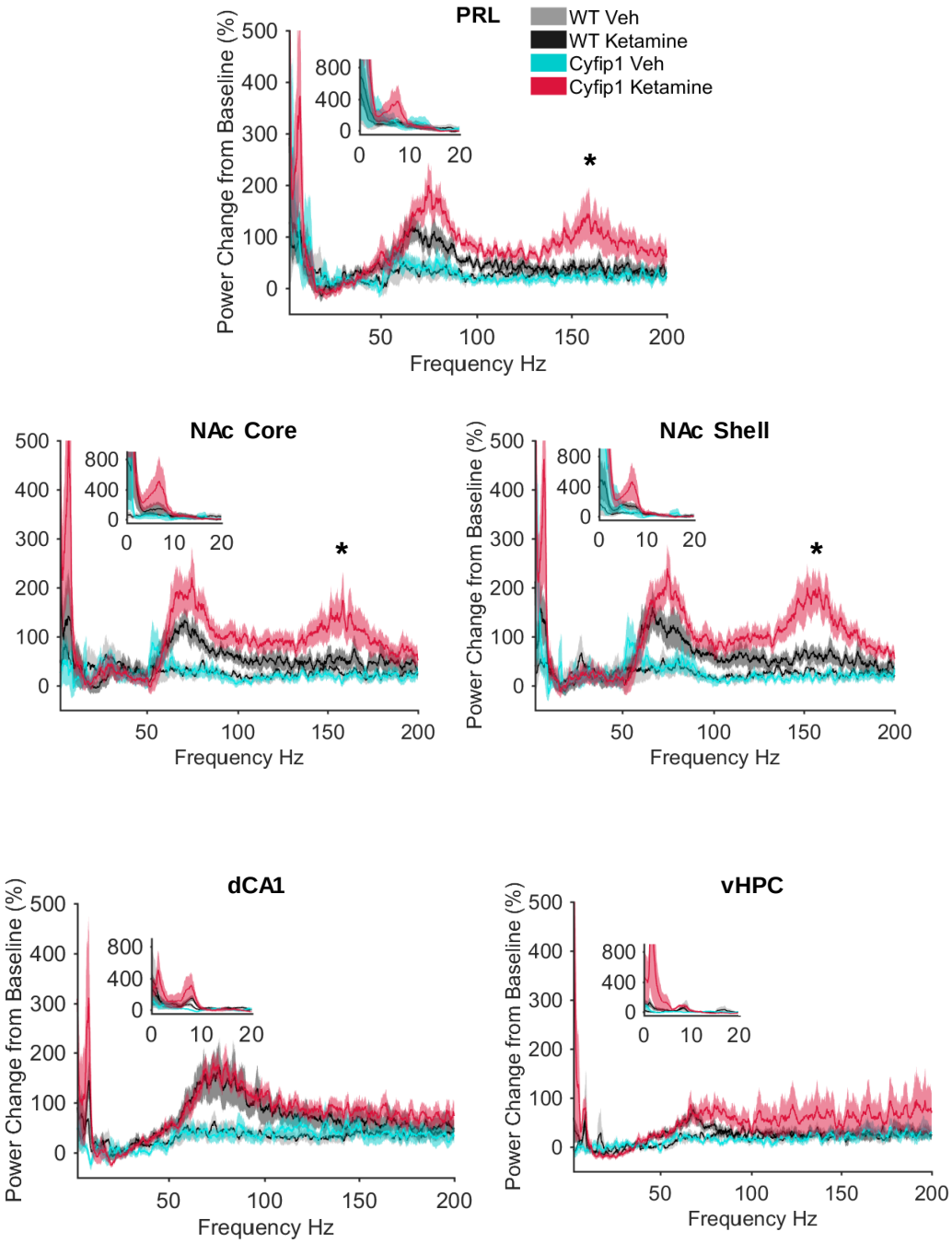

Figure 5.4 | **Power change spectra.** Spectral power changes are presented as a percentage change from pre-injection baseline. Inset are frequencies 0-20Hz. *p<0.05 for the genotype x treatment interaction. Veh = Vehicle injection. WT: n = 14, *Cyfip1*$^{+/-}$: n = 13.

The absence of a genotype effect on ketamine-induced hyperlocomotion suggests the enhanced HFOs seen in *Cyfip1*$^{+/-}$ rats are independent of movement, and this has been demonstrated by others (Hakami et al., 2009). Taken together, these data demonstrate similar power changes in gamma and HFO frequency bands to what

others have seen at this dose and highlight the heightened sensitivity of HFO-induction in the PRL and NAc of *Cyfip1*$^{+/-}$ rats following ketamine.

5.3.3 Phase-amplitude coupling

Given published findings of the effect of ketamine on hippocampal PAC (Caixeta et al., 2013; Michaels et al., 2018), and my observations of reduced theta-gamma coupling in *Cyfip1*$^{+/-}$ hippocampus (Chapter 3), I decided to explore the effect of ketamine on this phenomenon.

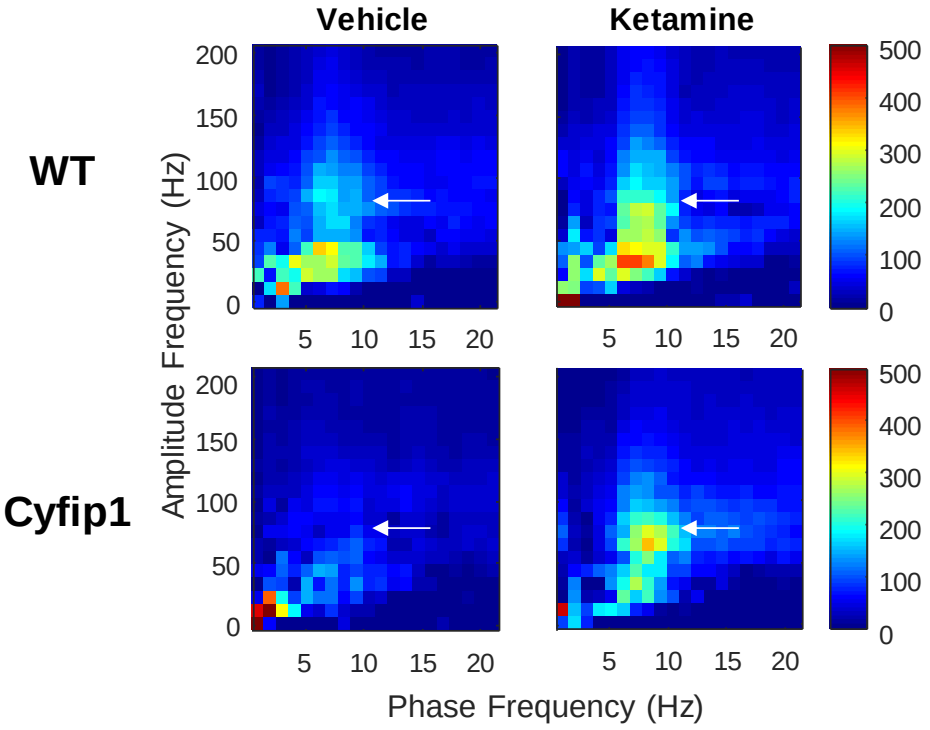

Figure 5.5 | **Hippocampal phase-amplitude coupling**. Group averaged comodulograms showing phase-amplitude coupling following a vehicle and following a ketamine injection. Arrows indicate theta-fast gamma region where genotype x ketamine interaction was significant (p = 0.032). WT: n = 14, *Cyfip1*$^{+/-}$: n = 13.

As described above, ketamine increased hippocampal gamma power in both WT and *Cyfip1*$^{+/-}$ animals and a similar outcome was seen for theta band oscillations, with a significant increase in dCA1 theta ($F_{1,23}$ = 1.53, p = 0.002; following removal of 2 Cyfip1 outliers). There was no main effect of genotype (p > 0.05) or interaction (p > 0.05). As in Chapter 3, gamma was divided into slow and fast bands for this

analysis. PAC data were log-transformed to bring the data within a normal distribution. Theta-slow gamma (25-60 Hz) PAC was similarly significantly increased by ketamine in both genotypes (drug effect: $F_{1,25}$ = 10.46, p = 0.003, genotype effect: $F_{1,25}$ = 0.004, p = 0.95, no interaction) (Figure 5.5). Theta-fast gamma (65-100 Hz) PAC showed a significant effect of ketamine ($F_{1,25}$ = 5.189, p = 0.032) and a significant genotype x ketamine interaction ($F_{1,25}$ = 4.612, p = 0.042), indicating a greater post-ketamine increase in PAC in *Cyfip1*$^{+/-}$ rats than in WTs. A Bonferroni-corrected Mann-Whitney U test showed that in the vehicle treatment, *Cyfip1*$^{+/-}$ PAC was significantly lower than in WT ($p<0.05$, following removal of 2 Cyfip1 outliers), with no difference in the drug condition ($p > 0.05$).

Theta-HFO (130-180 Hz) PAC, which is much weaker upon observation of the comodulograms, was also significantly increased by ketamine, but with no difference between genotypes (drug effect: $F_{1,25}$ = 9.88, p = 0.004, genotype effect: $F_{1,25}$ = 0.317, p = 0.58, no interaction).

5.4 Discussion

Results from this chapter show:

- Acute injection of 10mg/kg ketamine induces similar locomotor hyperactivity in both *Cyfip1*$^{+/-}$ rats and WTs.
- Ketamine leads to a similar increase in gamma power in PRL, hippocampus and NAc in both genotypes.
- Both genotypes show an increase in HFO oscillations following ketamine in PRL, NAc and dCA1, but this increase is augmented in *Cyfip1*$^{+/-}$ rats in PRL and NAc.
- Hippocampal theta-gamma PAC is increased by ketamine, and the increase is augmented in *Cyfip1*$^{+/-}$ rats for fast-gamma coupling.
- Hippocampal theta-HFO PAC is similarly increased by ketamine in both genotypes.

Thus *Cyfip1*$^{+/-}$ rats are hypersensitive to some effects of ketamine, notably the HFO-inducing and PAC strengthening effects. Since ketamine induced hyperlocomotion was not augmented in *Cyfip1*$^{+/-}$ rats, these effects are unlikely to be downstream of gross behavioural state changes caused by the drug. The overall effects observed here are largely in line with published findings. Hyperlocomotion is consistently found following acute sub-anaesthetic doses of NMDAR antagonists (Domino, 1964; Nicolás et al., 2011; Phillips et al., 2012b). A review of NMDAR antagonist effects on oscillatory activity in rodents found gamma to be consistently increased in cortex and hippocampus, with both increases and decreases seen in NAc (Hunt and Kasicki, 2013). In addition, EEG gamma power is increased in humans following ketamine administration (Hong et al., 2010). HFOs are consistently increased in multiple brain regions (Hunt and Kasicki, 2013; Hunt et al., 2006, 2011; Phillips et al., 2012b). In this study I found hippocampal theta power to increase following ketamine, but the literature has been mixed on this (Hunt and Kasicki, 2013), perhaps due to the close link between theta power and locomotion, which could change depending on dose.

As mentioned, a handful of studies with CNV animal models have explored the 'double-hit' model presented here, of a genetic risk coupled with an additional challenge of NMDAR antagonism. Of the two models that tested the effect of PCP/ketamine on hyperlocomotion, one found an augmented increase in mutants while the other did not (Didriksen et al., 2017; Nielsen et al., 2017). Of course, it would not necessarily be expected that these models all show a hypersensitivity to NMDAR antagonism-induced locomotion, as they each contribute to risk via different pathways, and not necessarily pathways that would lead to a similar hypersensitive phenotype. However, it is noteworthy that other models show a dissociation between effects on hyperlocomotion and other measures, as I have found here with the *Cyfip1*$^{+/-}$ rats: no effect on hyperlocomotion but enhanced ketamine-induced HFO and theta-gamma PAC compared to WT. Indeed, it has been argued that the hyperlocomotion phenotype is limited as a biomarker, as it does not map well onto the psychotic and cognitive phenotype seen in humans,

while electrophysiological markers may be more translatable (Phillips et al., 2012b).

Few double-hit models have investigated the impact of NMDAR antagonism on neural oscillations. Most notable are the experiments with the neurodevelopmental MAM model (Goda et al., 2015; Phillips et al., 2012b). Phillips et al. (2012) found that the same dose of ketamine as in the current study led to an augmented hyperactivity in the MAM rats, but a reduced increase in gamma power specifically in the visual cortex. This was linked to the finding that parvalbumin-positive interneuron density is reduced in the visual cortex but not in the motor cortex, where ketamine-induced gamma increase was normal. HFO, on the other hand, showed an augmented increase in MAM animals.

Goda et al. (2015) found slightly different results in the same model, although they recorded activity from the NAc *vs* cortical EEG in Phillips et al. (2012). Spontaneous HFO in the NAc was significantly increased in MAM rats, but this was not prominent in the cortical EEG recording. Unlike Phillips et al. (2012), they did not see a hyperlocomotion effect of MK801, nor an augmented increase of HFO. Instead they found a lack of MK801-induced increases in HFO frequency in MAM rats. Together, these findings indicate that an abnormal reaction to NMDAR antagonism has been observed in the MAM model, but with mixed findings between studies and across different brain regions. Again, as the contribution to risk in these models compared to the *Cyfip1*$^{+/-}$ rats is different, it would not be expected that their reaction to ketamine is necessarily identical. However, the two models have in common the finding of augmented HFO in cortical areas.

5.4.1 PAC

Theta-gamma and theta-HFO PAC was increased following ketamine, which is in line with the emerging literature indicating this effect of NMDAR antagonism (Caixeta et al., 2013; Cordon et al., 2015; Michaels et al., 2018). Caixeta et al. (2013) analysed PAC in the hippocampus and saw increased theta-fast gamma PAC at a 25mg/kg dose, and also increased theta-HFO PAC. However, the theta-HFO

coupling appeared much stronger here than in my results, where no clear hotspot for theta-HFO coupling is seen. Nevertheless, the basic pattern of ketamine-induced increase in theta-HFO coupling was present.

Interestingly, Michaels et al. (2018) found that the direction of change in PAC strength was modulated by running speed. They recorded hippocampal activity while animals ran laps on a rectangular track, and divided analyses into slow (<15cm/s) and fast (37-87cm/s) speeds. They found theta-fast gamma coupling increased following ketamine (30mg/kg) at slow speeds but decreased at fast speeds. This broadly aligns with my findings as it is unlikely my animals reached these fast speeds within their home cage. However, as LEDs were not tracked, and instead movement data were extracted from the video, it is not possible to ascertain this from the present dataset.

Theta-gamma PAC was increased more in *Cyfip1*$^{+/-}$ rats following ketamine than in WTs. Whereas in Chapter 3, theta-fast gamma PAC did not reach significance for being lower in *Cyfip1*$^{+/-}$ rats (only theta slow-gamma PAC did), in this experiment theta-fast gamma PAC in the vehicle condition was significantly lower in *Cyfip1*$^{+/-}$ rats and thus increased to be a similar level to WT following ketamine. This difference may be due to the different analysis windows used (multiple trials *vs* a 1 minute window) or different behavioural context (running on the maze *vs* in the homecage after an injection).

Increased theta-gamma coupling is associated with cognitive functions such as working memory (Lisman and Jensen, 2013; Montgomery and Buzsáki, 2007). Since NMDAR antagonism disrupts cognitive functions (Cadinu et al., 2018), the finding of increased theta-gamma PAC is somewhat difficult to interpret. However, an abnormally high level of PAC coupled with the increases in oscillatory power at theta, gamma and HFO together are likely to reflect an aberrant brain state, in which the dynamic information processing required for cognition is compromised.

5.4.2 Possible mechanisms leading to hypersensitivity to ketamine

It is currently unclear how *Cyfip1* haploinsufficiency could lead to enhanced HFO in prefrontal cortex and accumbens. The mechanism of HFO generation is also unknown, limiting the extent to which I can speculate on the role of *Cyfip1* low dosage. Given that several NMDAR antagonists have shown induced HFO (Phillips et al., 2012b), it is likely that HFO generation is linked to NMDARs. *Cyfip1* haploinsufficiency prevents spine remodelling downstream of NMDARs (Pathania et al., 2014), which provides evidence that other NMDAR-dependent pathways are affected by Cyfip1, which could mean that HFO generation could also be affected. It is possible that HFO, like gamma oscillations (Carlén et al., 2012), are also due predominantly to NMDARs on GABAergic interneurons. In this case, the low levels of Cyfip1 in GABAergic neurons (Pathania et al., 2014) may play a role. The GABAergic system is yet to be investigated in *Cyfip1* haploinsufficiency models, but deficits in the GABAergic system have been highlighted in *Fmr1* knockout models of Fragile X syndrome (Contractor et al., 2015; Nomura et al., 2017; Paluszkiewicz et al., 2011).

Of the several schizophrenia-relevant models that have been shown to have a heightened sensitivity to the effects of NMDAR antagonism on brain oscillations and hyperlocomotion (Didriksen et al., 2017; Goda et al., 2015; Ji et al., 2013; Jones et al., 2017; Kocsis, 2012; Nielsen et al., 2017; Phillips et al., 2012b), one model was able to demonstrate clear changes in NMDAR and interneurons that might mediate the heightened sensitivity. Mice carrying mutations in *Sp4*, a gene encoding a transcription factor, showed hyperlocomotion and enhanced gamma power in response to ketamine (Ji et al., 2013). This was thought to be mediated via the reduced NMDAR1 expression and down-regulated GAD67 protein also seen in *Sp4* mice, an enzyme important in GABA synthesis.

5.4.3 Conclusions and future directions

In this chapter I assessed whether *Cyfip1*$^{+/-}$ rats showed a heightened sensitivity to NMDAR antagonism by ketamine. It appears this is the case for some of the effects of ketamine, such as induced HFO and theta-gamma PAC, but not for others, such

as hyperlocomotion and enhanced gamma power. It is difficult to derive mechanistic insight from HFO, as their mechanism of generation is currently unknown. However, finding reduced theta-gamma PAC within the hippocampus in a different behavioural context extends the previous findings in Chapter 3, and the ketamine-induced augmented increase in PAC strength supports a hippocampal abnormality in *Cyfip1*$^{+/-}$ rats.

Emerging evidence suggests that ketamine can disrupt interactions between brain regions, such as cortico-cortico (Páleníček et al., 2011), hippocampal-cortical (Gass et al., 2014; Moran et al., 2015), and cortico-accumbal networks (Asif-Malik et al., 2017). For example, while hippocampal-prefrontal interactions were normal under baseline conditions in *Cyfip1*$^{+/-}$ rats (Chapter 3), it is possible that this network would show a heightened sensitivity following ketamine challenge.

6

Chapter 6 Circadian activity patterns and sleep neurophysiology in *Cyfip1*$^{+/-}$ rats

This chapter describes two studies investigating sleep patterns and sleep-dependent network activity in *Cyfip1*$^{+/-}$ rats. Infrared sensor-based actigraphy monitoring showed that *Cyfip1*$^{+/-}$ rats have normal circadian sleep and activity patterns. *In vivo* electrophysiology recordings during sleep revealed abnormal hippocampal ripples in *Cyfip1*$^{+/-}$ rats.

6.1 Introduction

6.1.1 Why study sleep?

Most – if not all – animals need some form of sleep to survive, yet the nature of sleep's many functions is still debated (Cirelli and Tononi, 2008). There are several key processes occurring during sleep that affect the brain, divided largely into memory processing (Rasch and Born, 2013; Tononi and Cirelli, 2006) and restorative processes (Inoué et al., 1995; Villafuerte et al., 2015; Vyazovskiy and Harris, 2013). In this chapter, I will focus on the memory roles of sleep.

Sleep disturbances and cognitive impairments – including in mnemonic functions – are common comorbidities in psychiatric disorders, including schizophrenia, autism and intellectual disability (Castelnovo et al., 2016; Kaskie et al., 2017). Given that memory consolidation seems to be one of sleep's key roles, it has been

suggested that these symptoms may be linked in psychiatric disorders by a common mechanism (Jagannath et al., 2013). Researchers investigating this link have found sleep neurophysiology to be a highly translatable measure of functional connectivity in the brain, and it has been presented as a strong candidate biomarker for psychiatric disorders such as schizophrenia for three independent reasons (Gardner et al., 2014). Firstly, characteristic coordinated network activity patterns spanning the neocortex, thalamus and hippocampus have regularly been found to be disrupted in psychiatric disorders, including schizophrenia, autism and intellectual disability (Castelnovo et al., 2018; Chan et al., 2017; Chouinard et al., 2004; D'Agostino et al., 2018; Demanuele et al., 2017; Ferrarelli and Tononi, 2017; Gruber and Wise, 2016; Manoach et al., 2016; Rockstroh et al., 2007; Tessier et al., 2015). Secondly, like other oscillatory mechanisms, sleep neurophysiology is evolutionarily highly conserved (Borbély and Achermann, 1999). Thirdly, these spontaneous circuit dynamics during sleep are less biased by waking behaviour, attention, and demands of any specific task (for a review see Gardner et al. (2014)). Patients with schizophrenia, autism and intellectual disability also experience disrupted circadian rhythms as well as sleep disturbances (Köse et al., 2017; Souders et al., 2009; Wulff et al., 2012), which is echoed in some psychiatric disorder-relevant animal models (Pritchett et al., 2012).

In this chapter I investigate the links between *Cyfip1* haploinsufficiency and circadian and sleep disturbances using actigraphy data and sleep neurophysiology recordings. First, I briefly review current understandings of the role of sleep and sleep oscillations in memory consolidation, and highlight how these processes have been disturbed in patient populations and rodent models.

6.1.2 Human and rodent sleep

6.1.2.1 Circadian rhythms

Sleep is regulated by two major influences: 1) the 24h endogenous oscillation of the circadian rhythm, driven by an internal clock in the suprachiasmatic nuclei (SCN) of the hypothalamus, which is entrained by the light-dark cycle; 2) the

homeostatic regulation of sleep, whereby sleep need accumulates during wake and dissipates during sleep (Borbély and Achermann, 1999; Fisher et al., 2013).

Humans and rats are both entrained by light, but their circadian rhythms differ, most obviously by rats being nocturnal. While they largely show an active phase during darkness and inactive phase during light, rats have polyphasic sleep, with many more sleep bouts throughout the 24 h cycle (Fisher et al., 2012). This might complicate the translation of any sleep bout phenotypes to the human context. Nevertheless, rodents are commonly used to model circadian rhythm disturbances (see below).

6.1.2.2 NREM sleep oscillations

While our circadian patterns differ, the neural circuit mechanisms driving and characterising human and rodent sleep are in many ways remarkably similar. Early sleep EEG experiments discovered characteristic neural oscillations can be used to distinguish sleep stages (Rechtschaffen and Kales, 1968). Sleep can broadly be divided into rapid-eye-movement (REM) sleep and non-REM (NREM) sleep (Berry et al., 2015). In humans, NREM can be further broken down into Stages N1-N3: N1 and N2 encompass lighter stages of sleep characterised by waxing and waning spindle oscillations at 8-15 Hz spreading from the thalamus to the cortex (McCormick and Bal, 1997), while N3 is dominated by slow wave oscillations at 0.25-4 Hz (Grey, 1963; Steriade et al., 1993a). In rats, NREM sleep is not subdivided and features both slow waves and spindles. REM sleep is characterized by brain activity that is very similar to that in wake coupled with decreased muscle tone (Figure 6.1).

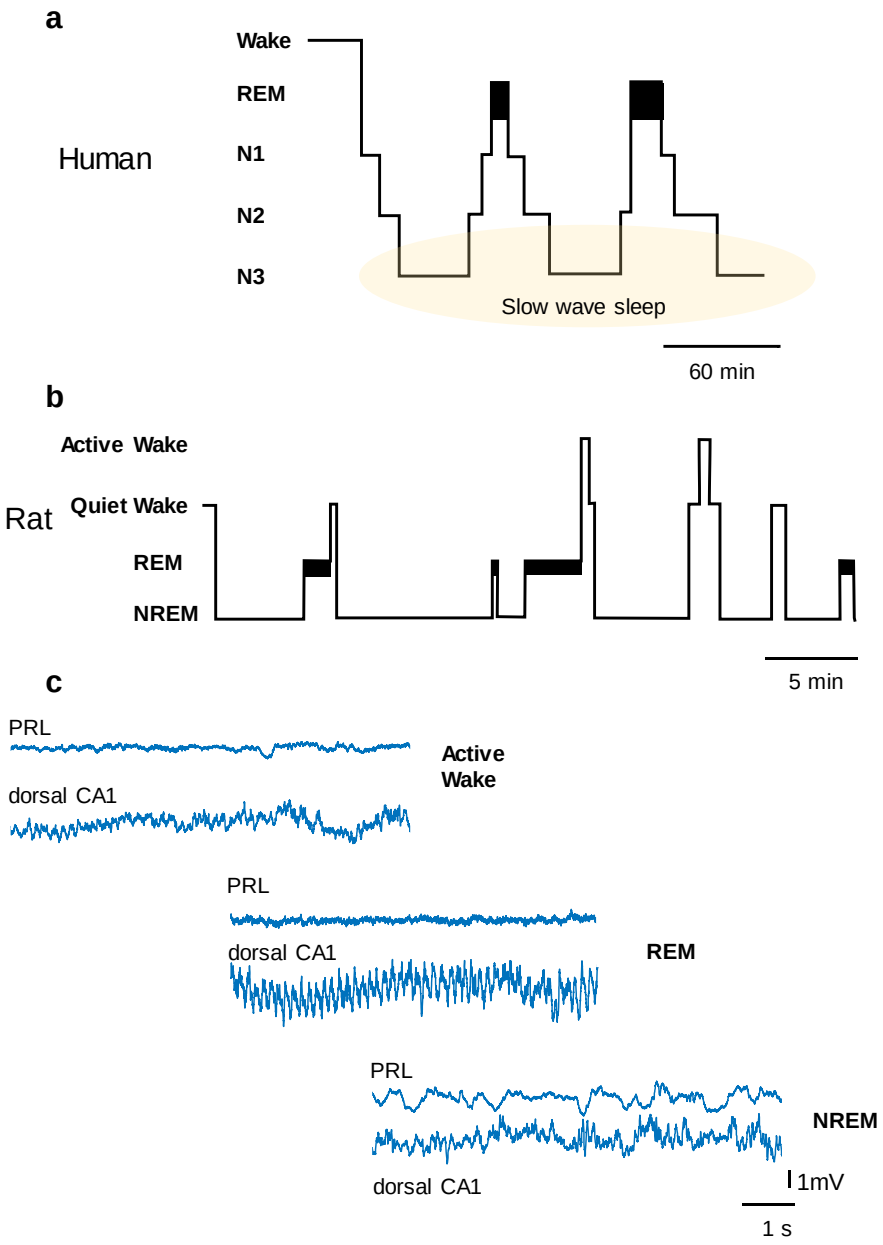

Figure 6.1 | **Human and rat sleep. a,** Human hypnogram showing time spent in different stages of sleep. N3 is also called slow wave sleep, characterised by these slow 1-4 Hz oscillations. Figure adapted from Rash and Born (2013). **b,** Rat hypnogram showing the stages that were scored for the current experiments. **c,** Raw traces from prelimbic cortex (PRL) and dorsal CA1 of the hippocampus during different brain states. Note theta (6-10 Hz) oscillation present in the dorsal CA1 during active wake and even more prominent in REM, and slow waves in the prelimbic cortex during NREM.

Slow waves are local field potential oscillations reflecting the synchronous transitions between high and low activity states, referred to as UP and DOWN states (Steriade et al., 1993a). During transitions to UP states (LFP positive half-waves),

populations of pyramidal cells are synchronously active, while transitions to DOWN (LFP negative half-waves) states signify the synchronous silencing of these neurons. Slow-waves are generated by a combination of intrinsic currents and synaptic currents in the thalamus and cortex (Crunelli and Hughes, 2010).

Spindles in the sigma frequency range also occur during NREM sleep. These waxing and waning, 0.5-3 s events are generated by the thalamic reticular nucleus (TRN). TRN GABAergic neurons show burst firing, which via thalamocortical glutamatergic projections entrain cortical neurons to oscillate at the spindle frequency (Steriade et al., 1993b). The thalamocortical feedback loop is completed by glutamatergic cortical projections onto NMDA receptors on TRN neurons (Contreras and Steriade, 1996), which aid in spindle coordination (McCormick and Bal, 1997).

Ripples are characteristic NREM oscillations seen in the hippocampus, but they can also occur during quiet rest (Buzsáki, 2015; Buzsáki et al., 1983). They are marked by a 2-4 Hz sharp-wave coupled with a high frequency oscillation at 140-200 Hz, and are most pronounced in the pyramidal cell layer of CA1. They are triggered by a temporary disinhibition leading to highly synchronous burst firing in a recurrent network in CA3 (Chrobak and Buzsáki, 1996), which generates the sharp-wave of the ripple. The bursting activity is propagated to the CA1 via the Schaffer collateral, generating the ripple recorded in this area (Buzsáki, 1986; Csicsvari et al., 2000).

Simultaneous recordings from cortex and hippocampus demonstrated that these NREM sleep events do not occur in isolation. There is in fact a precise temporal coordination between slow waves, spindles and ripples, seen in rodents and humans (Clemens et al., 2007; Siapas and Wilson, 1998; Sirota et al., 2003), where transitions to UP states are closely coupled with hippocampal ripples, followed by spindles (Figure 6.2).

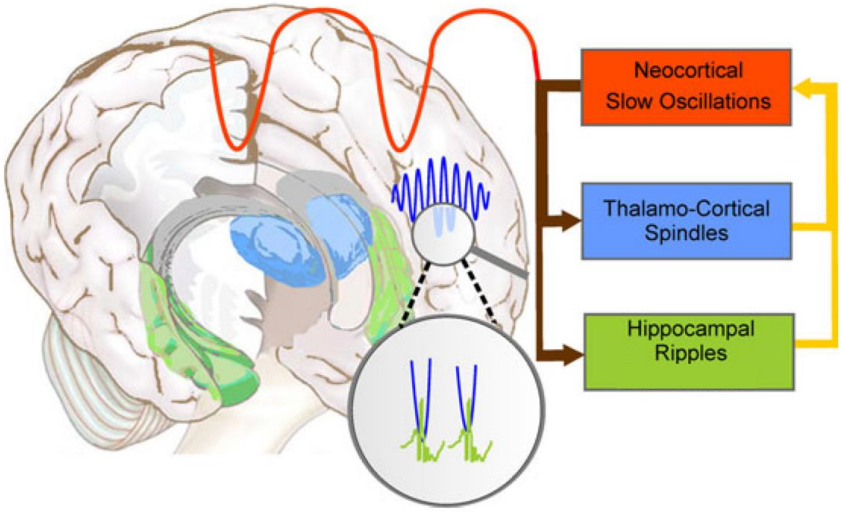

Figure 6.2 **| Coordinated NREM oscillation events in memory consolidation. E**vidence indicates that it is the concerted activity of NREM sleep oscillation events, slow waves, spindles and ripples, that is critical in memory consolidation, facilitating the transfer of recently encoded memories from the hippocampus to the prefrontal cortex. Figure adapted from Born and Wilhelm (2012).

6.1.2.3 Role of NREM sleep oscillations in memory consolidation

These characteristic NREM sleep oscillations have garnered particular attention as evidence suggests they play a role in memory consolidation. In particular, the active systems consolidation hypothesis posits that recent memory representations in the hippocampus are consolidated by 'replay' during subsequent NREM sleep, and thus transferred into the neocortex to be integrated to long-term memory (Rasch and Born, 2013). This was partially based on the landmark finding that hippocampal place cells active during a navigation task were reactivated in the same temporal order, albeit compressed time period, in subsequent rest or NREM sleep (Lee and Wilson, 2002; Skaggs et al., 1996; Wilson and McNaughton, 1994). Place cells during these 'replay' events are phase-locked to hippocampal ripples (Lee and Wilson, 2002), establishing a link between ripples and memory consolidation, likely mediated by ripple-induced LTP in between CA3 and CA1 neurons (Sadowski et al., 2016). Replay has since also been observed in the prefrontal cortex, suggesting a more prominent role of the cortex during encoding (Peyrache et al., 2009). REM sleep has also been implicated in memory consolidation, and while there are some reports of replay occurring during REM, this has not been

widely reproduced (Llewellyn and Hobson, 2015; Louie and Wilson, 2001). A further mechanism has been suggested for consolidation during sleep, whereby synaptic weights are homeostatically regulated thus improving the signal-to-noise ratio of replayed events (Tononi and Cirelli, 2006). These mechanisms could act in a complementary way to increase memory consolidation (Genzel and Robertson, 2015). There is growing evidence that the individual and concerted activity of slow waves, spindles and ripples have a direct role in memory processing.

6.1.2.4 Evidence for ripples in memory consolidation

Direct evidence linking hippocampal ripples to memory consolidation comes from studies where interruption of ripples by electrical stimulation during sleep or quiet rest impairs consolidation (Ego-Stengel and Wilson, 2010; Girardeau et al., 2009). Girardeau et al. (2009) detected ripples online during sleep following training on a spatial reference memory task. Using a single electrical pulse to the ventral hippocampal commissure they interrupted ripples, but importantly, did not disturb other sleep parameters. These animals showed deterioration in memory consolidation, while a control group who had electrical pulses delivered out of sync with ripples performed the same as unimplanted animals. Furthermore, the role of ripples in systems levels consolidation was revealed by experiments showing replay in the mPFC coincided with hippocampal ripples (Peyrache et al., 2009).

6.1.2.5 Evidence for spindles in memory consolidation

Consisting of a series of firing bursts from thalamocortical projections, spindles are well placed to trigger synaptic plasticity in the cortex. Applying a spindle-like train of stimuli to rat pyramidal cells in cortical slices, NMDA receptor-dependent short-term potentiation and L-type Ca^{2+} channel-dependent long-term potentiation is induced (Rosanova and Ulrich, 2005). By this mechanism, spindles are proposed to play a role in memory consolidation although evidence for this has been largely from correlational studies (Manoach et al., 2016). For example, increased spindle activity positively correlated with retention of a verbal task, memory recall and motor skills (Gais et al., 2002; Morin et al., 2008) with comparable findings in rats (Eschenko et al., 2006; Watts et al., 2012). Furthermore, increasing spindle activity

with pharmacological agents such as zolpidem (a sleep-promoting drug acting on $GABA_A$ receptors) improved the consolidation of declarative memories (Kaestner et al., 2013; Mednick et al., 2013). A direct and specific manipulation causally linking spindles to memory consolidation is yet to be published, although a recent conference abstract used an optogenetic approach to interfere with spindles in mice by silencing GABAergic neurons in the TRN, which led to decreased performance in recognition task (Katsuki et al., 2017).

Spindles have also been suggested to reflect basal intelligence levels, as spindle density correlates with IQ (Fang et al., 2017; Fogel and Smith, 2011). The finding that spindle density remains remarkably stable within subjects from night-to-night, suggesting a spindle 'fingerprint' (De Gennaro et al., 2005), supports the suggested link with IQ, but does not align with spindles being learning-dependent, i.e. involved in the consolidation of information acquired during the previous day. Spindles have also been noted to change over the course of development (Campbell and Feinberg, 2016), with a shift to higher frequencies occurring during adolescence, and reduced amplitude in the elderly (Guazzelli et al., 1986).

6.1.2.6 Evidence for slow waves in memory consolidation.

Increases in slow wave activity also correlate with post-sleep enhancements in both declarative, hippocampus-dependent tasks and non-declarative, hippocampus-independent memory (Miyamoto et al., 2017; Mölle et al., 2009). Moreover, when transcranial stimulation was used to increase the number of slow waves during NREM sleep in humans, memory was further enhanced (Marshall et al., 2006). A recent study in mice showed that following a floor-texture recognition task, optogenetic stimulation at slow wave frequency of the task-associated somatosensory and motor cortices, lead to enhanced memory consolidation, indicated by prolonged retention of a novelty recognition memory (Miyamoto et al., 2016).

6.1.2.7 Evidence for coordinated NREM oscillations in memory consolidation

While the findings described above point to the largely independent roles of each NREM oscillation in memory consolidation, recent evidence indicates that it is the *concerted* activity of NREM sleep oscillation events that is critical in memory consolidation, in facilitating the transfer of recently encoded memories from the hippocampus to the prefrontal cortex. Correlational studies had linked greater coordination of sleep oscillation events with improved consolidation in humans and rats (Johnson et al., 2010; Niknazar et al., 2015), but Maingret et al. (2016) were the first to demonstrate a causal link between the tight temporal correlation of slow waves, spindles and ripples by optogenetically manipulating their coordination. A novel object location task was used, whereby rats were exposed to two identical objects for a short period, and re-exposed 24 hours later, when one of the objects had been moved to the opposite corner. During sleep following the first exposure, online detection of ripple events triggered an electrical stimulation of the cortex, eliciting slow waves and spindles. Rats receiving the stimulation, explored the object in the novel location more than the unmoved one, indicating recall of the location memory. In contrast, unstimulated rats did not discriminate between the two, only if the duration of the first exposure was extended. This supports a consolidation mechanism whereby hippocampal ripples trigger reactivation of cell assemblies in the prefrontal cortex (Peyrache et al., 2009), whose target synapses would then be selectively isolated by the ensuing slow wave, and strengthened by synaptic plasticity during the incoming spindle (Maingret et al., 2016; Rosanova and Ulrich, 2005).

The generation of this concerted activity relies on the integrity of long-range connectivity between cortex, thalamus and hippocampus. Therefore, changes in the synchronization of these events can uncover deficits in the hippocampal-prefrontal network. Chapter 3 demonstrated that this network remains intact in *Cyfip1*$^{+/-}$ animals during behaviour, but analysis of the coordination of NREM sleep oscillations provides a new angle by which I can revisit the hippocampal-prefrontal network in a different behavioural state.

6.1.3 Disrupted sleep in psychiatric disorder

6.1.3.1 Psychiatric disorder patients

The accumulating evidence that sleep and specifically NREM sleep oscillations contribute to offline memory consolidation has led to the suggestion that cognitive impairments and sleep disruption seen in psychiatric disorders share a common mechanism (Jagannath et al., 2013; Pritchett et al., 2012). In this section, I will highlight evidence linking sleep disruptions on a macroscopic level looking at circadian rhythms, and a mesoscopic level looking at NREM oscillations, to the cognitive impairments seen in psychiatric disorders.

Sleep disruption is arguably one of the symptoms most damaging for quality of life of schizophrenia and other psychiatric patients (Cohrs, 2008; Hofstetter et al., 2005). Contrary to early observations, it appears unrelated to medication or lack of a social routine in schizophrenia (Wulff et al., 2012). Effects include difficulty in both falling asleep and staying asleep, with examples of early or delayed sleep, fragmented sleep, rest-activity patterns unregulated by the day, reduced sleep efficiency, and abnormal REM and NREM durations (Bromundt et al., 2011; Köse et al., 2017; Pritchett et al., 2012; Souders et al., 2017; Wulff et al., 2009a). Although circadian disruptions are not specific to schizophrenia, particular efforts have been made to link circadian-rhythm regulating genes to this disorder (Mansour et al., 2006; Takao et al., 2007; Zhang et al., 2011); however, circadian genes have not yet been implicated in genetic association studies (Ripke et al., 2014; Stefansson et al., 2009). Associations have been reported between disrupted sleep and cognitive performance in schizophrenia patients, both with medication (Bromundt et al., 2011; Göder et al., 2015; Wulff and Joyce, 2011) and without (Forest et al., 2007; Yang and Winkelman, 2006), while a recent study found poorer performance on a spatial declarative memory task in autistic children compared to controls after a night of sleep, suggesting poorer memory consolidation (Maski et al., 2015).

What is the relationship between sleep disruptions and cognitive symptoms? It appears that during the sleep patients are getting, NREM sleep oscillations critical for memory consolidation are disrupted (Hiatt et al., 1985). In particular,

schizophrenia patients show decreased spindle activity (Manoach et al., 2016). This has been observed in medicated (Ferrarelli et al., 2007; Göder et al., 2015; Seeck-Hirschner et al., 2010; Wamsley et al., 2012) and un-medicated patients (Manoach et al., 2014), as well as reduced spindle amplitude in (currently) healthy first-degree relatives (Keshavan et al., 2004; Manoach et al., 2014). Supporting their role in memory consolidation, several studies show a correlation between impaired enhancement of a finger-tapping motor sequence task and reduced spindle activity in preceding sleep (Barakat et al., 2011; Manoach et al., 2010; Nishida and Walker, 2007). Furthermore, various other neurodevelopmental and neurodegenerative disorders featuring cognitive deficits show abnormal spindle activity, including intellectual disability (Shibagaki et al., 1982), autism (Limoges et al., 2005), and Parkinson's with dementia (Latreille et al., 2015).

Sleep neurophysiology and/or actigraphy have not been studied in the context of the 15q11.2(BP1-BP2) deletion. However, it is noteworthy that a study of 14 cases carrying a duplication in the 15q11.2-q13 region reported sleep disturbances (Urraca et al., 2013). In addition, 10 of the 14 subjects had abnormal waking EEG signatures in the form of excessive beta (18-22Hz) epochs. There are sporadic reports of sleep problems in the literature regarding 15q11.2(BP1-BP2) deletion carriers (Burnside et al., 2011; Elert-Dobkowska et al., 2014) but no systematic investigations. A sleep study in the 15q11.2(BP1-BP2) deletion cohort is planned as part of the ongoing research programme at Cardiff University, and anecdotal reports from parents of children in this cohort have raised the issue of sleep disturbances.

6.1.3.2 Animal models

As discussed, the observation that schizophrenia goes hand in hand with sleep and circadian disruption has prompted the hypothesis that common mechanisms are involved in their pathogenesis (Jagannath et al., 2013; Pritchett et al., 2012). This would predict that animal models for schizophrenia should also show disrupted sleep and circadian rhythms. This prediction is being tested on a growing number of potential schizophrenia-relevant models, and they appear to support this

hypothesis. Furthermore, it has even been suggested that the circadian system might be causally relevant in the aetiology of psychiatric illness, following evidence of mania-like phenotypes in *Clock* mutant mice (Menet and Rosbash, 2011).

6.1.3.2.1 Circadian disruptions

A growing number of animal models have incorporated circadian phenotyping as part of their characterisation. Table 4 summarises the findings seen in some of these models, including the *Fmr1* KO mouse, which is of particularly interest due to the close molecular relationship between FMRP and CYFIP1. It is important to narrow down the nature of the circadian disruption, whether it affects inputs to the SCN, the SCN itself, or downstream processes. As an example, the blind-drunk (Bdr) mouse, which harbours a missense mutation in the neuronal SNARE synaptosomal-associated protein of 25 kDa (SNAP-25), has several schizophrenia-related endophenotypes and shows circadian disruption, with a phase advance and fragmented rest-activity rhythm. Bdr mouse activity patterns respond normally to a phase shift in light conditions, suggesting retinal inputs are intact. Clock gene rhythms are also unaffected in these mice, suggesting core SCN processes are intact. However, circadian rhythms of hormones such as arginine vasopressin and plasma corticosterone are phase-advanced, mirroring the sleep circadian phenotype, implicating processes downstream of the SCN in the disruption.

Table 4 Sleep and circadian findings in psychiatric disorder-relevant animal models

Model	**Sleep or circadian phenotype**	**Reference**
Blind-drunk mouse generates **SNAP-25** exocytotic disruption	Activity phase advance, fragmented rest-activity rhythm. Light induced phase-shift normal.	(Oliver et al., 2012)
Vipr2, 7q36.3 CNV.	Circadian period abnormally short, and is likely due to a disruption within the SCN or	(Hughes and Piggins 2008)

Protein and its receptor critical for circadian oscillations in SCN.	its outputs, as light-induced phase-shifts are normal.	
Fmr1/Fxr2 mutant mice	Mice lacking FMRP or related FXR2p, show shorter free-running period in constant darkness. Double mutant shows complete loss of rhythmicity in light:dark conditions.	(Zhang et al., 2008)
mGluR2 and **mGluR3** knockout mice	Reduced sleep time and increased sleep fragmentation.	(Pritchett et al., 2015a)
D-amino acid oxidase (**DAO**) knockout mouse	No circadian or sleep deficits	(Pritchett et al., 2015b)
STOP (stable tubule only polypeptide) null mutant mouse	Less time spent in NREM sleep, more fragmented sleep, especially in dark phase.	(Profitt et al., 2016)
Gain-of-function **DISC1** mice	Normal circadian entrainment of activity, but reduced overall wheel running. Reduced time asleep.	(Jaaro-Peled et al., 2016)

6.1.3.2.2 Sleep neurophysiology disruptions

Only a handful of studies have assessed sleep using electrophysiology methods in psychiatric disorder-relevant models. In addition to the circadian phenotype mentioned in Table 4, the STOP null mutant mouse showed increased slow wave power and reduced spindle power compared to WTs (Profitt et al., 2016). Kumar et al. (2015) recorded sleep EEG in the CACNA1c heterozygous (HET) knockout mouse. CACNA1c encodes a subunit of the widely expressed $Ca_v1.2$ voltage dependent L-type calcium channel and emerged as a candidate risk gene from the Psychiatric Genomics Consortium GWAS study. HET mice were found to have significantly lower EEG spectral power in beta to gamma frequencies both during wake and REM sleep. In addition, they noted a trend of higher slow wave activity during NREM sleep. Following a stress procedure (acute sleep deprivation or restraint stress), the recovery sleep in HET mice showed reduced REM sleep.

Suh et al. (2013) recorded single unit activity to characterize hippocampal activity in a forebrain specific calcineurin knockout mouse. Calcineurin, a phosphatase involved in synaptic plasticity, has been associated with schizophrenia in linkage analyses (Gerber et al., 2003). The authors reported specifically on awake ripples and found that knockout mice showed increased ripple power and density, together with abnormal over-reactivity of place cells during ripple events, and showing less replay of the recent spatial experience. These mice had previously been shown to exhibit an array of schizophrenia-relevant impairments (Miyakawa et al., 2003), including a severe working memory deficit (Zeng et al., 2001), and the authors attempt to link the ripple deficits seen in this model to the cognitive deficits in schizophrenia. An identical phenotype of increased waking ripple power and density was observed in a mouse model carrying a truncated human DISC1 gene, suggesting a convergence on the same neural phenotype via two unrelated genetic models (Altimus et al., 2015). Sleep activity was analysed in another DISC1 mouse model overexpressing full-length human DISC1, and showed reduced NREM and REM sleep with lower delta activity during recovery sleep following 2 h sleep deprivation (Jaaro-Peled et al., 2016). Another group made whole-cell recordings of L2/3 neurons *in vivo* in unanaesthetized *Fmr1* KO mice during sleep and saw a

doubling of neuronal firing probability during UP states, although prolonged UP states were not seen. In fact, these neurons had a 3-fold higher firing rate compared to WT in P14-16 animals at rest or asleep (Gonçalves et al., 2013).

In summary, emerging evidence of the link between cognitive deficits and the disrupted circadian rhythms and sleep neurophysiology seen in both patients and animal models of psychiatric disorders provides a strong general rationale to explore sleep characteristics in the *Cyfip1*$^{+/-}$ rats. This chapter reports on two experiments: an actigraphy study to investigate circadian sleep/activity patterns, and a sleep neurophysiology recording to assess any disruptions to characteristic NREM sleep oscillations and fine-scale sleep architecture.

6.2 Methods

6.2.1 Actigraphy

Actigraphy was monitored as described in Section 2.6 (page 75), in a holding room with 12:12 light/dark reverse light conditions (lights on at 8pm). Data were collected in four rounds of monitoring, as there were 12 sensors available, of which some malfunctioned and those data had to be discarded each round. The first 12 days of the first two monitoring rounds was discarded, as the time taken for animals to entrain to a reverse light room had not been taken into account, therefore these rounds provided 6 days of light-entrained monitoring. The last two rounds provided 24 days of light-entrained monitoring. Data was analysed as described in Chapter 2.

6.2.1.1 Validation of PIR-defined sleep

Simultaneous LFP and PIR monitoring was carried out for 3 rats to assess the effectiveness of using PIRs to identify sleep. The LFP recording was set up as previously described, with the animal in the home cage with a cage extender. A PIR sensor was fitted to the inside of a cardboard tube, which was fixed between the inside walls of the cage extender. The PIR was positioned to achieve the same field of view as in the actigraphy setup, 28cm from the floor of the cage and 17cm from the front of the cage.

6.2.2 Sleep electrophysiology recording session

Animals were implanted with LFP microdrives and sleep electrophysiology data was acquired as described in Chapter 2. Sleep was recorded before and after T maze running. Post-T maze sleep data were used for all analysis presented in this chapter. Sleep was scored offline, so sleep was roughly logged by visual inspection of the video feed and neural signal data, and recordings continued until an estimated 50-60 minutes of sleep had been accrued.

6.2.2.1 NREM oscillation events

Data were sleep-scored to isolate NREM epochs, where slow waves, spindles and ripples were detected as described in section 2.4. Mean frequency, amplitude and length of NREM events were calculated for each animal.

6.2.2.2 Delta/spindle power and coherence in 60 second NREM epoch

A 60 second NREM epoch on the PRL channel was extracted from the middle of the longest NREM bout for each animal, and confirmed as NREM sleep by eye. Delta and spindle power were calculated using the following parameters: bandwidth = 1 Hz, window = 3 s, constant = 1, providing five tapers and a moving window step of 0.05 s. The *mtspectrumsegc* function was used, splitting the epoch into 10 second sections, and averaging over these sections. Normalized power was used, as described in section 2.4, but results were not affected when analysis was run without normalization. Slow wave coherence between PRL and parietal cortex could be assessed in the subset of animals with a recording electrode in the parietal cortex using the *coherencysegc* function.

6.2.2.3 Ripple time-locked power spectrogram

Averaged power spectra and spectrograms were calculated for a 200ms window time-locked to the peak of detected ripples. The signal from the selected dorsal hippocampal electrode was bandpass filtered between 80-400 Hz using a Butterworth filter and the Matlab function *filtfilt.* Parameters were set as follows: bandwidth = 40 Hz, window = 0.03 s, constant = 1, moving window step = 0.001.

6.2.2.4 Coupling of NREM oscillation events

Temporal coupling was investigated between slow waves, spindles and ripples. Power in spindle and ripple frequency band was calculated as follows. Signals were bandpass filtered (10-16 Hz for spindles, 120-180 Hz for ripples) using Butterworth filters and the Matlab function *filtfilt*. Filtered data were Hilbert transformed and rectified to obtain the root mean squared (RMS) power envelope. For slow wave-spindle coupling, slow wave detections were used as a reference and the average spindle power envelope was calculated in a ± 1.5 second window surrounding the peak of the slow wave. Only negative half-wave detections were used as these transitions from UP to DOWN to UP state have been found to elicit a rebound in spindle power and a suppression of ripple power (Mölle et al., 2002, 2006). A bootstrap method using shuffled data tested the significance of coupling (Adhikari et al., 2010). The power envelope was randomly shifted by 5-10 seconds to create 500 shuffled data sets, which were tested for temporal coupling. Peaks in the power profile were used to assess coupling, as described below. Coupling was deemed significant if it surpassed 95% of the shuffled coupling values. The same method was used for slow wave-ripple coupling, with ripple power envelope calculated in a ± 0.5 second window. For ripple-spindle coupling, ripple detection times were used as a reference, with spindle power envelope calculated in a ±1.5 second window.

6.3 Results

6.3.1 Validation of PIR method: immobility-defined sleep under PIRs correlates well with LFP-scored sleep

Movement data can provide information about activity levels, but periods of immobility can also be used to infer sleep. In humans, actigraphy data has been shown to be an effective measure of gross sleep architecture, comparable to more sensitive sleep monitoring such as polysomnography (Baandrup and Jennum, 2015; Tahmasian et al., 2013). In mice, video monitoring studies have demonstrated that inactivity of ≥40s in mice can predict sleep with ~90% accuracy as compared to assessment using EEG/ EMG (Pack et al., 2007). Brown et al. (2016) also found greater than 95% correlation with sleep as assessed by immobility detected by

infrared sensor and sleep detected by EEG/EMG in mice. This method has only been validated in mice, therefore it was important to address this in the first study (to my knowledge) to use PIRs to monitor activity and infer sleep in rats.

To validate the PIR-defined sleep method in rats, I made simultaneous electrophysiological and PIR recordings in 3 WT animals, which showed a Pearson correlation coefficient of 0.9 ($p < 0.001$) (Figure 6.3). Behaviour scored by both methods is shown in Figure 6.3a. Using correlation, however, can be misleading to compare methods measuring the same variable, as it would be expected that their results would be correlated, yet this does not give an indication of agreement between two methods (Watson and Petrie, 2010). Therefore, as in Brown et al. (2016) I also used a Bland-Altman comparison of methods (Bland and Altman, 1986; Giavarina, 2015). Sleep periods were divided into 5 minute bins and the proportion of that bin scored as sleep was compared between the two methods. Figure 6.3b shows this measure plotted for both methods. The Bland-Altman comparison showed a reasonable agreement, with 95% of results measured by PIR lying between 93 s below or 124 s above the LFP data, as shown by the limits of agreement (Figure 6.3c). The mean of the differences was +15.64 s, (1 to 30 s 95% confidence interval), and the fact that the confidence interval does not overlap zero suggests there is a systematic difference with the PIR consistently scoring more sleep than LFP. This is likely due to the PIR detection missing awakenings when the animal does not move, suggesting the PIR detection would be less able to detect subtle effects of sleep fragmentation. Finally, degree of agreement between the 1682 ten second windows scored by each method was assessed by Cohen's kappa, which at 0.76 (95% CI: 0.73, 0.79), suggests substantial agreement (Watson and Petrie, 2010).

Overall, while it may be less sensitive when analysing individual sleep bouts and sleep fragmentation, these results show that the PIR data can be used as a reasonable indirect measure of sleep and circadian function in rats. In all subsequent analyses that refer to sleep from actigraphy data, I use this method of inferring sleep from immobility.

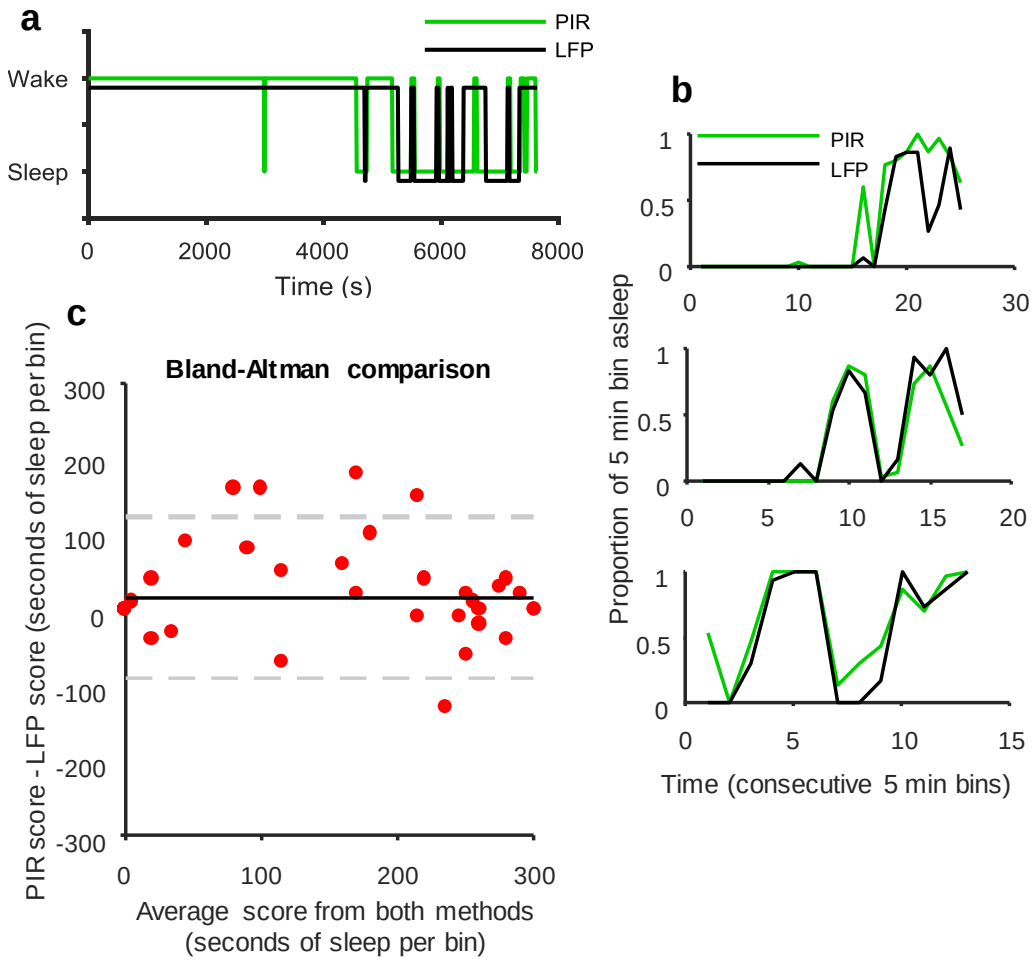

Figure 6.3 **| Validation of immobility-defined sleep from actigraphy monitoring. a,** Raw score data during one validation recording**,** showing sleep or wake as scored by PIR (green line shifted up) or LFP recording (black). Note how some LFP scored brief awakenings were missed by the PIR scoring. **b,** Data from three validation recordings showing proportion of each 5 minute bin spent asleep. Note general consistency between methods, with PIR tending to score more sleep per bin. **c,** Bland-Altman comparison of methods for scoring seconds spent asleep in each 5 minute bin. Solid line represents mean of the differences between methods. Dashed lines represent the limits of agreement (± 1.96 standard deviations), within which 95% of differences should fall. n = 3.

6.3.2 Actigraphy

Circadian rest/activity patterns were investigated in WT and *Cyfip1*$^{+/-}$ rats by monitoring movement in the homecage with PIR sensors over several days. PIR sensors provide an opportunity to measure homecage activity non-invasively, long-term and with low cost and low data storage requirements (Brown et al., 2016). It is also unaffected by the confounds of other common methods such as wheel-

running, e.g. motivation levels, novel object anxiety and motor impairment, which are not uncommon when studying disease models (Pritchett et al., 2015a).

Data are presented from four rounds of recordings, where 16 WTs and 18 *Cyfip1*$^{+/-}$ rats were monitored for between 6 and 24 days.

6.3.2.1 Activity

Interdaily stability, which indicates how consistent each animal's activity pattern is over days and thus how well it is synchronized to the light cycle, was normal in *Cyfip1*$^{+/-}$ rats ($p = 0.52$, t-test, two WT and 1 *Cyfip1* outlier did not affect this result) (Figure 6.4a and b). Intradaily variability, which measures transitions between rest and activity, therefore reflecting fragmentation of the rest-activity rhythm, was normal in *Cyfip1*$^{+/-}$ rats ($p = 0.42$, t-test, one *Cyfip1* outlier did not affect this result) (Figure 6.4a and b). Finally, relative amplitude, which captures the amplitude of the circadian rhythm was normal in *Cyfip1*$^{+/-}$ rats ($p = 0.38$, t-test, 3 *Cyfip1* outliers did not affect this result).

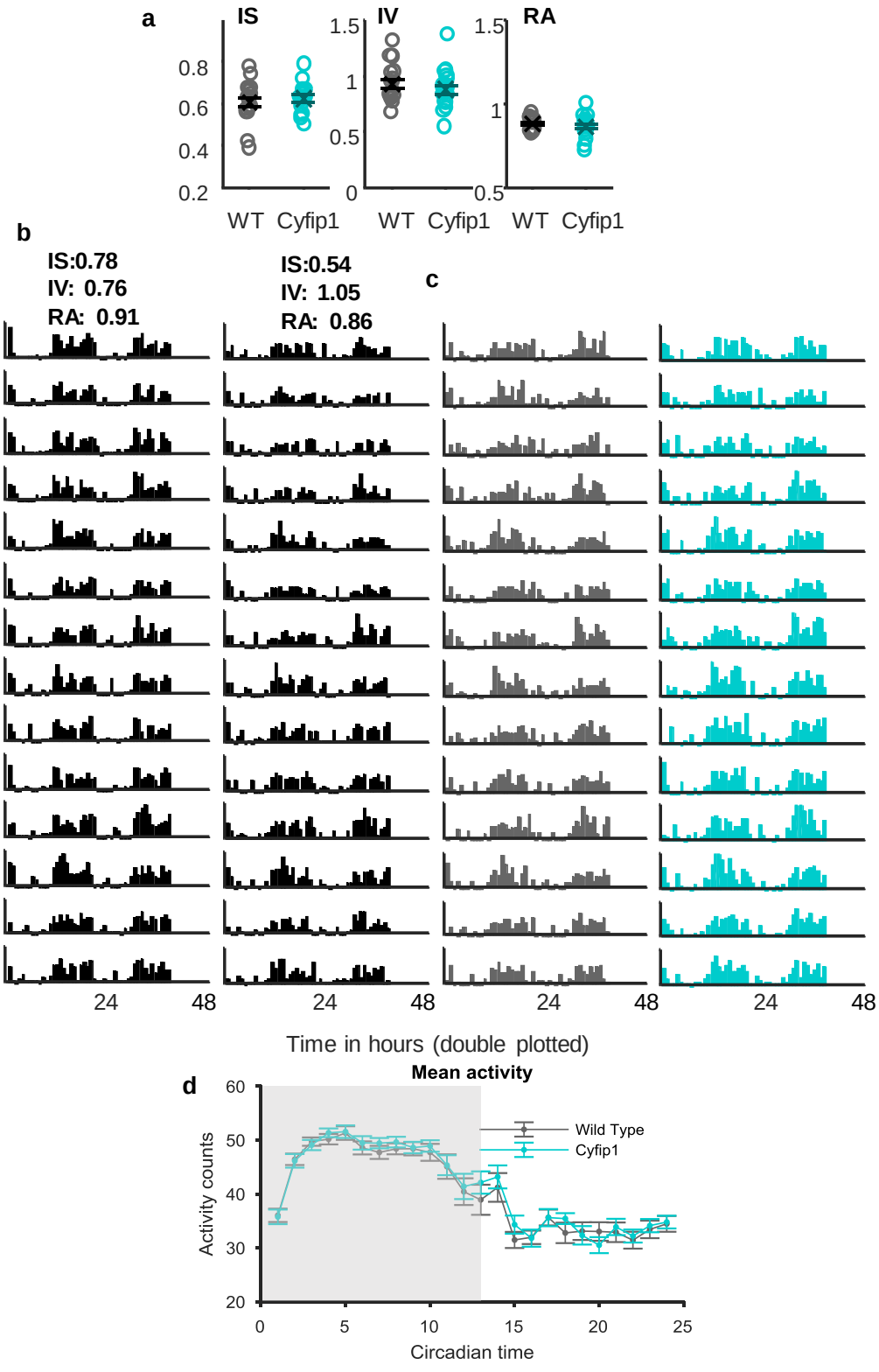

Figure 6.4 **| Activity patterns from actigraphy monitoring. a,** Interdaily stability, a measure of circadian entrainment, intradaily variability, a measure of fragmentation and relative amplitude of activity for WTs and *Cyfip1*$^{+/-}$ rats. **b,** Actograms to illustrate activity patterns with example interdaily stability and intradaily variability values. Actograms are

double-plotted, such that 48 hr is shown on each horizontal trace, with a 24 hr day shown both beneath and to the right of the preceding day. Bars indicate mean hourly activity counts. **c,** Representative actograms from one WT (grey) and one *Cyfip1*$^{+/-}$ rat (cyan). **d,** Hourly activity counts averaged over monitoring days and over animals. Shaded region indicates light off period. WT: n = 16, Cyfip1: n = 18.

Hourly activity counts were averaged over monitoring days to generate a circadian activity profile (Figure 6.4d). For activity analysis, the day was separated into four blocks of circadian time (hours 1-6, 7-12, 13-18, 19-24), and analysed by 2-way ANOVA. As expected, there was a significant main effect of time ($F_{3, 93} = 105.3$, $p < 0.001$), but no effect of genotype ($F_{1, 31} = 0.58$, $p = 0.45$) and no interaction ($F_{3, 93} = 0.26$, $p = 0.86$). One WT outlier did not affect this result.

A Lombe-Scargle periodogram, which reflects the periodicity of the activity rhythm, did not show a difference between genotypes in the strength of the 24 hour rhythm (24 hr amplitude: WT = 1844 ± 129, Cyfip1 = 1706 ± 134, p = 0.47, t-test, data not shown). Mean onset and offset times can highlight differences in the activity surrounding the light on/off times, and *Cyfip1*$^{+/-}$ rats had normal activity onset, with a trend for delayed activity offset (mean onset times: WT = 07:51 ± 6.6 min, Cyfip1 = 07:55 ± 14 min, p = 0.80, t-test; mean offset times: WT = 20:31 ± 11 min, Cyfip1 = 21:09 ± 13 min, p = 0.054, t-test, data not shown). Alpha duration estimates the duration of the active phase, and there was a trend for slightly longer duration in *Cyfip1*$^{+/-}$ rats, likely driven by the delayed activity offset time (WT: 12.65 ± 0.22 hrs, Cyfip1: 13.23 ± 0.19 hrs p = 0.068, data not shown).

6.3.2.2 Immobility-defined sleep

The proportion of time spent asleep per hour was averaged over monitoring days to generate a sleep profile (Figure 6.5a). Analysing over four time blocks, showed a significant main effect of time ($F_{3, 96} = 86.3$, $p < 0.001$), but no effect of genotype ($F_{1, 32} = 0.25$, $p = 0.62$) and no interaction ($F_{3, 96} = 0.13$, $p = 0.94$). This suggests that the amount of sleep was normal in *Cyfip1*$^{+/-}$ rats, but hourly sleep bout analysis is important to reveal how the sleep was accrued. For example, the same total amount of sleep can be achieved by lots of short sleep bouts, which would suggest sleep fragmentation, or fewer long sleep bouts.

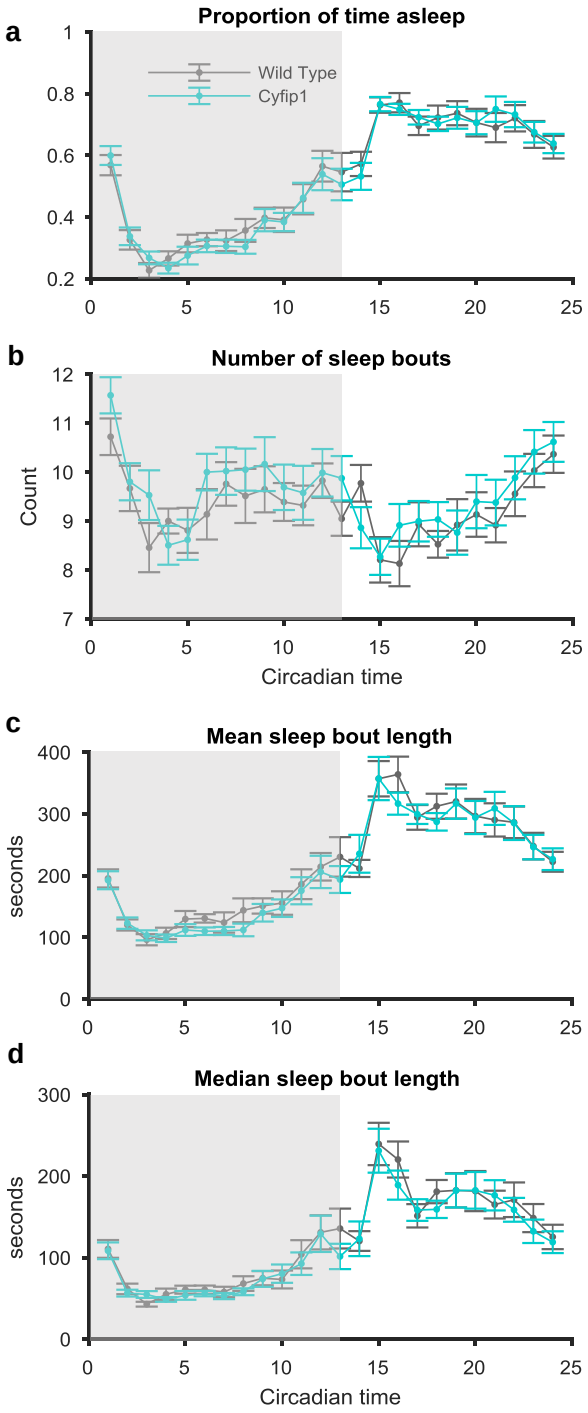

Figure 6.5 **| Immobility-defined sleep from actigraphy monitoring. a,** Proportion of each hour spent asleep. **b,** Hourly sleep bout number. **c,** Hourly mean sleep bout length. **d,** Hourly median sleep bout length. **a-d,** Data are averaged over monitoring days and over animals, shaded region represents lights off. WT: n = 16, Cyfip1: n = 18.

The distribution of hourly sleep bout lengths was positively skewed, therefore median sleep bout length was used for each animal (Figure 6.5c,d). As before, there

was a significant main effect of time over the four time blocks ($F_{3, 87} = 58.3$, $p < 0.001$), but no genotype effect ($F_{1, 29} = 2.0$, $p = 0.17$) or interaction ($F_{3, 87} = 0.87$, $p = 0.46$). Three WT outliers did not affect this result.

For the average hourly number of sleep bouts, the main effect of time did not reach significance ($F_{1.5, 49} = 3.09$, $p = 0.067$, with Greenhouse-Geisser correction) (Figure 6.5b). This reflects the fact that during the active phase, rats had 8-10 roughly 1 minute sleep bouts per hour, while during the inactive phase they had 8-10 longer sleep bouts. There was also no main effect of genotype ($F_{1, 32} = 1.44$, $p = 0.24$) or interaction ($F_{1.5, 49} = 0.03$, $p = 0.99$). It should be noted that these data failed the assumption of equality of error variance but without a non-parametric alternative, results are still reported.

In summary, these findings demonstrate that circadian activity and sleep patterns of *Cyfip1*$^{+/-}$ rats are normal, with no indication of fragmentation of sleep. Following this, I wanted to explore whether the *Cyfip1*$^{+/-}$ rats' sleep was normal at the level of limbic-cortical network activity central to sleep-dependent memory processing. Therefore, I carried out LFP sleep recordings to characterise sleep architecture, sleep fragmentation during a single sleep period, and sleep neurophysiology.

6.3.3 Sleep electrophysiology recordings

Sleep parameters were assessed during a sleep recording which followed the recording on the T maze experiment described in Chapter 3. This period was chosen as rats generally had a much shorter latency to sleep following the T maze task, than following the initial move to the experimental room, leading to a longer, more uninterrupted sleep recording. This is likely due to a combination of habituation to the experimental room during the T maze task, and a build-up of homeostatic sleep need.

6.3.3.1 Normal sleep architecture in Cyfip1 rats

One WT rat, (rat K.1) was excluded from sleep architecture analyses as he only achieved 16 minutes of sleep in a 3 hour session. I had issues with the

electrophysiology setup during this recording, having to disconnect and reconnect the animal to the system several times, and the handling likely impacted the fact that he did not sleep much. A second WT rat's sleep recording data were unfortunately corrupted, therefore has been removed. Thus, the following data refer to 12 WT and 12 *Cyfip1*$^{+/-}$ animals.

Gross sleep architecture was normal in *Cyfip1*$^{+/-}$ animals (Figure 6.6). Latency to sleep, measured as the time from the beginning of the recording session to the first sleep bout varied widely between animals, with a range of 11-50 minutes in WTs, and 9-47 minutes in *Cyfip1*$^{+/-}$ rats, with no overall difference between genotypes ($p = 0.14$, t-test, two *Cyfip1* outliers did not affect the result) (Figure 6.6a). Sleep efficiency was also similar in both groups ($p = 0.68$, t-test), measured as the proportion of time spent asleep from the first sleep bout until the end of the recording (Figure 6.6b).

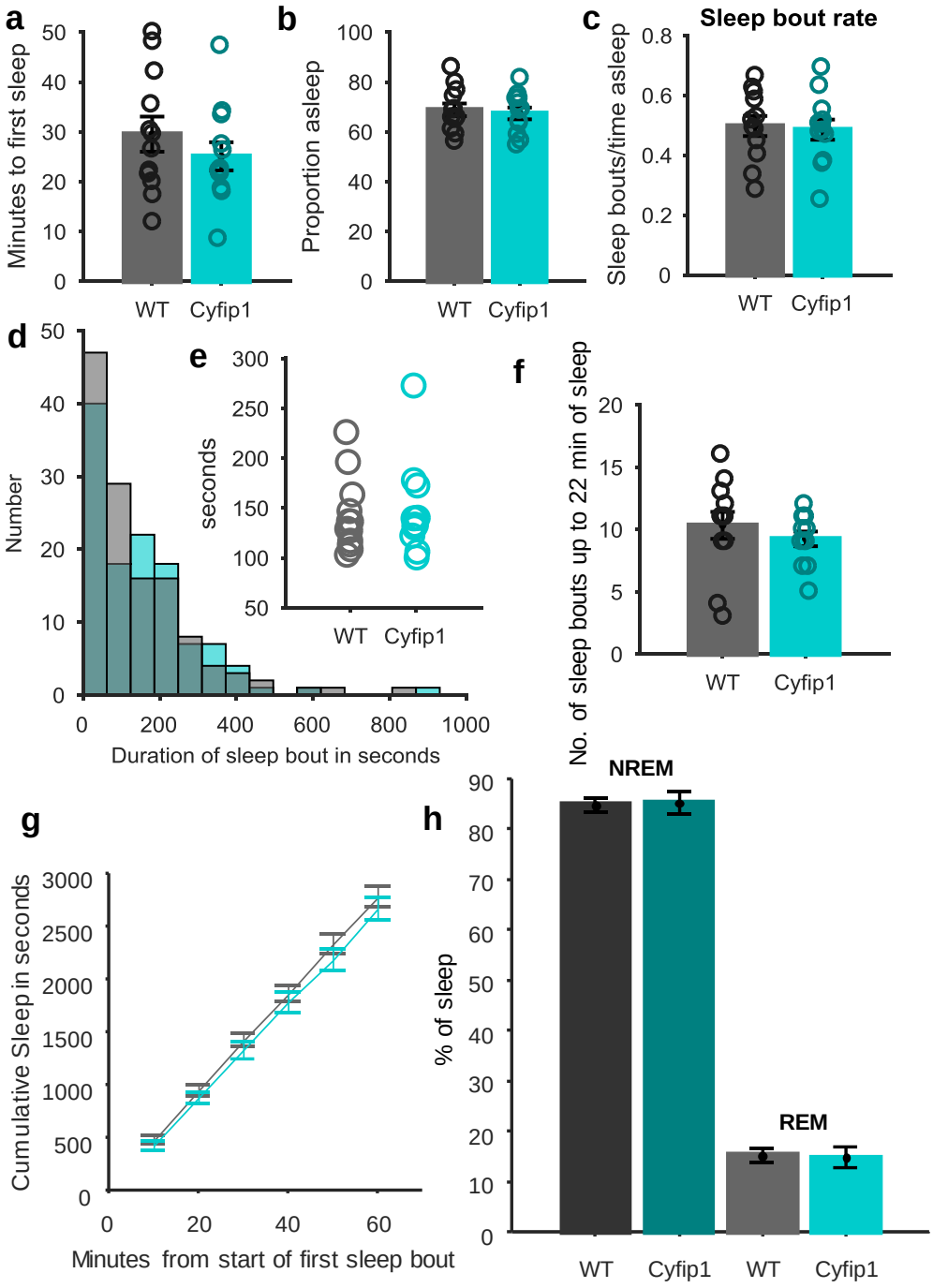

Figure 6.6 **| Sleep architecture from electrophysiology recording. a,** Sleep latency, measured as minutes from start of recording to first sleep bout. **b,** Proportion of recording spent asleep. **c,** Sleep bout rate, measured as the number of sleep bouts divided by the total amount of sleep. **d,** Distribution of sleep bout lengths for all WT and all *Cyfip1*$^{+/-}$ animals together. **e,** Mean sleep bout lengths. **f,** Number of sleep bouts up to 22 minutes of sleep, the minimum sleep duration achieved by all rats. **g,** Cumulative sleep in 10 minute blocks from start of first sleep bout, averaged over animals. **h,** Proportion of sleep spent in NREM and REM sleep. WT: n = 12, Cyfip1: n = 12.

There was no evidence for sleep fragmentation in *Cyfip1*$^{+/-}$ rats as assessed by 1) sleep bout rate, calculated as the number of sleep bouts divided by the total duration of sleep which was similar between genotypes (p = 0.8, t-test, Figure 6.6c), 2) mean sleep bout duration (p = 0.758, t-test, 1 *Cyfip1* outlier did not affect result, Figure 6.6e), 3) cumulative sleep during the recording, where sleep accumulated in the first 30 minutes since the first sleep bout was not different between genotypes (p = 0.48, t-test, Figure 6.6g), 4) number of sleep bouts required to achieve a certain amount of sleep (Figure 6.6f). For this latter measure, the shortest amount of sleep achieved by any rat (22 minutes) was taken as the sleep amount target, and the number of sleep bouts taken to reach this was the same in both groups (p = 0.39). The total time spent asleep was scored as NREM or REM, and the proportion of each was similar in both genotypes (WT: 85% NREM, *Cyfip1*: 84% NREM, p = 0.225, t-test, one *Cyfip1* outlier did not affect the result).

6.3.3.2 NREM sleep event parameters

Next I looked for any differences in characteristic NREM sleep oscillation events: cortical slow waves, thalamocortical spindles and hippocampal sharp-wave ripples. For each sleep oscillation event, average density (number of events per minute), amplitude, frequency and length were compared between genotypes (Table 5). Slow waves and spindles were detected on the PRL channel, using an automated detection algorithm as described in Chapter 2, while ripples were detected on the dorsal hippocampal channel (see Chapter 2).

6.3.3.3 PRL events: spindles and slow waves

Spindles were detected in all animals on the PRL channel and average waveforms for each animal appeared consistent, with no genotype differences in any parameter (Figure 6.7).

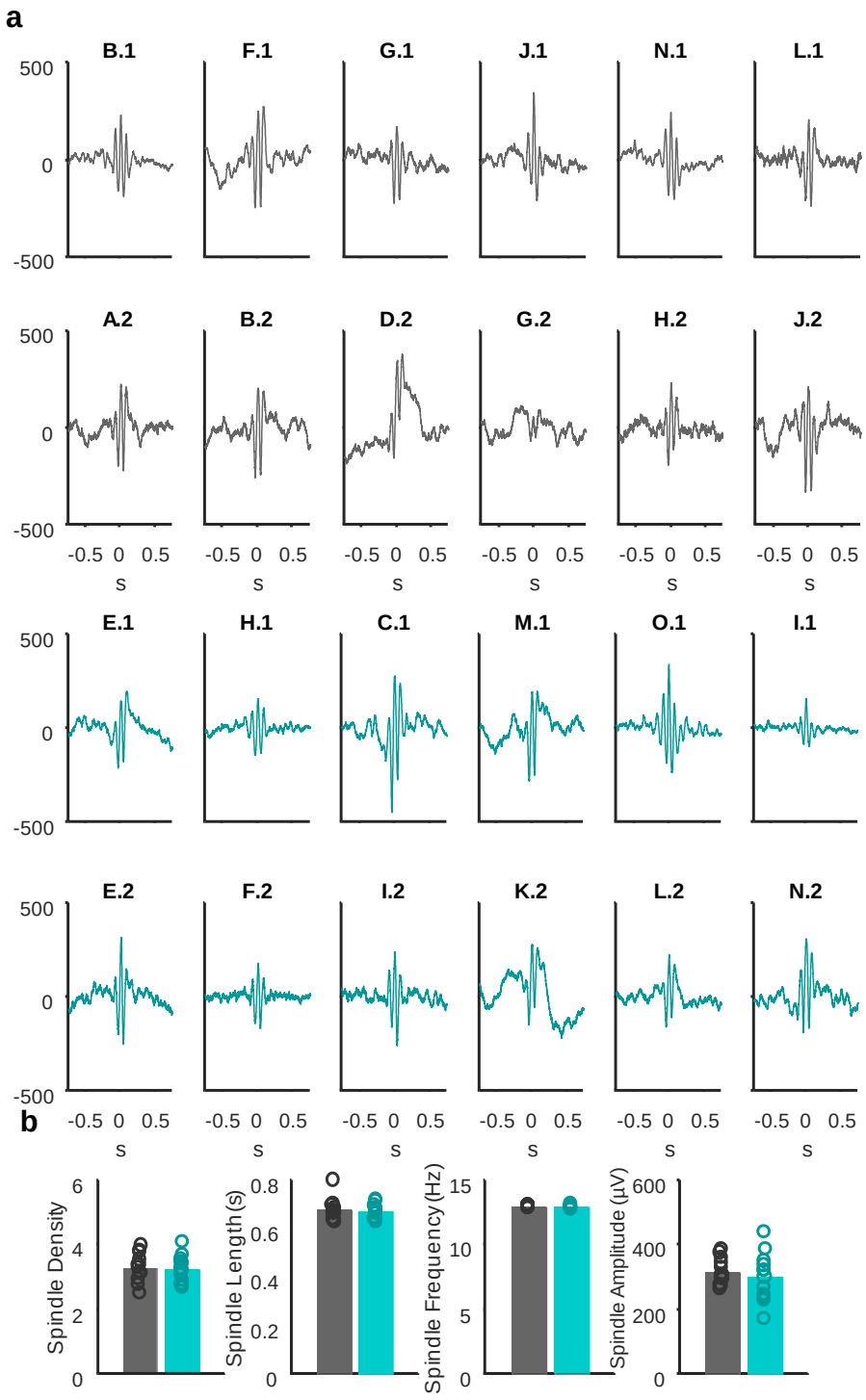

Figure 6.7 **| Spindles. a,** Average waveforms of detected spindles for WT (grey) and *Cyfip1*$^{+/-}$ rats (cyan). Y axis represents microvolts in this figure and all subsequent similar figures. **b,** Density, length, frequency and amplitude of spindles, WT in grey, Cyfip1 in cyan. WT: n = 12, Cyfip1: n = 12.

Slow waves were much more variable in amplitude, and also in the types of slow waves detected. Both negative and positive half-waves were detected, which reflect synchronous transitions between, and UP-DOWN- UP states (Figure 6.8Figure 6.8) and DOWN- UP- DOWN states (Figure 6.9) respectively. While the density of all slow wave types (positive and negative half-waves) was similar between rats ($p = 0.22$, t-test, data not shown), there was a wide variance in the ratio of negative to positive half-waves. Correlating half-wave amplitude with event density showed a significantly positive correlation for negative half-waves, but a negative correlation for positive half-waves (Figure 6.10a,b), suggesting the discrepancy is not due to an artefact of the detection algorithm. Rather, it appears that animals with lower amplitude slow waves overall have a lower ratio of negative to positive half-waves, likely due to individual differences in precise electrode location (Figure 6.10c).

It is possible that the polarity of slow waves is affected by electrode location, as it has been found that superficial layers of the cortex show inverted polarity of prelimbic oscillations (Contreras and Steriade, 1995; Peyrache et al., 2011). It would be important to eliminate animals where events analysed as negative half-waves in actual fact reflect UP states. However, it is near impossible to ascertain whether this is the case without multi-unit activity to confirm UP or DOWN states. I considered using the negative:positive ratio to exclude animals, but 1) there is no evidence that more superficial cortical layers would have more UP-DOWN-UP transitions, and 2) there were no clear clusters in the spread of the this variable. The only analysis where a polarity switch could become evident was in the slow wave-ripple or spindle coupling. As will be further explained below, these analyses led to the exclusion of WT rat B.1 from analyses relying on slow wave detection. Nevertheless, measures for both slow wave types are presented in Table 5, and no significant differences were found in any measures between genotypes.

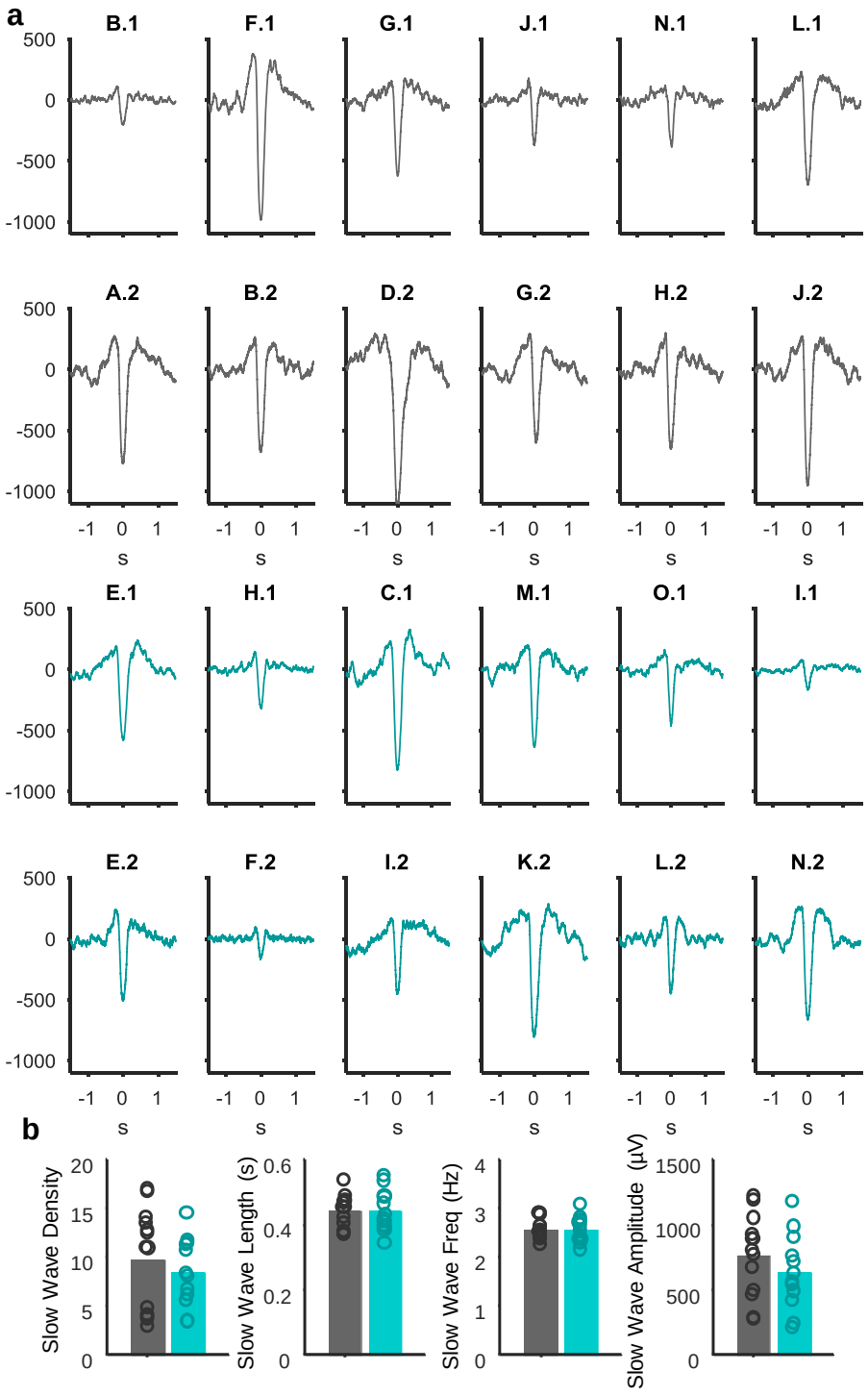

Figure 6.8 **| Slow waves: negative half waves. a,** Average waveforms of detected negative half-waves. **b,** Density, length, frequency and amplitude of negative half-waves, WT in grey, Cyfip1 in cyan. WT: n = 12, Cyfip1: n = 12.

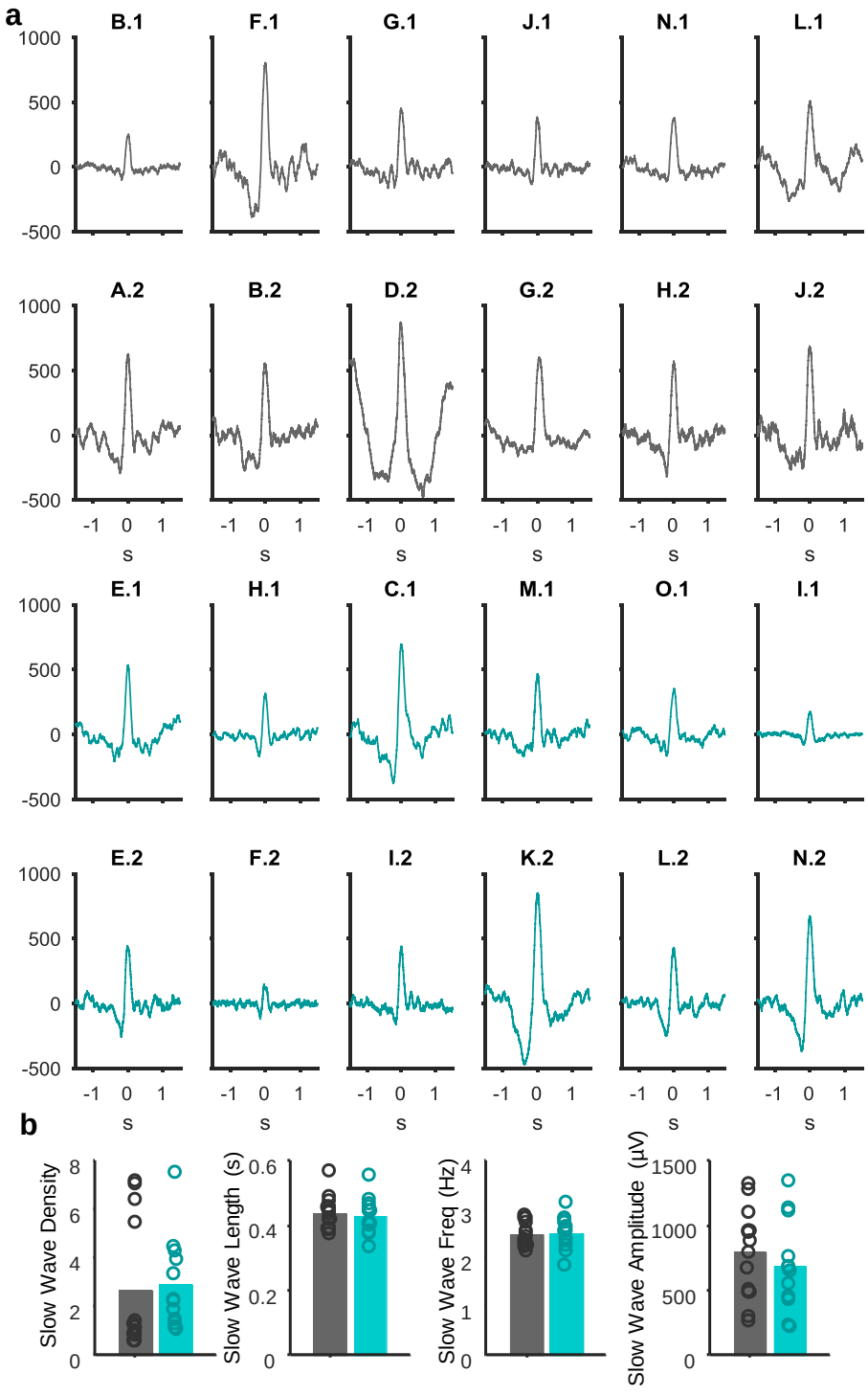

Figure 6.9 **| Slow waves: positive half waves. a,** Average waveforms of detected positive half-waves. **b,** Density, length, frequency and amplitude of positive half-waves, WT in grey, Cyfip1 in cyan. WT: n = 12, Cyfip1: n = 12.

Spectral power in the slow wave and spindle frequency ranges provides a measure of their prominence in the PRL signal. Consistent with the analyses of individual

events, in a 60 second NREM epoch, there were no genotype-related differences in slow wave power ($p = 0.247$, Mann-Whitney U test), or spindle power ($p = 0.62$) (Figure 6.10d).

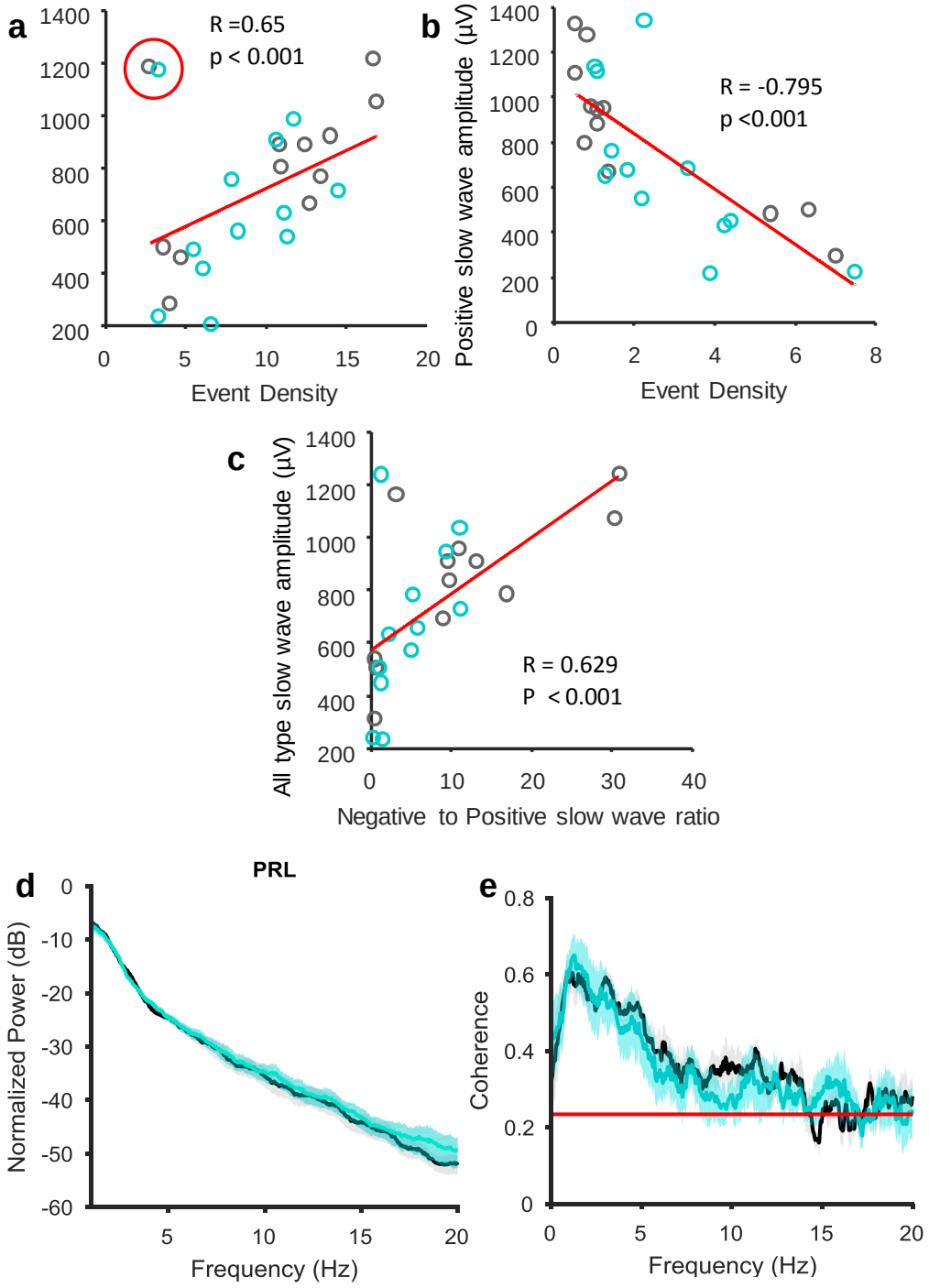

Figure 6.10 **| Slow waves: delta during NREM sleep. a,** Correlation between negative half-wave amplitude and density. Outliers are circled in red. **b,** Correlation between positive half-wave amplitude and density. **c,** Correlation between amplitude of all types of half-waves and the negative to positive half wave ratio. **d,** Power spectrum from 60 seconds of NREM sleep. WT (grey): n = 12, Cyfip1 (cyan): n = 12. **e,** Coherence spectrum between PRL and parietal cortex (in a subset of animals, WT: n=6, Cyfip1: n=6). Red line represents confidence level for significant coherence at p = 0.05.

Table 5 NREM oscillations

Cortical Slow Waves (positive half wave)				
	Density (events/min) ± SEM	**Amplitude (µV) ± SEM**	**Frequency (Hz) ± SEM**	**Length (s) ± SEM**
WT	2.66 ± 0.75	799 ± 95	2.48 ± 0.07	0.43 ± 0.01
Cyfip1$^{+/-}$	2.88 ± 0.54	682 ± 103	2.51 ± 0.10	0.43 ± 0.02
p value (t-test)	0.168 (Mann-Whitney test)	0.41	0.812	0.67

Cortical Slow Waves (negative half wave)				
	Density (events/min) ± SEM	**Amplitude (µV) ± SEM**	**Frequency (Hz) ± SEM**	**Length (s) ± SEM**
WT	9.78 ± 1.45	758 ± 86	2.57 ± 0.06	0.44 ± 0.01
Cyfip1$^{+/-}$	8.41 ± 1.02	630 ± 84	2.57 ± 0.08	0.44 ± 0.02

p value (t-test)	0.45	0.30	0.98	0.91

Thalamocortical Spindles

	Density (events/min) ± SEM	**Amplitude (μV) ± SEM**	**Frequency (Hz) ± SEM**	**Length (s) ± SEM**
WT	3.26 ± 0.12	314 ± 11	12.93 ± 0.02	0.67 ± 0.007
Cyfip1$^{+/-}$	3.22 ± 0.12	297 ± 22	12.88 ± 0.03	0.67 ± 0.009
p value (t-test)	0.79	0.49	0.19	0.75

Hippocampal Ripples

	Density (events/min) ± SEM	**Amplitude (μV) ± SEM**	**Frequency (Hz) ± SEM**	**Length (s) ± SEM**
WT	16.87 ± 1.1	278 ± 27	160.4 ± 1.14	0.080 ± 0.0008

Cyfip1$^{+/-}$	14.97 ± 1.5	192 ± 38	162.5 ± 1.17	0.078 ± 0.001
p value (t-test)	0.32	0.046 (Mann-Whitney test)	0.22	0.060

6.3.3.4 Slow wave propagation

Slow waves typically originate in the frontal cortex and can propagate towards the posterior cortex as a traveling wave (Massimini, 2004). The coherence of slow waves at different cortical sites can indicate whether this propagation is intact. Previously, a neurodevelopmental model of schizophrenia found significantly reduced slow wave coherence (Phillips et al., 2012a), indicating disrupted propagation. Only a subset of animals had a recording electrode in the posterior parietal cortex, therefore the group sizes were smaller for this analysis (WT: n=6, Cyfip1: n=6). For each animal, I looked at coherence between the PRL and parietal cortex channel in a 60 second window. Coherence in the slow wave frequency band was not significantly different between genotypes (p=0.78, t-test) (Figure 6.10e).

6.3.3.5 Slow wave-spindle coupling

A temporal coordination occurs between hippocampal and cortical networks during sleep, thought to be relevant for stabilization of memory traces. This coordination could be through the coupling of NREM sleep oscillation events, whereby ripples and slow waves are generally seen in close temporal proximity, and slow waves are closely followed by spindles (Maingret et al., 2016; Mölle et al., 2006; Siapas and Wilson, 1998; Sirota et al., 2003). These temporal relationships are also impaired in the MAM-E17 neurodevelopmental model of schizophrenia (Phillips et al., 2012a), therefore I analysed the coupling of NREM sleep oscillations.

To assess slow wave-spindle coupling, timestamps of detected negative half-slow waves were selected, as these are known to elicit a strong rebound in spindle power (Mölle et al., 2002, 2006). I assessed slow wave-triggered spindle power in each animal by calculating spindle power in a 3 s window centred on the negative peak of detected negative half waves, then averaging over all the windows (Figure 6.11). The pattern of spindle power surrounding slow waves was consistent with previous findings, with spindle power at a minimum during the down stroke of the negative half-wave, rebounding to a peak after the up stroke of the half-wave (Mölle et al., 2006; Phillips et al., 2012a). Individual slow wave-triggered spindle power traces are shown in Figure 6.11. 9 out of 11 WT and 11 out of 12 *Cyfip1*$^{+/-}$ rats showed significant slow wave-spindle coupling, with a bootstrap-determined significant difference between the negative peak and the positive peak in spindle power within a 500 ms window centred on 0. Group analysis showed no difference in the negative-to-positive peak amplitude of spindle power ($p = 0.37$, t-test). The fact that not all WT or *Cyfip1*$^{+/-}$ animals showed statistically significant coupling is likely due to a combination of factors, such as individual differences in pre-sleep behaviour which impact the level of memory consolidation, and therefore coupling seen in sleep, or differences in electrode position. This is observed by others too, for example ripple-spindle coupling was significant in 5 out of 6 control animals in the sleep study by Phillips et al. (2012).

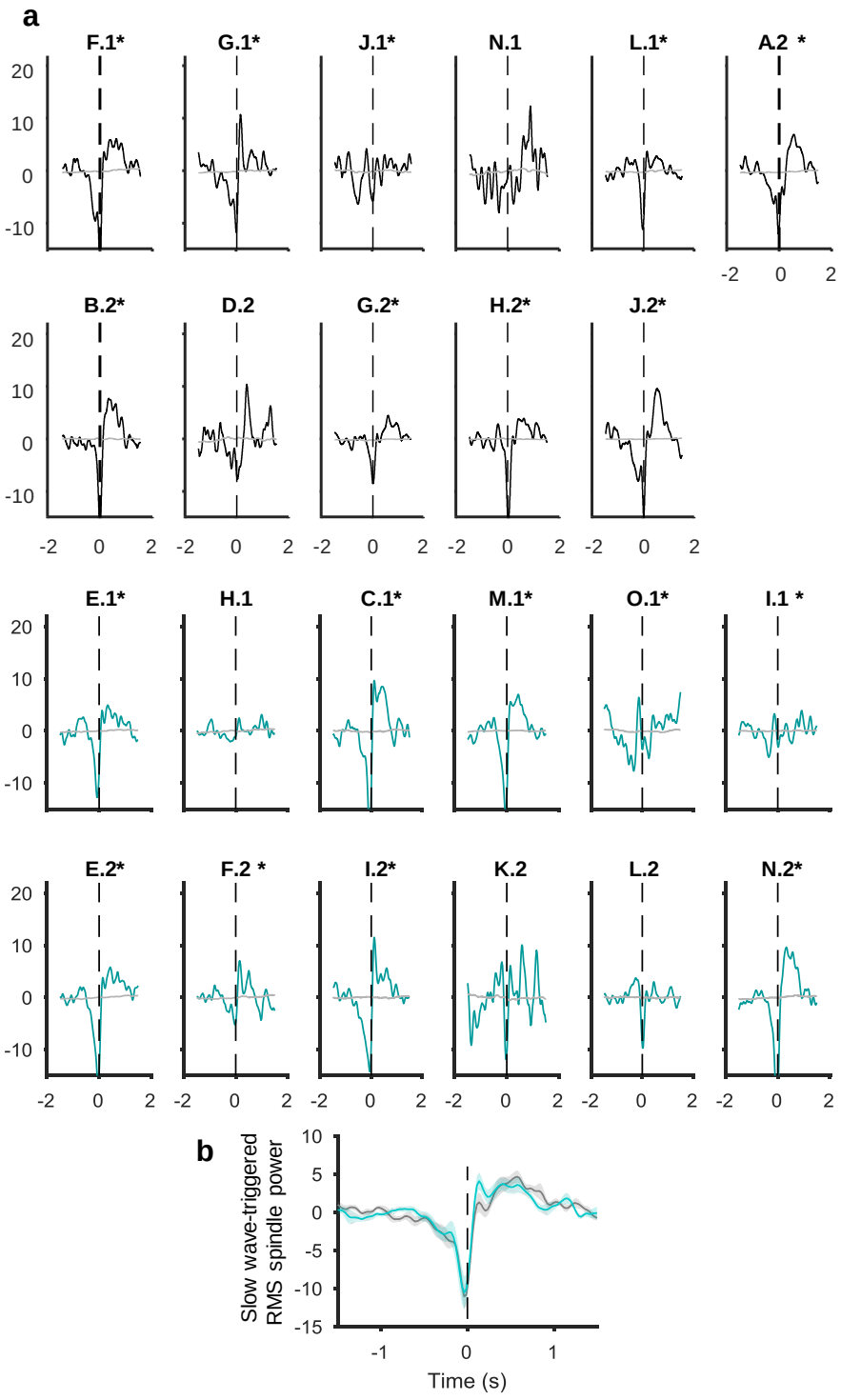

Figure 6.11 **| Slow wave-spindle coupling. a,** Slow wave-triggered root mean squared (RMS) spindle power, centred on the peak of the negative half-wave slow waves. All rats with an asterisk (*) showed a significant rebound in spindle power following the minimum at the slow wave peak, as determined by a bootstrapping method using shuffled data. WT in grey, Cyfip1 in cyan. Average shuffled data are shown in grey. Dotted line at 0 signifies the time of the negative half wave peak. **b,** Group averaged trace, shaded region represents ± SEM. Dotted line at 0 signifies the time of the negative half wave peak

6.3.3.6 Hippocampal events: Ripples

The presence and appearance of hippocampal ripples are particularly sensitive to electrode placement. Based on visual inspection of ripple average waveforms, putative ripple detection amplitudes <50 µA or with no overt ripple oscillation on the average waveform were not deemed acceptable, leading to the exclusion of one WT (rat G.2) and one *Cyfip1*$^{+/-}$ (rat H.1) animal for analyses relying on ripples (Figure 6.12). Histological confirmation of the location of electrode tips showed that G.2 appeared to have a normal lesion in the dorsal CA1, suggesting a fault with the electrode itself, while H.1 was more lateral and dorsal than other lesions (see General Methods for diagrams).

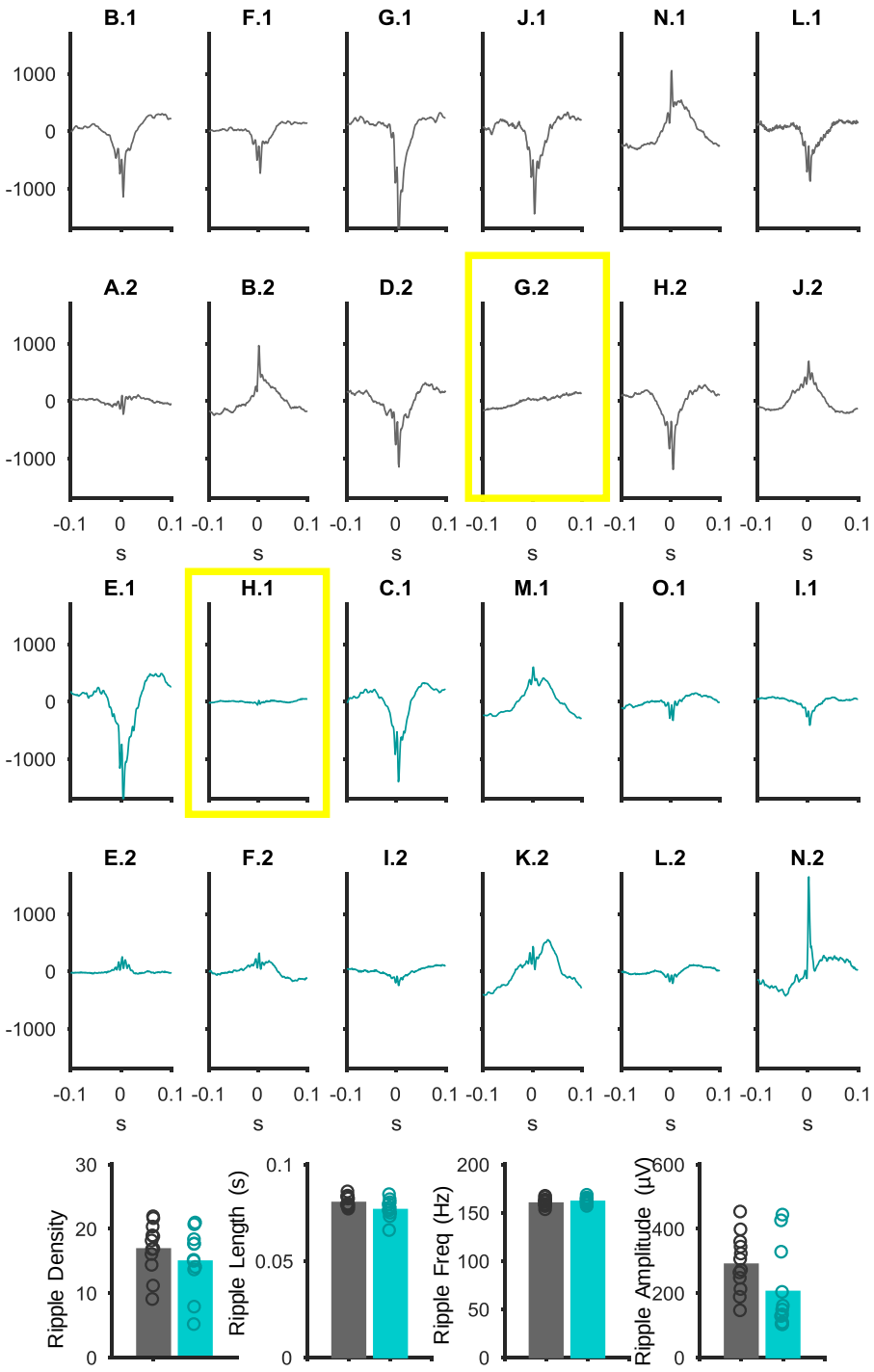

Figure 6.12 **| Ripples. a,** Average waveforms of detected ripples. Yellow boxes mark excluded animals. **b,** Density, length, amplitude, frequency and length of ripples, excluding rats G.3 and H.3, WT in grey, Cyfip1 in cyan.

NREM sleep recordings from remaining animals showed no genotype-dependent differences in ripple density, or frequency (Table 5); however, abnormalities in

other parameters were revealed (Figure 6.13). There was a trend for shorter ripples in *Cyfip1*$^{+/-}$ rats following the removal of one *Cyfip1* outlier ($p = 0.06$, t-test). With the mild outlier left in, reduced ripple length reached significance ($p = 0.031$, t-test). Ripple amplitude was significantly reduced in *Cyfip1*$^{+/-}$ rats, although this measure also captures the sharp wave amplitude, which is especially sensitive to electrode position relative to the CA1 pyramidal cell layer (Buzsáki, 1986). A better measure of ripple amplitude is power in the ripple frequency band. An 80 - 400 Hz bandpass filtered power spectrogram time-locked to ripple peak (see Methods) showed significantly reduced ripple power in *Cyfip1*$^{+/-}$ rats ($p = 0.044$, Mann-Whitney U test). A trend of reduced length and significantly reduced ripple power suggests weaker ripple generation, potentially due to deficiencies in local CA3-CA1 ripple-generating networks.

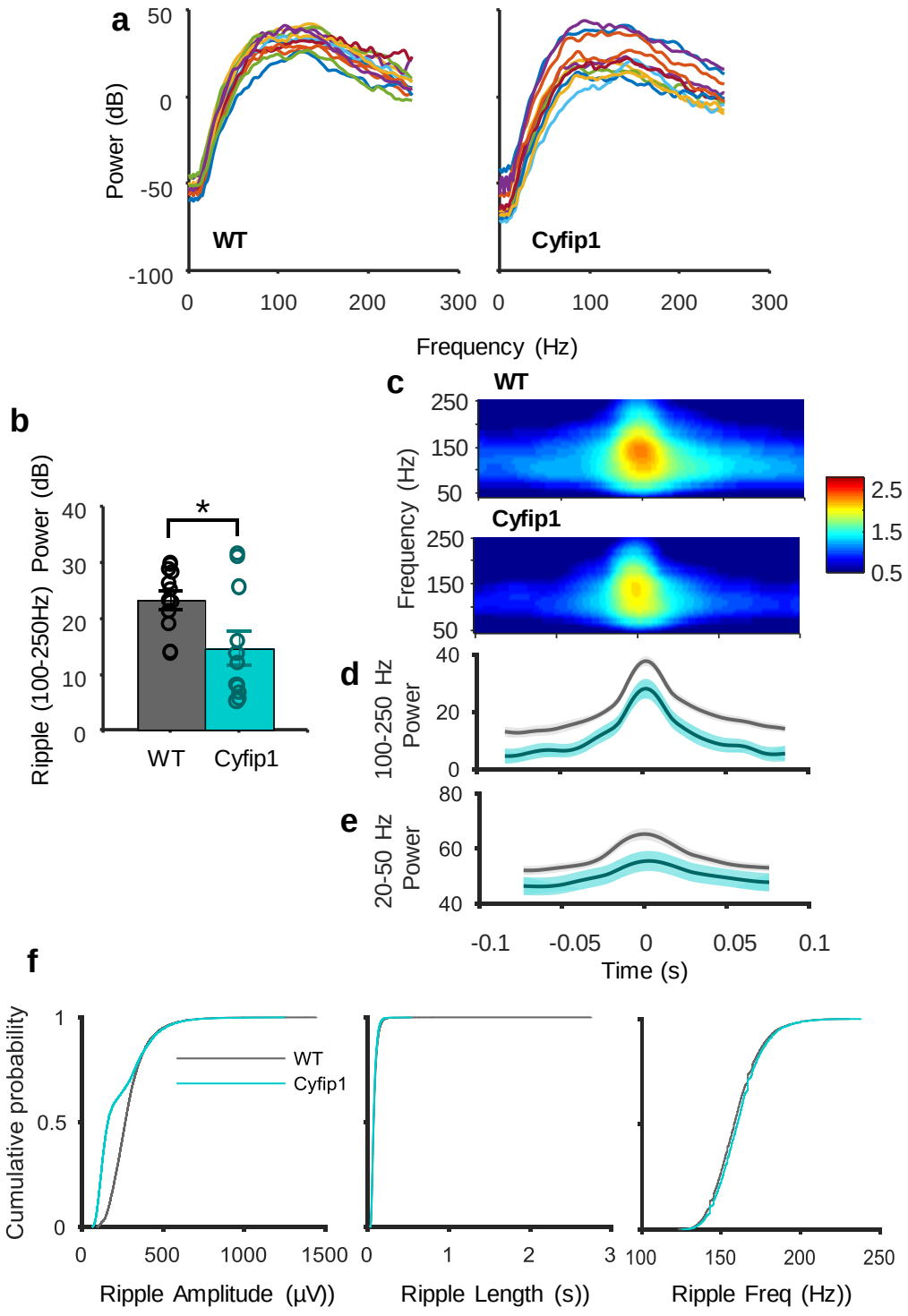

Figure 6.13 **| Ripple power. a,** Ripple time-locked power spectrum of bandpass filtered signal (80-400 Hz) from a 200 ms window, averaged over all ripples. Each line represents a different animal, excluding rats G.3 and H.3. **b,** Average ripple power (100-250 Hz) in the 200 ms window time-locked to the peak of detected ripples. **c,** Ripple time-locked power spectrograms of filtered (80-400 Hz) signal, averaged all ripples and over animals. **d,** Ripple power within the ripple time-locked 200 ms window in WT (grey) and Cyfip1 (cyan) rats. **e,**

Slow gamma power (20-50 Hz) within the ripple time-locked 200 ms window, colours as above. **f,** Cumulative probability plots.

What is the impact of weaker ripples on the incidence of replay and therefore memory consolidation in *Cyfip1*$^{+/-}$ rats? Without unit recordings it is difficult to know how abnormal ripples might be affecting the recruitment and reactivation of waking ensembles. One hint might come from a study that suggests slow gamma (20-50 Hz) is responsible for entraining CA3 and CA1 spiking, and found that the level of synchrony of slow gamma between CA1 and CA3 was predictive of the extent of replay occurring during the ripple (Carr et al., 2012). Therefore, I calculated gamma power in the 20-50Hz range during ripples from a power spectrogram time-locked to ripple peaks, and found it to be significantly reduced in *Cyfip1*$^{+/-}$ rats ($p = 0.035$, t-test). Slow gamma power was normal during behaviour (see Chapter 3) and during a 60 second NREM epoch gamma was not significantly reduced ($p = 0.07$, t-test, data not shown), suggesting the slow gamma power reduction is specific to ripple events. Given the suggested involvement of slow gamma coherence in replay, this might hint at deficient memory consolidation due to abnormal ripple information content.

6.3.3.7 Slow wave-ripple coupling

Analysing the coupling between cortical spindles and slow waves and hippocampal ripples provides another opportunity to assess functional coupling in the hippocampal-prelimbic network, this time during sleep. Nine out of 10 WT rats showed slow wave-ripple coupling, with a bootstrap-determined significant difference between the positive peak 500 ms prior to 0 and the negative peak within a 200 ms window centred on 0 (Figure 6.14). Only 7 out of 11 *Cyfip1*$^{+/-}$ rats passed this threshold for significance of coupling, although a Fisher's Exact test did not show a significant difference in the number with significant coupling ($p = 0.31$). Group analysis showed a trend for reduced coupling in *Cyfip1*$^{+/-}$ rats, as they showed a smaller positive-to-negative peak change of ripple power ($p = 0.099$, Mann-Whitney U Test). The distribution of *Cyfip1*$^{+/-}$ peak change values was non-normally distributed, reflecting high coupling in four animals. This is consistent

with the non-normal distribution of ripple power seen previously, suggesting some *Cyfip1*$^{+/-}$ rats show relatively normal ripples.

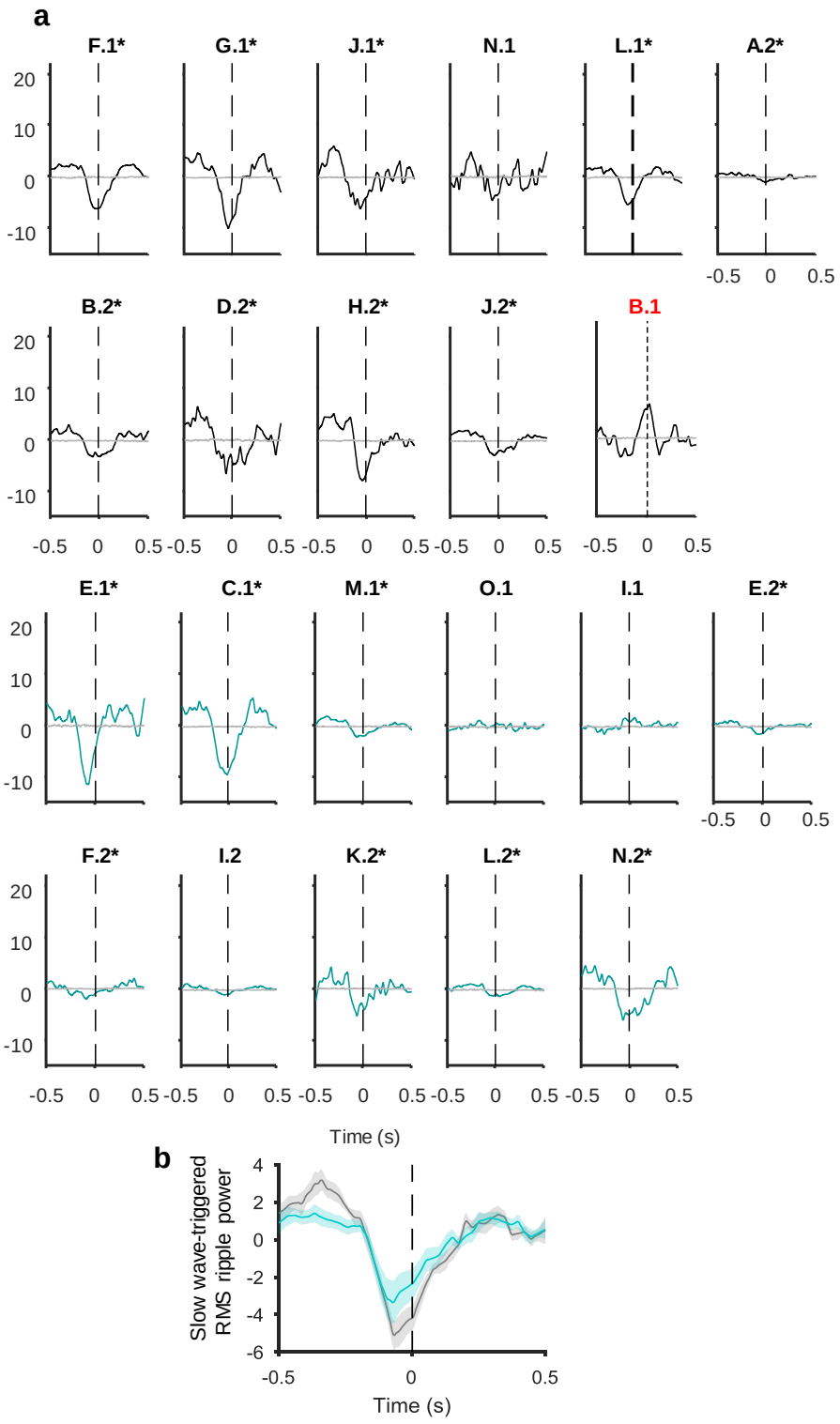

Figure 6.14 **| Slow wave-ripple coupling. a,** Slow wave-triggered ripple power, centred on the peak of the negative half-wave slow waves. All rats with an asterisk (*) showed a significant difference between peak ripple power prior to the slow wave and minimal ripple power around 0, the time of the negative half-wave peak, as determined by a bootstrapping method using shuffled data. WT in grey, Cyfip1 in cyan. Average shuffled data are shown

in grey. Dotted line at 0 signifies the time of the negative half wave peak. WT shown in dark grey, Cyfip1 in cyan. WT rat B.1 (red) was excluded, not opposite relationship of slow wave ripple coupling (see text). **b,** Group averaged data centred on the negative half-wave slow waves.

6.3.3.8 Exclusion of rat B.1

As mentioned above, WT rat B.1 was excluded from analyses relying on slow wave detections as it was suspected his PRL signal had a polarity shift. This was suggested by the fact that slow wave-spindle coupling was not significant and had an unusual profile compared to other rats. Furthermore, slow wave-ripple coupling was in fact significant but in the opposite direction to all the other animals: B.1 showed a positive peak in ripple activity where other animals had a minimum, suggesting that the detected negative half-wave did in fact represent an DOWN-UP-DOWN transition. As this could not be confirmed without multi-unit activity, this animal was excluded.

6.3.3.9 Ripple-spindle coupling

Ripple-spindle coupling was also present, again reflecting interaction in the hippocampal-prelimbic network (Figure 6.15). Spindle power peaked within a 200ms window of ripples times, as seen previously (Phillips et al., 2012a; Wierzynski et al., 2009). Rats lacking ripples (H.1 and G.2) were excluded from this analysis, but B.1 was included, as this analysis does not rely on slow wave detection and is unaffected by signal polarity. 8 out of 11 WT and 10 out of 11 *Cyfip1*$^{+/-}$ rats showed ripple-spindle coupling, with a bootstrap-determined significant positive peak within 200ms of 0. Group analysis showed no significant difference between positive peak of spindle power between groups ($p = 0.107$).

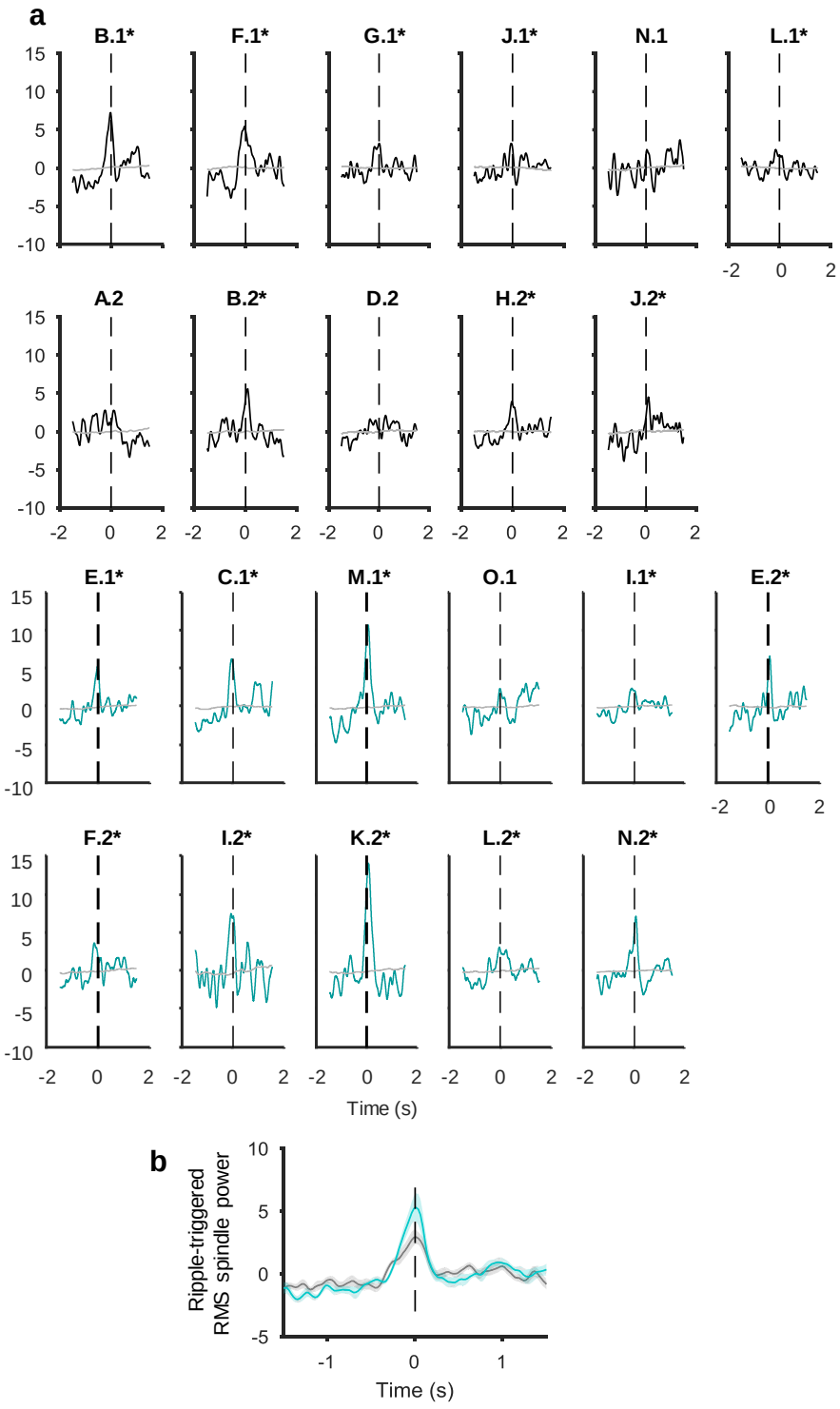

Figure 6.15 **| Ripple-spindle coupling. a,** Ripple-triggered spindle power, centred on the peak amplitude of the ripple. All rats with an asterisk (*) showed a significant maximum peak within 200 ms of 0, as determined by a bootstrapping method using shuffled data. WT in grey, Cyfip1 in cyan. Average shuffled data are shown in grey. Dotted line at 0 signifies the time of the ripple peak amplitude. **b,** Group averaged data centred on the peak of ripples.

The finding that ripple-triggered spindle power is normal in *Cyfip1*$^{+/-}$ rats suggests that the observed trend for reduced slow wave-ripple coupling is likely to stem from reduced ripple power, rather than a unique coupling deficit between hippocampus and prelimbic cortex. Therefore, these findings suggest that the hippocampal-prelimbic network is intact in *Cyfip1*$^{+/-}$ rats during NREM sleep, consistent with results in Chapter 3 where the network is unimpeded during behaviour.

6.4 Discussion

Results in this chapter found:

- PIRs provide a valid measure of immobility-defined sleep in rats.
- Normal circadian activity and immobility-defined sleep patterns in *Cyfip1*$^{+/-}$ rats.
- Normal sleep architecture during an *in vivo* electrophysiology recording.
- Slow wave and spindle properties were unchanged in *Cyfip1*$^{+/-}$ rats, including normal slow wave-spindle coupling.
- Hippocampal ripple power was reduced in *Cyfip1*$^{+/-}$ rats, although density and frequency remained stable, and low gamma (20-50 Hz) power was reduced specifically during ripples, hinting at abnormality in the informational content of ripples.
- The hippocampal-prefrontal network remains intact during NREM sleep, evidenced by normal ripple-spindle coupling, and the trend for reduced slow wave-ripple coupling in *Cyfip1*$^{+/-}$ rats is likely due to reduced ripple power.

6.4.1 Actigraphy

My hypothesis that *Cyfip1*$^{+/-}$ rats may have disrupted circadian rhythms was based on the abundance of psychiatric disorder-relevant genetic models showing disturbances including the *Fmr1*/*Fxr2* KO mouse. However, I did not observe any changes in circadian activity, as measured by non-parametric, circadian and hourly activity measure, nor sleep patterns, as assessed by immobility-defined sleep amount and sleep bouts. Sleep fragmentation, a common sleep disturbance in psychiatric disorders (Wulff et al., 2010), was not evident, and while the PIR-

determined sleep approach may be insufficient to detect subtle sleep fragmentation phenotypes, the lack of a sleep fragmentation effect in the LFP recording supports this conclusion.

There is currently no data on the sleep patterns or sleep neurophysiology of 15q11.2(BP1-BP2) deletion carriers; however, reports of sleep abnormalities in the literature associated with this locus (Burnside et al., 2011; Elert-Dobkowska et al., 2014; Urraca et al., 2013) and anecdotal reports of sleep disturbance from the parents of children in the Cardiff 15q11.2 cohort partly prompted this study. A systematic actigraphy and sleep neurophysiology study is planned for this cohort and it will be interesting to compare the finding in the *Cyfip1*$^{+/-}$ rat with the deletion carriers.

Thus it appears that circadian activity and sleep is normal in *Cyfip1*$^{+/-}$ rats, however, it is possible that challenging the robustness of these patterns may reveal differences. For example, it is possible that while under light-entrained conditions the circadian pattern appears normal, exposing animals to constant light conditions or constant darkness would reveal a deficit of the internal SCN-mediated circadian rhythm. This pattern of deficit was seen in the *Fmr1* KO mice, whereby under regular light conditions they appeared normal, but showed a significantly shorter free-running period than WT in constant darkness. Therefore, to fully rule out any circadian disruption, *Cyfip1*$^{+/-}$ rats should be tested under these conditions. In a similar vein, other studies have challenged sleep homeostasis by sleep deprivation to reveal phenotypes in recovery sleep (Jaaro-Peled et al., 2016; Kumar et al., 2015).

One limitation to using PIR actigraphy to assess circadian rhythms is that locomotor activity is an indirect measure of circadian rhythmicity, and is influenced by many other factors including motor deficits, anxiety and arousal levels. For example, it could be proposed that if *Cyfip1*$^{+/-}$ rats were in a state of hyperarousal leading to hyperlocomotion, they would appear to have normal activity levels. More direct measures of circadian activity could include monitoring *Clock* gene rhythms within the SCN.

In summary, PIR actigraphy monitoring revealed no circadian or sleep abnormalities in *Cyfip1*$^{+/-}$ rats. The validation of the immobility-defined sleep measure in rats establishes the PIR actigraphy system as a useful tool in screening other genetic model rats in our lab. In addition, rolling out the installation of these low-cost PIRs over all cages will lead to animal welfare benefits, for example by monitoring activity of animals recovering from surgery.

6.4.2 Sleep neurophysiology

Sleep electrophysiology recordings allowed a finer scale assessment of sleep in *Cyfip1*$^{+/-}$ rats. Consistent with normal actigraphy measures, sleep architecture in terms of sleep latency and NREM and REM proportion were normal in *Cyfip1*$^{+/-}$ rats. Consistent with normal PRL activity during wake, slow waves and spindle oscillations were unchanged in *Cyfip1*$^{+/-}$ rats. However, ripple oscillations in *Cyfip1*$^{+/-}$ rats were significantly weaker than in WTs, as determined by a trend of reduced length, and significantly reduced ripple power. Furthermore, slow gamma, thought to be involved in coordinating replay during ripples (Carr et al., 2012), was reduced specifically during ripples in *Cyfip1*$^{+/-}$ rats. What mechanism might underlie the weakening of ripples seen in *Cyfip1*$^{+/-}$ rats? One hint may lie in the abnormalities identified at Schaffer collateral-CA1 synapses by Bozdagi et al. (2012), the same CA3-CA1 network involved in ripple generation, where they observed enhanced mGluR-dependent LTD. Inhibition of this pathway is known to disrupt ripple generation (Nakashiba et al., 2009), so it is possible that enhanced LTD in this circuit reduces the ability of CA3 neurons to influence CA1. Although currently there is no evidence to link ripple generation to aberrant LTD at this synapse in *Cyfip1*$^{+/-}$ mice, it is interesting to note that common intra-hippocampal networks are being identified as abnormal in the *Cyfip1*$^{+/-}$ rat.

Only a handful of psychiatric disorder-relevant animal models have characterised hippocampal ripple properties to date. As mentioned, the calcineurin knockout and DISC1 mutant mouse models reported increased ripple power and density, but less replay of the recent spatial experience (Altimus et al., 2015; Suh et al., 2013). Further experiments should incorporate unit recordings to allow the informational

content of abnormal ripples to be examined in *Cyfip1*$^{+/-}$ rats. Furthermore, while core ripple properties were normal in MAM-E17 rats (Phillips et al., 2012a) further analysis found increased ripple activity specifically during wake (Bartsch & Jones, unpublished), supporting the idea that waking ripples are differentially modulated by psychiatric risk factors. Therefore, further analysis of my data should address properties of waking ripples in *Cyfip1*$^{+/-}$ rats.

A recent study using the *Fmr1*-KO mutant mouse showed that while the intrinsic properties of hippocampal CA1 place cells were normal, their firing relationship to LFP oscillations was abnormally weak, leading to weaker coordination among ensembles (Talbot et al., 2018). The authors did not analyse ripples or NREM sleep for this paper, but the findings could be predicted to extend to aberrant ripples, which would implicate the FMRP-related pathway in causing abnormal ripples. Malkki et al. (2016) assessed ripple properties in the *Arc/Arg3.1* knockout mouse model. As mentioned in Chapter 1, *Arc* is an mRNA target of CYFIP1/FMRP-mediated translation regulation, involved in homeostatic plasticity and actin polymerization. They found subtle abnormalities in *Arc/Arg3.1* KO ripples, including reduced ripple duration, which support the suggestion that disrupting the downstream protein pathway of Cyfip1 could lead to aberrant ripple generation.

It is currently unknown whether schizophrenia patients have normal ripples due to the difficulty of recording hippocampal signals in humans, although more general hippocampal dysfunction exists (Tamminga et al., 2010). However, since schizophrenia patients have pathological parvalbumin interneurons which cause alterations in gamma oscillations, it has been proposed that their role in ripple generation might lead to aberrant ripples (Buzsáki, 2015). Moreover, cognitive symptoms do point towards the disruption of memory consolidation mechanisms, implicating ripples as a key element to explore further. Overall, the weak ripple phenotype observed in *Cyfip1*$^{+/-}$ rats extends the sparse evidence base linking disrupted ripples to psychiatric risk.

6.4.3 Future directions

Next experiments should aim to corroborate the finding of abnormal ripples in *Cyfip1*$^{+/-}$ rats and investigate any behavioural consequences of ripple deficit. The non-normal distribution of ripple power seen in *Cyfip1*$^{+/-}$ rats, with some rats appearing to have normal ripples, might cast some doubt over the validity of this finding. Why might some *Cyfip1*$^{+/-}$ rats have normal ripples while others are impaired? A limitation of static LFP electrodes is the lack of certainty of their precise location, which in the case of ripples, can have a significant impact on their appearance. Further experiments using silicon probes would allow multi-layer recording and more precise identification of pyramidal layer location from observation of waveform shapes and characteristic burst mode firing (e.g. Sirota et al. 2003; Sullivan et al. 2011). If the abnormal ripple phenotype is confirmed, spiking properties of individual pyramidal cells and interneurons participating in the generation of abnormal ripples could be examined to further understand the origin of the pathophysiology, and ask whether replay is adversely affected.

It has been shown that abnormal ripples might lead to abnormal replay (Suh et al., 2013). It would be interesting to test whether the impact of abnormal *Cyfip1*$^{+/-}$ ripples on memory consolidation might manifest as a behavioural deficit in *Cyfip1*$^{+/-}$ rat recall performance following sleep. Successful recall in the novel object location task has been shown to be sensitive to sleep during the delay phase (Binder et al., 2012; Maingret et al., 2016). Therefore, I would hypothesise that *Cyfip1*$^{+/-}$ rats would be less able to distinguish the novel object location following sleep than WTs.

Finally, since this study assessed baseline properties of NREM sleep oscillation events, it would be interesting to investigate the impact of a novel experience/learning on sleep events. This can be achieved by comparing event properties in sleep before and after an experience that elicits memory consolidation. For example, following the learning of a novel association task, rats had increased amplitude, duration and density of ripples in post-learning sleep (Eschenko et al., 2008). Rats that did not learn the task showed reduced modulation of ripple activity.

Similar correlations exist with spindles (Fogel and Smith, 2006). The T maze task in this study was not expected to elicit a change in ripple or spindle activity, as it was a familiar environment, and no new rule learning was expected as the animals were well trained on the non-match-to-place rule.

In summary, results from this chapter reveal that *Cyfip1*$^{+/-}$ rats' activity patterns and sleep are largely unaffected, but they show a subtle, specific abnormal ripple phenotype. Together with the reduced intra-hippocampal theta-gamma coupling seen in Chapter 3, these findings point towards a local hippocampal network deficit. Future studies should address the single unit activity underlying this deficit, as well as any consequences of disrupted hippocampal networks on memory consolidation.

7

Chapter 7 Circadian patterns and sleep neurophysiology in the *Fmr1* knockout rat – a pilot study

This chapter describes a pilot actigraphy and neurophysiology study in a rat model of Fragile X Syndrome. Infrared sensor-based actigraphy monitoring showed that *Fmr1* knockout rats have normal circadian sleep and activity patterns. However, *in vivo* LFP recordings revealed fragmented sleep and elevated dCA1 ripple power in the *Fmr1* knockout model.

7.1 Introduction

CYFIP1 first drew the attention of the research community due to the finding that it is a binding partner of FMRP (Schenck et al., 2001b), and only later was CYFIP1 itself implicated as a risk gene for intellectual disability, autism and schizophrenia (Bittel et al., 2006; Butler, 2017; Stefansson et al., 2008). Fragile X syndrome, first described in 1943 (Martin and Bell, 1943), is caused by mutations in the *Fmr1* gene, leading to the loss of FMRP, the protein it encodes. Fragile X syndrome has since been recognised as one of the leading monogenetic causes of intellectual disability and Autism Spectrum Disorder (ASD), especially in boys due to its X-linked aetiology (Garber et al., 2008). This chapter investigates circadian activity patterns and sleep neurophysiology of the CRISPR/Cas9 generated *Fmr1* KO rat in an effort

to begin to compare and contrast the observed phenotypes with those seen in the *Cyfip1*$^{+/-}$ rat model.

7.1.1 Fragile X Syndrome

Fragile X syndrome is the most common heritable form of intellectual disability (ID), affecting 1 in 4000 males and 1 in 6000-8000 females (Crawford et al., 2001). The clinical phenotype is complex and variable, but includes intellectual disability, autism-related behaviours, anxiety, attention deficit hyperactivity disorder and hyperarousal to sensory stimuli (reviewed in Schneider et al. (2009)). The syndrome is caused by a CGG expansion in the *Fmr1* gene, resulting in near complete loss of function of FMRP. Healthy individuals have around 30 repeats, but when repeats exceed 200, the *Fmr1* gene is silenced due to hypermethylation of its promoter region (Coffee et al., 1999; Fu et al., 1991; Sutcliffe et al., 1992), and protein levels are reduced (Godler et al., 2010). Thus *Fmr1* KO animals model functional FMRP loss, but not through the same genetic mechanism. FMRP, together with CYFIP1, binds to mRNAs, many encoding synaptic proteins and regulates the translation of over 800 gene products (Darnell and Klann, 2013; Darnell et al., 2011). In the absence of FMRP, excess translation leads to disruptions in several aspects of neuronal function such as dendritic spine morphology (He and Portera-Cailliau, 2013), hippocampal and cortical plasticity (Huber et al., 2002; Li et al., 2002) and neuronal excitability (Contractor et al., 2015).

There are a number of parallel findings between the *Cyfip1*$^{+/-}$ and *Fmr1* KO mouse models (Bozdagi et al., 2012). mGluR activation leads to a release of FMRP-repression of translation resulting in LTD at glutamatergic synapses in hippocampal CA1 (Huber et al., 2000; Lüscher and Huber, 2010; Malenka and Bear, 2004). As in *Cyfip1*$^{+/-}$ mice, *Fmr1* KO mice have enhanced mGluR-dependent LTD, which is independent of protein synthesis (Bozdagi et al., 2012; Huber et al., 2002). Following from the known effects of FMRP-CYFIP1 repression on synaptic protein translation, *Fmr1* KO mice have increased translation of synaptic proteins, such as Arc (DeRubeis et al., 2013), which, as discussed in Chapter 1, leads to disruptions to normal synaptic plasticity (reviewed in Wilkerson et al. (2018)). There are

overlaps in the abnormal dendritic spine morphology seen in *Cyfip1*$^{+/-}$ mice and *Fmr1* KO mice, such as a greater number of long and immature dendritic spines (Galvez and Greenough, 2005; Irwin et al., 2002), although CYFIP1 also influences dendritic spine formation via the WAVE complex (DeRubeis et al., 2013; Pathania et al., 2014). The hallmark abnormal dendritic spines in Fragile X syndrome are likely caused by dysregulation of actin dynamics via Rac1 signalling (Arber et al., 1998; Castets et al., 2005; Yang et al., 1998). In addition, the enhanced extinction in inhibitory avoidance behaviour observed in *Cyfip1* is paralleled in *Fmr1* KO mice (Dölen et al., 2007).

Such changes to normal synaptic function lead to altered neural network function in Fragile X syndrome and might contribute to the 15q11.2 deletion phenotype, particularly their shared symptoms such as cognitive deficits and increased risk for autism.

7.1.2 Abnormal networks in Fragile X Syndrome

Functional and structural imaging studies in Fragile X syndrome patients have shown abnormal activation in a wide range of brain areas including prefrontal-striatal networks during impulse control tasks (Hoeft et al., 2007) and prefrontal cortex and hippocampus during working memory tasks (Greicius et al., 2004; Kwon et al., 2001) (reviewed in Lightbody & Reiss, (2009)). Neuroimaging studies have shown that functional connectivity between cognitive and affective brain networks is also compromised (Hall et al., 2013). EEG studies in Fragile X syndrome have largely focussed on measures relevant to sensory processing, finding abnormal auditory event-related potentials (reviewed in Sinclair et al. (2017) and comorbid epilepsy (Di Bonaventura et al., 2006; Musumeci et al., 2001). Recently, a number of studies have reported on baseline neural oscillations, finding increased gamma frequency band power (Ethridge et al., 2017; Wang et al., 2017), increased theta power (Van der Molen and Van der Molen, 2013) and a decrease in global functional connectivity in upper alpha and beta frequency bands (10-12 Hz, 13-30 Hz), but increased connectivity in the theta band in fronto-posterior long range and some short range interactions (van der Molen et al., 2014).

7.1.3 Abnormal networks in *Fmr1* KO rodent models

Electrophysiology data from rodent models point towards an imbalance between excitation and inhibition in cortical circuits underlying the symptoms of Fragile X syndrome and autism more broadly (Foss-Feig et al., 2017; Golden et al., 2018). In particular, there is a pattern of hypersynchrony in sensory cortices (Contractor et al., 2015) that leads to, for example, exaggerated sensory-evoked potentials (Lovelace et al., 2018) and a reduced threshold for audiogenic seizures (Rotschafer and Razak, 2013).

The increased EEG gamma band power seen in Fragile X syndrome (Ethridge et al., 2017; Wang et al., 2017) has recently been recapitulated in the *Fmr1* KO mouse (Lovelace et al., 2018; Sinclair et al., 2017a) and rat model (Berzhanskaya et al., 2017). Lovelace et al. (2018) found increased gamma (30-100 Hz) and delta (1-4 Hz) during resting state in auditory and frontal cortex in skull screw EEG recordings. The increase in gamma was independent of movement, while delta changes were only seen when the animals were moving. Berzhanskaya et al. (2017) recorded in visual cortex of juvenile *Fmr1* KO rats and found a similar increase in gamma and theta band power during resting state, also independent of movement, while WT animals saw a decrease in gamma power during quiet rest. The authors suggest this excessive synchronous activity in the gamma band represents a 'failure to inactivate'.

Another set of studies investigating abnormal circuits in the mouse model have focused on networks in the sensory cortex (Gibson et al., 2008; Gonçalves et al., 2013; Hays et al., 2011), revealing abnormalities in UP/DOWN states which are relevant to the generation of slow waves during NREM sleep (McCormick and Bal, 1997; Steriade et al., 1993b). Slice recordings from L4 and L5 excitatory neurons in *Fmr1* KO mice showed prolonged UP states, both evoked (Gibson et al., 2008) and naturally occurring (Hays et al., 2011). Prolonged UP states were also observed *in vivo* in adult *Fmr1* KO mice under urethane anaesthesia (Hays et al., 2011). Whole-cell recordings of L2/3 neurons *in vivo* in sleeping *Fmr1* KO mice revealed a doubling of neuronal firing probability during UP states, although prolonged UP

states were not seen. In fact, these neurons had a 3-fold higher firing rate compared to WT in P14-16 animals at rest or asleep (Gonçalves et al., 2013). This abnormally high firing rate during sleep may interfere with the memory consolidation processes occurring during NREM sleep, such as the temporal coordination of hippocampal-cortical NREM sleep oscillations which has been shown to facilitate memory consolidation (Contractor et al., 2015; Maingret et al., 2016).

While most studies in the *Fmr1* KO model have focussed on cortical oscillations, a number of studies reporting on hippocampal oscillations have emerged in recent years. A recent study recorded hippocampal CA1 place cell activity in freely moving *Fmr1* KO mice. They observed changes in synaptic plasticity, normal place fields, normal hippocampal theta and gamma power but a deficient relationship of CA1 neuronal firing to the local field potential, with *Fmr1* KO cells more weakly modulated than in WTs (Talbot et al., 2018). Another recent set of studies found slightly contrasting results. These authors did observe place cell impairments in the form of impaired place cell stability and reduced specificity of spatial representations (Arbab et al., 2017). In addition, they found abnormally increased theta power and increased slow gamma (20-50 Hz) synchrony between tetrodes in dCA1 (Arbab et al., 2018). Theta-gamma phase amplitude coupling has been found to be disrupted in a complex pattern linked to changes in cognitive demand (Radwan et al., 2016).

Given the disruptions to waking functional connectivity in patients and aberrant cortical and hippocampal circuits in animal models, investigation of the evolutionarily conserved NREM sleep oscillation events and their coordination is a useful tool to interrogate distributed network activity (see also Chapter 6). Indeed, sleep patterns and NREM sleep oscillations appear to be disrupted in Fragile X patients and animal models.

7.1.4 Disrupted sleep in Fragile X syndrome

Sleep abnormalities are regularly reported in Fragile X syndrome (Esbensen and Schwichtenberg, 2016; Picchioni et al., 2014). Findings include difficulty falling

asleep (increased sleep latency), reduced sleep time and fragmented sleep with frequent night awakenings (Gould et al., 2000; Kronk et al., 2010; Miano et al., 2008; Musumeci et al., 1995). The largest of these studies (n = 1295) reported that 32% of patients are affected, and of these 84% have two or more sleep problems, although almost half the patients were medicated for sleep problems so this may be an underestimate (Kronk et al., 2010). In addition, sleep problems correlated with behavioural phenotype severity (Kronk et al., 2010). Sleep neurophysiology in Fragile X syndrome has not been well studied, but polysomnography studies in small samples found a greater percentage of stage 1 NREM sleep and fewer REM epochs compared to healthy controls (Elia et al., 2000; Miano et al., 2008). In addition, Miano et al. (2008) identified abnormal slow wave patterns during NREM sleep.

Disrupted sleep has also been reported in the *Drosophila* model (*dfmr1*) and mouse models of Fragile X syndrome (Bushey et al., 2009; Zhang et al., 2008). In mice, the *Fmr1* deletion alone led to a modest deficit, with a shorter period length when in constant dark conditions, indicating normal entrainment or circadian activity when a light cue is present, but deficits when activity patterns rely on intrinsic, self-generated circadian rhythms. However, mutating both *Fmr1* and its paralog *Fxr1* results in a dramatic total loss of circadian rhythmicity (Zhang et al., 2008), highlighting the relevance of these proteins in circadian activity patterns. A home cage activity monitoring study found that adult *Fmr1* KO mice had decreased sleep during the inactive (light) phase, and this phenotype was exacerbated in the model with an additional mutation in *Fxr1* (Saré et al., 2017).

The known disruption of cortical networks coupled with the alteration in circadian rhythms and sleep in the *Fmr1* KO mouse (Saré et al., 2017; Zhang et al., 2008) as well as disturbed sleep in Fragile X syndrome patients (Kronk et al., 2010; Miano et al., 2008) drove an interest in investigating resting state cortical oscillations and sleep and circadian rhythm characteristics in the *Fmr1* KO rat.

7.2 Methods

7.2.1 Animals

Twelve 12-week-old male Long Evans rats (6 WT and 6 *Fmr1* KO) were obtained from Professor Peter Kind, University of Edinburgh, UK (Till et al., 2015). The rat model was generated using the CRISPR/Cas9 genome editing system. Animals were 4-6 months old during the experiments described. Surgical implantation for electrophysiological recording of LFP signals was as described in Chapter 2.

7.2.2 Actigraphy

Animals were 4 months old during the actigraphy experiment which took place prior to surgery (see Chapter 2 for details of the monitoring set up). Animals were moved into the reverse light room (12:12 light:dark, lights on at 8pm) and monitored for 31 days. Animals became entrained to the new light regime over the first 12 days (not unlike the human experience of jetlag), separating the recording into 12 days of 'jet lag' and 19 days of 'adjusted' recordings. Data was analysed as described in Chapter 2.

7.2.3 Surgery and data acquisition

Twelve five-month-old animals, 6 WT and 6 *Fmr1* KO, were implanted with chronic LFP microdrives for recording including electrodes in PRL, dCA1 and parietal cortex, as described in Chapter 2. Two animals died during the surgery, so data is reported for 5 WT and 5 *Fmr1* KO rats. Sleep recordings were conducted as described in Chapter 2.

7.2.3.1 Histological verification of electrode placement

Animals were terminally anaesthetised, lesioned, perfused and coronal sections were prepared as described in Chapter 2. Lesion sites were identified and cross-checked with the Rat Brain Atlas (Paxinos & Watson 2007) (Figure 7.1).

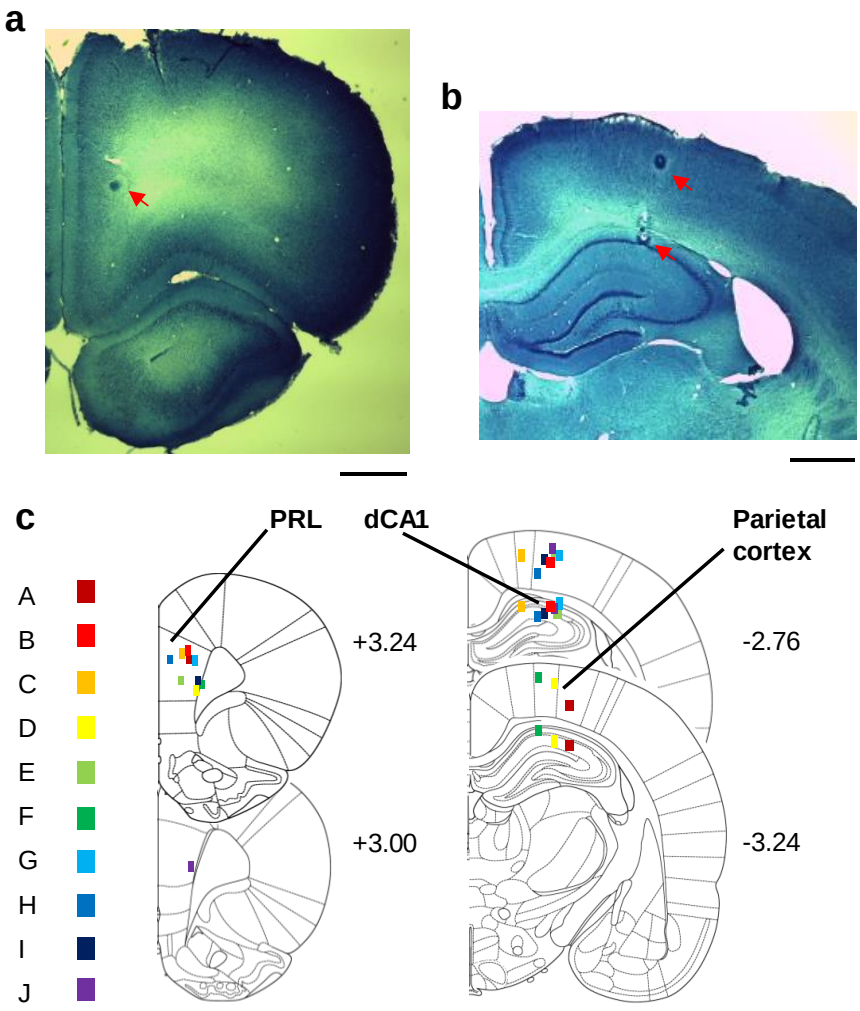

Figure 7.1 | **Histological verification of electrode placement.** Nissl-stained coronal sections with red arrows indicating lesions in **a**, PRL, **b**, dCA1 of hippocampus (lower) and parietal cortex (upper). Black scale bar = 1mm. **c,** Serial section diagrams of structures with the position of electrodes from each rat indicated with coloured squares. Distances from bregma in mm shown on right. Figures taken from the Rat Brain Atlas (Paxinos & Watson 2007).

7.2.4 LFP Data Analysis

Sleep/wake state detection was manually scored and slow waves, spindles and ripples were detected and their parameters calculated (see Chapter 2). Delta power and coherence in a 60 second NREM epoch, ripple time-locked power and the coupling of NREM oscillation events were calculated as described in Chapter 6 Methods. A 10 minute segment of data from the beginning of the recordings prior to sleep onset was extracted to analyse homecage waking data as described in Chapter 4 Methods.

7.3 Results

7.3.1 Actigraphy

To establish any differences in gross sleep architecture between *Fmr1* KO and WT rats, animals were monitored with PIR sensors in their home cages for 31 days. Actigraphy was monitored in 12 cages but three PIRs were faulty, therefore data is available from 9 rats, 5 KOs and 4 WTs. The recording began on the first day of the rats being transferred from a normal light room to a reverse light room (see Methods). This allowed me to observe how the activity of the animals adjusted to the 12-hour-shifted light conditions over ~12 days (referred to as 'jet lag period'), followed by normal, adjusted circadian patterns over the remaining days ('adjusted period').

7.3.1.1 Non-parametric measures comparing jet lag and adjusted period

To assess how animals adjusted to shifted light conditions, interdaily stability, relative amplitude and intradaily variability values (see Chapter 6 for details of these measures) were compared between genotypes across the jet lag period and the adjusted period (Figure 7.2).

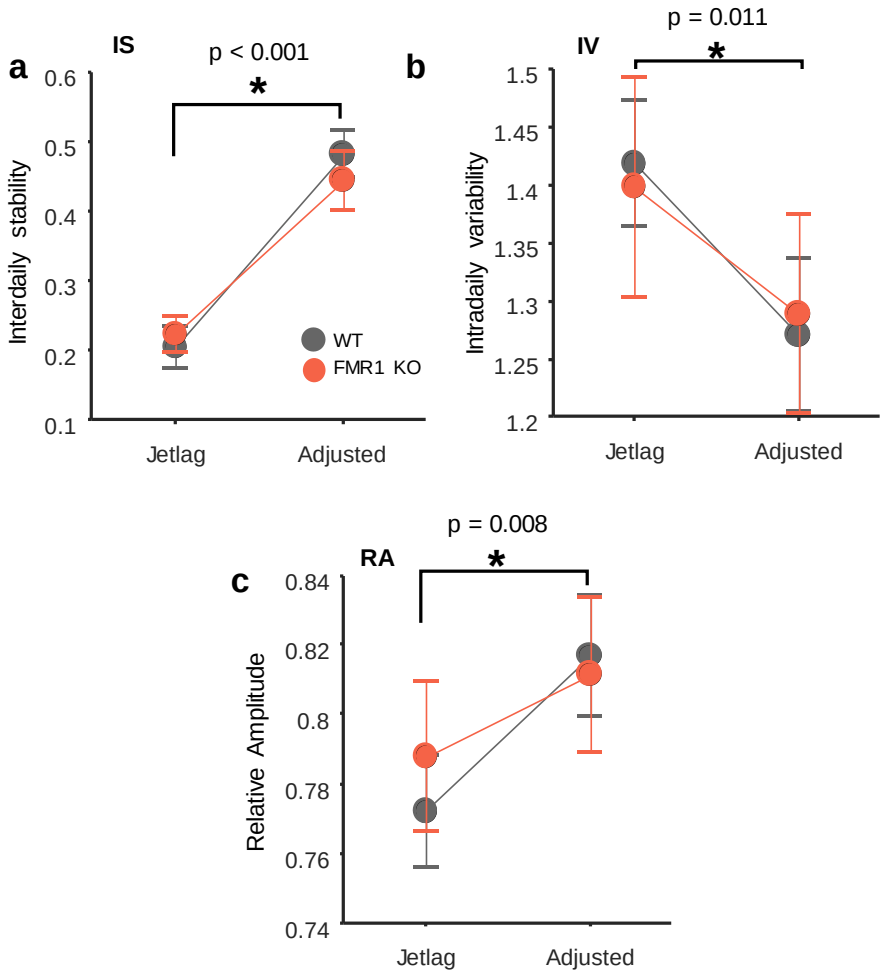

Figure 7.2 **| *Fmr1* KO and WT rats in jet lag and adjusted conditions.** Changes in nonparametric actigraphy measures between first 12 days of recording (jetlag period) and next 19 days of recording (adjusted period). Interdaily stability (**a**) and relative amplitude (**c**) were significantly lower in jetlag period. Intradaily variability was significantly higher in jetlag period (**b**). * denotes main effect of recording period. WT: n = 4, *Fmr1* KO: n = 5.

As expected, interdaily stability was significantly lower in the jet lag period than in the adjusted period ($F_{1,7}$ = 72.96, p<0.001) but there was no main effect of genotype ($F_{1,7}$ = 0.07, p>0.05) and no time x genotype interaction ($F_{1,7}$ = 0.97, p>0.05). Relative amplitude was significantly lower during the jet lag period ($F_{1,7}$ = 11.69, p = 0.008), but there was no main effect of genotype ($F_{1,7}$ = 0.035, p > 0.05) and no time x genotype interaction ($F_{1,7}$ = 1.24, p > 0.05). Intradaily variability was increased in the jet lag period compared to adjusted ($F_{1,7}$ = 11.69, p = 0.011), with no main effect of genotype ($F_{1,7}$ = 0.001, p > 0.05) and no time x genotype interaction ($F_{1,7}$ = 0.26, p > 0.05). Together, these measures indicate a less stable

and more fragmented rest-activity pattern in the jet lag period that is similar across genotypes.

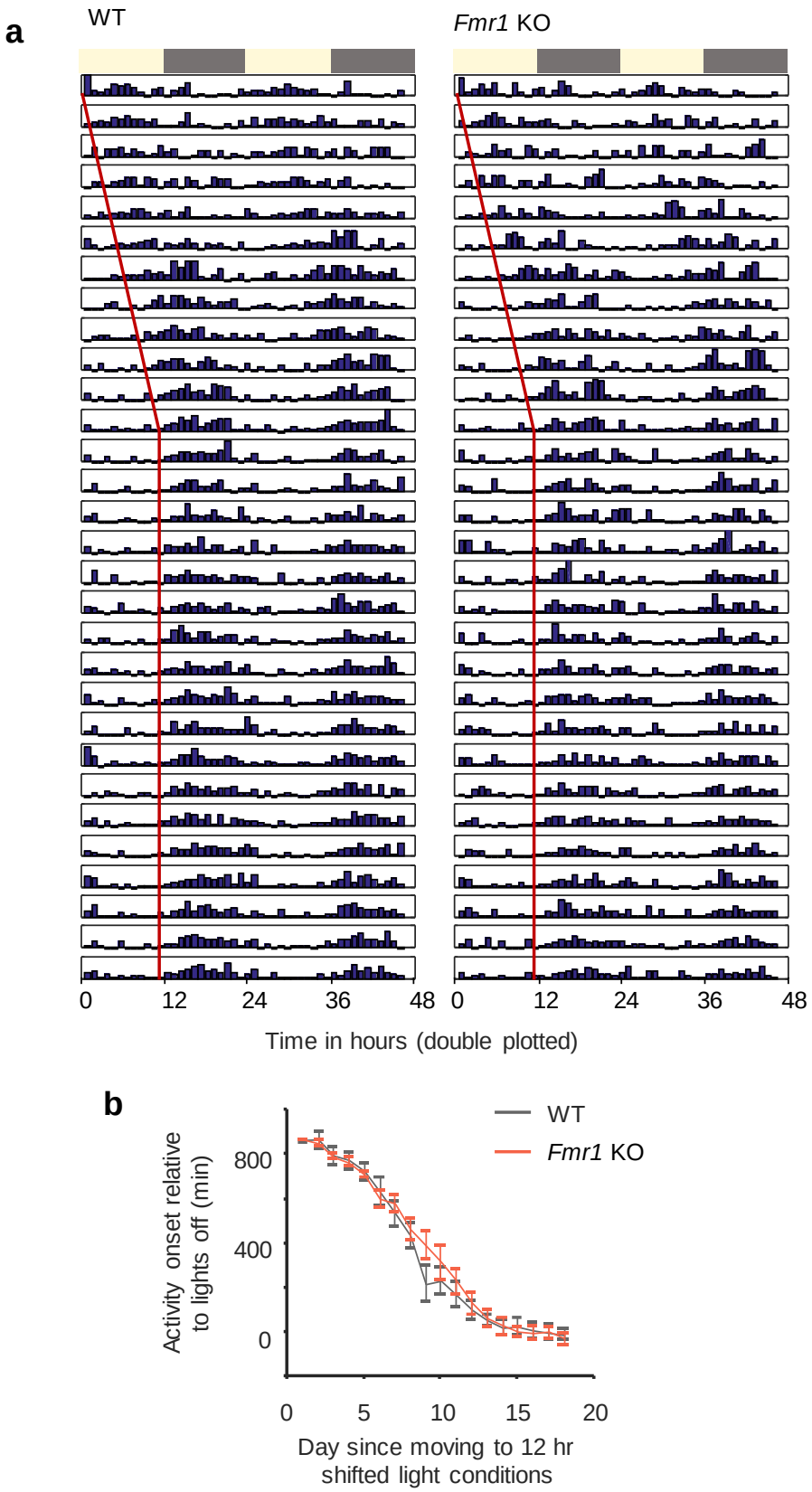
a
WT
Fmr1 KO
0
12
24
36
48
Time in hours (double plotted)
b
WT
Fmr1 KO
Activity onset relative to lights off (min)
800
400
0
0
5
10
15
20
Day since moving to 12 hr shifted light conditions

Figure 7.3 | **Re-entrainment to 12 hr shifted light cycle**. **a,** Actograms of a WT (left) and *Fmr1* KO (right) rat, plotted in 1 hr bins. Actograms are double plotted, such that 48 hr is shown on each horizontal trace, with a 24 hr day shown both beneath and to the right of the preceding day. Bars indicate mean hourly activity counts. Yellow and grey bars at top indicate light and dark periods respectively. Red line is aligned with points of onset of activity and indicates the adjustment of circadian activity patterns to the new light conditions. **b,** Activity onset times relative to the lights off time following transfer to the reverse light room. Note how as rats re-entrain, their activity onset aligns with lights off time. WT: n = 4, *Fmr1* KO: n = 5.

The shift of the onset of activity could also reveal changes in the way groups adapt to the shifted light cycle (Figure 7.3). Activity onset times relative to lights off time (8am) were calculated using the ClockLab actigraphy analysis package (www.actimetrics.com/products/clocklab/) and compared over days and between groups. As expected there was a significant effect of time ($F_{17,119} = 227$, $p < 0.001$), but no effect of genotype ($F_{1,7} = 0.17$, $p = 0.69$) or interaction ($p = 0.24$), suggesting that there are no differences between genotypes in their rate of re-entrainment (Figure 7.3b).

7.3.1.2 Activity

Subsequent analyses are restricted to the adjusted period to assess circadian activity and sleep patterns under normal conditions. Hourly activity counts were averaged over monitoring days to generate a circadian activity profile (Figure 7.4) and the day was separated into four blocks of circadian time (hours 1-6, 7-12, 13-18, 19-24). As expected, there was a significant main effect of time ($F_{3, 93} = 105.3$, $p < 0.001$), but no effect of genotype ($F_{1, 31} = 0.58$, $p = 0.45$) and no interaction ($F_{3, 93} = 0.26$, $p = 0.86$).

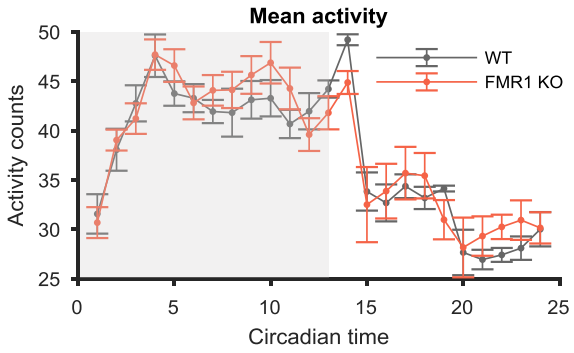

Figure 7.4 | **Hourly mean activity.** Hourly activity counts averaged over monitoring days and over animals. Shaded region indicates light off period. WT: n = 4, *Fmr1* KO: n = 5.

A Lombe-Scargle periodogram did not show a difference between genotypes in the strength of the 24 hour rhythm (24 hr amplitude: WT = 1232 ± 184, Cyfip1 = 1153 ± 232, p = 0.80, t-test, data not shown). *Fmr1* KO rats had normal activity onset and offset times (mean onset times: WT = 07:27 ± 8.6 min, *Fmr1* KO= 07:33 ± 12 min, p = 0.67, t-test; mean offset times: WT = 20:12 ± 13 min, *Fmr1* KO = 21:33 ± 31 min, p = 0.59, t-test, data not shown). The duration of the active phase (alpha) was normal in *Fmr1* KO rats (WT: 12.73 ± 0.13 hrs, *Fmr1* KO: 12.98 ± 0.65 hrs p = 0.74, data not shown).

7.3.1.3 Immobility-defined sleep

Fragile X Syndrome children commonly report frequent nocturnal awakenings, a marker of fragmented sleep (Kronk et al., 2010). To investigate whether the actigraphy data indicated any fragmentation or disruption of sleep in *Fmr1* KO rats, I analysed inferred sleep from epochs of immobility (see Chapter 6 for details) (Figure 7.5). The proportion of time spent asleep per hour in the four time blocks, averaged across days, showed a significant main effect of time ($F_{3, 21} = 54.2$, $p < 0.001$), but no effect of genotype ($F_{1, 7} = 0.15$, $p = 0.706$) and no interaction ($F_{3, 21} = 0.43$, $p = 0.73$). Similarly, measures that could indicate sleep fragmentation did not reveal a genotype effect: mean sleep bout number had a significant main effect of time ($F_{3, 21} = 21.9$, $p < 0.001$), no effect of genotype ($F_{1, 7} = 0.01$, $p = 0.92$) or interaction ($p > 0.05$); median sleep bout length showed a main effect of time ($F_{3,}$

$_{21}$ = 156, p < 0.001), no effect of genotype ($F_{1, 7}$ = 0.01, p = 0.55) or interaction (p > 0.05).

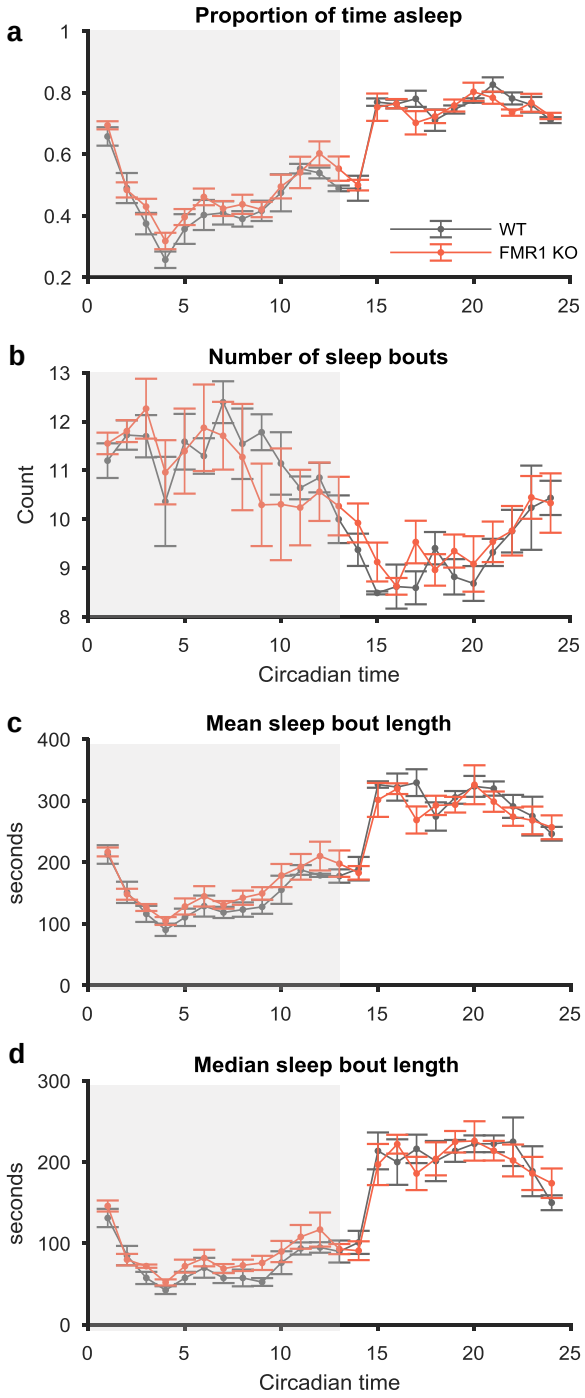

Figure 7.5 | **Immobility-defined sleep from actigraphy monitoring. a,** Proportion of each hour spent asleep. **b,** Hourly sleep bout number. **c** Hourly mean sleep bout length. **d,** Hourly

median sleep bout length. **a-d,** Data are averaged over monitoring days and over animals, shaded region represents lights off. WT: n = 4, *Fmr1* KO: n = 5.

7.3.2 Local field potential recording

The PIR sensor data described above afford a high-throughput, non-invasive measure of gross behaviour in relation to circadian time, but may not be sensitive to specific circuit abnormalities. To assess *Fmr1* KO rats at the neurophysiological level, I next recorded LFP in the homecage during wake and sleep from five *Fmr1* KO and five WT rats.

7.3.2.1 Wake

Cortical gamma and theta/delta power have been shown to be increased in *Fmr1* KO rats and mice (Berzhanskaya et al., 2017; Lovelace et al., 2018; Sinclair et al., 2017b), while hippocampal theta and gamma power appear normal in one study (Talbot et al., 2018), but increased theta power was seen by others (Arbab et al., 2018). Therefore, I compared WT and *Fmr1* KO power spectra from a 10 minute home cage wake segment from PRL and parietal cortical regions and dCA1 of hippocampus (Figure 7.6). Consistent with Talbot et al. (2018), theta (6-10 Hz) and gamma (30-90 Hz) power were normal in dCA1 (theta: $p = 0.67$, gamma: $p = 0.35$). However, inconsistent with published data, cortical regions also did not show any genotype-dependent differences in theta or gamma power ($p>0.05$, t-tests).

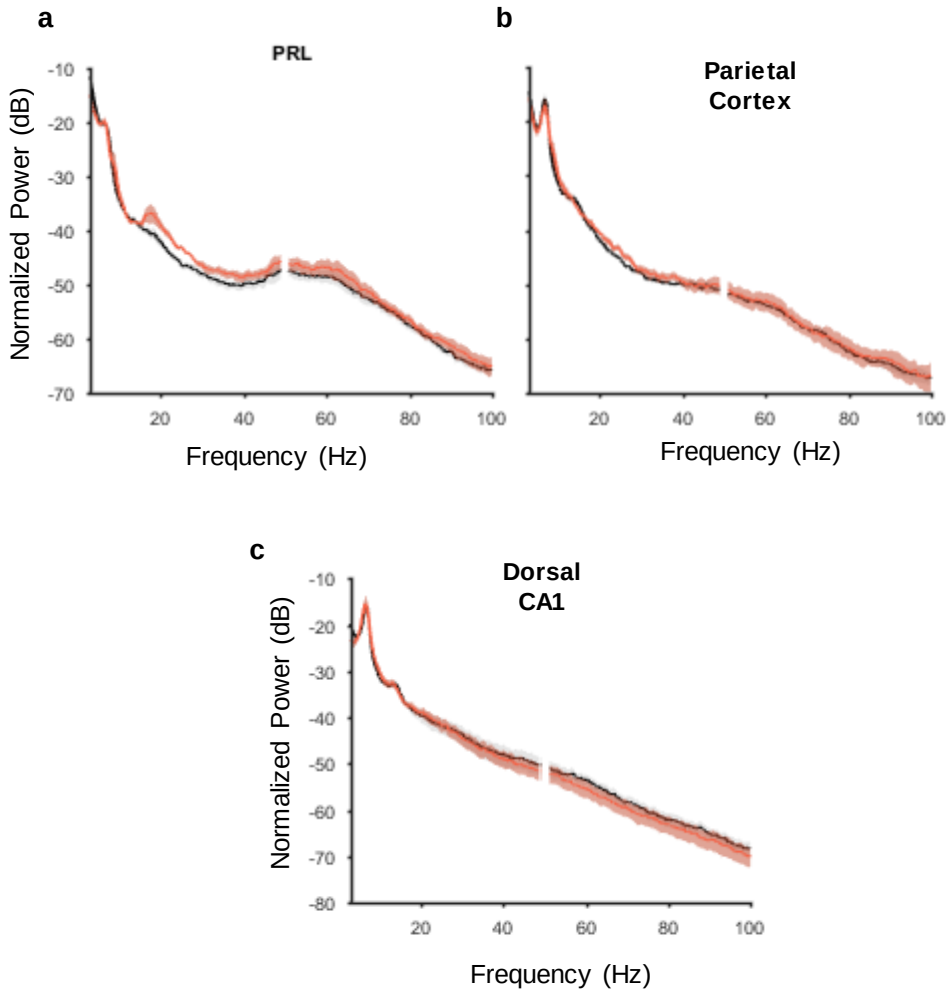

Figure 7.6 **| Waking power spectra.** Power spectra from a 10 minute waking epoch from the beginning of the recording, in PRL cortex (**a**), parietal cortex (**b**) and dCA1 of the hippocampus (**c**). WT: n = 5, *Fmr1* KO: n = 5.

7.3.2.2 Sleep

7.3.2.2.1 Sleep fragmentation

Using a direct measure of sleep from LFP recording, I investigated whether sleep was fragmented by analysing sleep bouts (Figure 7.7). Sleep fragmentation was assessed by four measures as in Chapter 6. Sleep bout rate was on average greater in *Fmr1* KO rats but this was not significant (p = 0.29) (Figure 7.7c). However, mean sleep bout duration was significantly reduced in *Fmr1* KO rats (p = 0.027) (Figure 7.7d and e). Cumulative sleep curves diverged (Figure 7.7g), and the number of sleep bouts required to achieve 50 minutes of sleep (all rats had at least 50 minutes of sleep) was significantly greater in *Fmr1* KO rats than in WTs (p =

0.021) Figure 7.7f). This would suggest sleep bouts are shorter in *Fmr1* KO rats, which can be seen in a histogram of sleep bout durations (Figure 7.7d). Indeed, comparing the average number of short sleep bouts (thresholded as <400 seconds long) showed that *Fmr1* KO rats had more short sleep bouts than WT rats (p=0.032) (Figure 7.7h).

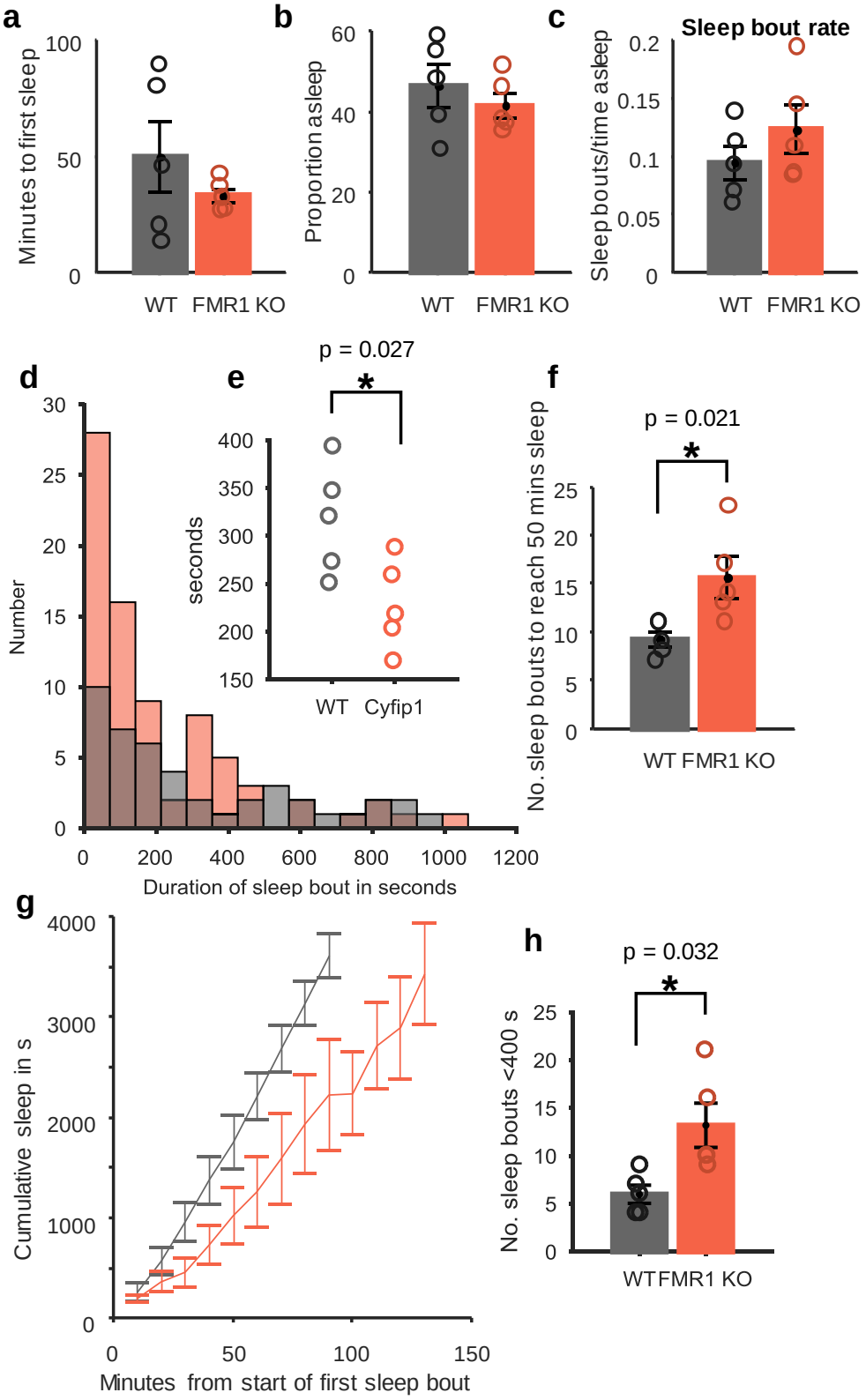

Figure 7.7 **| Sleep architecture from electrophysiology recording. a,** Sleep latency, measured as minutes from start of recording to first sleep bout. **b,** Proportion of recording

spent asleep. **c,** Sleep bout rate, measured as the number of sleep bouts divided by the total amount of sleep. **d,** Distribution of sleep bout lengths for all WT and all *Fmr1* KO animals together. **e,** Mean sleep bout lengths. **f,** Number of sleep bouts up to 50 minutes of sleep, the minimum sleep duration achieved by all rats. **g,** Cumulative sleep in 10 minute blocks from start of first sleep bout, averaged over animals. **h,** Number of short sleep bouts (<400s) up to 50 minutes of sleep. WT: n = 5, *Fmr1* KO: n = 5.

I next assessed whether this fragmented sleep phenotype affected other commonly measured aspects of the sleep architecture, such as sleep latency (time from start of recording to first sleep bout) and NREM vs REM distribution. Sleep latency was normal in *Fmr1* KO rats (Figure 7.7a), with both genotypes taking 30-50 minutes to sleep (33 ± 6.8 min for *Fmr1* KO, 50 ± 34 min for WT, independent samples t-test, $p>0.05$). Sleep efficiency (proportion of time spent asleep from the first sleep bout until the end of the recording) was also similar across groups ($p > 0.05$) (Figure 7.7b). The relative durations of NREM and REM sleep of the total sleep time was the same for both genotypes ($p > 0.05$) (Figure 7.8).

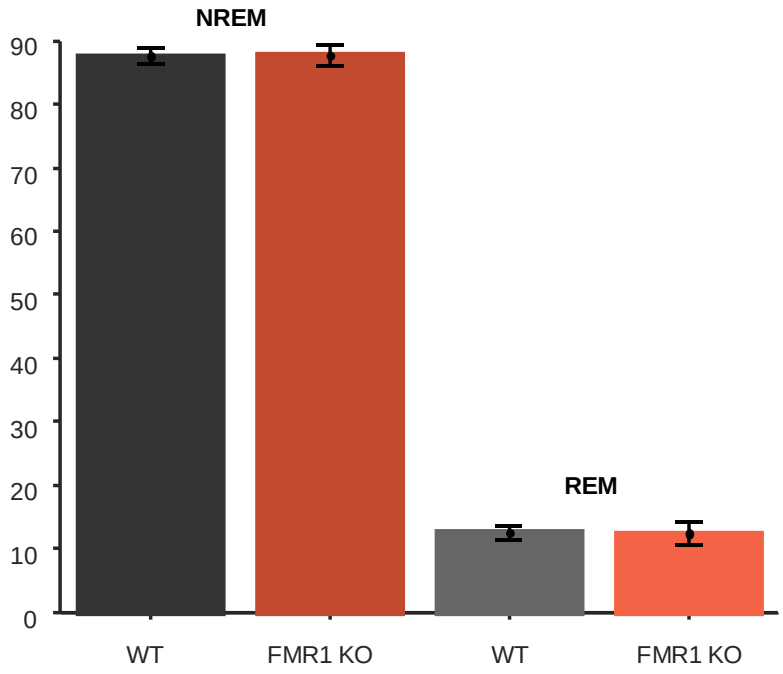

Figure 7.8 | **Proportion of sleep spent in NREM and REM sleep**. WT: n = 5, *Fmr1* KO: n = 5.

7.3.2.3 NREM sleep event parameters

I analysed characteristic NREM sleep oscillation events in *Fmr1* KO and WT rats, which may be affected by fragmentation of sleep. Any differences in slow wave properties would be particularly interesting, as previous findings from *Fmr1* KO mice suggest abnormalities in cortical UP states (Gibson et al., 2008; Gonçalves et al., 2013; Hays et al., 2011), which underlie slow wave generation. As in Chapter 6, both positive and negative half-waves could be detected (Figure 7.9 and Figure 7.10). Similarly to rat B.1 in Chapter 6, of the 10 animals in this chapter, one animal's data indicated a polarity switch: rat D showed 1) low amplitude slow waves, 2) low negative:positive half-wave density ratio as seen in the slow wave density figures (Figure 7.9 and Figure 7.10), 3) no negative-half wave spindle coupling (see below). This combination of features aligns with excluded rat B.1 in Chapter 6, and thus led to the exclusion of rat D from analyses relying on slow wave detection.

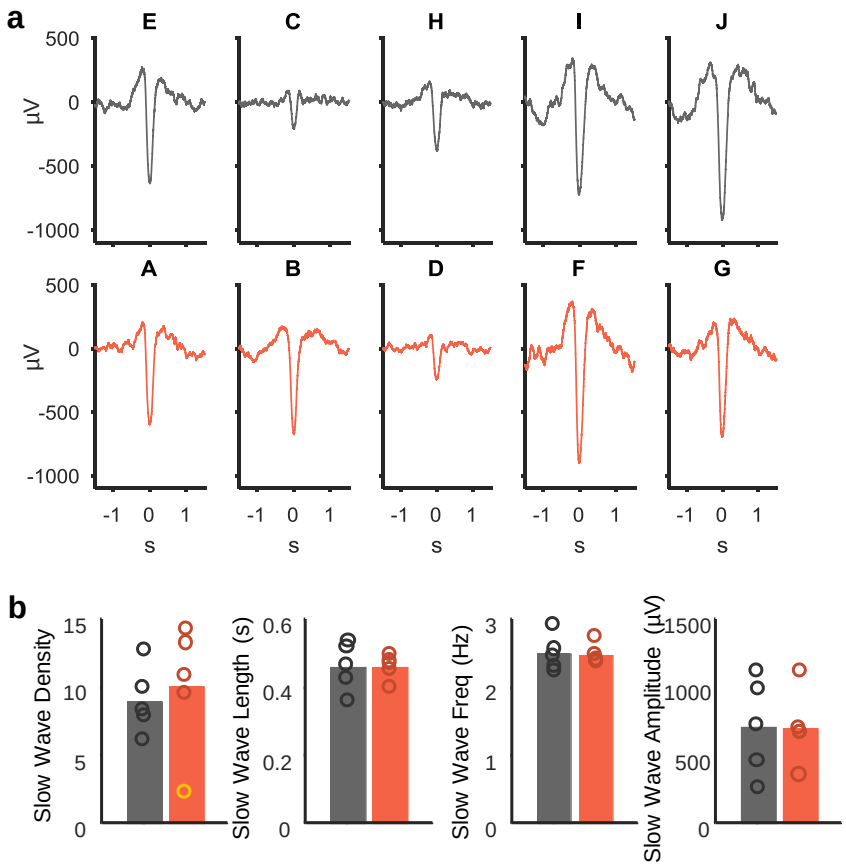

Figure 7.9 **| Slow waves: negative half waves. a,** Average waveforms of detected negative half-waves. Letters above figure denotes animal ID. **b,** Density, length, frequency and amplitude of negative half-waves, WT in grey, *Fmr1* KO in orange. Note Rat D has an abnormally low negative half-wave density (marked in yellow). WT: n = 5, *Fmr1* KO: n = 5

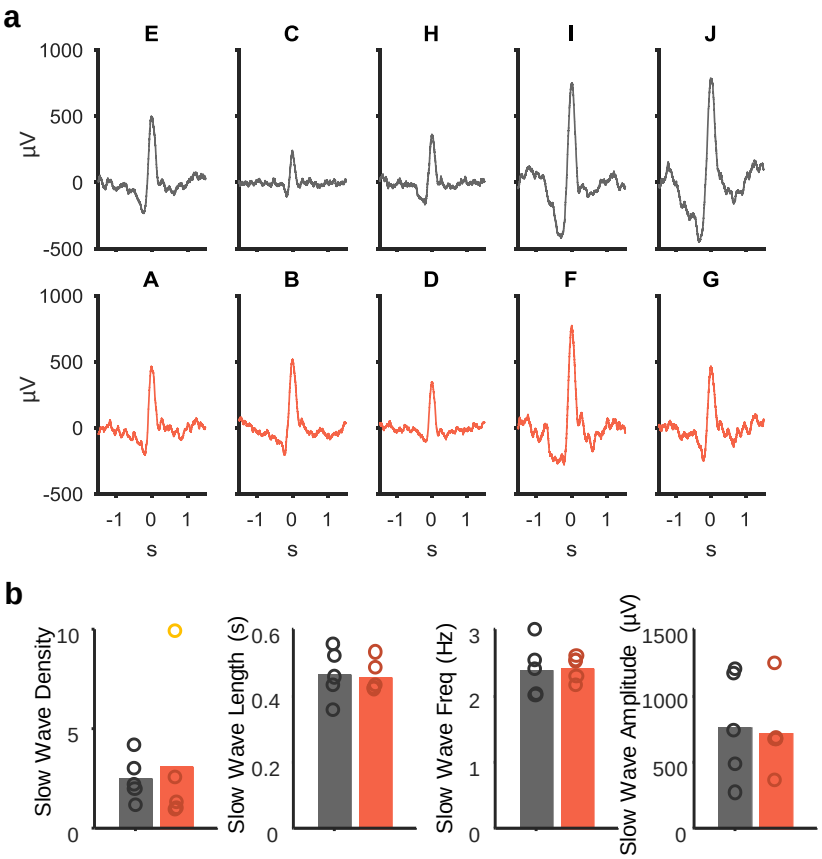

Figure 7.10 **| Slow waves: positive half waves. a,** Average waveforms of detected positive half-waves. Letters above figure denotes animal ID. **b,** Density, length, frequency and amplitude of positive half-waves, WT in grey, *Fmr1* KO in orange. Note Rat D has an abnormally high positive half-wave density (marked in yellow). WT: n = 5, *Fmr1* KO: n = 5

No significant differences were found in either type of slow wave amplitude, frequency or length (Table 2). Thalamocortical spindles, detected on the PRL channel, showed no significant differences in event density, amplitude, frequency or length (Table 2) (Figure 7.11).

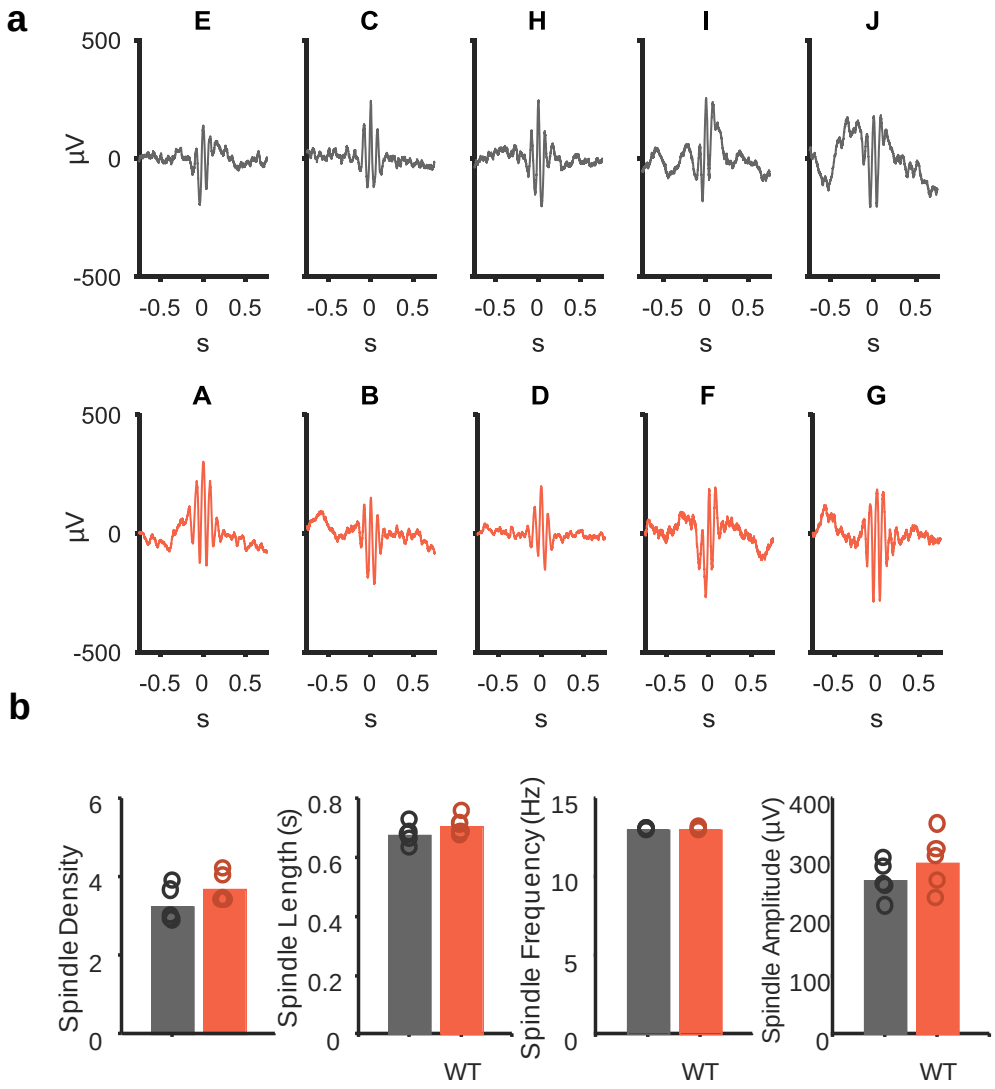

Figure 7.11 **| Spindles. a,** Average waveforms of detected spindles for WT (grey) and *Fmr1* KO rats (orange). **b,** Density, length, amplitude, frequency and length of spindles, WT in grey, *Fmr1* KO in orange. WT: n = 5, *Fmr1* KO: n = 5

Table 2

Cortical Slow Waves (positive half wave)				
	Density (events/min) ± SEM	Amplitude (µV) ± SEM	Frequency (Hz) ± SEM	Length (s) ± SEM

WT	2.48±0.51	766±183	2.43±0.12	0.50±0.01
***Fmr1* KO**	1.43±0.37	814±142	2.40±0.04	0.50±0.02
Independent samples t-test, p value	0.156	0.85	0.80	0.98
Cortical Slow Waves (negative half wave)				
WT	9.00±1.13	709±160	2.43±0.12	0.50±0.01
***Fmr1* KO**	11.97±1.08	787±112	2.40±0.04	0.50±0.02
Independent samples t-test, p value	0.105	0.71	0.80	0.98
Thalamocortical Spindles				
	Density (events/min) ± SEM	**Amplitude (µV) ± SEM**	**Frequency (Hz) ± SEM**	**Length (s) ± SEM**
WT	3.26±0.20	259±14	13.0±0.03	0.67±0.02
***Fmr1* KO**	3.69±0.17	290±21	13.0±0.04	0.70±0.02
Independent samples t-test, p value	0.15	0.26	0.58	0.16

Hippocampal Ripples				
	Density (events/min) ± SEM	**Amplitude (µV) ± SEM**	**Frequency (Hz) ± SEM**	**Length (s) ± SEM**
WT	17.6±0.98	170±50	155±0.59	0.079±0.002
***Fmr1* KO**	17.1±0.93	221±41	154±0.91	0.079±0.001
Independent samples t-test, p value	0.74	0.46	0.13	0.89

Consistent with no effect on detected slow waves and spindles, a 60 second NREM epoch showed no genotype-related differences in PRL slow wave power ($p = 0.98$), or spindle power ($p = 0.45$) (Figure 7.12a and Figure 7.12b).

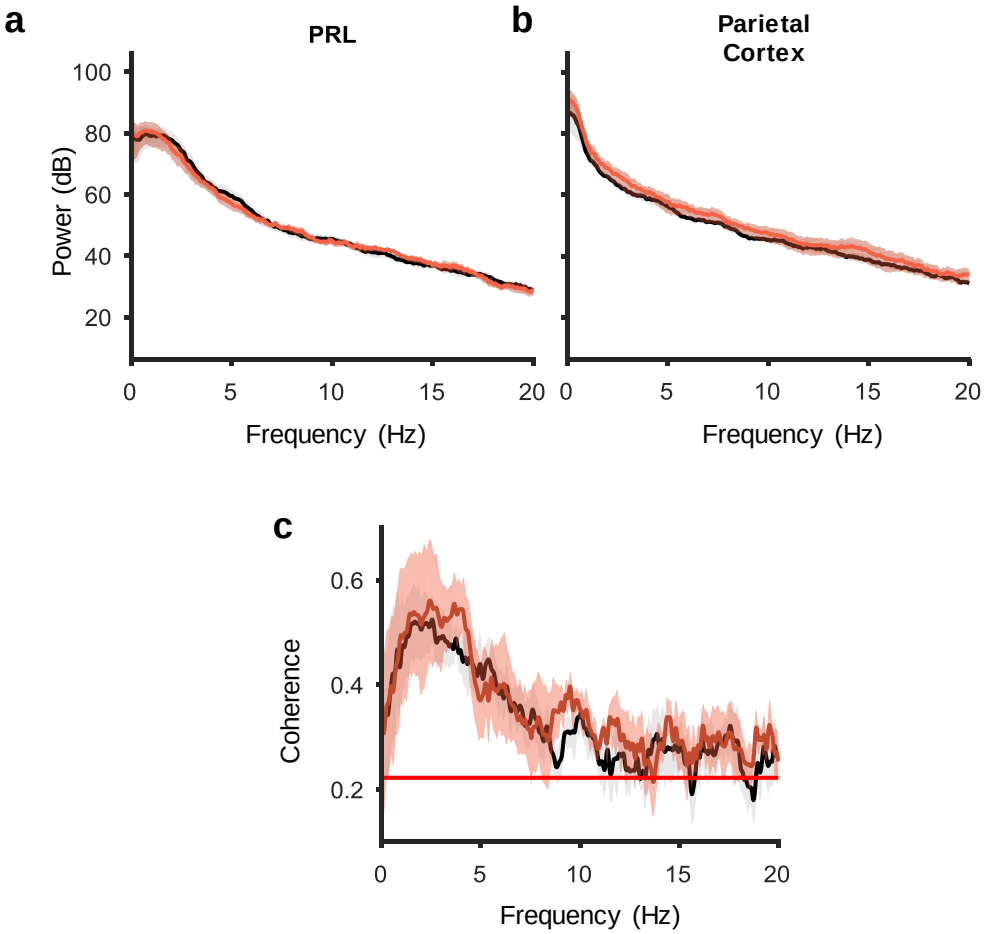

Figure 7.12 | **NREM sleep cortical power spectra.** Power spectra from prelimic (PRL, **a**) and parietal cortex **(b)** from a 60 s epoch of NREM sleep. **c**, Coherence spectrum between PRL and parietal cortex. Red line represents confidence level at p = 0.05. WT in grey, *Fmr1* KO in orange. WT: n = 5, *Fmr1* KO: n = 5

7.3.2.4 Normal slow wave propagation in Fmr1 KO rats

The coherence of slow waves at different cortical sites can indicate whether anterior to posterior cortical slow wave propagation is intact (Massimini, 2004). Slow wave coherence between PRL and parietal cortex was assessed as a measure of slow wave propagation in a 60 s NREM epoch. Coherence in the slow wave frequency band was not significantly different between genotypes (p=0.74) (Figure 7.12c).

7.3.2.5 Slow wave-spindle coupling

I next investigated the temporal coordination between corticothalamic and hippocampal-cortical NREM oscillations in *Fmr1* KO rats.

The pattern of spindle power surrounding slow waves was consistent with findings seen in Chapter 6 and published data (Mölle et al., 2006; Phillips et al., 2012a) (Figure 7.13). Notably, all rats except rat D showed significant slow wave-spindle coupling, with a bootstrap-determined significant difference between the negative peak and the positive peak in spindle power within a 500 ms window centred on 0, supporting his exclusion from the data.

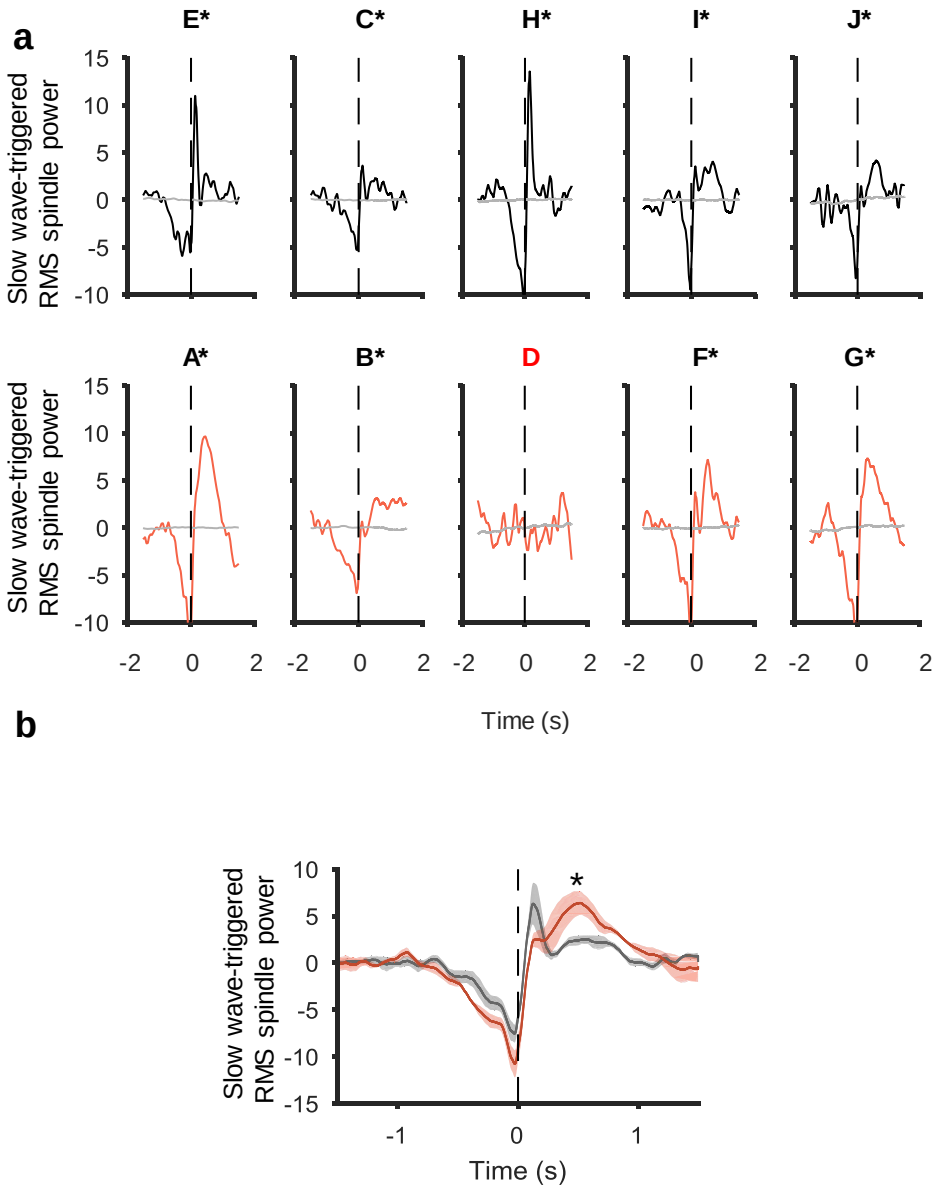

Figure 7.13 **| Slow wave-spindle coupling. a,** Slow wave-triggered root mean squared (RMS) spindle power, centred on the peak of the negative half-wave slow waves. All rats with an asterisk (*) showed a significant rebound in spindle power following the minimum at the slow wave peak, as determined by a bootstrapping method using shuffled data. WT in grey, *Fmr1* KO in orange Average shuffled data is shown in grey. Dotted line at 0 signifies the time of the negative half wave peak. **b,** Group averaged trace, shaded region represents ± SEM. Dotted line at 0 signifies the time of the negative half wave peak. * denotes significant difference in 'delayed peak' >300ms from 0. WT: n = 5, *Fmr1* KO: n = 4.

Comparing the negative-to-positive peak amplitude of spindle power found no difference between groups ($p = 0.88$). While neither the absolute minimum value nor the maximum values within the 500 ms window were different ($p > 0.05$), the

profile of spindle power following a slow wave looked different in *Fmr1* KO rats, with a 'delayed peak'. Therefore, I compared the maximum spindle power in a later window, beyond 300 ms from the slow wave within which the 'early peak' occurred and found *Fmr1* KO rats had a significantly larger 'delayed peak' ($p = 0.023$). However, comparing this figure to the equivalent in the Cyfip1 study (Figure 6.11), both groups show a dominant 'delayed peak' that is similar in amplitude as the 'early peak'. Hence, the discrepancy seen here may be a consequence of the low n in this pilot study and precludes any definitive conclusion that slow wave-spindle coupling is abnormal in *Fmr1* KO rats.

7.3.2.6 Hippocampal ripples

Ripples were detected on the dCA1 channel and their presence was confirmed in each animal by inspection of the average waveforms (Figure 7.14a). There were no genotype-dependent differences in ripple density, frequency or length (Figure 7.14b). An 80 - 400 Hz bandpass filtered power spectrogram time-locked to ripple peak (see Chapter 6 Methods) (Figure 7.15a and Figure 7.15c) revealed a trend for increased ripple frequency power in *Fmr1* KO rats ($p = 0.095$, Mann-Whitney U test); however, following the removal of 2 outliers (one in each group), the difference reached significance ($p = 0.013$, t-test) (Figure 7.15b). Ripple-associated gamma power was normal ($p = 0.46$) (Figure 7.15e).

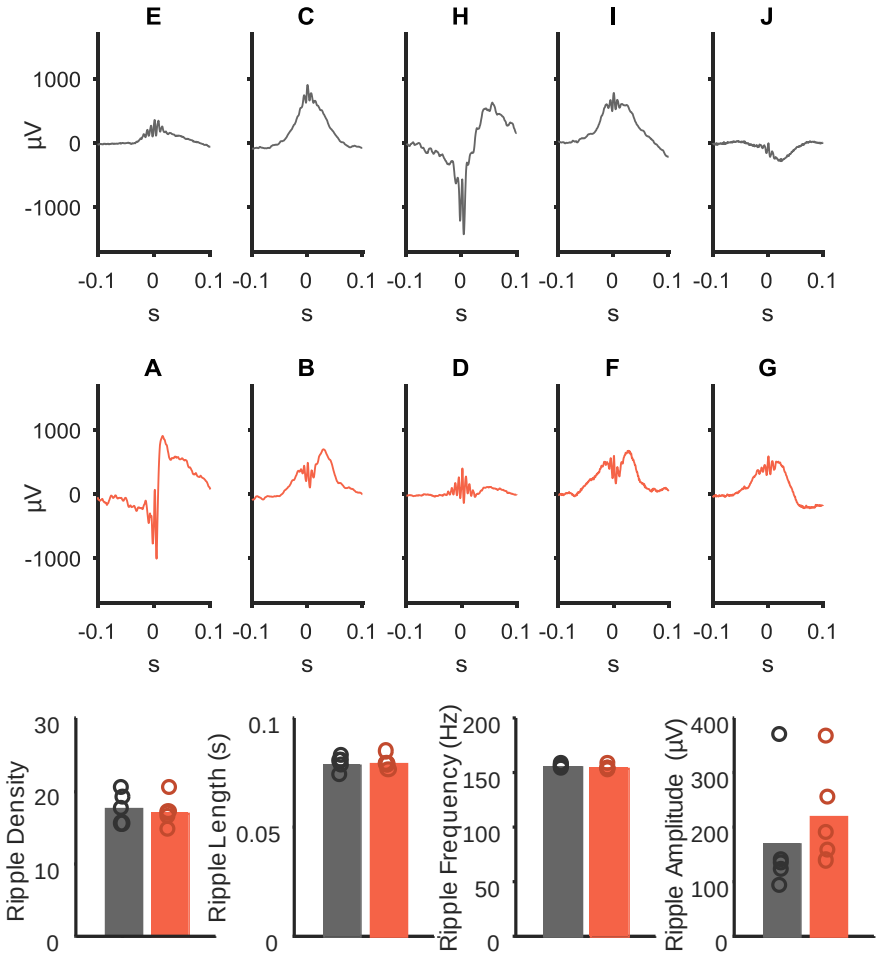

Figure 7.14 **| Ripples. a,** Average waveforms of detected ripples. **b,** Density, length, amplitude, frequency and length of ripples, WT in grey, *Fmr1* KO in orange. WT: n = 5, *Fmr1* KO: n = 5

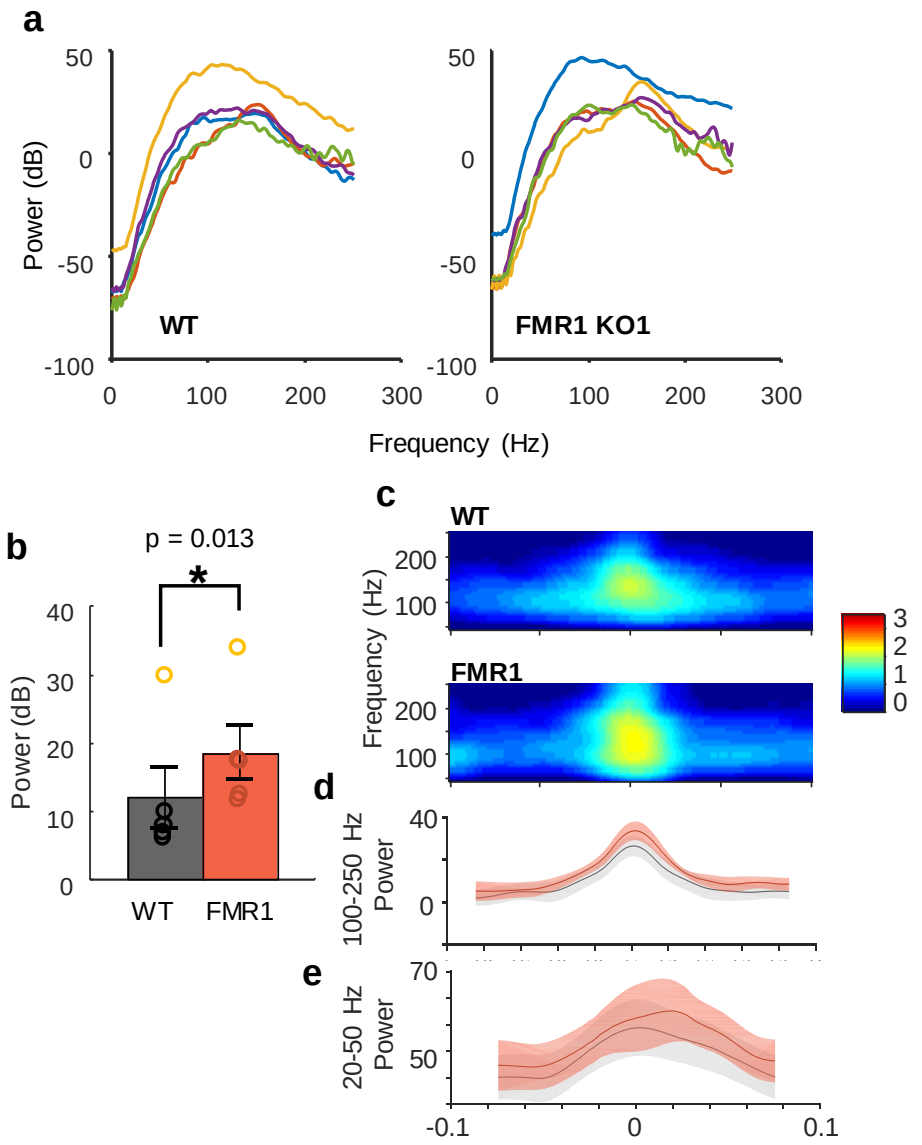

Figure 7.15 **| Ripple power. a,** Ripple time-locked power spectrum of bandpass filtered signal (80-400 Hz) from a 200 ms window, averaged over all ripples. Each line represents a different animal. **b,** Average ripple power (100-250 Hz) in the 200ms window time-locked to the peak of detected ripples. Outliers are marked in yellow and were not included in the statistical test shown (p = 0.095 with outliers included). **c,** Ripple time-locked power spectrograms of filtered (80-400 Hz) signal, averaged all ripples and over animals. **d,** Ripple power within the ripple time-locked 200ms window in WT (grey) and *Fmr1* KO (orange) rats. **e,** Slow gamma power (20-50 Hz) within the ripple time-locked 200ms window, colours as above. WT: n = 5, *Fmr1* KO: n = 5.

7.3.2.7 Slow wave-ripple coupling

Cortical-hippocampal coupling during sleep can be assessed by analysing slow wave-ripple coupling. Four out of five WT rats showed significant slow wave-ripple coupling, with a bootstrap-determined significant difference between the

positive peak 500 ms prior to 0 and the negative peak within a 200 ms window centred on 0 (Figure 7.16). In the *Fmr1* KO group, the only rat that did not show coupling was rat D, who had been excluded from group analysis for reasons outlined above. Group analysis showed no difference in the positive-to-negative peak change of ripple power (p = 0.96, t-test, result unaffected by a WT outlier).

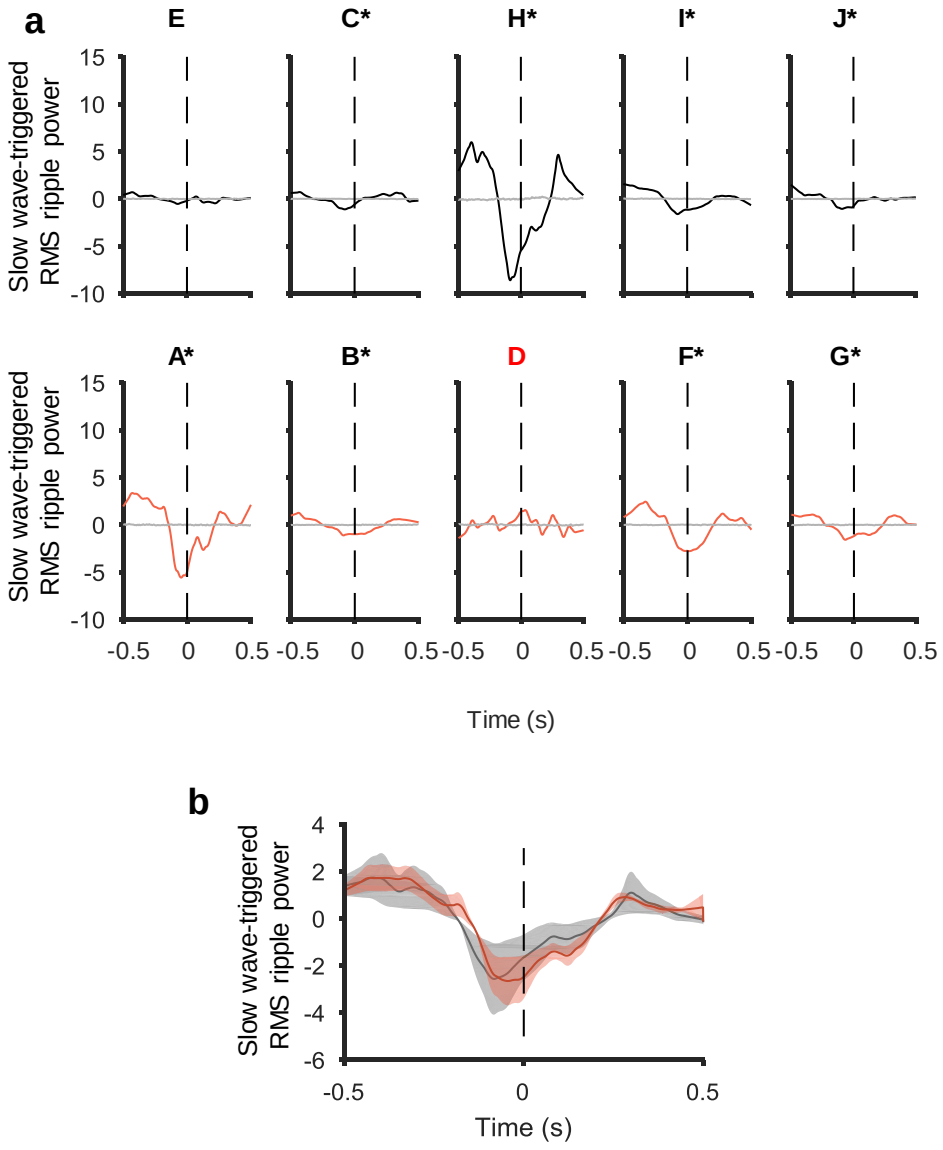

Figure 7.16 **| Slow wave-ripple coupling. a,** Slow wave-triggered ripple power, centred on the peak of the negative half-wave slow waves. All rats with an asterisk (*) showed a significant difference between peak ripple power prior to the slow wave and minimal ripple power around 0, the time of the negative half-wave peak, as determined by a bootstrapping method using shuffled data. Average shuffled data is shown in grey. Dotted line at 0 signifies the time of the negative half wave peak. WT shown in dark grey, *Fmr1* KO in orange. Rat D (red) was excluded, note lack of relationship in slow wave ripple coupling

(see text). **b,** Group averaged data centred on the negative half-wave slow waves. WT: n = 5, *Fmr1* KO: n = 4.

7.3.2.8 Ripple-spindle coupling

Spindle-ripple coupling was present in 4 out of 5 animals in both genotypes. Rat D was included in this analysis as it does not rely on slow wave detection and is unaffected by signal polarity. Group analysis showed no significant difference between the positive peak of spindle power between groups (p = 0.107) (Figure 7.17).

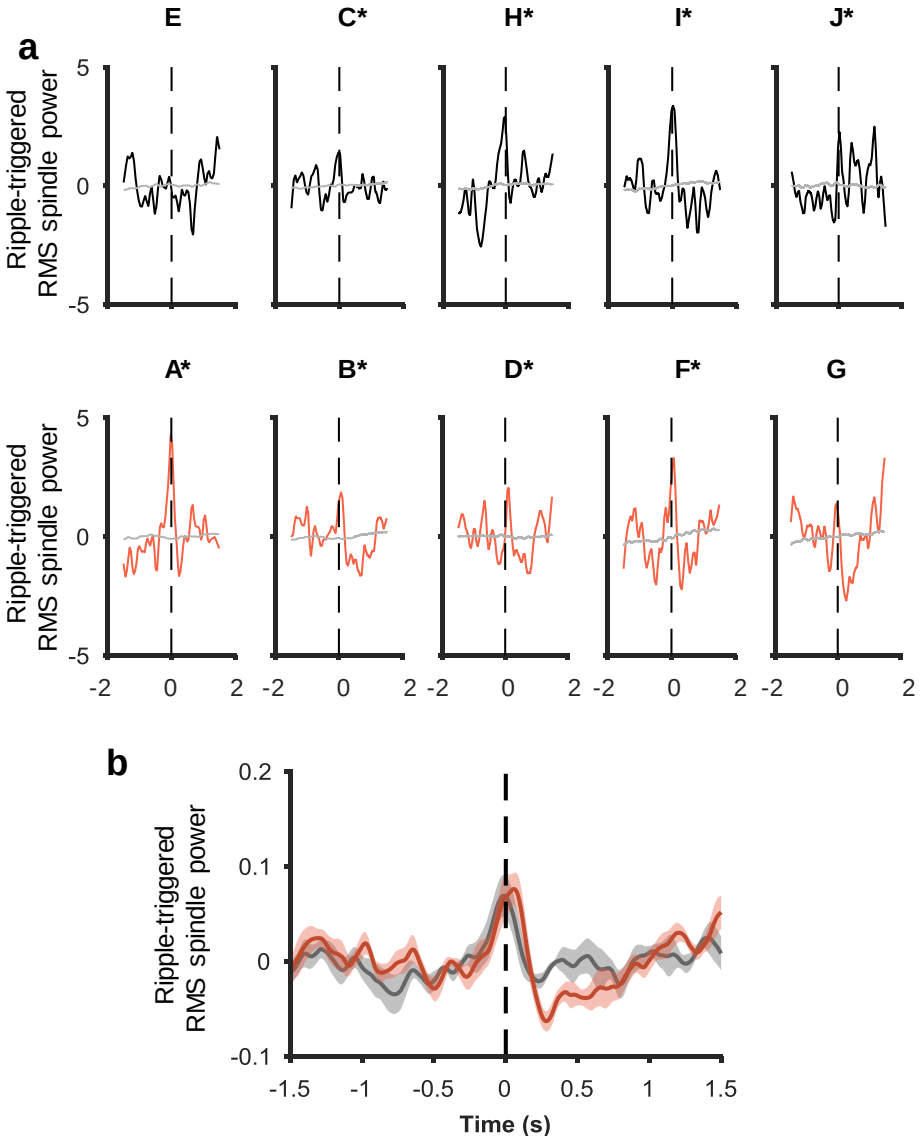

Figure 7.17 **| Ripple-spindle coupling. a,** Ripple-triggered spindle power, centred on the peak amplitude of the ripple. All rats with an asterisk (*) showed a significant maximum

peak within 200 ms of 0, as determined by a bootstrapping method using shuffled data. Average shuffled data is shown in grey. Dotted line at 0 signifies the time of the ripple peak amplitude. **b,** Group averaged data centred on the peak of ripples. WT: n = 5, *Fmr1* KO: n = 5

7.4 Discussion

Pilot results in this chapter show:

- *Fmr1* KO rats show similar nonparametric circadian measures to WTs under 'jet lag' and 'adjusted' conditions, with a similar rate of re-entrainment.
- Circadian activity and immobility-defined sleep patterns appear normal in *Fmr1* KO rats.
- Waking cortical and hippocampal theta and gamma power are normal in *Fmr1* KO rats.
- In the context of a light phase *in vivo* electrophysiology recording, *Fmr1* KO rats show fragmented sleep with more frequent short sleep bouts.
- Slow wave and spindle properties were unchanged in *Fmr1* KO rats.
- Ripple power was increased in *Fmr1* KO rats.
- Slow wave-spindle coupling, slow wave-ripple coupling and spindle-ripple coupling is present in both genotypes.

Circadian rhythm and sleep disturbances are seen in several psychiatric conditions associated with cognitive impairment, including Fragile X Syndrome (Jagannath et al., 2013; Kronk et al., 2010). Indeed, *Fmr1* and its vertebrate paralog *Fxr2* are necessary for normal circadian behaviour in mice (Zhang et al., 2008). Furthermore, *Fmr1* KO mice have been shown to have aberrant UP/DOWN states, which give rise to the slow wave oscillation during NREM sleep (Gibson et al., 2008; Gonçalves et al., 2013; Hays et al., 2011), suggesting that the nature of their already disrupted sleep may also be abnormal.

The finding that circadian rhythms in acclimatized light conditions appeared normal in FMR1 KO rats, with no indication of a fragmented sleep phenotype, is similar to the findings in *Cyfip1*$^{+/-}$ rats, which may be expected due to the close molecular interaction between these proteins. In the mouse study investigating circadian rhythms, mice carrying only the *Fmr1* mutation had normal circadian activity patterns in regular light conditions (Zhang et al., 2008). In this study, animals were then challenged with a change in light conditions, housing them in constant

darkness. Loss of FMRP was found to affect the period of the free-running circadian rhythm, reducing its duration compared to WT. While I was not able to run the constant darkness experiment, I hypothesised that the challenge of shifting the light cycle by 12 hours (jetlag period) may draw out a difference in the way the animals adjust their circadian activity pattern. However, there appeared to be no difference in the re-entrainment to the new light conditions between genotypes. Importantly, this context still had light cues to help entrain circadian rhythms, whereas the constant darkness experiment is able to test the intrinsic circadian rhythm in the absence of light cues.

A recent study using a very similar home cage monitoring set up (using infrared beam breaks to monitor movement rather than passive infrared monitoring) and near-identical immobility-inferred sleep detection to the current study, found decreased sleep during the light phase (Saré et al., 2017), which I did not see in this dataset (no change in proportion of time spent asleep in 2nd two time blocks (Figure 7.5a)). The authors observed this phenotype at several time points (P70, P180), so it is unlikely to be related to age of the animals. The discrepancy could be attributed to species differences, or due to the slight difference in the activity monitoring set up used.

In contrast to the apparently normal sleep phenotype seen in the actigraphy data, sleep bout data from the electrophysiology recordings revealed a fragmentation of sleep phenotype in the *Fmr1* KO rats. The discrepancy between the results obtained from actigraphy and electrophysiological recordings may be attributed to the differences in sensitivity between the two techniques. While the PIR sensors were reasonable at capturing sleep bouts, the simultaneous PIR and electrophysiology recordings shown in Chapter 6 demonstrated that they were less sensitive at picking up small movements that indicate an interruption of a sleep bout, leading to a possible overestimation of sleep bout durations. However, it is also possible that the sleep during the 3 hour electrophysiology recording may not be of the same quality as usual due to moving the animal to a different room. While animals were habituated to the environment, the presence of the tether may lead to a more

disturbed sleep than normal. Wireless recording setups would get around this potential confound, in addition to allowing longer term electrophysiology recordings.

Nevertheless, the results from the sleep recording indicating fragmented sleep are robust (although preliminary), with a number of different measures, such as reduced mean sleep bout length, and greater number of sleep bouts, pointing towards a fragmented phenotype. This finding is consistent with the patient data: the largest Fragile X patient actigraphy study to date cites frequent night-time awakenings as one of the most prominent sleep disturbances (Kronk et al., 2010). In contrast, *Cyfip1*$^{+/-}$ rats did not have fragmented sleep, suggesting these proteins may have diverging roles in the control of sleep fragmentation.

Sleep architecture, in terms of the amount of NREM and REM sleep, was unaltered in *Fmr1* KO rats, which is in contrast to a small study in Fragile X syndrome patients that described a change in sleep architecture, with increased stage 1 NREM and reduced REM, but no fragmentation of sleep (Miano et al., 2008). It is possible that the relatively short duration of the electrophysiology recording compared to a full night of polysomnography was not enough to reveal differences in the rats. Alternatively, it could be attributed to species differences, and it has been shown that chronic sleep fragmentation can occur without alterations in NREM and REM sleep duration and distribution (Ramesh et al., 2012).

Studies in *Fmr1* KO mice describe abnormal UP/DOWN states, showing increased firing rates during UP states *in vivo* (Gonçalves et al., 2013) and prolonged duration of UP states (Gibson et al., 2008; Hays et al., 2011). Given that UP/DOWN state transitions underlie the slow wave oscillation, it was somewhat surprising to find no changes in the slow wave parameters investigated, particularly slow wave amplitude and length. A possible explanation, beyond species differences, could be the difference in age of the rats used in my study. Gonçalves et al. (2013) used mice at postnatal days 14-16 for *in vivo* recordings, while my rats were 4-6 months old. Furthermore, these observations of altered UP states were made in somatosensory

cortex, whereas my analyses focused on the PRL site, although I believe this is unlikely to be the cause of the discrepancy, given the high level of coherence between different cortical areas. The high PRL-parietal slow wave coherence seen in both *Fmr1* KO and WT rats further supports the finding that slow wave oscillations and their propagation remain intact in this model.

Properties of thalamocortical spindle events were also unchanged in *Fmr1* KO rats, as were the coupling relationships between NREM sleep events, consistent with the conserved coordination of these events seen in the *Cyfip1*$^{+/-}$ rats. Hippocampal ripples had greater power in *Fmr1* KO rats, although this followed removal of 2 outliers leaving just n = 4 *Fmr1* KO and n = 4 WT, therefore this is likely underpowered and should be investigated further in a larger cohort. The reported alterations in hippocampal synaptic plasticity and pyramidal cell dendrite morphology in *Fmr1* KO rats (Till et al., 2015), together with evidence for impaired GABAergic inhibition of CA1 (Sabanov et al., 2017), abnormal place cell properties (Arbab et al., 2017) and a weakened relationship between hippocampal pyramidal neuron spike firing and the phase of ongoing theta and gamma oscillations (Talbot et al., 2018), could manifest as abnormal ripple characteristics in this model. While abnormal ripples were also found in the *Cyfip1*$^{+/-}$ rat model, where ripple power and length was reduced, the direction of change is in the opposite direction in this model.

Waking theta and gamma in PRL and parietal cortical regions were normal in *Fmr1* KO rats, which is inconsistent with findings from rodents (Berzhanskaya et al., 2017; Lovelace et al., 2018; Sinclair et al., 2017a) and humans (Ethridge et al., 2017; Wang et al., 2017). While the rodent studies suggest these findings might be independent of movement, both theta and gamma oscillations are influenced by locomotion so it would be important to investigate the effects relative to locomotor activity. In my study, no tracking data was available from the homecage recording precluding this analysis. Waking oscillations in the hippocampus were normal in the current study, which is similar to that seen in mice by one study (Talbot et al., 2018), but is inconsistent with increased theta seen by another group (Arbab et al.,

2018). Further experiments will be required to establish how the species, strain and behavioural contexts can affect hippocampal oscillations.

7.5 Conclusions and future directions

This pilot study is the first, to the best of my knowledge, to investigate actigraphy and sleep neurophysiology in the *Fmr1* KO rat. The findings here demonstrate that *Fmr1* KO rats show a fragmented sleep phenotype in acute sleep recordings, coupled with data pointing toward abnormally high ripple power, while NREM oscillation coupling and circadian activity patterns remain broadly intact. Waking oscillations appear normal in *Fmr1* KO rats in contrast to published data.

The conserved circadian patterns and waking oscillations are consistent with the findings in *Cyfip1*$^{+/-}$ rats seen in Chapter 6. It is interesting to find preliminary evidence for an abnormal ripple phenotype as ripples are also disrupted in *Cyfip1*$^{+/-}$ rats, albeit in the opposite direction. Together with emerging findings suggesting a hippocampal deficit in *Fmr1* KO rats, future studies should explore ripple properties in a larger cohort to confirm this finding and test any relationship between abnormal ripples and impaired memory consolidation.

8

Chapter 8 General Discussion

This chapter draws together the results from Chapters 3-7 to discuss how my findings contribute to the understanding of *Cyfip1*'s role in neuronal networks.

8.1 Summary of principal findings

The aim of this thesis was to explore the impacts of haploinsufficiency in *Cyfip1*, a gene associated with neuropsychiatric illness, on the network activity of hippocampus, prefrontal cortex and nucleus accumbens during behaviours these brain regions mediate. The key findings are:

- Chapter 3 shows that *Cyfip1*$^{+/-}$ rats were able to achieve normal performance accuracy in a discrete-trial alternation T maze task, but ran more slowly than WTs and took longer to reach criterion when tested over several days. Hippocampal-prefrontal interactions on the maze appeared normal, but theta-gamma phase-amplitude coupling within dorsal CA1 was reduced in *Cyfip1*$^{+/-}$ rats.
- Chapter 4 described disrupted interactions between NAc Shell and the vHPC and IL. Gamma coherence between vHPC and NAc Shell was significantly reduced in *Cyfip1*$^{+/-}$ rats, during baseline behaviour but most prominently during approach to reward points. Conversely, infralimbic cortex and nucleus accumbens shell showed increased coherence in the beta

frequency band. Preliminary evidence points towards a disruption to behaviour in the novel object location task, where *Cyfip1*$^{+/-}$ rats did not significantly discriminate the novel location object.

- Chapter 5 shows that *Cyfip1*$^{+/-}$ rats show an exaggerated response to acute ketamine injection in the form of an enhanced surge in high frequency oscillations compared to WT rats in NAc and PRL. In addition, hippocampal dCA1 theta-gamma coupling was augmented to a greater extent in *Cyfip1*$^{+/-}$ rats than WTs.
- Chapter 6 shows that, while circadian patterns and sleep architecture were normal, *Cyfip1*$^{+/-}$ rats had reduced hippocampal ripple power during NREM sleep, which could impact memory consolidation.
- Chapter 7 reports on a pilot study in *Fmr1* KO rats, a model that is highly relevant to *Cyfip1* given the close molecular interactions between these proteins. *Fmr1* KO rats show fragmented sleep, characterised by more numerous and shorter sleep bouts and preliminary evidence suggests an increase in ripple power compared to WTs.

Contrary to my initial hypothesis, hippocampal-prefrontal network appears intact in *Cyfip1*$^{+/-}$ rats, as evidenced by three findings: 1) typical LFP coherence during the T maze; 2) intact hippocampal theta-prefrontal gamma phase-amplitude coupling; 3) normal coordination of NREM sleep oscillations in the form of intact ripple-spindle coupling. It is possible that the no-delay T maze task used in Chapter 3 imposes relatively low cognitive demand, which failed to reveal any deficit in this network during a task where it was minimally engaged. In contrast, Sigurdsson et al. (2010) saw behavioural and network deficits in *Df(16)A*$^{+/-}$ mice in a similar task with a 10 second delay. However, if this network can be shown to function normally even under more challenging circumstances (e.g. with a delay or a more difficult task), it suggests that haploinsufficiency of CYFIP1 does not contribute to potential disruptions in this network in 15q11.2(BP1-BP2) deletion carriers diagnosed with, for example, schizophrenia.

Whilst convergent evidence points to disrupted hippocampal-prefrontal interactions in schizophrenia, there are fewer studies of these networks in autism and intellectual disability, disorders for which the 15q11.2 deletion confers an even greater risk. Behaviourally, it appears that while performance of the T maze was normal, acquisition of the task was slower in *Cyfip1*$^{+/-}$ rats. Some parallels can be drawn with the behavioural findings in undiagnosed 15q11.2(BP1-BP2) deletion carriers, who were able to perform normally in a spatial working memory test, but suffer from learning disabilities (dyslexia, dyscalculia) and lower IQ (Stefansson et al., 2014).

Rather than a hippocampal-prefrontal deficit, the evidence from the experiments in this thesis points towards a hippocampal and hippocampal-accumbal network deficit. Evidence for disrupted hippocampal activity arose in several chapters. Theta-gamma phase amplitude coupling in dCA1 is reduced in *Cyfip1*$^{+/-}$ rats, both during the T maze task in Chapter 3 and in the homecage prior to ketamine injection in Chapter 5. Hippocampal theta-gamma coupling is thought to facilitate memory processing (Colgin, 2015) and its disruption has been reported in various models of cognitive disfunction (Booth et al., 2016; Zhang et al., 2016).

In Chapter 6, reduced hippocampal ripples point towards a deficit in the ripple generating CA3-CA1 network, which is the same synapse at which Bozdagi et al. (2012) observe abnormal synaptic plasticity in *Cyfip1*$^{+/-}$ mice. The preliminary evidence from Chapter 7 showing abnormal ripples in the *Fmr1* KO rat, together with published findings suggesting a hippocampal deficit in the *Fmr1* KO rodent model (Radwan et al., 2016; Sabanov et al., 2017; Talbot et al., 2018; Till et al., 2015), suggest that hippocampal abnormalities are common to both models, and thus might arise via the interaction of CYFIP1 and FMRP. Indeed, ripples are also abnormal in an *Arc* KO mouse model (Malkki et al., 2016), an important mRNA target of the FMRP/CYFIP1 translation regulator complex.

Further to a disrupted hippocampus, robust evidence from Chapter 4 suggests the vHPC-NAc Shell network is impaired by *Cyfip1* haploinsufficiency . The response

of this network to arrival at the reward point is diminished (as seen in the diminished coherence peak), and coherence is more generally reduced in multiple further behavioural contexts. Further evidence for abnormalities in the NAc Shell come from Chapter 5, where acute ketamine elicited an exaggerated surge of high frequency oscillations, and the most substantial effect was seen in NAc Shell. While the exact mechanism of generation of high frequency oscillations is unknown, NMDA receptors are assumed to be involved. It has been shown that *Cyfip1* haploinsufficiency impacts processes downstream of NMDA receptors, such as NMDA receptor-induced spine-remodelling (Pathania et al., 2014), opening up the possibility that *Cyfip1* affects HFO generation. In addition, NMDA receptor-blockade causes increased dopamine release in the prefrontal cortex and nucleus accumbens (Kokkinou et al., 2018) via the disinhibition of dopaminergic neurons in the ventral tegmental area (Lisman et al., 2008; Lodge and Grace, 2011). Thus, aberrant signalling downstream of NMDA receptors could lead to dopaminergic deficits in *Cyfip1*$^{+/-}$ rats.If dopaminergic disruption is indeed present in *Cyfip1*$^{+/-}$ rats, it is of interest to note that a recent paper linked dopamine to aberrant modulation of phase amplitude coupling (Andino-Pavlovsky et al., 2017). This study found that light-induced uncaging of dopamine in freely behaving rats led to a shift of theta-gamma coupling to delta-gamma coupling in the mPFC. Changes in dopamine could therefore be envisaged to lead to the reduced theta-gamma coupling seen in *Cyfip1*$^{+/-}$ rat hippocampus. Furthermore, dopamine has been shown to have an important role in maintaining coupling between different brain regions (Benchenane et al., 2010; Dzirasa et al., 2009; Xu et al., 2016), and while the hippocampal-prefrontal interaction appears intact, this presents a way in which altered dopamine could lead to the aberrant coupling of hippocampus and prefrontal cortex to nucleus accumbens in the *Cyfip1*$^{+/-}$ rat. The results in Chapter 4 also revealed abnormal interaction between the IL and NAc Shell, with increased beta coherence between these regions at the reward point. Increasing the excitation in IL has been shown to increase IL-NAc gamma coherence and repress reward-seeking behaviour, as measured by sucrose preference and place preference tasks (Ferenczi et al., 2016).

By what mechanism could CYFIP1 lead to disrupted coherence between two brain regions? The exact mechanisms of how dysconnectivity between brain regions arises is unclear, but it is likely that both local synaptic and long range anatomical scaffolding changes play a role, both of which are known to be disrupted by Cyfip1 haploinsufficiency (Bozdagi et al., 2012; DeRubeis et al., 2013; Hsiao et al., 2016; Pathania et al., 2014; Schenck et al., 2003). A clear mechanism has been identified in another psychiatric risk model related to 22q11.2 microdeletion syndrome: *Df16(A)*$^{+/-}$ mouse modelling the CNV, and the *Zdhhc8*$^{+/-}$ mouse, deficient in a key gene within the 22q11.2 region (Mukai et al., 2015; Sigurdsson et al., 2010; Tamura et al., 2016). The authors demonstrated that intact axonal growth and axonal arborization of ventral hippocampal axons targeting the mPFC is necessary for normal coherence between these regions and normal performance of a spatial working memory task (Mukai et al., 2015; Tamura et al., 2016). Given the axonal growth and branching deficits observed in *dcyfip1* haploinsufficient drosophila (Schenck et al., 2003), coupled with the known synaptic deficits including both pre- and post-synaptic abnormalities observed in heterozygous mouse models and human induced pluripotent stem cells (Bozdagi et al., 2012; DeRubeis et al., 2013; Hsiao et al., 2016; Pathania et al., 2014; Yoon et al., 2014), it is possible that similar anatomical and synaptic deficits could lead to aberrant network interactions in the *Cyfip1*$^{+/-}$ rat.

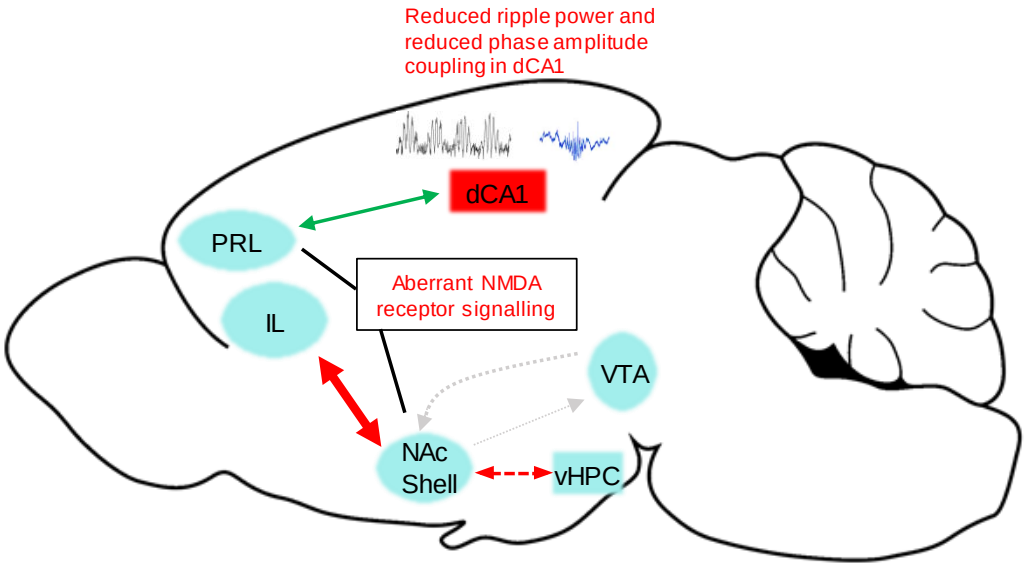

Figure 8.1 | **Summary of network deficits in *Cyfip1*$^{+/-}$ rats**. IL-NAc Shell coherence in the beta band is increased (thick red arrow). Conversely, vHPC-NAc Shell gamma coherence is reduced (thin dashed red arrow). PRL-hippocampal network is intact (green arrow) as shown by normal theta coherence, normal phase amplitude coupling across regions and normal coordination of ripples and spindles during NREM sleep. dCA1 shows weaker ripple power and reduced theta-gamma coupling. Ketamine elicits an exaggerated surge of high frequency oscillations in the PRL and NAc Shell and Core, suggesting NMDA receptor signalling is abnormal. Abnormal NMDA activation on GABAergic neurons in the nucleus accumbens could lead to changes in dopaminergic via disinhibition of the ventral tegmental area (this is hypothetical so marked with grey dotted arrows.)

8.2 Limitations of LFP

The work in this thesis is based on recordings of LFPs from a number of different brain regions. There is still debate in the literature about the spatial resolution of LFPs, whether it represents highly localised events and to what extent they are influenced by volume-conducted currents (Friston et al., 2015b; Kajikawa and Schroeder, 2011; Sirota et al., 2008). In these experiments, this is particularly pertinent to the striking reward-related gamma oscillations observed in the nucleus accumbens, and the debate about their origin (Berke, 2009; Carmichael et al., 2017; van der Meer and Redish, 2009a). Recording simultaneous single unit activity with tetrodes or silicon probes would have allowed assessment of spike-LFP coherence, which can help indicate whether a signal is locally generated.

Recording multiunit activity would be useful for detecting slow waves in Chapters 6 and 7. Two animals showed a suspected polarity switch in their prelimbic cortex

signal, but without multiunit activity recording, this could not be confirmed, and therefore their data had to be excluded.

LFP findings from subcortical structures in animal models can be more challenging to translate to human findings, mainly due to the limited number of studies with depth recordings in patients undergoing surgery for epilepsy (Anderson et al., 2010; Axmacher et al., 2010; Cohen et al., 2009b). However, the ability to record from a number of regions simultaneously with a high spatial and temporal resolution can arguably lead to a better understanding of behaviour-dependent brain activity than, for example, rodent fMRI.

8.3 Use of genetically altered animals as tools in neuropsychiatric research

When using rodents in psychiatric research, it is important to acknowledge that it is impossible for a rodent model to recapitulate the full phenotypic spectrum of a psychiatric disorder for a number of reasons (Nestler and Hyman, 2010). Firstly, given the extensive anatomical differences between rodent and humans, particularly in the complexity of the prefrontal cortex (Carlén, 2017; Uylings and van Eden, 1990; Uylings et al., 2003), a region implicated in most psychiatric disorders, it is unlikely that rodents are capable of harbouring psychiatric illness as humans do (Wong and Josselyn, 2015). Second, clinical diagnoses rely exclusively on reporting of subjective experience and currently no diagnostic biomarkers exist. Thirdly, the heterogeneous nature of many psychiatric conditions like schizophrenia, autism and depression, and the substantial overlap between them (Cross-Disorder Group of the Psychiatric Genomics Consortium, 2013; Gandal et al., 2018), complicates the validation of any rodent models. Therefore, preclinical psychiatric research has shifted from attempting to model specific disorders, rather attempting "a more piecemeal recreation of the disorder's components" (Arguello and Gogos, 2006). Furthermore, it is argued that perhaps genetically altered animals should not be considered as models at all, but tools to understand the molecular-, systems- and behavioural-level consequences of the genetic manipulation (Davis and Isles, 2014; Nestler and Hyman, 2010).

As such, in the narrowest sense the aim of generating the novel *Cyfip1*$^{+/-}$ rat model is to understand the neurobiological consequences of haploinsufficiency of this gene. Eventually, it is hoped that by understanding the molecular pathways and circuit level deficits *Cyfip1* haploinsufficiency may cause, we might identify pathophysiology that is common not only to 15q11.2 deletion carriers, but to a subset of sufferers of schizophrenia, autism and intellectual disability.

8.4 Future Directions

The results in this thesis prompt some experiments that could help further understand the impact of *Cyfip1* haploinsufficiency on brain networks and behaviour.

8.4.1 Behaviour

Considering the behavioural findings in Chapter 3, the discrete-trial alternation T maze does not require extensive training to perform at high accuracy, and likely imposes limited cognitive demand (although the run type modulation of hippocampal-prelimbic coherence does suggest it is engaging this network). It would be interesting to run a task with a higher cognitive demand, such as a radial arm maze, where working memory and reference memory could simultaneously be tested, engaging both hippocampal-prefrontal interactions and hippocampal function, which appears to be disrupted in this model.

Two observations prompt further investigation into the vigour of reward-seeking behaviour. Firstly, slower running on the maze might suggest the groups are not matched for incentive value of the sucrose reward. Secondly, the increased coherence between IL-NAc Shell may act to reduce reward seeking behaviour (Ferenczi et al., 2016; Liu et al., 2016) which could be tested using a sucrose preference test.

Further behavioural tasks that warrant investigation are ones that harness the vHPC-NAc Shell circuit that is deficient in *Cyfip1*$^{+/-}$ rats. Firstly, the novel object location task should be repeated with larger group sizes to replicate the current finding that

suggests *Cyfip1*$^{+/-}$ rats may fail to discriminate the novel location object. Further behavioural tasks that tax this network include a place-preference conditioning task that has been shown to depend specifically on the interaction between vHPC and NAc Shell (Ito et al., 2008). In addition, hippocampal-accumbal interactions were found to be critical to a task involving decision-making with time trade-offs (Abela et al., 2015). Using a disconnection paradigm, the authors found that in animals where the vHPC and NAc interaction was not intact, animals were much less tolerant of a delay for a larger reward and instead chose the smaller, immediately available reward, suggesting the reduced coherence phenotype observed in *Cyfip1*$^{+/-}$ rats could affect this kind of decision-making.

Finally, it would be worth exploring any behavioural consequences of abnormal hippocampal ripples during NREM sleep in *Cyfip1*$^{+/-}$ rats, where I would hypothesise that memory consolidation during sleep is impaired by weak ripples. The novel object location task is known to be sensitive to disruptions of NREM sleep oscillations during the delay phase (Binder et al., 2012; Maingret et al., 2016), thus this would be a good place to start.

8.4.2 Hippocampal-prefrontal network during acquisition

The finding that *Cyfip1*$^{+/-}$ rats took longer to achieve criterion performance on the T maze, together with evidence from other models (*Df(16)A*$^{+/-}$ and *Zdhhc8*$^{+/}$, (Mukai et al., 2015; Sigurdsson et al., 2010)) showing that hippocampal-prefrontal theta coherence prior to training could predict days to criterion and that coherence improved throughout training, prompts the question whether this network is aberrant during task acquisition in *Cyfip1*$^{+/-}$ rats. One could hypothesise that *Cyfip1*$^{+/-}$ theta coherence is impaired at baseline, but improves during training in parallel with learning, raising the level of functional connectivity into the normal range. This could be tested by making recordings prior to and during behavioural training, ideally on a more difficult task that requires a longer training period.

8.4.3 Consequences of cortical-hippocampal-accumbens network disruption

The increased beta coherence between IL and NAc Shell together with reduced vHPC-NAc Shell gamma coherence in *Cyfip1*$^{+/-}$ rats suggests a broader disruption to the cortical-hippocampal-accumbal network, which is important in facilitating flexible behaviour (Floresco et al., 2009). Indeed, unpublished data from Dr. Josephine Haddon shows a reversal learning deficit in a visual discrimination task in *Cyfip1*$^{+/-}$ rats that is hypothesised to be due to network level deficits. While the network deficit finding requires more investigation using single unit recordings, a rescue experiment can be envisaged where the abnormal coherence levels are restored in parallel with normalising the reversal learning deficit. For example, in *Df(16)A*$^{+/-}$ mice, where understanding of the mechanism of disrupted hippocampal-prefrontal connectivity is much more advanced, developmental inhibition of Gsk3 was able to rescue reduced hippocampal-prefrontal theta coherence and behavioural deficits (Tamura et al., 2016).

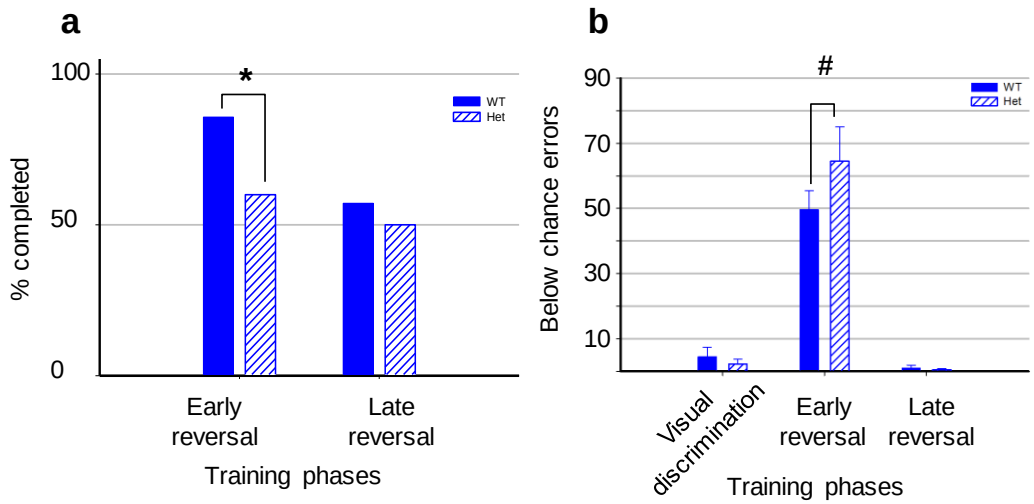

Figure 8.2 | **Reversal learning deficits in *Cyfip1*$^{+/-}$ rats.** *Cyfip1*$^{+/-}$ (Het) rats are **a,** less likely to complete the early reversal phase and **b,** make more errors during the early stages of reversal. Courtesy of Dr. Josephine Haddon, Cardiff University.

8.4.4 Hippocampal recordings

The current findings highlighted multiple hippocampal deficits: reduced hippocampal theta-gamma phase amplitude coupling and weaker ripple during

NREM sleep. Simultaneous unit recordings from hippocampal CA3 and CA1, a network within which slow gamma synchrony is important for memory retrieval (Colgin et al., 2009; Montgomery and Buzsáki, 2007; Schomburg et al., 2014), could shed light on the specific nature of hippocampal oscillation disruption. Following up on the attenuated hippocampal ripple phenotype, it would be important to record single units in the dCA1 to examine the spiking properties of individual pyramidal cells and interneurons which together generate ripples. In addition, if analysis of awake ripples confirms the ripple deficit, this would lend support for abnormal ripple generation mechanisms and also allow comparison with published findings in other psychiatric disorder-relevant models (Suh et al., 2013).

In addition, given the disruptions in the hippocampal-accumbal network, it may be hypothesised that the selective consolidation of salient events through simultaneous replay in these structures (Lansink et al., 2009; Pennartz et al., 2004) could be compromised. This could be explored using dual site single unit recordings in hippocampus and NAc.

8.4.5 Recordings during development

Autism, intellectual disability and schizophrenia are considered neurodevelopmental disorders, where early disturbed brain development can lead to mental illness (Owen et al., 2011). The neonatal ventral hippocampal lesion model of schizophrenia highlights how an early insult to hippocampal circuit development leads to the emergence of schizophrenia-related network changes and behavioural phenotypes in early adulthood (reviewed in Tseng, Chambers, and Lipska 2009). CYFIP1 also appears to have a role in synaptic development, as seen in the switch from predominantly pre-synaptic deficits in younger animals (<P21) to post-synaptic deficits later in life (>P21) (Bozdagi et al., 2012; Hsiao et al., 2016). Notably, hippocampal spatial representations, such as place cells and grid cells, are still under development in the first 4-5 postnatal weeks (Ainge and Langston, 2012; Langston et al., 2010). Thus, it could be proposed that if the hippocampal deficits seen in *Cyfip1*$^{+/-}$ rats emerge at a critical period during network development, they could lead to the circuit- and behavioural-level changes

seen in adulthood. Similarly, disruptions to the hippocampal-accumbal network could arise early during development which could lead to the reduced coherence and reduced response to reward seen in adulthood. Therefore, simultaneous single unit recordings from hippocampus and LFP recording from NAc in developing *Cyfip1*$^{+/-}$ rats could shed light on the developmental origins of the 15q11.2 phenotype.

8.4.6 Dopamine dysregulation

Impaired network activity of vHPC could lead to disrupted dopamine regulation (Goto and Grace, 2008; Grace, 2016; Lodge and Grace, 2011). It would be important to ascertain whether dopamine levels are abnormal in Cyfip1 rats by voltammetry (e.g. Papageorgiou et al. 2016; Syed et al. 2016) or recording neural activity of ventral tegmental area neurons.

8.4.7 Further investigation of heightened sensitivity to ketamine

The augmented increase in HFO following ketamine in *Cyfip1*$^{+/-}$ rats implicate abnormal NMDA receptor functioning. If high frequency oscillations, like gamma oscillations, are driven by parvalbumin-positive (PV) interneurons, which are also thought to be a major target of NMDAR antagonists, it would be important to assess PV interneuron density in *Cyfip1*$^{+/-}$ rat, as in the MAM rat model, where aberrant ketamine-evoked gamma oscillations were linked to a region-specific decrease in PV staining (Phillips et al., 2012b).

8.4.8 Gene-environment interactions

Gene-environment interactions play an important role in the development of psychiatric disorders. One example is early life stress, which has been shown to increase the risk of developing a neuropsychiatric disorder in later life (Pechtel and Pizzagalli, 2011), via a possible mechanism of epigenetics (Lewis and Olive, 2014). The juvenile (pre-pubescent) brain may be particularly susceptible, with brain regions undergoing extended postnatal development, such as the hippocampus, being especially vulnerable (Teicher et al., 2012). Animal models of juvenile stress also show behavioural changes in adults, including hippocampal-dependent

behaviours (Brydges et al., 2012, 2014). A growing body of research indicates that genetic mutations and an additional environmental insult, including early life stressors, have synergistic contributions to psychiatric disorder-related phenotypes (reviewed in Moran et al. 2016). Previously, I ran a study investigating delayed discrete-trial alternation in WT rats exposed to juvenile stress and found no performance deficit (data not included in this thesis). Future experiments could address whether the combined impact of *Cyfip1* haploinsufficiency and juvenile stress would together lead to a spatial working memory deficit.

8.4.9 Next steps with 15q11.2 deletion carriers

The current finding of disruption to the cortical-hippocampal-accumbens network in the *Cyfip1*$^{+/-}$ rat might offer a useful starting point for functional connectivity analysis for future fMRI studies in 15q11.2 deletion carriers. As changes in the rats were most prominent during reward anticipation and receipt, subjects could perform a reward anticipation task as in Bossong et al. (2018). Parallel fMRI studies in the *Cyfip1*$^{+/-}$ rats would aid comparison between rodent and human.

8.4.10 Postscript

Very recently, following the completion of the work in this thesis and immediately before its submission, I have become aware of ongoing work by my colleagues in Cardiff examining factors which influence the molecular Cyfip1 phenotype in *Cyfip1*$^{+/-}$ rats. This work is in its early stages but an emerging picture is that whilst the *Cyfip1*$^{+/-}$ rat model is consistently haploinsufficient at the mRNA levels as assessed across a wide range of brain regions and preparations (whole brain homogenates, synaptosome preparations) there is more variability in terms of protein levels, such that (according to the data collected so far), whilst there is always a consistent reduction in mean protein levels in brain tissue from *Cyfip1*$^{+/-}$ animals, variability in levels can result in non-significant group differences. It should be emphasised that this work, constituting a large screen of various brain regions, preparations, stages of development and environmental conditions, is incomplete and needs to be confirmed with further antibodies and methods in addition to Western Blot (e.g. ELISA).

However, it seems important to note these initial findings in case they are eventually confirmed, in which case they may suggest varying degrees of compensation at the protein level (presumably arising from expression from the normal Cyfip1 locus) in different brain regions. The functional consequences of this brain region specific (and even more speculatively, cell specific) effect would then become of interest, and possible differences in the impact of the *Cyfip1* mutation on brain networks which might also be sensitive to developmental stage would need to be considered. However, again it should be emphasised that the experiments in Cardiff are incomplete and that significant group differences in protein levels have been observed, as of course, have significant group effects of genotype on electrophysiological and behavioural phenotypes.

8.5 Conclusions

This thesis has made novel contributions to understanding the impact of *Cyfip1* haploinsufficiency on neural network interactions in rats, which can be summarised as follows:

- *Cyfip1*$^{+/-}$ rats have deficits in acquisition of a working memory task, but hippocampal-prefrontal interactions remain intact in well-trained animals.
- *Cyfip1*$^{+/-}$ rats show several hippocampal deficits, such as reduced theta-gamma phase amplitude coupling and reduced ripple power. The closely related *Fmr1* KO rat also shows abnormal hippocampal ripples.
- The hippocampal-cortical-accumbal network is disrupted in *Cyfip1*$^{+/-}$ rats, with reduced vHPC-NAc Shell gamma coherence and increased IL-NAc Shell beta coherence. Preliminary evidence suggests a deficit in the novel object location task.
- Circadian patterns and sleep architecture appear normal in *Cyfip1*$^{+/-}$ rats.

Collectively, these findings suggest that CYFIP1 has an important role in normal functioning of a number of brain regions and networks implicated in psychiatric disorders. These network changes may be linked to the increased psychiatric risk conferred by the 15q11.2 deletion in humans and provide a

framework within which to focus mechanistic studies bridging CYFIP1's molecular functions to brain and behaviour phenotypes.

References

Abbott, L.F., and Nelson, S.B. (2000). Synaptic plasticity: taming the beast. Nat. Neurosci. *3 Suppl*, 1178–1183.

Abdelmoity, A.T., LePichon, J.-B., Nyp, S.S., Soden, S.E., Daniel, C.A., and Yu, S. (2012). 15q11.2 Proximal Imbalances Associated With a Diverse Array of Neuropsychiatric Disorders and Mild Dysmorphic Features. J. Dev. Behav. Pediatr. *33*, 570–576.

Abekhoukh, S., Sahin, H.B., Grossi, M., Zongaro, S., Maurin, T., Madrigal, I., Kazue-Sugioka, D., Raas-Rothschild, A., Doulazmi, M., Carrera, P., et al. (2017). New insights into the regulatory function of CYFIP1 in the context of WAVE- and FMRP-containing complexes. Dis. Model. Mech. *10*, 463–474.

Abela, A.R., Duan, Y., and Chudasama, Y. (2015). Hippocampal interplay with the nucleus accumbens is critical for decisions about time. Eur. J. Neurosci. *42*, 2224–2233.

Abi-Dargham, A., Gil, R., Krystal, J., Baldwin, R.M., Seibyl, J.P., Bowers, M., van Dyck, C.H., Charney, D.S., Innis, R.B., and Laruelle, M. (1998). Increased striatal dopamine transmission in schizophrenia: confirmation in a second cohort. Am. J. Psychiatry *155*, 761–767.

Abi-Saab, W., D'Souza, D., Moghaddam, B., and Krystal, J. (1998). The NMDA Antagonist Model for Schizophrenia: Promise and Pitfalls. Pharmacopsychiatry *31*, 104–109.

Acheson, A., Farrar, A.M., Patak, M., Hausknecht, K.A., Kieres, A.K., Choi, S., de Wit, H., and Richards, J.B. (2006). Nucleus accumbens lesions decrease sensitivity to rapid changes in the delay to reinforcement. Behav. Brain Res. *173*, 217–228.

Adhikari, A., Sigurdsson, T., Topiwala, M.A., and Gordon, J.A. (2010). Cross-correlation of instantaneous amplitudes of field potential oscillations: a straightforward method to estimate the directionality and lag between brain areas. J. Neurosci. Methods *191*, 191–200.

Adler, C.M., Malhotra, A.K., Elman, I., Goldberg, T., Egan, M., Pickar, D., and Breier, A. (1999). Comparison of Ketamine-Induced Thought Disorder in Healthy

Volunteers and Thought Disorder in Schizophrenia. Am. J. Psychiatry *156*, 1646–1649.

Aggleton, J.P., Kenn, S., Warburton, E.C., and Bussey, T.J. (1997). Extensive cytotoxic lesions involving both the rhinal cortices and area TE impair recognition but spare spatial alternation in the rat. Brain Res. Bull. *43*, 279–287.

Ahmed, O.J., and Mehta, M.R. (2012). Running Speed Alters the Frequency of Hippocampal Gamma Oscillations. J. Neurosci. *32*, 7373–7383.

Ainge, J.A., and Langston, R.F. (2012). Ontogeny of neural circuits underlying spatial memory in the rat. Front. Neural Circuits *6*, 8.

Ainge, J.A., Van Der Meer, M.A.A., Langston, R.F., and Wood, E.R. (2007a). Exploring the role of context-dependent hippocampal activity in spatial alternation behavior. Hippocampus *17*, 988–1002.

Ainge, J.A., Tamosiunaite, M., Woergoetter, F., and Dudchenko, P.A. (2007b). Hippocampal CA1 place cells encode intended destination on a maze with multiple choice points. J. Neurosci. *27*, 9769–9779.

Akbarian, S., Kim, J.J., Potkin, S.G., Hagman, J.O., Tafazzoli, A., Bunney, W.E., and Jones, E.G. (1995). Gene expression for glutamic acid decarboxylase is reduced without loss of neurons in prefrontal cortex of schizophrenics. Arch. Gen. Psychiatry *52*, 258–266.

Alexander, G.E., and Crutcher, M.D. (1990). Functional architecture of basal ganglia circuits: neural substrates of parallel processing. Trends Neurosci. *13*, 266–271.

Altimus, C., Harrold, J., Jaaro-Peled, H., Sawa, A., and Foster, D.J. (2015). Disordered Ripples Are a Common Feature of Genetically Distinct Mouse Models Relevant to Schizophrenia. Mol. Neuropsychiatry *1*, 52–59.

American Psychiatric Association (2013). Diagnostic and statistical manual of mental disorders (DSM-5®) (American Psychiatric Publishing, Inc).

Anderson, K.L., Rajagovindan, R., Ghacibeh, G.A., Meador, K.J., and Ding, M. (2010). Theta Oscillations Mediate Interaction between Prefrontal Cortex and Medial Temporal Lobe in Human Memory. Cereb. Cortex *20*, 1604–1612.

Andino-Pavlovsky, V., Souza, A.C., Scheffer-Teixeira, R., Tort, A.B.L., Etchenique, R., and Ribeiro, S. (2017). Dopamine Modulates Delta-Gamma Phase-Amplitude Coupling in the Prefrontal Cortex of Behaving Rats. Front. Neural Circuits *11*, 29.

Anis, N.A., Berry, S.C., Burton, N.R., and Lodge, D. (1983). The dissociative anaesthetics, ketamine and phencyclidine, selectively reduce excitation of central mammalian neurones by N-methyl-aspartate. Br. J. Pharmacol. *79*, 565–575.

Apicella, P., Ljungberg, T., Scarnati, E., and Schultz, W. (1991). Responses to reward in monkey dorsal and ventral striatum. Exp. Brain Res. *85*, 491–500.

Arbab, T., Pennartz, C.M., and Battaglia, F.P. (2017). Impaired hippocampal representation of place in the Fmr1-knockout mouse model of Fragile X syndrome. bioRxiv 191775.

Arbab, T., Battaglia, F.P., Pennartz, C.M.A., and Bosman, C.A. (2018). Abnormal hippocampal theta and gamma hypersynchrony produces network and spike timing disturbances in the Fmr1-KO mouse model of Fragile X syndrome. Neurobiol. Dis. *114*, 65–73.

Arber, S., Barbayannis, F.A., Hanser, H., Schneider, C., Stanyon, C.A., Bernard, O., and Caroni, P. (1998). Regulation of actin dynamics through phosphorylation of cofilin by LIM-kinase. Nature *393*, 805–809.

Arguello, P.A., and Gogos, J.A. (2006). Modeling madness in mice: one piece at a time. Neuron *52*, 179–196.

Arnone, D., McIntosh, A.M., Tan, G.M.Y., and Ebmeier, K.P. (2008). Meta-analysis of magnetic resonance imaging studies of the corpus callosum in schizophrenia. Schizophr. Res. *101*, 124–132.

Asif-Malik, A., Dautan, D., Young, A.M.J., and Gerdjikov, T. V. (2017). Altered cortico-striatal crosstalk underlies object recognition memory deficits in the sub-chronic phencyclidine model of schizophrenia. Brain Struct. Funct. *222*, 3179–3190.

Aultman, J.M., and Moghaddam, B. (2001). Distinct contributions of glutamate and dopamine receptors to temporal aspects of rodent working memory using a clinically relevant task. Psychopharmacology (Berl). *153*, 353–364.

Avsar, K.B., Weller, R.E., Cox, J.E., Reid, M.A., White, D.M., and Lahti, A.C. (2013). An fMRI investigation of delay discounting in patients with schizophrenia. Brain Behav. *3*, 384–401.

Axmacher, N., Mormann, F., Fernández, G., Elger, C.E., and Fell, J. (2006). Memory formation by neuronal synchronization. Brain Res. Rev. *52*, 170–182.

Axmacher, N., Schmitz, D.P., Wagner, T., Elger, C.E., and Fell, J. (2008). Interactions between medial temporal lobe, prefrontal cortex, and inferior temporal regions during visual working memory: a combined intracranial EEG and functional magnetic resonance imaging study. J. Neurosci. *28*, 7304–7312.

Axmacher, N., Henseler, M.M., Jensen, O., Weinreich, I., Elger, C.E., and Fell, J. (2010). Cross-frequency coupling supports multi-item working memory in the human hippocampus. Proc. Natl. Acad. Sci. U. S. A. *107*, 3228–3233.

Baandrup, L., and Jennum, P.J. (2015). A validation of wrist actigraphy against polysomnography in patients with schizophrenia or bipolar disorder. Neuropsychiatr. Dis. Treat. *11*, 2271–2277.

Baddeley, A.D., and Hitch, G. (1974). Working memory. Psychol. Learn. Motiv. - Adv. Res. Theory *8*, 47–89.

Baeg, E.H., Kim, Y.B., Huh, K., Mook-Jung, I., Kim, H.T., and Jung, M.W. (2003). Dynamics of population code for working memory in the prefrontal cortex. Neuron *40*, 177–188.

Bähner, F., and Meyer-Lindenberg, A. (2017). Hippocampal–prefrontal connectivity as a translational phenotype for schizophrenia. Eur. Neuropsychopharmacol. *27*, 93–106.

Bähner, F., Demanuele, C., Schweiger, J., Gerchen, M.F., Zamoscik, V., Ueltzhöffer, K., Hahn, T., Meyer, P., Flor, H., Durstewitz, D., et al. (2015). Hippocampal-dorsolateral prefrontal coupling as a species-conserved cognitive mechanism: a human translational imaging study. Neuropsychopharmacology *40*, 1674–1681.

Baiano, M., David, A., Versace, A., Churchill, R., Balestrieri, M., and Brambilla, P. (2007). Anterior cingulate volumes in schizophrenia: A systematic review and a meta-analysis of MRI studies. Schizophr. Res. *93*, 1–12.

Baliki, M.N., Mansour, A., Baria, A.T., Huang, L., Berger, S.E., Fields, H.L., and Apkarian, A.V. (2013). Parceling human accumbens into putative core and shell dissociates encoding of values for reward and pain. J. Neurosci. *33*, 16383–16393.

Bamford, N.S., Wightman, R.M., and Sulzer, D. (2018). Dopamine's Effects on Corticostriatal Synapses during Reward-Based Behaviors. Neuron *97*, 494–510.

Bannerman, D.., Rawlins, J.N.., McHugh, S.., Deacon, R.M.., Yee, B.., Bast, T., Zhang, W.-N., Pothuizen, H.H.., and Feldon, J. (2004). Regional dissociations within the hippocampus—memory and anxiety. Neurosci. Biobehav. Rev. *28*, 273–283.

Bannerman, D.M., Yee, B.K., Good, M.A., Heupel, M.J., Iversen, S.D., and Rawlins, J.N. (1999). Double dissociation of function within the hippocampus: a comparison of dorsal, ventral, and complete hippocampal cytotoxic lesions. Behav. Neurosci. *113*, 1170–1188.

Bannerman, D.M., Deacon, R.M.J., Offen, S., Friswell, J., Grubb, M., and Rawlins, J.N.P. (2002). Double dissociation of function within the hippocampus: spatial memory and hyponeophagia. Behav. Neurosci. *116*, 884–901.

Barakat, M., Doyon, J., Debas, K., Vandewalle, G., Morin, A., Poirier, G., Martin, N., Lafortune, M., Karni, A., Ungerleider, L.G., et al. (2011). Fast and slow spindle involvement in the consolidation of a new motor sequence. Behav. Brain Res. *217*, 117–121.

Bardo, M.T. (1998). Neuropharmacological mechanisms of drug reward: beyond dopamine in the nucleus accumbens. Crit. Rev. Neurobiol. *12*, 37–67.

Barker, G.R.I., Bird, F., Alexander, V., and Warburton, E.C. (2007). Recognition memory for objects, place, and temporal order: a disconnection analysis of the role of the medial prefrontal cortex and perirhinal cortex. J. Neurosci. *27*, 2948–2957.

Barker, G.R.I., Banks, P.J., Scott, H., Ralph, G.S., Mitrophanous, K.A., Wong, L.-F., Bashir, Z.I., Uney, J.B., and Warburton, E.C. (2017). Separate elements of episodic memory subserved by distinct hippocampal–prefrontal connections. Nat. Neurosci. *20*, 242–250.

Barnes, S.A., Der-Avakian, A., and Young, J.W. (2017). Preclinical Models to Investigate Mechanisms of Negative Symptoms in Schizophrenia. Schizophr. Bull. *43*, 706–711.

Barr, M.S., Farzan, F., Tran, L.C., Chen, R., Fitzgerald, P.B., and Daskalakis, Z.J. (2010). Evidence for excessive frontal evoked gamma oscillatory activity in schizophrenia during working memory. Schizophr. Res. *121*, 146–152.

Barr, M.S., Rajji, T.K., Zomorrodi, R., Radhu, N., George, T.P., Blumberger, D.M., and Daskalakis, Z.J. (2017). Impaired theta-gamma coupling during working memory performance in schizophrenia. Schizophr. Res. *189*, 104–110.

Bayer, H.M., and Glimcher, P.W. (2005). Midbrain Dopamine Neurons Encode a Quantitative Reward Prediction Error Signal. Neuron *47*, 129–141.

Becker, A., Peters, B., Schroeder, H., Mann, T., Huether, G., and Grecksch, G. (2003). Ketamine-induced changes in rat behaviour: A possible animal model of schizophrenia. Prog. Neuro-Psychopharmacology Biol. Psychiatry *27*, 687–700.

Beier, K.T., Steinberg, E.E., DeLoach, K.E., Xie, S., Miyamichi, K., Schwarz, L., Gao, X.J., Kremer, E.J., Malenka, R.C., and Luo, L. (2015). Circuit Architecture of VTA Dopamine Neurons Revealed by Systematic Input-Output Mapping. Cell *162*, 622–634.

Belluscio, M.A., Mizuseki, K., Schmidt, R., Kempter, R., and Buzsaki, G. (2012). Cross-Frequency Phase-Phase Coupling between Theta and Gamma Oscillations in the Hippocampus. J. Neurosci. *32*, 423–435.

Belujon, P., and Grace, A.A. (2014). Restoring mood balance in depression: ketamine reverses deficit in dopamine-dependent synaptic plasticity. Biol. Psychiatry *76*, 927–936.

Belujon, P., Patton, M.H., and Grace, A.A. (2014). Role of the prefrontal cortex in altered hippocampal-accumbens synaptic plasticity in a developmental animal model of schizophrenia. Cereb. Cortex *24*, 968–977.

Benchenane, K., Peyrache, A., Khamassi, M., Tierney, P.L., Gioanni, Y., Battaglia, F.P., and Wiener, S.I. (2010). Coherent Theta Oscillations and Reorganization of Spike Timing in the Hippocampal- Prefrontal Network upon Learning. Neuron *66*, 921–936.

Benchenane, K., Tiesinga, P.H., and Battaglia, F.P. (2011). Oscillations in the prefrontal cortex: a gateway to memory and attention. Curr. Opin. Neurobiol. *21*, 475–485.

Benetti, S., Mechelli, A., Picchioni, M., Broome, M., Williams, S., and McGuire, P. (2009). Functional integration between the posterior hippocampus and prefrontal cortex is impaired in both first episode schizophrenia and the at risk mental state. Brain *132*, 2426–2436.

Berendse, H.W., Groenewegen, H.J., and Lohman, A.H. (1992). Compartmental distribution of ventral striatal neurons projecting to the mesencephalon in the rat. J. Neurosci. *12*, 2079–2103.

Berger, S.M., and Bartsch, D. (2014). The role of L-type voltage-gated calcium channels Cav1.2 and Ca v1.3 in normal and pathological brain function. Cell Tissue Res. *357*, 463–476.

Berke, J.D. (2009). Fast oscillations in cortical-striatal networks switch frequency following rewarding events and stimulant drugs. Eur. J. Neurosci. *30*, 848–859.

Berridge, K.C. (2007). The debate over dopamine's role in reward: the case for incentive salience. Psychopharmacology (Berl). *191*, 391–431.

Berridge, K.C., and Robinson, T.E. (1998). What is the role of dopamine in reward: Hedonic impact, reward learning, or incentive salience? Brain Res. Rev. *28*, 309–369.

Berry, R.B., Gamaldo, C.E., Harding, S.M., Brooks, R., Lloyd, R.M., Vaughn, B. V., and Marcus, C.L. (2015). AASM scoring manual version 2.2 updates: New chapters for scoring infant sleep staging and home sleep apnea testing. J. Clin. Sleep Med. *11*, 1253–1254.

Bersani, F.S., Minichino, A., Fojanesi, M., Gallo, M., Maglio, G., Valeriani, G., Biondi, M., and Fitzgerald, P.B. (2014). Cingulate Cortex in Schizophrenia: its relation with negative symptoms and psychotic onset. A review study. Eur. Rev. Med. Pharmacol. Sci. *18*, 3354–3367.

Berzhanskaya, J., Phillips, M.A., Gorin, A., Lai, C., Shen, J., and Colonnese, M.T. (2017). Disrupted Cortical State Regulation in a Rat Model of Fragile X Syndrome. Cereb. Cortex *27*, 1386–1400.

Bevins, R.A. (2001). Novelty Seeking and Reward: Implications for the Study of High-Risk Behaviors. Curr. Dir. Psychol. Sci. *10*, 189–193.

Bevins, R.A., and Besheer, J. (2005). Novelty reward as a measure of anhedonia.

Neurosci. Biobehav. Rev. *29*, 707–714.

Bevins, R.A., Besheer, J., Palmatier, M.I., Jensen, H.C., Pickett, K.S., and Eurek, S. (2002). Novel-object place conditioning: behavioral and dopaminergic processes in expression of novelty reward. Behav. Brain Res. *129*, 41–50.

Binder, S., Baier, P.C., Mölle, M., Inostroza, M., Born, J., and Marshall, L. (2012). Sleep enhances memory consolidation in the hippocampus-dependent object-place recognition task in rats. Neurobiol. Learn. Mem. *97*, 213–219.

Birrell, J.M., and Brown, V.J. (2000). Medial frontal cortex mediates perceptual attentional set shifting in the rat. J. Neurosci. *20*, 4320–4324.

Bitanihirwe, B.K.Y., Lim, M.P., Kelley, J.F., Kaneko, T., and Woo, T.U.W. (2009). Glutamatergic deficits and parvalbumin-containing inhibitory neurons in the prefrontal cortex in schizophrenia. BMC Psychiatry *9*, 71.

Bittel, D.C., Kibiryeva, N., and Butler, M.G. (2006). Expression of 4 genes between chromosome 15 breakpoints 1 and 2 and behavioral outcomes in Prader-Willi syndrome. Pediatrics *118*, e1276-83.

Blaha, C.D., Yang, C.R., Floresco, S.B., Barr, A.M., and Phillips, A.G. (1997). Stimulation of the ventral subiculum of the hippocampus evokes glutamate receptor-mediated changes in dopamine efflux in the rat nucleus accumbens. Eur. J. Neurosci. *9*, 902–911.

Blaiss, C.A., and Janak, P.H. (2009). The nucleus accumbens core and shell are critical for the expression, but not the consolidation, of Pavlovian conditioned approach. Behav. Brain Res. *200*, 22–32.

Bland, J.M., and Altman, D.G. (1986). Statistical methods for assessing agreement between two methods of clinical measurement. Lancet *1*, 307–310.

Bonaccorso, C.M., Spatuzza, M., Dimarco, B., Gloria, A., Barrancotto, G., Cupo, A., Musumeci, S.A., D'Antoni, S., Bardoni, B., and Catania, M. V (2015). Fragile X mental retardation protein (FMRP) interacting proteins exhibit different expression patterns during development. Int. J. Dev. Neurosci.

Di Bonaventura, C., Mari, F., Pierallini, A., Mecarelli, O., Randi, F., Manfredi, M., Prencipe, M., and Giallonardo, A.T. (2006). Status epilepticus in a patient with fragile X syndrome: electro-clinical features and peri-ictal neuroimaging. Epileptic

Disord. *8*, 195–199.

Booth, C., Witton, J., Nowacki, J., Tsaneva-Atanasova, K., Jones, M.W., Randall, A.D., and Brown, J.T. (2016). Alterations to intrinsic pyramidal neuron properties and temporoammonic synaptic plasticity underlie deficits in hippocampal network function in a mouse model of tauopathy. J. Neurosci. *36*, 350–363.

Bora, E., Fornito, A., Radua, J., Walterfang, M., Seal, M., Wood, S.J., Yücel, M., Velakoulis, D., and Pantelis, C. (2011). Neuroanatomical abnormalities in schizophrenia: a multimodal voxelwise meta-analysis and meta-regression analysis. Schizophr. Res. *127*, 46–57.

Borbély, A.A., and Achermann, P. (1999). Sleep homeostasis and models of sleep regulation. J. Biol. Rhythms *14*, 557–568.

Born, J., and Wilhelm, I. (2012). System consolidation of memory during sleep. Psychol. Res. *76*, 192–203.

Bossong, M.G., Wilson, R., Appiah-Kusi, E., McGuire, P., and Bhattacharyya, S. (2018). Human Striatal Response to Reward Anticipation Linked to Hippocampal Glutamate Levels. Int. J. Neuropsychopharmacol.

Bozdagi, O., Sakurai, T., Dorr, N., Pilorge, M., Takahashi, N., and Buxbaum, J.D. (2012). Haploinsufficiency of Cyfip1 produces fragile X-like phenotypes in mice. PLoS One *7*, e42422.

Bracci, E., Centonze, D., Bernardi, G., and Calabresi, P. (2003). Voltage-dependent membrane potential oscillations of rat striatal fast-spiking interneurons. J. Physiol. *549*, 121–130.

Bragin, A., Jandó, G., Nádasdy, Z., Hetke, J., Wise, K., and Buzsáki, G. (1995). Gamma (40-100 Hz) oscillation in the hippocampus of the behaving rat. J. Neurosci. *15*, 47–60.

Bramham, C.R., Jensen, K.B., and Proud, C.G. (2016). Tuning Specific Translation in Cancer Metastasis and Synaptic Memory: Control at the MNK–eIF4E Axis. Trends Biochem. Sci. *41*, 847–858.

Brincat, S.L., and Miller, E.K. (2015). Frequency-specific hippocampal-prefrontal interactions during associative learning. Nat. Neurosci. *18*, 576–581.

Brito, G.N., Davis, B.J., Stopp, L.C., and Stanton, M.E. (1983). Memory and the septo-hippocampal cholinergic system in the rat. Psychopharmacology (Berl). *81*, 315–320.

Brito, L.S., Yamasaki, E.N., Paumgartten, F.J., and Brito, G.N. (1987). Continuous and discrete T-maze alternation in rats: effects of intertrial and interrun intervals. Brazilian J. Med. Biol. Res. *20*, 125–135.

Britt, J.P., Benaliouad, F., McDevitt, R.A., Stuber, G.D., Wise, R.A., and Bonci, A. (2012). Synaptic and behavioral profile of multiple glutamatergic inputs to the nucleus accumbens. Neuron *76*, 790–803.

Brog, J.S., Salyapongse, A., Deutch, A.Y., and Zahm, D.S. (1993). The patterns of afferent innervation of the core and shell in the "Accumbens" part of the rat ventral striatum: Immunohistochemical detection of retrogradely transported fluoro-gold. J. Comp. Neurol. *338*, 255–278.

Bromundt, V., Koster, M., Georgiev-Kill, A., Opwis, K., Wirz-Justice, A., Stoppe, G., and Cajochen, C. (2011). Sleep-wake cycles and cognitive functioning in schizophrenia. Br J Psychiatry *198*, 269–276.

Brown, A.S., and Derkits, E.J. (2010). Prenatal infection and schizophrenia: a review of epidemiologic and translational studies. Am. J. Psychiatry *167*, 261–280.

Brown, L.A., Hasan, S., Foster, R.G., Peirson, S.N., Brown, L.A., Hasan, S., Foster, R.G., and Peirson, S.N. (2016). COMPASS: Continuous Open Mouse Phenotyping of Activity and Sleep Status. Wellcome Open Res. *1*, 2.

Brydges, N.M., Hall, L., Nicolson, R., Holmes, M.C., and Hall, J. (2012). The effects of juvenile stress on anxiety, cognitive bias and decision making in adulthood: a rat model. PLoS One *7*, e48143.

Brydges, N.M., Wood, E.R., Holmes, M.C., and Hall, J. (2014). Prepubertal stress and hippocampal function: sex-specific effects. Hippocampus *24*, 684–692.

Burgos-Robles, A., Vidal-Gonzalez, I., Santini, E., and Quirk, G.J. (2007). Consolidation of Fear Extinction Requires NMDA Receptor-Dependent Bursting in the Ventromedial Prefrontal Cortex. Neuron *53*, 871–880.

Burnside, R.D., Pasion, R., Mikhail, F.M., Carroll, A.J., Robin, N.H., Youngs, E.L., Gadi, I.K., Keitges, E., Jaswaney, V.L., Papenhausen, P.R., et al. (2011).

Microdeletion/microduplication of proximal 15q11.2 between BP1 and BP2: a susceptibility region for neurological dysfunction including developmental and language delay. Hum. Genet. *130*, 517–528.

Burwell, R.D., and Amaral, D.G. (1998). Cortical afferents of the perirhinal, postrhinal, and entorhinal cortices of the rat. J. Comp. Neurol. *398*, 179–205.

Bushey, D., Tononi, G., and Cirelli, C. (2009). The Drosophila Fragile X Mental Retardation Gene Regulates Sleep Need. J. Neurosci. *29*, 1948–1961.

Butler, M.G. (2017). Clinical and genetic aspects of the 15q11.2 BP1–BP2 microdeletion disorder. J. Intellect. Disabil. Res. *61*, 568–579.

Butterly, D.A., Petroccione, M.A., and Smith, D.M. (2012). Hippocampal context processing is critical for interference free recall of odor memories in rats. Hippocampus *22*, 906–913.

Buzsáki, G. (1986). Hippocampal sharp waves: their origin and significance. Brain Res. *398*, 242–252.

Buzsáki, G. (2002). Theta oscillations in the hippocampus. Neuron *33*, 325–340.

Buzsáki, G. (2015). Hippocampal sharp wave-ripple: A cognitive biomarker for episodic memory and planning. Hippocampus *25*, 1073–1188.

Buzsáki, G., and Draguhn, A. (2004). Neuronal oscillations in cortical networks. Science *304*, 1926–1929.

Buzsáki, G., and Moser, E.I. (2013). Memory, navigation and theta rhythm in the hippocampal-entorhinal system. Nat. Neurosci. *16*, 130–138.

Buzsáki, G., and Watson, B.O. (2012). Brain rhythms and neural syntax: Implications for efficient coding of cognitive content and neuropsychiatric disease. Dialogues Clin. Neurosci. *14*, 345–367.

Buzsáki, G., Leung, L.W., and Vanderwolf, C.H. (1983). Cellular bases of hippocampal EEG in the behaving rat. Brain Res. *287*, 139–171.

Buzsáki, G., Buhl, D.L., Harris, K.D., Csicsvari, J., Czéh, B., and Morozov, A. (2003). Hippocampal network patterns of activity in the mouse. Neuroscience *116*,

201–211.

Buzsáki, G., Anastassiou, C.A., and Koch, C. (2012). The origin of extracellular fields and currents — EEG, ECoG, LFP and spikes. Nat. Rev. Neurosci. *13*, 407–420.

Buzsáki, G., Logothetis, N., and Singer, W. (2013). Scaling brain size, keeping timing: evolutionary preservation of brain rhythms. Neuron *80*, 751–764.

Cadinu, D., Grayson, B., Podda, G., Harte, M.K., Doostdar, N., and Neill, J.C. (2018). NMDA receptor antagonist rodent models for cognition in schizophrenia and identification of novel drug treatments, an update. Neuropharmacology.

Caixeta, F. V., Cornélio, A.M., Scheffer-Teixeira, R., Ribeiro, S., and Tort, A.B.L. (2013). Ketamine alters oscillatory coupling in the hippocampus. Sci. Rep. *3*, 2348.

Callicott, J.H., Feighery, E.L., Mattay, V.S., White, M.G., Chen, Q., Baranger, D.A.A., Berman, K.F., Lu, B., Song, H., Ming, G., et al. (2013). DISC1 and SLC12A2 interaction affects human hippocampal function and connectivity. J. Clin. Invest. *123*, 2961–2964.

Campbell, I.G., and Feinberg, I. (2016). Maturational Patterns of Sigma Frequency Power Across Childhood and Adolescence: A Longitudinal Study. Sleep *39*, 193–201.

Canolty, R.T., and Knight, R.T. (2010). The functional role of cross-frequency coupling. Trends Cogn. Sci. *14*, 506–515.

Canolty, R.T., Edwards, E., Dalal, S.S., Soltani, M., Nagarajan, S.S., Kirsch, H.E., Berger, M.S., Barbaro, N.M., and Knight, R.T. (2006). High gamma power is phase-locked to theta oscillations in human neocortex. Science *313*, 1626–1628.

Caravaggio, F., Fervaha, G., Iwata, Y., Plitman, E., Chung, J.K., Nakajima, S., Mar, W., Gerretsen, P., Kim, J., Chakravarty, M.M., et al. (2018). Amotivation is associated with smaller ventral striatum volumes in older patients with schizophrenia. Int. J. Geriatr. Psychiatry *33*, 523–530.

Cardin, J.A., Carlén, M., Meletis, K., Knoblich, U., Zhang, F., Deisseroth, K., Tsai, L.-H., and Moore, C.I. (2009). Driving fast-spiking cells induces gamma rhythm and controls sensory responses. Nature *459*, 663–667.

Cardinal, R.N., Pennicott, D.R., Sugathapala, C.L., Robbins, T.W., and Everitt, B.J. (2001). Impulsive Choice Induced in Rats by Lesions of the Nucleus Accumbens Core. Science (80-.). *292*, 2499–2501.

Carelli, R.M., and Deadwyler, S.A. (1994). A comparison of nucleus accumbens neuronal firing patterns during cocaine self-administration and water reinforcement in rats. J. Neurosci. *14*, 7735–7746.

Carlén, M. (2017). What constitutes the prefrontal cortex? Science (80-.). *358*, 478–482.

Carlén, M., Meletis, K., Siegle, J.H., Cardin, J.A., Futai, K., Vierling-Claassen, D., Rühlmann, C., Jones, S.R., Deisseroth, K., Sheng, M., et al. (2012). A critical role for NMDA receptors in parvalbumin interneurons for gamma rhythm induction and behavior. Mol. Psychiatry *17*, 537–548.

Carmichael, J.E., Gmaz, J.M., and van der Meer, M.A.A. (2017). Gamma Oscillations in the Rat Ventral Striatum Originate in the Piriform Cortex. J. Neurosci. *37*, 7962–7974.

Carr, M.F., Karlsson, M.P., and Frank, L.M. (2012). Transient Slow Gamma Synchrony Underlies Hippocampal Memory Replay. Neuron *75*, 700–713.

Carracedo, L.M., Kjeldsen, H., Cunnington, L., Jenkins, A., Schofield, I., Cunningham, M.O., Davies, C.H., Traub, R.D., and Whittington, M.A. (2013). A neocortical delta rhythm facilitates reciprocal interlaminar interactions via nested theta rhythms. J. Neurosci. *33*, 10750–10761.

Cassel, J.-C., Pereira de Vasconcelos, A., Loureiro, M., Cholvin, T., Dalrymple-Alford, J.C., and Vertes, R.P. (2013). The reuniens and rhomboid nuclei: neuroanatomy, electrophysiological characteristics and behavioral implications. Prog. Neurobiol. *111*, 34–52.

Castelnovo, A., Agostino, A.D., Casetta, C., Sarasso, S., and Ferrarelli, F. (2016). Sleep Spindle Deficit in Schizophrenia : Contextualization of Recent Findings. Curr. Psychiatry Rep. *18*, 72.

Castelnovo, A., Graziano, B., Ferrarelli, F., and D'Agostino, A. (2018). Sleep spindles and slow waves in schizophrenia and related disorders: Main findings, challenges and future perspectives. Eur. J. Neurosci.

Castets, M., Schaeffer, C., Bechara, E., Schenck, A., Khandjian, E.W., Luche, S., Moine, H., Rabilloud, T., Mandel, J.-L., and Bardoni, B. (2005). FMRP interferes with the Rac1 pathway and controls actin cytoskeleton dynamics in murine fibroblasts. Hum. Mol. Genet. *14*, 835–844.

Catanese, J., Carmichael, J.E., and van der Meer, M.A.A. (2016). Low- and high-gamma oscillations deviate in opposite directions from zero-phase synchrony in the limbic corticostriatal loop. J. Neurophysiol. *116*, 5–17.

Catts, V.S., Lai, Y.L., Weickert, C.S., Weickert, T.W., and Catts, S. V (2016). A quantitative review of the postmortem evidence for decreased cortical N-methyl-D-aspartate receptor expression levels in schizophrenia: How can we link molecular abnormalities to mismatch negativity deficits? Biol. Psychol. *116*, 57–67.

Chai, J.-H., Locke, D.P., Greally, J.M., Knoll, J.H.M., Ohta, T., Dunai, J., Yavor, A., Eichler, E.E., and Nicholls, R.D. (2003). Identification of four highly conserved genes between breakpoint hotspots BP1 and BP2 of the Prader-Willi/Angelman syndromes deletion region that have undergone evolutionary transposition mediated by flanking duplicons. Am. J. Hum. Genet. *73*, 898–925.

Chan, M.S., Chung, K.F., Yung, K.P., and Yeung, W.F. (2017). Sleep in schizophrenia: A systematic review and meta-analysis of polysomnographic findings in case-control studies. Sleep Med. Rev. *32*, 69–84.

Chang, J.Y., Chen, L., Luo, F., Shi, L.H., and Woodward, D.J. (2002). Neuronal responses in the frontal cortico-basal ganglia system during delayed matching-to-sample task: Ensemble recording in freely moving rats. Exp. Brain Res. *142*, 67–80.

Chao, O.Y., Huston, J.P., Li, J.-S., Wang, A.-L., and de Souza Silva, M.A. (2016). The medial prefrontal cortex-lateral entorhinal cortex circuit is essential for episodic-like memory and associative object-recognition. Hippocampus *26*, 633–645.

Chaste, P., Klei, L., Sanders, S.J.S., Hus, V., Murtha, M.T., Lowe, J.K., Willsey, A.J., Moreno-De-Luca, D., Yu, T.W., Fombonne, E., et al. (2015). A Genome-wide Association Study of Autism Using the Simons Simplex Collection: Does Reducing Phenotypic Heterogeneity in Autism Increase Genetic Homogeneity? Biol. Psychiatry *77*, 775–784.

Chen, X., Shu, S., and Bayliss, D.A. (2009). HCN1 Channel Subunits Are a

Molecular Substrate for Hypnotic Actions of Ketamine. J. Neurosci. *29*, 600–609.

Chen, Z., Resnik, E., McFarland, J.M., Sakmann, B., and Mehta, M.R. (2011). Speed Controls the Amplitude and Timing of the Hippocampal Gamma Rhythm. PLoS One *6*, e21408.

Chouinard, S., Poulin, J., Stip, E., and Godbout, R. (2004). Sleep in untreated patients with schizophrenia: a meta-analysis. Schizophr. Bull. *30*, 957–967.

Chowdhury, S., Shepherd, J.D., Okuno, H., Lyford, G., Petralia, R.S., Plath, N., Kuhl, D., Huganir, R.L., and Worley, P.F. (2006). Arc/Arg3.1 interacts with the endocytic machinery to regulate AMPA receptor trafficking. Neuron *52*, 445–459.

Chrobak, J.J., and Buzsáki, G. (1996). High-frequency oscillations in the output networks of the hippocampal-entorhinal axis of the freely behaving rat. J. Neurosci. *16*, 3056–3066.

Chung, L., Wang, X., Zhu, L., Towers, A., Kim, I.H., and Jiang, Y.-H. (2015). Parental origin impairment of synaptic functions and behaviors in cytoplasmic FMRP interacting protein 1 (Cyfip1) deficiency mice. Brain Res. *1629*, 340–350.

Churchwell, J.C., and Kesner, R.P. (2011). Hippocampal-prefrontal dynamics in spatial working memory: interactions and independent parallel processing. Behav. Brain Res. *225*, 389–395.

Cingolani, L.A., and Goda, Y. (2008). Actin in action: the interplay between the actin cytoskeleton and synaptic efficacy. Nat. Rev. Neurosci. *9*, 344–356.

Cirelli, C., and Tononi, G. (2008). Is Sleep Essential? PLoS Biol. *6*, e216.

Clemens, Z., Molle, M., Eross, L., Barsi, P., Halasz, P., and Born, J. (2007). Temporal coupling of parahippocampal ripples, sleep spindles and slow oscillations in humans. Brain *130*, 2868–2878.

Clinton, S.M., Sucharski, I.L., and Finlay, J.M. (2006). Desipramine attenuates working memory impairments induced by partial loss of catecholamines in the rat medial prefrontal cortex. Psychopharmacology (Berl). *183*, 404–412.

Coffee, B., Zhang, F., Warren, S.T., and Reines, D. (1999). Acetylated histones are associated with FMR1 in normal but not fragile X-syndrome cells. Nat. Genet. *22*,

98–101.

Cohen, M.X., Elger, C.E., and Fell, J. (2009a). Oscillatory activity and phase-amplitude coupling in the human medial frontal cortex during decision making. J. Cogn. Neurosci. *21*, 390–402.

Cohen, M.X., Axmacher, N., Lenartz, D., Elger, C.E., Sturm, V., and Schlaepfer, T.E. (2009b). Good vibrations: cross-frequency coupling in the human nucleus accumbens during reward processing. J. Cogn. Neurosci. *21*, 875–889.

Cohen, S.M., Tsien, R.W., Goff, D.C., and Halassa, M.M. (2015). The impact of NMDA receptor hypofunction on GABAergic neurons in the pathophysiology of schizophrenia. Schizophr. Res. *167*, 98–107.

Cohrs, S. (2008). Sleep disturbances in patients with schizophrenia : impact and effect of antipsychotics. CNS Drugs *22*, 939–962.

Colgin, L.L. (2011). Oscillations and hippocampal-prefrontal synchrony. Curr. Opin. Neurobiol. *21*, 467–474.

Colgin, L.L. (2015). Theta-gamma coupling in the entorhinal-hippocampal system. Curr. Opin. Neurobiol. *31*, 45–50.

Colgin, L.L., Denninger, T., Fyhn, M., Hafting, T., Bonnevie, T., Jensen, O., Moser, M.-B., and Moser, E.I. (2009). Frequency of gamma oscillations routes flow of information in the hippocampus. Nature *462*, 353–357.

Contractor, A., Klyachko, V.A., and Portera-Cailliau, C. (2015). Altered Neuronal and Circuit Excitability in Fragile X Syndrome. Neuron *87*, 699–715.

Contreras, D., and Steriade, M. (1995). Cellular basis of EEG slow rhythms: a study of dynamic corticothalamic relationships. J. Neurosci. *15*, 604–622.

Contreras, D., and Steriade, M. (1996). Spindle oscillation in cats: the role of corticothalamic feedback in a thalamically generated rhythm. J. Physiol. *490*, 159–179.

Cooper, S., Robison, A.J., and Mazei-Robison, M.S. (2017). Reward Circuitry in Addiction. Neurotherapeutics *14*, 687–697.

Corbit, L.H., and Balleine, B.W. (2011). The general and outcome-specific forms of Pavlovian-instrumental transfer are differentially mediated by the nucleus accumbens core and shell. J. Neurosci. *31*, 11786–11794.

Cordon, I., Nicolás, M.J., Arrieta, S., Lopetegui, E., López-Azcárate, J., Alegre, M., Artieda, J., and Valencia, M. (2015). Coupling in the cortico-basal ganglia circuit is aberrant in the ketamine model of schizophrenia. Eur. Neuropsychopharmacol. *25*, 1375–1387.

Cortesi, F., Giannotti, F., Ivanenko, A., and Johnson, K. (2010). Sleep in children with autistic spectrum disorder. Sleep Med. *11*, 659–664.

Cousijn, H., Tunbridge, E.M., Rolinski, M., Wallis, G., Colclough, G.L., Woolrich, M.W., Nobre, A.C., and Harrison, P.J. (2015). Modulation of hippocampal theta and hippocampal-prefrontal cortex function by a schizophrenia risk gene. Hum. Brain Mapp. *36*, 2387–2395.

Cox, D., and Butler, M. (2015). The 15q11.2 BP1–BP2 Microdeletion Syndrome: A Review. Int. J. Mol. Sci. *16*, 4068–4082.

Crawford, D.C., Acuña, J.M., and Sherman, S.L. (2001). FMR1 and the fragile X syndrome: Human genome epidemiology review. Genet. Med. *3*, 359–371.

Cross-Disorder Group of the Psychiatric Genomics Consortium (2013). Identification of risk loci with shared effects on five major psychiatric disorders: a genome-wide analysis. Lancet *381*, 1371–1379.

Crunelli, V., and Hughes, S.W. (2010). The slow (1 Hz) rhythm of non-REM sleep: A dialogue between three cardinal oscillators. Nat. Neurosci. *13*, 9–17.

Csicsvari, J., Hirase, H., Mamiya, A., and Buzsáki, G. (2000). Ensemble patterns of hippocampal CA3-CA1 neurons during sharp wave-associated population events. Neuron *28*, 585–594.

Culbreth, A.J., Westbrook, A., Xu, Z., Barch, D.M., and Waltz, J.A. (2016). Intact Ventral Striatal Prediction Error Signaling in Medicated Schizophrenia Patients. Biol. Psychiatry Cogn. Neurosci. Neuroimaging *1*, 474–483.

Czerniawski, J., Yoon, T., and Otto, T. (2009). Dissociating space and trace in dorsal and ventral hippocampus. Hippocampus *19*, 20–32.

D'Agostino, A., Castelnovo, A., Cavallotti, S., Casetta, C., Marcatili, M., Gambini, O., Canevini, M., Tononi, G., Riedner, B., Ferrarelli, F., et al. (2018). Sleep endophenotypes of schizophrenia: slow waves and sleep spindles in unaffected first-degree relatives. Npj Schizophr. *4*, 2.

Dalley, J.W., Cardinal, R.N., and Robbins, T.W. (2004). Prefrontal executive and cognitive functions in rodents: neural and neurochemical substrates. Neurosci. Biobehav. Rev. *28*, 771–784.

Dalley, J.W., Everitt, B.J., and Robbins, T.W. (2011). Impulsivity, compulsivity, and top-down cognitive control. Neuron *69*, 680–694.

Darnell, J.C., and Klann, E. (2013). The translation of translational control by FMRP: therapeutic targets for FXS. Nat. Neurosci. *16*, 1530–1536.

Darnell, J.C., Van Driesche, S.J., Zhang, C., Hung, K.Y.S., Mele, A., Fraser, C.E., Stone, E.F., Chen, C., Fak, J.J., Chi, S.W., et al. (2011). FMRP Stalls Ribosomal Translocation on mRNAs Linked to Synaptic Function and Autism. Cell *146*, 247–261.

Davis, B.A., and Isles, A.R. (2014). Modelling the genetic contribution to mental illness: a timely end for the psychiatric rodent? Eur. J. Neurosci. *39*, 1933–1942.

Dejean, C., Sitko, M., Girardeau, P., Bennabi, A., Caillé, S., Cador, M., Boraud, T., and Le Moine, C. (2017). Memories of Opiate Withdrawal Emotional States Correlate with Specific Gamma Oscillations in the Nucleus Accumbens. Neuropsychopharmacology *42*, 1157–1168.

Demanuele, C., Bartsch, U., Baran, B., Khan, S., Vangel, M.G., Cox, R., Hämäläinen, M., Jones, M.W., Stickgold, R., and Manoach, D.S. (2017). Coordination of Slow Waves With Sleep Spindles Predicts Sleep-Dependent Memory Consolidation in Schizophrenia. Sleep *40*.

DeRubeis, S., Pasciuto, E., Li, K.W., Fernández, E., DiMarino, D., Buzzi, A., Ostroff, L.E., Klann, E., Zwartkruis, F.J.T., Komiyama, N.H., et al. (2013). CYFIP1 coordinates mRNA translation and cytoskeleton remodeling to ensure proper dendritic Spine formation. Neuron *79*, 1169–1182.

Deserno, L., Schlagenhauf, F., and Heinz, A. (2016). Striatal dopamine, reward, and decision making in schizophrenia. Dialogues Clin. Neurosci. *18*, 77–89.

Dias, R., and Aggleton, J.P. (2000). Effects of selective excitotoxic prefrontal lesions on acquisition of nonmatching- and matching-to-place in the T-maze in the rat: Differential involvement of the prelimbic-infralimbic and anterior cingulate cortices in providing behavioural flexibility. Eur. J. Neurosci. *12*, 4457–4466.

Dickerson, D., Wolff, A.R., and Bilkey, D.K. (2010). Abnormal long-range neural synchrony in a maternal immune activation animal model of schizophrenia. J. Neurosci. *30*, 12424–12431.

Didriksen, M., Fejgin, K., Nilsson, S.R.O., Birknow, M.R., Grayton, H.M., Larsen, P.H., Lauridsen, J.B., Nielsen, V., Celada, P., Santana, N., et al. (2017). Persistent gating deficit and increased sensitivity to NMDA receptor antagonism after puberty in a new mouse model of the human 22q11.2 microdeletion syndrome: a study in male mice. J. Psychiatry Neurosci. *42*, 48–58.

Dölen, G. (2015). Autism: Oxytocin, serotonin, and social reward. Soc. Neurosci. *10*, 450–465.

Dölen, G., Osterweil, E., Rao, B.S.S., Smith, G.B., Auerbach, B.D., Chattarji, S., and Bear, M.F. (2007). Correction of Fragile X Syndrome in Mice. Neuron *56*, 955–962.

Dolleman-Van Der Weel, M.J., and Witter, M.P. (1996). Projections from the nucleus reuniens thalami to the entorhinal cortex, hippocampal field CA1, and the subiculum in the rat arise from different populations of neurons. J. Comp. Neurol. *364*, 637–650.

Domino, E.F. (1964). Neurobiology of Phencyclidine (Sernyl), A Drug With An Unusual Spectrum of Pharmacological Activity. Int. Rev. Neurobiol. *6*, 303–347.

Donnelly, N.A., Holtzman, T., Rich, P.D., Nevado-Holgado, A.J., Fernando, A.B.P., Van Dijck, G., Holzhammer, T., Paul, O., Ruther, P., Paulsen, O., et al. (2014). Oscillatory activity in the medial prefrontal cortex and nucleus accumbens correlates with impulsivity and reward outcome. PLoS One *9*, e111300.

Doornbos, M., Sikkema-Raddatz, B., Ruijvenkamp, C.A.L., Dijkhuizen, T., Bijlsma, E.K., Gijsbers, A.C.J., Hilhorst-Hofstee, Y., Hordijk, R., Verbruggen, K.T., Kerstjens-Frederikse, W.S.S. (Mieke., et al. (2009). Nine patients with a microdeletion 15q11.2 between breakpoints 1 and 2 of the Prader-Willi critical region, possibly associated with behavioural disturbances. Eur. J. Med. Genet. *52*, 108–115.

Dowd, E.C., and Barch, D.M. (2010). Anhedonia and Emotional Experience in Schizophrenia: Neural and Behavioral Indicators. Biol. Psychiatry *67*, 902–911.

Dudchenko, P.A. (2001). How do animals actually solve the T maze? Behav. Neurosci. *115*, 850–860.

Düzel, E., Penny, W.D., and Burgess, N. (2010). Brain oscillations and memory. Curr. Opin. Neurobiol. *20*, 143–149.

Dzirasa, K., Ramsey, A.J., Takahashi, D.Y., Stapleton, J., Potes, J.M., Williams, J.K., Gainetdinov, R.R., Sameshima, K., Caron, M.G., and Nicolelis, M.A.L. (2009). Hyperdopaminergia and NMDA receptor hypofunction disrupt neural phase signaling. J. Neurosci. *29*, 8215–8224.

Eacott, M.J., and Norman, G. (2004). Integrated memory for object, place, and context in rats: a possible model of episodic-like memory? J. Neurosci. *24*, 1948–1953.

Ego-Stengel, V., and Wilson, M.A. (2010). Disruption of ripple-associated hippocampal activity during rest impairs spatial learning in the rat. Hippocampus *20*, 1–10.

Eichenbaum, H. (2004). Hippocampus: cognitive processes and neural representations that underlie declarative memory. Neuron *44*, 109–120.

Eichenbaum, H. (2017). Prefrontal-hippocampal interactions in episodic memory. Nat. Rev. Neurosci. *18*, 547–558.

Eichenbaum, H., and Cohen, N.J. (2014). Can We Reconcile the Declarative Memory and Spatial Navigation Views on Hippocampal Function? Neuron *83*, 764–770.

Eichenbaum, H., Kuperstein, M., Fagan, A., and Nagode, J. (1987). Cue-sampling and goal-approach correlates of hippocampal unit activity in rats performing an odor-discrimination task. J. Neurosci. *7*, 716–732.

Eichenbaum, H., Dudchenko, P., Wood, E., Shapiro, M., and Tanila, H. (1999). The hippocampus, memory, and place cells: is it spatial memory or a memory space? Neuron *23*, 209–226.

Elert-Dobkowska, E., Stepniak, I., Rajkiewicz, M., Krysa, W., Rakowicz, M., Hoffman-Zacharska, D., Lipczynska-Lojkowska, W., Zaremba, J., and Sulek, A. (2014). Familial 15q11.2 Micro deletions are not Fully Penetrant in Two Cases with Hereditary Spastic Paraplegia and Dysmorphic Features. J. Genet. Syndr. Gene Ther. *5*.

Elia, M., Ferri, R., Musumeci, S.A., Del Gracco, S., Bottitta, M., Scuderi, C., Miano, G., Panerai, S., Bertrand, T., and Grubar, J.C. (2000). Sleep in subjects with autistic disorder: a neurophysiological and psychological study. Brain Dev. *22*, 88–92.

Engel, A.K., and Fries, P. (2010). Beta-band oscillations — signalling the status quo? Curr. Opin. Neurobiol. *20*, 156–165.

Engel, A.K., and Singer, W. (2001). Temporal binding and the neural correlates of sensory awareness. Trends Cogn. Sci. *5*, 16–25.

van Erp, T.G.M., Hibar, D.P., Rasmussen, J.M., Glahn, D.C., Pearlson, G.D., Andreassen, O.A., Agartz, I., Westlye, L.T., Haukvik, U.K., Dale, A.M., et al. (2016). Subcortical brain volume abnormalities in 2028 individuals with schizophrenia and 2540 healthy controls via the ENIGMA consortium. Mol. Psychiatry *21*, 585.

Esbensen, A.J., and Schwichtenberg, A.J. (2016). Sleep in Neurodevelopmental Disorders. In International Review of Research in Developmental Disabilities, pp. 153–191.

Eschenko, O., Mölle, M., Born, J., and Sara, S.J. (2006). Elevated sleep spindle density after learning or after retrieval in rats. J. Neurosci. *26*, 12914–12920.

Eschenko, O., Ramadan, W., Mölle, M., Born, J., and Sara, S.J. (2008). Sustained increase in hippocampal sharp-wave ripple activity during slow-wave sleep after learning. Learn. Mem. *15*, 222–228.

Esslinger, C., Walter, H., Kirsch, P., Erk, S., Schnell, K., Arnold, C., Haddad, L., Mier, D., Opitz von Boberfeld, C., Raab, K., et al. (2009). Neural mechanisms of a genome-wide supported psychosis variant. Science *324*, 605.

Ethridge, L.E., White, S.P., Mosconi, M.W., Wang, J., Pedapati, E. V., Erickson, C.A., Byerly, M.J., and Sweeney, J.A. (2017). Neural synchronization deficits linked to cortical hyper-excitability and auditory hypersensitivity in fragile X

syndrome. Mol. Autism *8*, 22.

Everitt, B.J., Morris, K.A., O'Brien, A., and Robbins, T.W. (1991). The basolateral amygdala-ventral striatal system and conditioned place preference: Further evidence of limbic-striatal interactions underlying reward-related processes. Neuroscience *42*, 1–18.

Fang, Z., Sergeeva, V., Ray, L.B., Viczko, J., Owen, A.M., and Fogel, S.M. (2017). Sleep Spindles and Intellectual Ability: Epiphenomenon or Directly Related? J. Cogn. Neurosci. *29*, 167–182.

Fanselow, M.S., and Dong, H.-W. (2010). Are the Dorsal and Ventral Hippocampus Functionally Distinct Structures? Neuron *65*, 7–19.

Feigenbaum, J.D., Polkey, C.E., and Morris, R.G. (1996). Deficits in spatial working memory after unilateral temporal lobectomy in man. Neuropsychologia *34*, 163–176.

Fejgin, K., Nielsen, J., Birknow, M.R., Bastlund, J.F., Nielsen, V., Lauridsen, J.B., Stefansson, H., Steinberg, S., Sorensen, H.B.D., Mortensen, T.E., et al. (2014). A mouse model that recapitulates cardinal features of the 15q13.3 microdeletion syndrome including schizophrenia- and epilepsy-related alterations. Biol. Psychiatry *76*, 128–137.

Felix, R., and Levin, E.D. (1997). Nicotinic antagonist administration into the ventral hippocampus and spatial working memory in rats. Neuroscience *81*, 1009–1017.

Fell, J., and Axmacher, N. (2011). The role of phase synchronization in memory processes. Nat. Rev. Neurosci. *12*, 105–118.

Fell, J., Klaver, P., Lehnertz, K., Grunwald, T., Schaller, C., Elger, C.E., and Fernández, G. (2001). Human memory formation is accompanied by rhinal–hippocampal coupling and decoupling. Nat. Neurosci. *4*, 1259–1264.

Ferenczi, E.A., Zalocusky, K.A., Liston, C., Grosenick, L., Warden, M.R., Amatya, D., Katovich, K., Mehta, H., Patenaude, B., Ramakrishnan, C., et al. (2016). Prefrontal cortical regulation of brainwide circuit dynamics and reward-related behavior. Science (80-.). *351*, aac9698-aac9698.

Ferrarelli, F. (2015). Sleep in Patients With Schizophrenia. Curr. Sleep Med.

Reports *1*, 150–156.

Ferrarelli, F., and Tononi, G. (2017). Reduced sleep spindle activity point to a TRN-MD thalamus-PFC circuit dysfunction in schizophrenia. Schizophr. Res. *180*, 36–43.

Ferrarelli, F., Huber, R., Peterson, M.J., Massimini, M., Murphy, M., Riedner, B.A., Watson, A., Bria, P., and Tononi, G. (2007). Reduced sleep spindle activity in schizophrenia patients. Am. J. Psychiatry *164*, 483–492.

Fisher, S.P., Godinho, S.I.H., Pothecary, C.A., Hankins, M.W., Foster, R.G., and Peirson, S.N. (2012). Rapid Assessment of Sleep-Wake Behavior in Mice. J. Biol. Rhythms *27*, 48–58.

Fisher, S.P., Foster, R.G., and Peirson, S.N. (2013). The Circadian Control of Sleep. In Handbook of Experimental Pharmacology, pp. 157–183.

Fletcher, P.C., and Frith, C.D. (2009). Perceiving is believing: a Bayesian approach to explaining the positive symptoms of schizophrenia. Nat. Rev. Neurosci. *10*, 48–58.

Floresco, S.B. (2007). Dopaminergic regulation of limbic-striatal interplay. J. Psychiatry Neurosci. *32*, 400–411.

Floresco, S.B. (2015). The Nucleus Accumbens: An Interface Between Cognition, Emotion, and Action. Annu. Rev. Psychol. *66*, 25–52.

Floresco, S.B., and Phillips, A.G. (1999). Dopamine and hippocampal input to the nucleus accumbens play an essential role in the search for food in an unpredictable environment. Psychobiology *27*, 277–286.

Floresco, S.B., Seamans, J.K., and Phillips, A.G. (1997). Selective roles for hippocampal, prefrontal cortical, and ventral striatal circuits in radial-arm maze tasks with or without a delay. J. Neurosci. *17*, 1880–1890.

Floresco, S.B., Blaha, C.D., Yang, C.R., and Phillips, A.G. (2001a). Modulation of hippocampal and amygdalar-evoked activity of nucleus accumbens neurons by dopamine: cellular mechanisms of input selection. J. Neurosci. *21*, 2851–2860.

Floresco, S.B., Todd, C.L., and Grace, A.A. (2001b). Glutamatergic afferents from

the hippocampus to the nucleus accumbens regulate activity of ventral tegmental area dopamine neurons. J. Neurosci. *21*, 4915–4922.

Floresco, S.B., Ghods-Sharifi, S., Vexelman, C., and Magyar, O. (2006). Dissociable Roles for the Nucleus Accumbens Core and Shell in Regulating Set Shifting. J. Neurosci. *26*, 2449–2457.

Floresco, S.B., Block, A.E., and Tse, M.T.L. (2008). Inactivation of the medial prefrontal cortex of the rat impairs strategy set-shifting, but not reversal learning, using a novel, automated procedure. Behav. Brain Res. *190*, 85–96.

Floresco, S.B., Zhang, Y., and Enomoto, T. (2009). Neural circuits subserving behavioral flexibility and their relevance to schizophrenia. Behav. Brain Res. *204*, 396–409.

Fogel, S.M., and Smith, C.T. (2006). Learning-dependent changes in sleep spindles and Stage 2 sleep. J. Sleep Res. *15*, 250–255.

Fogel, S.M., and Smith, C.T. (2011). The function of the sleep spindle: A physiological index of intelligence and a mechanism for sleep-dependent memory consolidation. Neurosci. Biobehav. Rev. *35*, 1154–1165.

Forest, G., Poulin, J., Daoust, A.-M., Lussier, I., Stip, E., and Godbout, R. (2007). Attention and non-REM sleep in neuroleptic-naive persons with schizophrenia and control participants. Psychiatry Res. *149*, 33–40.

Forsingdal, A., Fejgin, K., Nielsen, V., Werge, T., and Nielsen, J. (2016). 15q13.3 homozygous knockout mouse model display epilepsy-, autism- and schizophrenia-related phenotypes. Transl. Psychiatry *6*, e860–e860.

Foss-Feig, J.H., Adkinson, B.D., Ji, J.L., Yang, G., Srihari, V.H., McPartland, J.C., Krystal, J.H., Murray, J.D., and Anticevic, A. (2017). Searching for Cross-Diagnostic Convergence: Neural Mechanisms Governing Excitation and Inhibition Balance in Schizophrenia and Autism Spectrum Disorders. Biol. Psychiatry *81*, 848–861.

Fox, M.D., and Raichle, M.E. (2007). Spontaneous fluctuations in brain activity observed with functional magnetic resonance imaging. Nat. Rev. Neurosci. *8*, 700–711.

Frank, L.M., Brown, E.N., and Wilson, M. (2000). Trajectory encoding in the

hippocampus and entorhinal cortex. Neuron *27*, 169–178.

French, S.J., and Totterdell, S. (2003). Individual nucleus accumbens-projection neurons receive both basolateral amygdala and ventral subicular afferents in rats. Neuroscience *119*, 19–31.

Fries, P. (2005). A mechanism for cognitive dynamics: neuronal communication through neuronal coherence. Trends Cogn. Sci. *9*, 474–480.

Fries, P., Nikolić, D., and Singer, W. (2007). The gamma cycle. Trends Neurosci. *30*, 309–316.

Friese, U., Köster, M., Hassler, U., Martens, U., Trujillo-Barreto, N., and Gruber, T. (2013). Successful memory encoding is associated with increased cross-frequency coupling between frontal theta and posterior gamma oscillations in human scalp-recorded EEG. Neuroimage *66*, 642–647.

Friston, K.J., and Frith, C.D. (1995). Schizophrenia: a disconnection syndrome? Clin. Neurosci. *3*, 89–97.

Friston, K., Brown, H.R., Siemerkus, J., and Stephan, K.E. (2016). The dysconnection hypothesis (2016). Schizophr. Res. *176*, 83–94.

Friston, K.J., Bastos, A.M., Pinotsis, D., and Litvak, V. (2015a). LFP and oscillations—what do they tell us? Curr. Opin. Neurobiol. *31*, 1–6.

Friston, K.J., Bastos, A.M., Pinotsis, D., and Litvak, V. (2015b). LFP and oscillations-what do they tell us? Curr. Opin. Neurobiol. *31*, 1–6.

Fromer, M., Pocklington, A.J., Kavanagh, D.H., Williams, H.J., Dwyer, S., Gormley, P., Georgieva, L., Rees, E., Palta, P., Ruderfer, D.M., et al. (2014). De novo mutations in schizophrenia implicate synaptic networks. Nature *506*, 179–184.

Fu, Y.H., Kuhl, D.P., Pizzuti, A., Pieretti, M., Sutcliffe, J.S., Richards, S., Verkerk, A.J., Holden, J.J., Fenwick, R.G., and Warren, S.T. (1991). Variation of the CGG repeat at the fragile X site results in genetic instability: resolution of the Sherman paradox. Cell *67*, 1047–1058.

Fuccillo, M. V. (2016). Striatal Circuits as a Common Node for Autism

Pathophysiology. Front. Neurosci. *10*, 27.

Funahashi, S. (2017). Working Memory in the Prefrontal Cortex. Brain Sci. *7*, 49.

Fuster, J.M., and Alexander, G.E. (1971). Neuron activity related to short-term memory. Science *173*, 652–654.

Gais, S., Mölle, M., Helms, K., and Born, J. (2002). Learning-dependent increases in sleep spindle density. J. Neurosci. *22*, 6830–6834.

Galvez, R., and Greenough, W.T. (2005). Sequence of abnormal dendritic spine development in primary somatosensory cortex of a mouse model of the fragile X mental retardation syndrome. Am. J. Med. Genet. A *135*, 155–160.

Gandal, M.J., Haney, J.R., Parikshak, N.N., Leppa, V., Ramaswami, G., Hartl, C., Schork, A.J., Appadurai, V., Buil, A., Werge, T.M., et al. (2018). Shared molecular neuropathology across major psychiatric disorders parallels polygenic overlap. Science (80-.). *359*, 693–697.

Garber, K.B., Visootsak, J., and Warren, S.T. (2008). Fragile X syndrome. Eur.J Hum.Genet. *16*, 666–672.

Gardner, R.J., Kersanté, F., Jones, M.W., and Bartsch, U. (2014). Neural oscillations during non-rapid eye movement sleep as biomarkers of circuit dysfunction in schizophrenia. Eur. J. Neurosci. *39*, 1091–1106.

Gass, N., Schwarz, A.J., Sartorius, A., Schenker, E., Risterucci, C., Spedding, M., Zheng, L., Meyer-Lindenberg, A., and Weber-Fahr, W. (2014). Sub-Anesthetic Ketamine Modulates Intrinsic BOLD Connectivity Within the Hippocampal-Prefrontal Circuit in the Rat. Neuropsychopharmacology *39*, 895–906.

Gazzaley, A., Rissman, J., and D'Esposito, M. (2004). Functional connectivity during working memory maintenance. Cogn. Affect. Behav. Neurosci. *4*, 580–599.

Geng, H.-Y., Zhang, J., Yang, J.-M., Li, Y., Wang, N., Ye, M., Chen, X.-J., Lian, H., and Li, X.-M. (2017). *Erbb4* Deletion from Medium Spiny Neurons of the Nucleus Accumbens Core Induces Schizophrenia-Like Behaviors via Elevated GABA $_{A}$ Receptor α1 Subunit Expression. J. Neurosci. *37*, 7450–7464.

De Gennaro, L., Ferrara, M., Vecchio, F., Curcio, G., and Bertini, M. (2005). An

electroencephalographic fingerprint of human sleep. Neuroimage *26*, 114–122.

Genovese, G., Fromer, M., Stahl, E.A., Ruderfer, D.M., Chambert, K., Landén, M., Moran, J.L., Purcell, S.M., Sklar, P., Sullivan, P.F., et al. (2016). Increased burden of ultra-rare protein-altering variants among 4,877 individuals with schizophrenia. Nat. Neurosci. *19*, 1433–1441.

Genzel, L., and Robertson, E.M. (2015). To Replay, Perchance to Consolidate. PLoS Biol. *13*, e1002285.

Gerber, D.J., Hall, D., Miyakawa, T., Demars, S., Gogos, J.A., Karayiorgou, M., and Tonegawa, S. (2003). Evidence for association of schizophrenia with genetic variation in the 8p21.3 gene, PPP3CC, encoding the calcineurin gamma subunit. Proc. Natl. Acad. Sci. U. S. A. *100*, 8993–8998.

Giavarina, D. (2015). Understanding Bland Altman analysis. Biochem. Medica *25*, 141–151.

Gibson, J.R., Bartley, A.F., Hays, S.A., and Huber, K.M. (2008). Imbalance of Neocortical Excitation and Inhibition and Altered UP States Reflect Network Hyperexcitability in the Mouse Model of Fragile X Syndrome. J. Neurophysiol. *100*, 2615–2626.

Gilmour, G., Dix, S., Fellini, L., Gastambide, F., Plath, N., Steckler, T., Talpos, J., and Tricklebank, M. (2012). NMDA receptors, cognition and schizophrenia – Testing the validity of the NMDA receptor hypofunction hypothesis. Neuropharmacology *62*, 1401–1412.

Girardeau, G., Benchenane, K., Wiener, S.I., Buzsáki, G., and Zugaro, M.B. (2009). Selective suppression of hippocampal ripples impairs spatial memory. Nat. Neurosci. *12*, 1222–1223.

Girirajan, S., Rosenfeld, J.A., Coe, B.P., Parikh, S., Friedman, N., Goldstein, A., Filipink, R.A., McConnell, J.S., Angle, B., Meschino, W.S., et al. (2012). Phenotypic Heterogeneity of Genomic Disorders and Rare Copy-Number Variants.

Goda, S.A., Olszewski, M., Piasecka, J., Rejniak, K., Whittington, M.A., Kasicki, S., and Hunt, M.J. (2015). Aberrant high frequency oscillations recorded in the rat nucleus accumbens in the methylazoxymethanol acetate neurodevelopmental model of schizophrenia. Prog. Neuro-Psychopharmacology Biol. Psychiatry *61*, 44–51.

Göder, R., Graf, A., Ballhausen, F., Weinhold, S., Baier, P.C., Junghanns, K., and Prehn-Kristensen, A. (2015). Impairment of sleep-related memory consolidation in schizophrenia: relevance of sleep spindles? Sleep Med. *16*, 564–569.

Godler, D.E., Tassone, F., Loesch, D.Z., Taylor, A.K., Gehling, F., Hagerman, R.J., Burgess, T., Ganesamoorthy, D., Hennerich, D., Gordon, L., et al. (2010). Methylation of novel markers of fragile X alleles is inversely correlated with FMRP expression and FMR1 activation ratio. Hum. Mol. Genet. *19*, 1618–1632.

Godsil, B.P., Kiss, J.P., Spedding, M., and Jay, T.M. (2013). The hippocampal–prefrontal pathway: The weak link in psychiatric disorders? Eur. Neuropsychopharmacol. *23*, 1165–1181.

Gold, J.M., Waltz, J.A., Prentice, K.J., Morris, S.E., and Heerey, E.A. (2008). Reward Processing in Schizophrenia: A Deficit in the Representation of Value. Schizophr. Bull. *34*, 835–847.

Golden, C.E., Buxbaum, J.D., and De Rubeis, S. (2018). Disrupted circuits in mouse models of autism spectrum disorder and intellectual disability. Curr. Opin. Neurobiol. *48*, 106–112.

Goldman-Rakic, P.S. (1995). Cellular basis of working memory. Neuron *14*, 477–485.

Gonçalves, B.S.B., Adamowicz, T., Louzada, F.M., Moreno, C.R., and Araujo, J.F. (2015). A fresh look at the use of nonparametric analysis in actimetry. Sleep Med. Rev. *20*, 84–91.

Gonçalves, J.T., Anstey, J.E., Golshani, P., and Portera-Cailliau, C. (2013). Circuit level defects in the developing neocortex of Fragile X mice. Nat. Neurosci. *16*, 903–909.

Gonzalez-Burgos, G., Cho, R.Y., and Lewis, D.A. (2015). Alterations in Cortical Network Oscillations and Parvalbumin Neurons in Schizophrenia. Biol. Psychiatry *77*, 1031–1040.

Goonawardena, A. V, Heiss, J., Glavis-Bloom, C., Trube, G., Borroni, E., Alberati, D., and Wallace, T.L. (2016). Alterations in High-Frequency Neuronal Oscillations in a Cynomolgus Macaque Test of Sustained Attention Following NMDA Receptor Antagonism. Neuropsychopharmacology *41*, 1319–1328.

Gordon, J.A. (2011). Oscillations and hippocampal–prefrontal synchrony. Curr. Opin. Neurobiol. *21*, 486–491.

Goto, Y., and Grace, A.A. (2005). Dopamine-dependent interactions between limbic and prefrontal cortical plasticity in the nucleus accumbens: Disruption by cocaine sensitization. Neuron *47*, 255–266.

Goto, Y., and Grace, A.A. (2008). Limbic and cortical information processing in the nucleus accumbens. Trends Neurosci. *31*, 552–558.

Goto, Y., and O'Donnell, P. (2001). Synchronous activity in the hippocampus and nucleus accumbens in vivo. J. Neurosci. *21*, RC131.

Gottesman, I.I. (1991). Schizophrenia genesis: The origins of madness (New York, NY, US: W H Freeman/Times Books/ Henry Holt & Co.).

Gould, E.L., Loesch, D.Z., Martin, M.J., Hagerman, R.J., Armstrong, S.M., and Huggins, R.M. (2000). Melatonin profiles and sleep characteristics in boys with fragile X syndrome: a preliminary study. Am. J. Med. Genet. *95*, 307–315.

Goytain, A., Hines, R.M., El-Husseini, A., and Quamme, G.A. (2007). NIPA1(SPG6), the basis for autosomal dominant form of hereditary spastic paraplegia, encodes a functional Mg2+ transporter. J. Biol. Chem. *282*, 8060–8068.

Grace, A.A. (2000). Gating of information flow within the limbic system and the pathophysiology of schizophrenia. Brain Res. Brain Res. Rev. *31*, 330–341.

Grace, A.A. (2016). Dysregulation of the dopamine system in the pathophysiology of schizophrenia and depression. Nat. Rev. Neurosci. *17*, 524–532.

Grady, C.L., McIntosh, A.R., and Craik, F.I.M. (2003). Age-related differences in the functional connectivity of the hippocampus during memory encoding. Hippocampus *13*, 572–586.

Granon, S., Vidal, C., Thinus-Blanc, C., Changeux, J.P., and Poucet, B. (1994). Working memory, response selection, and effortful processing in rats with medial prefrontal lesions. Behav. Neurosci. *108*, 883–891.

Gratten, J. (2016). Rare variants are common in schizophrenia. Nat. Neurosci. *19*, 1426–1428.

Green, M.F., Kern, R.S., Braff, D.L., and Mintz, J. (2000). Neurocognitive deficits and functional outcome in schizophrenia: Are we measuring the "right stuff"? Schizophr. Bull. *26*, 119–136.

Gregoriou, G.G., Gotts, S.J., Zhou, H., and Desimone, R. (2009). High-Frequency, long-range coupling between prefrontal and visual cortex during attention. Science (80-.). *324*, 1207–1210.

Greicius, M.D., Boyett-Anderson, J.M., Menon, V., and Reiss, A.L. (2004). Reduced basal forebrain and hippocampal activation during memory encoding in girls with fragile X syndrome. Neuroreport *15*, 1579–1583.

Grey, W.W. (1963). The living brain.

Griffin, A.L. (2015). Role of the thalamic nucleus reuniens in mediating interactions between the hippocampus and medial prefrontal cortex during spatial working memory. Front. Syst. Neurosci. *9*, 29.

Griffin, A.L., and Berry, S.D. (2004). Inactivation of the Anterior Cingulate Cortex Impairs Extinction of Rabbit Jaw Movement Conditioning and Prevents Extinction-Related Inhibition of Hippocampal Activity. Learn. Mem. *11*, 604–610.

Griffin, A.L., Owens, C.B., Peters, G.J., Adelman, P.C., and Cline, K.M. (2012). Spatial representations in dorsal hippocampal neurons during a tactile-visual conditional discrimination task. Hippocampus *22*, 299–308.

Grimm, O., Heinz, A., Walter, H., Kirsch, P., Erk, S., Haddad, L., Plichta, M.M., Romanczuk-Seiferth, N., Pöhland, L., Mohnke, S., et al. (2014). Striatal Response to Reward Anticipation. JAMA Psychiatry *71*, 531.

Groenewegen, H.J., Vermeulen-Van der Zee, E., te Kortschot, A., and Witter, M.P. (1987). Organization of the projections from the subiculum to the ventral striatum in the rat. A study using anterograde transport of Phaseolus vulgaris leucoagglutinin. Neuroscience *23*, 103–120.

Groenewegen, H.J., Berendse, H.W., and Haber, S.N. (1993). Organization of the output of the ventral striatopallidal system in the rat: ventral pallidal efferents. Neuroscience *57*, 113–142.

Groenewegen, H.J., Mulder, A.B., Beijer, A.V.J., Wright, C.I., Silva, F.H.L. Da, and Pennartz, C.M. a. (1999). Hippocampal and amygdaloid interactions in the

nucleus accumbens. Psychobiology *27*, 149–164.

Gross, B.A., Walsh, C.M., Turakhia, A.A., Booth, V., Mashour, G.A., and Poe, G.R. (2009). Open-source logic-based automated sleep scoring software using electrophysiological recordings in rats. J. Neurosci. Methods *184*, 10–18.

Gruber, R., and Wise, M.S. (2016). Sleep Spindle Characteristics in Children with Neurodevelopmental Disorders and Their Relation to Cognition. Neural Plast. *2016*, 1–27.

Gruber, A.J., Hussain, R.J., and O'Donnell, P. (2009). The nucleus accumbens: A switchboard for goal-directed behaviors. PLoS One *4*, e5062.

Grunze, H.C., Rainnie, D.G., Hasselmo, M.E., Barkai, E., Hearn, E.F., McCarley, R.W., and Greene, R.W. (1996). NMDA-dependent modulation of CA1 local circuit inhibition. J. Neurosci. *16*, 2034–2043.

Guazzelli, M., Feinberg, I., Aminoff, M., Fein, G., Floyd, T.C., and Maggini, C. (1986). Sleep spindles in normal elderly: comparison with young adult patterns and relation to nocturnal awakening, cognitive function and brain atrophy. Electroencephalogr. Clin. Neurophysiol. *63*, 526–539.

Haenschel, C., and Linden, D. (2011). Exploring intermediate phenotypes with EEG: working memory dysfunction in schizophrenia. Behav Brain Res *216*, 481–495.

Haenschel, C., Bittner, R.A., Waltz, J., Haertling, F., Wibral, M., Singer, W., Linden, D.E.J., and Rodriguez, E. (2009). Cortical oscillatory activity is critical for working memory as revealed by deficits in early-onset schizophrenia. J. Neurosci. *29*, 9481–9489.

Hakami, T., Jones, N.C., Tolmacheva, E.A., Gaudias, J., Chaumont, J., Salzberg, M., O'Brien, T.J., and Pinault, D. (2009). NMDA receptor hypofunction leads to generalized and persistent aberrant γ oscillations independent of hyperlocomotion and the state of consciousness. PLoS One *4*.

Hall, R.C.W. (1995). Global Assessment of Functioning. Psychosomatics *36*, 267–275.

Hall, J., Trent, S., Thomas, K.L., O'Donovan, M.C., and Owen, M.J. (2015). Genetic risk for schizophrenia: Convergence on synaptic pathways involved in

plasticity. Biol. Psychiatry *77*, 52–58.

Hall, S.S., Jiang, H., Reiss, A.L., and Greicius, M.D. (2013). Identifying Large-Scale Brain Networks in Fragile X Syndrome. JAMA Psychiatry *70*, 1215.

Hallock, H.L., and Griffin, A.L. (2013). Dynamic coding of dorsal hippocampal neurons between tasks that differ in structure and memory demand. Hippocampus *23*, 169–186.

Hallock, H.L., Wang, A., and Griffin, A.L. (2016). Ventral Midline Thalamus Is Critical for Hippocampal-Prefrontal Synchrony and Spatial Working Memory. J. Neurosci. *36*, 8372–8389.

Hampson, R.E., Heyser, C.J., and Deadwyler, S.A. (1993). Hippocampal cell firing correlates of delayed-match-to-sample performance in the rat. Behav. Neurosci. *107*, 715–739.

Hamra, F.K. (2010). Gene targeting: Enter the rat. Nature *467*, 161–163.

Hao, Y., Yan, Q., Liu, H., Xu, L., Xue, Z., Song, X., Kaneko, Y., Jiang, T., Liu, Z., and Shan, B. (2009). Schizophrenia patients and their healthy siblings share disruption of white matter integrity in the left prefrontal cortex and the hippocampus but not the anterior cingulate cortex. Schizophr. Res. *114*, 128–135.

Harris, A.Z., and Gordon, J.A. (2015). Long-Range Neural Synchrony in Behavior. Annu. Rev. Neurosci. *38*, 171–194.

Hartung, H., Cichon, N., De Feo, V., Riemann, S., Schildt, S., Lindemann, C., Mulert, C., Gogos, J.A., and Hanganu-Opatz, I.L. (2016). From Shortage to Surge: A Developmental Switch in Hippocampal–Prefrontal Coupling in a Gene–Environment Model of Neuropsychiatric Disorders. Cereb. Cortex *26*, 4265–4281.

Harvey, P.-O., Pruessner, J., Czechowska, Y., and Lepage, M. (2007). Individual differences in trait anhedonia: a structural and functional magnetic resonance imaging study in non-clinical subjects. Mol. Psychiatry *12*, 767–775.

Hays, S.A., Huber, K.M., and Gibson, J.R. (2011). Altered neocortical rhythmic activity states in Fmr1 KO mice are due to enhanced mGluR5 signaling and involve changes in excitatory circuitry. J. Neurosci. *31*, 14223–14234.

He, C.X., and Portera-Cailliau, C. (2013). The trouble with spines in fragile X syndrome: density, maturity and plasticity. Neuroscience *251*, 120–128.

Heckenast, J.R., Wilkinson, L.S., and Jones, M.W. (2015). Decoding Advances in Psychiatric Genetics: A Focus on Neural Circuits in Rodent Models. In Advances in Genetics, pp. 75–106.

Heidbreder, C.A., and Groenewegen, H.J. (2003). The medial prefrontal cortex in the rat: evidence for a dorso-ventral distinction based upon functional and anatomical characteristics. Neurosci. Biobehav. Rev. *27*, 555–579.

Hiatt, J.F., Floyd, T.C., Katz, P.H., and Feinberg, I. (1985). Further evidence of abnormal non-rapid-eye-movement sleep in schizophrenia. Arch. Gen. Psychiatry *42*, 797–802.

Hietala, J., Syvälahti, E., Vuorio, K., Räkköläinen, V., Bergman, J., Haaparanta, M., Solin, O., Kuoppamäki, M., Kirvelä, O., and Ruotsalainen, U. (1995). Presynaptic dopamine function in striatum of neuroleptic-naive schizophrenic patients. Lancet (London, England) *346*, 1130–1131.

Hill, D.F., Parent, K.L., Atcherley, C.W., Cowen, S.L., and Heien, M.L. (2017). Differential release of dopamine in the nucleus accumbens evoked by low-versus high-frequency medial prefrontal cortex stimulation. Brain Stimul. *11*, 426–434.

Hirano, S., Nakhnikian, A., Hirano, Y., Oribe, N., Kanba, S., Onitsuka, T., Levin, M., and Spencer, K.M. (2018). Phase-Amplitude Coupling of the Electroencephalogram in the Auditory Cortex in Schizophrenia. Biol. Psychiatry Cogn. Neurosci. Neuroimaging *3*, 69–76.

Hoeft, F., Hernandez, A., Parthasarathy, S., Watson, C.L., Hall, S.S., and Reiss, A.L. (2007). Fronto-striatal dysfunction and potential compensatory mechanisms in male adolescents with fragile X syndrome. Hum. Brain Mapp. *28*, 543–554.

Hofstetter, J.R., Lysaker, P.H., and Mayeda, A.R. (2005). Quality of sleep in patients with schizophrenia is associated with quality of life and coping. BMC Psychiatry *5*, 13.

Hölscher, C., Schmid, S., Pilz, P.K.D., Sansig, G., van der Putten, H., and Plappert, C.F. (2004). Lack of the metabotropic glutamate receptor subtype 7 selectively impairs short-term working memory but not long-term memory. Behav. Brain Res. *154*, 473–481.

Homayoun, H., and Moghaddam, B. (2007). NMDA Receptor Hypofunction Produces Opposite Effects on Prefrontal Cortex Interneurons and Pyramidal Neurons. J. Neurosci. *27*, 11496–11500.

Hong, L.E., Summerfelt, A., Buchanan, R.W., O'Donnell, P., Thaker, G.K., Weiler, M.A., and Lahti, A.C. (2010). Gamma and Delta Neural Oscillations and Association with Clinical Symptoms under Subanesthetic Ketamine. Neuropsychopharmacology *35*, 632–640.

Hoover, W.B., and Vertes, R.P. (2007). Anatomical analysis of afferent projections to the medial prefrontal cortex in the rat. Brain Struct. Funct. *212*, 149–179.

Horev, G., Ellegood, J., Lerch, J.P., Son, Y.-E.E., Muthuswamy, L., Vogel, H., Krieger, A.M., Buja, A., Henkelman, R.M., Wigler, M., et al. (2011). Dosage-dependent phenotypes in models of 16p11.2 lesions found in autism. Proc. Natl. Acad. Sci. U. S. A. *108*, 17076–17081.

Horst, N.K., and Laubach, M. (2012). Working with memory: evidence for a role for the medial prefrontal cortex in performance monitoring during spatial delayed alternation. J. Neurophysiol. *108*, 3276–3288.

Horsthemke, B., and Wagstaff, J. (2008). Mechanisms of imprinting of the Prader-Willi/Angelman region. Am. J. Med. Genet. A *146A*, 2041–2052.

Howe, M.W., Atallah, H.E., McCool, A., Gibson, D.J., and Graybiel, A.M. (2011). Habit learning is associated with major shifts in frequencies of oscillatory activity and synchronized spike firing in striatum. Proc. Natl. Acad. Sci. *108*, 16801–16806.

Howes, O.D., and Kapur, S. (2009). The dopamine hypothesis of schizophrenia: version III--the final common pathway. Schizophr. Bull. *35*, 549–562.

Hsiao, K., Harony-Nicolas, H., Buxbaum, J.D., Bozdagi-Gunal, O., and Benson, D.L. (2016). Cyfip1 Regulates Presynaptic Activity during Development. J. Neurosci. *36*, 1564–1576.

Hsieh, L.-T., and Ranganath, C. (2014). Frontal midline theta oscillations during working memory maintenance and episodic encoding and retrieval. Neuroimage *85*, 721–729.

Huber, K.M., Kayser, M.S., and Bear, M.F. (2000). Role for rapid dendritic protein synthesis in hippocampal mGluR-dependent long-term depression. Science *288*,

1254–1257.

Huber, K.M., Gallagher, S.M., Warren, S.T., and Bear, M.F. (2002). Altered synaptic plasticity in a mouse model of fragile X mental retardation. Proc. Natl. Acad. Sci. *99*, 7746–7750.

Huerta, P.T., and Lisman, J.E. (1995). Bidirectional synaptic plasticity induced by a single burst during cholinergic theta oscillation in CA1 in vitro. Neuron *15*, 1053–1063.

Huganir, R.L., and Nicoll, R.A. (2013). AMPARs and synaptic plasticity: the last 25 years. Neuron *80*, 704–717.

Hughes, J.R. (2007). Autism: The first firm finding = underconnectivity? Epilepsy Behav. *11*, 20–24.

Hunt, M.J., and Kasicki, S. (2013). A systematic review of the effects of NMDA receptor antagonists on oscillatory activity recorded in vivo. J. Psychopharmacol. *27*, 972–986.

Hunt, M.J., Raynaud, B., and Garcia, R. (2006). Ketamine Dose-Dependently Induces High-Frequency Oscillations in the Nucleus Accumbens in Freely Moving Rats. Biol. Psychiatry *60*, 1206–1214.

Hunt, M.J., Falinska, M., Łęski, S., Wójcik, D.K., and Kasicki, S. (2011). Differential effects produced by ketamine on oscillatory activity recorded in the rat hippocampus, dorsal striatum and nucleus accumbens. J. Psychopharmacol. *25*, 808–821.

Hunt, M.J., Olszewski, M., Piasecka, J., Whittington, M.A., and Kasicki, S. (2015). Effects of NMDA receptor antagonists and antipsychotics on high frequency oscillations recorded in the nucleus accumbens of freely moving mice. Psychopharmacology (Berl). *232*, 4525–4535.

Hunt, M.J., Kopell, N.J., Traub, R.D., and Whittington, M.A. (2017). Aberrant Network Activity in Schizophrenia. Trends Neurosci. *40*, 371–382.

Hyman (2010). Working memory performance correlates with prefrontal-hippocampal theta interactions but not with prefrontal neuron firing rates. Front. Integr. Neurosci. *4*, 2.

Hyman, S.E. (2014). Revitalizing psychiatric therapeutics. Neuropsychopharmacology *39*, 220–229.

Hyman, S.E. (2018). The daunting polygenicity of mental illness: making a new map. Philos. Trans. R. Soc. Lond. B. Biol. Sci. *373*.

Hyman, J.M., Wyble, B.P., Goyal, V., Rossi, C.A., and Hasselmo, M.E. (2003). Stimulation in hippocampal region CA1 in behaving rats yields long-term potentiation when delivered to the peak of theta and long-term depression when delivered to the trough. J. Neurosci. *23*, 11725–11731.

Hyman, J.M., Zilli, E.A., Paley, A.M., and Hasselmo, M.E. (2005). Medial prefrontal cortex cells show dynamic modulation with the hippocampal theta rhythm dependent on behavior. Hippocampus *15*, 739–749.

Hyman, J.M., Ma, L., Balaguer-Ballester, E., Durstewitz, D., and Seamans, J.K. (2012). Contextual encoding by ensembles of medial prefrontal cortex neurons. Proc. Natl. Acad. Sci. *109*, 5086–5091.

Inoué, S., Honda, K., and Komoda, Y. (1995). Sleep as neuronal detoxification and restitution. Behav. Brain Res. *69*, 91–96.

Insel, T.R. (2010). Rethinking schizophrenia. Nature *468*.

Insel, T.R. (2012). Next-generation treatments for mental disorders. Sci. Transl. Med. *4*, 155ps19.

International Schizophrenia Consortium. (2008). Rare chromosomal deletions and duplications increase risk of schizophrenia. Nature *455*, 237–241.

Irwin, S.A., Idupulapati, M., Gilbert, M.E., Harris, J.B., Chakravarti, A.B., Rogers, E.J., Crisostomo, R.A., Larsen, B.P., Mehta, A., Alcantara, C.J., et al. (2002). Dendritic spine and dendritic field characteristics of layer V pyramidal neurons in the visual cortex of fragile-X knockout mice. Am. J. Med. Genet. *111*, 140–146.

Ito, R., Robbins, T.W., Pennartz, C.M., and Everitt, B.J. (2008). Functional interaction between the hippocampus and nucleus accumbens shell is necessary for the acquisition of appetitive spatial context conditioning. J. Neurosci. *28*, 6950–6959.

Izumi, N., Fumoto, K., Izumi, S., and Kikuchi, A. (2008). GSK-3beta regulates proper mitotic spindle formation in cooperation with a component of the gamma-tubulin ring complex, GCP5. J. Biol. Chem. *283*, 12981–12991.

Jaaro-Peled, H., Altimus, C., LeGates, T., Cash-Padgett, T., Zoubovsky, S., Hikida, T., Ishizuka, K., Hattar, S., Mongrain, V., and Sawa, A. (2016). Abnormal wake/sleep pattern in a novel gain-of-function model of DISC1. Neurosci. Res. *112*, 63–69.

Jagannath, A., Peirson, S.N., and Foster, R.G. (2013). Sleep and circadian rhythm disruption in neuropsychiatric illness. Curr. Opin. Neurobiol. *23*, 888–894.

Jan, Y.-N., and Jan, L.Y. (2010). Branching out: mechanisms of dendritic arborization. Nat. Rev. Neurosci. *11*, 316–328.

Javitt, D.C. (1987). Negative schizophrenic symptomatology and the PCP (phencyclidine) model of schizophrenia. Hillside J. Clin. Psychiatry *9*, 12–35.

Javitt, D.C., and Zukin, S.R. (1991). Recent advances in the phencyclidine model of schizophrenia. Am. J. Psychiatry *148*, 1301–1308.

Jay, T.M., and Witter, M.P. (1991). Distribution of hippocampal CA1 and subicular efferents in the prefrontal cortex of the rat studied by means of anterograde transport of Phaseolus vulgaris-leucoagglutinin. J. Comp. Neurol. *313*, 574–586.

Jay, T.M., Glowinski, J., and Thierry, A.M. (1989). Selectivity of the hippocampal projection to the prelimbic area of the prefrontal cortex in the rat. Brain Res. *505*, 337–340.

Ji, B., Wang, X., Pinto-Duarte, A., Kim, M., Caldwell, S., Young, J.W., Behrens, M.M., Sejnowski, T.J., Geyer, M.A., and Zhou, X. (2013). Prolonged Ketamine Effects in Sp4 Hypomorphic Mice: Mimicking Phenotypes of Schizophrenia. PLoS One *8*, e66327.

Jiang, Y., Zhang, Y., Zhang, P., Sang, T., Zhang, F., Ji, T., Huang, Q., Xie, H., Du, R., Cai, B., et al. (2012). NIPA2 located in 15q11.2 is mutated in patients with childhood absence epilepsy. Hum. Genet. *131*, 1217–1224.

Johnson, L.A., Euston, D.R., Tatsuno, M., and McNaughton, B.L. (2010). Stored-Trace Reactivation in Rat Prefrontal Cortex Is Correlated with Down-to-Up State Fluctuation Density. J. Neurosci. *30*, 2650–2661.

Jones, M.W., and Wilson, M.A. (2005). Theta rhythms coordinate hippocampal-prefrontal interactions in a spatial memory task. PLoS Biol. *3*, 1–13.

Jones, K.A., Menniti, F.S., and Sivarao, D. V (2015). Translational psychiatry--light at the end of the tunnel. Ann. N. Y. Acad. Sci. *1344*, 1–11.

Jones, N.C., Hudson, M., Foreman, J., Rind, G., Hill, R., Manning, E.E., and van den Buuse, M. (2017). Brain-derived neurotrophic factor haploinsufficiency impairs high-frequency cortical oscillations in mice. Eur. J. Neurosci.

Jonides, J., and Nee, D.E. (2006). Brain mechanisms of proactive interference in working memory. Neuroscience *139*, 181–193.

Jung, M.W., Qin, Y., McNaughton, B.L., and Barnes, C.A. (1998a). Firing characteristics of deep layer neurons in prefrontal cortex in rats performing spatial working memory tasks. Cereb. Cortex *8*, 437–450.

Jung, M.W., Qin, Y., McNaughton, B.L., and Barnes, C.A. (1998b). Firing characteristics of deep layer neurons in prefrontal cortex in rats performing spatial working memory tasks. Cereb. Cortex *8*, 437–450.

Jutras, M.J., and Buffalo, E.A. (2010). Synchronous neural activity and memory formation. Curr. Opin. Neurobiol. *20*, 150–155.

Jutras, M.J., Fries, P., and Buffalo, E.A. (2009). Gamma-band synchronization in the macaque hippocampus and memory formation. J. Neurosci. *29*, 12521–12531.

Kaestner, E.J., Wixted, J.T., and Mednick, S.C. (2013). Pharmacologically increasing sleep spindles enhances recognition for negative and high-arousal memories. J. Cogn. Neurosci. *25*, 1597–1610.

Kajikawa, Y., and Schroeder, C.E. (2011). How Local Is the Local Field Potential? Neuron *72*, 847–858.

Kalenscher, T., Lansink, C.S., Lankelma, J. V., and Pennartz, C.M.A. (2010). Reward-Associated Gamma Oscillations in Ventral Striatum Are Regionally Differentiated and Modulate Local Firing Activity. J. Neurophysiol. *103*, 1658–1672.

Kang, H.J., Voleti, B., Hajszan, T., Rajkowska, G., Stockmeier, C.A., Licznerski,

P., Lepack, A., Majik, M.S., Jeong, L.S., Banasr, M., et al. (2012). Decreased expression of synapse-related genes and loss of synapses in major depressive disorder. Nat. Med. *18*, 1413–1417.

Kantrowitz, J.T., and Javitt, D.C. (2010). N-methyl-d-aspartate (NMDA) receptor dysfunction or dysregulation: The final common pathway on the road to schizophrenia? Brain Res. Bull. *83*, 108–121.

Kapur, S. (2003). Psychosis as a state of aberrant salience: a framework linking biology, phenomenology, and pharmacology in schizophrenia. Am. J. Psychiatry *160*, 13–23.

Kapur, S. (2004). How antipsychotics become anti-'psychotic' - From dopamine to salience to psychosis. Trends Pharmacol. Sci. *25*, 402–406.

Kapur, S., and Seeman, P. (2002). NMDA receptor antagonists ketamine and PCP have direct effects on the dopamine D2 and serotonin 5-HT2 receptors—implications for models of schizophrenia. Mol. Psychiatry *7*, 837–844.

Karayiorgou, M., Flint, J., Gogos, J.A., and Malenka, R.C. (2012). The best of times, the worst of times for psychiatric disease. Nat. Neurosci. *15*, 811–812.

Kasai, H., Fukuda, M., Watanabe, S., Hayashi-Takagi, A., and Noguchi, J. (2010). Structural dynamics of dendritic spines in memory and cognition. Trends Neurosci. *33*, 121–129.

Kaskie, R.E., Graziano, B., and Ferrarelli, F. (2017). Schizophrenia and sleep disorders: links, risks, and management challenges. Nat. Sci. Sleep *9*, 227–239.

Katsuki, F., McNally, J., Thankachan, S., McKenna, J., Brown, R., Strecker, R., and McCarley, R. (2017). 0218 Optogenetic manipulation of parvalbumin containing GABAergic neurons in the thalamic reticular nucleus alters declarative and non-declarative memories in mice. In Sleep, (Oxford University Press), pp. A80–A81.

Katzner, S., Nauhaus, I., Benucci, A., Bonin, V., Ringach, D.L., and Carandini, M. (2009). Local Origin of Field Potentials in Visual Cortex. Neuron *61*, 35–41.

Kay, L.M. (2003). Two species of gamma oscillations in the olfactory bulb: dependence on behavioral state and synaptic interactions. J. Integr. Neurosci. *2*, 31–44.

Keedwell, P.A., Andrew, C., Williams, S.C.R., Brammer, M.J., and Phillips, M.L. (2005). The Neural Correlates of Anhedonia in Major Depressive Disorder. Biol. Psychiatry *58*, 843–853.

Keefe, R.S.E., Bilder, R.M., Davis, S.M., Harvey, P.D., Palmer, B.W., Gold, J.M., Meltzer, H.Y., Green, M.F., Capuano, G., Stroup, T.S., et al. (2007). Neurocognitive Effects of Antipsychotic Medications in Patients With Chronic Schizophrenia in the CATIE Trial. Arch. Gen. Psychiatry *64*, 633.

Keistler, C., Barker, J.M., and Taylor, J.R. (2015). Infralimbic prefrontal cortex interacts with nucleus accumbens shell to unmask expression of outcome-selective Pavlovian-to-instrumental transfer. Learn. Mem. *22*, 509–513.

Kelly, K.M. (2004). Spike–wave Discharges: Absence or Not, a Common Finding in Common Laboratory Rats. Epilepsy Curr. *4*, 176–177.

Kendler, K.S., and Eaves, L.J. (2005). Psychiatric genetics. In Review of Psychiatry Series, (Arlington, VA, US: American Psychiatric Publishing, Inc), p.

Keppel, G., and Underwood, B.J. (1962). Proactive inhibition in short-term retention of single items. J. Verbal Learning Verbal Behav. *1*, 153–161.

Keshavan, M.S., Diwadkar, V.A., Montrose, D.M., Stanley, J.A., and Pettegrew, J.W. (2004). Premorbid characterization in schizophrenia: the Pittsburgh High Risk Study. World Psychiatry *3*, 163–168.

Kikuchi, M., Hashimoto, T., Nagasawa, T., Hirosawa, T., Minabe, Y., Yoshimura, M., Strik, W., Dierks, T., and Koenig, T. (2011). Frontal areas contribute to reduced global coordination of resting-state gamma activities in drug-naïve patients with schizophrenia. Schizophr. Res. *130*, 187–194.

Kim, H., Sul, J.H., Huh, N., Lee, D., and Jung, M.W. (2009). Role of striatum in updating values of chosen actions. J. Neurosci. *29*, 14701–14712.

Kim, J.W., Lee, Y.S., Han, D.H., Min, K.J., Lee, J., and Lee, K. (2015). Diagnostic utility of quantitative EEG in un-medicated schizophrenia. Neurosci. Lett. *589*, 126–131.

Kirihara, K., Rissling, A.J., Swerdlow, N.R., Braff, D.L., and Light, G.A. (2012). Hierarchical organization of gamma and theta oscillatory dynamics in schizophrenia. Biol. Psychiatry *71*, 873–880.

Kirov, G. (2015). CNVs in neuropsychiatric disorders. Hum. Mol. Genet. *24*, R45–R49.

Kirov, G., Pocklington, A.J., Holmans, P., Ivanov, D., Ikeda, M., Ruderfer, D., Moran, J., Chambert, K., Toncheva, D., Georgieva, L., et al. (2012). De novo CNV analysis implicates specific abnormalities of postsynaptic signalling complexes in the pathogenesis of schizophrenia. Mol. Psychiatry *17*, 142–153.

Kirov, G., Rees, E., Walters, J.T.R., Escott-Price, V., Georgieva, L., Richards, A.L., Chambert, K.D., Davies, G., Legge, S.E., Moran, J.L., et al. (2014). The penetrance of copy number variations for schizophrenia and developmental delay. Biol. Psychiatry *75*, 378–385.

Kittelberger, K., Hur, E.E., Sazegar, S., Keshavan, V., and Kocsis, B. (2012). Comparison of the effects of acute and chronic administration of ketamine on hippocampal oscillations: relevance for the NMDA receptor hypofunction model of schizophrenia. Brain Struct. Funct. *217*, 395–409.

Knutson, B., Bjork, J.M., Fong, G.W., Hommer, D., Mattay, V.S., and Weinberger, D.R. (2004). Amphetamine modulates human incentive processing. Neuron *43*, 261–269.

Kobayashi, K., Kuroda, S., Fukata, M., Nakamura, T., Nagase, T., Nomura, N., Matsuura, Y., Yoshida-Kubomura, N., Iwamatsu, A., and Kaibuchi, K. (1998). p140Sra-1 (specifically Rac1-associated protein) is a novel specific target for Rac1 small GTPase. J. Biol. Chem. *273*, 291–295.

Kocsis, B. (2012). Differential Role of NR2A and NR2B Subunits in N-Methyl-D-Aspartate Receptor Antagonist-Induced Aberrant Cortical Gamma Oscillations. Biol. Psychiatry *71*, 987–995.

Kohls, G., Schulte-Rüther, M., Nehrkorn, B., Müller, K., Fink, G.R., Kamp-Becker, I., Herpertz-Dahlmann, B., Schultz, R.T., and Konrad, K. (2013). Reward system dysfunction in autism spectrum disorders. Soc. Cogn. Affect. Neurosci. *8*, 565–572.

Kokkinou, M., Ashok, A.H., and Howes, O.D. (2018). The effects of ketamine on dopaminergic function: meta-analysis and review of the implications for neuropsychiatric disorders. Mol. Psychiatry *23*, 59–69.

Kolb, B., Buhrmann, K., Mcdonald, R., and Sutherland, R.J. (1994). Dissociation of the medial prefrontal, posterior parietal, and posterior temporal cortex for spatial

navigation and recognition memory in the rat. Cereb. Cortex *4*, 664–680.

Korotkova, T., Fuchs, E.C., Ponomarenko, A., von Engelhardt, J., and Monyer, H. (2010). NMDA Receptor Ablation on Parvalbumin-Positive Interneurons Impairs Hippocampal Synchrony, Spatial Representations, and Working Memory. Neuron *68*, 557–569.

Köse, S., Yılmaz, H., Ocakoğlu, F.T., and Özbaran, N.B. (2017). Sleep problems in children with autism spectrum disorder and intellectual disability without autism spectrum disorder. Sleep Med. *40*, 69–77.

Koshiyama, D., Fukunaga, M., Okada, N., Yamashita, F., Yamamori, H., Yasuda, Y., Fujimoto, M., Ohi, K., Fujino, H., Watanabe, Y., et al. (2018). Role of subcortical structures on cognitive and social function in schizophrenia. Sci. Rep. *8*, 1183.

Köster, F., Schinke, B., Niemann, S., and Hermans-Borgmeyer, I. (1998). Identification of shyc, a novel gene expressed in the murine developing and adult nervous system. Neurosci. Lett. *252*, 69–71.

Köster, M., Friese, U., Schöne, B., Trujillo-Barreto, N., and Gruber, T. (2014). Theta-gamma coupling during episodic retrieval in the human EEG. Brain Res. *1577*, 57–68.

Krivosheya, D., Tapia, L., Levinson, J.N., Huang, K., Kang, Y., Hines, R., Ting, A.K., Craig, A.M., Mei, L., Bamji, S.X., et al. (2008). ErbB4-neuregulin signaling modulates synapse development and dendritic arborization through distinct mechanisms. J. Biol. Chem. *283*, 32944–32956.

Kronk, R., Bishop, E.E., Raspa, M., Bickel, J.O., Mandel, D.A., and Bailey, D.B. (2010). Prevalence, nature, and correlates of sleep problems among children with fragile X syndrome based on a large scale parent survey. Sleep *33*, 679–687.

Krystal, J.H., Karper, L.P., Seibyl, J.P., Freeman, G.K., Delaney, R., Bremner, J.D., Heninger, G.R., Bowers, M.B., and Charney, D.S. (1994). Subanesthetic effects of the noncompetitive NMDA antagonist, ketamine, in humans. Psychotomimetic, perceptual, cognitive, and neuroendocrine responses. Arch. Gen. Psychiatry *51*, 199–214.

Krystal, J.H., Perry, E.B., Gueorguieva, R., Belger, A., Madonick, S.H., Abi-Dargham, A., Cooper, T.B., MacDougall, L., Abi-Saab, W., and D'Souza, D.C.

(2005). Comparative and Interactive Human Psychopharmacologic Effects of Ketamine and Amphetamine. Arch. Gen. Psychiatry *62*, 985.

Kubicki, M., McCarley, R., Westin, C.F., Park, H.J., Maier, S., Kikinis, R., Jolesz, F.A., and Shenton, M.E. (2007). A review of diffusion tensor imaging studies in schizophrenia. J. Psychiatr. Res. *41*, 15–30.

Kumar, D., Dedic, N., Flachskamm, C., Voulé, S., Deussing, J.M., and Kimura, M. (2015). Cacna1c (Cav1.2) Modulates Electroencephalographic Rhythm and Rapid Eye Movement Sleep Recovery. Sleep.

Kwon, H., Menon, V., Eliez, S., Warsofsky, I.S., White, C.D., Dyer-Friedman, J., Taylor, A.K., Glover, G.H., and Reiss, A.L. (2001). Functional neuroanatomy of visuospatial working memory in fragile X syndrome: relation to behavioral and molecular measures. Am. J. Psychiatry *158*, 1040–1051.

Lahti, A., Koffel, B., LaPorte, D., and Tamminga, C.A. (1995). Subanesthetic Doses of Ketamine Stimulate Psychosis in Schizophrenia. Neuropsychopharmacology *13*, 9–19.

Lakatos, P., Shah, A.S., Knuth, K.H., Ulbert, I., Karmos, G., and Schroeder, C.E. (2005). An oscillatory hierarchy controlling neuronal excitability and stimulus processing in the auditory cortex. J. Neurophysiol. *94*, 1904–1911.

Lancaster, T.M., Ihssen, N., Brindley, L.M., Tansey, K.E., Mantripragada, K., O'Donovan, M.C., Owen, M.J., and Linden, D.E.J. (2016a). Associations between polygenic risk for schizophrenia and brain function during probabilistic learning in healthy individuals. Hum. Brain Mapp. *37*, 491–500.

Lancaster, T.M., Linden, D.E., Tansey, K.E., Banaschewski, T., Bokde, A.L.W., Bromberg, U., Büchel, C., Cattrell, A., Conrod, P.J., Flor, H., et al. (2016b). Polygenic Risk of Psychosis and Ventral Striatal Activation During Reward Processing in Healthy Adolescents. JAMA Psychiatry *73*, 852–861.

Lancaster, T.M., Dimitriadis, S.L., Tansey, K.E., Perry, G., Ihssen, N., Jones, D.K., Singh, K.D., Holmans, P., Pocklington, A., Davey Smith, G., et al. (2018). Structural and Functional Neuroimaging of Polygenic Risk for Schizophrenia: A Recall-by-Genotype–Based Approach. Schizophr. Bull.

Lange, F., Seer, C., and Kopp, B. (2017). Cognitive flexibility in neurological disorders: Cognitive components and event-related potentials. Neurosci. Biobehav.

Rev. *83*, 496–507.

Langston, R.F., and Wood, E.R. (2010). Associative recognition and the hippocampus: differential effects of hippocampal lesions on object-place, object-context and object-place-context memory. Hippocampus *20*, 1139–1153.

Langston, R.F., Ainge, J.A., Couey, J.J., Canto, C.B., Bjerknes, T.L., Witter, M.P., Moser, E.I., and Moser, M.-B. (2010). Development of the Spatial Representation System in the Rat. Science (80-.). *328*, 1576–1580.

Lansink, C.S., Goltstein, P.M., Lankelma, J. V., McNaughton, B.L., and Pennartz, C.M.A. (2009). Hippocampus Leads Ventral Striatum in Replay of Place-Reward Information. PLoS Biol. *7*, e1000173.

Lansink, C.S., Meijer, G.T., Lankelma, J. V, Vinck, M.A., Jackson, J.C., and Pennartz, C.M.A. (2016). Reward Expectancy Strengthens CA1 Theta and Beta Band Synchronization and Hippocampal-Ventral Striatal Coupling. J. Neurosci. *36*, 10598–10610.

Latreille, V., Carrier, J., Lafortune, M., Postuma, R.B., Bertrand, J.-A., Panisset, M., Chouinard, S., and Gagnon, J.-F. (2015). Sleep spindles in Parkinson's disease may predict the development of dementia. Neurobiol. Aging *36*, 1083–1090.

Lavoie, A.M., and Mizumori, S.J. (1994). Spatial, movement- and reward-sensitive discharge by medial ventral striatum neurons of rats. Brain Res. *638*, 157–168.

Leblond, C.S., Heinrich, J., Delorme, R., Proepper, C., Betancur, C., Huguet, G., Konyukh, M., Chaste, P., Ey, E., Rastam, M., et al. (2012). Genetic and functional analyses of SHANK2 mutations suggest a multiple hit model of autism spectrum disorders. PLoS Genet. *8*, e1002521.

Lee, A.K., and Wilson, M.A. (2002). Memory of Sequential Experience in the Hippocampus during Slow Wave Sleep. Neuron *36*, 1183–1194.

Lee, I., Griffin, A.L., Zilli, E.A., Eichenbaum, H., and Hasselmo, M.E. (2006). Gradual Translocation of Spatial Correlates of Neuronal Firing in the Hippocampus toward Prospective Reward Locations. Neuron *51*, 639–650.

Lee, J., Hudson, M.R., O'Brien, T.J., Nithianantharajah, J., and Jones, N.C. (2017). Local NMDA receptor hypofunction evokes generalized effects on gamma and high-frequency oscillations and behavior. Neuroscience *358*, 124–136.

Lee, S., Ripke, S., Neale, B.M., Faraone, S. V., Purcell, S.M., Perlis, R.H., Mowry, B.J., Thapar, A., Goddard, M.E., Witte, J.S., et al. (2013). Genetic relationship between five psychiatric disorders estimated from genome-wide SNPs. Nat. Genet. *45*, 984–994.

Legault, M., and Wise, R.A. (1999). Injections of N-methyl-D-aspartate into the ventral hippocampus increase extracellular dopamine in the ventral tegmental area and nucleus accumbens. Synapse *31*, 241–249.

Lewis, C.R., and Olive, M.F. (2014). Early-life stress interactions with the epigenome. Behav. Pharmacol. *25*, 1.

Lewis, D.A., Hashimoto, T., and Volk, D.W. (2005). Cortical inhibitory neurons and schizophrenia. Nat. Rev. Neurosci. *6*, 312–324.

Li, H.H., Roy, M., Kuscuoglu, U., Spencer, C.M., Halm, B., Harrison, K.C., Bayle, J.H., Splendore, A., Ding, F., Meltzer, L.A., et al. (2009). Induced chromosome deletions cause hypersociability and other features of Williams-Beuren syndrome in mice. EMBO Mol. Med. *1*, 50–65.

Li, J., Pelletier, M.R., Perez Velazquez, J.-L., and Carlen, P.L. (2002). Reduced Cortical Synaptic Plasticity and GluR1 Expression Associated with Fragile X Mental Retardation Protein Deficiency. Mol. Cell. Neurosci. *19*, 138–151.

Li, J., Kuo, T., Hsieh, I., and Yang, C. (2012a). Changes in hippocampal theta rhythm and their correlations with speed during different phases of voluntary wheel running in rats. Neuroscience *213*, 54–61.

Li, N., Lee, B., Liu, R.-J., Banasr, M., Dwyer, J.M., Iwata, M., Li, X.-Y., Aghajanian, G., and Duman, R.S. (2010). mTOR-dependent synapse formation underlies the rapid antidepressant effects of NMDA antagonists. Science *329*, 959–964.

Li, S., Bai, W., Liu, T., Yi, H., and Tian, X. (2012b). Increases of theta–low gamma coupling in rat medial prefrontal cortex during working memory task. Brain Res. Bull. *89*, 115–123.

Lightbody, A.A., and Reiss, A.L. (2009). Gene, brain, and behavior relationships in fragile X syndrome: Evidence from neuroimaging studies. Dev. Disabil. Res. Rev. *15*, 343–352.

Limoges, E., Mottron, L., Bolduc, C., Berthiaume, C., and Godbout, R. (2005). Atypical sleep architecture and the autism phenotype. Brain *128*, 1049–1061.

Lin, P., Wang, X., Zhang, B., Kirkpatrick, B., Öngür, D., Levitt, J.J., Jovicich, J., Yao, S., and Wang, X. (2018). Functional dysconnectivity of the limbic loop of frontostriatal circuits in first-episode, treatment-naive schizophrenia. Hum. Brain Mapp. *39*, 747–757.

Lindén, H., Tetzlaff, T., Potjans, T.C., Pettersen, K.H., Grün, S., Diesmann, M., and Einevoll, G.T. (2011). Modeling the Spatial Reach of the LFP. Neuron *72*, 859–872.

Lindström, L.H., Gefvert, O., Hagberg, G., Lundberg, T., Bergström, M., Hartvig, P., and Långström, B. (1999). Increased dopamine synthesis rate in medial prefrontal cortex and striatum in schizophrenia indicated by L-(beta-11C) DOPA and PET. Biol. Psychiatry *46*, 681–688.

von der Lippe, C., Rustad, C., Heimdal, K., and Rødningen, O.K. (2011). 15q11.2 microdeletion – Seven new patients with delayed development and/or behavioural problems. Eur. J. Med. Genet. *54*, 357–360.

Lisman, J.E., and Jensen, O. (2013). The Theta-Gamma Neural Code. Neuron *77*, 1002–1016.

Lisman, J.E., Coyle, J.T., Green, R.W., Javitt, D.C., Benes, F.M., Heckers, S., and Grace, A.A. (2008). Circuit-based framework for understanding neurotransmitter and risk gene interactions in schizophrenia. Trends Neurosci. *31*, 234–242.

Liu, Z., Wang, Y., Cai, L., Li, Y., Chen, B., Dong, Y., and Huang, Y.H. (2016). Prefrontal Cortex to Accumbens Projections in Sleep Regulation of Reward. J. Neurosci. *36*, 7897–7910.

Lladó-Pelfort, L., Celada, P., and Artigas, F. (2014). P.1.a.010 Brain oscillatory patterns in 22q11 transgenic mice model. Interaction with non-competitive NMDA receptor antagonists. Eur. Neuropsychopharmacol. *24*, S158–S159.

Llewellyn, S., and Hobson, J.A. (2015). Not only…but also: REM sleep creates and NREM Stage 2 instantiates landmark junctions in cortical memory networks. Neurobiol. Learn. Mem. *122*, 69–87.

Lodge, D.J., and Grace, A.A. (2006). The Hippocampus Modulates Dopamine

Neuron Responsivity by Regulating the Intensity of Phasic Neuron Activation. Neuropsychopharmacology *31*, 1356–1361.

Lodge, D.J., and Grace, A.A. (2007). Aberrant hippocampal activity underlies the dopamine dysregulation in an animal model of schizophrenia. J. Neurosci. *27*, 11424–11430.

Lodge, D.J., and Grace, A.A. (2011). Hippocampal dysregulation of dopamine system function and the pathophysiology of schizophrenia. Trends Pharmacol. Sci. *32*, 507–513.

Logothetis, N.K., Eschenko, O., Murayama, Y., Augath, M., Steudel, T., Evrard, H.C., Besserve, M., and Oeltermann, A. (2013). Hippocampal-cortical interaction during periods of subcortical silence. Nature *491*, 547–553.

López-Bendito, G., Cautinat, A., Sánchez, J.A., Bielle, F., Flames, N., Garratt, A.N., Talmage, D.A., Role, L.W., Charnay, P., Marín, O., et al. (2006). Tangential neuronal migration controls axon guidance: a role for neuregulin-1 in thalamocortical axon navigation. Cell *125*, 127–142.

Louie, K., and Wilson, M.A. (2001). Temporally structured replay of awake hippocampal ensemble activity during rapid eye movement sleep. Neuron *29*, 145–156.

Lovelace, J.W., Ethell, I.M., Binder, D.K., and Razak, K.A. (2018). Translation-relevant EEG phenotypes in a mouse model of Fragile X Syndrome. Neurobiol. Dis. *115*, 39–48.

Luby, E.D., Cohen, B.D., Rosenbaum, G., Gottlieb, J.S., and Kelley, R. (1959). Study of a new schizophrenomimetic drug; sernyl. A. M. A. Arch. Neurol. Psychiatry *81*, 363–369.

Luchicchi, A., Lecca, S., Melis, M., De Felice, M., Cadeddu, F., Frau, R., Muntoni, A.L., Fadda, P., Devoto, P., and Pistis, M. (2016). Maternal immune activation disrupts dopamine system in the offspring. Int. J. Neuropsychopharmacol. *19*, 1–10.

Lüscher, C., and Huber, K.M. (2010). Group 1 mGluR-dependent synaptic long-term depression: mechanisms and implications for circuitry and disease. Neuron *65*, 445–459.

Lüscher, C., and Malenka, R.C. (2012). NMDA receptor-dependent long-term potentiation and long-term depression (LTP/LTD). Cold Spring Harb. Perspect. Biol. *4*.

Madrigal, I., Rodríguez-Revenga, L., Xunclà, M., and Milà, M. (2012). 15q11.2 microdeletion and FMR1 premutation in a family with intellectual disabilities and autism. Gene *508*, 92–95.

Maier, R., Moser, G., Chen, G.-B., Ripke, S., Coryell, W., Potash, J.B., Scheftner, W.A., Shi, J., Weissman, M.M., Hultman, C.M., et al. (2015). Joint Analysis of Psychiatric Disorders Increases Accuracy of Risk Prediction for Schizophrenia, Bipolar Disorder, and Major Depressive Disorder. Am. J. Hum. Genet. *96*, 283–294.

Mailly, P., Aliane, V., Groenewegen, H.J., Haber, S.N., and Deniau, J.-M. (2013). The rat prefrontostriatal system analyzed in 3D: evidence for multiple interacting functional units. J. Neurosci. *33*, 5718–5727.

Maingret, N., Girardeau, G., Todorova, R., Goutierre, M., and Zugaro, M.M. (2016). Hippocampo-cortical coupling mediates memory consolidation during sleep. Nat Neurosci *19*, 959–964.

Malenka, R.C. (1994). Synaptic plasticity in the hippocampus: LTP and LTD. Cell *78*, 535–538.

Malenka, R.C., and Bear, M.F. (2004). LTP and LTD: An embarrassment of riches. Neuron *44*, 5–21.

Malhotra, D., and Sebat, J. (2012). CNVs: harbingers of a rare variant revolution in psychiatric genetics. Cell *148*, 1223–1241.

Malhotra, A.K., Pinals, D.A., Adler, C.M., Elman, I., Clifton, A., Pickar, D., and Breier, A. (1997). Ketamine-induced exacerbation of psychotic symptoms and cognitive impairment in neuroleptic-free schizophrenics. Neuropsychopharmacology *17*, 141–150.

Malkki, H.A.I., Mertens, P.E.C., Lankelma, J. V., Vinck, M., van Schalkwijk, F.J., van Mourik-Donga, L.B., Battaglia, F.P., Mahlke, C., Kuhl, D., and Pennartz, C.M.A. (2016). Effects of Arc/Arg3.1 gene deletion on rhythmic synchronization of hippocampal CA1 neurons during locomotor activity and sleep. Neurobiol. Learn. Mem. *131*, 155–165.

Manoach, D.S., Thakkar, K.N., Stroynowski, E., Ely, A., McKinley, S.K., Wamsley, E., Djonlagic, I., Vangel, M.G., Goff, D.C., and Stickgold, R. (2010). Reduced overnight consolidation of procedural learning in chronic medicated schizophrenia is related to specific sleep stages. J. Psychiatr. Res. *44*, 112–120.

Manoach, D.S., Demanuele, C., Wamsley, E.J., Vangel, M., Montrose, D.M., Miewald, J., Kupfer, D., Buysse, D., Stickgold, R., and Keshavan, M.S. (2014). Sleep spindle deficits in antipsychotic-naïve early course schizophrenia and in non-psychotic first-degree relatives. Front. Hum. Neurosci. *8*, 762.

Manoach, D.S., Pan, J.Q., Purcell, S.M., and Stickgold, R. (2016). Reduced Sleep Spindles in Schizophrenia: A Treatable Endophenotype That Links Risk Genes to Impaired Cognition? Biol. Psychiatry *80*, 599–608.

Mansbach, R.S. (1991). Effects of NMDA receptor ligands on sensorimotor gating in the rat. Eur. J. Pharmacol. *202*, 61–66.

Mansour, H.A., Wood, J., Logue, T., Chowdari, K. V, Dayal, M., Kupfer, D.J., Monk, T.H., Devlin, B., and Nimgaonkar, V.L. (2006). Association study of eight circadian genes with bipolar I disorder, schizoaffective disorder and schizophrenia. Genes. Brain. Behav. *5*, 150–157.

Di Marino, D., Chillemi, G., De Rubeis, S., Tramontano, A., Achsel, T., and Bagni, C. (2015). MD and Docking Studies Reveal That the Functional Switch of CYFIP1 is Mediated by a Butterfly-like Motion. J. Chem. Theory Comput. *11*, 3401–3410.

Markram, H., Lübke, J., Frotscher, M., and Sakmann, B. (1997). Regulation of synaptic efficacy by coincidence of postsynaptic APs and EPSPs. Science *275*, 213–215.

Markus, E.J., Qin, Y.L., Leonard, B., Skaggs, W.E., McNaughton, B.L., and Barnes, C.A. (1995). Interactions between location and task affect the spatial and directional firing of hippocampal neurons. J. Neurosci. *15*, 7079–7094.

Marshall, L., Helgadóttir, H., Mölle, M., and Born, J. (2006). Boosting slow oscillations during sleep potentiates memory. Nature *444*, 610–613.

Martin, J.P., and Bell, J. (1943). A Pedigree of Mental Defect Showing Sex-Linkage. J. Neurol. Psychiatry *6*, 154–157.

Maski, K., Holbrook, H., Manoach, D., Hanson, E., Kapur, K., and Stickgold, R.

(2015). Sleep Dependent Memory Consolidation in Children with Autism Spectrum Disorder. Sleep *38*, 1955–1963.

Massimini, M. (2004). The Sleep Slow Oscillation as a Traveling Wave. J. Neurosci. *24*, 6862–6870.

Maurer, L., Tang, H., Haumesser, J.K., Altschüler, J., Kühn, A.A., Spranger, J., and van Riesen, C. (2017). High-fat diet-induced obesity and insulin resistance are characterized by differential beta oscillatory signaling of the limbic cortico-basal ganglia loop. Sci. Rep. *7*, 15555.

Maurin, Y., Banrezes, B., Menetrey, A., Mailly, P., and Deniau, J.M. (1999). Three-dimensional distribution of nigrostriatal neurons in the rat: relation to the topography of striatonigral projections. Neuroscience *91*, 891–909.

Mayberg, H.S., Lozano, A.M., Voon, V., McNeely, H.E., Seminowicz, D., Hamani, C., Schwalb, J.M., and Kennedy, S.H. (2005). Deep Brain Stimulation for Treatment-Resistant Depression. Neuron *45*, 651–660.

McBride, W.J., Murphy, J.M., and Ikemoto, S. (1999). Localization of brain reinforcement mechanisms: intracranial self-administration and intracranial place-conditioning studies. Behav. Brain Res. *101*, 129–152.

McCarroll, S.A., and Hyman, S.E. (2013). Progress in the genetics of polygenic brain disorders: significant new challenges for neurobiology. Neuron *80*, 578–587.

McCarthy, S.E., McCombie, W.R., and Corvin, A. (2014). Unlocking the treasure trove: from genes to schizophrenia biology. Schizophr. Bull. *40*, 492–496.

McCormick, D.A., and Bal, T. (1997). SLEEP AND AROUSAL: Thalamocortical Mechanisms. Annu. Rev. Neurosci. *20*, 185–215.

McDonald, C., and Murray, R.M. (2000). Early and late environmental risk factors for schizophrenia. Brain Res. Brain Res. Rev. *31*, 130–137.

McFarland, W.L., Teitelbaum, H., and Hedges, E.K. (1975). Relationship between hippocampal theta activity and running speed in the rat. J. Comp. Physiol. Psychol. *88*, 324–328.

McHugh, S.B., Niewoehner, B., Rawlins, J.N.P., and Bannerman, D.M. (2008).

Dorsal hippocampal N-methyl-D-aspartate receptors underlie spatial working memory performance during non-matching to place testing on the T-maze. Behav. Brain Res. *186*, 41–47.

McNally, J.M., and McCarley, R.W. (2016). Gamma band oscillations. Curr. Opin. Psychiatry *29*, 202–210.

Mednick, S.C., McDevitt, E.A., Walsh, J.K., Wamsley, E., Paulus, M., Kanady, J.C., and Drummond, S.P.A. (2013). The critical role of sleep spindles in hippocampal-dependent memory: a pharmacology study. J. Neurosci. *33*, 4494–4504.

van der Meer, M.A.A., and Redish, A.D. (2009a). Low and High Gamma Oscillations in Rat Ventral Striatum have Distinct Relationships to Behavior, Reward, and Spiking Activity on a Learned Spatial Decision Task. Front. Integr. Neurosci. *3*, 9.

van der Meer, M.A.A., and Redish, A.D. (2009b). Covert Expectation-of-Reward in Rat Ventral Striatum at Decision Points. Front. Integr. Neurosci. *3*, 1.

van der Meer, M.A.A., and Redish, A.D. (2011). Theta phase precession in rat ventral striatum links place and reward information. J. Neurosci. *31*, 2843–2854.

van der Meer, M.A.A., Kalenscher, T., Lansink, C.S., Pennartz, C.M.A., Berke, J.D., and Redish, A.D. (2010). Integrating early results on ventral striatal gamma oscillations in the rat. Front. Neurosci. *4*, 300.

Menet, J.S., and Rosbash, M. (2011). When brain clocks lose track of time: Cause or consequence of neuropsychiatric disorders. Curr. Opin. Neurobiol. *21*, 849–857.

Messaoudi, E., Kanhema, T., Soulé, J., Tiron, A., Dagyte, G., da Silva, B., and Bramham, C.R. (2007). Sustained Arc/Arg3.1 synthesis controls long-term potentiation consolidation through regulation of local actin polymerization in the dentate gyrus in vivo. J. Neurosci. *27*, 10445–10455.

Meyer-Lindenberg, A.S., Olsen, R.K., Kohn, P.D., Brown, T., Egan, M.F., Weinberger, D.R., and Berman, K.F. (2005). Regionally specific disturbance of dorsolateral prefrontal-hippocampal functional connectivity in schizophrenia. Arch. Gen. Psychiatry *62*, 379–386.

Miano, S., Bruni, O., Elia, M., Scifo, L., Smerieri, A., Trovato, A., Verrillo, E.,

Terzano, M.G., and Ferri, R. (2008). Sleep phenotypes of intellectual disability: A polysomnographic evaluation in subjects with Down syndrome and Fragile-X syndrome. Clin. Neurophysiol. *119*, 1242–1247.

Michaels, T.I., Long, L.L., Stevenson, I.H., Chrobak, J.J., and Chen, C.-M.A. (2018). Effects of chronic ketamine on hippocampal cross-frequency coupling: implications for schizophrenia pathophysiology. Eur. J. Neurosci.

Middleton, S.J., Racca, C., Cunningham, M.O., Traub, R.D., Monyer, H., Knöpfel, T., Schofield, I.S., Jenkins, A., and Whittington, M.A. (2008). High-Frequency Network Oscillations in Cerebellar Cortex. Neuron *58*, 763–774.

Milner, B. (1963). Effects of Different Brain Lesions on Card Sorting: The Role of the Frontal Lobes. Arch. Neurol. *9*, 90–100.

Mitra, P., and Bokil, H. (2008). Observed Brain Dynamics (New York: Oxford University Press).

Miyakawa, T., Leiter, L.M., Gerber, D.J., Gainetdinov, R.R., Sotnikova, T.D., Zeng, H., Caron, M.G., and Tonegawa, S. (2003). Conditional calcineurin knockout mice exhibit multiple abnormal behaviors related to schizophrenia. Proc. Natl. Acad. Sci. U. S. A. *100*, 8987–8992.

Miyamoto, D., Hirai, D., Fung, C.C.A., Inutsuka, A., Odagawa, M., Suzuki, T., Boehringer, R., Adaikkan, C., Matsubara, C., Matsuki, N., et al. (2016). Top-down cortical input during NREM sleep consolidates perceptual memory. Science *352*, 1315–1318.

Miyamoto, D., Hirai, D., and Murayama, M. (2017). The Roles of Cortical Slow Waves in Synaptic Plasticity and Memory Consolidation. Front. Neural Circuits *11*, 92.

Miyazaki, K., Mogi, E., Araki, N., and Matsumoto, G. (1998). Reward-quality dependent anticipation in rat nucleus accumbens. Neuroreport *9*, 3943–3948.

Mogenson, G.J., Jones, D.L., and Yim, C.Y. (1980). From motivation to action: functional interface between the limbic system and the motor system. Prog. Neurobiol. *14*, 69–97.

van der Molen, M.J.W., Stam, C.J., and van der Molen, M.W. (2014). Resting-state EEG oscillatory dynamics in fragile X syndrome: abnormal functional connectivity

and brain network organization. PLoS One *9*, e88451.

Van der Molen, M.J.W., and Van der Molen, M.W. (2013). Reduced alpha and exaggerated theta power during the resting-state EEG in fragile X syndrome. Biol. Psychol. *92*, 216–219.

Mölle, M., Marshall, L., Gais, S., and Born, J. (2002). Grouping of spindle activity during slow oscillations in human non-rapid eye movement sleep. J. Neurosci. *22*, 10941–10947.

Mölle, M., Yeshenko, O., Marshall, L., Sara, S.J., and Born, J. (2006). Hippocampal sharp wave-ripples linked to slow oscillations in rat slow-wave sleep. J. Neurophysiol. *96*, 62–70.

Mölle, M., Eschenko, O., Gais, S., Sara, S.J., and Born, J. (2009). The influence of learning on sleep slow oscillations and associated spindles and ripples in humans and rats. Eur. J. Neurosci. *29*, 1071–1081.

Montgomery, S.M., and Buzsáki, G. (2007). Gamma oscillations dynamically couple hippocampal CA3 and CA1 regions during memory task performance. Proc. Natl. Acad. Sci. U. S. A. *104*, 14495–14500.

Moorman, D.E., James, M.H., McGlinchey, E.M., and Aston-Jones, G. (2015). Differential roles of medial prefrontal subregions in the regulation of drug seeking. Brain Res. *1628*, 130–146.

Moran, P., Stokes, J., Marr, J., Bock, G., Desbonnet, L., Waddington, J., and O'Tuathaigh, C. (2016). Gene × Environment Interactions in Schizophrenia: Evidence from Genetic Mouse Models. Neural Plast. *2016*, 2173748.

Moran, R.J., Jones, M.W., Blockeel, A.J., Adams, R.A., Stephan, K.E., and Friston, K.J. (2015). Losing Control Under Ketamine: Suppressed Cortico-Hippocampal Drive Following Acute Ketamine in Rats. Neuropsychopharmacology *40*, 268–277.

Morin, A., Doyon, J., Dostie, V., Barakat, M., Hadj Tahar, A., Korman, M., Benali, H., Karni, A., Ungerleider, L.G., and Carrier, J. (2008). Motor sequence learning increases sleep spindles and fast frequencies in post-training sleep. Sleep *31*, 1149–1156.

Morris, R.G.M., Black, A.H., and Okeefe, J. (1976). Hippocampal Eeg During a Ballistic Movement. Neurosci Lett *3*, 102.

Morris, R.W., Vercammen, A., Lenroot, R., Moore, L., Langton, J.M., Short, B., Kulkarni, J., Curtis, J., O'Donnell, M., Weickert, C.S., et al. (2012). Disambiguating ventral striatum fMRI-related BOLD signal during reward prediction in schizophrenia. Mol. Psychiatry *17*, 235, 280–289.

Moser, M.B., Moser, E.I., Forrest, E., Andersen, P., and Morris, R.G. (1995). Spatial learning with a minislab in the dorsal hippocampus. Proc. Natl. Acad. Sci. U. S. A. *92*, 9697–9701.

Moussa, R., Poucet, B., Amalric, M., and Sargolini, F. (2011). Contributions of dorsal striatal subregions to spatial alternation behavior. Learn. Mem. *18*, 444–451.

Mukai, J., Liu, H., Burt, R.A., Swor, D.E., Lai, W.-S., Karayiorgou, M., and Gogos, J.A. (2004). Evidence that the gene encoding ZDHHC8 contributes to the risk of schizophrenia. Nat. Genet. *36*, 725–731.

Mukai, J., Dhilla, A., Drew, L.J., Stark, K.L., Cao, L., MacDermott, A.B., Karayiorgou, M., and Gogos, J.A. (2008). Palmitoylation-dependent neurodevelopmental deficits in a mouse model of 22q11 microdeletion. Nat. Neurosci. *11*, 1302–1310.

Mukai, J., Tamura, M., Fénelon, K., Rosen, A.M., Spellman, T.J., Kang, R., MacDermott, A.B., Karayiorgou, M., Gordon, J.A., and Gogos, J.A. (2015). Molecular Substrates of Altered Axonal Growth and Brain Connectivity in a Mouse Model of Schizophrenia. Neuron *86*, 680–695.

Murray, G.K., Corlett, P.R., Clark, L., Pessiglione, M., Blackwell, A.D., Honey, G., Jones, P.B., Bullmore, E.T., Robbins, T.W., and Fletcher, P.C. (2008). Substantia nigra/ventral tegmental reward prediction error disruption in psychosis. Mol. Psychiatry *13*, 239, 267–276.

Musumeci, S.A., Ferri, R., Elia, M., DalGracco, S., Scuderi, C., Stefanini, M.C., Castano, A., and Azan, G. (1995). Sleep neurophysiology in fragile X patients. Dev. Brain Dysfunct. *8*, 218–222.

Musumeci, S.A., Ferri, R., Scuderi, C., Bosco, P., and Elia, M. (2001). Seizures and epileptiform EEG abnormalities in FRAXE syndrome. Clin. Neurophysiol. *112*, 1954–1955.

Muthukumaraswamy, S.D., Shaw, A.D., Jackson, L.E., Hall, J., Moran, R., and Saxena, N. (2015). Evidence that Subanesthetic Doses of Ketamine Cause

Sustained Disruptions of NMDA and AMPA-Mediated Frontoparietal Connectivity in Humans. J. Neurosci. *35*, 11694–11706.

Myroshnychenko, M., Seamans, J.K., Phillips, A.G., and Lapish, C.C. (2017). Temporal Dynamics of Hippocampal and Medial Prefrontal Cortex Interactions During the Delay Period of a Working Memory-Guided Foraging Task. Cereb. Cortex *27*, 5331–5342.

Nagase, T., Kikuno, R., and Ohara, O. (2001). Prediction of the coding sequences of unidentified human genes. XXI. The complete sequences of 60 new cDNA clones from brain which code for large proteins. DNA Res. *8*, 179–187.

Nakashiba, T., Buhl, D.L., McHugh, T.J., and Tonegawa, S. (2009). Hippocampal CA3 Output Is Crucial for Ripple-Associated Reactivation and Consolidation of Memory. Neuron *62*, 781–787.

Nakatani, J., Tamada, K., Hatanaka, F., Ise, S., Ohta, H., Inoue, K., Tomonaga, S., Watanabe, Y., Chung, Y.J., Banerjee, R., et al. (2009). Abnormal behavior in a chromosome-engineered mouse model for human 15q11-13 duplication seen in autism. Cell *137*, 1235–1246.

Napoli, I., Mercaldo, V., Boyl, P.P., Eleuteri, B., Zalfa, F., De Rubeis, S., Di Marino, D., Mohr, E., Massimi, M., Falconi, M., et al. (2008). The fragile X syndrome protein represses activity-dependent translation through CYFIP1, a new 4E-BP. Cell *134*, 1042–1054.

Nason, M.W., Adhikari, A., Bozinoski, M., Gordon, J.A., and Role, L.W. (2011). Disrupted Activity in the Hippocampal–Accumbens Circuit of Type III Neuregulin 1 Mutant Mice. Neuropsychopharmacology *36*, 488–496.

Nebel, R.A., Zhao, D., Pedrosa, E., Kirschen, J., Lachman, H.M., Zheng, D., and Abrahams, B.S. (2016). Reduced CYFIP1 in Human Neural Progenitors Results in Dysregulation of Schizophrenia and Epilepsy Gene Networks. PLoS One *11*, e0148039.

Nee, D.E., and Jonides, J. (2008). Neural correlates of access to short-term memory. Proc. Natl. Acad. Sci. U. S. A. *105*, 14228–14233.

Need, A.C., and Goldstein, D.B. (2014). Schizophrenia Genetics Comes of Age. Neuron *83*, 760–763.

Nelson, A.J.D., Thur, K.E., Marsden, C.A., and Cassaday, H.J. (2010). Dissociable roles of dopamine within the core and medial shell of the nucleus accumbens in memory for objects and place. Behav. Neurosci. *124*, 789–799.

Nestler, E.J., and Hyman, S.E. (2010). Animal models of neuropsychiatric disorders. Nat. Neurosci. *13*, 1161–1169.

Neymotin, S.A., Lazarewicz, M.T., Sherif, M., Contreras, D., Finkel, L.H., and Lytton, W.W. (2011). Ketamine Disrupts Theta Modulation of Gamma in a Computer Model of Hippocampus. J. Neurosci. *31*, 11733–11743.

Nicola, S.M. (2010). The flexible approach hypothesis: unification of effort and cue-responding hypotheses for the role of nucleus accumbens dopamine in the activation of reward-seeking behavior. J. Neurosci. *30*, 16585–16600.

Nicola, S.M., Surmeier, D.J., and Malenka, R.C. (2000). Dopaminergic Modulation of Neuronal Excitability in the Striatum and Nucleus Accumbens. Annu. Rev. Neurosci. *23*, 185–215.

Nicolás, M.J., López-Azcárate, J., Valencia, M., Alegre, M., Pérez-Alcázar, M., Iriarte, J., and Artieda, J. (2011). Ketamine-induced oscillations in the motor circuit of the rat basal ganglia. PLoS One *6*, e21814.

Nielsen, J., Fejgin, K., Sotty, F., Nielsen, V., Mørk, A., Christoffersen, C.T., Yavich, L., Lauridsen, J.B., Clausen, D., Larsen, P.H., et al. (2017). A mouse model of the schizophrenia-associated 1q21.1 microdeletion syndrome exhibits altered mesolimbic dopamine transmission. Transl. Psychiatry *7*, 1261.

Niknazar, M., Krishnan, G.P., Bazhenov, M., and Mednick, S.C. (2015). Coupling of Thalamocortical Sleep Oscillations Are Important for Memory Consolidation in Humans. PLoS One *10*, e0144720.

Nilsson, S.R., Fejgin, K., Gastambide, F., Vogt, M.A., Kent, B.A., Nielsen, V., Nielsen, J., Gass, P., Robbins, T.W., Saksida, L.M., et al. (2016a). Assessing the Cognitive Translational Potential of a Mouse Model of the 22q11.2 Microdeletion Syndrome. Cereb. Cortex *26*, 3991–4003.

Nilsson, S.R.O., Celada, P., Fejgin, K., Thelin, J., Nielsen, J., Santana, N., Heath, C.J., Larsen, P.H., Nielsen, V., Kent, B.A., et al. (2016b). A mouse model of the 15q13.3 microdeletion syndrome shows prefrontal neurophysiological dysfunctions and attentional impairment. Psychopharmacology (Berl). *233*, 2151–

2163.

Nishida, M., and Walker, M.P. (2007). Daytime naps, motor memory consolidation and regionally specific sleep spindles. PLoS One *2*, e341.

Nishida, H., Takahashi, M., and Lauwereyns, J. (2014). Within-session dynamics of theta-gamma coupling and high-frequency oscillations during spatial alternation in rat hippocampal area CA1. Cogn. Neurodyn. *8*, 363–372.

Nomura, T., Musial, T.F., Marshall, J.J., Zhu, Y., Remmers, C.L., Xu, J., Nicholson, D.A., and Contractor, A. (2017). Delayed Maturation of Fast-Spiking Interneurons Is Rectified by Activation of the TrkB Receptor in the Mouse Model of Fragile X Syndrome. J. Neurosci. *37*, 11298–11310.

O'Donnell, P., and Grace, A.A. (1995). Synaptic interactions among excitatory afferents to nucleus accumbens neurons: hippocampal gating of prefrontal cortical input. J. Neurosci. *15*, 3622–3639.

O'Keefe, J., and Nadel, L. (1978). The hippocampus as a cognitive map.

O'Keefe, J., and Recce, M.L. (1993). Phase relationship between hippocampal place units and the EEG theta rhythm. Hippocampus *3*, 317–330.

O'Neill, P.-K., Gordon, J.A., and Sigurdsson, T. (2013). Theta Oscillations in the Medial Prefrontal Cortex Are Modulated by Spatial Working Memory and Synchronize with the Hippocampus through Its Ventral Subregion. J. Neurosci. *33*, 14211–14224.

O'Reilly, C., Lewis, J.D., and Elsabbagh, M. (2017). Is functional brain connectivity atypical in autism? A systematic review of EEG and MEG studies. PLoS One *12*, e0175870.

Oguro-Ando, A., Rosensweig, C., Herman, E., Nishimura, Y., Werling, D., Bill, B.R., Berg, J.M., Gao, F., Coppola, G., Abrahams, B.S., et al. (2015). Increased CYFIP1 dosage alters cellular and dendritic morphology and dysregulates mTOR. Mol. Psychiatry *20*, 1069–1078.

Okada, N., Fukunaga, M., Yamashita, F., Koshiyama, D., Yamamori, H., Ohi, K., Yasuda, Y., Fujimoto, M., Watanabe, Y., Yahata, N., et al. (2016). Abnormal asymmetries in subcortical brain volume in schizophrenia. Mol. Psychiatry *21*, 1460–1466.

Oliver, P.L., Sobczyk, M. V, Maywood, E.S., Edwards, B., Lee, S., Livieratos, A., Oster, H., Butler, R., Godinho, S.I.H., Wulff, K., et al. (2012). Disrupted circadian rhythms in a mouse model of schizophrenia. Curr. Biol. *22*, 314–319.

Olney, J.W., Newcomer, J.W., and Farber, N.B. (1999). NMDA receptor hypofunction model of schizophrenia. J. Psychiatr. Res. *33*, 523–533.

Olszewski, M., Dolowa, W., Matulewicz, P., Kasicki, S., and Hunt, M.J. (2013a). NMDA receptor antagonist-enhanced high frequency oscillations: Are they generated broadly or regionally specific? Eur. Neuropsychopharmacol. *23*, 1795–1805.

Olszewski, M., Piasecka, J., Goda, S.A., Kasicki, S., and Hunt, M.J. (2013b). Antipsychotic compounds differentially modulate high-frequency oscillations in the rat nucleus accumbens: A comparison of first- and second-generation drugs. Int. J. Neuropsychopharmacol. *16*, 1009–1020.

Olton, D.S., and Werz, M.A. (1978). Hippocampal function and behavior: spatial discrimination and response inhibition. Physiol Behav *20*, 597–605.

Olton, D.S., Becker, J.T., and Handelmann, G.E. (1979). Hippocampus, space, and memory. Behav. Brain Sci. *2*, 313–322.

Onslow, A.C.E., Bogacz, R., and Jones, M.W. (2011). Quantifying phase-amplitude coupling in neuronal network oscillations. Prog. Biophys. Mol. Biol. *105*, 49–57.

Otto, T., and Eichenbaum, H. (1992). Neuronal activity in the hippocampus during delayed non-match to sample performance in rats: Evidence for hippocampal processing in recognition memory. Hippocampus *2*, 323–334.

Owen, M.J. (2014). New Approaches to Psychiatric Diagnostic Classification. Neuron *84*, 564–571.

Owen, M.J., O'Donovan, M.C., Thapar, A., and Craddock, N. (2011). Neurodevelopmental hypothesis of schizophrenia. Br. J. Psychiatry *198*, 173–175.

Owesson-White, C.A., Ariansen, J., Stuber, G.D., Cleaveland, N.A., Cheer, J.F., Wightman, R.M., and Carelli, R.M. (2009). Neural encoding of cocaine-seeking behavior is coincident with phasic dopamine release in the accumbens core and shell. Eur. J. Neurosci. *30*, 1117–1127.

Pack, A.I., Galante, R.J., Maislin, G., Cater, J., Metaxas, D., Lu, S., Zhang, L., Smith, R. Von, Kay, T., Lian, J., et al. (2007). Novel method for high-throughput phenotyping of sleep in mice. Physiol. Genomics *28*, 232–238.

Páleníček, T., Fujáková, M., Brunovský, M., Balíková, M., Horáček, J., Gorman, I., Tylš, F., Tišlerová, B., Soš, P., Bubeníková-Valešová, V., et al. (2011). Electroencephalographic spectral and coherence analysis of ketamine in rats: correlation with behavioral effects and pharmacokinetics. Neuropsychobiology *63*, 202–218.

Paluszkiewicz, S.M., Martin, B.S., and Huntsman, M.M. (2011). Fragile X Syndrome: The GABAergic System and Circuit Dysfunction. Dev. Neurosci. *33*, 349–364.

Palva, J.M., Palva, S., and Kaila, K. (2005). Phase Synchrony among Neuronal Oscillations in the Human Cortex. J. Neurosci. *25*, 3962–3972.

Papageorgiou, G.K., Baudonnat, M., Cucca, F., and Walton, M.E. (2016). Mesolimbic Dopamine Encodes Prediction Errors in a State-Dependent Manner. Cell Rep. *15*, 221–228.

Park, S., and Holzman, P.S. (1992). Schizophrenics show spatial working memory deficits. Arch Gen Psychiatry. *49*, 975–982.

Parkinson, J.A., Willoughby, P.J., Robbins, T.W., and Everitt, B.J. (2000). Disconnection of the anterior cingulate cortex and nucleus accumbens core impairs Pavlovian approach behavior: further evidence for limbic cortical-ventral striatopallidal systems. Behav. Neurosci. *114*, 42–63.

Pastalkova, E., Itskov, V., Amarasingham, A., and Buzsaki, G. (2008). Internally Generated Cell Assembly Sequences in the Rat Hippocampus. Science (80-.). *321*, 1322–1327.

Pastoll, H., Solanka, L., van Rossum, M.C.W., and Nolan, M.F. (2013). Feedback inhibition enables θ-nested γ oscillations and grid firing fields. Neuron *77*, 141–154.

Pathania, M., Davenport, E.C., Muir, J., Sheehan, D.F., Lopez-Domenech, G., Kittler, J.T., and Transl, P. (2014). The autism and schizophrenia associated gene CYFIP1 is critical for the maintenance of dendritic complexity and the stabilization of mature spines. Transl. Psychiatry.

Patterson, P.H. (2009). Immune involvement in schizophrenia and autism: etiology, pathology and animal models. Behav. Brain Res. *204*, 313–321.

Pawlowski, L., Mathé, J.M., and Svensson, T.H. (1990). Phencyclidine activates rat A10 dopamine neurons but reduces burst activity and causes regularization of firing. Acta Physiol. Scand. *139*, 529–530.

Paxinos, G., and Watson, C. (2007). The Rat Brain in Stereotaxic Coordinates (Elsevier Inc.).

Pechtel, P., and Pizzagalli, D.A. (2011). Effects of early life stress on cognitive and affective function: an integrated review of human literature. Psychopharmacology (Berl). *214*, 55–70.

Peebles, C.L., Yoo, J., Thwin, M.T., Palop, J.J., Noebels, J.L., and Finkbeiner, S. (2010). Arc regulates spine morphology and maintains network stability in vivo. Proc. Natl. Acad. Sci. U. S. A. *107*, 18173–18178.

van Pelt, S., Boomsma, D.I., and Fries, P. (2012). Magnetoencephalography in twins reveals a strong genetic determination of the peak frequency of visually induced γ-band synchronization. J. Neurosci. *32*, 3388–3392.

Pennartz, C.M.A., Groenewegen, H.J., and Lopes da Silva, F.H. (1994). The nucleus accumbens as a complex of functionally distinct neuronal ensembles: An integration of behavioural, electrophysiological and anatomical data. Prog. Neurobiol. *42*, 719–761.

Pennartz, C.M.A., Lee, E., Verheul, J., Lipa, P., Barnes, C.A., and McNaughton, B.L. (2004). The ventral striatum in off-line processing: ensemble reactivation during sleep and modulation by hippocampal ripples. J. Neurosci. *24*, 6446–6456.

Pennartz, C.M.A., Berke, J.D., Graybiel, A.M., Ito, R., Lansink, C.S., van der Meer, M., Redish, A.D., Smith, K.S., and Voorn, P. (2009). Corticostriatal Interactions during Learning, Memory Processing, and Decision Making. J. Neurosci. *29*, 12831–12838.

Pennartz, C.M.A., Ito, R., Verschure, P.F.M.J., Battaglia, F.P., and Robbins, T.W. (2011). The hippocampal-striatal axis in learning, prediction and goal-directed behavior. Trends Neurosci. *34*, 548–559.

Penzes, P., Cahill, M.E., Jones, K.A., VanLeeuwen, J.-E., and Woolfrey, K.M.

(2011). Dendritic spine pathology in neuropsychiatric disorders. Nat. Neurosci. *14*, 285–293.

De Peri, L., Crescini, A., Deste, G., Fusar-Poli, P., Sacchetti, E., and Vita, A. (2012). Brain structural abnormalities at the onset of schizophrenia and bipolar disorder: a meta-analysis of controlled magnetic resonance imaging studies. Curr. Pharm. Des. *18*, 486–494.

Pessiglione, M., Seymour, B., Flandin, G., Dolan, R.J., and Frith, C.D. (2006). Dopamine-dependent prediction errors underpin reward-seeking behaviour in humans. Nature *442*, 1042–1045.

Peters, J., Kalivas, P.W., and Quirk, G.J. (2009). Extinction circuits for fear and addiction overlap in prefrontal cortex. Learn. Mem. *16*, 279–288.

Pettersson-Yeo, W., Allen, P., Benetti, S., McGuire, P., and Mechelli, A. (2011). Dysconnectivity in schizophrenia: where are we now? Neurosci. Biobehav. Rev. *35*, 1110–1124.

Peyrache, A., Khamassi, M., Benchenane, K., Wiener, S.I., and Battaglia, F.P. (2009). Replay of rule-learning related neural patterns in the prefrontal cortex during sleep. Nat. Neurosci. *12*, 919–926.

Peyrache, A., Battaglia, F.P., and Destexhe, A. (2011). Inhibition recruitment in prefrontal cortex during sleep spindles and gating of hippocampal inputs. Proc. Natl. Acad. Sci. *108*, 17207–17212.

Phillips, K.G., and Uhlhaas, P.J. (2015). Neural oscillations as a translational tool in schizophrenia research: rationale, paradigms and challenges. J. Psychopharmacol. *29*, 155–168.

Phillips, K.G., Bartsch, U., McCarthy, A.P., Edgar, D.M., Tricklebank, M.D., Wafford, K.A., and Jones, M.W. (2012a). Decoupling of Sleep-Dependent Cortical and Hippocampal Interactions in a Neurodevelopmental Model of Schizophrenia. Neuron *76*, 526–533.

Phillips, K.G., Cotel, M.C., McCarthy, A.P., Edgar, D.M., Tricklebank, M., O'Neill, M.J., Jones, M.W., and Wafford, K.A. (2012b). Differential effects of NMDA antagonists on high frequency and gamma EEG oscillations in a neurodevelopmental model of schizophrenia. Neuropharmacology *62*, 1359–1370.

Picchioni, D., Reith, R., Nadel, J., and Smith, C. (2014). Sleep, Plasticity and the Pathophysiology of Neurodevelopmental Disorders: The Potential Roles of Protein Synthesis and Other Cellular Processes. Brain Sci. *4*, 150–201.

Picinelli, C., Lintas, C., Piras, I.S., Gabriele, S., Sacco, R., Brogna, C., and Persico, A.M. (2016). Recurrent 15q11.2 BP1-BP2 microdeletions and microduplications in the etiology of neurodevelopmental disorders. Am. J. Med. Genet. Part B Neuropsychiatr. Genet. *171*, 1088–1098.

Pinault, D. (2008). N-methyl d-aspartate receptor antagonists ketamine and MK-801 induce wake-related aberrant gamma oscillations in the rat neocortex. Biol. Psychiatry *63*, 730–735.

Del Pino, I., García-Frigola, C., Dehorter, N., Brotons-Mas, J.R., Alvarez-Salvado, E., Martínez de Lagrán, M., Ciceri, G., Gabaldón, M.V., Moratal, D., Dierssen, M., et al. (2013). Erbb4 deletion from fast-spiking interneurons causes schizophrenia-like phenotypes. Neuron *79*, 1152–1168.

Pocklington, A.J., Rees, E., Walters, J.T.R., Han, J., Kavanagh, D.H., Chambert, K.D., Holmans, P., Moran, J.L., McCarroll, S.A., Kirov, G., et al. (2015). Novel Findings from CNVs Implicate Inhibitory and Excitatory Signaling Complexes in Schizophrenia. Neuron *86*, 1203–1214.

Popov, T., Wienbruch, C., Meissner, S., Miller, G.A., and Rockstroh, B. (2015). A mechanism of deficient interregional neural communication in schizophrenia. Psychophysiology *52*, 648–656.

Pritchett, D., Wulff, K., Oliver, P.L., Bannerman, D.M., Davies, K.E., Harrison, P.J., Peirson, S.N., and Foster, R.G. (2012). Evaluating the links between schizophrenia and sleep and circadian rhythm disruption. J. Neural Transm. *119*, 1061–1075.

Pritchett, D., Jagannath, A., Brown, L.A., Tam, S.K.E., Hasan, S., Gatti, S., Harrison, P.J., Bannerman, D.M., Foster, R.G., and Peirson, S.N. (2015a). Deletion of Metabotropic Glutamate Receptors 2 and 3 (mGlu2 & mGlu3) in Mice Disrupts Sleep and Wheel-Running Activity, and Increases the Sensitivity of the Circadian System to Light. PLoS One *10*, e0125523.

Pritchett, D., Hasan, S., Tam, S.K.E., Engle, S.J., Brandon, N.J., Sharp, T., Foster, R.G., Harrison, P.J., Bannerman, D.M., and Peirson, S.N. (2015b). d -amino acid oxidase knockout (Dao −/−) mice show enhanced short-term memory performance

and heightened anxiety, but no sleep or circadian rhythm disruption. Eur. J. Neurosci. *41*, 1167–1179.

Profitt, M.F., Deurveilher, S., Robertson, G.S., Rusak, B., and Semba, K. (2016). Disruptions of Sleep/Wake Patterns in the Stable Tubule Only Polypeptide (STOP) Null Mouse Model of Schizophrenia. Schizophr. Bull. *42*, 1207–1215.

Purcell, S.M., Moran, J.L., Fromer, M., Ruderfer, D., Solovieff, N., Roussos, P., O'Dushlaine, C., Chambert, K., Bergen, S.E., Kähler, A., et al. (2014). A polygenic burden of rare disruptive mutations in schizophrenia. Nature *506*, 185–190.

Qiu, A., Tuan, T.A., Woon, P.S., Abdul-Rahman, M.F., Graham, S., and Sim, K. (2010). Hippocampal-cortical structural connectivity disruptions in schizophrenia: An integrated perspective from hippocampal shape, cortical thickness, and integrity of white matter bundles. Neuroimage *52*, 1181–1189.

Quan, M., Lee, S.-H., Kubicki, M., Kikinis, Z., Rathi, Y., Seidman, L.J., Mesholam-Gately, R.I., Goldstein, J.M., McCarley, R.W., Shenton, M.E., et al. (2013). White matter tract abnormalities between rostral middle frontal gyrus, inferior frontal gyrus and striatum in first-episode schizophrenia. Schizophr. Res. *145*, 1–10.

Radua, J., Schmidt, A., Borgwardt, S., Heinz, A., Schlagenhauf, F., McGuire, P., and Fusar-Poli, P. (2015). Ventral Striatal Activation During Reward Processing in Psychosis. JAMA Psychiatry *72*, 1243.

Radwan, B., Dvorak, D., and Fenton, A.A. (2016). Impaired cognitive discrimination and discoordination of coupled theta-gamma oscillations in Fmr1 knockout mice. Neurobiol. Dis. *88*, 125–138.

Ragozzino, M.E., Detrick, S., and Kesner, R.P. (1999). Involvement of the prelimbic-infralimbic areas of the rodent prefrontal cortex in behavioral flexibility for place and response learning. J. Neurosci. *19*, 4585–4594.

Rainier, S., Chai, J.-H., Tokarz, D., Nicholls, R.D., and Fink, J.K. (2003). NIPA1 Gene Mutations Cause Autosomal Dominant Hereditary Spastic Paraplegia (SPG6). Am. J. Hum. Genet. *73*, 967–971.

Rajagopal, L., Massey, B.W., Huang, M., Oyamada, Y., and Meltzer, H.Y. (2013). The Novel Object Recogniton Test in Rodents in Relation to Cognitive Impairment in Schizophrenia. Curr Pharm Des *15*, 15.

Rajasethupathy, P., Sankaran, S., Marshel, J.H., Kim, C.K., Ferenczi, E., Lee, S.Y., Berndt, A., Ramakrishnan, C., Jaffe, A., Lo, M., et al. (2015). Projections from neocortex mediate top-down control of memory retrieval. Nature *526*, 653–659.

Ramesh, V., Nair, D., Zhang, S.X.L., Hakim, F., Kaushal, N., Kayali, F., Wang, Y., Li, R.C., Carreras, A., and Gozal, D. (2012). Disrupted sleep without sleep curtailment induces sleepiness and cognitive dysfunction via the tumor necrosis factor-α pathway. J. Neuroinflammation *9*, 601.

Rasch, B., and Born, J. (2013). About sleep's role in memory. Physiol. Rev. *93*, 681–766.

Rasetti, R., Sambataro, F., Chen, Q., Callicott, J.H., Mattay, V.S., and Weinberger, D.R. (2011). Altered Cortical Network Dynamics. Arch. Gen. Psychiatry *68*, 1207.

Rauch, A., Wieczorek, D., Graf, E., Wieland, T., Endele, S., Schwarzmayr, T., Albrecht, B., Bartholdi, D., Beygo, J., Di Donato, N., et al. (2012). Range of genetic mutations associated with severe non-syndromic sporadic intellectual disability: an exome sequencing study. Lancet *380*, 1674–1682.

Rausch, F., Mier, D., Eifler, S., Esslinger, C., Schilling, C., Schirmbeck, F., Englisch, S., Meyer-Lindenberg, A., Kirsch, P., and Zink, M. (2014). Reduced activation in ventral striatum and ventral tegmental area during probabilistic decision-making in schizophrenia. Schizophr. Res. *156*, 143–149.

Rawlins, J.N., and Olton, D.S. (1982). The septo-hippocampal system and cognitive mapping. Behav. Brain Res. *5*, 331–358.

Rechtschaffen, A., and Kales, A. (1968). A Manual of Standardized Terminology, Techniques and Scoring System for Sleep Stages of Human Subjects (Washington DC: Public Health Service, US Government Printing Office).

Redgrave, P., Prescott, T.J., and Gurney, K. (1999). Is the short-latency dopamine response too short to signal reward error? Trends Neurosci. *22*, 146–151.

Redish, A.D. (2016). Vicarious trial and error. Nat. Rev. Neurosci. *17*, 147–159.

Rees, E., Walters, J.T.R., Georgieva, L., Isles, A.R., Chambert, K.D., Richards, A.L., Mahoney-Davies, G., Legge, S.E., Moran, J.L., McCarroll, S.A., et al. (2014). Analysis of copy number variations at 15 schizophrenia-associated loci. Br. J. Psychiatry *204*, 108–114.

Rees, E., O'Donovan, M.C., and Owen, M.J. (2015). Genetics of schizophrenia. Curr. Opin. Behav. Sci. *2*, 8–14.

Rich, E.L., and Shapiro, M. (2009). Rat prefrontal cortical neurons selectively code strategy switches. J. Neurosci. *29*, 7208–7219.

Richter, A., Petrovic, A., Diekhof, E.K., Trost, S., Wolter, S., and Gruber, O. (2015). Hyperresponsivity and impaired prefrontal control of the mesolimbic reward system in schizophrenia. J. Psychiatr. Res. *71*, 8–15.

Rigotti, M., Barak, O., Warden, M.R., Wang, X.-J., Daw, N.D., Miller, E.K., and Fusi, S. (2013). The importance of mixed selectivity in complex cognitive tasks. Nature *497*, 585–590.

Ripke, S., Neale, B.M., Corvin, A., Walters, J.T.R., Farh, K.H., Holmans, P.A., Lee, P., Bulik-Sullivan, B., Collier, D.A., Huang, H., et al. (2014). Biological Insights From 108 Schizophrenia-Associated Genetic Loci. Nature *511*, 421–427.

Rissman, J., Gazzaley, A., and D'Esposito, M. (2008). Dynamic adjustments in prefrontal, hippocampal, and inferior temporal interactions with increasing visual working memory load. Cereb. Cortex *18*, 1618–1629.

Rivolta, D., Heidegger, T., Scheller, B., Sauer, A., Schaum, M., Birkner, K., Singer, W., Wibral, M., and Uhlhaas, P.J. (2015). Ketamine Dysregulates the Amplitude and Connectivity of High-Frequency Oscillations in Cortical–Subcortical Networks in Humans: Evidence From Resting-State Magnetoencephalography-Recordings. Schizophr. Bull. *41*, 1105–1114.

Robbins, T.W., and Everitt, B.J. (1996). Neurobehavioural mechanisms of reward and motivation. Curr. Opin. Neurobiol. *6*, 228–236.

Robinson, T.E., and Berridge, K.C. (1993). The neural basis of drug craving: an incentive-sentitization theory of addition. Brain Res. Rev. *18*, 247–291.

Rockstroh, B.S., Wienbruch, C., Ray, W.J., and Elbert, T. (2007). Abnormal oscillatory brain dynamics in schizophrenia: a sign of deviant communication in neural network? BMC Psychiatry *7*, 44.

Roitman, M.F., Wheeler, R.A., and Carelli, R.M. (2005). Nucleus accumbens neurons are innately tuned for rewarding and aversive taste stimuli, encode their predictors, and are linked to motor output. Neuron *45*, 587–597.

Rosanova, M., and Ulrich, D. (2005). Pattern-specific associative long-term potentiation induced by a sleep spindle-related spike train. J. Neurosci. *25*, 9398–9405.

Rosen, A.M., Spellman, T., and Gordon, J.A. (2015). Electrophysiological endophenotypes in rodent models of schizophrenia and psychosis. Biol. Psychiatry *77*, 1041–1049.

Rosti, R.O., Sadek, A.A., Vaux, K.K., and Gleeson, J.G. (2014). The genetic landscape of autism spectrum disorders. Dev. Med. Child Neurol. *56*, 12–18.

Rotschafer, S., and Razak, K. (2013). Altered auditory processing in a mouse model of fragile X syndrome. Brain Res. *1506*, 12–24.

Rotzer, S., Kucian, K., Martin, E., von Aster, M., Klaver, P., and Loenneker, T. (2008). Optimized voxel-based morphometry in children with developmental dyscalculia. Neuroimage *39*, 417–422.

Rudd, D.S., Axelsen, M., Epping, E.A., Andreasen, N.C., and Wassink, T.H. (2014). A genome-wide CNV analysis of schizophrenia reveals a potential role for a multiple-hit model. Am. J. Med. Genet. Part B Neuropsychiatr. Genet. *165*, 619–626.

Ruddy, R.M., Chen, Y., Milenkovic, M., and Ramsey, A.J. (2015). Differential effects of NMDA receptor antagonism on spine density. Synapse *69*, 52–56.

Russell, N.A., Horii, A., Smith, P.F., Darlington, C.L., and Bilkey, D.K. (2006). Lesions of the vestibular system disrupt hippocampal theta rhythm in the rat. J. Neurophysiol. *96*, 4–14.

Rutter, L., Carver, F.W., Holroyd, T., Nadar, S.R., Mitchell-Francis, J., Apud, J., Weinberger, D.R., and Coppola, R. (2009). Magnetoencephalographic gamma power reduction in patients with schizophrenia during resting condition. Hum. Brain Mapp. *30*, 3254–3264.

Sabanov, V., Braat, S., D'Andrea, L., Willemsen, R., Zeidler, S., Rooms, L., Bagni, C., Kooy, R.F., and Balschun, D. (2017). Impaired GABAergic inhibition in the hippocampus of Fmr1 knockout mice. Neuropharmacology *116*, 71–81.

Sadowski, J.H.L.P., Jones, M.W., and Mellor, J.R. (2016). Sharp-Wave Ripples Orchestrate the Induction of Synaptic Plasticity during Reactivation of Place Cell

Firing Patterns in the Hippocampus. Cell Rep. *14*, 1916–1929.

Salamone, J.D., Correa, M., Mingote, S.M., and Weber, S.M. (2005). Beyond the reward hypothesis: alternative functions of nucleus accumbens dopamine. Curr. Opin. Pharmacol. *5*, 34–41.

Sams-Dodd, F. (1995). Distinct effects of d-amphetamine and phencyclidine on the social behaviour of rats. Behav. Pharmacol. *6*, 55–65.

Sanders, S.J., Murtha, M.T., Gupta, A.R., Murdoch, J.D., Raubeson, M.J., Willsey, A.J., Ercan-Sencicek, A.G., DiLullo, N.M., Parikshak, N.N., Stein, J.L., et al. (2012). De novo mutations revealed by whole-exome sequencing are strongly associated with autism. Nature *485*, 237–241.

Sanderson, D.J., and Bannerman, D.M. (2012). The role of habituation in hippocampus-dependent spatial working memory tasks: Evidence from GluA1 AMPA receptor subunit knockout mice. Hippocampus *22*, 981–994.

Sapkota, K., Mao, Z., Synowicki, P., Lieber, D., Liu, M., Ikezu, T., Gautam, V., and Monaghan, D.T. (2016). GluN2D N-Methyl-d-Aspartate Receptor Subunit Contribution to the Stimulation of Brain Activity and Gamma Oscillations by Ketamine: Implications for Schizophrenia. J. Pharmacol. Exp. Ther. *356*, 702–711.

Saré, R.M., Harkless, L., Levine, M., Torossian, A., Sheeler, C.A., and Smith, C.B. (2017). Deficient Sleep in Mouse Models of Fragile X Syndrome. Front. Mol. Neurosci. *10*, 280.

Saunders, B.T., and Robinson, T.E. (2012). The role of dopamine in the accumbens core in the expression of Pavlovian-conditioned responses. Eur. J. Neurosci. *36*, 2521–2532.

Schacter, G.B., Yang, C.R., Innis, N.K., and Mogenson, G.J. (1989). The role of the hippocampal-nucleus accumbens pathway in radial-arm maze performance. Brain Res. *494*, 339–349.

Schenck, Bardoni, B., Moro, A., Bagni, C., and Mandel, J.L. (2001a). A highly conserved protein family interacting with the fragile X mental retardation protein (FMRP) and displaying selective interactions with FMRP-related proteins FXR1P and FXR2P. Proc. Natl. Acad. Sci. U. S. A. *98*, 8844–8849.

Schenck, A., Bardoni, B., Moro, A., Bagni, C., and Mandel, J.L. (2001b). A highly

conserved protein family interacting with the fragile X mental retardation protein (FMRP) and displaying selective interactions with FMRP-related proteins FXR1P and FXR2P. Proc. Natl. Acad. Sci. U. S. A. *98*, 8844–8849.

Schenck, A., Bardoni, B., Langmann, C., Harden, N., Mandel, J.L., and Giangrande, A. (2003). CYFIP/Sra-1 controls neuronal connectivity in Drosophila and links the Rac1 GTPase pathway to the fragile X protein. Neuron *38*, 887–898.

Schlagenhauf, F., Huys, Q.J.M., Deserno, L., Rapp, M.A., Beck, A., Heinze, H.-J., Dolan, R., and Heinz, A. (2014). Striatal dysfunction during reversal learning in unmedicated schizophrenia patients. Neuroimage *89*, 171–180.

Schmiedt, C., Brand, A., Hildebrandt, H., and Basar-Eroglu, C. (2005). Event-related theta oscillations during working memory tasks in patients with schizophrenia and healthy controls. Brain Res. Cogn. Brain Res. *25*, 936–947.

Schneider, A., Hagerman, R.J., and Hessl, D. (2009). Fragile X syndrome - From genes to cognition. Dev. Disabil. Res. Rev. *15*, 333–342.

Schomburg, E., and Fernández-Ruiz, A. (2014). Theta phase segregation of input-specific gamma patterns in entorhinal-hippocampal networks. Neuron *84*, 470–485.

Schomburg, E.W., Fernández-Ruiz, A., Mizuseki, K., Berényi, A., Anastassiou, C.A., Koch, C., and Buzsáki, G. (2014). Theta phase segregation of input-specific gamma patterns in entorhinal-hippocampal networks. Neuron *84*, 470–485.

Schultz, W., Apicella, P., Scarnati, E., and Ljungberg, T. (1992). Neuronal activity in monkey ventral striatum related to the expectation of reward. J. Neurosci. *12*, 4595–4610.

Schultz, W., Dayan, P., and Montague, P.R. (1997). A neural substrate of prediction and reward. Science *275*, 1593–1599.

Scoville, W.B., and Milner, B. (1957). Loss of recent memory after bilateral hippocampal lesions. J. Neurol. Neurosurg. Psychiatry *20*, 11–21.

Seeck-Hirschner, M., Baier, P.C., Sever, S., Buschbacher, A., Aldenhoff, J.B., and Göder, R. (2010). Effects of daytime naps on procedural and declarative memory in patients with schizophrenia. J. Psychiatr. Res. *44*, 42–47.

Sekar, A., Bialas, A.R., de Rivera, H., Davis, A., Hammond, T.R., Kamitaki, N., Tooley, K., Presumey, J., Baum, M., Van Doren, V., et al. (2016). Schizophrenia risk from complex variation of complement component 4. Nature *advance on*.

Sempere Pérez, A., Manchón Trives, I., Palazón Azorín, I., Alcaraz Más, L., Pérez Lledó, E., and Galán Sánchez, F. (2011). 15Q11.2 (BP1-BP2) microdeletion, a new syndrome with variable expressivity. An. Pediatr. (Barcelona, Spain 2003) *75*, 58–62.

Sesack, S.R., and Grace, A.A. (2010). Cortico-Basal Ganglia Reward Network: Microcircuitry. Neuropsychopharmacology *35*, 27–47.

Setlow, B., Schoenbaum, G., and Gallagher, M. (2003). Neural encoding in ventral striatum during olfactory discrimination learning. Neuron *38*, 625–636.

Shaw, F.-Z. (2004). Is spontaneous high-voltage rhythmic spike discharge in Long Evans rats an absence-like seizure activity? J. Neurophysiol. *91*, 63–77.

Shaw, A.D., Saxena, N., E. Jackson, L., Hall, J.E., Singh, K.D., and Muthukumaraswamy, S.D. (2015). Ketamine amplifies induced gamma frequency oscillations in the human cerebral cortex. Eur. Neuropsychopharmacol. *25*, 1136–1146.

Shepherd, A.M., Laurens, K.R., Matheson, S.L., Carr, V.J., and Green, M.J. (2012). Systematic meta-review and quality assessment of the structural brain alterations in schizophrenia. Neurosci. Biobehav. Rev. *36*, 1342–1356.

Shibagaki, M., Kiyono, S., and Watanabe, K. (1982). Spindle evolution in normal and mentally retarded children: a review. Sleep *5*, 47–57.

Shoji, H., Hagihara, H., Takao, K., Hattori, S., and Miyakawa, T. (2012). T-maze Forced Alternation and Left-right Discrimination Tasks for Assessing Working and Reference Memory in Mice. J. Vis. Exp.

Siapas, A.G., and Wilson, M.A. (1998). Coordinated interactions between hippocampal ripples and cortical spindles during slow-wave sleep. Neuron *21*, 1123–1128.

Siapas, A.G., Lubenov, E. V, and Wilson, M.A. (2005). Prefrontal phase locking to hippocampal theta oscillations. Neuron *46*, 141–151.

Sigurdsson, T., and Duvarci, S. (2015). Hippocampal-Prefrontal Interactions in Cognition, Behavior and Psychiatric Disease. Front. Syst. Neurosci. *9*, 190.

Sigurdsson, T., Stark, K.L., Karayiorgou, M., Gogos, J.A., and Gordon, J.A. (2010). Impaired hippocampal–prefrontal synchrony in a genetic mouse model of schizophrenia. Nature *464*, 763–767.

Sinclair, D., Oranje, B., Razak, K.A., Siegel, S.J., and Schmid, S. (2017a). Sensory processing in autism spectrum disorders and Fragile X syndrome—From the clinic to animal models. Neurosci. Biobehav. Rev. *76*, 235–253.

Sinclair, D., Featherstone, R., Naschek, M., Nam, J., Du, A., Wright, S., Pance, K., Melnychenko, O., Weger, R., Akuzawa, S., et al. (2017b). GABA-B Agonist Baclofen Normalizes Auditory-Evoked Neural Oscillations and Behavioral Deficits in the Fmr1 Knockout Mouse Model of Fragile X Syndrome. Eneuro *4*, ENEURO.0380-16.2017.

Singh, T., Kurki, M.I., Curtis, D., Purcell, S.M., Crooks, L., McRae, J., Suvisaari, J., Chheda, H., Blackwood, D., Breen, G., et al. (2016). Rare loss-of-function variants in SETD1A are associated with schizophrenia and developmental disorders. Nat. Neurosci. *19*, 571–577.

Sirota, A., Csicsvari, J., Buhl, D., and Buzsaki, G. (2003). Communication between neocortex and hippocampus during sleep in rodents. Proc. Natl. Acad. Sci. *100*, 2065–2069.

Sirota, A., Montgomery, S., Fujisawa, S., Isomura, Y., Zugaro, M., and Buzsáki, G. (2008). Entrainment of neocortical neurons and gamma oscillations by the hippocampal theta rhythm. Neuron *60*, 683–697.

Skaggs, W.E., McNaughton, B.L., Wilson, M.A., and Barnes, C.A. (1996). Theta phase precession in hippocampal neuronal populations and the compression of temporal sequences. Hippocampus *6*, 149–172.

Smith, D.M., and Mizumori, S.J.Y. (2006). Hippocampal place cells, context, and episodic memory. Hippocampus *16*, 716–729.

Sohal, V.S., Zhang, F., Yizhar, O., and Deisseroth, K. (2009). Parvalbumin neurons and gamma rhythms enhance cortical circuit performance. Nature *459*, 698–702.

Van Someren, E.J.W., Swaab, D.F., Colenda, C.C., Cohen, W., McCall, W. V, and

Rosenquist, P.B. (1999). Bright light therapy: improved sensitivity to its effects on rest-activity rhythms in Alzheimer patients by application of nonparametric methods. Chronobiol. Int. *16*, 505–518.

Sorg, C., Manoliu, A., Neufang, S., Myers, N., Peters, H., Schwerthöffer, D., Scherr, M., Mühlau, M., Zimmer, C., Drzezga, A., et al. (2013). Increased intrinsic brain activity in the striatum reflects symptom dimensions in schizophrenia. Schizophr. Bull. *39*, 387–395.

Souders, M.C., Mason, T.B.A., Valladares, O., Bucan, M., Levy, S.E., Mandell, D.S., Weaver, T.E., and Pinto-Martin, J. (2009). Sleep behaviors and sleep quality in children with autism spectrum disorders. Sleep *32*, 1566–1578.

Souders, M.C., Zavodny, S., Eriksen, W., Sinko, R., Connell, J., Kerns, C., Schaaf, R., and Pinto-Martin, J. (2017). Sleep in Children with Autism Spectrum Disorder. Curr. Psychiatry Rep. *19*, 34.

Spellman, T.J., and Gordon, J. a (2015). Synchrony in schizophrenia: a window into circuit-level pathophysiology. Curr. Opin. Neurobiol. *30*, 17–23.

Spellman, T., Rigotti, M., Ahmari, S.E., Fusi, S., Gogos, J.A., and Gordon, J.A. (2015). Hippocampal-prefrontal input supports spatial encoding in working memory. Nature *522*, 309–314.

Sperner-Unterweger, B., and Fuchs, D. (2015). Schizophrenia and psychoneuroimmunology: an integrative view. Curr. Opin. Psychiatry *28*, 201–206.

Srinath, R., and Ray, S. (2014). Effect of amplitude correlations on coherence in the local field potential. J. Neurophysiol. *112*, 741–751.

Stanton, M.E., Thomas, G.J., and Brito, G.N. (1984). Posterodorsal septal lesions impair performance on both shift and stay working memory tasks. Behav. Neurosci. *98*, 405–415.

Stark, K.L., Xu, B., Bagchi, A., Lai, W.-S., Liu, H., Hsu, R., Wan, X., Pavlidis, P., Mills, A.A., Karayiorgou, M., et al. (2008). Altered brain microRNA biogenesis contributes to phenotypic deficits in a 22q11-deletion mouse model. Nat. Genet. *40*, 751–760.

Stefansson, H., Sarginson, J., Kong, A., Yates, P., Steinthorsdottir, V., Gudfinnsson, E., Gunnarsdottir, S., Walker, N., Petursson, H., Crombie, C., et al.

(2003). Association of Neuregulin 1 with Schizophrenia Confirmed in a Scottish Population. Am. J. Hum. Genet. *72*, 83–87.

Stefansson, H., Rujescu, D., Cichon, S., Pietilainen, O.P., Ingason, A., Steinberg, S., Fossdal, R., Sigurdsson, E., Sigmundsson, T., Buizer-Voskamp, J.E., et al. (2008). Large recurrent microdeletions associated with schizophrenia. Nature. *455*, 232–236.

Stefansson, H., Ophoff, R.A., Steinberg, S., Andreassen, O.A., Cichon, S., Rujescu, D., Werge, T., Pietiläinen, O.P.H., Mors, O., Mortensen, P.B., et al. (2009). Common variants conferring risk of schizophrenia. Nature *460*, 744–747.

Stefansson, H., Meyer-Lindenberg, A., Steinberg, S., Magnusdottir, B., Morgen, K., Arnarsdottir, S., Bjornsdottir, G., Walters, G.B., Jonsdottir, G.A., Doyle, O.M., et al. (2014). CNVs conferring risk of autism or schizophrenia affect cognition in controls. Nature *505*, 361–366.

Steffenach, H.-A., Sloviter, R.S., Moser, E.I., and Moser, M.-B. (2002). Impaired retention of spatial memory after transection of longitudinally oriented axons of hippocampal CA3 pyramidal cells. Proc. Natl. Acad. Sci. U. S. A. *99*, 3194–3198.

Steiner, A.P., and Redish, A.D. (2014). Behavioral and neurophysiological correlates of regret in rat decision-making on a neuroeconomic task. Nat. Neurosci. *17*, 995–1002.

Steriade, M., Nuñez, A., and Amzica, F. (1993a). A novel slow (< 1 Hz) oscillation of neocortical neurons in vivo: depolarizing and hyperpolarizing components. J. Neurosci. *13*, 3252–3265.

Steriade, M., McCormick, D.A., and Sejnowski, T.J. (1993b). Thalamocortical oscillations in the sleeping and aroused brain. Science *262*, 679–685.

Steward, O., and Worley, P.F. (2001). Selective targeting of newly synthesized Arc mRNA to active synapses requires NMDA receptor activation. Neuron *30*, 227–240.

Stopper, C.M., and Floresco, S.B. (2015). Dopaminergic Circuitry and Risk/Reward Decision Making: Implications for Schizophrenia. Schizophr. Bull. *41*, 9–14.

Strange, B.A., Witter, M.P., Lein, E.S., and Moser, E.I. (2014). Functional

organization of the hippocampal longitudinal axis. Nat. Rev. Neurosci. *15*, 655–669.

Stujenske, J.M., Likhtik, E., Topiwala, M.A., and Gordon, J.A. (2014). Fear and Safety Engage Competing Patterns of Theta-Gamma Coupling in the Basolateral Amygdala. Neuron *83*, 919–933.

Suh, J., Foster, D.J., Davoudi, H., Wilson, M.A., and Tonegawa, S. (2013). Impaired hippocampal ripple-associated replay in a mouse model of schizophrenia. Neuron *80*, 484–493.

Sullivan, D., Csicsvari, J., Mizuseki, K., Montgomery, S., Diba, K., and Buzsáki, G. (2011). Relationships between hippocampal sharp waves, ripples, and fast gamma oscillation: influence of dentate and entorhinal cortical activity. J. Neurosci. *31*, 8605–8616.

Sullivan, P.F., Daly, M.J., and O'Donovan, M. (2012). Genetic architectures of psychiatric disorders: the emerging picture and its implications. Nat. Rev. Genet. *13*, 537–551.

Sullivan, P.F., Agrawal, A., Bulik, C.M., Andreassen, O.A., Børglum, A.D., Breen, G., Cichon, S., Edenberg, H.J., Faraone, S. V., Gelernter, J., et al. (2018). Psychiatric Genomics: An Update and an Agenda. Am. J. Psychiatry *175*, 15–27.

Sutcliffe, J.S., Nelson, D.L., Zhang, F., Pieretti, M., Caskey, C.T., Saxe, D., and Warren, S.T. (1992). DNA methylation represses FMR-1 transcription in fragile X syndrome. Hum. Mol. Genet. *1*, 397–400.

Sutherland, R.J., Whishaw, I.Q., and Kolb, B. (1983). A behavioural analysis of spatial localization following electrolytic, kainate- or colchicine-induced damage to the hippocampal formation in the rat. Behav. Brain Res. *7*, 133–153.

Syed, E.C.J., Grima, L.L., Magill, P.J., Bogacz, R., Brown, P., and Walton, M.E. (2016). Action initiation shapes mesolimbic dopamine encoding of future rewards. Nat. Neurosci. *19*, 34–36.

Tabuchi, E.T., Mulder, A.B., and Wiener, S.I. (2000). Position and behavioral modulation of synchronization of hippocampal and accumbens neuronal discharges in freely moving rats. Hippocampus *10*, 717–728.

Tagliabue, E., Pouvreau, T., Eybrard, S., Meyer, F., and Louilot, A. (2017).

Dopaminergic responses in the core part of the nucleus accumbens to subcutaneous MK801 administration are increased following postnatal transient blockade of the prefrontal cortex. Behav. Brain Res. *335*, 191–198.

Tahmasian, M., Khazaie, H., Golshani, S., and Avis, K.T. (2013). Clinical application of actigraphy in psychotic disorders: A systematic review. Curr. Psychiatry Rep. *15*, 359.

Takao, T., Tachikawa, H., Kawanishi, Y., Mizukami, K., and Asada, T. (2007). CLOCK gene T3111C polymorphism is associated with Japanese schizophrenics: A preliminary study. Eur. Neuropsychopharmacol. *17*, 273–276.

Talbot, Z.N., Sparks, F.T., Dvorak, D., Curran, B.M., Alarcon, J.M., and Fenton, A.A. (2018). Normal CA1 Place Fields but Discoordinated Network Discharge in a Fmr1-Null Mouse Model of Fragile X Syndrome. Neuron *97*, 684–697.

Tam, G.W.C., van de Lagemaat, L.N., Redon, R., Strathdee, K.E., Croning, M.D.R., Malloy, M.P., Muir, W.J., Pickard, B.S., Deary, I.J., Blackwood, D.H.R., et al. (2010). Confirmed rare copy number variants implicate novel genes in schizophrenia. Biochem. Soc. Trans. *38*, 445–451.

Tamminga, C.A., Vogel, M., Gao, X., Lahti, A.C., and Holcomb, H.H. (2000). The limbic cortex in schizophrenia: focus on the anterior cingulate. Brain Res. Brain Res. Rev. *31*, 364–370.

Tamminga, C.A., Stan, A.D., and Wagner, A.D. (2010). The Hippocampal Formation in Schizophrenia. Am. J. Psychiatry *167*, 1178–1193.

Tamura, M., Mukai, J., Gordon, J.A., and Gogos, J.A. (2016). Developmental Inhibition of Gsk3 Rescues Behavioral and Neurophysiological Deficits in a Mouse Model of Schizophrenia Predisposition. Neuron *89*, 1100–1109.

Tamura, M., Spellman, T.J., Rosen, A.M., Gogos, J.A., and Gordon, J.A. (2017). Hippocampal-prefrontal theta-gamma coupling during performance of a spatial working memory task. Nat. Commun. *8*, 2182.

Tandon, R., Nasrallah, H.A., and Keshavan, M.S. (2009). Schizophrenia, "just the facts" 4. Clinical features and conceptualization. Schizophr. Res. *110*, 1–23.

Teicher, M.H., Anderson, C.M., and Polcari, A. (2012). Childhood maltreatment is associated with reduced volume in the hippocampal subfields CA3, dentate gyrus,

and subiculum. Proc. Natl. Acad. Sci. U. S. A. *109*, E563-72.

Tessier, S., Lambert, A., Chicoine, M., Scherzer, P., Soulières, I., and Godbout, R. (2015). Intelligence measures and stage 2 sleep in typically-developing and autistic children. Int. J. Psychophysiol. *97*, 58–65.

Thelin, J., Halje, P., Nielsen, J., Didriksen, M., Petersson, P., and Bastlund, J.F. (2017). The translationally relevant mouse model of the 15q13.3 microdeletion syndrome reveals deficits in neuronal spike firing matching clinical neurophysiological biomarkers seen in schizophrenia. Acta Physiol. *220*, 124–136.

Till, S.M., Asiminas, A., Jackson, A.D., Katsanevaki, D., Barnes, S.A., Osterweil, E.K., Bear, M.F., Chattarji, S., Wood, E.R., Wyllie, D.J.A., et al. (2015). Conserved hippocampal cellular pathophysiology but distinct behavioural deficits in a new rat model of FXS. Hum. Mol. Genet. *24*, 5977–5984.

Tononi, G., and Cirelli, C. (2006). Sleep function and synaptic homeostasis. Sleep Med. Rev. *10*, 49–62.

Tort, A.B.L., Kramer, M.A., Thorn, C., Gibson, D.J., Kubota, Y., Graybiel, A.M., and Kopell, N.J. (2008). Dynamic cross-frequency couplings of local field potential oscillations in rat striatum and hippocampus during performance of a T-maze task. Proc. Natl. Acad. Sci. U. S. A. *105*, 20517–20522.

Tort, A.B.L., Komorowski, R.W., Manns, J.R., Kopell, N.J., and Eichenbaum, H. (2009). Theta-gamma coupling increases during the learning of item-context associations. Proc. Natl. Acad. Sci. U. S. A. *106*, 20942–20947.

Tseng, K.Y., Chambers, R.A., and Lipska, B.K. (2009). The neonatal ventral hippocampal lesion as a heuristic neurodevelopmental model of schizophrenia. Behav. Brain Res. *204*, 295–305.

Uhlhaas, P.J., and Singer, W. (2010). Abnormal neural oscillations and synchrony in schizophrenia. Nat Rev Neurosci *11*, 100–113.

Urraca, N., Cleary, J., Brewer, V., Pivnick, E.K., McVicar, K., Thibert, R.L., Schanen, N.C., Esmer, C., Lamport, D., and Reiter, L.T. (2013). The interstitial duplication 15q11.2-q13 syndrome includes autism, mild facial anomalies and a characteristic EEG signature. Autism Res. *6*, 268–279.

Uylings, H.B., and van Eden, C.G. (1990). Qualitative and quantitative comparison

of the prefrontal cortex in rat and in primates, including humans. Prog. Brain Res. *85*, 31–62.

Uylings, H.B.M., Groenewegen, H.J., and Kolb, B. (2003). Do rats have a prefrontal cortex? Behav. Brain Res. *146*, 3–17.

Van, L., Boot, E., and Bassett, A.S. (2017). Update on the 22q11.2 deletion syndrome and its relevance to schizophrenia. Curr. Opin. Psychiatry *30*, 191–196.

Vanderwolf, C.H. (1969). Hippocampal electrical activity and voluntary movement in the rat. Electroencephalogr. Clin. Neurophysiol. *26*, 407–418.

Vanlerberghe, C., Petit, F., Malan, V., Vincent-Delorme, C., Bouquillon, S., Boute, O., Holder-Espinasse, M., Delobel, B., Duban, B., Vallee, L., et al. (2015). 15q11.2 microdeletion (BP1-BP2) and developmental delay, behaviour issues, epilepsy and congenital heart disease: a series of 52 patients. Eur. J. Med. Genet. *58*, 140–147.

Verhoeff, M.E., Blanken, L.M.E., Kocevska, D., Mileva-Seitz, V.R., Jaddoe, V.W. V., White, T., Verhulst, F., Luijk, M.P.C.M., and Tiemeier, H. (2018). The bidirectional association between sleep problems and autism spectrum disorder: a population-based cohort study. Mol. Autism *9*, 8.

Vertes, R.P. (2004). Differential projections of the infralimbic and prelimbic cortex in the rat. Synapse *51*, 32–58.

Vertes, R.P., Hoover, W.B., Szigeti-Buck, K., and Leranth, C. (2007). Nucleus reuniens of the midline thalamus: Link between the medial prefrontal cortex and the hippocampus. Brain Res. Bull. *71*, 601–609.

Villafuerte, G., Miguel-Puga, A., Murillo Rodríguez, E., Machado, S., Manjarrez, E., and Arias-Carrión, O. (2015). Sleep Deprivation and Oxidative Stress in Animal Models: A Systematic Review. Oxid. Med. Cell. Longev. *2015*, 1–15.

Voorn, P., Vanderschuren, L.J.M.J., Groenewegen, H.J., Robbins, T.W., and Pennartz, C.M.A. (2004). Putting a spin on the dorsal-ventral divide of the striatum. Trends Neurosci. *27*, 468–474.

Vyazovskiy, V. V., and Harris, K.D. (2013). Sleep and the single neuron: the role of global slow oscillations in individual cell rest. Nat. Rev. Neurosci. *14*, 443–451.

Walsh, T., Mcclellan, J.M., Mccarthy, S.E., Addington, A.M., Sarah, B., Cooper, G.M., Nord, A.S., Kusenda, M., Malhotra, D., Bhandari, A., et al. (2008). Rare Structural Multiple Pathways Genes Variants Disrupt in Neurodevelopmental. Science *320*, 539–543.

Waltz, J.A., and Gold, J.M. (2016). Motivational Deficits in Schizophrenia and the Representation of Expected Value. Curr. Top. Behav. Neurosci. *27*, 375–410.

Wamsley, E.J., Tucker, M.A., Shinn, A.K., Ono, K.E., McKinley, S.K., Ely, A. V, Goff, D.C., Stickgold, R., and Manoach, D.S. (2012). Reduced sleep spindles and spindle coherence in schizophrenia: mechanisms of impaired memory consolidation? Biol. Psychiatry *71*, 154–161.

Wang, G.-W., and Cai, J.-X. (2006a). Disconnection of the hippocampal-prefrontal cortical circuits impairs spatial working memory performance in rats. Behav. Brain Res. *175*, 329–336.

Wang, G.-W., and Cai, J.-X. (2006b). Disconnection of the hippocampal–prefrontal cortical circuits impairs spatial working memory performance in rats. Behav. Brain Res. *175*, 329–336.

Wang, J., Ethridge, L.E., Mosconi, M.W., White, S.P., Binder, D.K., Pedapati, E. V., Erickson, C.A., Byerly, M.J., and Sweeney, J.A. (2017). A resting EEG study of neocortical hyperexcitability and altered functional connectivity in fragile X syndrome. J. Neurodev. Disord. *9*, 11.

Wang, J.M., Koldewyn, K., Hashimoto, R.-I., Schneider, A., Le, L., Tassone, F., Cheung, K., Hagerman, P., Hessl, D., and Rivera, S.M. (2012). Male carriers of the FMR1 premutation show altered hippocampal-prefrontal function during memory encoding. Front. Hum. Neurosci. *6*, 297.

Watson, P.F., and Petrie, A. (2010). Method agreement analysis: A review of correct methodology. Theriogenology *73*, 1167–1179.

Watts, A., Gritton, H.J., Sweigart, J., and Poe, G.R. (2012). Antidepressant suppression of non-REM sleep spindles and REM sleep impairs hippocampus-dependent learning while augmenting striatum-dependent learning. J. Neurosci. *32*, 13411–13420.

Wernicke, C. (1906). Grundrisse der Psychiatrie.

Whittington, M.A., and Traub, R.D. (2003). Interneuron Diversity series: Inhibitory interneurons and network oscillations in vitro. Trends Neurosci. *26*, 676–682.

Wierzynski, C.M., Lubenov, E. V, Gu, M., and Siapas, A.G. (2009). State-dependent spike-timing relationships between hippocampal and prefrontal circuits during sleep. Neuron *61*, 587–596.

Wilkerson, J.R., Albanesi, J.P., and Huber, K.M. (2018). Roles for Arc in metabotropic glutamate receptor-dependent LTD and synapse elimination: Implications in health and disease. Semin. Cell Dev. Biol. *77*, 51–62.

Wilson, C.J. (1993). The generation of natural firing patterns in neostriatal neurons. Prog. Brain Res. *99*, 277–297.

Wilson, M.A., and McNaughton, B.L. (1994). Reactivation of hippocampal ensemble memories during sleep. Science *265*, 676–679.

Witter, M.P., Wouterlood, F.G., Naber, P.A., and Van Haeften, T. (2000). Anatomical organization of the parahippocampal-hippocampal network. Ann. N. Y. Acad. Sci. *911*, 1–24.

Wolf, D.H., Gur, R.C., Valdez, J.N., Loughead, J., Elliott, M.A., Gur, R.E., and Ragland, J.D. (2007). Alterations of fronto-temporal connectivity during word encoding in schizophrenia. Psychiatry Res. *154*, 221–232.

Wolf, R.C., Vasic, N., Sambataro, F., Höse, A., Frasch, K., Schmid, M., and Walter, H. (2009). Temporally anticorrelated brain networks during working memory performance reveal aberrant prefrontal and hippocampal connectivity in patients with schizophrenia. Prog. Neuropsychopharmacol. Biol. Psychiatry *33*, 1464–1473.

De Wolf, V., Brison, N., Devriendt, K., and Peeters, H. (2013). Genetic counseling for susceptibility loci and neurodevelopmental disorders: the del15q11.2 as an example. Am. J. Med. Genet. A *161A*, 2846–2854.

Won, G.H., Kim, J.W., Choi, T.Y., Lee, Y.S., Min, K.J., and Seol, K.H. (2018). Theta-phase gamma-amplitude coupling as a neurophysiological marker in neuroleptic-naïve schizophrenia. Psychiatry Res. *260*, 406–411.

Wong, A.H.C., and Josselyn, S.A. (2015). Caution when diagnosing your mouse with schizophrenia: the use and misuse of model animals for understanding psychiatric disorders. Biol. Psychiatry.

Woo, T.-U.W., Walsh, J.P., and Benes, F.M. (2004). Density of glutamic acid decarboxylase 67 messenger RNA-containing neurons that express the N-methyl-D-aspartate receptor subunit NR2A in the anterior cingulate cortex in schizophrenia and bipolar disorder. Arch. Gen. Psychiatry *61*, 649–657.

Wood, E.R., Dudchenko, P. a, Robitsek, R.J., and Eichenbaum, H. (2000). Hippocampal neurons encode information about different types of memory episodes occurring in the same location. Neuron *27*, 623–633.

Wulff, K., and Joyce, E. (2011). Circadian rhythms and cognition in schizophrenia. Br. J. Psychiatry *198*, 250–252.

Wulff, K., Porcheret, K., Cussans, E., and Foster, R.G. (2009a). Sleep and circadian rhythm disturbances: multiple genes and multiple phenotypes. Curr. Opin. Genet. Dev. *19*, 237–246.

Wulff, K., Gatti, S., Wettstein, J.G., and Foster, R.G. (2010). Sleep and circadian rhythm disruption in psychiatric and neurodegenerative disease. Nat. Rev. Neurosci. *11*, 589–599.

Wulff, K., Dijk, D.-J., Middleton, B., Foster, R.G., and Joyce, E.M. (2012). Sleep and circadian rhythm disruption in schizophrenia. Br. J. Psychiatry *200*, 308–316.

Wulff, P., Ponomarenko, A.A., Bartos, M., Korotkova, T.M., Fuchs, E.C., Bähner, F., Both, M., Tort, A.B.L., Kopell, N.J., Wisden, W., et al. (2009b). Hippocampal theta rhythm and its coupling with gamma oscillations require fast inhibition onto parvalbumin-positive interneurons. Proc. Natl. Acad. Sci. U. S. A. *106*, 3561–3566.

Xi, D., Zhang, W., Wang, H.X., Stradtman, G.G., and Gao, W.J. (2009). Dizocilpine (MK-801) induces distinct changes of N-methyl-d-aspartic acid receptor subunits in parvalbumin-containing interneurons in young adult rat prefrontal cortex. Int. J. Neuropsychopharmacol. *12*, 1395–1408.

Xu, X., Zheng, C., An, L., Wang, R., and Zhang, T. (2016). Effects of Dopamine and Serotonin Systems on Modulating Neural Oscillations in Hippocampus-Prefrontal Cortex Pathway in Rats. Brain Topogr. *29*, 539–551.

Yang, C., and Winkelman, J.W. (2006). Clinical significance of sleep EEG abnormalities in chronic schizophrenia. Schizophr. Res. *82*, 251–260.

Yang, N., Higuchi, O., Ohashi, K., Nagata, K., Wada, A., Kangawa, K., Nishida,

E., and Mizuno, K. (1998). Cofilin phosphorylation by LIM-kinase 1 and its role in Rac-mediated actin reorganization. Nature *393*, 809–812.

Yoon, K.J., Nguyen, H.N., Ursini, G., Zhang, F., Kim, N.S., Wen, Z., Makri, G., Nauen, D., Shin, J.H., Park, Y., et al. (2014). Modeling a genetic risk for schizophrenia in iPSCs and Mice reveals neural stem cell deficits associated with adherens junctions and polarity. Cell Stem Cell *15*, 79–91.

Young, C.K., and McNaughton, N. (2009). Coupling of theta oscillations between anterior and posterior midline cortex and with the hippocampus in freely behaving rats. Cereb. Cortex *19*, 24–40.

Zahm, D.S. (2000). An integrative neuroanatomical perspective on some subcortical substrates of adaptive responding with emphasis on the nucleus accumbens. Neurosci. Biobehav. Rev. *24*, 85–105.

Zahm, D.S., and Brog, J.S. (1992). On the significance of subterritories in the "accumbens" part of the rat ventral striatum. Neuroscience *50*, 751–767.

Zanos, P., Moaddel, R., Morris, P.J., Georgiou, P., Fischell, J., Elmer, G.I., Alkondon, M., Yuan, P., Pribut, H.J., Singh, N.S., et al. (2016). NMDAR inhibition-independent antidepressant actions of ketamine metabolites. Nature *533*, 481–486.

Zarate, C.A., and Machado-Vieira, R. (2017). Ketamine: translating mechanistic discoveries into the next generation of glutamate modulators for mood disorders. Mol. Psychiatry *22*, 324–327.

Zeng, H., Chattarji, S., Barbarosie, M., Rondi-Reig, L., Philpot, B.D., Miyakawa, T., Bear, M.F., and Tonegawa, S. (2001). Forebrain-specific calcineurin knockout selectively impairs bidirectional synaptic plasticity and working/episodic-like memory. Cell *107*, 617–629.

Zhang, J., Fang, Z., Jud, C., Vansteensel, M.J., Kaasik, K., Lee, C.C., Albrecht, U., Tamanini, F., Meijer, J.H., Oostra, B.A., et al. (2008). Fragile X-related proteins regulate mammalian circadian behavioral rhythms. Am. J. Hum. Genet. *83*, 43–52.

Zhang, L., Jones, C.R., Ptacek, L.J., and Fu, Y.-H. (2011). The Genetics of the Human Circadian Clock. In Advances in Genetics, pp. 231–247.

Zhang, X., Zhong, W., Brankačk, J., Weyer, S.W., Müller, U.C., Tort, A.B.L., and

Draguhn, A. (2016). Impaired theta-gamma coupling in APP-deficient mice. Sci. Rep. *6*, 21948.

Zhao, L., Wang, D., Wang, Q., Rodal, A.A., and Zhang, Y.Q. (2013a). Drosophila cyfip Regulates Synaptic Development and Endocytosis by Suppressing Filamentous Actin Assembly. PLoS Genet. *9*, e1003450.

Zhao, Q., Li, T., Zhao, X., Huang, K., Wang, T., Li, Z., Ji, J., Zeng, Z., Zhang, Z., Li, K., et al. (2013b). Rare CNVs and tag SNPs at 15q11.2 are associated with schizophrenia in the Han Chinese population. Schizophr. Bull. *39*, 712–719.

Zhong, C., Du, C., Hancock, M., Mertz, M., Talmage, D.A., and Role, L.W. (2008). Presynaptic type III neuregulin 1 is required for sustained enhancement of hippocampal transmission by nicotine and for axonal targeting of alpha7 nicotinic acetylcholine receptors. J. Neurosci. *28*, 9111–9116.

Zhou, Y., Shu, N., Liu, Y., Song, M., Hao, Y., Liu, H., Yu, C., Liu, Z., and Jiang, T. (2008). Altered resting-state functional connectivity and anatomical connectivity of hippocampus in schizophrenia. Schizophr. Res. *100*, 120–132.

van der Zwaag, B., Staal, W.G., Hochstenbach, R., Poot, M., Spierenburg, H.A., de Jonge, M. V, Verbeek, N.E., van 't Slot, R., van Es, M.A., Staal, F.J., et al. (2010). A co-segregating microduplication of chromosome 15q11.2 pinpoints two risk genes for autism spectrum disorder. Am. J. Med. Genet. B. Neuropsychiatr. Genet. *153B*, 960–966.

Appendix 1

Creation of the *Cyfip1*$^{+/-}$ rat

CRISPR-Cas9 targeting

Proprietary bioinformatics software (Horizon Discovery, St. Louis, USA) was used to design a short guide RNA (sgRNA) targeting a Protospacer Adjacent Motif (PAM) sequence within exon 7 of the rat *Cyfip1* gene (GGCAGATCCACAATCCATCCagg, Figure A1) on chromosome 1.

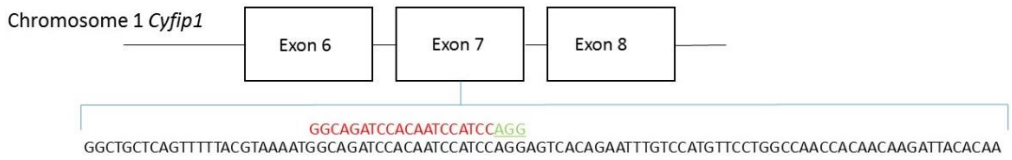

Figure A1 | **Targeting of the Cyfip1 gene with sgRNA in exon 7**. Targeting of the sgRNA was restricted to the first two thirds of the Open Reading Frame of the Cyfip1 rat gene (first 21 of 32 exons, Refseq: NC_005100.4, NM_001107517.1). Upstream targeting at the 5'end was also avoided due to the possible presence of cryptic promoters. The guide was designed and selected with the use of a commercially available online CRISPR design tool (commercial algorithm) to locate the appropriate PAM sequences and ideal locations for the sgRNA. An oligo was generated containing the specific guide sequence along with the appropriate scaffold and the oligo then acted as a template in an *in vitro* transfection (IVT) reaction to generate the sgRNA.

An initial *in vitro* assessment of efficiency of the sgRNA-Cas9 was performed by nucleofecting the sgRNA-Cas9 into rat C6 glial cells. Genomic DNA (gDNA) PCR products were subsequently generated from nucleofected C6 cells using primers flanking the sgRNA site (FOR: GCCAAAGCTTCCCCTAAAGT; REV: TGGGCGTCAAGTACATTCTG; 497bp amplicon). gDNA PCR products were screened for non-homologous end joining (NHEJ) activity and deletion mutations using the SURVEYOR Cel-1 Mutation Detection Assay (Integrated DNA Technologies, following manufacturer's instructions, Figure A2).

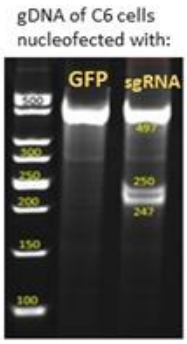

Figure A2 | **gDNA screening.** gDNA was obtained from C6 glial cells nucleofected with sgRNA-Cas9 and Green Fluorescent Protein (GFP). C6 cells nucleofected with GFP only acted as a visual positive of successful nucleofection (cells fluoresce green) and a genetic negative control of NHEJ activity. Meanwhile, NHEJ activity is observed in C6 cells nucleofected with sgRNA-Cas9 via the observation of smaller cel-1 bands and the relative intensity of these bands compared to the intensity of the larger WT band (497 bp) can be used to estimate NHEJ activity.

Embryonic microinjection of sgRNA-Cas9

Embryo donor female Long Evans rats were super-ovulated with pregnant mare serum (PMS) and given human chorionic gonadotrophin (HCG) 48hrs post PMS administration. Females were immediately mated to stud males after HCG administration. Embryo donor females were euthanized 18-24 hrs after mating and their one-cell fertilized embryos were isolated by harvesting the reproductive tract and rupturing the ampulae. A total of 270 embryos were then put in culture media in a CO2 incubator until ready for microinjection. All 270 one-cell stage embryos were microinjected with the validated sgRNA-Cas9 over four sessions and then implanted into synchronized pseudopregnant Long Evans recipient females, resulting in 18 live births.

Positive founders and confirmation of 4bp deletion

Of the 18 live births, 7 pups demonstrated NHEJ activity (39% efficiency) as measured by the SURVEYOR assay (with gDNA derived from P14 tissue biopsies). To further identify positive founders, sequencing experiments of the gDNA PCR products were performed and revealed one positive female showing a 4bp out of frame heterozygous deletion in exon 7 of the *Cyfip1* gene at location Chromosome 1: 36974-36977 and a resulting bioinformatics prediction of an early

stop codon in exon 8 (Figure A3). Therefore, the efficiency ratio of generating rats carrying the required deletion was 5.5% (1 from 18 live births).

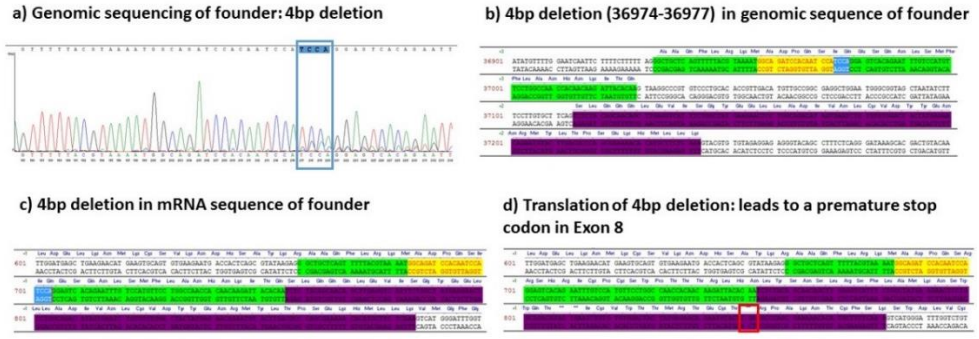

Figure A3 | **Genomic sequencing of the *Cyfip1* 4bp heterozygous deletion founder. a,** Manual reading of each double peak in the sequencing chromatograph (ABI Sequence Scanner) show that upstream of the deletion, sequences from the WT and modified allele are identical. At the site of the deletion i) the sequence read becomes mixed and ii) the sequence of the secondary peaks from the modified allele align with WT sequence, except they occur 4bp further upstream. This reveals the size and position of the modified allele. **b,** The 4bp deletion in the founder genomic sequence is highlighted in blue (Exon 7 highlighted in green; sgRNA site highlighted in yellow; exon 8 highlighted in purple) **c,** 4bp deletion in the mRNA sequence of the founder. **d,** The translation of mRNA from the 4bp-deleted sequence is bioinformatically predicted to create an early stop codon in Exon 8 (indicated by ***)

Assessment of potential off-target effects

The top 10 potential off-target (OT) sites, based on the sgRNA sequence used (GGCAGATCCACAATCCATCCagg), were generated and ranked using the MIT website http://crispr.mit.edu/ and corresponding gDNA PCR primer pairs were designed to flank each potential OT site (Figure A4a). Extracted gDNA from the founder animal and WT controls were used as templates for PCR, before each gDNA PCR product underwent the SURVEYOR assay (Figure A4b). The lack of NHEJ activity, as indicated by a lack of smaller secondary products, revealed no evidence for genomic disruptions at the selected sites and was further confirmed by sequencing the 10 OT site gDNA products (data not shown).

a) Top 10 potential off-target sites (MIT) for sgRNA

	Off Target Sequence	genomic coordinates	F primer	R primer
Injected gRNA sequence	GGCAGATCCACAATCCATCC**AGG**	chr1: 115302084-115302106		
OT Site 1	GGAAAATCCACCATCCATCCTGG	chr2: 95670408-95670430	ttgaaggcaggaacttctgg	tgacagatgcaccaagtgtt
OT Site 2	GTATCATCCACAATCCATCCAAG	chr4: 111917803-111917825	agtcactgctgccaaatcct	tacacccctccccacaaata
OT Site 3	GCCAAATCCACAATCCATGCCAG	chr14: 5746379-5746401	ttctttatgcccctgtcctg	gctttcacatgggggtctaa
OT Site 4	CTCAGAAACACAATCCATCCCAG	chr3: 86410011-86410033	tcccattttgcagatggact	ctttcaccttggaggctgtt
OT Site 5	TGTACAGCCACAATCCATCCAAG	chr8: 44004281-44004303	gatggtgtagaacacccaactg	ccaccatagctcaccgaaat
OT Site 6	GTCCGAACCCCAATCCATCCTAG	chr2: 84878323-84878345	ctgggaagcataaagggaag	ttgcagctattttgtcccagt
OT Site 7	TGGAAATCCACAATCCATCTCAG	chr2: 216880248-216880270	caccaggatccccaagtcta	ctgcctcaaaatcccagtgt
OT Site 8	AGCAGATCCAGATTCCATCCAGG	chr4: 70983405-70983427	gccattctgggataccatgt	acctctgtgggaagcaaaga
OT Site 9	AGCATAACCAGAATCCATCCGGG	chr11: 78421166-78421188	tcctctcttgcctcccagta	cgcaggacaagtgtgtgatt
OT Site10	TGCATACCCAGAATCCATCCTAG	chr6: 129397603-129397625	cagagcaggtgtgtggaaga	cgtttaatcagcgagtgcag

b) SURVEYOR assay of Top 10 potential off-target sites

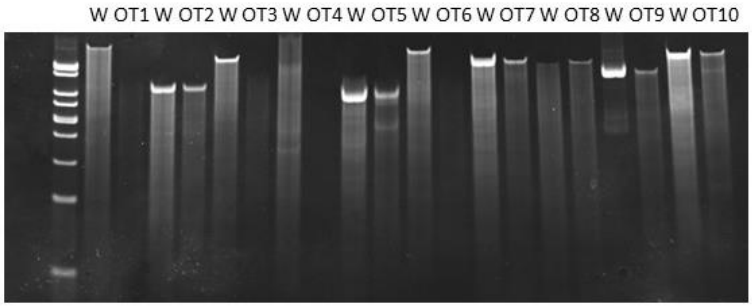

Figure A4 | **In silico identification of the Top 10 sgRNA off-target sites and NHEJ activity assessed by the SURVEYOR assay. a,** The top 10 OT sites were computed by taking into account the following i) total number of mismatches (either 3-4 mistmatches, highlighted in red), ii) mismatch absolute position (to accommodate for the relatively high disturbance of mismatches falling close to the PAM site) and iii) mean pairwise distance between mismatches to account for the steric effect of closely neighbouring mismatches in disrupting sgRNA -DNA interaction. A total of 156 off-target sites were found, although only 14 of which were intragenic. Corresponding PCR primer pairs were designed to flank the top 10 potential off target sites. **b,** Using extracted gDNA from the founder animal and WT controls, gDNA products were made to flank each potential OT site (~300-500bp amplicon) and run on the SURVEYOR assay. None of the 10 OT sites tested revealed NHEJ activity and this was later corroborated with sequencing data.

Breeding, re-derivation and maintenance at Charles River, UK

The F1 founder female was mated with male wild types at Horizon Discovery and generated F2 progeny containing the mutation confirming germline transmission. A total of five male positives were exported to Charles River, Lyon, France for re-derivation by embryo transfer. The resulting specific pathogen free (SPF) progeny were sent to Charles River, Margate, UK for routine breeding and generation of experimental groups for phenotypic testing. The standard breeding protocol was a heterozygous (Het) x WT cross giving rise to 1:1 average Het/WT progeny allowing full use of the litter and the generation of litter-mate controls. In most cases and unless otherwise stated, the genetic modification was transmitted through the male, resulting in the litters being raised by WT dams. On occasion, transmission was

through the female, this was to check for parent-of-origin effects. No POE have been found to press (personal communication from Cardiff). The model is viable and Charles River have reported no adverse (overt) effects on breeding performance, development, general health, and in addition no deviation from the expected Mendelian 1:1 ratio of Hets to WTs and no skewing of the sex ratios (personal communication from Cardiff).

PCR Genotyping

Genotyping was carried out twice, an initial assay from tissue sent from Charles River prior to transport of the rats to Bristol and then a further confirmatory assay post-mortem; in both cases the genotyping was carried out by colleagues in Cardiff. DNA was extracted using Qiagen DNEasy Blood & Tissue Kit, Cat No./ID: 69506 and PCR carried out using a 2-primer design with primer sequences: **Forward** - TAGGGCTGCTCAGTTTTTACG, **Reverse** - TTGTTGTGGTTGG CCAGGAA. For the cycling conditions 2ul of sample was added to 23ul of PCR Mastermix solution (12.5ul Promega GoTaq® G2 Green Mastermix M7822, M7823, 1ul of each primer and 8.5ul nuclease-free water) and placed in a thermal cycler under the following conditions: 1. 95^0C for 10:00, 2. 95^0C for 00:40, 3. 60^0C for 00:40, 4. 72^0C for 00:60, 5. Go to steps 2-4, 40 times, 6. 72^0C for 05:00, 7. 8^0C for ever.

The resulting PCR products for the mutant and WT sequences differed by 8bp, which produces a single band (WT) or a double band (Het), see Figure A5. To achieve this level of resolution, 10ul PCR product and 3ul Promega 6X Blue/Orange Loading Dye (G1881) were pipetted into a well in a 4% agarose gel and run for 1.5-2 hours at 150v.

Figure A5 | Gel image showing PCR products from and WT rats using ear tissue; WT products show as a single band, products as a double band, using this 2-primer design there was 100% concordance between the initial and post mortem genotype determinations.

Molecular verification and characterisation of the rat model

qPCR

The effect of the heterozygous genomic premature stop codon on transcription was tested by measuring *Cyfip1* mRNA gene expression in the brain tissue of via quantitative real-time PCR using the StepOnePlus System (Applied Biosystems, ThermoFisher Scientific). Rats were sacrificed by carbon dioxide inhalation and whole brains from mutant adult males were extracted (4.5-5 months old), alongside WT littermate controls (n = 10 / genotype). Prefrontal cortex (PFC) and hippocampal regions from both brain hemispheres were dissected free-hand and frozen on dry ice before storage at -80°C. RNA was extracted from the hippocampus and PFC (one hemisphere only) using RNeasy Kits (Qiagen), followed by DNase treatment of RNA (TURBO DNA-free Kit, Ambion, Life Technologies) and cDNA synthesis (RNA to cDNA EcoDry Premix, Random Hexamers, Clontech). cDNA was then prepared for SYBR-green (SensiFAST, HI-ROX, Bioline)-based quantitative real-time PCR with *Cyfip1*-specific primers (FOR: GAGGAGAATAAGTCCCGGTGG, REV: GTAGCGTGCCAGCTCAGAAA; targeting exon 11-12, oligonucleotides synthesised by Sigma-Aldrich). *Gapdh* and *Hprt* were used as housekeeper genes (Gapdh FOR: TCTCTGCTCCTCCCTGTTCT, Gapdh REV: TACGGCCAAATCCGTTCACA; Hprt FOR: TCCTCCTCAGACCGCTTTTC, Hprt REV: ATCACTAATCACGACGCTGGG) and the ΔΔCt method was used in order

to quantify normalised fold-change of mRNA gene expression (and graphed as 2-ΔΔCt). All primers were bioinformatically designed and assessed to span at least one exon-exon boundary and to match only for its target mRNA sequence in rat (primer-BLAST and nBLAST, NCBI). Primer efficiencies were experimentally determined through a dilution series of brain region-specific wildtype cDNA (efficiency of 90-110% was required, annealing temperature set at 60°C).

As illustrated in Figure A6, quantification by qPCR confirmed that the genomic disruption of *Cyfip1* leads to reduced *Cyfip1* mRNA expression in *Cyfip1* Het rats, with a reduction seen in both the PFC and hippocampus compared to WTs (PFC GENE $F_{(1,19)}$=41.259, P=0.0001; HIPP GENE $F_{(1,19)}$=26.74 P=0.0001, 1-way ANOVA on transformed ΔΔCt data and normality assessed by Shapiro-Wilk tests).

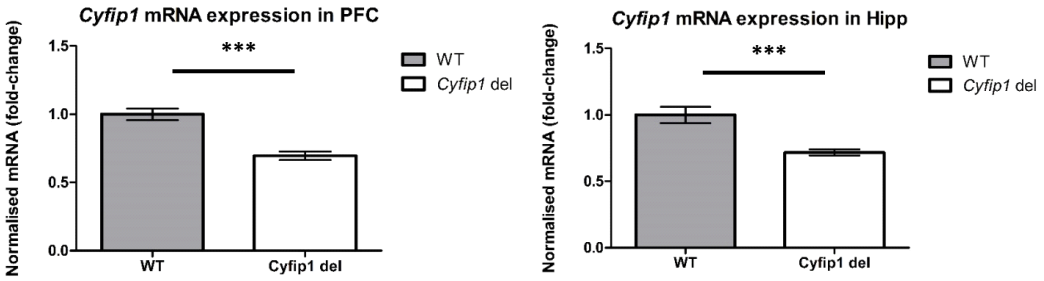

Figure A6 | mRNA levels determined by qPCR in brain tissue (PFC, prefrontal cortex; Hipp, hippocampus) from adult (4.5-5 months) WT and (n=10/genotype); *** p < 0.001

Western Blot

Semi-quantitative western blotting assays were employed to determine whether Cyfip1 protein was reduced in the brain of Cyfip1$^{+/-}$ rats. Hippocampal tissue dissected previously for the transcript analysis (other hemisphere, n = 10/genotype), was homogenized manually with a glass Dounce homogeniser in 1 ml of ice-cold lysis RIPA buffer (RIPA Lysis and Extraction Buffer, ThermoFisher Scientific) containing protease inhibitors (cOmplete Mini EDTA-free Protease Inhibitor, Roche, 1 tablet/ 10 ml RIPA). The homogenates were centrifuged at 12,000 rpm for 20 minutes at 4°C and aliquots of supernatant containing proteins stored at -80°C. A total of 40 µg of protein (quantified using Pierce BCA Protein Kit Assay, as per

manufacturer's instructions, ThermoFisher Scientific) in Laemmli sample buffer containing 1/20 β-mercaptoethanol (Bio-rad) were denatured at 95°C for 5 min prior to separation on a 4-12% gradient Bis-Tris Midi gel (NuPAGE, ThermoFisher Scientific) in 1x Bolt MES SDS Running Buffer (ThermoFisher Scientific) at a constant voltage of 115 V for 1 hr. Transfer was performed in 1 x Bolt Transfer Buffer (ThermoFisher Scientific) to Amersham Protran nitrocellulose membranes (GE Healthcare Life Sciences) at a constant voltage of 85 V for 2 hr 15 min at 4°C. Blots were blocked in 5% non-fat milk (Blocking Agent, Amersham, GE Healthcare Life Sciences) in 0.01 M Tris buffered saline solution containing 0.2% Tween 20 (TBST), and this TBST solution was used for all subsequent washes. Primary and fluorescent secondary antibodies were similarly diluted in TBST containing 0.2% Tween 20 and 5% milk and they were used at the following concentrations: Cyfip1 (AB6046, Millipore), 1:1,000; GAPDH (ab8245, Abcam), 1:5,000; IRDye® 680RD Goat anti-Rabbit IgG (Li-Cor, 926-68071), 1:15,000 and IRDye® 680RD Donkey anti-Mouse IgG (Li-Cor, 926-68072), 1:15,000. Incubation of blots in primary antibody solutions were at 4°C overnight, whilst fluorescent secondary antibodies were for 1 hr at RT. Blots were visualised using the 700nm channel of the Odyssey CLx Imaging System (Li-Cor). Software analysis (Image Studio, Li-Cor) was used for densitometry of each protein target and normalised to the loading control GAPDH.

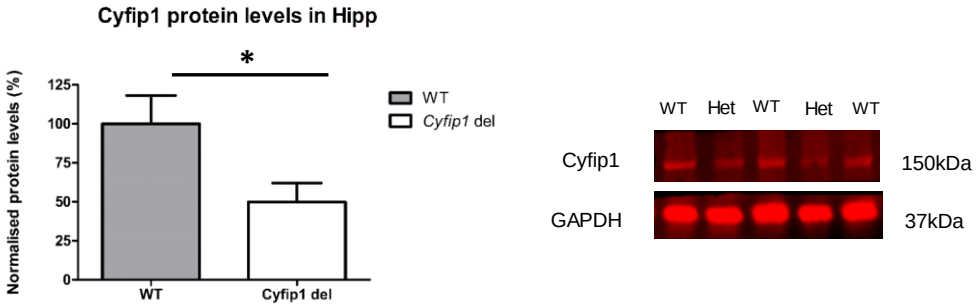

Figure A7 | Cyfip1 protein levels determined by Western Blot in brain tissue (Hipp, hippocampus) from adult (4.5-5 months) wild-type and Cyfip1 Het (n=10/genotype); *p<0.05

Figure A7 shows data from Western Blot indicating reduced Cyfip1 protein levels in hippocampal tissue of compared with WTs (hippocampal protein: $F_{1,18} = 4.996$,

p = 0.039, 1-way ANOVA, 1 Cyfip1 sample was> 2 SDs from the group mean and excluded as an outlier).